ERDC/CRREL TR-22-5

US Army Corps of Engineers®
Engineer Research and Development Center

ERDC
ENGINEER RESEARCH & DEVELOPMENT CENTER

Engineering for Polar Operations, Logistics, and Research (EPOLAR)

Continued Investigation of Thermal and Lidar Surveys of Building Infrastructure

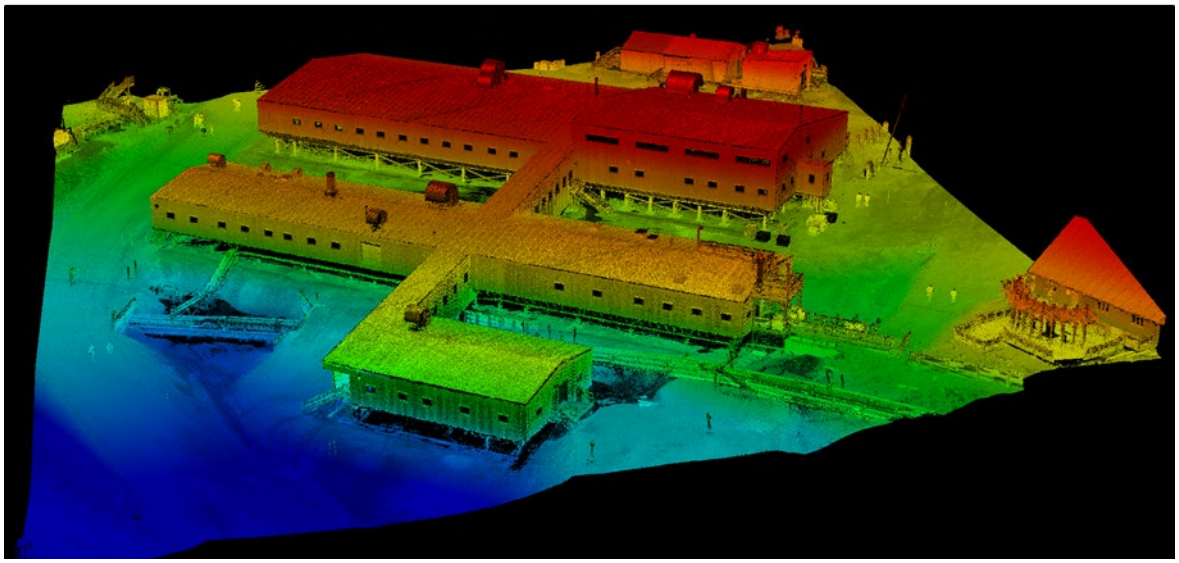
Crary Lab and Wet Utility Corridor, McMurdo Station, Antarctica

Adam L. LeWinter, Elias J. Deeb, Dominic L. Filiano, and David C. Finnegan

March 2022







Cold Regions Research and Engineering Laboratory

Approved for public release; distribution is unlimited.

The U.S. Army Engineer Research and Development Center (ERDC) solves the nation's toughest engineering and environmental challenges. ERDC develops innovative solutions in civil and military engineering, geospatial sciences, water resources, and environmental sciences for the Army, the Department of Defense, civilian agencies, and our nation's public good. Find out more at www.erdc.usace.army.mil.

To search for other technical reports published by ERDC, visit the ERDC online library at https://erdclibrary.on.worldcat.org/discovery.

Engineering for Polar Operations, Logistics, and Research (EPOLAR)

ERDC/CRREL TR-22-5
March 2022

Continued Investigation of Thermal and Lidar Surveys of Building Infrastructure

Crary Lab and Wet Utility Corridor, McMurdo Station, Antarctica

Adam L. LeWinter, Elias J. Deeb, Dominic L. Filiano and David C. Finnegan

U.S. Army Engineer Research and Development Center (ERDC)
Cold Regions Research and Engineering Laboratory (CRREL)
72 Lyme Road
Hanover, NH 03755-1290

Final Report

Approved for public release; distribution is unlimited.

Prepared for National Science Foundation, Office of Polar Programs
2415 Eisenhower Avenue
Alexandria, VA 22314

Under Engineering for Polar Operations, Logistics, and Research (EPOLAR)
Customer Order No. 1564557, ANT-19-11, "Continued Investigation of Thermal and Lidar Surveys of Building Infrastructure: Crary Lab and Wet Utility Corridor, McMurdo Station, Antarctica"

Abstract

We conducted a combined lidar and thermal infrared survey from both ground-based and Unmanned Aerial System (UAS) platforms at McMurdo Station, Antarctica, in February 2020 to assess the building thermal envelope and infrastructure of the Crary Lab and the wet utility corridor (utilidor). These high-accuracy, coregistered data produced a 3-D model with assigned temperature values for measured surfaces, useful in identifying thermal anomalies and areas for potential improvements and for assessing building and utilidor infrastructure by locating and quantifying areas settlement and structural anomalies.

The ground-based survey of the Crary Lab was similar to previous work performed by the team at both Palmer (2015) and South Pole (2017) Stations. The UAS platform focused on approximately 10,500 linear-feet of utilidor throughout McMurdo Station. The datasets of the two survey areas overlapped, allowing us to combine them into a single, georeferenced 3-D model of McMurdo Station. Coincident exterior temperature and atmospheric measurements and Global Navigation Satellite System real-time kinematic surveys provided further insights.

Finally, we assessed the thermal envelope of the Crary Lab and the structural features of the utilidor. The resulting dataset is available for analysis and quantification.

DISCLAIMER: The contents of this report are not to be used for advertising, publication, or promotional purposes. Citation of trade names does not constitute an official endorsement or approval of the use of such commercial products. All product names and trademarks cited are the property of their respective owners. The findings of this report are not to be construed as an official Department of the Army position unless so designated by other authorized documents.

DESTROY THIS REPORT WHEN NO LONGER NEEDED. DO NOT RETURN IT TO THE ORIGINATOR.

Contents

Abstract ii

Figures and Tables v

Preface x

1 Introduction 1

1.1 Background 1
1.2 Objectives 3
1.3 Approach 3

2 Lidar/TIR System Description 5

2.1 Lidar scanner 5
2.2 TIR camera 6
2.3 Unmanned Aerial System 7

3 Data Acquisition 10

3.1 External temperature measurements 10
3.2 Interior measurements 13
3.3 GNSS control survey 14
3.4 Handheld electro-optical imagery 14
3.5 Lidar/TIR system 15
3.6 UAS data acquisition 17

4 Data Processing 19

4.1 TLS lidar scans registration and georeferencing 19
4.2 TLS TIR radiometric value registration 20
4.3 TLS data products 21
4.4 UAS data processing 22
4.4.1 Trajectory processing 22
4.4.2 Lidar point cloud processing 23
4.4.3 Visible-spectrum image processing 23
4.4.4 TIR image processing 24
4.5 UAS data products 25

5 Results 27

5.1 Crary Lab—exterior surface thermal analysis 27
5.2 UAS results and discussion 34
5.2.1 Lidar point cloud and digital elevation model results 34
5.2.2 Utilidor point cloud analysis 37
5.2.3 Visible-spectrum colorized point cloud 42
5.2.4 Longwave TIR colorized point cloud 43

6 Conclusion and Recommendations 47

References 49

Acronyms and Abbreviations 50

Appendix A: CRREL Lidar/TIR System Data Acquisition Procedure 52

Appendix B: CRREL RiCOPTER Operation Checklists 54

Appendix C: Crary Lab Features Catalog 58

Report Documentation Page 265

Figures and Tables

Figures

1 Riegl VZ-1000 TLS lidar scanner (front and side views) used in the lidar/TIR system. The sensor is portable and light enough for one person to carry and set up in the field 5

2 *Left*: FOV of the lidar sensor (*blue shaded area*) compared with the FOV of the TIR (*red shaded area*). While the lidar sensor has a wider FOV, the typical setup of the system places the focus object (building) within the narrower TIR FOV, providing full coverage from both sensors. *Right*: Lidar/TIR system in use 7

3 Example panoramic thermal image, colored by temperature (−15 °C to 5 °C), of a portion of the Phase 1 Crary Lab, McMurdo. The image is composed from individual images collected by the TIR camera that are automatically referenced and stitched together to generate the product. In general, this example thermal image captures consistent temperature values on similarly oriented building surfaces with expected higher temperatures around loading docks, doors, and windows 7

4 RiCOPTER UAS setup at McMurdo Station with VUX-1UAV lidar sensor, FLIR Tau2 thermal infrared camera, Sony A7R-III optical camera, and Applanix APX-20 inertial measurement unit mounted to the belly of the aircraft 8

5 Crary Lab survey map indicating the location of scan positions (*red triangles*), reflectors (*green circles*), and external-air-temperature sensor placement (*red circles*) 11

6 Air-temperature measurements from eight sensors temporarily installed around the exterior of the Crary Lab. Timing of the TLS scan positions are identified as *dashed black lines*. Variation in temperatures is due to sensor location and the effects of solar exposure and winds. Sensor #20045687 was attached to the tripod with the instrument package and shows the influence of bringing the instruments inside when not in use 12

7 Plot of 10-minute air-temperature measurements for 3–7 February 2020 from the McMurdo AWOS (*solid black line*) alongside the temporary exterior temperature HOBO sensors (*various solid colored lines*) and the TLS scan timing (*black dashed lines)* 12

8 Example of interior air temperatures provided by the automated monitoring system for Phase 1 (*top*) and Phases 2 and 3 (*bottom*) Crary Lab spaces 13

9 A 10 cm cylinder reflector temporarily installed during the Crary Lab lidar/TIR survey. The reflectors, with 10 cm height and diameter dimensions, provide reference coordinates used to tie the 3-D model to a global coordinate system 14

10 Electro-optical image (*right*) captured of the Crary Lab compared to the intensity-colored 3-D model (*left*), highlighting the utility of capturing true-color images in conjunction with the lidar/TIR data acquisition. The electro-optical imagery is helpful in identifying specific building and infrastructure materials and for providing visual context of the survey area 15

11 CRREL's lidar/TIR system at McMurdo Station 16

12 Example 2-D panoramic TIR images collected from two perspectives of the Crary Lab, colored by a −15 °C to +5 °C color scale 16

13 Visualization of the coarse registration process in which an unregistered scan is roughly aligned to a registered, georeferenced baseline scan. Utilidor-ScanPos001 (*left*) was tied to the WGS84 APS coordinate system using reflectors and the GNSS RTK survey. Crary-ScanPos015 (*right*) was captured from a position of significant overlap relative to Utilidor-ScanPos001. Common features are manually identified between each point cloud (yellow dots), and Crary-ScanPos015's position and orientation are subsequently modified 20

14 TLS point cloud data of the Crary Lab was collected from 21 different scan positions. Each resulting point cloud covered a portion of the Station. *Left*: Image shows eight of these point clouds, colored by scan position. *Right*: After registration and georeferencing, the individual scans combine to create a complete 3-D model of the Station 20

15 A 3-D model captured of the Crary Lab colored by intensity (*left*) and temperature (*right*). Mapping the TIR imagery onto the 3-D model visually represents thermal variations 21

16 Plot of the resulting UAS lidar point cloud overlaid on the McMurdo Station 2018–2019 survey map with the four lift trajectories displayed. Note that the PIC/VO programed the flight trajectories for automated flight, focusing on the main areas of the McMurdo Station utilidor. Because of the wide FOV of the lidar scanner, the majority of the station was collected even though the flight locations were spatially limited. The point cloud is colored by intensity 22

17 Sample image captured by the onboard Sony A7R-III visible-spectrum camera at McMurdo Station. A section of the utilidor, the Chalet, and lower section of the Crary Lab is visible. The UAS payload captures coincident lidar point clouds, visible spectrum imagery, and longwave TIR imagery during flight 23

18 FLIR Tau2 longwave TIR image overlaid on an image captured by the Sony A7R visible-spectrum camera. This figure illustrates the smaller detector size in the Tau2, resulting in a lower-resolution image compared to the Sony camera. The temperature color scale for the image is −15 °C to 25 °C 24

19 Orthorectified image derived from images captured by the FLIR Tau2 during the wastewater lift. Areas of direct solar exposure are evident by the high temperature (bright yellow/orange sections), while shadowed areas or surfaces of low reflectance are indicated by darker sections. The temperature color scale for the image is −15 °C to 25 °C 25

20 Construction phases and subdivision of the Crary Lab for the purpose of analyzing the exterior surface thermal results. Phase 1, 2, and 3 along with the Phase 1–2 and Phase 2–3 connectors are identified 27

21 Crary Lab construction phases labeled with respect to the construction phase and compass aspect as it pertains to subsequent 3-D thermal example figures 28

22 A 3-D thermal model of Phase 1, North, Loading Dock 01 (P1N-LD-01). *Top left*: Phase 1, North, highlighted in *red* on the Crary Lab map. *Bottom*: Thermal image across Phase 1, North, at a −15 °C to −5 °C scale with focus section identified with a *red box*. *Top right*: Focus section highlighted P1N-LD-01 29

23 A 3-D thermal model of Phase 1, North, Door 04 (P1N-D-04). *Top left*: Phase 1, North, highlighted in *red* on the Crary Lab map. *Bottom*: Thermal image across Phase 1, North, at a −15 °C to −5 °C scale with focus section identified with a *red box*. *Top right*: Focus section highlighted P1N-D-04 30

24 A 3-D thermal model of Phase 1, West, Window 03 (P1W-W-03). *Top left*: Phase 1, West, highlighted in *red* on the Crary Lab map. *Bottom*: Thermal image across Phase 1, West, at a −15 °C to −5 °C scale with focus section identified with a *red box*. *Top right*: Focus section highlighted P1W-W-03 30

25 A 3-D thermal model of Phase 1, Southwest, Window 01 (P1SW-W-01). *Top left*: Phase 1, Southwest, highlighted in *red* on the Crary Lab map. *Bottom*: Thermal image across Phase 1, Southwest, at a −15 °C to −5 °C scale with focus section identified with a *red box*. *Top right*: Focus section highlighted P1SW-W-01 31

26 A 3-D thermal model of Phase 1, Southwest, Window 05 (P1W-W-05). *Top left*: Phase 1, Southwest, highlighted in *red* on the Crary Lab map. *Bottom*: Thermal image across Phase 1, Southwest, at a −15 °C to −5 °C scale with focus section identified with a *red box*. *Top right*: Focus section highlighted P1SW-W-05 31

27 A 3-D thermal model of Phase 1, Southwest, Window 11 (P1W-W-11). *Top left*: Phase 1, Southwest, highlighted in *red* on the Crary Lab map. *Bottom*: Thermal image across Phase 1, Southwest, at a −15 °C to −5 °C scale with focus section identified with a *red box*. *Top right*: Focus section highlighted P1SW-W-11 32

28 A 3-D thermal model of Phase 3, North, Window 01 (P3N-W-01). *Top left*: Phase 3, North, highlighted in *red* on the Crary Lab map. *Bottom*: Thermal image across Phase 3, North, at a −15 °C to −5 °C scale with focus section identified with a *white box*. *Top right*: Focus section highlighted P3N-W-01 32

29 A 3-D thermal model of Phase 2, East, Loading Dock 01 (P2E-LD-01). *Top left*: Phase 2, East, highlighted in *red* on the Crary Lab map. *Bottom*: Thermal image across Phase 2, East, at a −15 °C to −5 °C scale with focus section identified with a *white box*. *Top right*: Focus section highlighted P2E-LD-01 33

30 A 3-D thermal model near Phase 2, Northeast, Window 04 (P2NE-W-04). *Top left*: Phase 2, Northeast, highlighted in *red* on the Crary Lab map. *Bottom*: Thermal image across Phase 2, Northeast, at a −15 °C to −5 °C scale with focus section identified with a *red box*. *Top right*: Focus section highlighted P2NE-W-04 33

31 Oblique view (looking north) of the resulting lidar point cloud of McMurdo Station captured by the UAS. The point cloud is colored by height (relative scale) and shaded by surface intensity (range-independent surface reflectance). Areas with lower surface intensity are darker, while areas with high intensity are lighter 34

32 Oblique view (looking northeast) of the resulting lidar point cloud of McMurdo Station, focused on the Crary Lab, captured by the UAS. The point cloud is colored by height (relative scale) and shaded by surface intensity (range-independent surface reflectance). Areas with lower surface intensity are darker, while areas with high intensity are lighter. The roof surfaces from the UAS lidar point cloud were used to fill in the gaps from the TLS survey, which was unable to capture roof features due to line-of-sight limitations 35

33 Lidar point cloud from the full FOV dataset, colored by height and shaded by intensity, overlaid on the McMurdo Station 2018–2019 survey map. Of note are the power and communication cables throughout the station, visible as lower-intensity (darker) lines 35

34 Lidar point cloud from the full FOV dataset, colored by density, overlaid on the McMurdo Station 2018–2019 survey map. Areas with less than 100 pts/m^2 are colored *blue*, while areas with greater than 1000 pts/m^2 are colored *red*. Areas of high point densities correspond to sections below the UAS flight lines 36

35 A 0.3 m bare-earth digital elevation model (DEM) derived from the full FOV dataset, colored by height, overlaid on the McMurdo Station 2018–2019 survey map. Ground points were identified using a bare-earth-extraction algorithm 36

36 Building outlines (*red*) and roof vectors (*yellow*) overlaid on the 0.3 m bare-earth DEM derived from the full FOV dataset. The DEM uses a hillshade colorization. This data product is overlaid on the McMurdo Station 2018–2019 survey map. Building outlines and roof vectors were identified using a building extraction tool in Quick Terrain Model 37

37 Isolated point cloud covering surfaces representing the McMurdo Station utilidor (colored *red*), overlaid on the McMurdo Station 2018–2019 survey map. The utilidor surfaces were isolated from the larger full FOV point cloud dataset in an effort to simplify future analysis of the utilidor features 38

38 Oblique view of the lidar point cloud from a section of the utilidor below the Crary Lab, colored by height and shaded by intensity (range-independent surface reflectance). A cross section of the utilidor is show by the inset image, showing the level of detail achieved from the UAS lidar point cloud. Individual sections of insulation, pipes, and conduit can be identified within the cross-sectional point cloud 38

39 Utilidor profiles derived from the lidar point cloud. *Top*: Profiles 1–5 overlaid on the McMurdo Station 2018–2019 survey map. Profiles are individually colored. *Bottom*: cross-sectional view of the utilidor for Profiles 1–5. Points are colored by classification (*green* is ground points, *red* and *blue* are nonground points). Where applicable, the length of the utilidor section and the corresponding slope is noted within the cross-sectional view (e.g., P1 length = 131.7 m with a slope of 1.151°) 39

40 Utilidor profiles derived from the lidar point cloud. *Top*: Profiles 6–10 overlaid on the McMurdo Station 2018–2019 survey map. Profiles are individually colored. *Bottom*: cross-sectional view of the utilidor for Profiles 6–10. Points are colored by classification (*green* is ground points, *red* and *blue* are nonground points). Where applicable, the length of the utilidor section and the corresponding slope is noted within the cross-sectional view (e.g., P10 length = 76.74 m with a slope of 1.10°) 40

41 Utilidor profiles derived from the lidar point cloud. *Top*: Profiles 11–15 overlaid on the McMurdo Station 2018–2019 survey map. Profiles are individually colored. *Bottom*: cross-sectional view of the utilidor for Profiles 11–15. Points are colored by classification (*green* is ground points, *red* and *blue* are nonground points). Where applicable, the length of the utilidor section and the corresponding slope is noted within the cross-sectional view (e.g., P11 length = 69.05 m with a slope of 0.88°) 41

42 Utilidor profiles derived from the lidar point cloud. *Top*: Profiles 16–20 overlaid on the McMurdo Station 2018–2019 survey map. Profiles are individually colored. *Bottom*: cross-sectional view of the utilidor for Profiles 16–20. Points are colored by classification (*green* is ground points, *red* and *blue* are nonground points). Where applicable, the length of the utilidor section and the corresponding slope is noted within the cross-sectional view (e.g., P16 length = 77.26 m with a slope of 2.69°).....42

43 Plot of the resulting point cloud data captured by UAS at McMurdo Station overlaid on the McMurdo Station 2018–2019 survey map, colored by visible-spectrum imagery. Since the FOV of the Sony A7R-III camera is spatially limited compared to the FOV of the lidar sensor, the resulting point cloud with RGB color values is also more spatially limited 43

44 *Left*: Oblique view of the lidar point cloud near the helipad at McMurdo Station, colored by visible-spectrum imagery. *Right*: Same view as left image, colored by height (blue to red = low to high height) and shaded by intensity (dark to light = low to high intensity).....43

45 Plot of the resulting point cloud data captured by UAS at McMurdo Station overlaid on the McMurdo Station 2018–2019 survey map, colored by TIR imagery 44

46 Example of the TIR colorization process. *Top left*: Oblique view of the upper helipad area at McMurdo Station, colored by intensity. *Top right*: The same view colored by TIR-derived temperature values (temperature scale is −15 °C to 25 °C). *Bottom*: The same view as the top images, colored by temperature (dark to light = low to high temperature) and shaded by intensity (dark to light = low to high intensity).....44

47 Orthorectified image from the helipad lift. Temperature scale is −15 °C to 25 °C. Sections of the utilidor are identifiable by the lower-temperature (darker) linear surfaces.....45

48 Orthorectified image from the wastewater lift. Temperature scale is −15 °C to 25 °C. Sections of the utilidor are identifiable by the lower-temperature (darker) linear surfaces.....45

49 Orthorectified image from the dormitory lift. Temperature scale is −15 °C to 25 °C. Sections of the utilidor are identifiable by the lower-temperature (darker) linear surfaces.....46

50 Orthorectified image from the carpentry shop lift. Temperature scale is −15 °C to 25 °C. Sections of the utilidor are identifiable by the lower-temperature (darker) linear surfaces.....46

Tables

1 Specifications of the Riegl VUX-1UAV lidar scanner.....9

2 Specifications of the Applanix APX-20 IMU.....9

3 Specifications of the FLIR Tau2 longwave TIR camera.....9

4 Specifications for the Sony A7R-III visible-spectrum camera.....9

5 Mission list and parameters for RiCOPTER deployment at McMurdo Station 17

6 Crary Lab perspective view nomenclature 29

Preface

This study was conducted for the National Science Foundation, Office of Polar Programs, Antarctic Infrastructure and Logistics (NSF-OPP-AIL), under Engineering for Polar Operations, Logistics, and Research (EPOLAR) Customer Order No. 1564557, ANT-19-11, "Continued Investigation of Thermal and Lidar Surveys of Building Infrastructure: Crary Lab and Wet Utility Corridor, McMurdo Station, Antarctica." The technical monitor was Ms. Margaret Knuth, Chief Program Manager, NSF-OPP, U.S. Antarctic Program.

The work was performed by the Lidar and Wetlands Group of the Remote Sensing / GIS Center of Expertise (RS/GIS CX), U.S. Army Engineer Research and Development Center, Cold Regions Research and Engineering Laboratory (ERDC-CRREL). At the time of publication, Dr. Elias Deeb was lead for the Lidar and Wetlands Group; Mr. David Finnegan was director, RS/GIS CX; and Dr. Rosa Affleck was the program manager for the Antarctic EPOLAR program. The acting deputy director of ERDC-CRREL was Mr. Bryan E. Baker, and the director was Dr. Joseph L. Corriveau.

COL Teresa A. Schlosser was commander of ERDC, and Dr. David W. Pittman was the director.

1 Introduction

1.1 Background

With plans for modernization of McMurdo Station underway, opportunity to further assess energy efficiency (e.g., building thermal envelope) of existing and new infrastructure is essential to assist the National Science Foundation, Office of Polar Programs, Antarctic Infrastructure and Logistics (NSF-OPP-AIL) team in making decisions that will help control operational budgets. As an example, coordinated lidar and thermal infrared (TIR) surveys of building infrastructure at Palmer (Deeb and LeWinter 2018) and Amundsen-Scott South Pole (LeWinter et al. 2018) Stations highlighted building deficiencies and superior building performance, respectively. These surveys, at centimeter accuracy and resolution, also provided a 3-D model for planned construction activities and the assessment of building infrastructure, such as South Pole Station settlement measurements. Moreover, for renovations currently planned, interrogating the thermal signature of 3-D building models prior to and following renovations would allow a more accurate estimate of return on investment of the executed renovations and of any future building improvements under consideration.

Located on the bare volcanic rock of Hut Point Peninsula, McMurdo Station is the largest Antarctic station. With a harbor, nearby landing strips on the ice shelf, and a helicopter pad, it is the logistics hub of the U.S. Antarctic Program (USAP). It supports multidisciplinary research across the Antarctic continent for both domestic interests of NSF and collaborations across international partnerships. The horizontal infrastructure at McMurdo Station ranges in size from shacks to three-story structures and serves a variety of purposes (dormitories, administrative buildings, power and water distillation plants, and warehouses). This diversity brings many challenges when maintaining building temperatures at a comfortable working level; and there is added difficulty, and therefore cost, of supplying the station with heating fuel. Energy efficiency of building infrastructure plays a crucial role in operating remote stations like McMurdo for USAP.

As part of the Antarctic Infrastructure Modernization for Science initiative, NSF-OPP-AIL has identified energy efficiency as a key priority. To evaluate the current condition, potential maintenance required, and architectural design performance in the harsh Antarctic environment, NSF-OPP-

AIL has deemed it prudent to assess existing infrastructure. Moreover, this effort builds on previous work by the U.S. Army Engineer Research and Development Center, Cold Regions Research and Engineering Laboratory (ERDC-CRREL) to integrate and develop advanced processing techniques to fuse the disparate lidar and TIR datasets. The system combines both spatial and thermal measurements of target surfaces as a comprehensive tool for assessing building envelopes and as a means of separating geometric and radiometric influences from one another.

TIR is a passive, nondestructive and stand-off method to identify thermal variations across building surfaces that contribute to heat loss and building inefficiencies. With a highly sensitive (0.05°C at 30°C*) detector, small thermal anomalies can be quantified. Lidar is a fast and accurate technology capable of obtaining from a ground-based sensor 3-D measurements at high spatial and temporal resolutions with millimeter-scale accuracy and ranges exceeding 6 km. In addition, lidar also measures surface reflectance values at each measured surface point, corresponding to wavelength characteristics and surface reflectance properties (wood, aluminum, concrete, etc.). Because the surface reflectance of the transmitted laser pulse varies with different building materials, a comparison between the reflectance and thermal values helps to identify building materials that are more or less energy efficient. In addition, the resulting 3-D point cloud may be used to make precise measurements, to identify areas of change when referenced to previously collected data, and to compare with architectural drawings for assessing construction quality. Furthermore, when collected with high-accuracy Global Navigation Satellite System (GNSS) position data, it is possible to tie the point cloud to a global coordinate system.

TIR and lidar surveys are commonplace in the fields of building envelope assessments and spatial measurements, respectively. Phetteplace (2007) presented findings from infrared surveys conducted between 2005 and 2007 of the South Pole Elevated Station. However, if collected independently, it is both labor intensive and difficult to merge these datasets to produce a 3-D thermal model. CRREL's integrated lidar/TIR system collects these two disparate datasets coincidently. With known spatial relations and error between sensors, along with laser and camera calibrations,

* For a full list of the spelled-out forms of the units of measure used in this document, please refer to *U.S. Government Publishing Office Style Manual*, 31st ed. (Washington, DC: U.S Government Publishing Office, 2016), 248–252, https://www.govinfo.gov/content/pkg/GPO-STYLEMANUAL-2016/pdf/GPO-STYLEMANUAL-2016.pdf.

it is possible to accurately combine these measurements. Combining the data products derived from TIR, lidar, and GNSS produces a 3-D thermal model that includes the thermal signature, a range-independent surface reflectance value, and an absolute location for each individual measurement in space.

1.2 Objectives

For this effort, we aimed to deploy the lidar/TIR system during the austral summer to conduct surveys of the Crary Lab by using a ground-based, tripod configuration and an unmanned aerial system (UAS) for the aboveground wet utility corridor (utilidor). From these data, CRREL can provide comprehensive 3-D models with thermal signatures assigned to each individual lidar point measurement. These data may then be used to assess the building envelope and utilidor insulation by identifying any thermal anomalies, which indicate a deficiency in the insulation or building material and design, and to identify any infrastructure concerns due to building settlement and ice-sheet movement.

Previous studies at South Pole Station (LeWinter et al. 2018) required a system capable of operating in extreme cold. Daily mean temperatures in February at McMurdo Station range from approximately –17°C to –8°C. Therefore, based on minimum operating temperatures of –10°C and –15°C for the lidar scanner and TIR camera, respectively, we considered it reasonable to not actively heat the lidar/TIR system during these acquisitions; and the previously designed thermal jacket was not required.

1.3 Approach

To realize the objectives of this effort, we carried out the following tasks:

- Deployed both a ground-based and UAS lidar/TIR system to McMurdo Station in February 2020 to collect thermal and spatial measurements of the exterior of the Crary Lab and approximately 10,500 linear-feet of aboveground utilidor. These data were tied to a global coordinate system (WGS84 APS* [EPSG†:3031] with WGS84 ellipsoid height) utilizing GNSS real-time kinematic (RTK) equipment.

* World Geodetic System 1984 Antarctic Polar Stereographic

† European Petroleum Survey Group

- Collected environmental conditions by using existing measurement infrastructure (permanent weather station sensors) alongside temporarily deployed temperature and relative humidity sensors
- Used a handheld electro-optical camera (Nikon D800) to collect standard imagery for both reference and documentation of identified areas of thermal deficiencies
- Processed all collected data, combining the lidar, TIR, and GNSS measurements to produce a 3-D model (LAZ file format) of the Crary Lab, the utilidor, and the McMurdo Station as a whole
- Analyzed resulting data to identify building thermal envelope anomalies, deficiencies, and infrastructure concerns for both the Crary Lab and the utilidor while suggesting courses of action to mitigate any identified issues and to confirm the effectiveness of current building material and design techniques

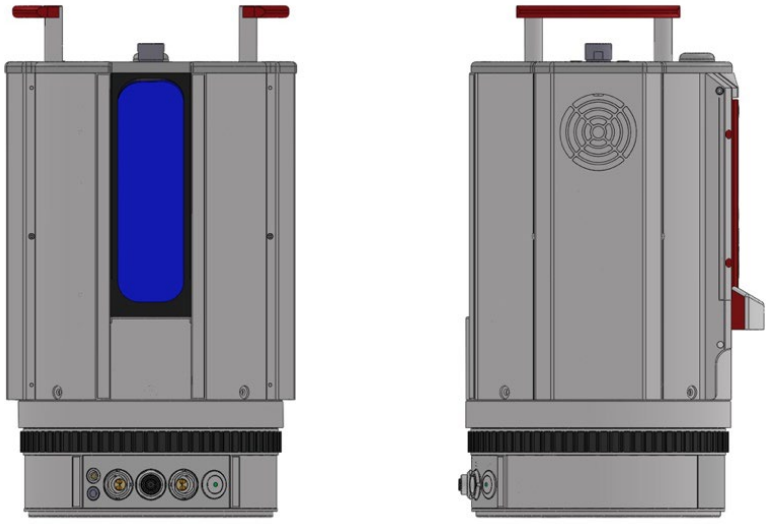
We conducted the above data collection tasks on-site at McMurdo Station and all postprocessing and analysis tasks at the CRREL offices in Hanover, New Hampshire. Within this report, we discuss the data collected and resulting analysis to inform USAP for future maintenance of McMurdo Station.

2 Lidar/TIR System Description

2.1 Lidar scanner

We chose a Riegl VZ-1000 terrestrial laser scanner (TLS) as the lidar sensor (Figure 1), which had performed well when deployed in 2015 at Palmer Station and in 2017 at South Pole Station. The VZ-1000 also provides the mounting platform, rotating stage, and power supply for the TIR sensor. The VZ-1000 is a full-waveform, time-of-flight sensor capable of capturing multiple range measurements per individual laser pulse. This better represents measured surfaces compared to discrete or single-return lidar sensors by capturing a higher point density (typically measured by points per square meter) and allowing for measurements through partially obstructing objects (fencing, windows, and blowing snow). The sensor uses a 1550 nm wavelength pulsed laser (Class 1 laser, eye safe) to measure range and surface reflectance of target objects. With a 360° × 100° (horizontal and vertical, respectively) field of view (FOV) and a maximum pulse rate of 300 kHz, the scanner captures a full FOV in as little as 8 seconds with a maximum measurement range of 1400 m and an accuracy and precision of 8 mm and 5 mm, respectively.

Figure 1. Riegl VZ-1000 TLS lidar scanner (front and side views) used in the lidar/TIR system. The sensor is portable and light enough for one person to carry and set up in the field.



The acquisition parameters, including laser pulse rate and angular step width (vertical/horizontal angle between consecutive laser pulses), for the scanner are configurable based on the desired measurement range, time of

scan acquisition, target-object albedo, and resulting point density. At the highest pulse rate (300 kHz) and smallest angular increment (0.0024°), the scanner is capable of capturing tens of thousands of point measurements per square meter, resulting in subcentimeter point spacing.

2.2 TIR camera

Hard mounted on the top of the lidar sensor is an InfraTec VarioCAM HD 880 TIR camera. Using an uncooled microbolometer, 1024 × 768 pixel focal-plane array with a 7.5–14 μm spectral range, the camera has a measurement range of –40°C to 1200°C, a measurement accuracy of ±1.5% of reading when surface temperatures are below 0°C, and a thermal resolution better than 0.05°C at 30°C (Figure 2). To best match the lidar vertical FOV (100°), a wide-angle 15 mm lens (60° × 47° FOV) was used. By mounting the camera in a portrait orientation (camera rotated 90°) onto the lidar sensor, this produces a 10° and 30° shadow below and above level, respectively, compared to the lidar data (Figure 2). To mitigate this data shadow, we selected the system setup positions to keep the building within the TIR FOV with multiple setup positions used to fully capture the target surfaces.

For the best control of TIR image acquisition, the camera is operated independently from the lidar scanner, relying on the scanner for only power and system rotation, allowing for full panoramic image acquisition. The resulting images are output in a proprietary .irb file format, which is imported into InfraTec's IRBIS 3 software package, built to support image analysis and exploitation of InfraTec TIR imagery (Figure 3). These images preserve per-pixel calibrated radiometric values (temperature), which are converted to absolute temperature values. These images are then exported for further use.

Figure 2. *Left*: FOV of the lidar sensor (*blue shaded area*) compared with the FOV of the TIR (*red shaded area*). While the lidar sensor has a wider FOV, the typical setup of the system places the focus object (building) within the narrower TIR FOV, providing full coverage from both sensors. *Right*: Lidar/TIR system in use.

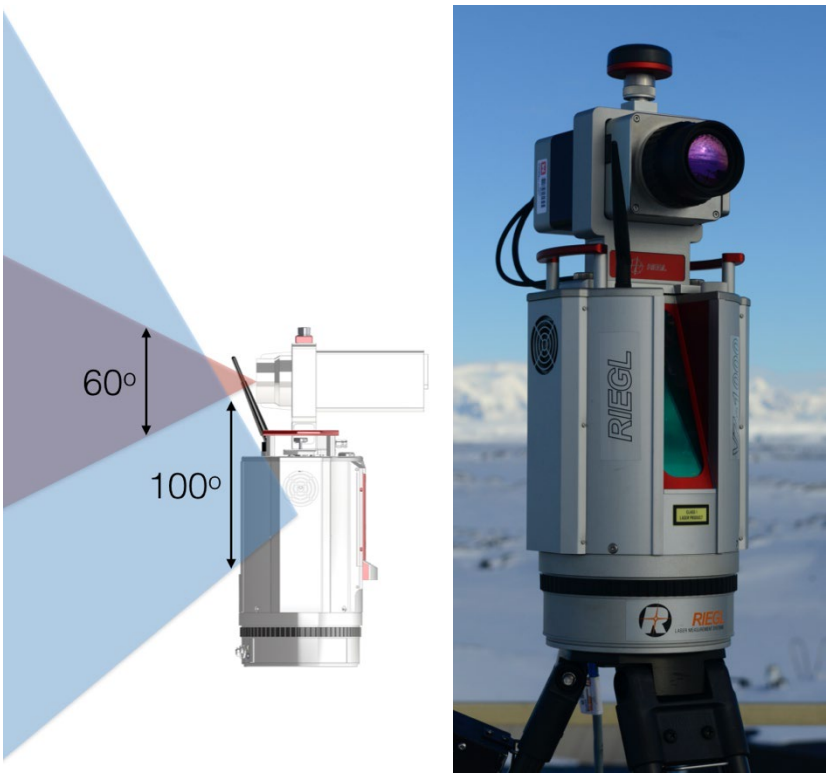
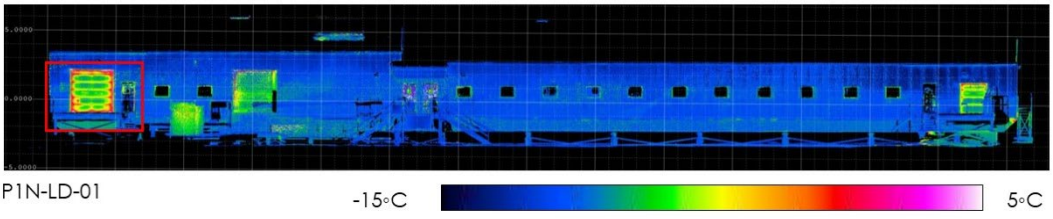


Figure 3. Example panoramic thermal image, colored by temperature (−15 °C to 5 °C), of a portion of the Phase 1 Crary Lab, McMurdo. The image is composed from individual images collected by the TIR camera that are automatically referenced and stitched together to generate the product. In general, this example thermal image captures consistent temperature values on similarly oriented building surfaces with expected higher temperatures around loading docks, doors, and windows.



2.3 Unmanned Aerial System

We chose a Riegl RiCOPTER with a VUX-1UAV unmanned laser scanning (ULS) system for the UAS data collection at McMurdo Station, specifically for capturing the roof surfaces over the Crary Lab and detailed lidar, visible-spectrum imagery, and TIR imagery along the McMurdo utilidor (Figure 4). The Riegl RiCOPTER is a Class II (<25 kg max takeoff

weight) multirotor UAS system produced by Riegl LMS GmbH. The UAS is operated by a designated pilot in command (PIC) and visual observer (VO). Takeoff, dynamic alignment, and landing flight procedures are conducted through manual flight operations by the PIC, while data acquisition flight lines are flown using an automated flight plan carried out by an onboard flight controller, uploaded to the UAS by the VO during flight start-up procedures.

Figure 4. RiCOPTER UAS setup at McMurdo Station with VUX-1UAV lidar sensor, FLIR Tau2 thermal infrared camera, Sony A7R-III optical camera, and Applanix APX-20 inertial measurement unit mounted to the belly of the aircraft.



The payload for the McMurdo deployment included a Riegl VUX-1UAV lidar scanner with integrated FLIR Tau2 thermal camera, Sony A7R-III high-resolution visible-spectrum optical camera, and an Applanix APX-20 high-precision inertial measurement unit (IMU). Tables 1–4 show sensor specifications for the VUX-1UAV and accessory sensors. The laser scanner has a 360° FOV, with a portion of that FOV necessarily obstructed by the UAS airframe above. The scanner has a maximum pulse rate of 550 kHz with an accuracy and precision of 10 mm and 5 mm, respectively. The IMU logs the sensors position and orientation in time (trajectory), and when combined with a static GNSS base station collecting positional data at 1 Hz is capable of achieving positional accuracies of 0.02–0.05 m for the aircraft trajectory. When the lidar data is combined with the IMU trajectory, typical point cloud accuracies are within 0.02–0.08 m.

Table 1. Specifications of the Riegl VUX-1UAV lidar scanner.

VUX-1UAV Parameters	Specification
Laser Wavelength	1550 nm
Target Operating Altitude	70–80 m
Accuracy	10 mm
Precision	5 mm
Pulse Repetition Frequency	550 kHz
Scan Angle	360° (full FOV); 110° (used FOV)
Beam Divergence	0.5 milliradian

Table 2. Specifications of the Applanix APX-20 IMU.

APX-20 Parameters	Specification
Weight	0.68 kg
Size	85 × 85 × 66 mm
Embedded GNSS	L1/L2, GPS, GLONASS, BeiDou, Galileo, QZSS, SBAS, L-Band
Power	5 V direct current
Output Refreshing Rate	200 Hz
Time Tagging	Pulse per second output
Heading Accuracy	0.035°
Roll and Pitch Accuracy	0.015°
Position Accuracy	0.02–0.05 m

Table 3. Specifications of the FLIR Tau2 longwave TIR camera.

FLIR Tau2 Parameters	Specification
Detector	640 × 512 vanadium oxide microbolometer
Pixel Size	17 µm
Spectral Band	7.5–13 µm
Performance	<50 mK @ f/1.0

Table 4. Specifications for the Sony A7R-III visible-spectrum camera.

Sony A7R-III Parameters	Specification
Megapixels	42.4
Sensor Size	35.9 × 24.0 mm
Pixel Dimensions	7952 × 5304
Pixel Size	4.51 µm
Body Dimensions	126.9 × 95.6 × 73.7 mm

3 Data Acquisition

We collected survey data 2–7 February 2020 at McMurdo Station. While we made every effort to collect these data in stable, consistent environmental conditions (wind, solar exposure, cloud cover, lack of precipitation, etc.), the challenges of rapidly changing atmospheric conditions and the reality of a full 24 hours of daylight resulted in variations of thermal conditions throughout the acquisition. The "Results" portion of this report further details the effects of these variations, especially that of direct solar exposure during the TIR measurements.

Along with the lidar/TIR data acquisition from both ground-based and UAS platforms and supporting GNSS measurements, we performed additional on-site measurements to support processing and analysis of the 3-D thermal building envelope. In particular, interior and exterior temperature measurements aid in the analysis of the building performance with respect to temperature gradients from inside the Crary Lab to the external surfaces. In addition to placing temporary sensors outside of the building, we leveraged the extensive environmental monitoring built into the Crary Lab and received temperature logs from multiple locations from station management. Further, in an effort to provide visual context to potential areas of interest within the 3-D model, we captured images from each scan position and of any identified thermal anomalies by using a handheld digital camera. Figure 5 shows the distribution of measurements with respect to the Crary Lab.

3.1 External temperature measurements

A set of eight HOBO Pro v2 sensors were temporarily distributed on, below, and around the Crary Lab to log exterior air temperatures from different aspects of the building during the survey. The sensors, which are housed in a weatherproof enclosure and have internal logging capability, a temperature measurement range of –40°C to 70°C, an accuracy of ±0.21°C over 0°C–50°C, and a resolution of ± 0.02°C, were sampled at 1Hz. Refer to Figure 5 for placement locations.

Figure 6 plots all external air-temperature measurements during the survey period along with the timing of TLS scanning locations. Variations in temperature measurements are due to different conditions at each location, including aspect, solar exposure, wind, and proximity to warmer objects (e.g., building surfaces, vehicles, and infrastructure). These

measurements are referenced when assessing the 3-D thermal model, providing in situ data for comparing and validating TIR measurements and thermal-deficiency findings.

Archived and real-time meteorological data from McMurdo Station is publicly available through the Antarctic Meteorological Research Center and Automatic Weather Station programs within USAP (http://amrc.ssec.wisc.edu/). The McMurdo Station Automated Weather Observation System (AWOS station ID: ZCMA) is located at 77.85° S, 166.67° E, 33 m. Figure 7 shows the 10-minute air temperatures from the ZCMA station for 3–7 February 2020 alongside the temporary exterior temperature HOBO sensors and the TLS scan timing. During this period, there were minimum and maximum temperatures of approximately –7°C and +6°C, respectively. The general trend of ZCMA temperatures agrees with deployed HOBO air-temperature sensors; however, because the HOBO sensors were deployed on building infrastructure, some do exhibit higher apparent temperatures by almost 10°C when in direct sunlight as compared to the cooler air temperatures from the ZCMA station.

Figure 5. Crary Lab survey map indicating the location of scan positions (*red triangles*), reflectors (*green circles*), and external-air-temperature sensor placement (*red circles*).

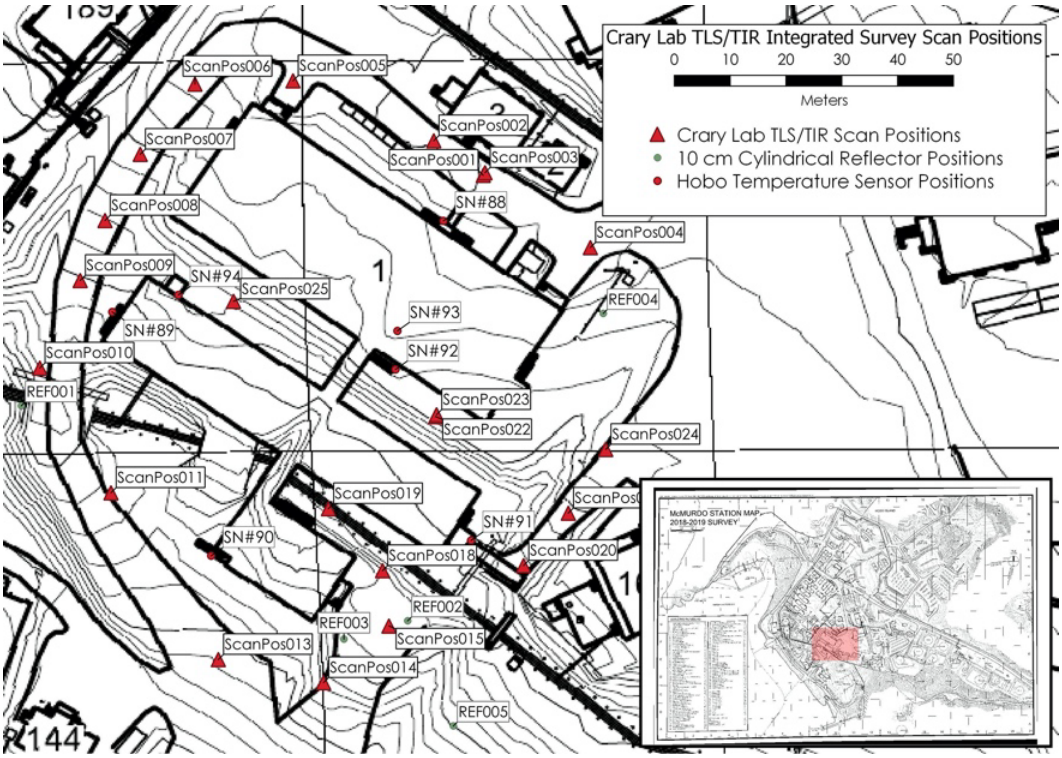
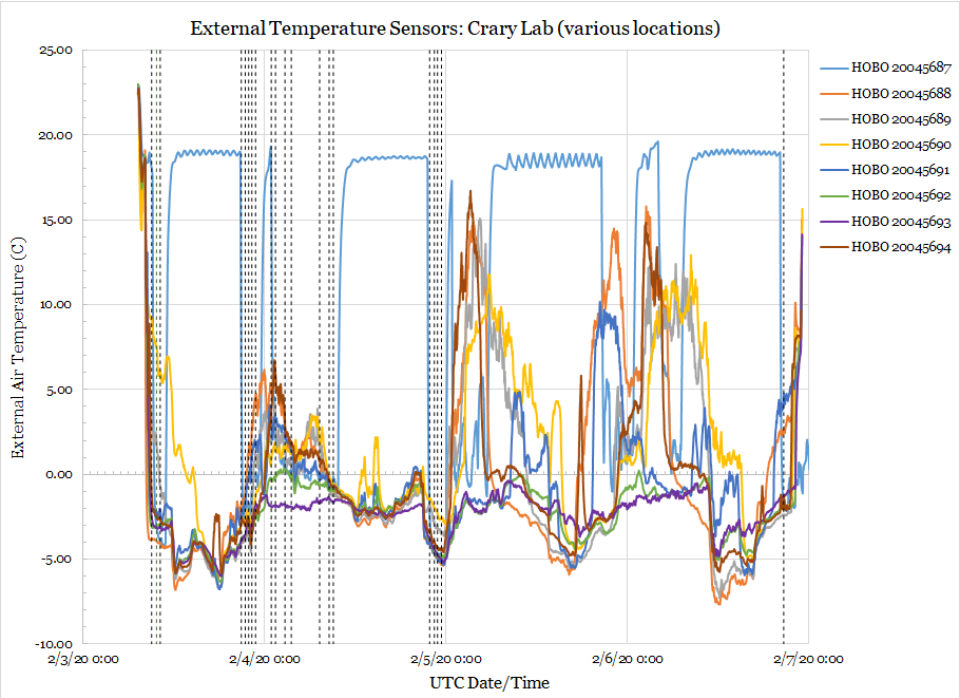
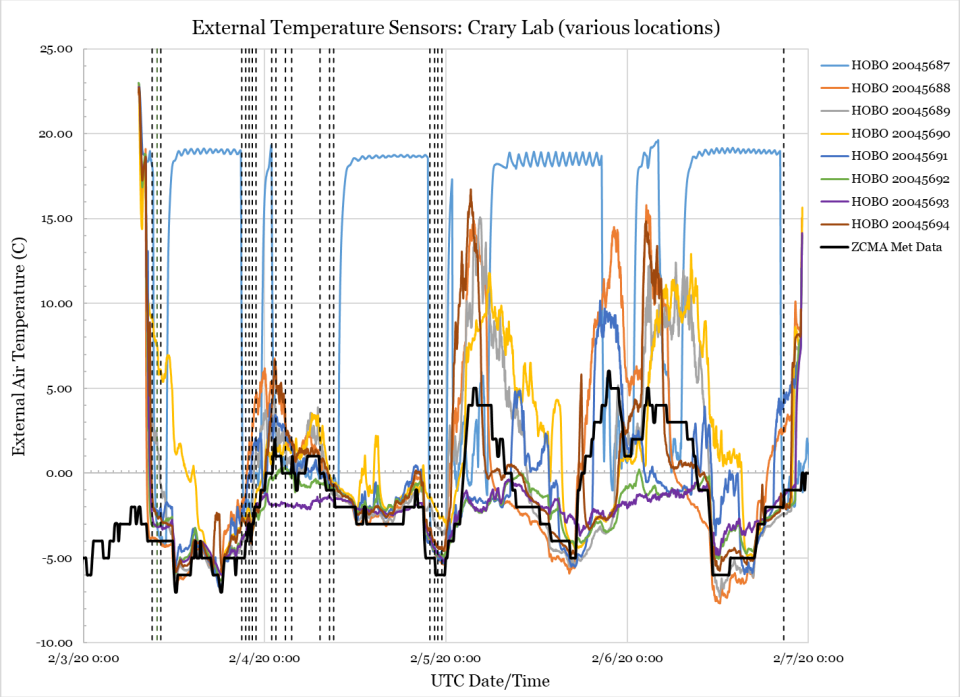


Figure 6. Air-temperature measurements from eight sensors temporarily installed around the exterior of the Crary Lab. Timing of the TLS scan positions are identified as *dashed black lines*. Variation in temperatures is due to sensor location and the effects of solar exposure and winds. Sensor #20045687 was attached to the tripod with the instrument package and shows the influence of bringing the instruments inside when not in use.



Note: UTC = Coordinated Universal Time

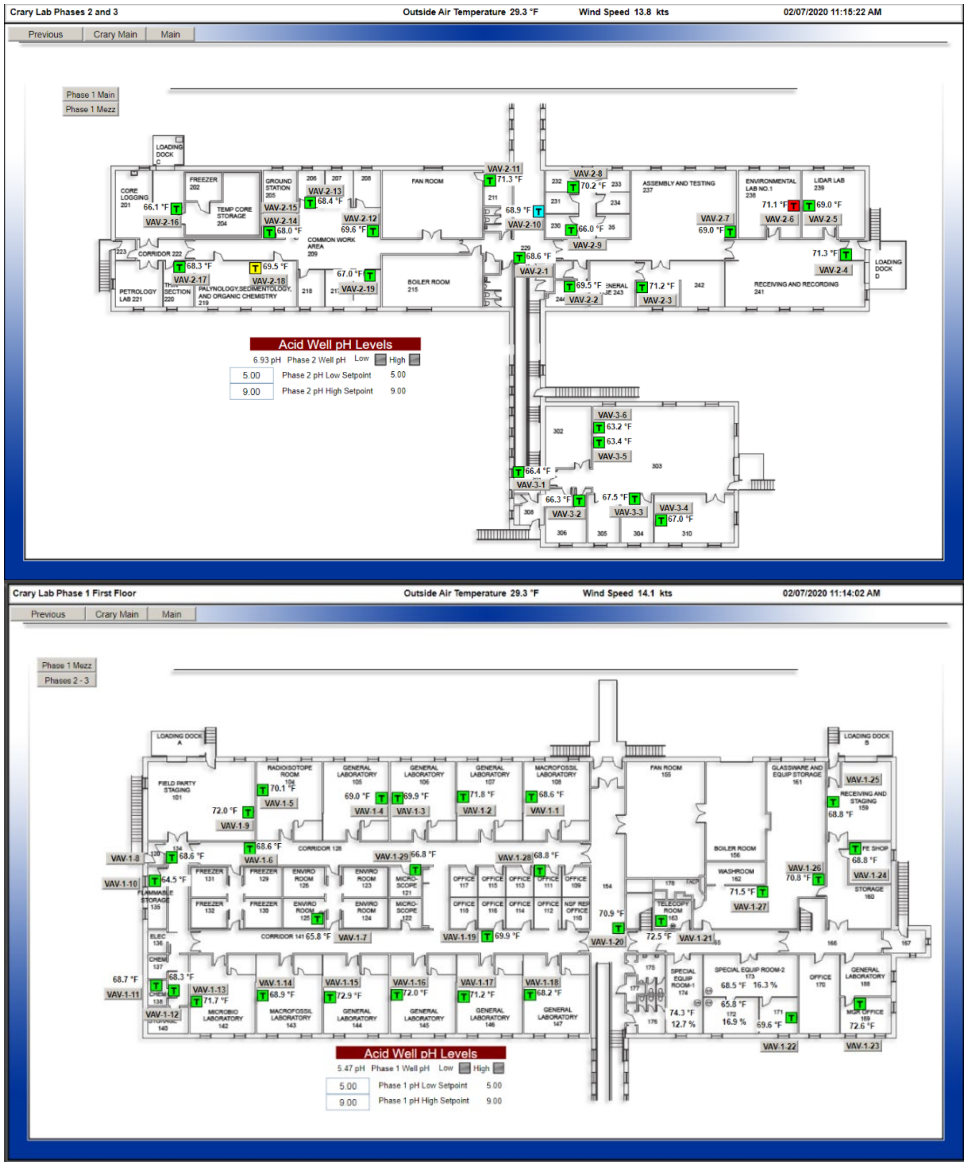
Figure 7. Plot of 10-minute air-temperature measurements for 3–7 February 2020 from the McMurdo AWOS (*solid black line*) alongside the temporary exterior temperature HOBO sensors (*various solid colored lines*) and the TLS scan timing (*black dashed lines)*.



3.2 Interior measurements

Figure 8 depicts an example of the automated monitoring system of interior temperatures for Phase 1, 2, and 3 Crary Lab spaces. Despite exterior temperatures being higher than average during some of the deployment dates, this example shows that for even a relatively high exterior temperature (about –1°C on 7 February 2020), there is still a significant temperature gradient between the exterior temperature and indoor air temperatures (ranging from a high of 21°C to a low of 15°C). In general, these data may be used for reference where any thermal anomalies are identified in the 3-D thermal model, as discussed in section 5, "Results."

Figure 8. Example of interior air temperatures provided by the automated monitoring system for Phase 1 (*top*) and Phases 2 and 3 (*bottom*) Crary Lab spaces.



3.3 GNSS control survey

To account for the absolute location and orientation of the Crary Lab with respect to a global coordinate system and to provide a baseline 3-D dataset that future studies may leverage for spatial comparison (settlement observations), we performed a GNSS control survey. This process, referred to as georeferencing, was completed for the Crary Lab lidar/TIR survey by collecting RTK survey measurements of temporary reflectors placed in the scanner's FOV (Figure 9). For further discussion regarding the general georeferencing techniques employed during the McMurdo lidar surveys, please refer to Deeb and LeWinter (2018) and LeWinter et al. (2018), as the techniques used for the McMurdo Station survey were based on those two previous projects.

Figure 9. A 10 cm cylinder reflector temporarily installed during the Crary Lab lidar/TIR survey. The reflectors, with 10 cm height and diameter dimensions, provide reference coordinates used to tie the 3-D model to a global coordinate system.



3.4 Handheld electro-optical imagery

While the reflectance-colored 3-D model derived from the lidar scanner provides sufficient distinction between differing surfaces, it is still beneficial to capture true-color images to assist in identifying specific building materials (Figure 10). Using a Nikon D800 DSLR with a 14–24 mm lens, we collected handheld electro-optical imagery at each scan position and

for areas on the Elevated Station exterior identified with either damage or thermal deficiencies. The image-naming convention is McMurdo_EO_Pos_scan position_xxx.JPG.

Figure 10. Electro-optical image (*right*) captured of the Crary Lab compared to the intensity-colored 3-D model (*left*), highlighting the utility of capturing true-color images in conjunction with the lidar/TIR data acquisition. The electro-optical imagery is helpful in identifying specific building and infrastructure materials and for providing visual context of the survey area.



3.5 Lidar/TIR system

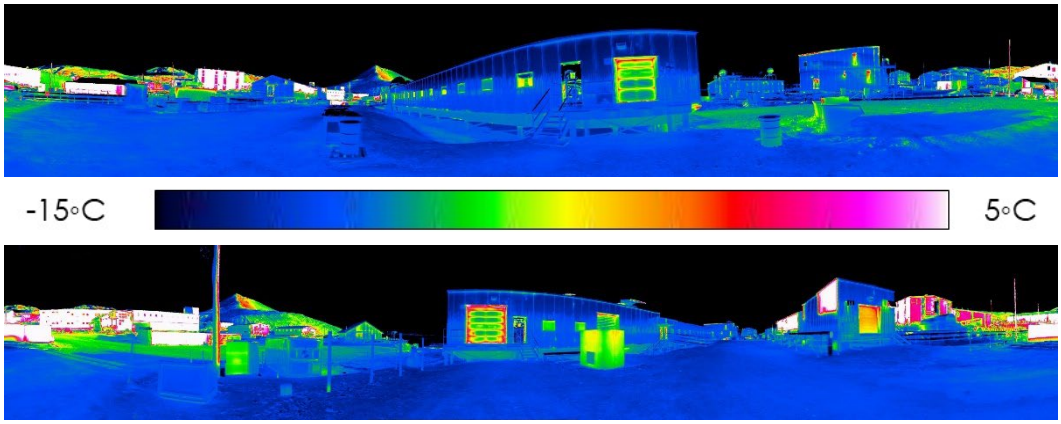
The lidar/TIR system includes a Riegl VZ-1000 laser scanner, InfraTec VarioCAM HD TIR camera, and Trimble R10 for GNSS measurements (Figure 11). The system was mounted to a fiberglass survey tripod, which is both lightweight and less prone to thermal expansion and contraction compared to similar metal tripods. External batteries were used to power both the lidar and TIR sensors. Both lidar and TIR sensors were controlled by a ruggedized PC. The lidar sensor connected via wireless communication while the TIR was connected via Ethernet cable to the PC.

For each scan position, we made efforts to visually level the tripod; though, as a result of the data processing and georeferencing procedure, it was not necessary to perfectly level the system for each scan. At each scan position, we captured a high-resolution scan with the following scanning parameters: a 100° vertical × 360° horizontal FOV, a 0.03° angular increment (both vertically and horizontally), and a 300 kHz pulse repetition rate. The range from scanner position to target building surface varied but was typically 5–10 m. These scan parameters resulted in roughly 8–28-million points per scan, with centimeter-scale point spacing on the building surface. At the conclusion of each lidar scan, we captured TIR images with a 40° horizontal overlap to ensure total coverage of the scan area. Figure 12 displays examples of panoramic TIR images captured from two separate scan positions. 0 documents detailed acquisition procedures.

Figure 11. CRREL's lidar/TIR system at McMurdo Station.



Figure 12. Example 2-D panoramic TIR images collected from two perspectives of the Crary Lab, colored by a −15°C to +5°C color scale.



Because of line-of-sight limitations of both sensors and the complicated building footprint, multiple scan positions were required to capture the exterior of the Crary Lab. While we made every effort to minimize shadowed areas and thus data gaps, some sections of the building were obstructed by ground vehicles, exterior infrastructure, and scanner position limitations (e.g., where the scanner could be safely set up and operated). We collected these data in five acquisition sessions to optimize atmospheric conditions (solar exposure, wind, and temperature).

3.6 UAS data acquisition

For the UAS data acquisition, we collected coincident lidar, visible-spectrum imagery, longwave TIR imagery, and high-accuracy position and orientation trajectories during each lift (flight). We divided the areas of interest at McMurdo Station selected for UAS lidar data acquisition into four focus areas: helipad, wastewater, dormitory, and carpentry shop (Table 5). This was in part due to limited flight duration at low temperatures as a result of battery capacity degradation, in addition to flight procedures requiring the PIC and VO to remain within visual line of sight of the aircraft at all times. In addition, the UAS can safely fly at or below sustained winds of 8 m/s. To ensure both the safety of the aircraft and stability of the payload, UAS lifts at McMurdo Station were conducted during times of calm-to-moderate winds without precipitation present.

Table 5. Mission list and parameters for RiCOPTER deployment at McMurdo Station.

Mission Name	Date/Time (Local)	Wind Speed (m/s)	Pressure (mbar)	Temp (°C)	Relative Humidity (%)
1—Helipad	2/5/20 19:30	1.5	980.9	4.0	29.2
2—Wastewater	2/5/20 20:25	Calm	980.9	4.0	29.2
3—Dormitory	2/6/20 04:35	1.5	979.2	−6.0	37.4
4—Carpentry Shop	2/6/20 20:30	2.1	973.6	5.2	29.5

For each lift, the PIC and VO completed an operation checklist, which includes systematically logging environmental conditions; checking the aircraft and payload for any damage or physical issues; assessing the airspace for any potential obstructions or anomalies; and upon flight, logging timing and duration of each phase of the flight (e.g., static alignment duration and liftoff time). See 0 for the operation checklists for each lift conducted at McMurdo Station. Each lift includes the following phases:

- Start-up static alignment: Prior to takeoff of the UAS, a 5-minute static logging of position and orientation measurements from the IMU was collected and used for calibration of the IMU sensor.
- Dynamic alignment: Upon takeoff of the UAS, flight procedure in which the aircraft is flown in a figure-eight pattern to further calibrate the IMU. This procedure improves the overall accuracy of the resulting trajectory file.
- Data acquisition: PIC triggers the lidar and cameras during automated flight lines, collecting records that include raw lidar point

cloud data and individual camera images from both visible-spectrum and TIR cameras.
- Final static alignment: Upon landing, the IMU sensor performs an additional 5-minute static logging of position and orientation measurements.

When the UAS landed, the PIC and VO downloaded the collected data from the lidar sensor, IMU, and both cameras. To ensure a successful mission, the IMU trajectories were field processed and an initial point cloud was produced and run through a visual quality assessment by the PIC and VO. The camera imagery was manually reviewed to ensure proper coverage and exposure.

4 Data Processing

4.1 TLS lidar scans registration and georeferencing

Due to line-of-sight limitations and the Crary Lab's exterior complexity (multiple phases and facets), it was necessary to collect TLS data from 21 separate scan positions. Similarly, to collect TLS data on sections of the utilidor, we collected data from 29 separate scan positions. Further, to produce a combined 3-D model requires registration and georeferencing of these disparate datasets. Registration is the process of tying individual point clouds from separate scan positions to each other whereas georeferencing refers to the process of tying the point clouds to a global coordinate system. For the McMurdo Station survey, we conducted these processes simultaneously.

Using four 10 cm cylinder reflectors and the GNSS RTK survey data, the first utilidor scan position (Utilidor-ScanPos001) was tied to the WGS84 APS coordinate system. Given that the reflectors were scanned from this scan position, the centroid XYZ coordinates (X = longitude, Y = latitude, Z = elevation) of each cylinder was measured and identifiable within the point cloud. The XYZ coordinates measured by the GNSS survey were then assigned to the reflector positions in the point cloud. This established the baseline georeferenced scan to which all remaining scans are registered.

The subsequent scans (Crary Lab scan positions 001–025, utilidor scan positions 002–025, and upper utilidor scan positions 001–004) were tied to the baseline georeferenced scan (Utilidor-ScanPos001) through a two-step process: coarse registration and multistation adjustment (MSA). Coarse registration involves identifying a minimum of four common points between overlapping scans to roughly align the point clouds together. The baseline scan's position and orientation are locked while the unregistered scan's position and orientation are allowed to be modified. For example, Utilidor-ScanPos001 and Crary-ScanPos021 were acquired from locations with many similar point measurements from which to identify common points (Figure 13). This process, while helpful for roughly aligning multiple point clouds, is limited by the user's ability to select common points and results in typical positional errors on the centimeter-to-meter scale.

Following coarse registration, MSA is run to improve the positional accuracy of the point cloud registration. MSA uses a planar filter algorithm that identifies planar features within each point cloud and then iteratively aligns

the unregistered scan data to the baseline point cloud. This process involves initial user input, including the minimum number of points required to define a plane and the minimum and maximum search radius between separate point clouds to identify similar planar features. The calculated planes from different scans are then aligned, resulting in a typical positional error between multiple point clouds in the subcentimeter scale (Figure 14).

Figure 13. Visualization of the coarse registration process in which an unregistered scan is roughly aligned to a registered, georeferenced baseline scan. Utilidor-ScanPos001 (*left*) was tied to the WGS84 APS coordinate system using reflectors and the GNSS RTK survey. Crary-ScanPos015 (*right*) was captured from a position of significant overlap relative to Utilidor-ScanPos001. Common features are manually identified between each point cloud (yellow dots), and Crary-ScanPos015's position and orientation are subsequently modified.

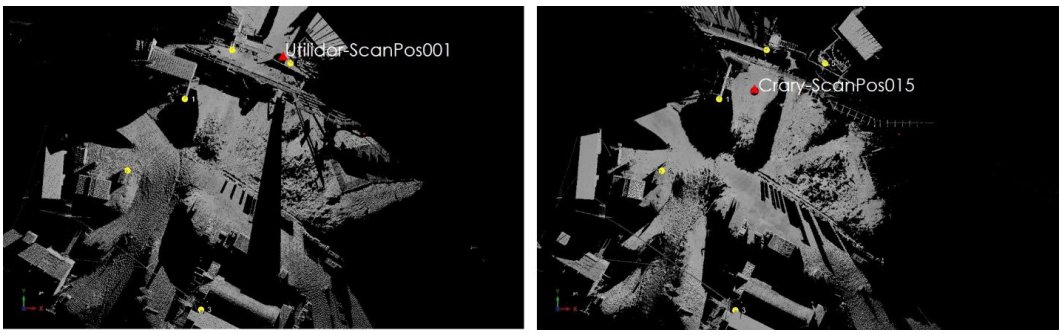
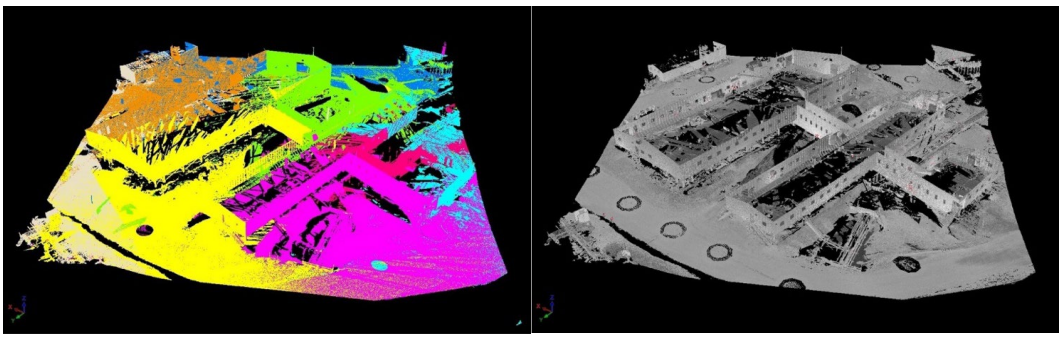


Figure 14. TLS point cloud data of the Crary Lab was collected from 21 different scan positions. Each resulting point cloud covered a portion of the Station. *Left*: Image shows eight of these point clouds, colored by scan position. *Right*: After registration and georeferencing, the individual scans combine to create a complete 3-D model of the Station.

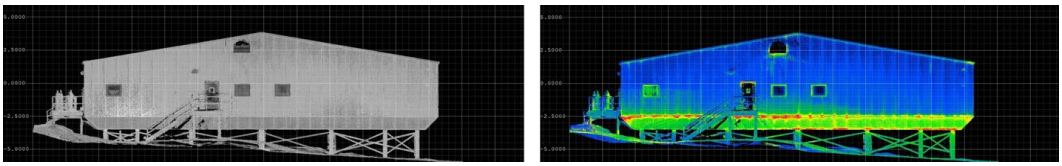


4.2 TLS TIR radiometric value registration

Each scan position has associated TIR imagery covering the same FOV as the lidar point cloud. The temperature values measured by the TIR sensor can be mapped and assigned to each individual point measurement using a camera calibration (Figure 15). This allows each pixel of the thermal image to be assigned to each individual lidar measurement based on the scan angle of the laser. For each point cloud, the thermal value is written to the

LAS file format GPS Time field for dynamic visualization in 3-D point cloud viewing applications. In addition, a continuous color scale from blue to red, based on temperature, is used to set the red-green-blue (RGB) fields in the LAS file. This is useful for 3-D model viewers that are unable to colorize point clouds by their GPS Time values.

Figure 15. A 3-D model captured of the Crary Lab colored by intensity (*left*) and temperature (*right*). Mapping the TIR imagery onto the 3-D model visually represents thermal variations.



4.3 TLS data products

The data processing steps produced specific data products. Each scan position provides the following deliverables:

1. Full-resolution georeferenced point clouds from each scan position, with reflectance and temperature values assigned to each point measurement—Temperature values are located in the GPS Time field in the LAS-zipped (.laz) file format. RGB values represent a fixed-scale temperature colorization. Naming convention: YYMMDD_HHMMSS.laz.

2. A 1 cm subsampled, georeferenced point cloud from each scan position, with reflectance and temperature values assigned to each point measurement—Octree filter subsampling is applied to the point cloud, averaging all point values (XYZ, reflectance, and temperature) into 1 cm cubes. RGB values represent a fixed-scale temperature colorization. Naming convention: YYMMDD_HHMMSS-1cmSample.laz.

3. A 1 cm subsampled, georeferenced point cloud of all scan positions combined, with reflectance and temperature values assigned to each point measurement—Octree filter subsampling is applied to the point cloud, averaging all point values (XYZ, reflectance, and temperature) into 1 cm cubes. RGB values represent a fixed-scale temperature colorization. Naming convention: 2020-02-Crary-Lab-1cmSample.laz.

4. Set of TIR images in both proprietary InfraTec file format (IRB) and fixed color scale (JPG) file format—Naming convention: ScanPosXXX – ImageXXX.irb/.jpg.

5. Set of electro-optical images in JPG file format taken from each scan position location and any detail images of observed exterior damage or thermal deficiency—Naming Convention: McMurdo_EO_Pos_scan position_XXX.jpg.

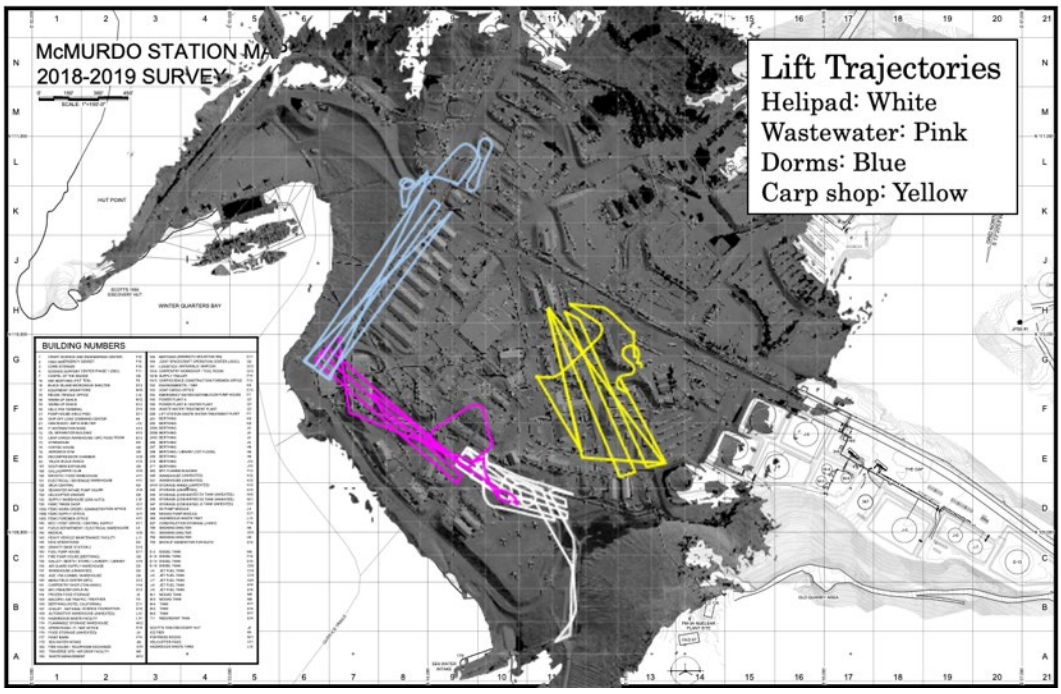
4.4 UAS data processing

The following section describes the tasks completed to go from the raw collected data from each individual sensor deployed in the UAS payload (lidar, IMU, visible-spectrum camera, and TIR camera) to a georeferenced point cloud with attributes associated with the external cameras.

4.4.1 Trajectory processing

We improved the IMU position and orientation file using a static GNSS base station for reference. This process was completed in the Applanix POSPac MMS processing software. A smoothed best estimate trajectory (SBET) file with accuracy assessment was exported for use within the lidar point cloud processing software suite (Figure 16).

Figure 16. Plot of the resulting UAS lidar point cloud overlaid on the McMurdo Station 2018–2019 survey map with the four lift trajectories displayed. Note that the PIC/VO programed the flight trajectories for automated flight, focusing on the main areas of the McMurdo Station utilidor. Because of the wide FOV of the lidar scanner, the majority of the station was collected even though the flight locations were spatially limited. The point cloud is colored by intensity.



4.4.2 Lidar point cloud processing

Lidar point cloud measurements were projected into a global coordinate system reference frame using the resulting SBET file from the IMU. We used the WGS84 APS (EPSG:3031) with WGS84 ellipsoid heights (meters) coordinate reference system for these data. In addition, we ran the point cloud through initial filtering to remove in-air noise (caused by dust and moisture) and oblique angle measurements (FOV was limited to 110°, or 55° off nadir on each side). This processing was completed in Riegl's RiPROCESS software suite.

4.4.3 Visible-spectrum image processing

Using event markers (time-synced events within the IMU trajectory file), we imported individual visible-spectrum camera images into the RiPROCESS project, and the RGB pixel values were assigned to the lidar point cloud using a known camera mounting and lens calibration. This results in a colorized point cloud based on the images collected by the onboard Sony A7R-III camera (Figure 17).

Figure 17. Sample image captured by the onboard Sony A7R-III visible-spectrum camera at McMurdo Station. A section of the utilidor, the Chalet, and lower section of the Crary Lab is visible. The UAS payload captures coincident lidar point clouds, visible spectrum imagery, and longwave TIR imagery during flight.



4.4.4 TIR image processing

Unlike the visible-spectrum imagery, the TIR images collected by the onboard FLIR Tau2 camera require separate processing first to extract a temperature-scaled image (Figure 18). The individual images captured by the Tau2 were converted using Thermoviewer software to radiometric JPG files with set temperature color scales of −15°C to 25°C for the helipad, wastewater, and carpentry shop lifts and −15°C to 10°C for the dormitory lift. We used the different temperature scales in an effort to optimize contrast between varying surfaces because of the changing solar exposure during the flights (the dormitory flight has more cloud coverage). Once the radiometric JPG files were created, we used Open Drone Map (https://www.opendronemap.org/webodm/) to create orthorectified thermal images for each lift. These orthorectified images were then projected onto the lidar point clouds, creating a point cloud with TIR colorization (Figure 19). This final process was completed using Quick Terrain Modeler software.

Figure 18. FLIR Tau2 longwave TIR image overlaid on an image captured by the Sony A7R visible-spectrum camera. This figure illustrates the smaller detector size in the Tau2, resulting in a lower-resolution image compared to the Sony camera. The temperature color scale for the image is −15 °C to 25 °C.

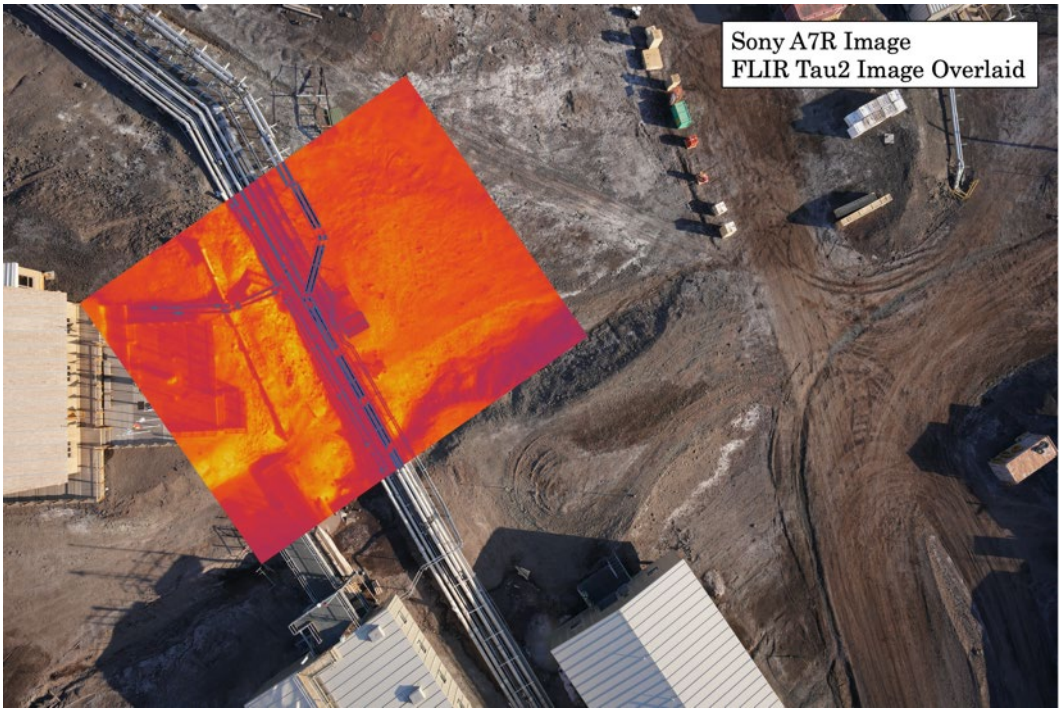
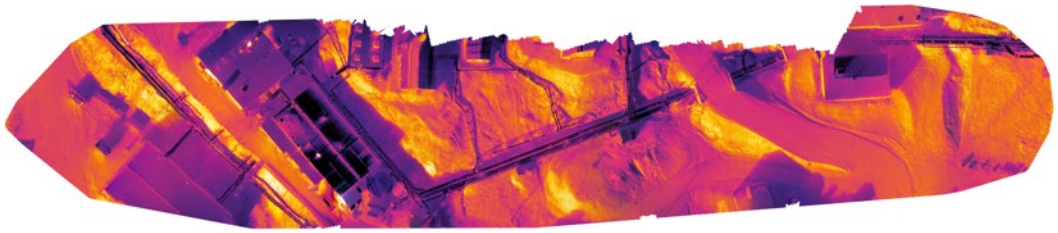


Figure 19. Orthorectified image derived from images captured by the FLIR Tau2 during the wastewater lift. Areas of direct solar exposure are evident by the high temperature (bright yellow/orange sections), while shadowed areas or surfaces of low reflectance are indicated by darker sections. The temperature color scale for the image is −15°C to 25°C.



4.5 UAS data products

The UAS data collection resulted in the following data products:

1. Raw longwave TIR images—This product includes images with embedded XML metadata recorded directly by the FLIR Tau2 camera for each lift.

2. Raw visible-spectrum images—This product includes images recorded directly by the Sony A7R-III camera for each lift.

3. Full FOV point cloud—This dataset includes all points within the full width FOV of the lidar sensor without point colorization from either the visible-spectrum camera or longwave TIR camera. LAZ files are divided by lift (e.g., helipad, wastewater, dorms, and carpentry shop) with the naming convention 202002-McMurdo-lift name-Full-FOV.laz. These data are classified as ground, buildings, and unclassified.

4. Visible-spectrum colorized point cloud—This dataset includes all points that fall within the visible-spectrum camera FOV (which is narrower than the lidar sensor FOV). LAZ files are divided by lift (e.g., helipad, wastewater, dorms, and carpentry shop) with the naming convention 202002-McMurdo-lift name-RGB.laz. In addition, a combined LAZ file merging all lifts was produced, named 202002-McMurdo-RGB.laz.

5. TIR colorized point cloud—This dataset includes all points that fall within the longwave TIR camera FOV (which is narrower than the lidar sensor FOV). LAZ files are divided by lift (e.g., helipad, wastewater, dorms, and carpentry shop) with the naming convention 202002-McMurdo-lift name-TIR.laz. In addition, a combined LAZ file merging all lifts was produced, named 202002-McMurdo-TIR.laz.

6. Isolated utilidor point cloud—This dataset, Named 202002-McMurdo-ULS-utilidor.laz, includes all points from the full FOV point clouds that cover the utilidor sections, isolated to provide a lower-file-size point cloud for utilidor analysis..

7. Isolated Crary Lab point cloud— Named 202002-McMurdo-Crary-ULS.laz, this includes all points from the full FOV point clouds that cover the Crary Lab, used to fill in the roof surfaces for the Crary Lab TLS dataset.

8. TIR orthorectified images—These are orthorectified images from the longwave TIR camera, processed by lift. Both an IMG and a TIF file were produced for each lift. The naming convention is 202002-McMurdo-lift name-TIR-orthophoto.file extension (e.g., 202002-McMurdo-Helipad-TIR-orthophoto.img).

9. Digital surface model (DSM) GeoTIFF—Based on the full FOV point cloud, this is a 0.3 m digital surface model produced from all points, named 202002-McMurdo.DSM.tif.

10. Digital terrain model (DTM) GeoTIFF—Based on the full FOV point cloud, this is a 0.3 m DTM produced from ground classified points, named 202002-McMurdo.DTM.tif.

11. Building outlines and roof vector files: These building outlines and roof vectors, produced in Quick Terrain Modeler, include all buildings within the full FOV point clouds, in both DXF and SHP file format.

5 Results

5.1 Crary Lab—exterior surface thermal analysis

The 3-D thermal model of the Crary Lab can be divided by the phase of building construction and aspect of the wings being reviewed (Figure 20). For the purposes of analysis, the layout uses a grid-north orientation, and each construction phase is labeled with respect to the compass aspect (Figure 21). While some expected thermal deficiencies exist around windows and doors, overall the Crary Lab thermal envelope appears to be reasonable. Figures 22–30 provide examples around the Crary Lab for a selection of windows, doors, and other features (soffits, exhausts, etc.). Appendix C provides a full catalog of each existing feature.

Figure 20. Construction phases and subdivision of the Crary Lab for the purpose of analyzing the exterior surface thermal results. Phase 1, 2, and 3 along with the Phase 1–2 and Phase 2–3 connectors are identified.

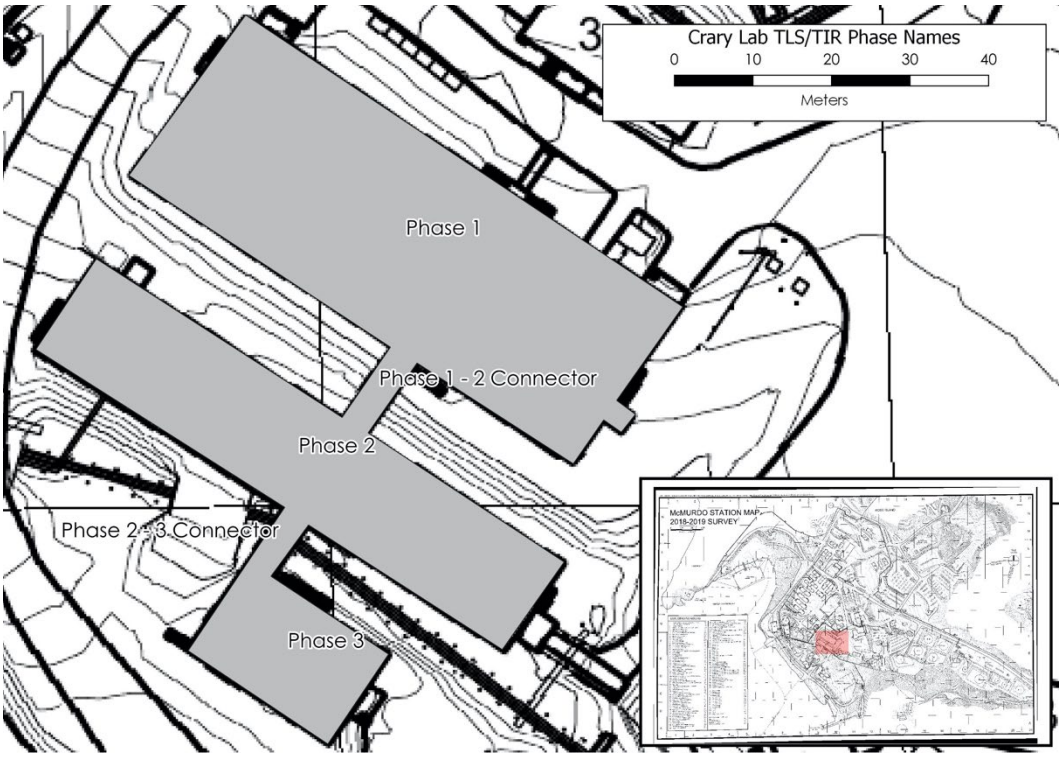
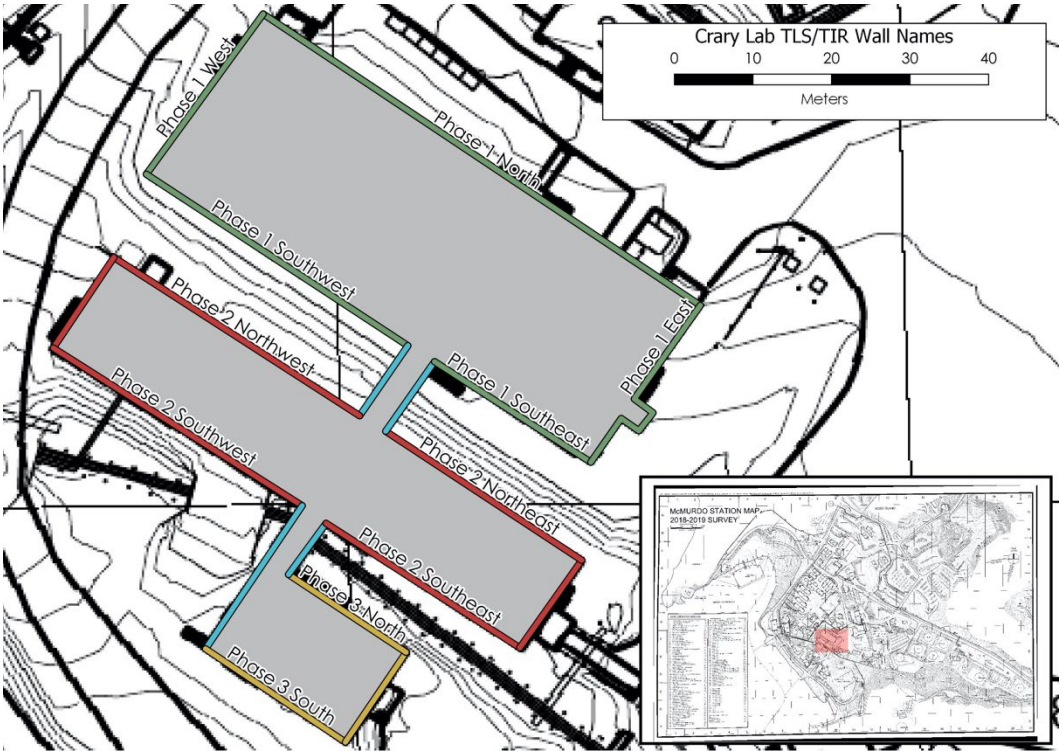


Figure 21. Crary Lab construction phases labeled with respect to the construction phase and compass aspect as it pertains to subsequent 3-D thermal example figures.



Each perspective view is named using the following nomenclature:

(Phase + Compass Direction)-(Feature)-(Integer Identifier)

Example: P1N-W-01,

where

P1 = the construction phase,
N = the compass direction of the building side,
W = the feature type being investigated (windows in this example), and
01 = an integer identifier. Table 6 shows valid values for these different fields.

Table 6. Crary Lab perspective view nomenclature.

Field	Valid Values	Description
Phase	P1	Phase 1
	P2	Phase 2
	P3	Phase 3
	P4	Phase 4
	P2C	Phase 2 Connector
	P3C	Phase 3 Connector
Direction	N	North
	NW	Northwest
	W	West
	SW	Southwest
	S	South
	SE	Southeast
	E	East
	NE	Northeast
Type	W	Windows
	D	Doors
	LD	Loading Docks
Identifier	##	Integer Value

Figure 22. A 3-D thermal model of Phase 1, North, Loading Dock 01 (P1N-LD-01). *Top left*: Phase 1, North, highlighted in *red* on the Crary Lab map. *Bottom*: Thermal image across Phase 1, North, at a −15 °C to −5 °C scale with focus section identified with a *red box*. *Top right*: Focus section highlighted P1N-LD-01.

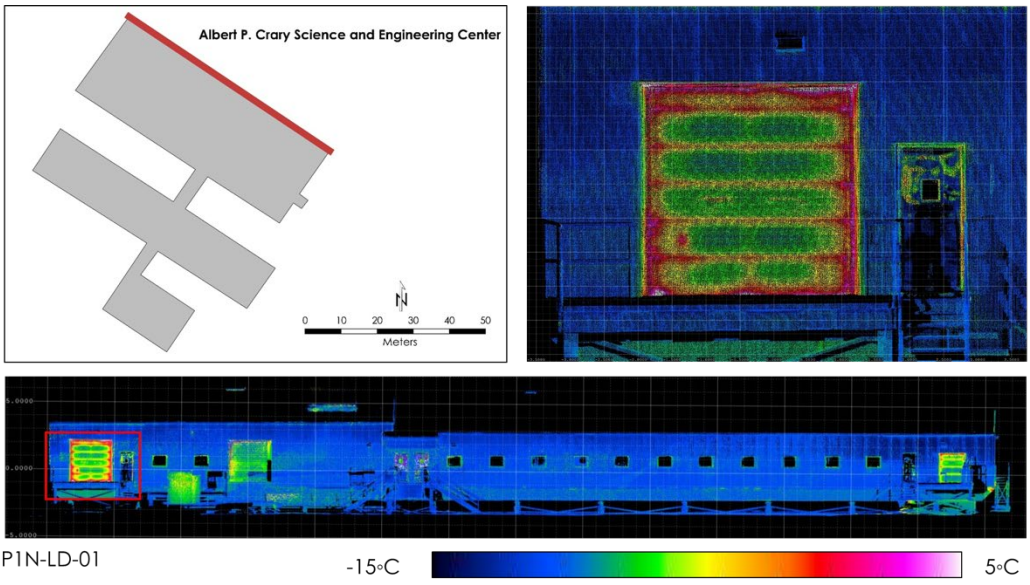


Figure 23. A 3-D thermal model of Phase 1, North, Door 04 (P1N-D-04). *Top left*: Phase 1, North, highlighted in *red* on the Crary Lab map. *Bottom*: Thermal image across Phase 1, North, at a −15 °C to −5 °C scale with focus section identified with a *red box*. *Top right*: Focus section highlighted P1N-D-04.

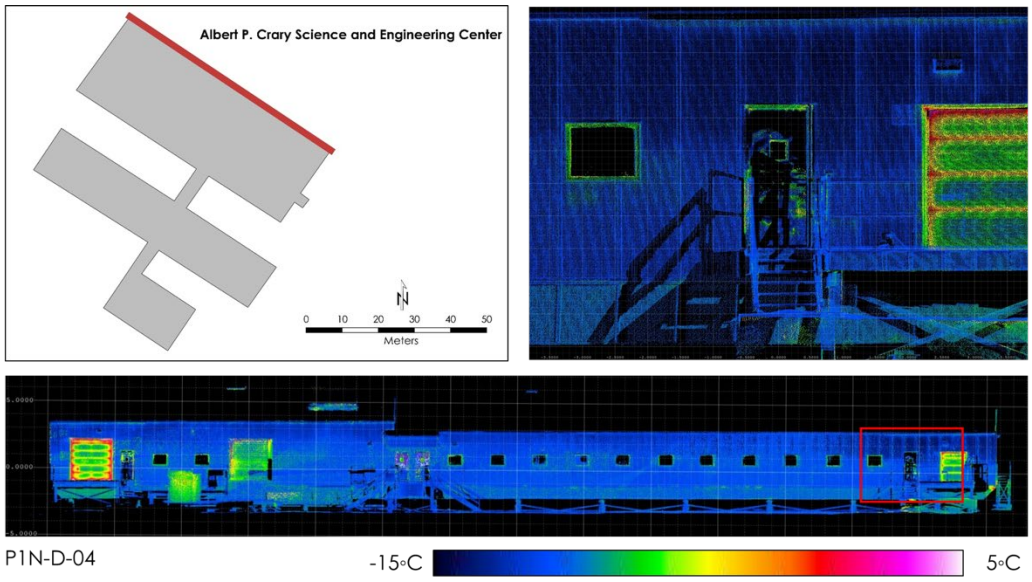


Figure 24. A 3-D thermal model of Phase 1, West, Window 03 (P1W-W-03). *Top left*: Phase 1, West, highlighted in *red* on the Crary Lab map. *Bottom*: Thermal image across Phase 1, West, at a −15 °C to −5 °C scale with focus section identified with a *red box*. *Top right*: Focus section highlighted P1W-W-03.

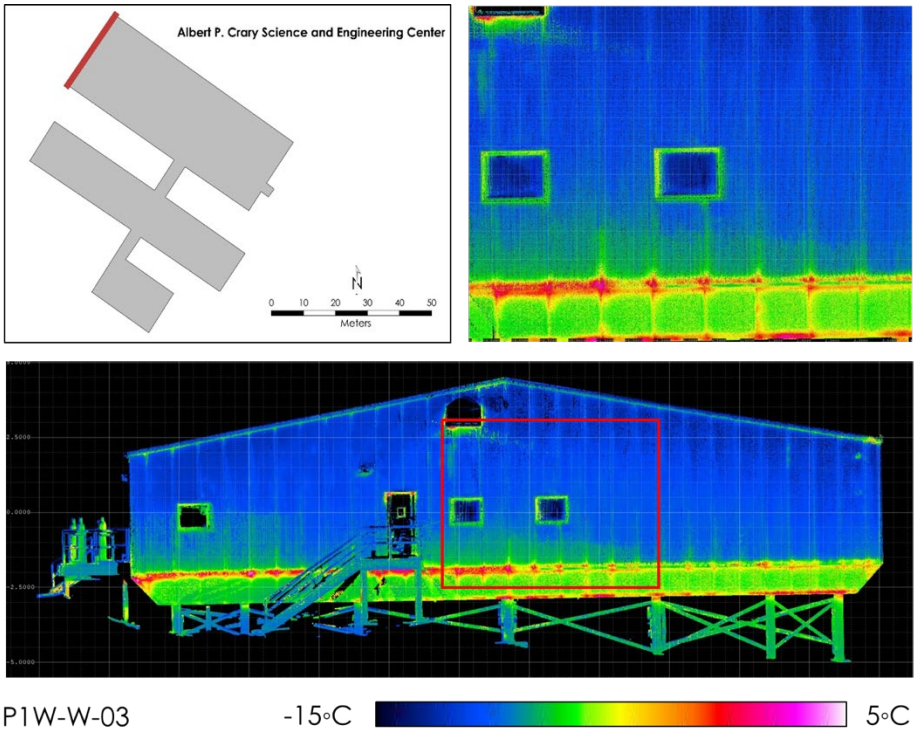


Figure 25. A 3-D thermal model of Phase 1, Southwest, Window 01 (P1SW-W-01). *Top left*: Phase 1, Southwest, highlighted in *red* on the Crary Lab map. *Bottom*: Thermal image across Phase 1, Southwest, at a −15 °C to −5 °C scale with focus section identified with a *red box*. *Top right*: Focus section highlighted P1SW-W-01.

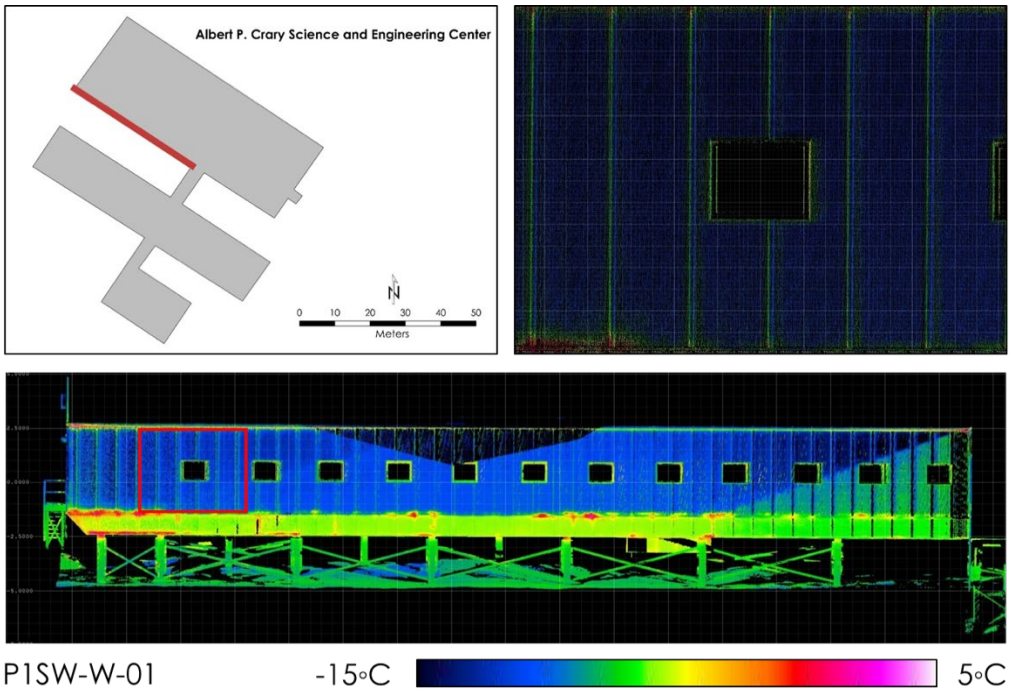


Figure 26. A 3-D thermal model of Phase 1, Southwest, Window 05 (P1W-W-05). *Top left*: Phase 1, Southwest, highlighted in *red* on the Crary Lab map. *Bottom*: Thermal image across Phase 1, Southwest, at a −15 °C to −5 °C scale with focus section identified with a *red box*. *Top right*: Focus section highlighted P1SW-W-05.

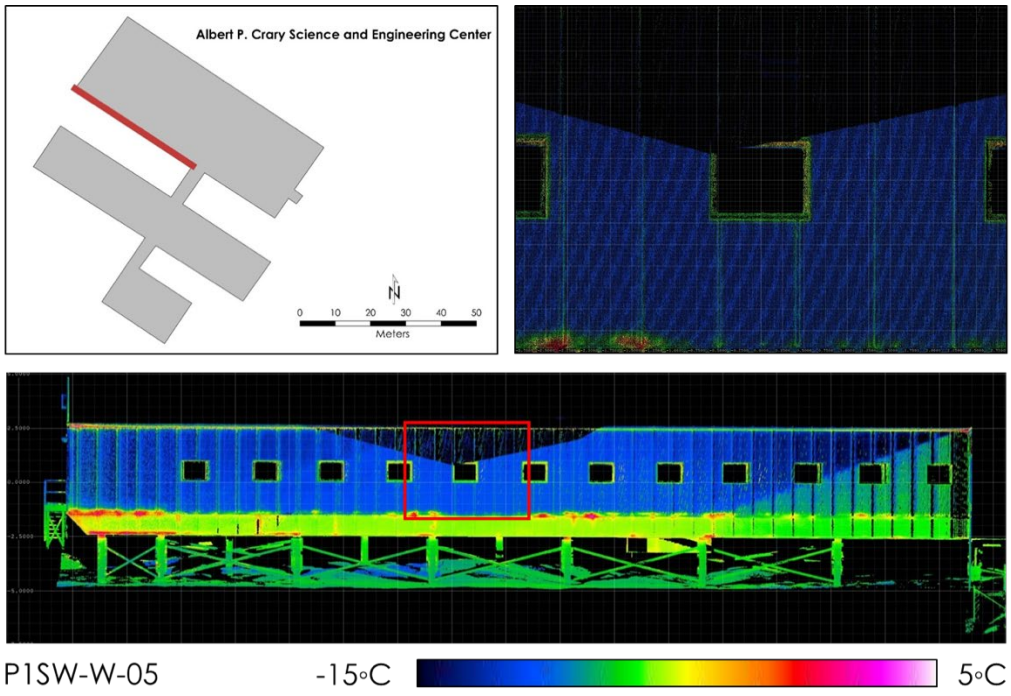


Figure 27. A 3-D thermal model of Phase 1, Southwest, Window 11 (P1W-W-11). *Top left*: Phase 1, Southwest, highlighted in *red* on the Crary Lab map. *Bottom*: Thermal image across Phase 1, Southwest, at a −15 °C to −5 °C scale with focus section identified with a *red box*. *Top right*: Focus section highlighted P1SW-W-11.

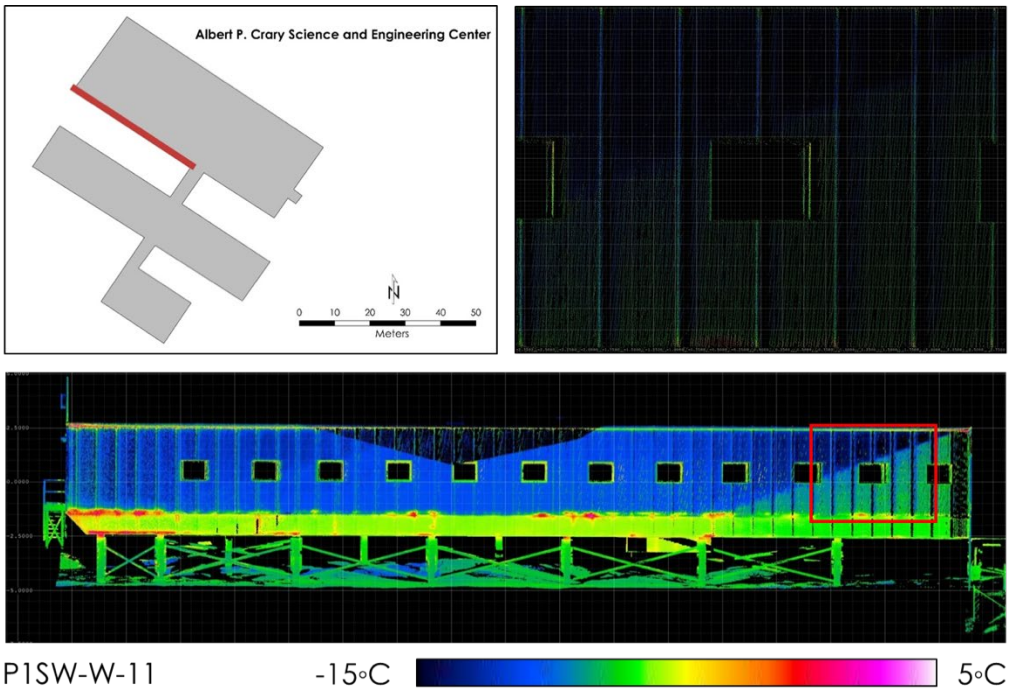


Figure 28. A 3-D thermal model of Phase 3, North, Window 01 (P3N-W-01). *Top left*: Phase 3, North, highlighted in *red* on the Crary Lab map. *Bottom*: Thermal image across Phase 3, North, at a −15 °C to −5 °C scale with focus section identified with a *white box*. *Top right*: Focus section highlighted P3N-W-01.

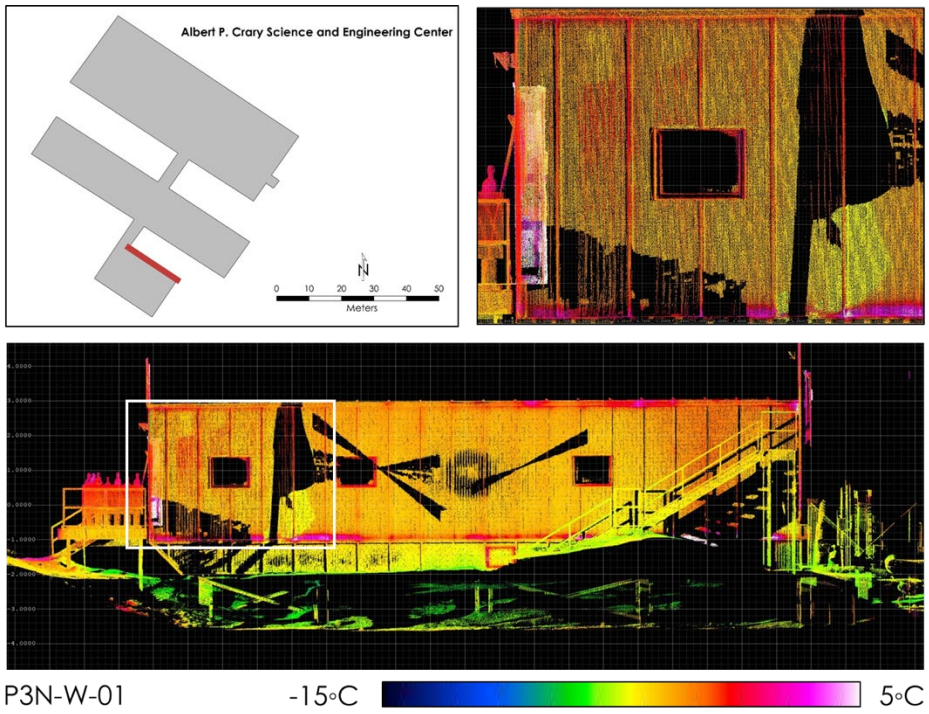


Figure 29. A 3-D thermal model of Phase 2, East, Loading Dock 01 (P2E-LD-01). *Top left*: Phase 2, East, highlighted in *red* on the Crary Lab map. *Bottom*: Thermal image across Phase 2, East, at a −15 °C to −5 °C scale with focus section identified with a *white box*. *Top right*: Focus section highlighted P2E-LD-01.

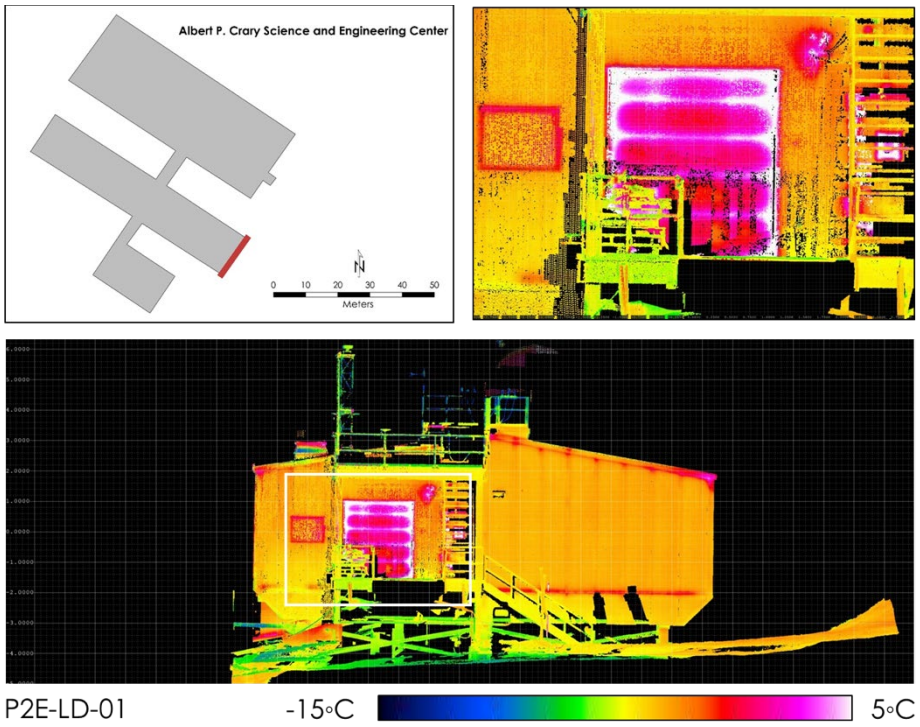
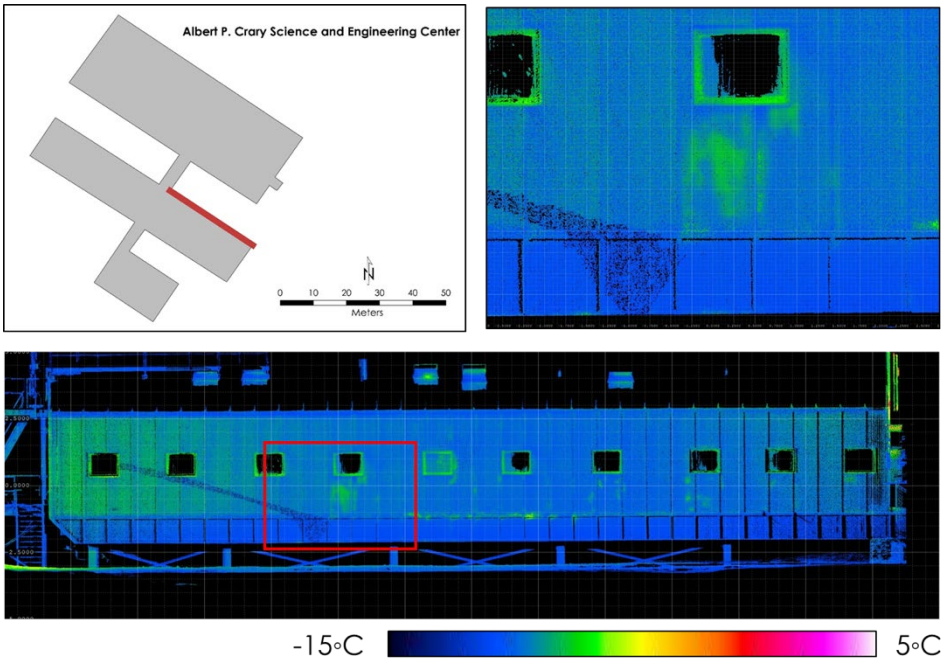


Figure 30. A 3-D thermal model near Phase 2, Northeast, Window 04 (P2NE-W-04). *Top left*: Phase 2, Northeast, highlighted in *red* on the Crary Lab map. *Bottom*: Thermal image across Phase 2, Northeast, at a −15 °C to −5 °C scale with focus section identified with a *red box*. *Top right*: Focus section highlighted P2NE-W-04.



5.2 UAS results and discussion

We successfully conducted four UAS flights, collecting lidar, visible-spectrum images, and longwave TIR images coincidently. With these data, we have provided a collection of fused data products to best visualize and assess the current condition of McMurdo Station and the utilidor. Because of the wide FOV of the lidar scanner, we were able to capture the majority of the McMurdo Station area even with limited flight lines focused over subsections of the utilidor. These data provide a detailed spatial representation of McMurdo Station and can be the basis for further analysis to quantify the current physical state of the station topography, buildings, and utilidor sections. In this results section, we present examples of the fused data products. Further, we provide profile samples from the utilidor in an effort to quantify utilidor slope over sections of the infrastructure and to qualitatively assess the condition of the utilidor. With the data products delivered with this report, we provide NSF and its contractors the capability and tools to analyze these data in greater detail.

5.2.1 Lidar point cloud and digital elevation model results

Figures 31–36 are samples from the UAS survey, including views of the point cloud and resulting data products derived from the point cloud.

Figure 31. Oblique view (looking north) of the resulting lidar point cloud of McMurdo Station captured by the UAS. The point cloud is colored by height (relative scale) and shaded by surface intensity (range-independent surface reflectance). Areas with lower surface intensity are darker, while areas with high intensity are lighter.

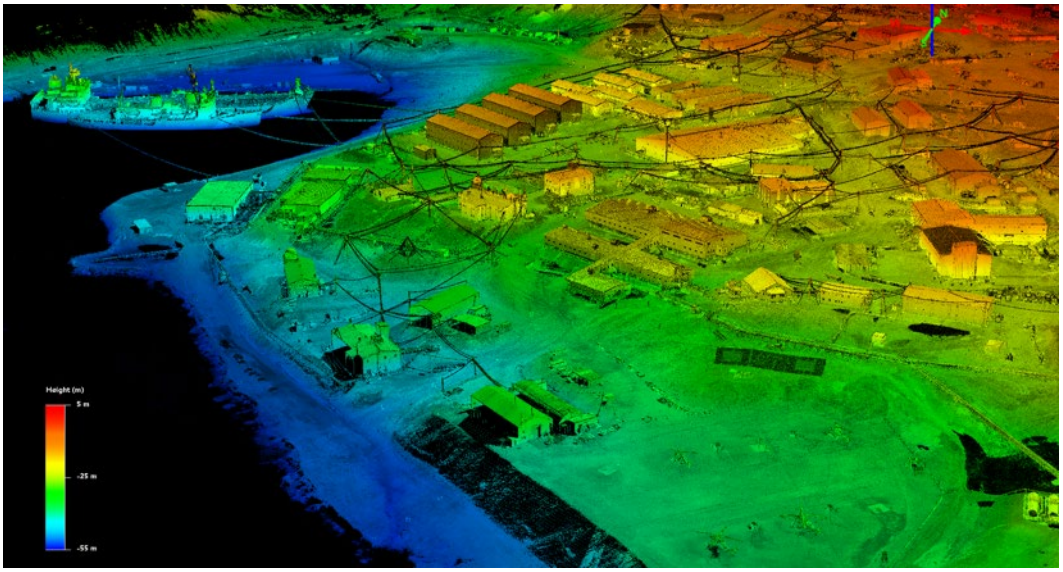


Figure 32. Oblique view (looking northeast) of the resulting lidar point cloud of McMurdo Station, focused on the Crary Lab, captured by the UAS. The point cloud is colored by height (relative scale) and shaded by surface intensity (range-independent surface reflectance). Areas with lower surface intensity are darker, while areas with high intensity are lighter. The roof surfaces from the UAS lidar point cloud were used to fill in the gaps from the TLS survey, which was unable to capture roof features due to line-of-sight limitations.

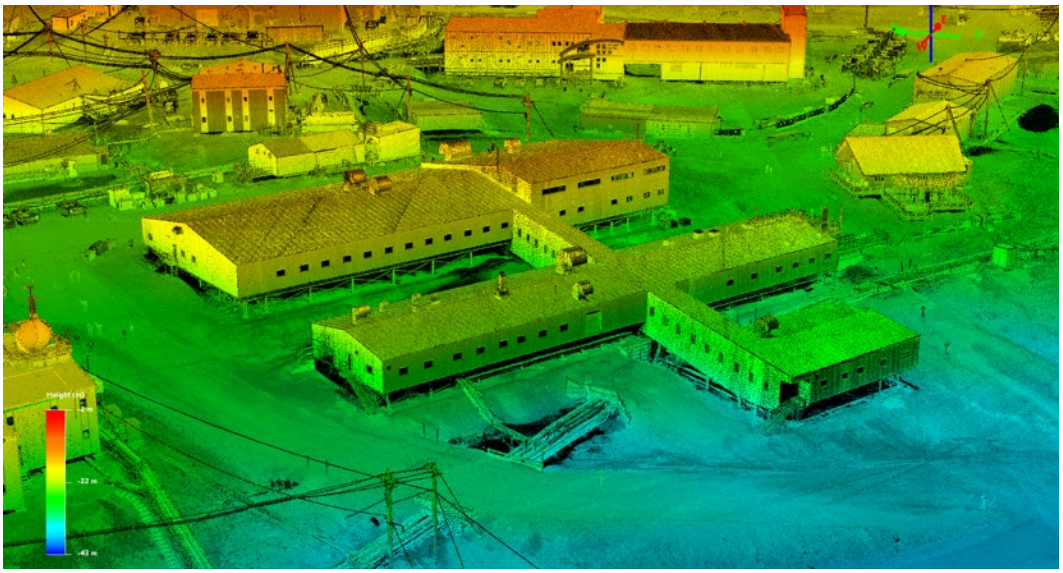


Figure 33. Lidar point cloud from the full FOV dataset, colored by height and shaded by intensity, overlaid on the McMurdo Station 2018–2019 survey map. Of note are the power and communication cables throughout the station, visible as lower-intensity (darker) lines.

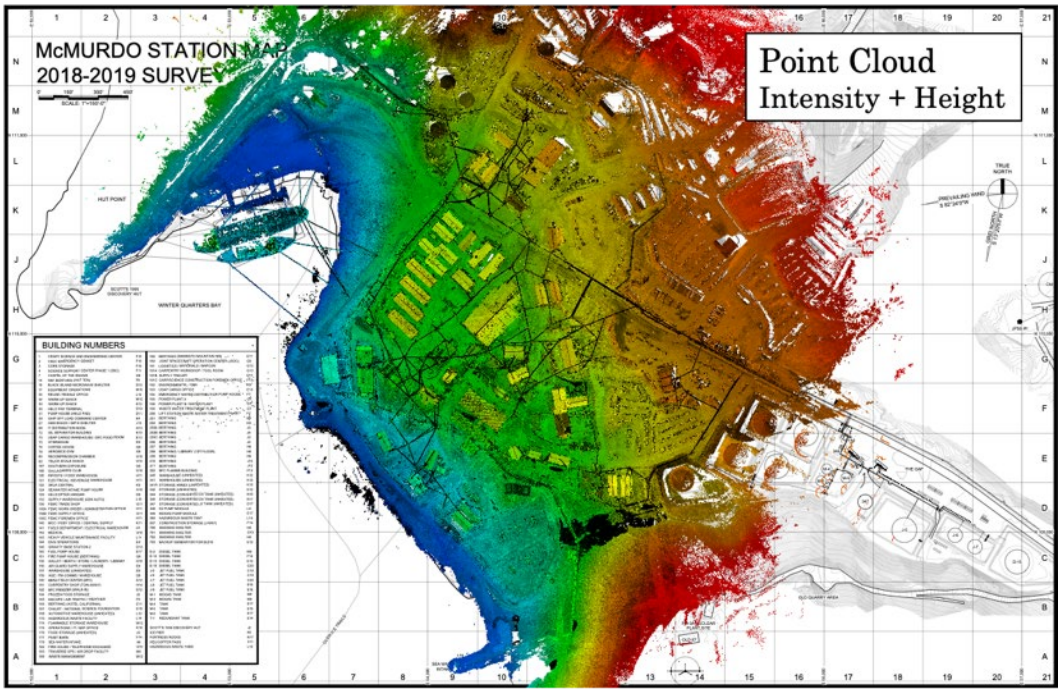


Figure 34. Lidar point cloud from the full FOV dataset, colored by density, overlaid on the McMurdo Station 2018–2019 survey map. Areas with less than 100 pts/m² are colored *blue*, while areas with greater than 1000 pts/m² are colored *red*. Areas of high point densities correspond to sections below the UAS flight lines.

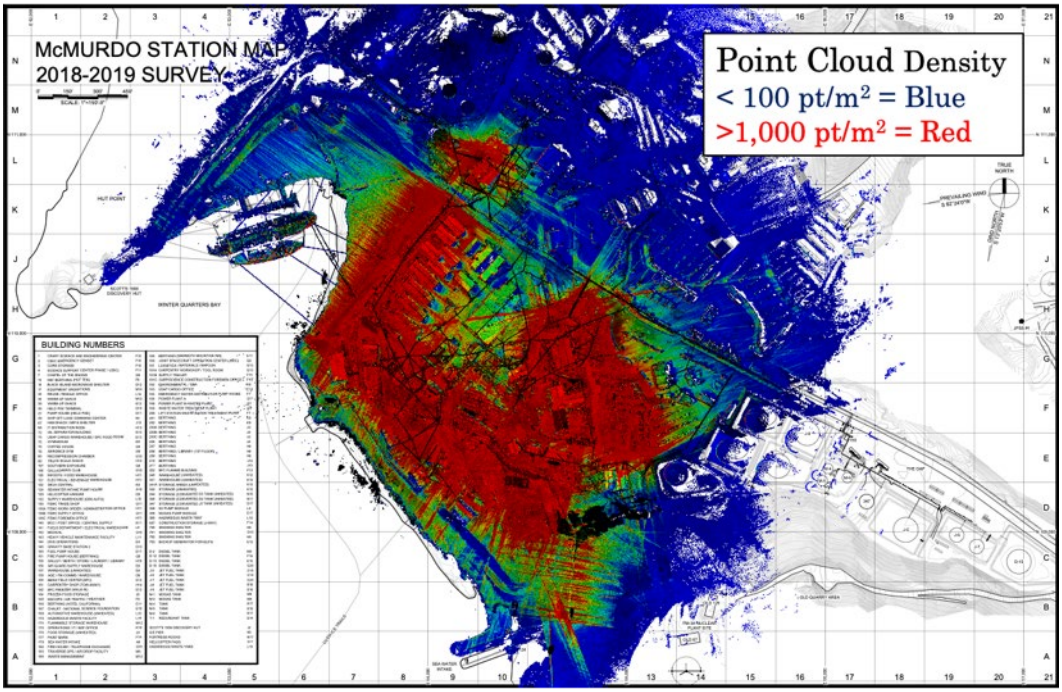


Figure 35. A 0.3 m bare-earth digital elevation model (DEM) derived from the full FOV dataset, colored by height, overlaid on the McMurdo Station 2018–2019 survey map. Ground points were identified using a bare-earth-extraction algorithm.

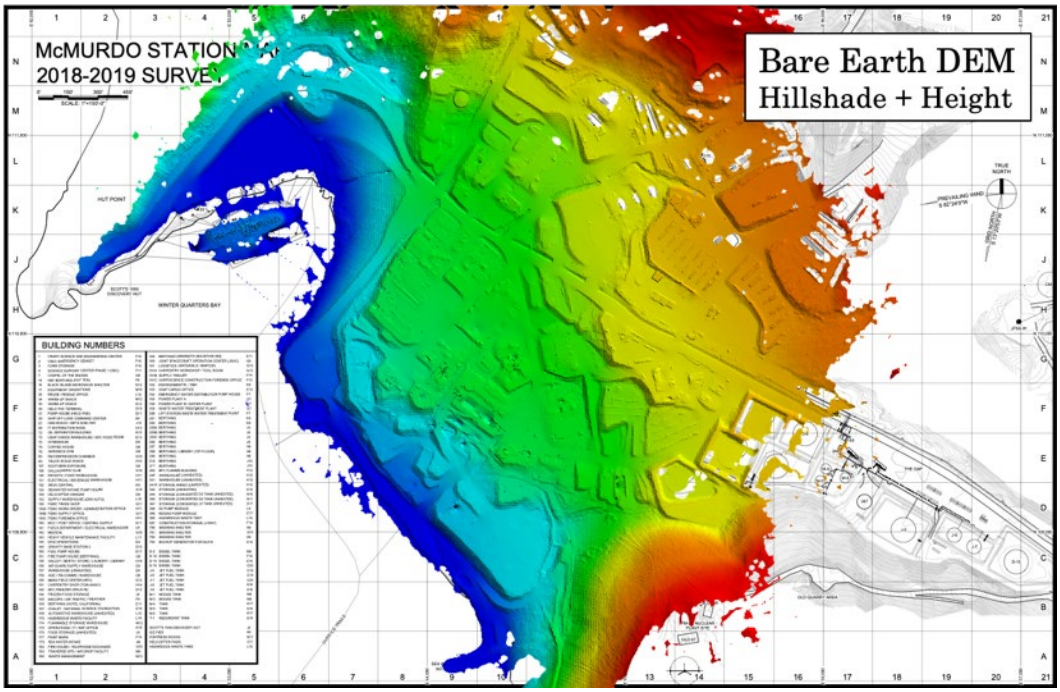
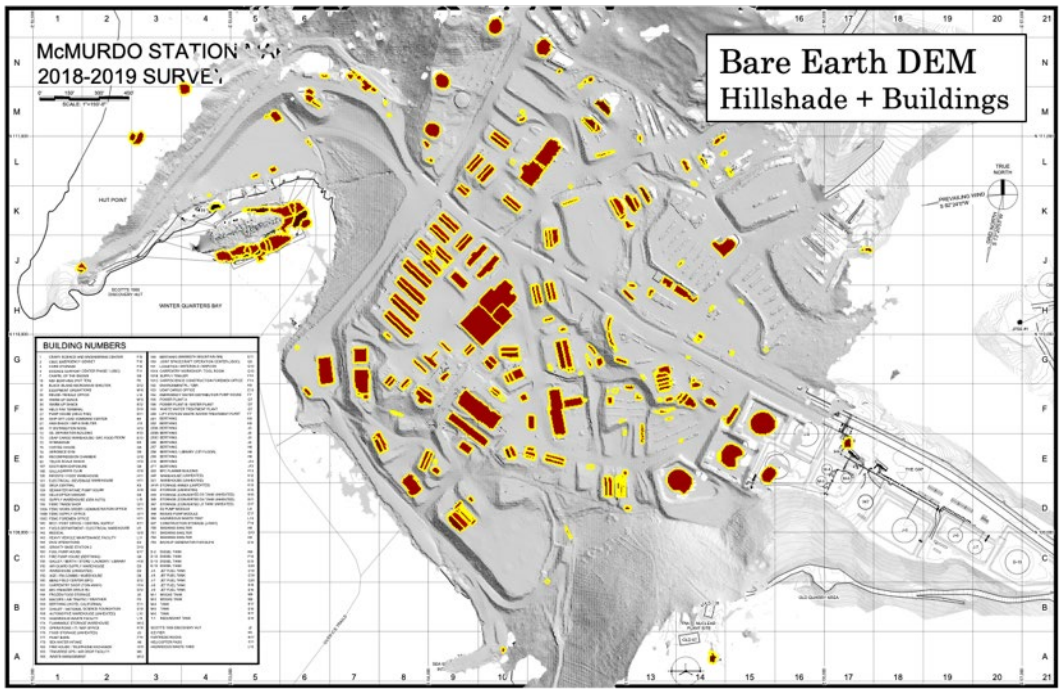


Figure 36. Building outlines (*red*) and roof vectors (*yellow*) overlaid on the 0.3 m bare-earth DEM derived from the full FOV dataset. The DEM uses a hillshade colorization. This data product is overlaid on the McMurdo Station 2018–2019 survey map. Building outlines and roof vectors were identified using a building extraction tool in Quick Terrain Model.



5.2.2 Utilidor point cloud analysis

Figures 37–42 are samples from the UAS survey, focused on the utilidor, including views of the point cloud and resulting data products derived from the point cloud.

Figure 37. Isolated point cloud covering surfaces representing the McMurdo Station utilidor (colored *red*), overlaid on the McMurdo Station 2018–2019 survey map. The utilidor surfaces were isolated from the larger full FOV point cloud dataset in an effort to simplify future analysis of the utilidor features.

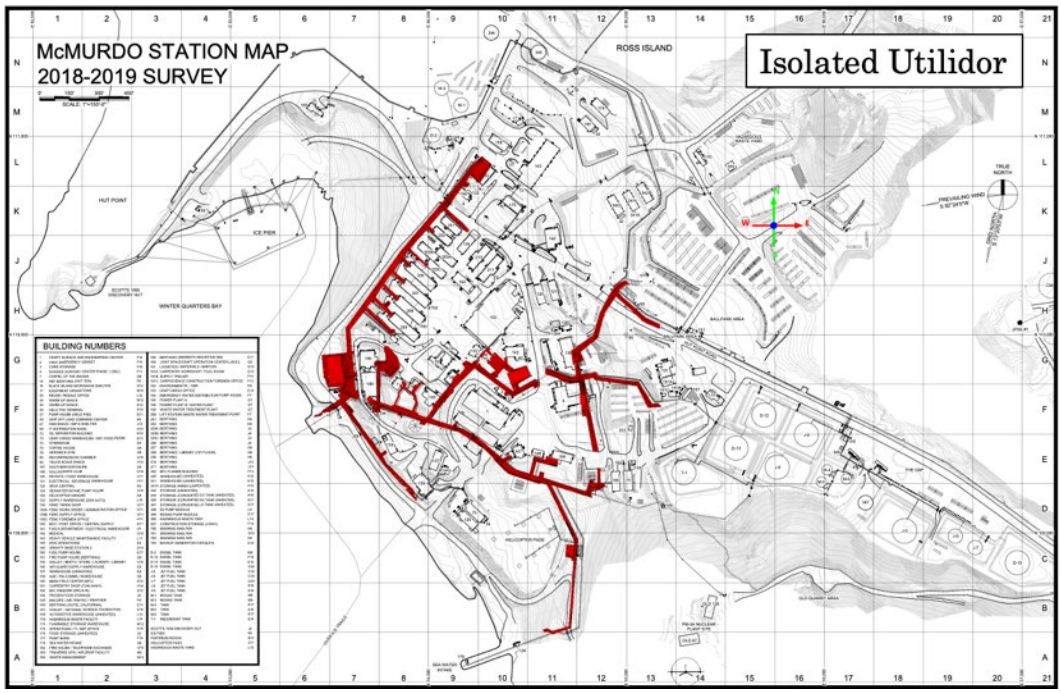


Figure 38. Oblique view of the lidar point cloud from a section of the utilidor below the Crary Lab, colored by height and shaded by intensity (range-independent surface reflectance). A cross section of the utilidor is show by the inset image, showing the level of detail achieved from the UAS lidar point cloud. Individual sections of insulation, pipes, and conduit can be identified within the cross-sectional point cloud.

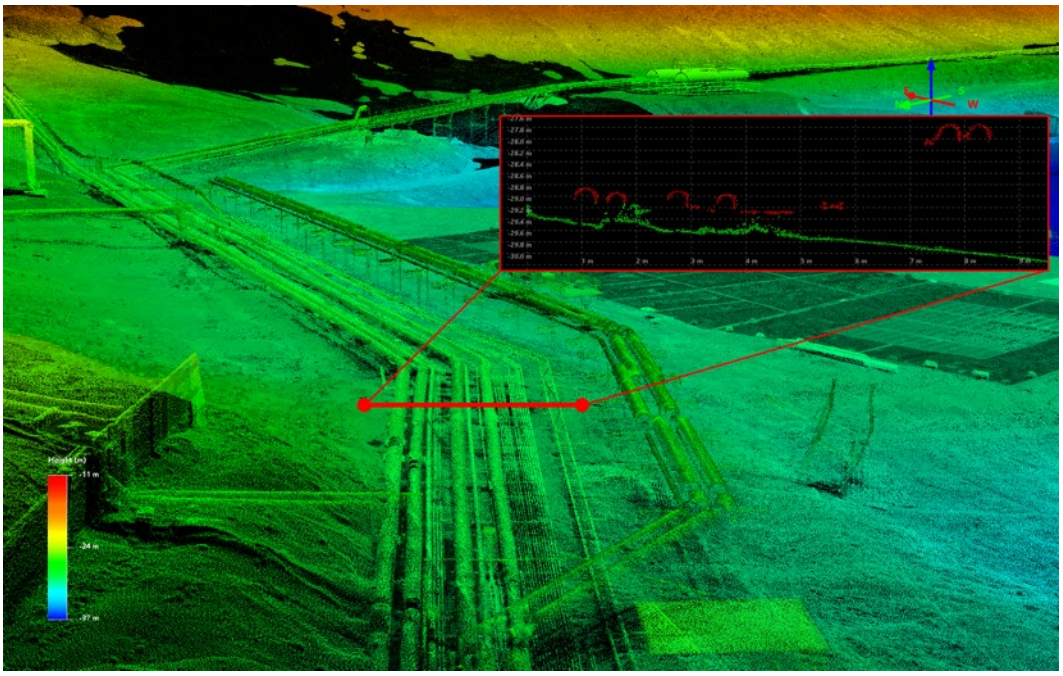


Figure 39. Utilidor profiles derived from the lidar point cloud. *Top*: Profiles 1–5 overlaid on the McMurdo Station 2018–2019 survey map. Profiles are individually colored. *Bottom*: cross-sectional view of the utilidor for Profiles 1–5. Points are colored by classification (*green* is ground points, *red* and *blue* are nonground points). Where applicable, the length of the utilidor section and the corresponding slope is noted within the cross-sectional view (e.g., P1 length = 131.7 m with a slope of 1.151°).

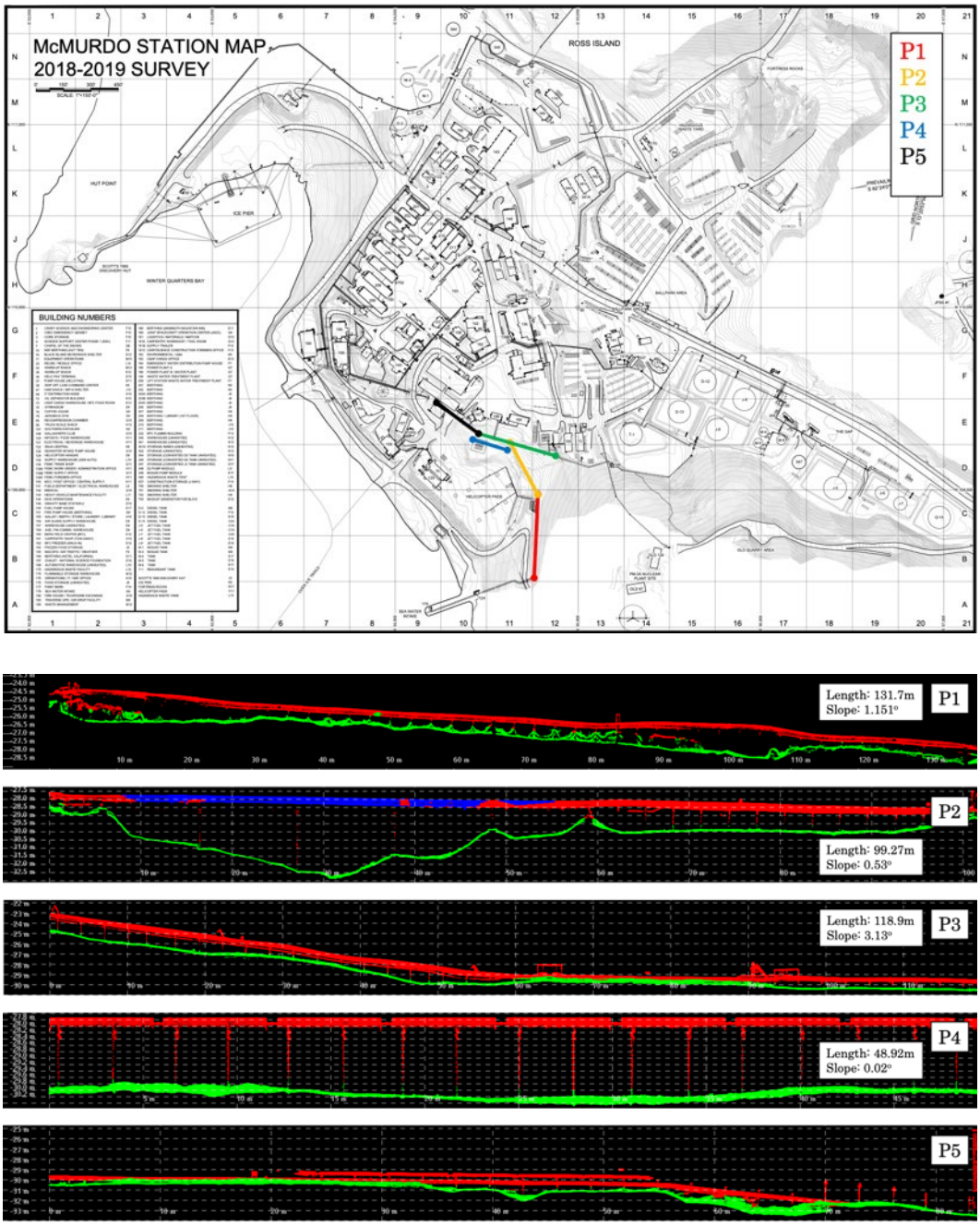


Figure 40. Utilidor profiles derived from the lidar point cloud. *Top*: Profiles 6–10 overlaid on the McMurdo Station 2018–2019 survey map. Profiles are individually colored. *Bottom*: cross-sectional view of the utilidor for Profiles 6–10. Points are colored by classification (*green* is ground points, *red* and *blue* are nonground points). Where applicable, the length of the utilidor section and the corresponding slope is noted within the cross-sectional view (e.g., P10 length = 76.74 m with a slope of 1.10°).

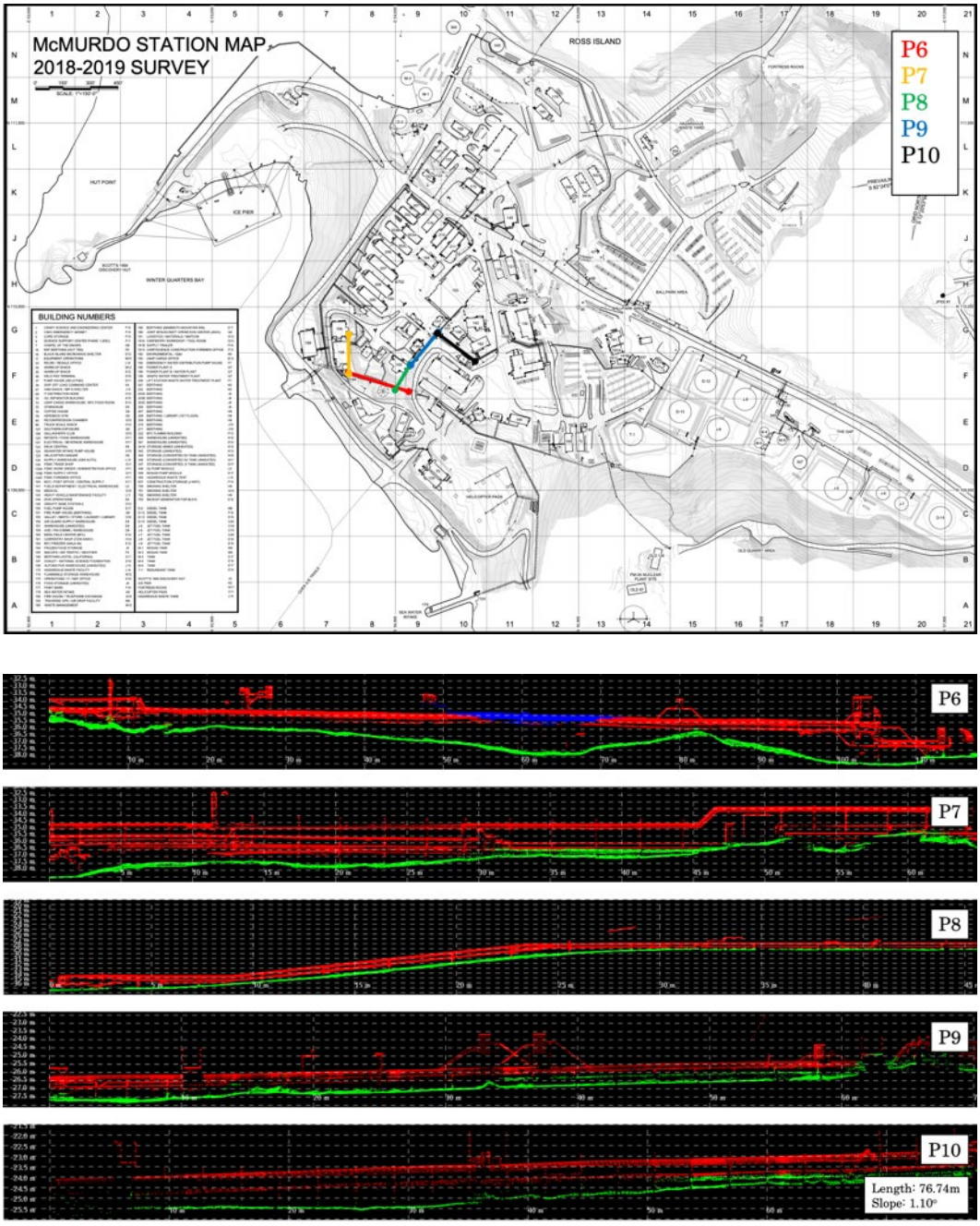


Figure 41. Utilidor profiles derived from the lidar point cloud. *Top*: Profiles 11–15 overlaid on the McMurdo Station 2018–2019 survey map. Profiles are individually colored. *Bottom*: cross-sectional view of the utilidor for Profiles 11–15. Points are colored by classification (*green* is ground points, *red* and *blue* are nonground points). Where applicable, the length of the utilidor section and the corresponding slope is noted within the cross-sectional view (e.g., P11 length = 69.05 m with a slope of 0.88°).

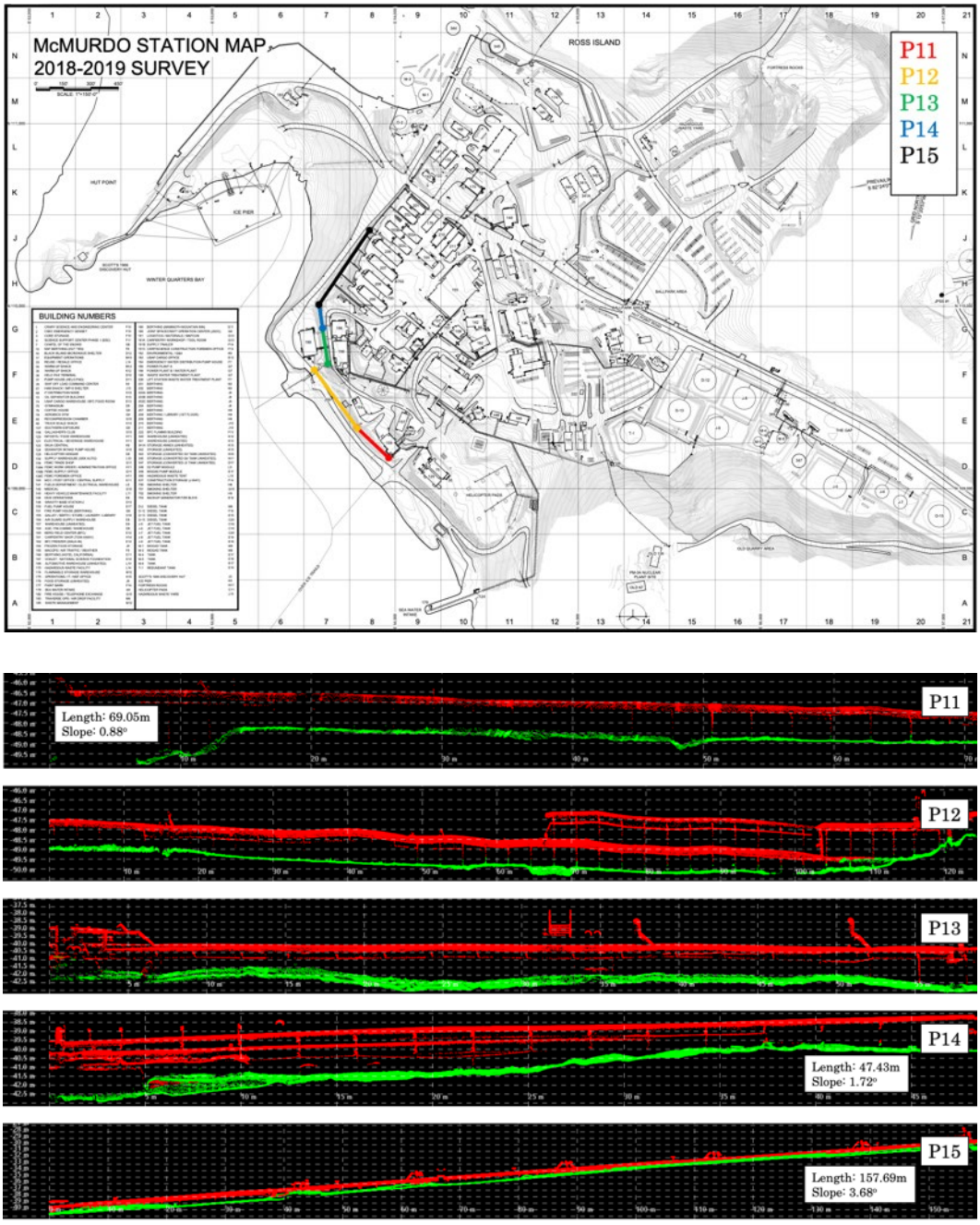
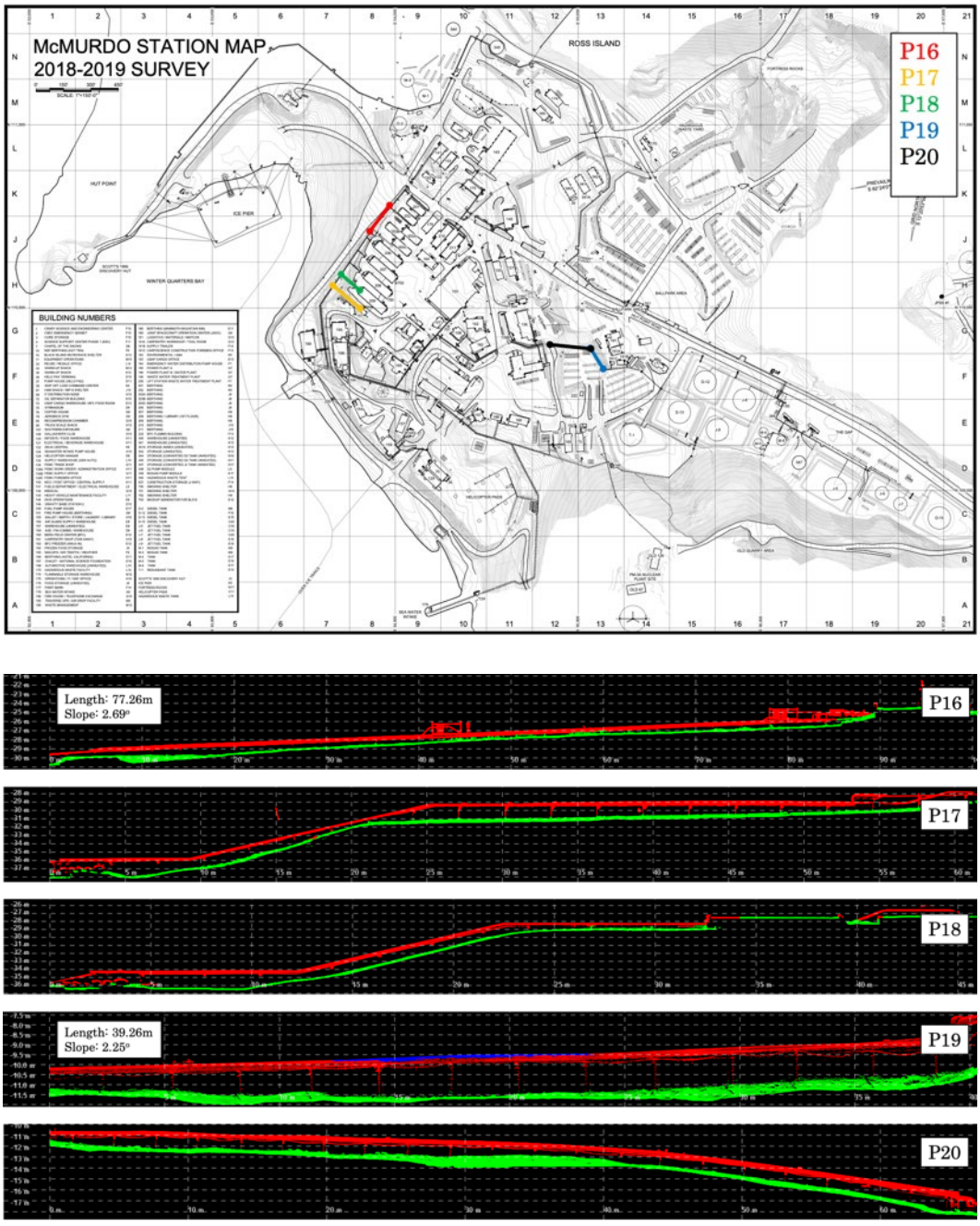


Figure 42. Utilidor profiles derived from the lidar point cloud. *Top*: Profiles 16–20 overlaid on the McMurdo Station 2018–2019 survey map. Profiles are individually colored. *Bottom*: cross-sectional view of the utilidor for Profiles 16–20. Points are colored by classification (*green* is ground points, *red* and *blue* are nonground points). Where applicable, the length of the utilidor section and the corresponding slope is noted within the cross-sectional view (e.g., P16 length = 77.26 m with a slope of 2.69°).



5.2.3 Visible-spectrum colorized point cloud

Figures 43 and 44 are samples from the UAS survey, including views of the point cloud colorized by the visible-spectrum camera.

Figure 43. Plot of the resulting point cloud data captured by UAS at McMurdo Station overlaid on the McMurdo Station 2018–2019 survey map, colored by visible-spectrum imagery. Since the FOV of the Sony A7R-III camera is spatially limited compared to the FOV of the lidar sensor, the resulting point cloud with RGB color values is also more spatially limited.

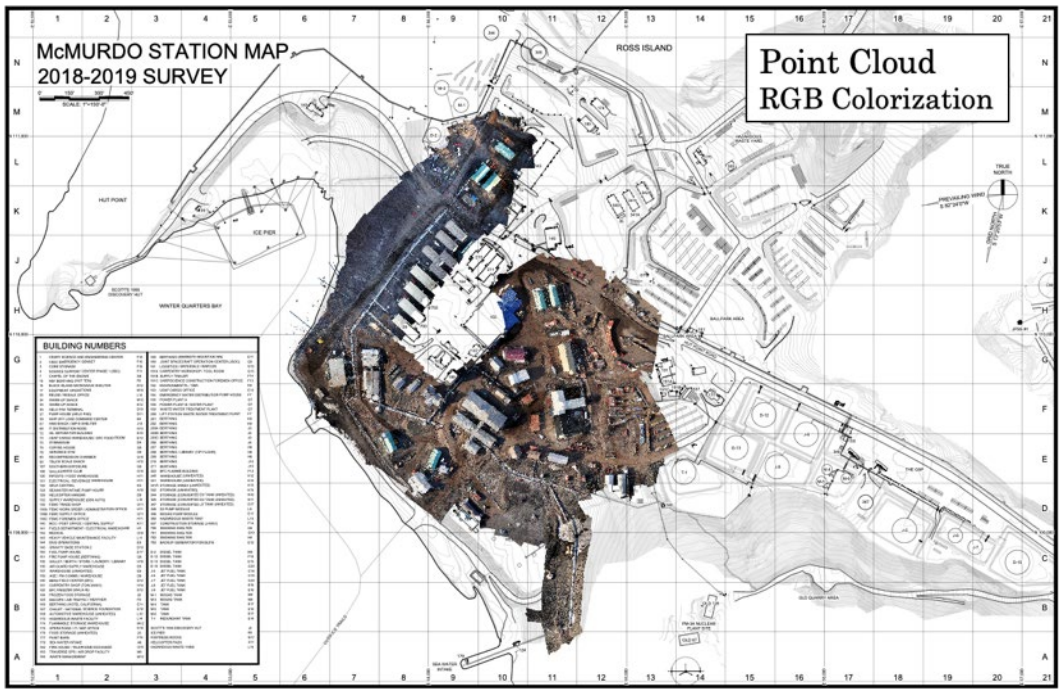
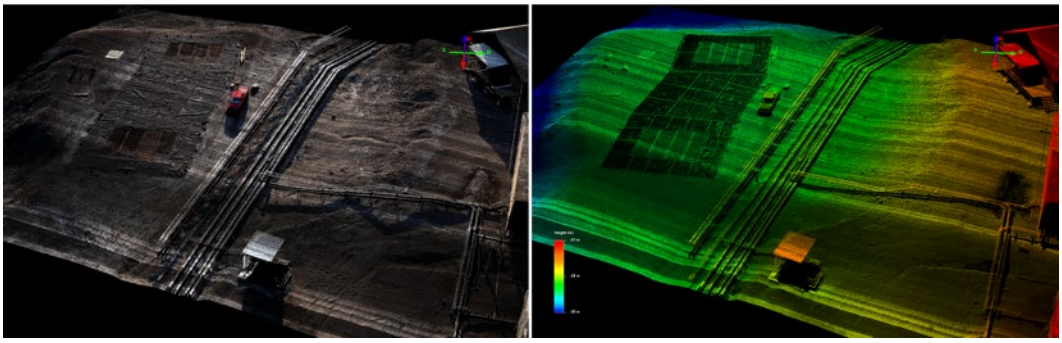


Figure 44. *Left*: Oblique view of the lidar point cloud near the helipad at McMurdo Station, colored by visible-spectrum imagery. *Right*: Same view as left image, colored by height (blue to red = low to high height) and shaded by intensity (dark to light = low to high intensity).



5.2.4 Longwave TIR colorized point cloud

Figures 45–50 are samples from the UAS survey, including views of the point cloud colorized by the TIR camera.

Figure 45. Plot of the resulting point cloud data captured by UAS at McMurdo Station overlaid on the McMurdo Station 2018–2019 survey map, colored by TIR imagery.

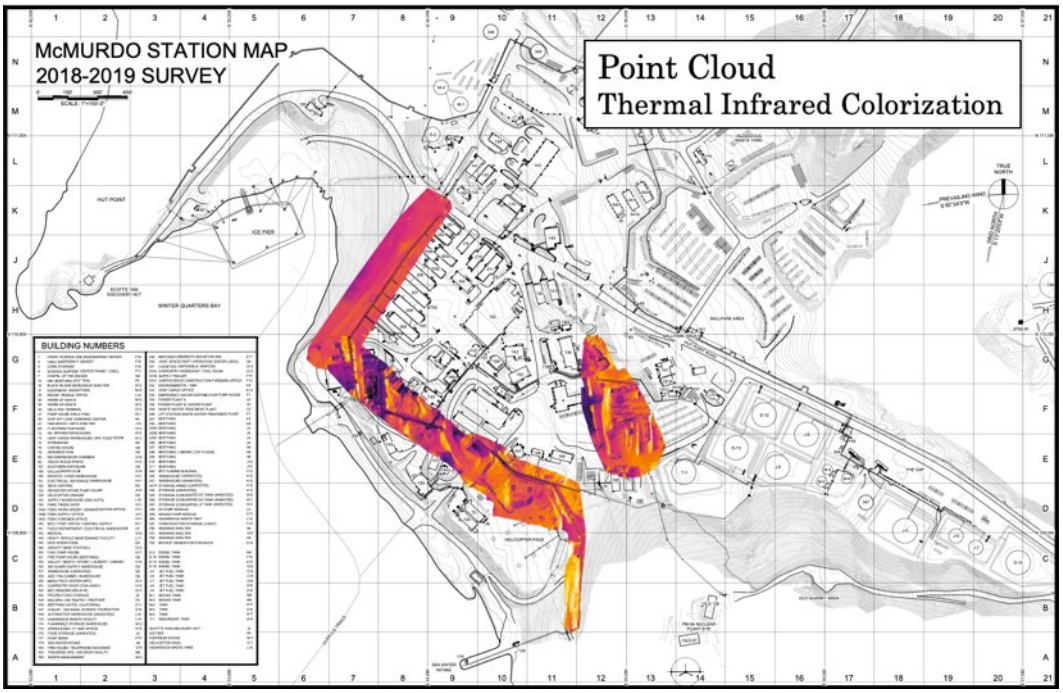


Figure 46. Example of the TIR colorization process. *Top left*: Oblique view of the upper helipad area at McMurdo Station, colored by intensity. *Top right*: The same view colored by TIR-derived temperature values (temperature scale is −15 °C to 25 °C). *Bottom*: The same view as the top images, colored by temperature (dark to light = low to high temperature) and shaded by intensity (dark to light = low to high intensity).

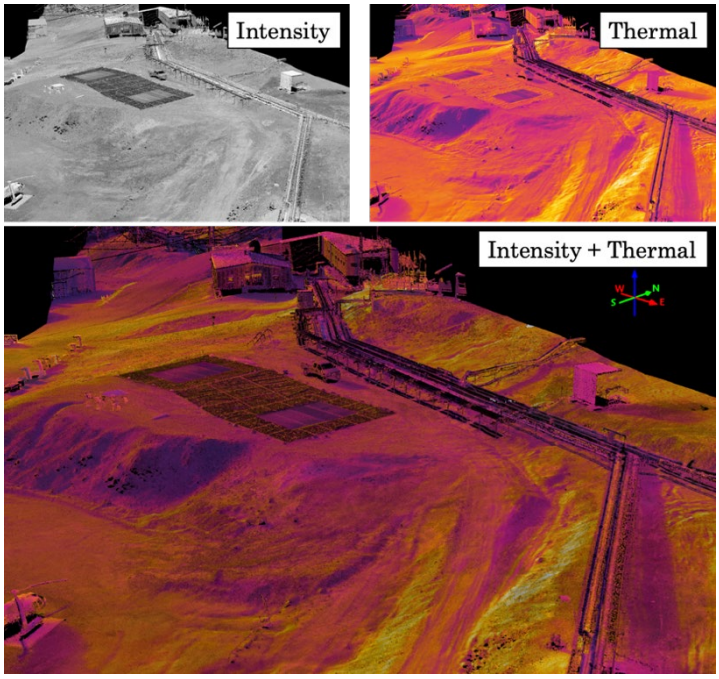


Figure 47. Orthorectified image from the helipad lift. Temperature scale is −15 °C to 25 °C. Sections of the utilidor are identifiable by the lower-temperature (darker) linear surfaces.

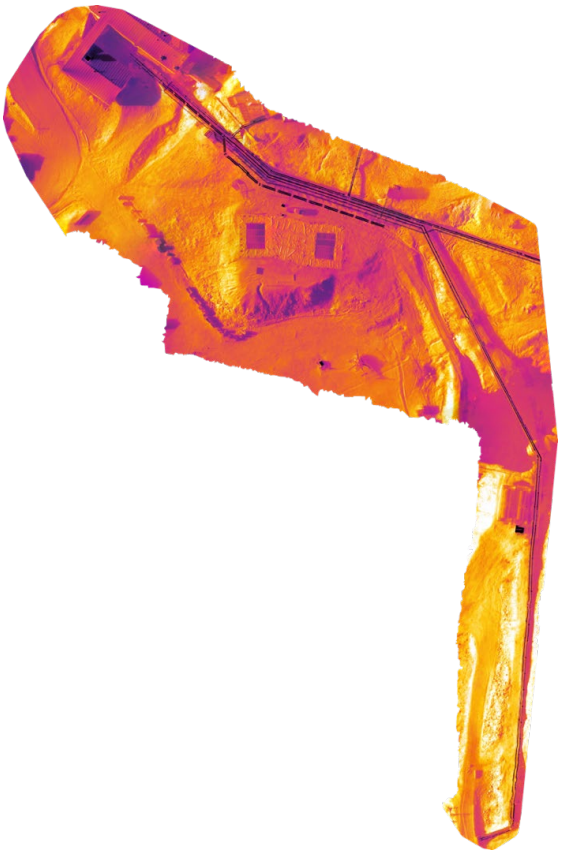


Figure 48. Orthorectified image from the wastewater lift. Temperature scale is −15 °C to 25 °C. Sections of the utilidor are identifiable by the lower-temperature (darker) linear surfaces.

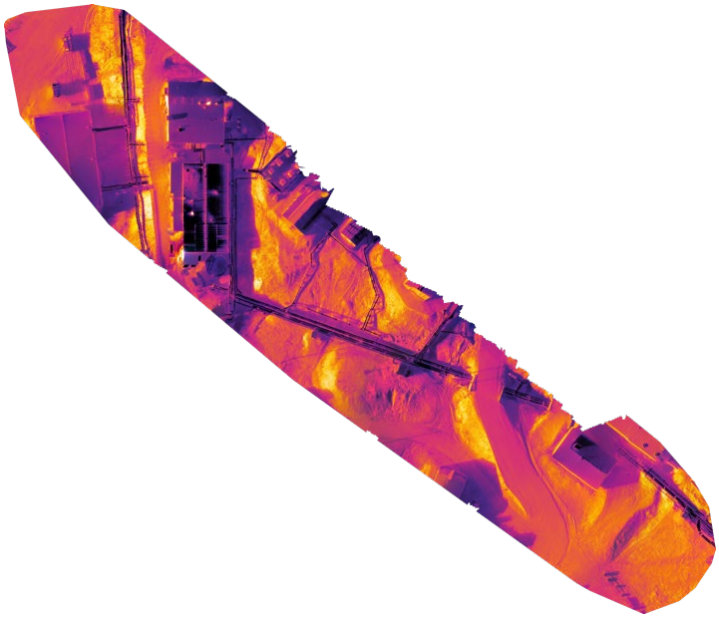


Figure 49. Orthorectified image from the dormitory lift. Temperature scale is −15 °C to 25 °C. Sections of the utilidor are identifiable by the lower-temperature (darker) linear surfaces.

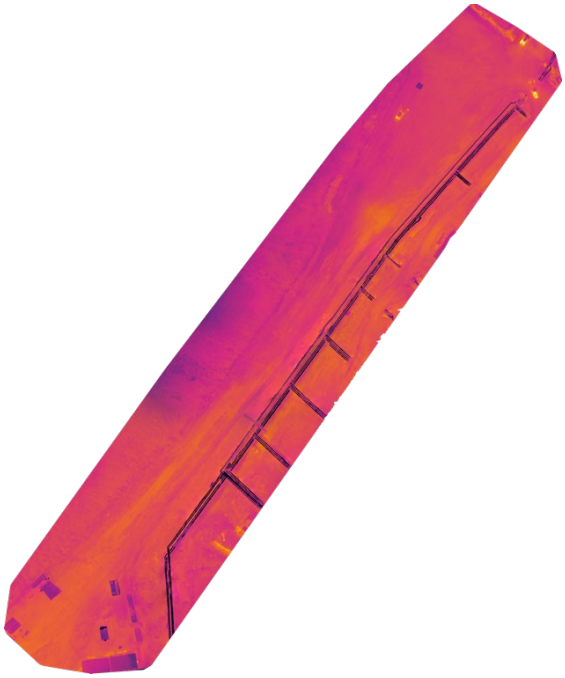
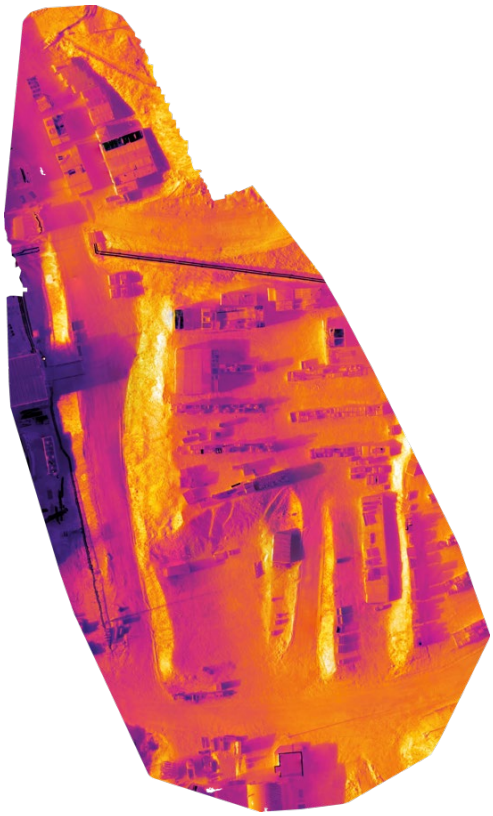


Figure 50. Orthorectified image from the carpentry shop lift. Temperature scale is −15 °C to 25 °C. Sections of the utilidor are identifiable by the lower-temperature (darker) linear surfaces.



6 Conclusion and Recommendations

Between 2 and 7 February 2020, we collected a 3-D thermal model of the Crary Lab and wet utility corridor at McMurdo Station, Antarctica, by using a combined terrestrial lidar/TIR scanning system and unmanned lidar/TIR/electro-optical system in an effort to identify deficiencies in the building thermal envelope and to collect information for future structural assessments. These data are intended to assist USAP determine potential thermal-deficiency remediation steps, confirm effective design and construction techniques, and prioritize ongoing efforts in the modernization of McMurdo Station. We collected supporting data to assist in processing and interpreting the lidar/TIR results, including exterior and interior air-temperature measurements, RTK GNSS measurements of lidar reflectors, and handheld DSLR images.

We presented the results and preliminary 3-D thermal models to NSF during the data processing and analysis period of the project, summarizing our initial findings. Further data processing has produced a full 3-D thermal model representing the exterior surfaces of the Crary Lab and the utilidor at centimeter-scale point spacing. Every individual point measurement in these point clouds was assigned a temperature value based on coincident TIR imagery. Further, the UAS point clouds have been assigned RGB color values from the onboard visible-spectrum camera. With the addition of the ULS data, we provide a more complete 3-D model of the Crary Lab exterior surface by including the roof in the final model. This is an improvement over past efforts at Palmer Station (2015) and South Pole Station (2017) where only TLS surveys were conducted. Finally, with the wide FOV of the ULS sensor, we successfully captured the majority of McMurdo Station at centimeter-scale detail and accuracy. These data should prove useful in future modernization and development of McMurdo Station as they provide a high-resolution baseline spatial reference for planning and design purposes.

Overall, the Crary Lab's design and construction provides a tight thermal envelope with little significant heat loss observed by the lidar/TIR system. In addition to the samples included in section 5.1, we have provided an exhaustive catalog (Appendix C: Crary Lab Features Catalog) of all the Crary Lab windows, doors, loading docks and other features (vents, soffits, etc.) with any thermal anomalies or areas of structural or surface damage indicated. In general, we observe areas of higher surface thermal values and

heat loss in the transition sections of the exterior walls of the Crary Lab where the walls change from vertical to overhanging, minor heat loss at windows and doors, and larger heat loss at loading dock doors.

Given the homogeneity of the building's exterior through consistent use of the same windows and doors and the repeating patterns for the building's phases, individual TIR images without the spatial reference provided by the lidar point cloud would be difficult to associate with specific locations on the building in follow-up analysis. The combined lidar/TIR dataset avoids this difficulty through its 3-D data products.

With the ULS results over the utilidor, we find that the point cloud data provide a detailed reference for analyzing the individual pipes, insulated tubes, conduit, and supporting structures. From these data, users may calculate the slope of the utilidor sections and identify areas of undulation or elevation issues (e.g., backflow of gravity-fed pipes due to support structure settlement or sagging). With the great detail provided by the ULS data, we recommend further analysis and quantification of metrics of interest (e.g., elevation differences and slope limits) by NSF personnel and support staff. Section 5.2.2 provides twenty sample cross sections along the utilidor, but additional analysis of the point cloud data using the provided data products outlined in section 4.5 will likely reveal areas of interest. The coincident TIR imagery provides an additional visual feature in identifying and separating utilidor surfaces from surrounding ground surfaces; but given the presence of direct solar exposure and the influence of surface reflectivity on the resulting thermal images, these data should be used for relative analysis only, not absolute temperature values.

The final point clouds are available for NSF-personnel and contractor access only. Contact the authors for data access instructions and additional data visualization and analysis recommendations. With these data collected at McMurdo Station, Antarctica, NSF has access to high-accuracy, high-resolution 3-D and TIR products over select sites at McMurdo Station for further analysis and exploitation. These data assist in validating best practices for Antarctic infrastructure development and provide real-world observations of existing infrastructure performance in austere environments.

References

Deeb, E. J., and A. L. LeWinter. 2018. *Building Envelope Assessment Using Thermal Infrared and Lidar Scanning: Palmer Station, Antarctica*. ERDC/CRREL TR-18-9. Hanover, NH: U.S. Army Engineer Research and Development Center, Cold Regions Research and Engineering Laboratory. https://hdl.handle.net/11681/27353.

LeWinter, A. L., D. C. Finnegan, E. J. Deeb, and P. J. Gadomski. 2018. *Building Envelope and Infrastructure Assessment Using an Integrated Thermal Imaging and Lidar Scanning System: Amundsen-Scott South Pole Station, Antarctica*. ERDC/CRREL TR-18-10. Hanover, NH: U.S. Army Engineer Research and Development Center, Cold Regions Research and Engineering Laboratory. https://hdl.handle.net/11681/27385.

Phetteplace, G. 2007. *Infrared Survey of the Elevated Station 2006–2007 Season, South Pole, Antarctica*. ERDC/CRREL LR-07-09. Hanover, NH: U.S. Army Engineer Research and Development Center, Cold Regions Research and Engineering Laboratory.

Acronyms and Abbreviations

AIL	Antarctic Infrastructure and Logistics
APS	Antarctic Polar Sterographic
AWOS	Automated Weather Observation System
CRREL	U.S. Army Cold Regions Research and Engineering Laboratory
DEM	Digital Elevation Model
DSM	Digital Surface Model
DTM	Digital Terrain Model
EPOLAR	Engineering for Polar Operations, Logistics, and Research
EPSG	European Petroleum Survey Group
ERDC	Engineer Research and Development Center
FOV	Field of View
GNSS	Global Navigation Satellite System
GriD	Geospatial Repository and Data Management System
IMU	Inertial Measurement Unit
MSA	Multi-Station Adjustment
NSF	National Science Foundation
OPP	Office of Polar Programs
PIC	Pilot in Command
RGB	Red-Green-Blue
RS/GIS CX	Remote Sensing/GIS Center of Expertise
RTK	Real-Time Kinematic
SBET	Smoothed Best Estimate Trajectory
TIR	Thermal Infrared

TLS	Terrestrial Laser Scanner
UAS	Unmanned Aerial System
ULS	Unmanned Laser Scanning
USAP	U.S. Antarctic Program
UTC	Coordinated Universal Time
VO	Visual Observer
WGS84	World Geodetic System 1984
XYZ	Longitude, Latitude, Elevation

Appendix A: CRREL Lidar/TIR System Data Acquisition Procedure

A.1 Overview

This appendix describes the acquisition procedure for capturing coregistered thermal images using the InfraTec VarioCAM HD camera and Riegl VZ-1000 TLS.

A.2 Acquisition PC Setup

A.2.1 Network

1. Set the LAN networks connection to the following settings:
   a. IP address: 192.168.2.2
   b. Subnet mask: 255.255.255.0
2. Ensure both RiSCAN Pro and IRBIS 3 Professional are installed.
3. When the scanner is powered, select the Wi-Fi S9998518, password 123456789.
4. Connect the InfraTec Ethernet cable to the laptop, and then check connection via command prompt if necessary.

A.2.2 RiSCAN Pro Setup

1. Create a new project.
2. In the project attributes, set the following:
   a. Instrument Tab, Scanner IP: 10.0.0.1 (if using wireless) and 192.168.2.125 (if using network cable)
   b. Camera model: Custom camera
3. Set image acquisition to external software:
   a. "Tools"> "Options"> "Image Acquisition"
   b. Image acquisition controlled by: Software (this specifies that external software triggers the camera as opposed to RiSCAN Pro)
4. Set Camera and Mounting calibrations:
   a. Camera: Result calibration nikonD700_2505549_20mm_Final _4256x2832
   b. Mounting: Result mounting nikonD700_2505549_20mm_Final

A.2.3 InfraTec IRBIS 3 Professional Setup

1. Camera IP address is preset to 192.168.2.15.

2. Open IRBIS 3 Professional.
3. Ensure that the scanner is powered and the camera is initialized.
4. In the Camera tab, select "Connect."
5. Use VarioCAM HD; the camera will connect and display a live image.
6. Select the "Remote" tab to display the focus options.
7. Go to the "View" tab.
8. Select the "Scale" tab.
9. Return to the "Camera" tab.
10. Use the "Live" tab to see a live view.
11. In the "Snap" tab, ensure it is set to "Premium and Auto Save."

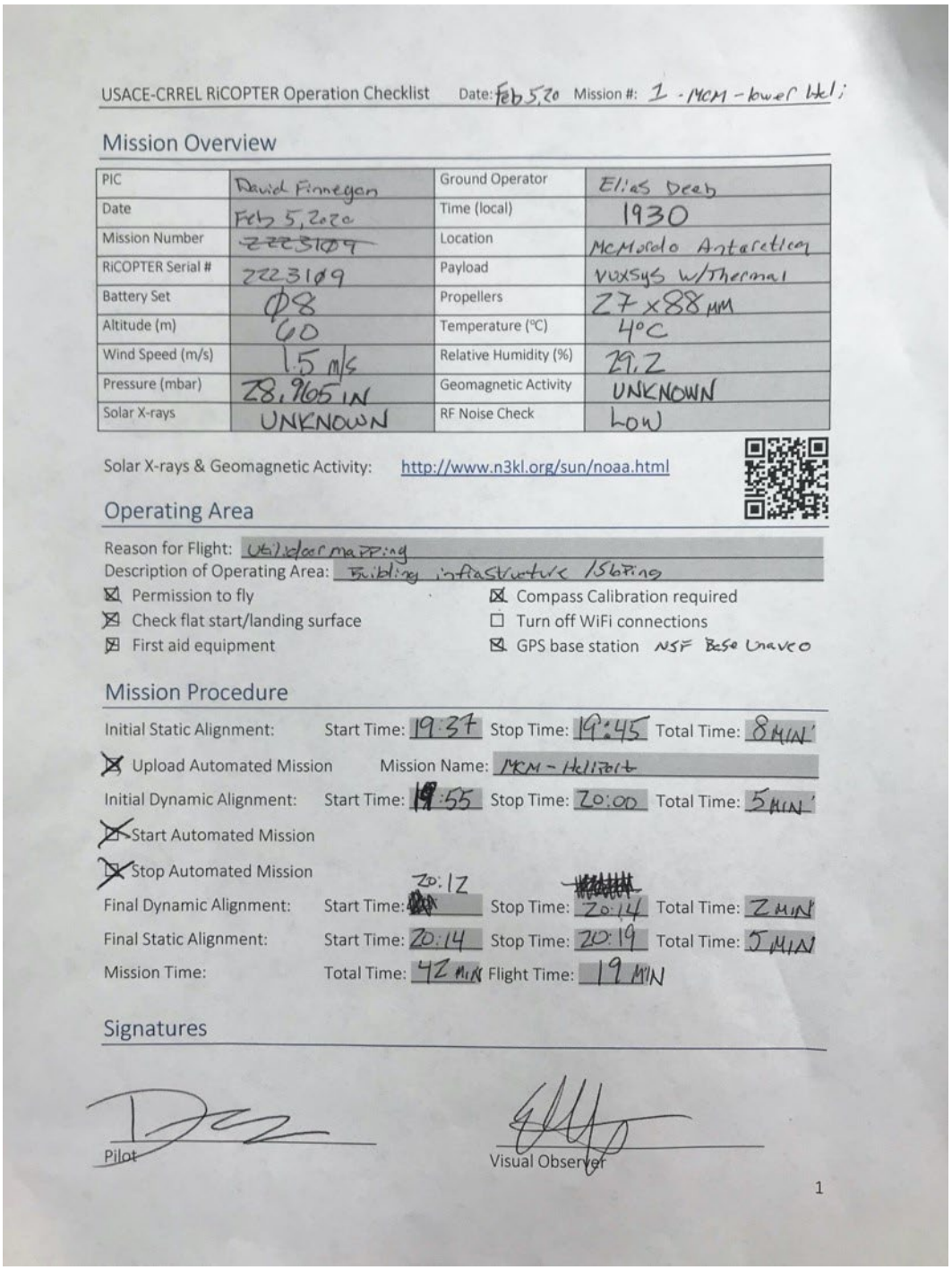
A.3 Hardware Setup

1. Attach the scanner to the survey tripod.
2. Attach the InfraTec VarioCAM HD TIR camera to the scanner.

A.4 Collection of Data

1. In RiSCAN Pro, collect a scan with settings appropriate to the project, but do not acquire the images automatically.
2. After the scan is complete, right-click the scan and select "Image Acquisition." (If using the network cable with the scanner, switch project to wireless [10.0.0.1], disconnect the scanner network cable, and connect the InfraTec network cable.)
3. Use the "NikonD700_2505549_20mm_Final Scanner" camera calibration/mounting file.
4. Use a 40% overlap to ensure good coverage of the scan area.
5. The scanner will move to the first image phi angle and prompt the user to capture the image.
6. Go into IRBIS 3 and focus the camera; then select "Snap," and verify that the new image with naming convention YYMMDD_HHMMSS.irb was saved.
7. Back in RiSCAN Pro, select "OK" to proceed with the next image.
8. Proceed for all images.
9. End the scan position, and proceed to the next position.

Appendix B: CRREL RiCOPTER Operation Checklists



USACE-CRREL RiCOPTER Operation Checklist Date: Feb 5,20 Mission #: 1 - MCM - lower Wkl

Mission Overview

PIC	David Finnegan	Ground Operator	Elias Deeb
Date	Feb 5, 2020	Time (local)	1930
Mission Number	~~2223109~~	Location	McMurdo Antarctica
RiCOPTER Serial #	2223109	Payload	VUXSYS w/Thermal
Battery Set	Ø8	Propellers	27 x 88 MM
Altitude (m)	60	Temperature (°C)	4°C
Wind Speed (m/s)	1.5 M/S	Relative Humidity (%)	29.2
Pressure (mbar)	28.965 IN	Geomagnetic Activity	UNKNOWN
Solar X-rays	UNKNOWN	RF Noise Check	LOW

Solar X-rays & Geomagnetic Activity: http://www.n3kl.org/sun/noaa.html

Operating Area

Reason for Flight: Utility/door mapping
Description of Operating Area: Building infrastructure 156ing

- [x] Permission to fly
- [x] Check flat start/landing surface
- [x] First aid equipment
- [x] Compass Calibration required
- [ ] Turn off WiFi connections
- [x] GPS base station NSF Base Unavco

Mission Procedure

Initial Static Alignment: Start Time: 19:37 Stop Time: 19:45 Total Time: 8 MIN

- [x] Upload Automated Mission — Mission Name: MCM - Helitak

Initial Dynamic Alignment: Start Time: 19:55 Stop Time: 20:00 Total Time: 5 MIN

- [x] Start Automated Mission
- [x] Stop Automated Mission

Final Dynamic Alignment: Start Time: 20:12 Stop Time: 20:14 Total Time: 2 MIN

Final Static Alignment: Start Time: 20:14 Stop Time: 20:19 Total Time: 5 MIN

Mission Time: Total Time: 42 MIN Flight Time: 19 MIN

Signatures

Pilot

Visual Observer

1

USACE-CRREL RiCOPTER Operation Checklist Date: 2/5/20 Mission #: 2

Mission Overview

PIC	DAVID FINNEGAN	Ground Operator	ELIAS DERS
Date	2/5/20	Time (local)	2025
Mission Number	2	Location	McMURDO BACKUP HELIPAD
RiCOPTER Serial #	OSPREY	Payload	FLIR TAU/HASELBLATT/UAV VUX
Battery Set	01	Propellers	27 x 8.8 CM
Altitude (m)	85M	Temperature (°C)	4.0
Wind Speed (m/s)	CALM	Relative Humidity (%)	3.5
Pressure (mbar)	28.965 IN	Geomagnetic Activity	UNKNOWN
Solar X-rays	UNKNOWN	RF Noise Check	GOOD

Solar X-rays & Geomagnetic Activity: http://www.n3kl.org/sun/noaa.html

Operating Area

Reason for Flight: McMURDO UTILIDOR

Description of Operating Area: BUILDING INFRASTRUCTURE

- [X] Permission to fly
- [X] Check flat start/landing surface
- [X] First aid equipment
- [X] Compass Calibration required
- [X] Turn off WiFi connections
- [X] GPS base station UNAVCO McMURDO BASE STATION

Mission Procedure

Initial Static Alignment: Start Time: 2040 Stop Time: 20:45 Total Time: 5 MIN

- [X] Upload Automated Mission Mission Name: MCM - POWER PLANT

Initial Dynamic Alignment: Start Time: 20:45 Stop Time: 20:48 Total Time: 3MIN

- [X] Start Automated Mission
- [X] Stop Automated Mission

Final Dynamic Alignment: Start Time: 2055 Stop Time: 2058 Total Time: 3 MIN

Final Static Alignment: Start Time: 2058 Stop Time: 2103 Total Time: 5 MIN

Mission Time: Total Time: 23 Flight Time: 10

Signatures

Pilot

Visual Observer

1

USACE-CRREL RiCOPTER Operation Checklist Date: 2/6/20 Mission #: 1

Mission Overview

PIC	DAVID FINNEGAN	Ground Operator	ELIAS DEEB
Date	2/6/20	Time (local)	0435
Mission Number	1	Location	MCM
RiCOPTER Serial #	OSPREY	Payload	UAVUX/FLIR/SONY A7
Battery Set	01	Propellers	27 X 8.8 CM
Altitude (m)	60M	Temperature (°C)	20°C
Wind Speed (m/s)	1.5 M/S	Relative Humidity (%)	37.4%
Pressure (mbar)	979.2	Geomagnetic Activity	UNKNOWN
Solar X-rays	UNKNOWN	RF Noise Check	LOW

Solar X-rays & Geomagnetic Activity: http://www.n3kl.org/sun/noaa.html

Operating Area

Reason for Flight: MCM DOEM SURVEY
Description of Operating Area: BUILDING INFRASTRUCTURE

- [x] Permission to fly
- [x] Check flat start/landing surface
- [x] First aid equipment
- [x] Compass Calibration required *NOT REQUIRED
- [x] Turn off WiFi connections
- [x] GPS base station

Mission Procedure

0445

Initial Static Alignment: Start Time: ~~0435~~ Stop Time: ~~0440~~ Total Time: ~~4:50~~

- [x] Upload Automated Mission — Mission Name: DORMS MCM

Initial Dynamic Alignment: Start Time: 0450 Stop Time: 0455 Total Time: 5 MIN

- [x] Start Automated Mission
- [x] Stop Automated Mission

Final Dynamic Alignment: Start Time: 0500 Stop Time: 0505 Total Time: 5 MIN

Final Static Alignment: Start Time: 0505 Stop Time 0510 Total Time: 5 MIN

Mission Time: Total Time: 20' Flight Time: 15'

Signatures

Pilot

Visual Observer

1

USACE-CRREL RiCOPTER Operation Checklist Date: 2/6/20 Mission #: 2

Mission Overview

PIC	DAVID FINNEGAN	Ground Operator	ELIAS DEEB
Date	2/6/20	Time (local)	20:30
Mission Number	2	Location	MCM CARP SHOP
RiCOPTER Serial #	OSPREY	Payload	UAV VUX/FLIR TAU/SONY α7r
Battery Set	#1	Propellers	27 x 8.8 cm
Altitude (m)	60m	Temperature (°C)	5.2°C
Wind Speed (m/s)	< 1 m/s	Relative Humidity (%)	29.5%
Pressure (mbar)	973.6 mbar	Geomagnetic Activity	UNKNOWN
Solar X-rays	UNKNOWN	RF Noise Check	LOW

Solar X-rays & Geomagnetic Activity: http://www.n3kl.org/sun/noaa.html

Operating Area

Reason for Flight: MCM INFRASTRUCTURE PROJECT
Description of Operating Area: BUILDINGS + CARGO

- [x] Permission to fly
- [x] Check flat start/landing surface
- [x] First aid equipment
- [ ] Compass Calibration required
- [x] Turn off WiFi connections
- [x] GPS base station UNAVCO MCM

Mission Procedure

Initial Static Alignment: Start Time: 20:45 Stop Time: 20:50 Total Time: 5 MIN

- [x] Upload Automated Mission Mission Name: CarpShop

Initial Dynamic Alignment: Start Time: 20:50 Stop Time: 20:53 Total Time: 3 MIN

- [x] Start Automated Mission
- [x] Stop Automated Mission

Final Dynamic Alignment: Start Time: 21:00 Stop Time: 21:03 Total Time: 3 MIN

Final Static Alignment: Start Time: 21:03 Stop Time: 21:08 Total Time: 5 MIN

Mission Time: Total Time: 25 MIN Flight Time: 13 MIN

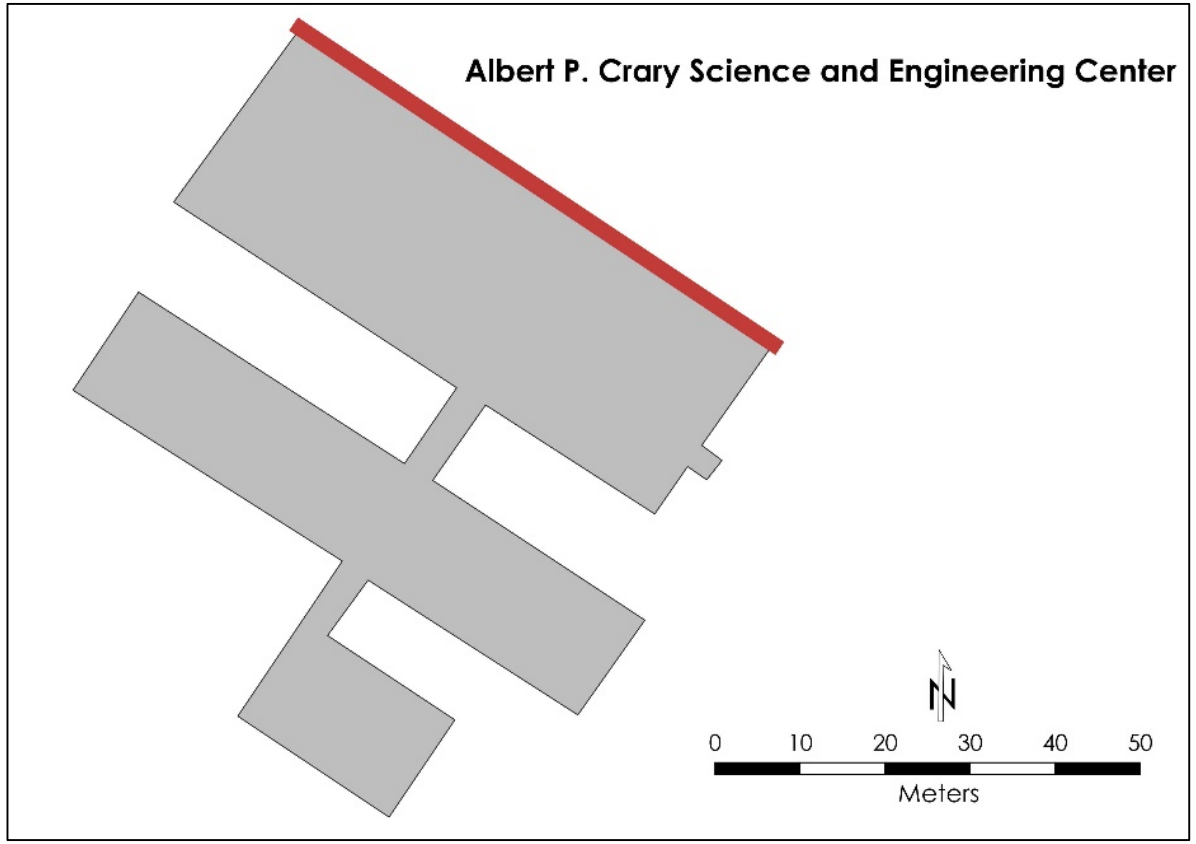
Signatures

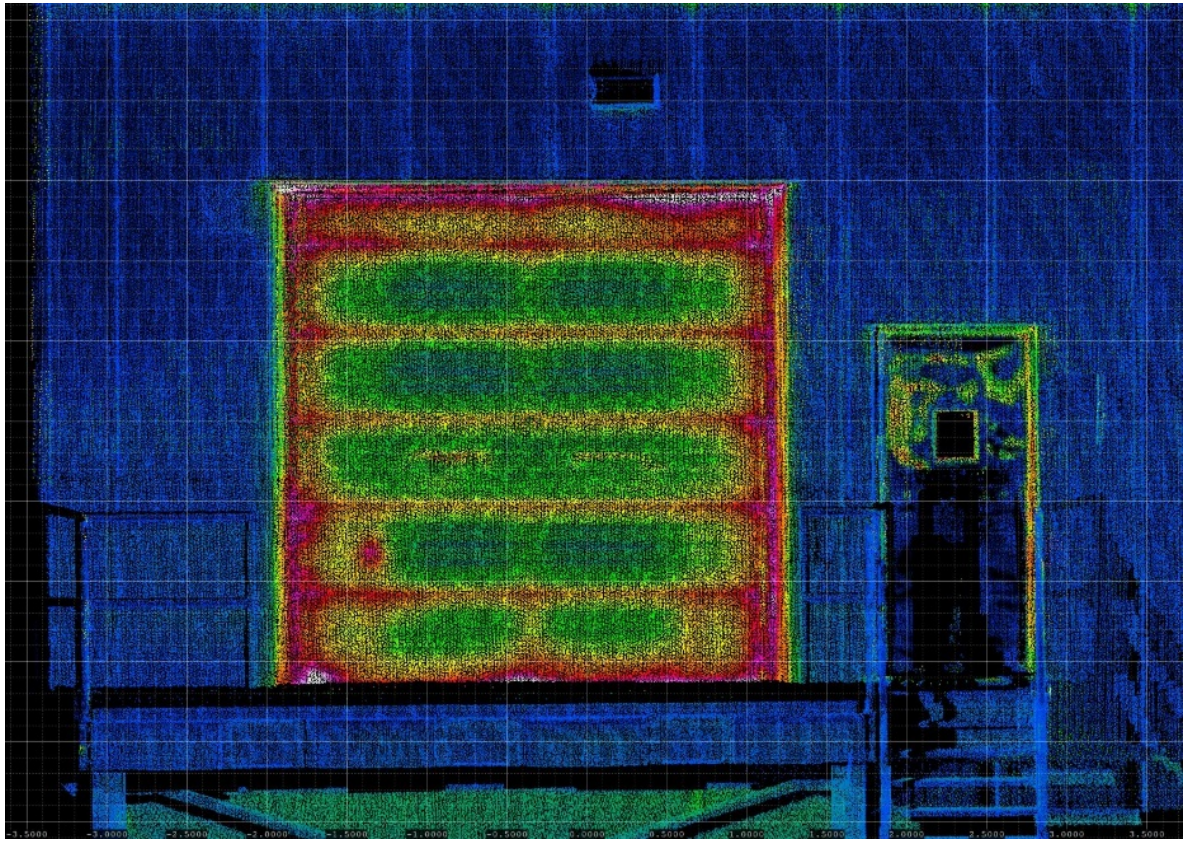
Pilot

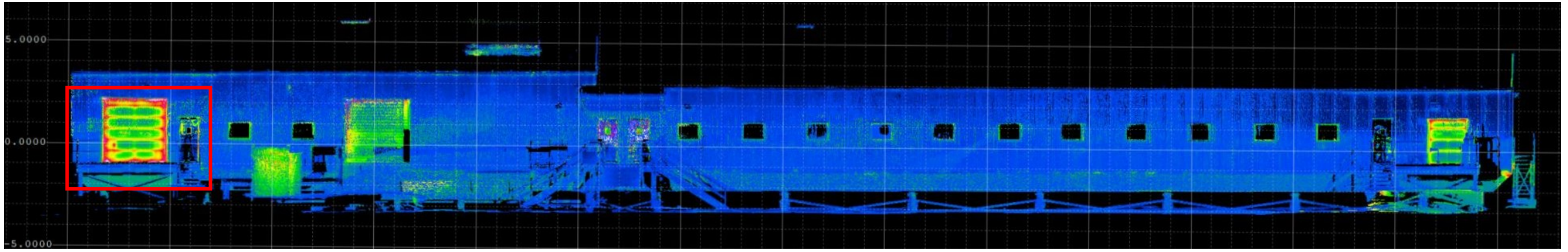
Visual Observer

1

Appendix C: Crary Lab Features Catalog





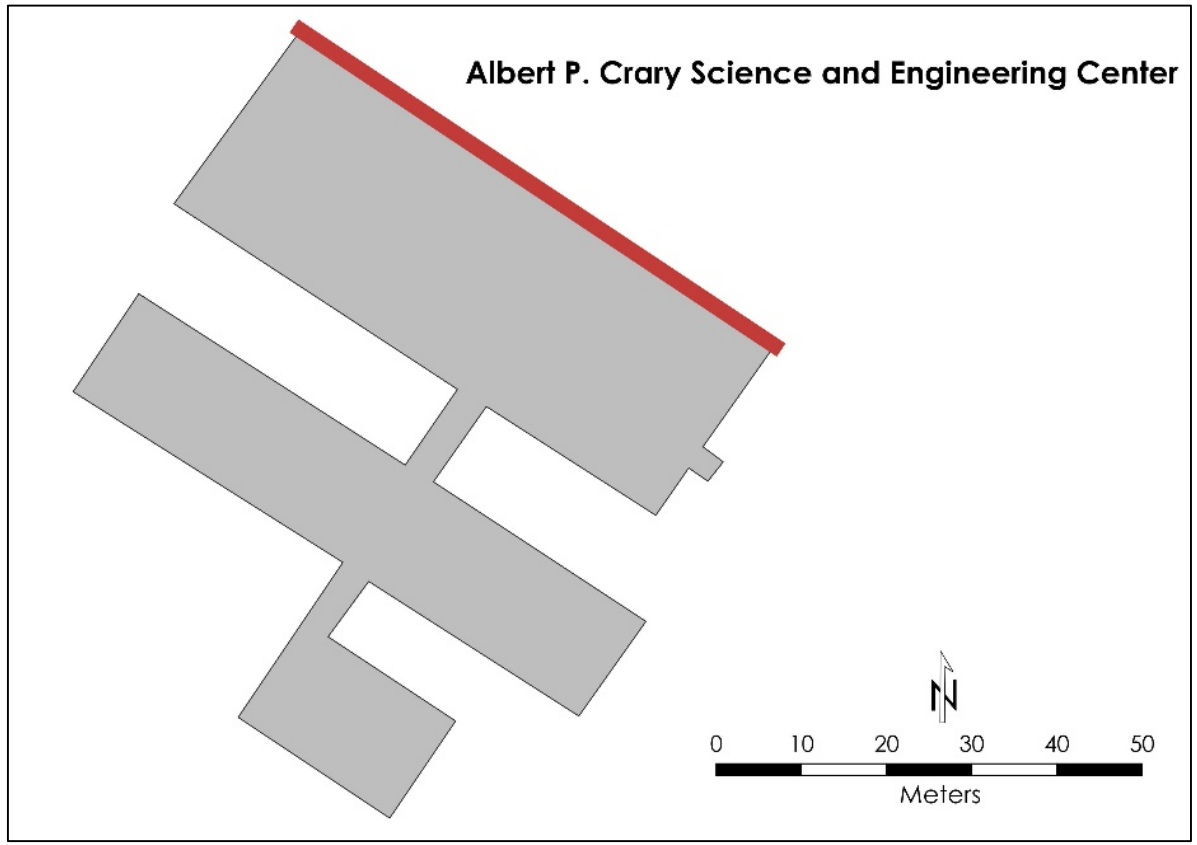


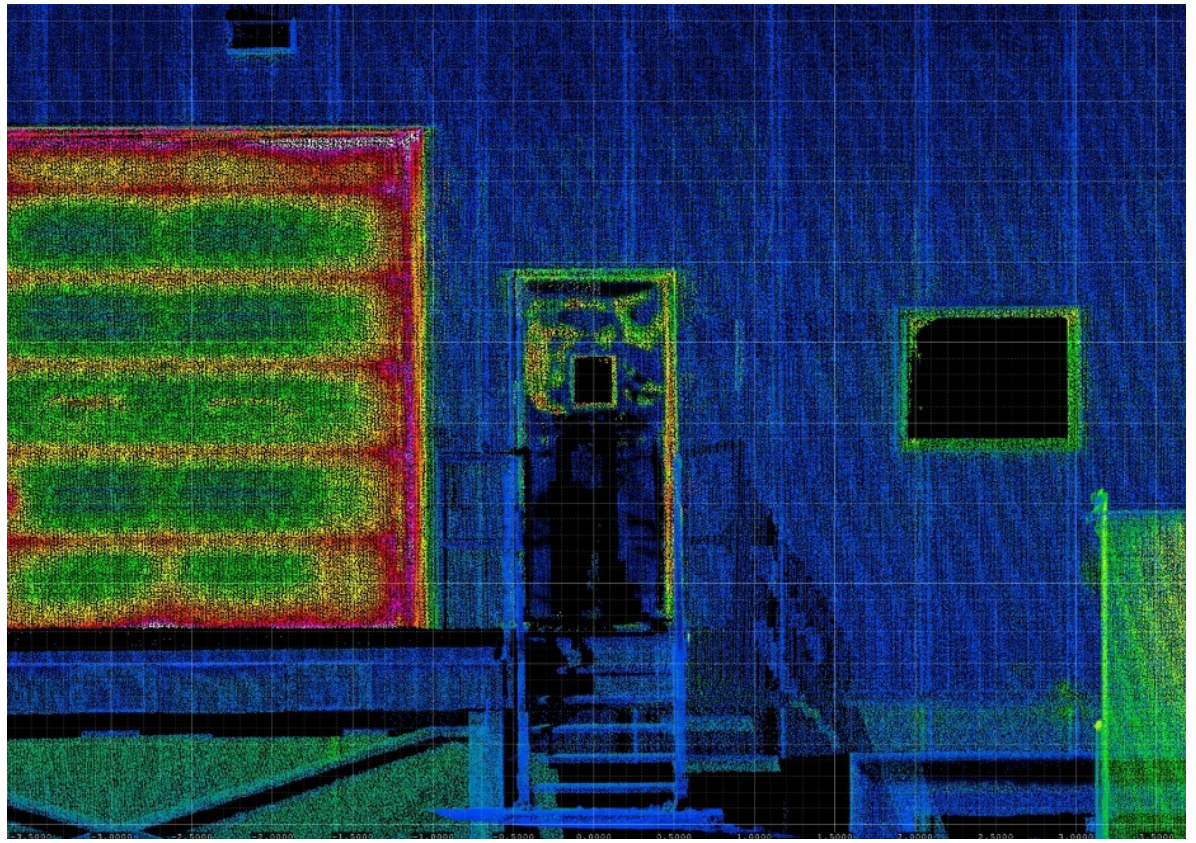
P1N-LD-01

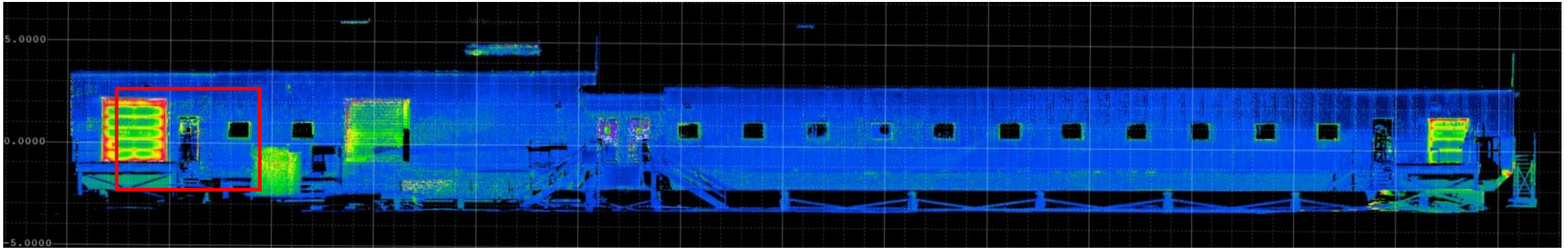
-15◦C



5◦C





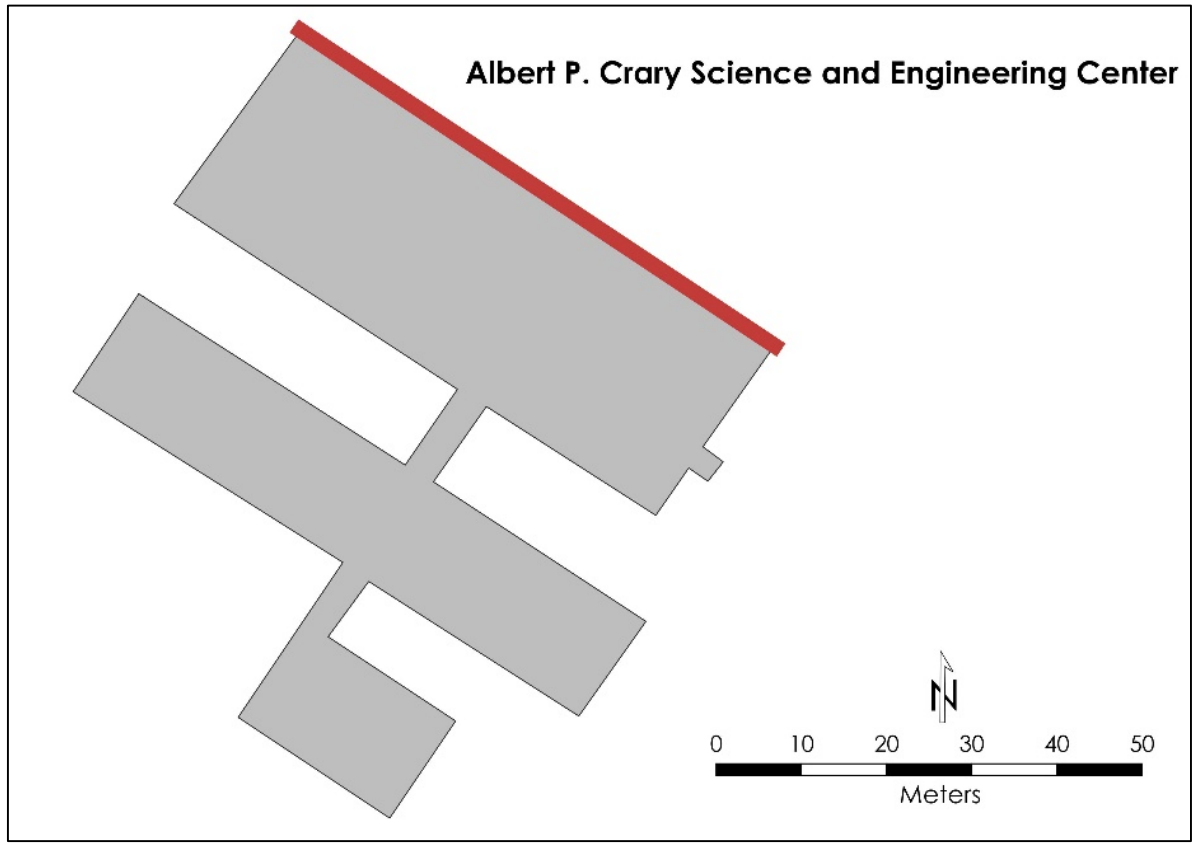


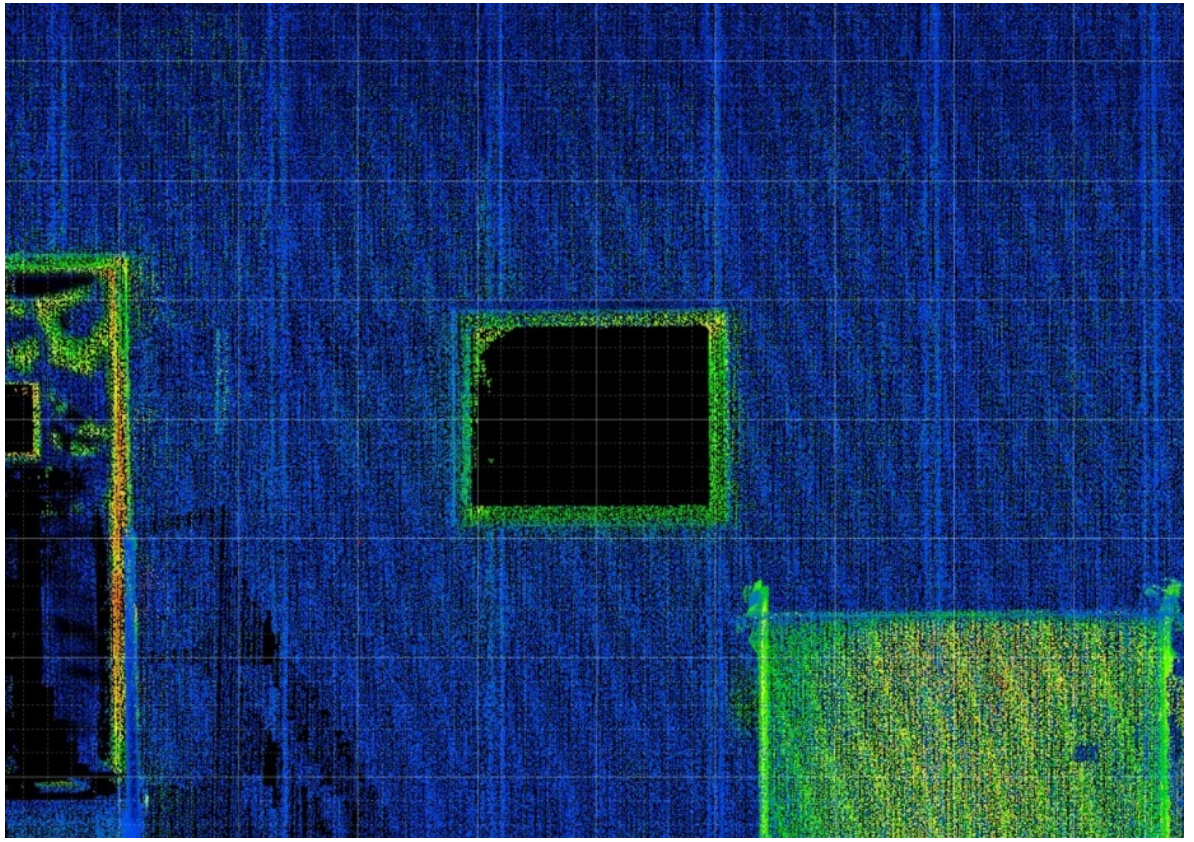
P1N-D-01

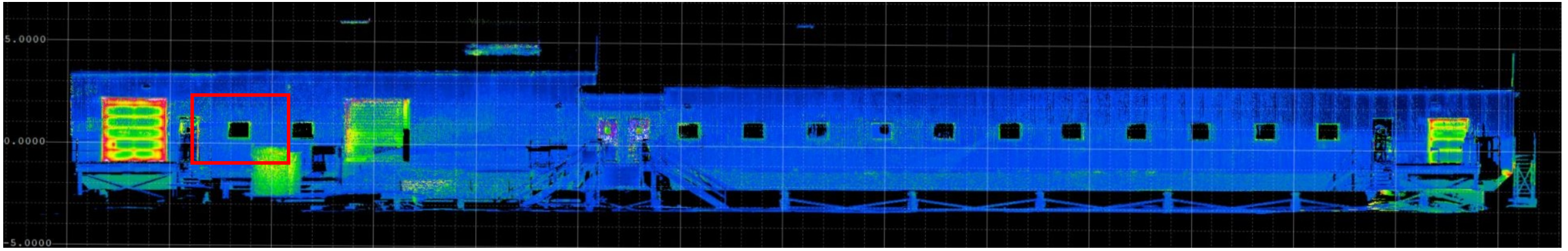
-15◦C



5◦C





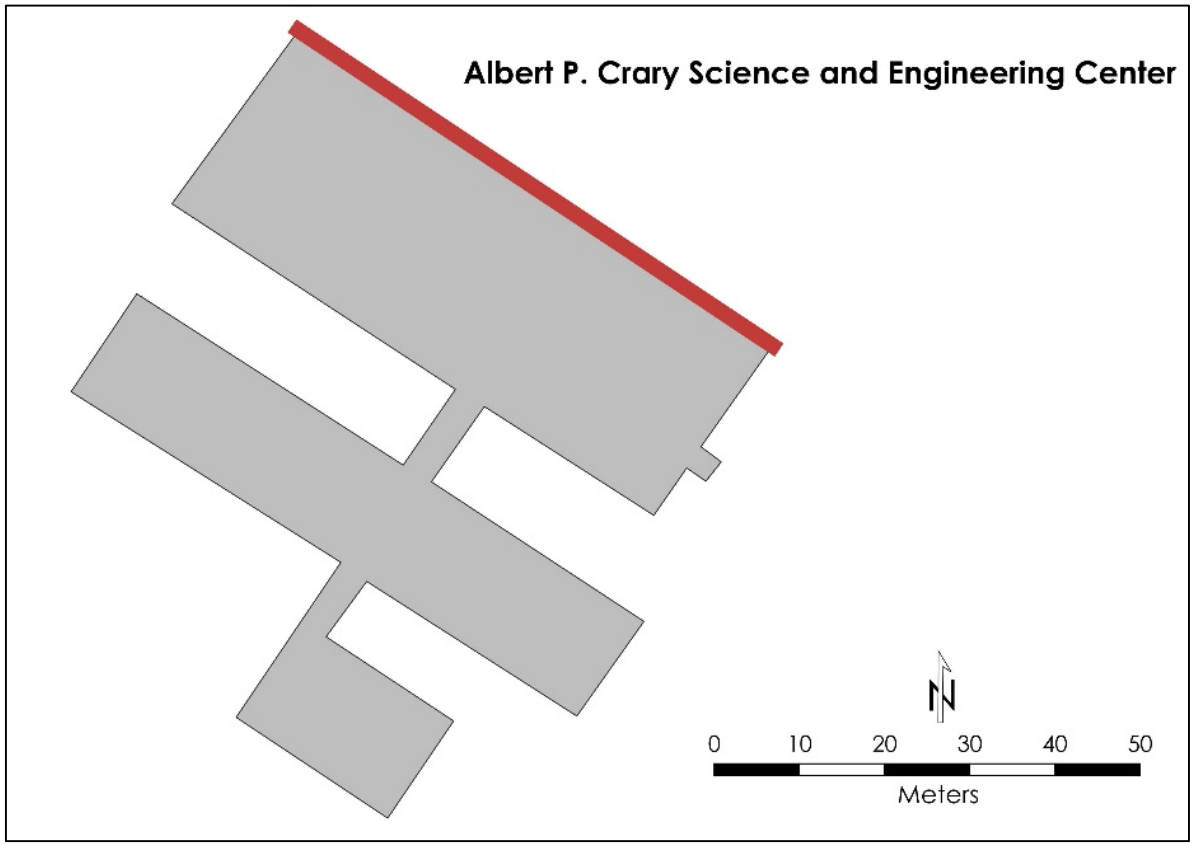


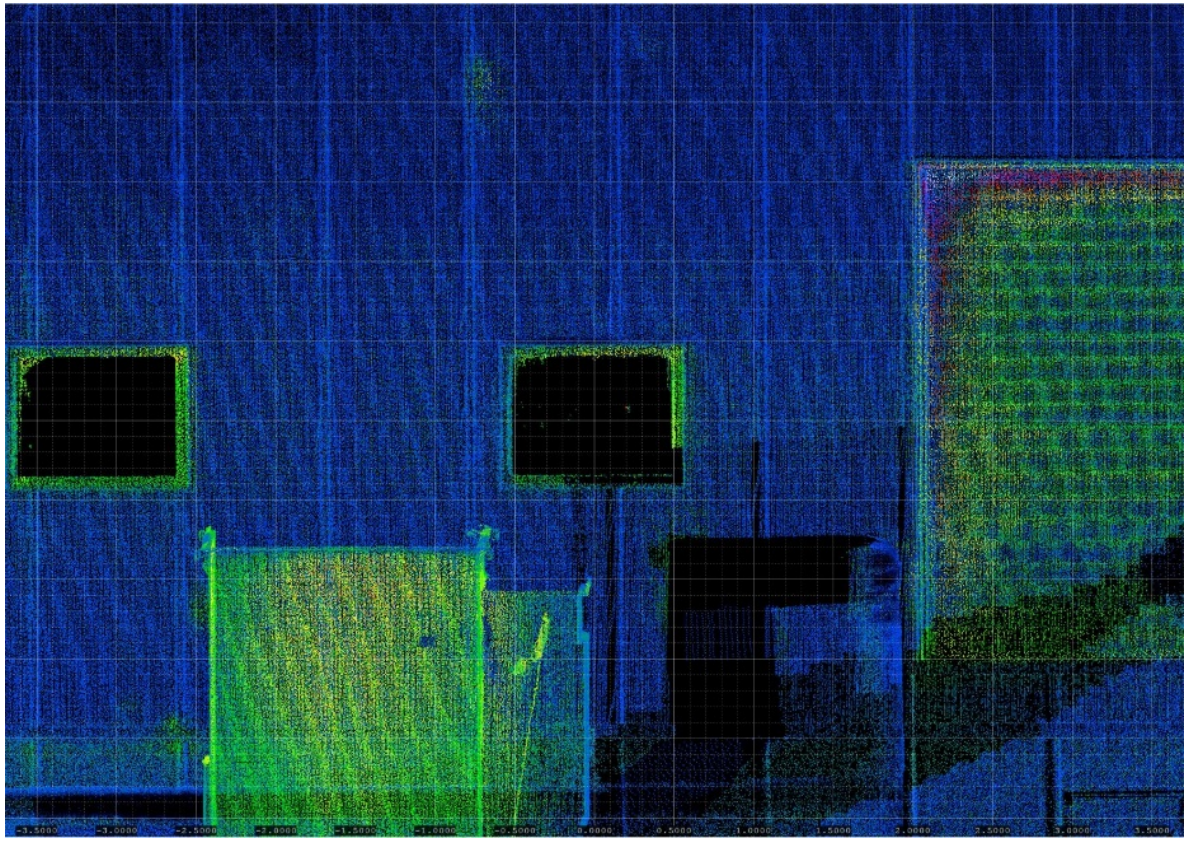
P1N-W-01

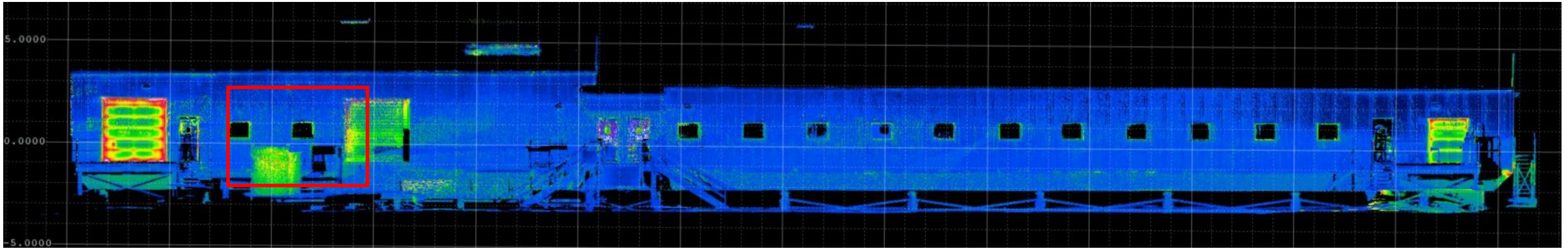
-15◦C



5◦C





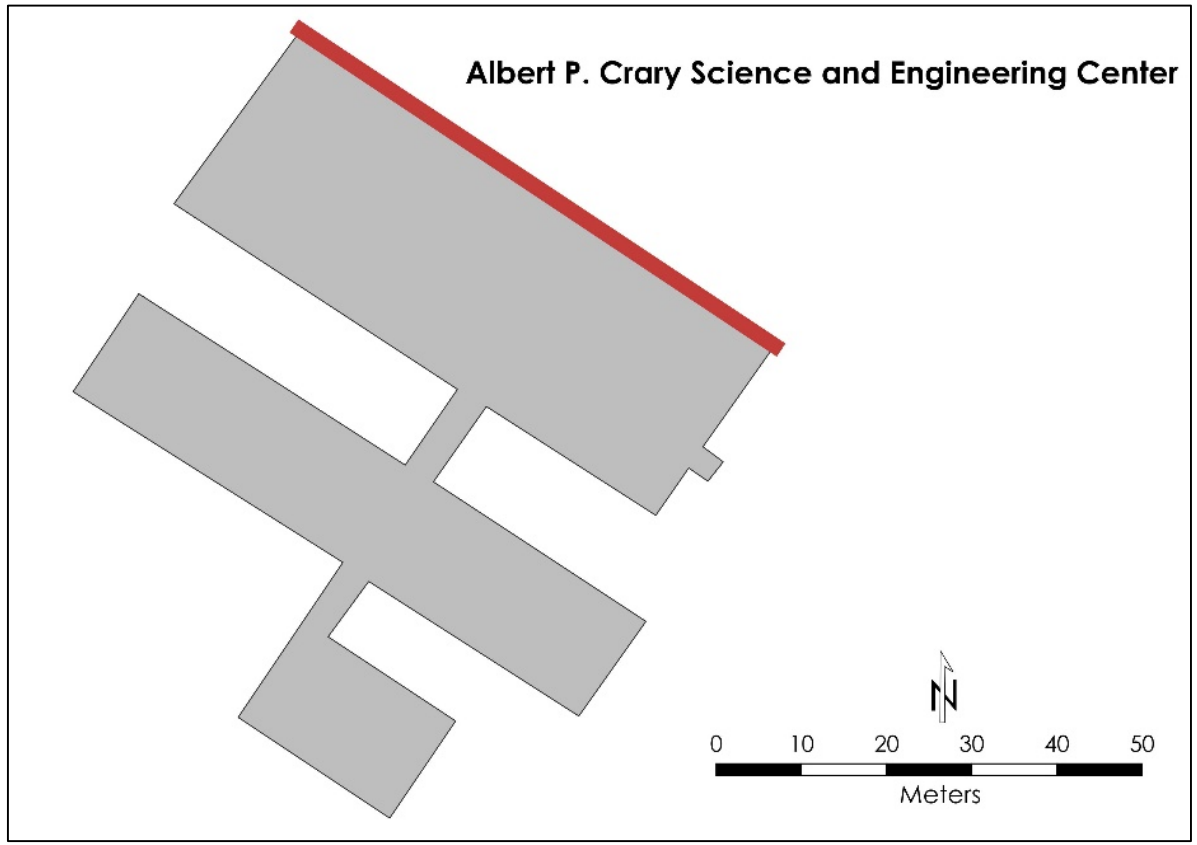


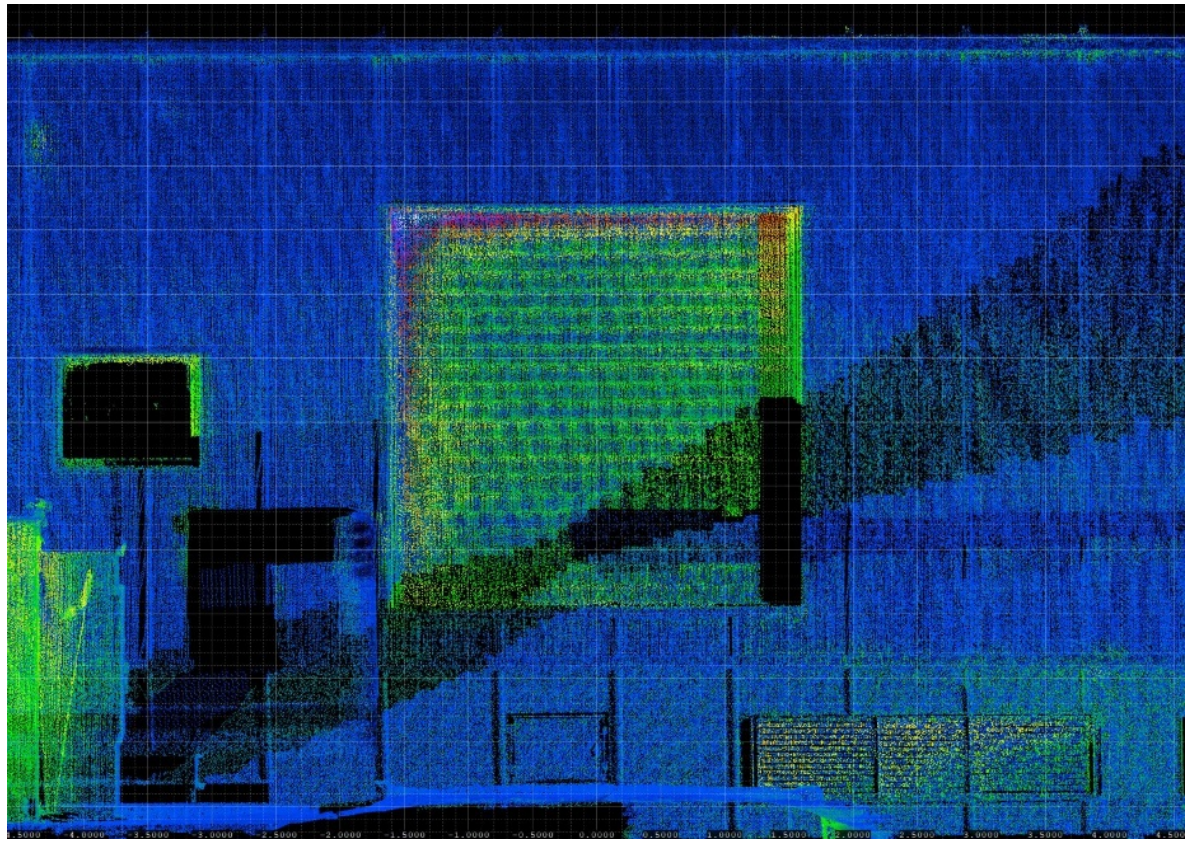
P1N-W-02

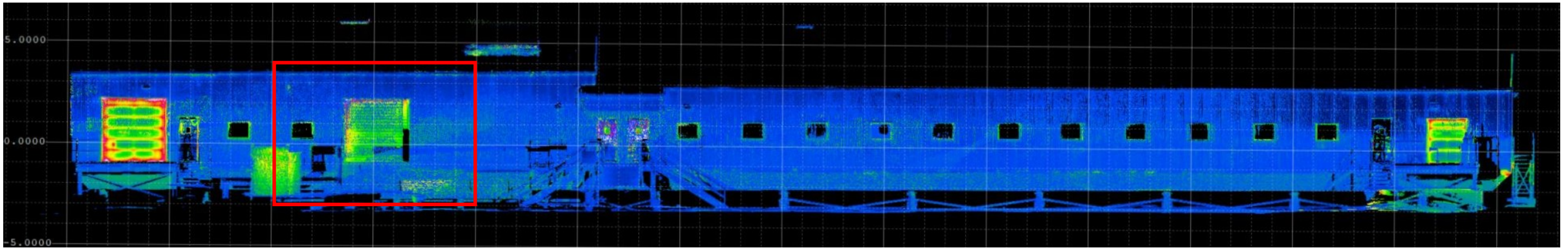
-15◦C



5◦C

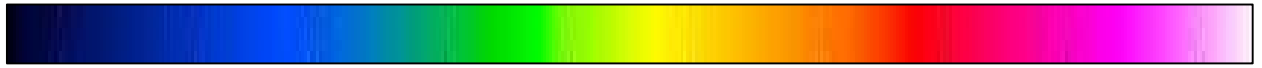




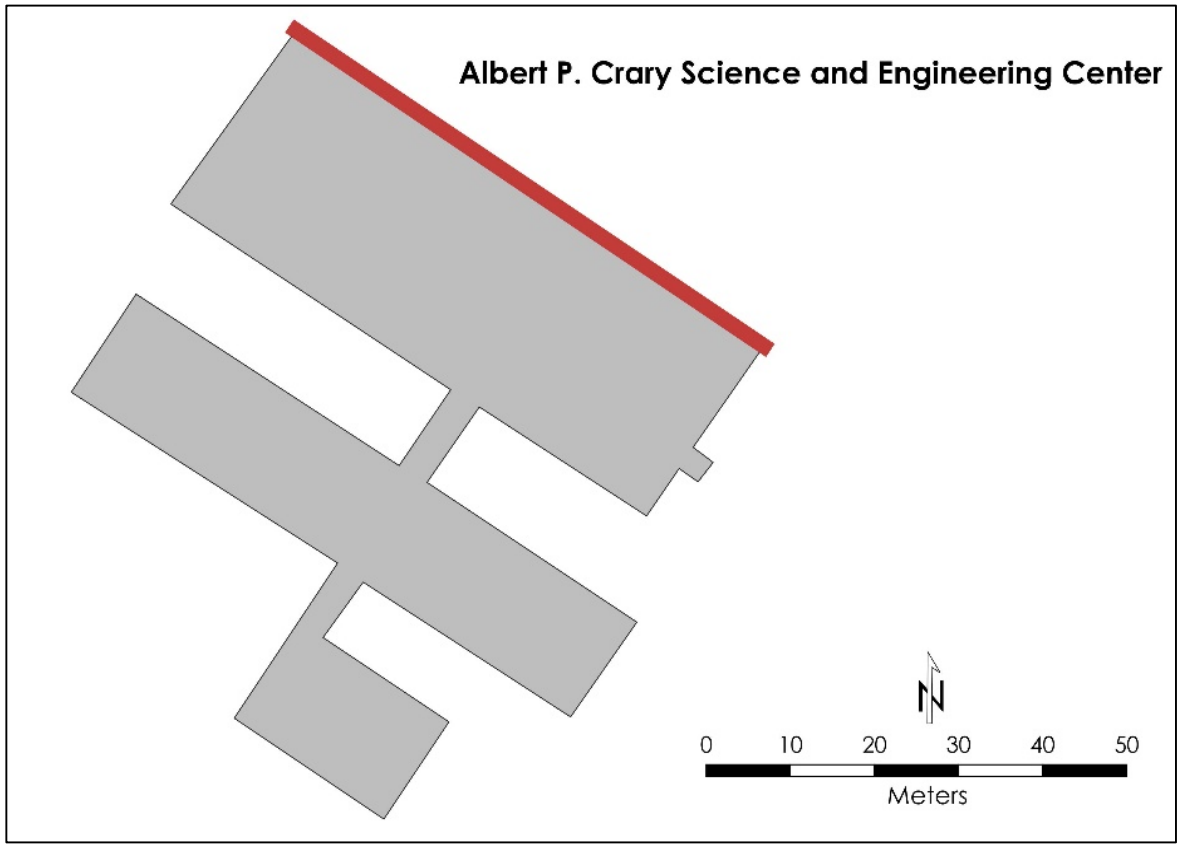


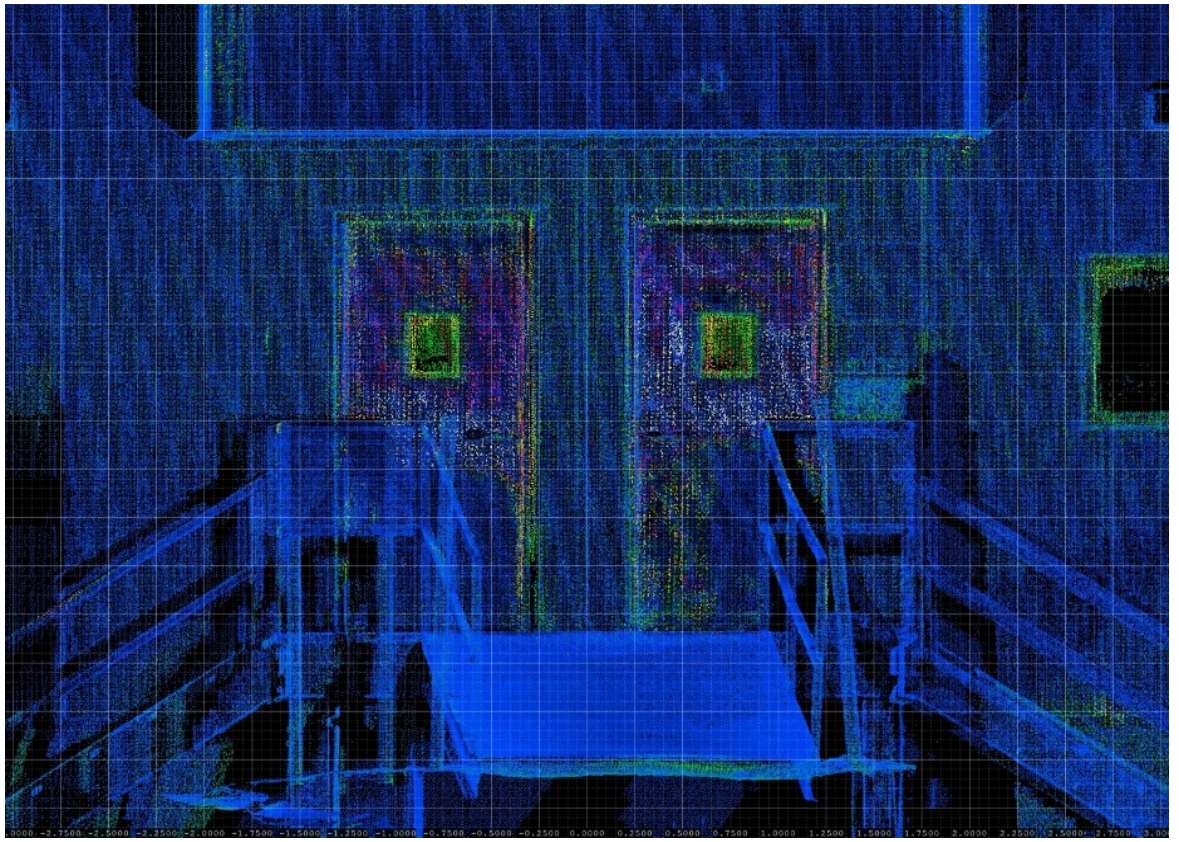
P1N-LD-02

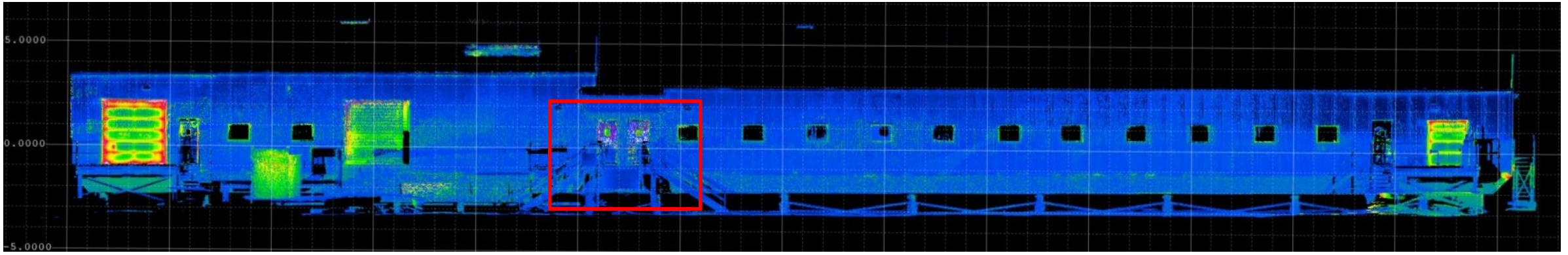
-15◦C



5◦C





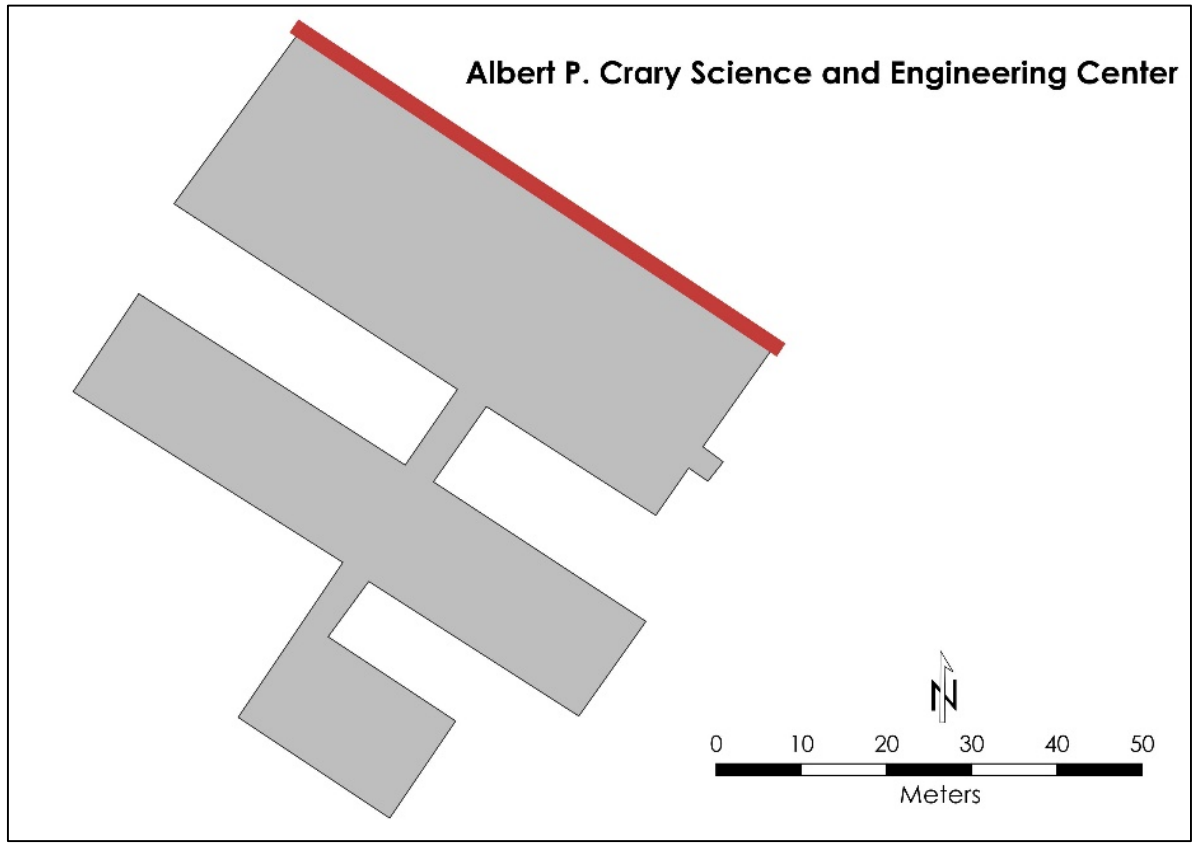


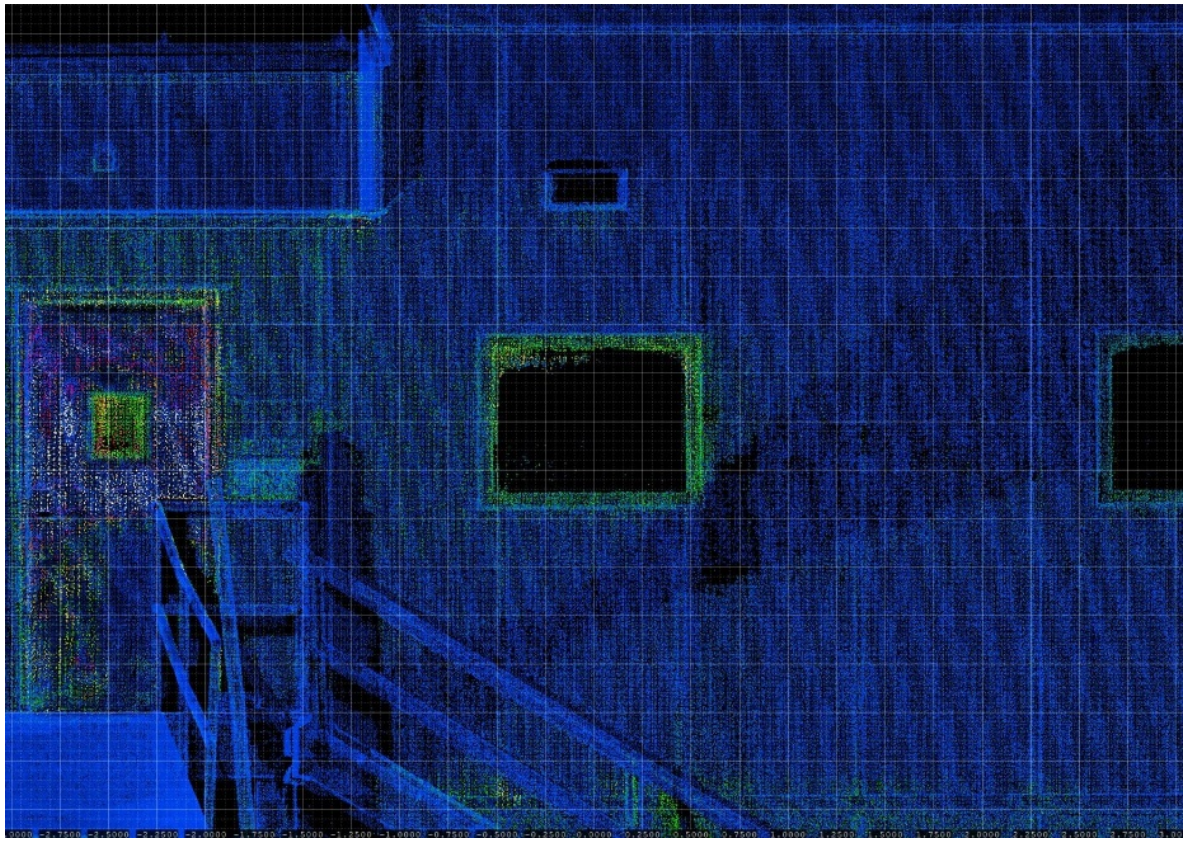
P1N-D-02 & P1N-D-03

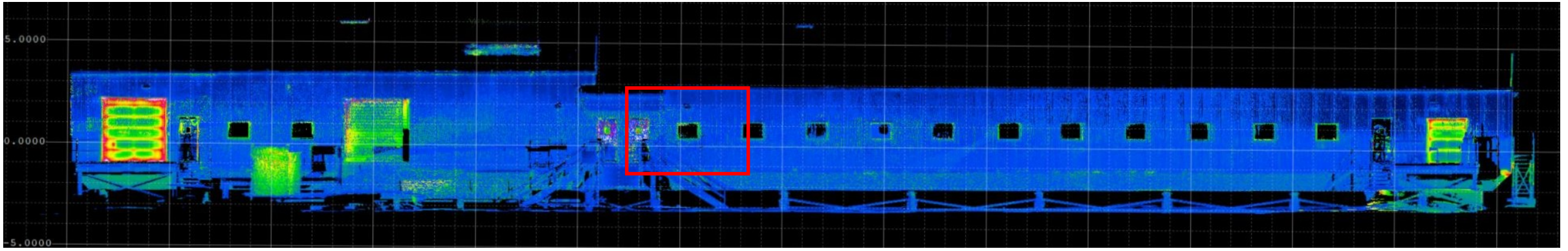
-15°C



5°C





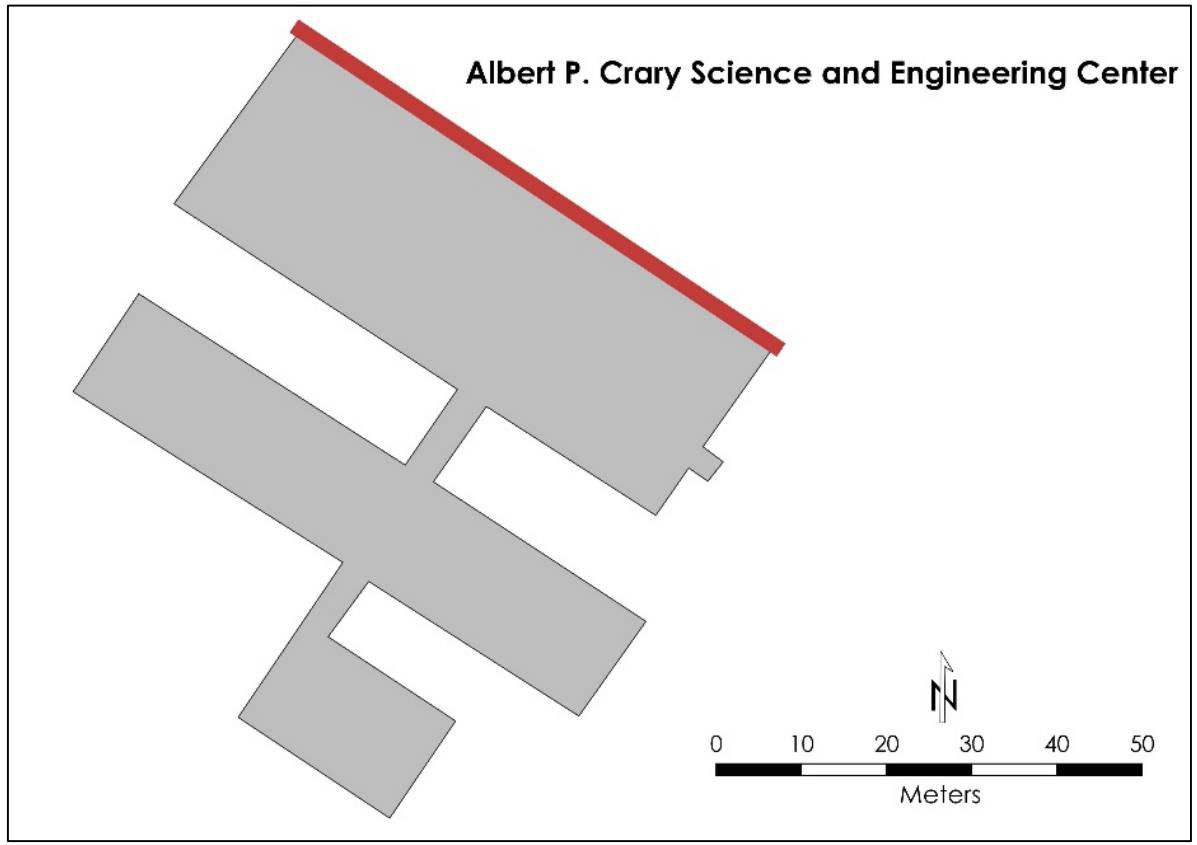


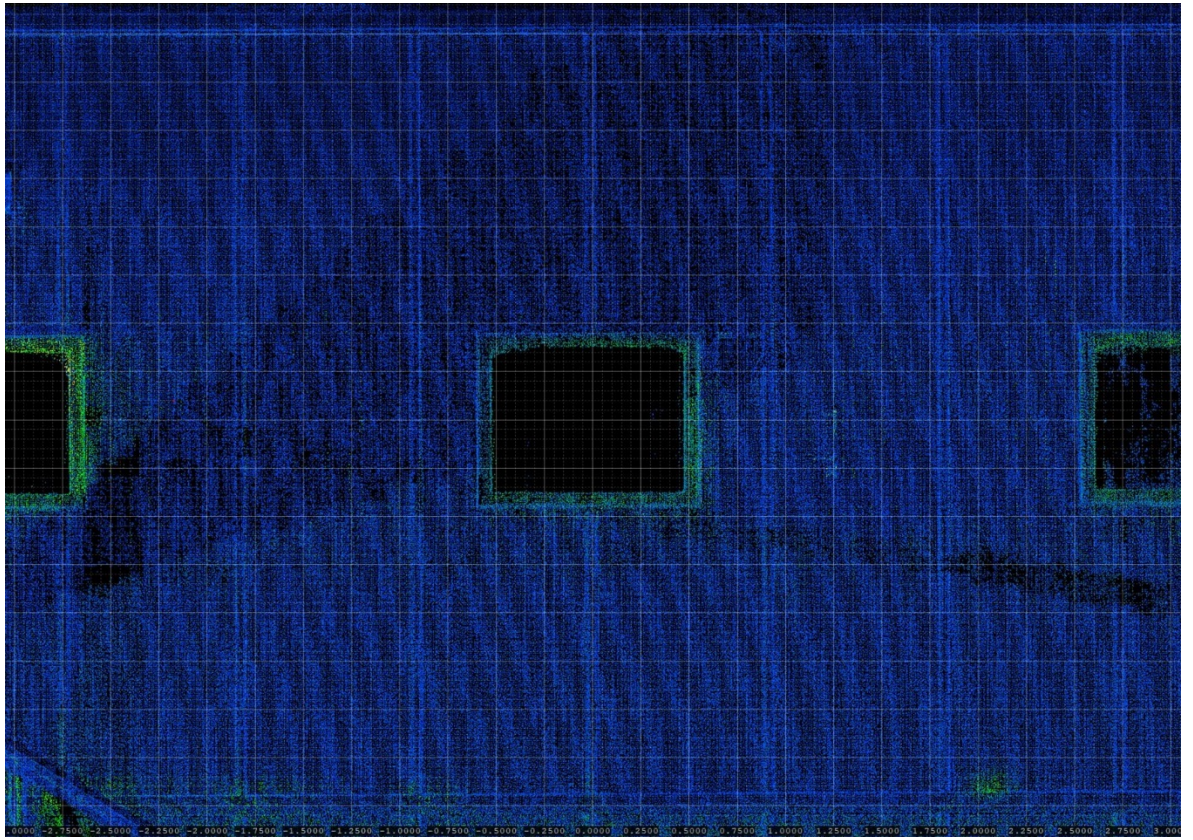
P1N-W-03

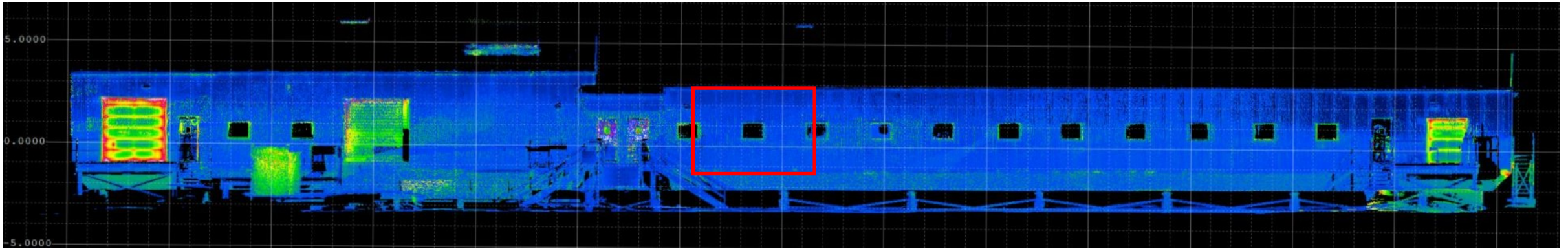
-15◦C



5◦C





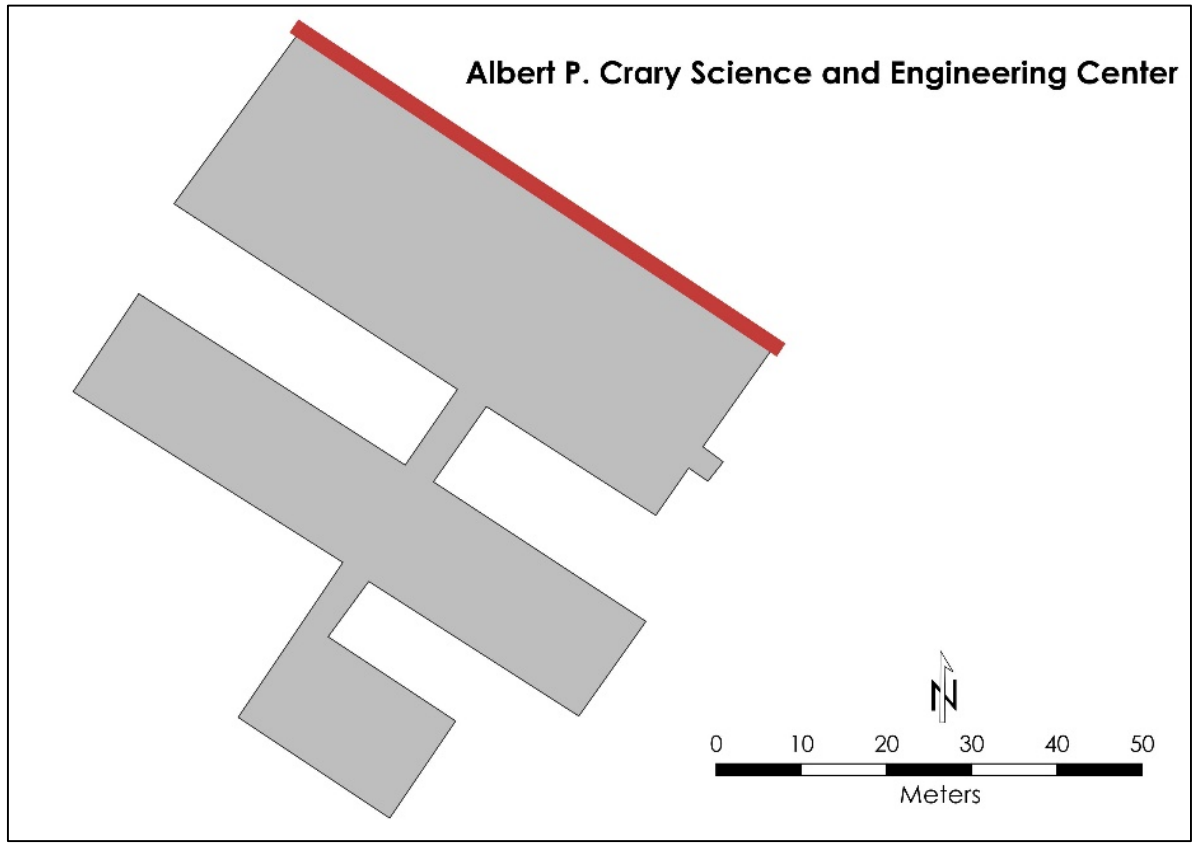


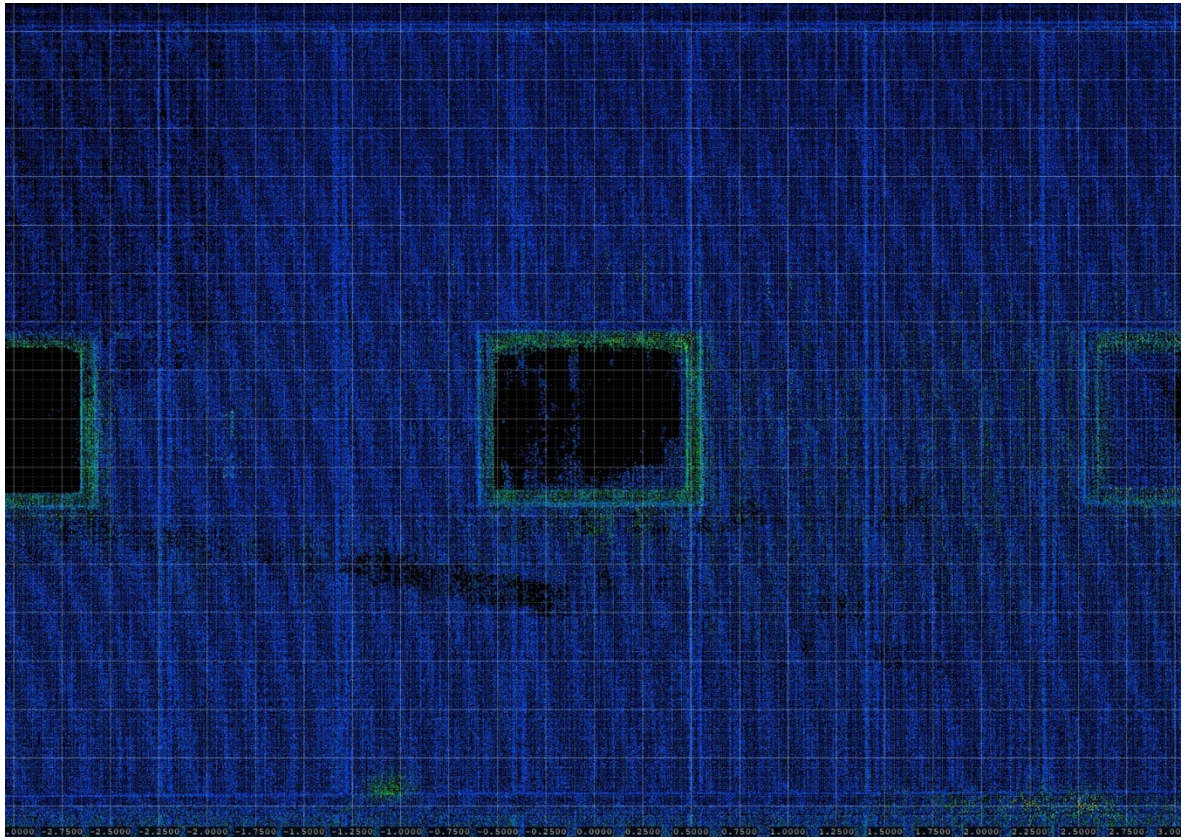
P1N-W-04

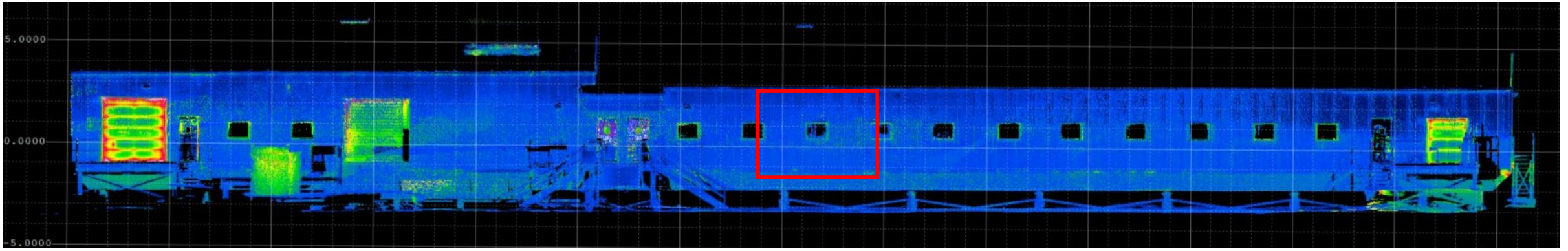
-15◦C



5◦C





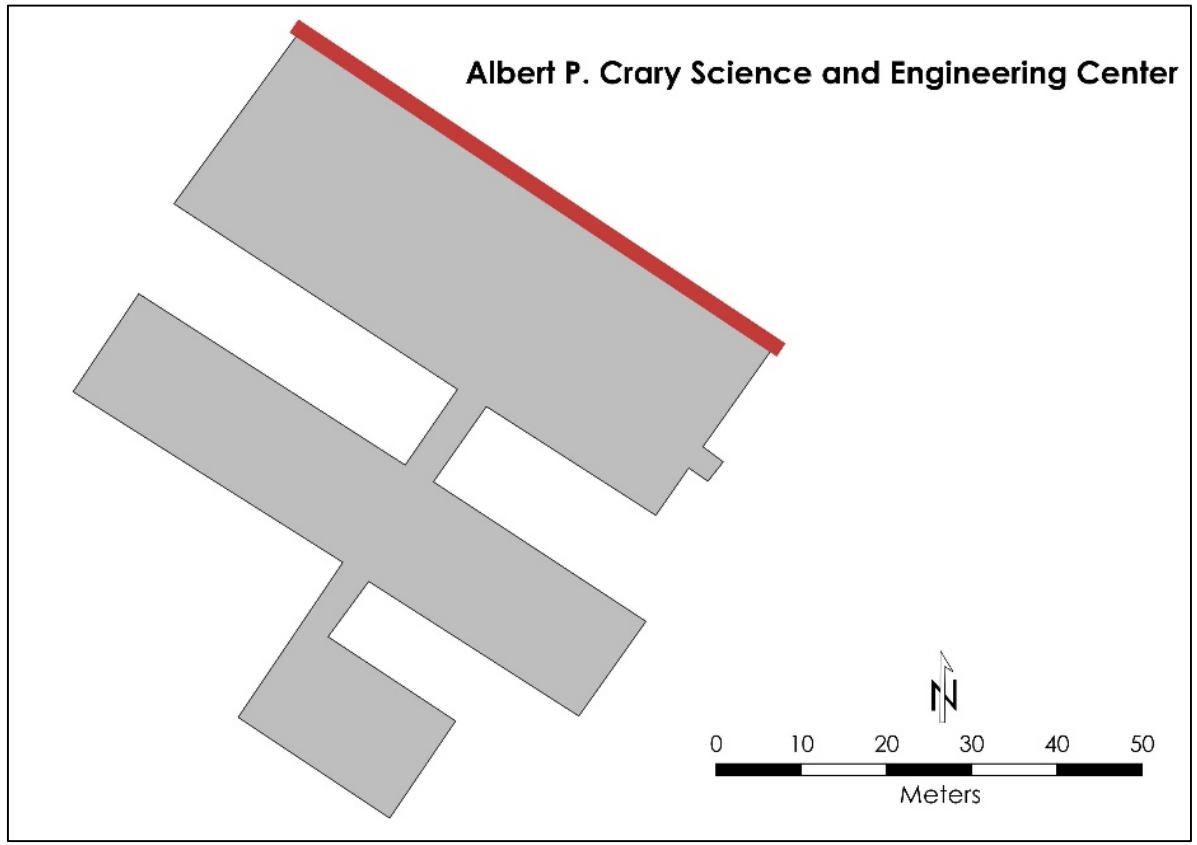


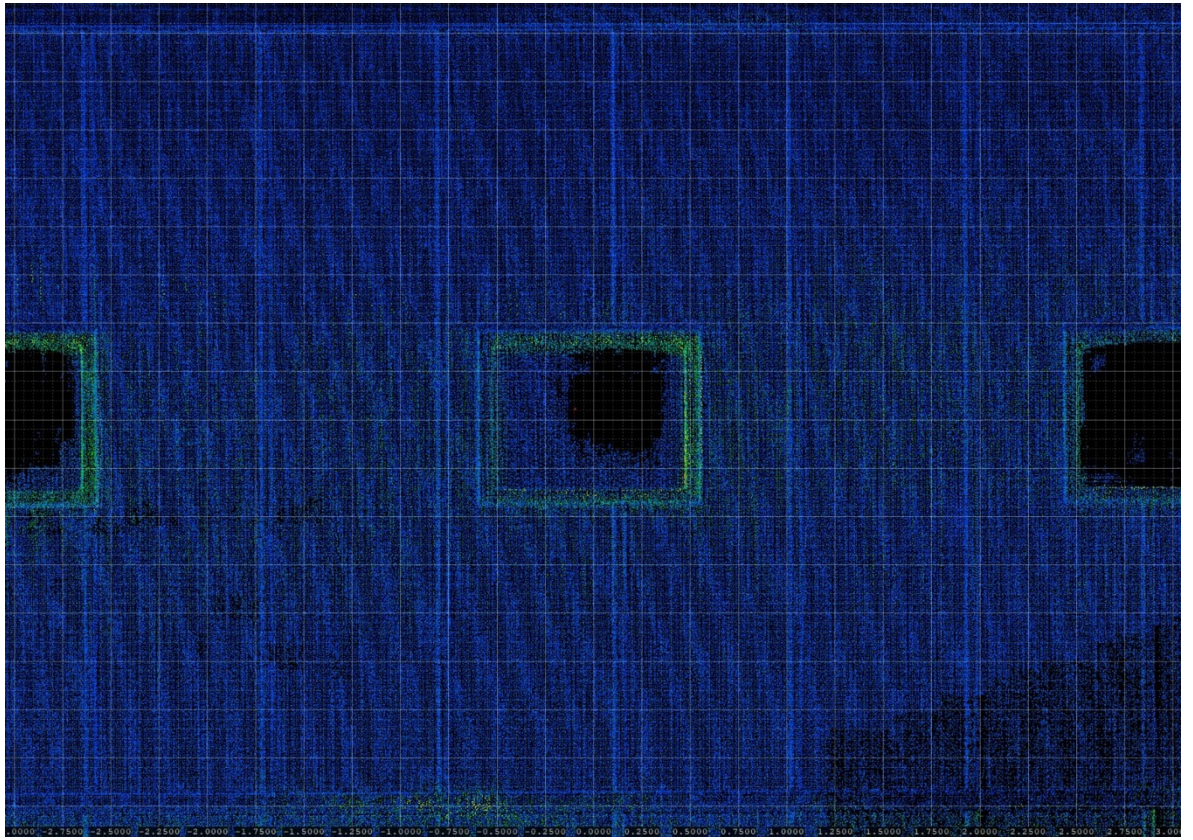
P1N-W-05

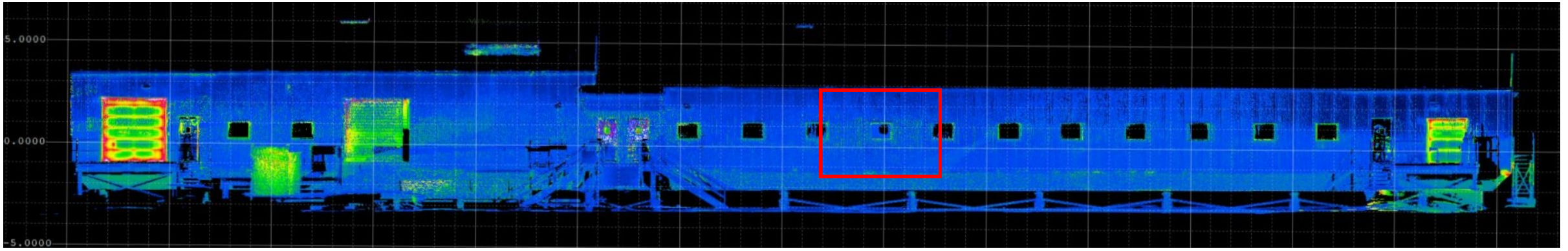
-15◦C



5◦C





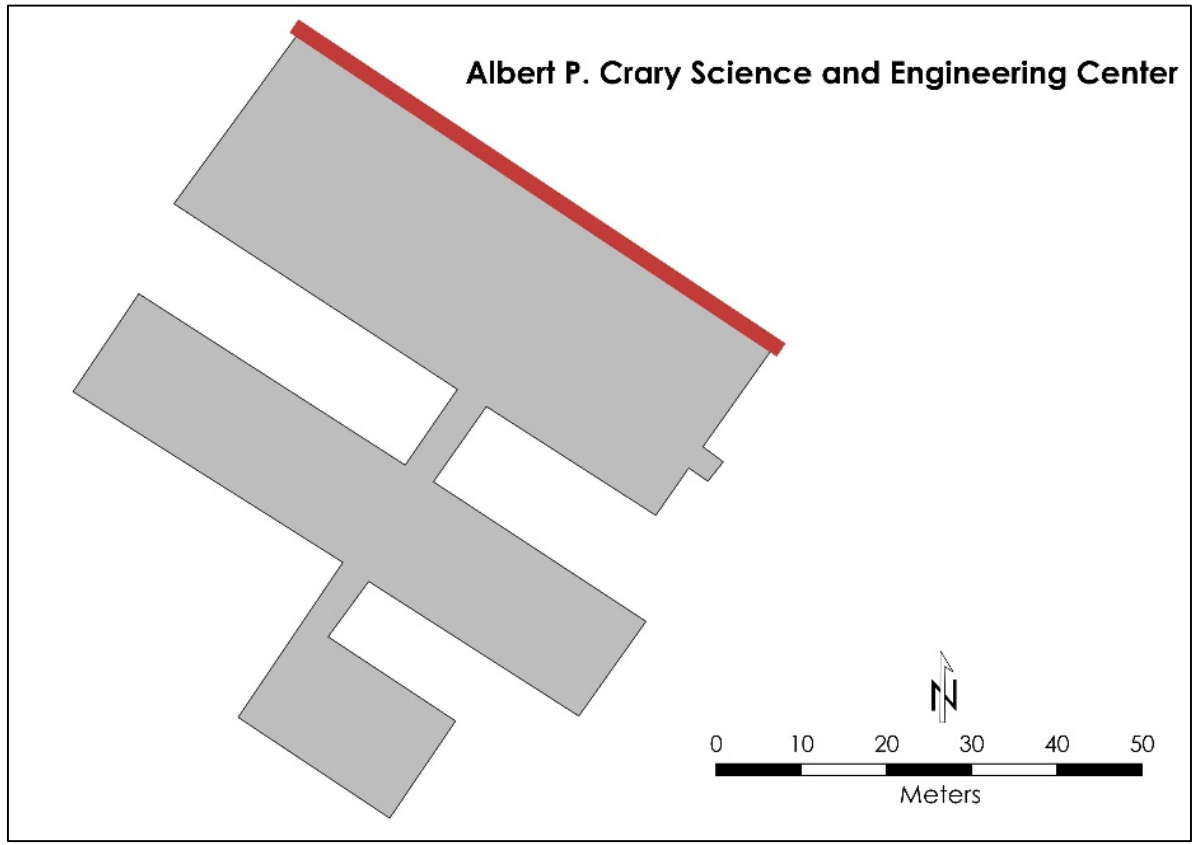


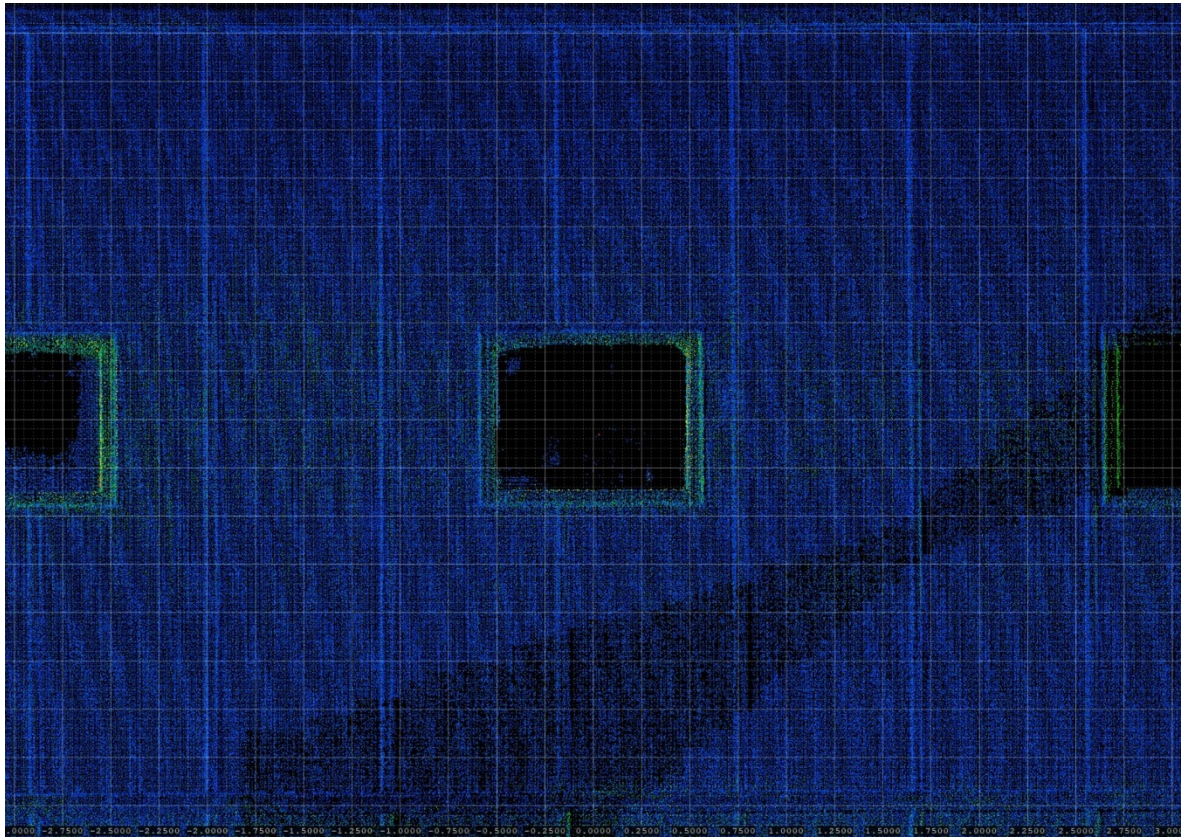
P1N-W-06

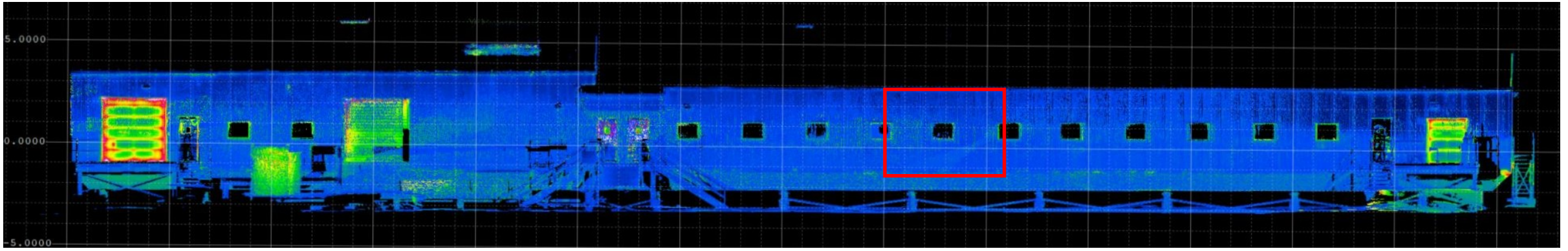
-15◦C



5◦C





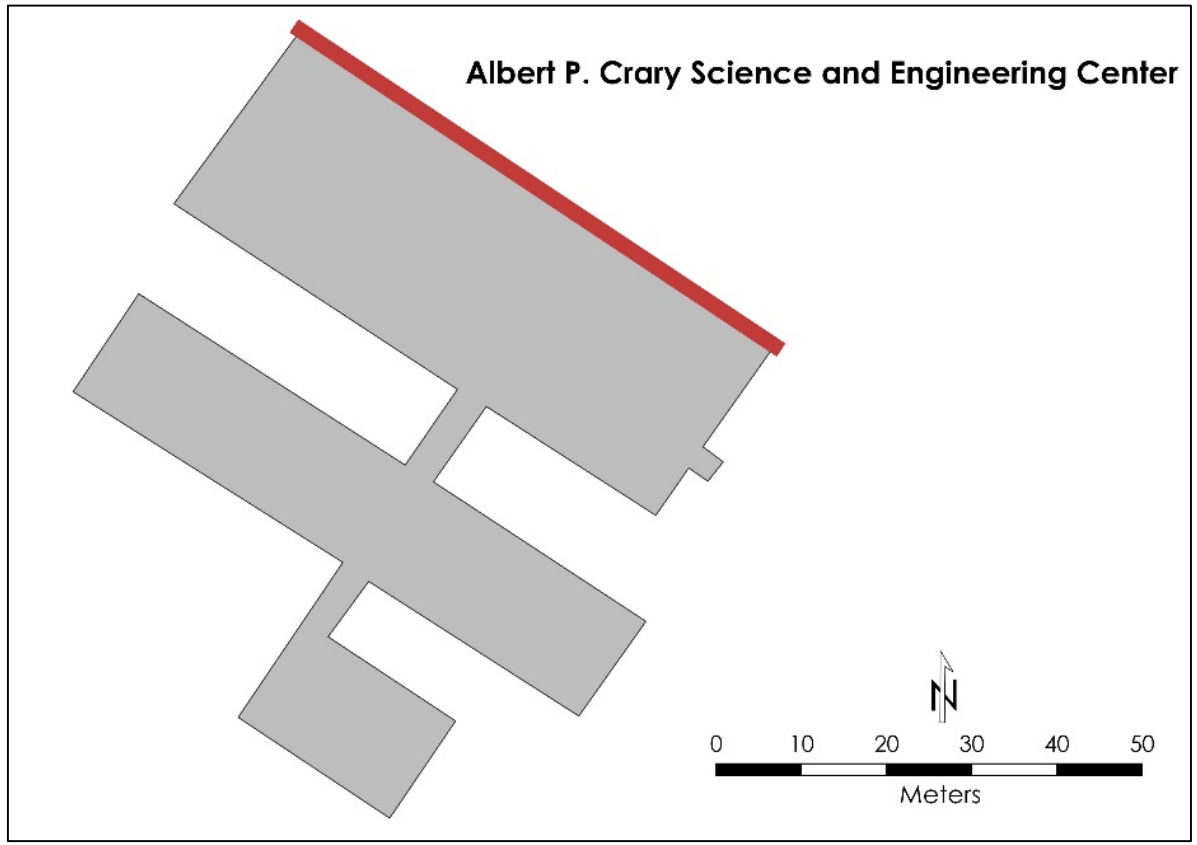


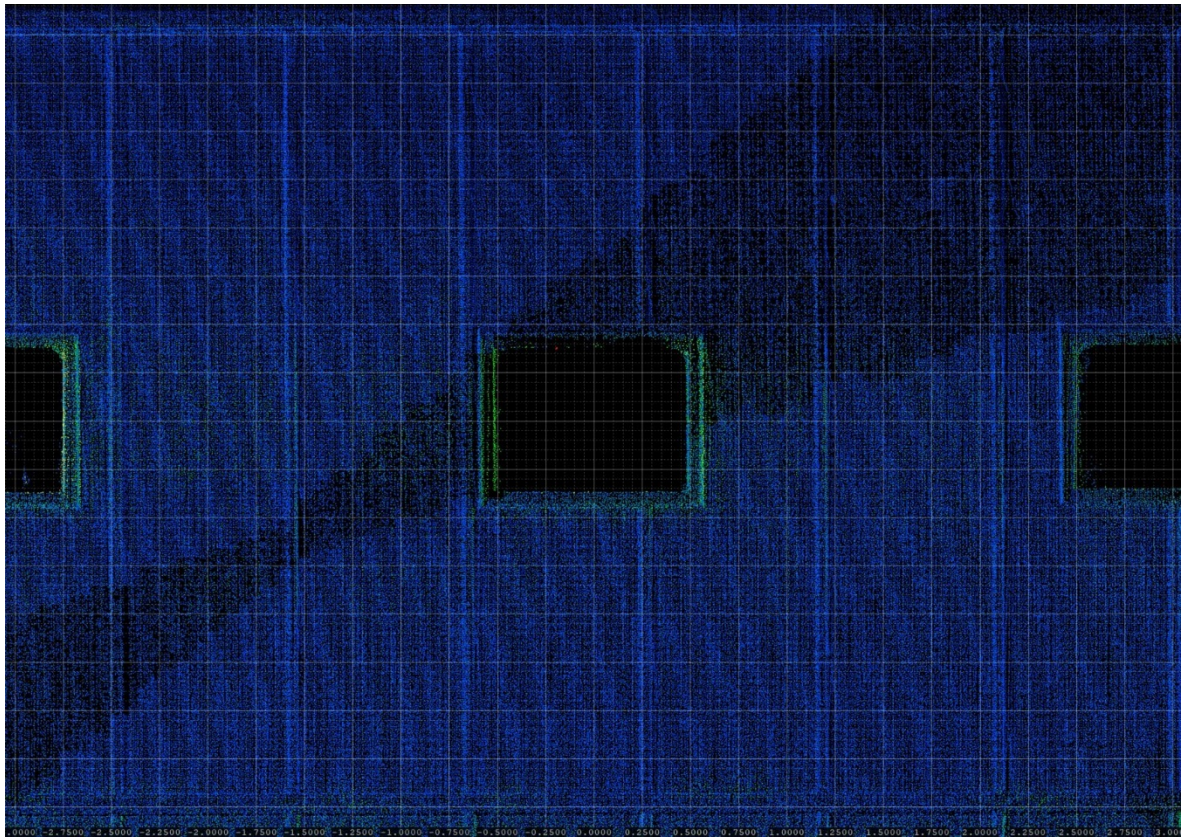
P1N-W-07

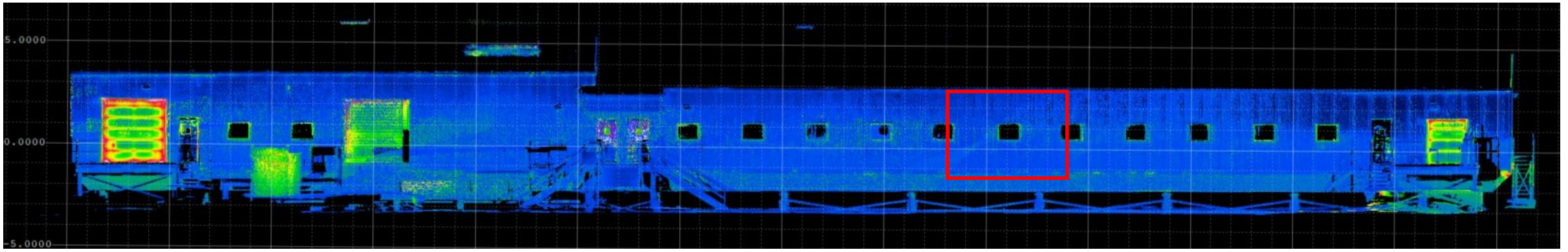
-15◦C



5◦C

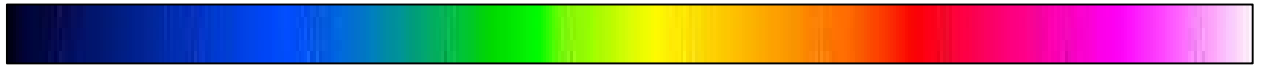




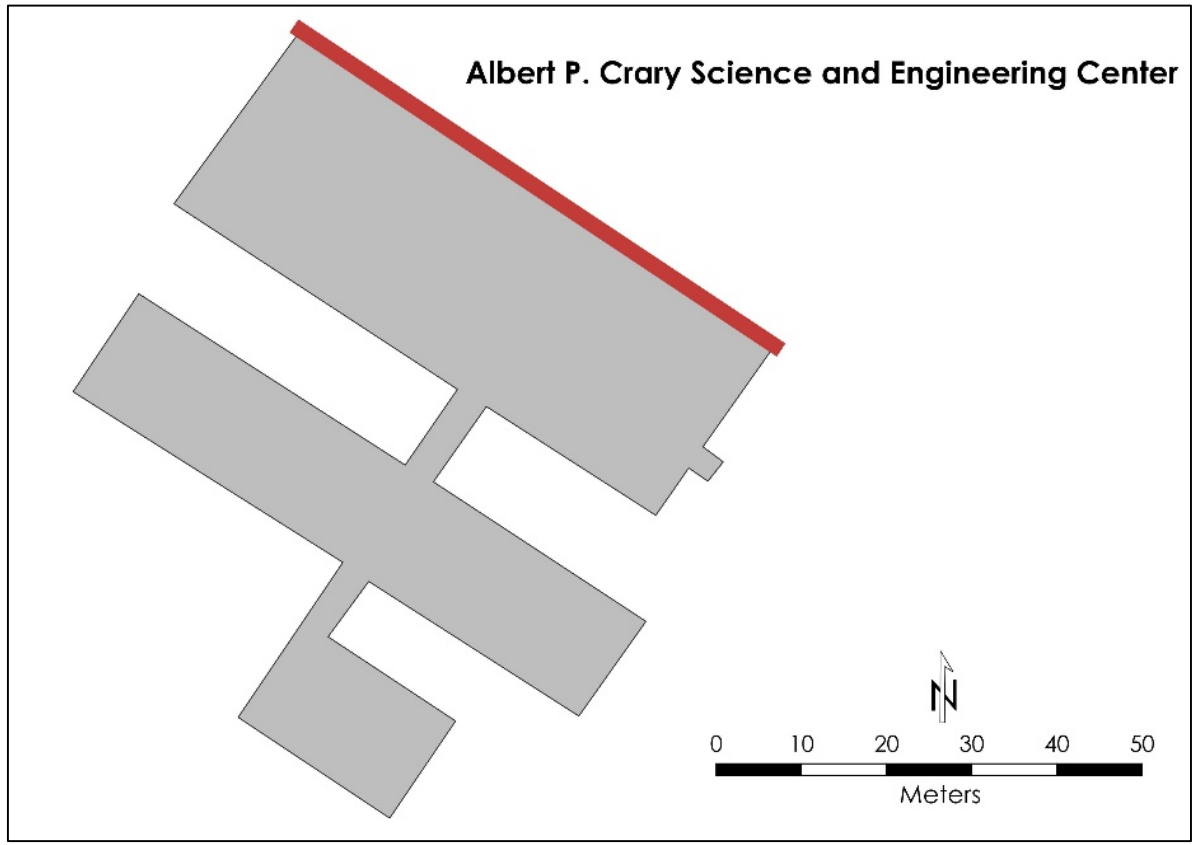


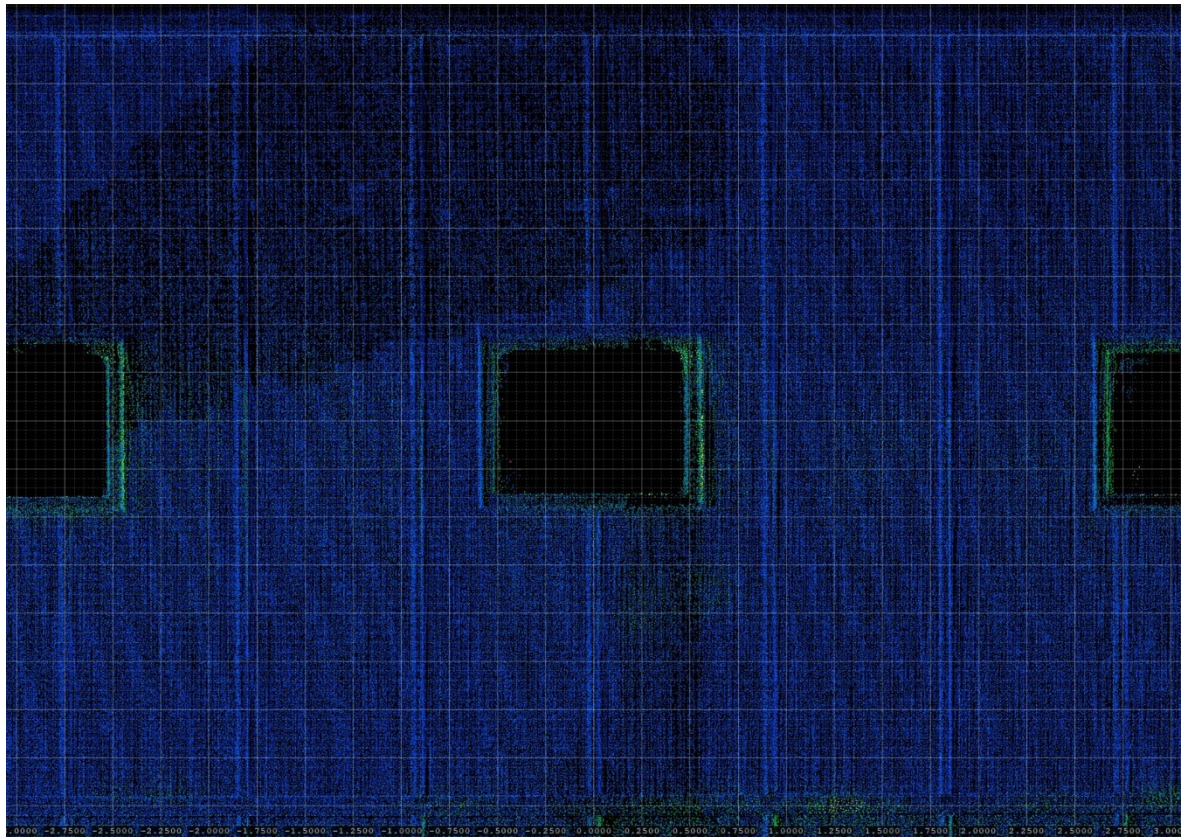
P1N-W-08

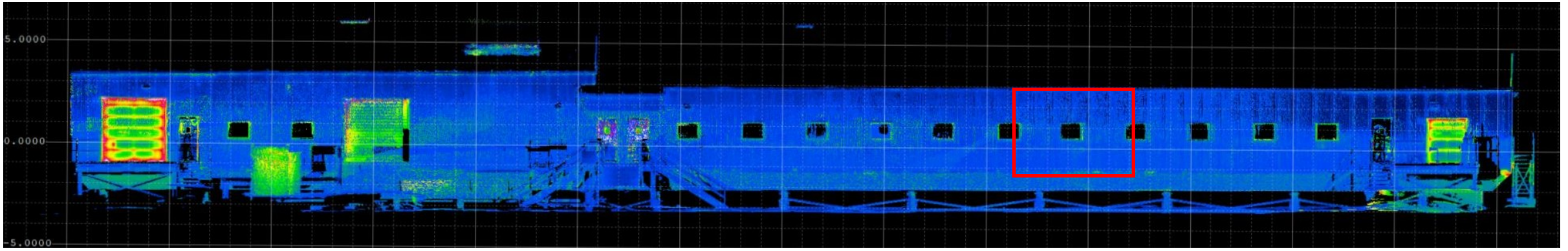
-15◦C



5◦C





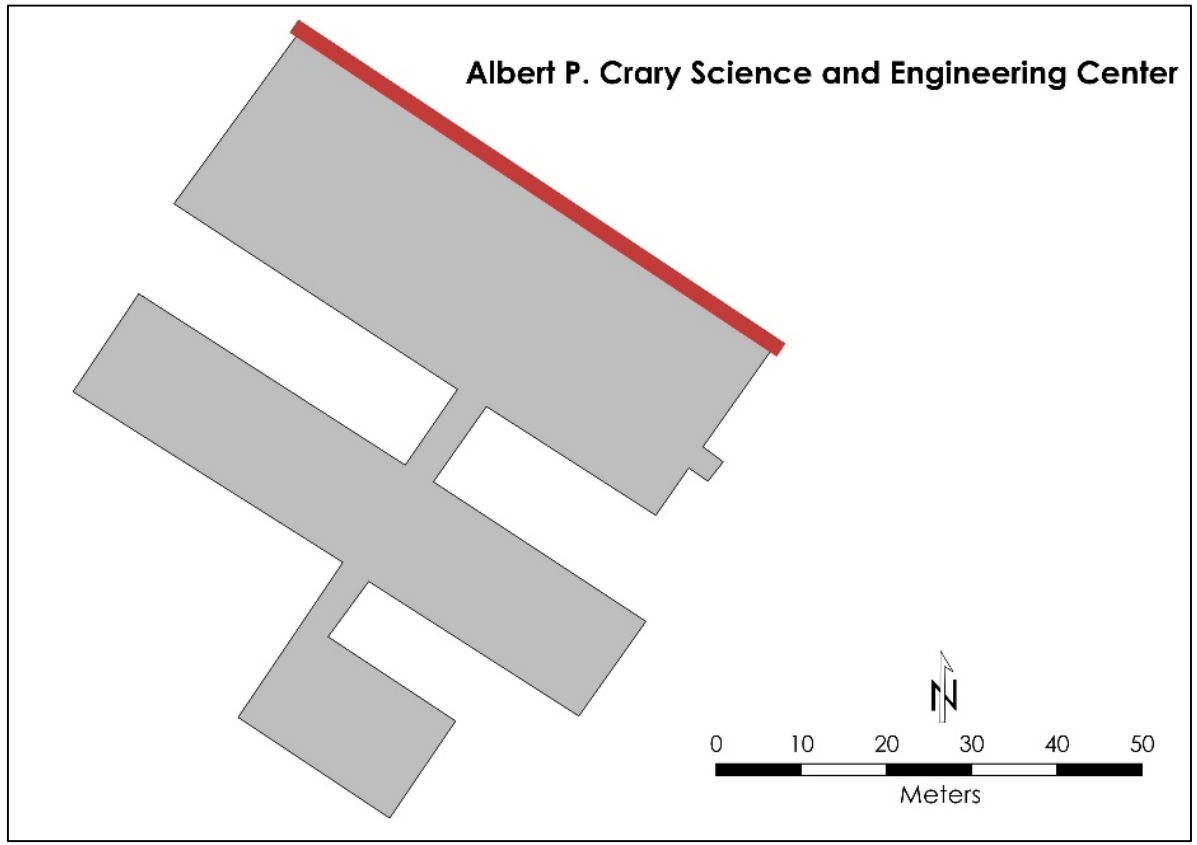


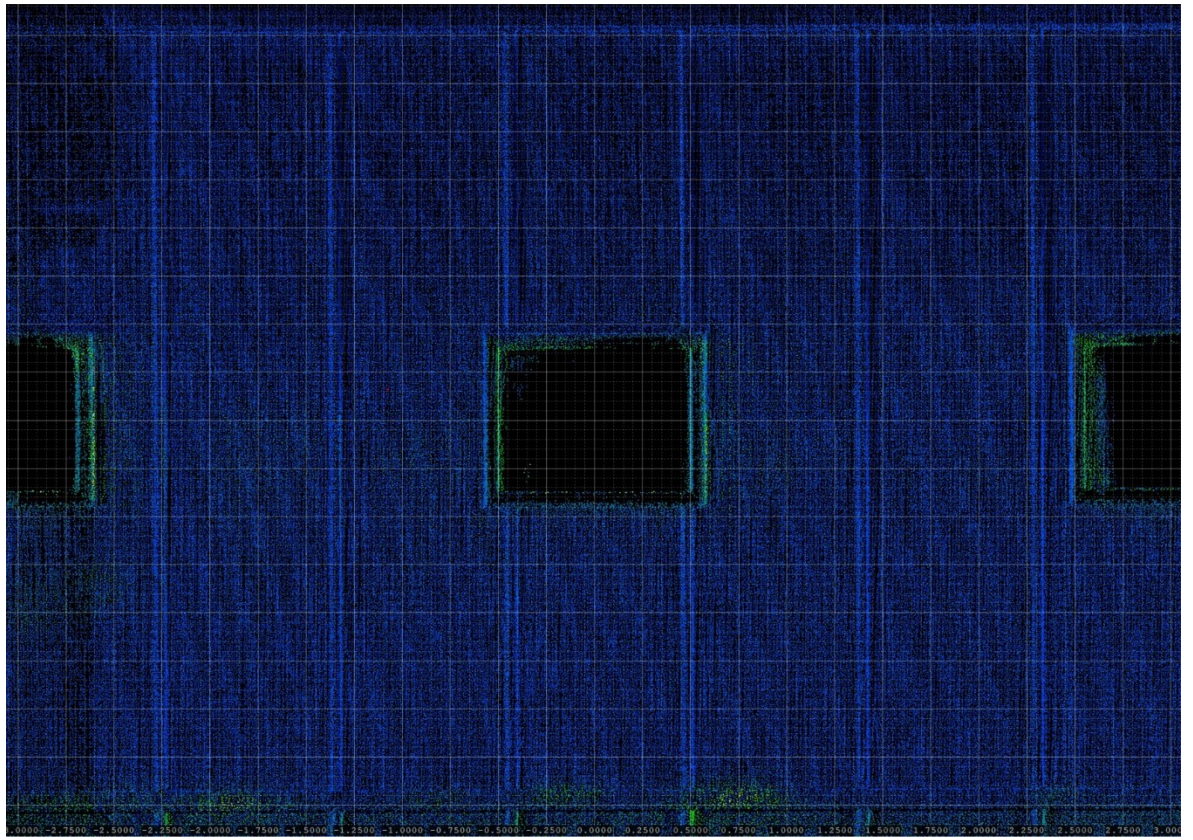
P1N-W-09

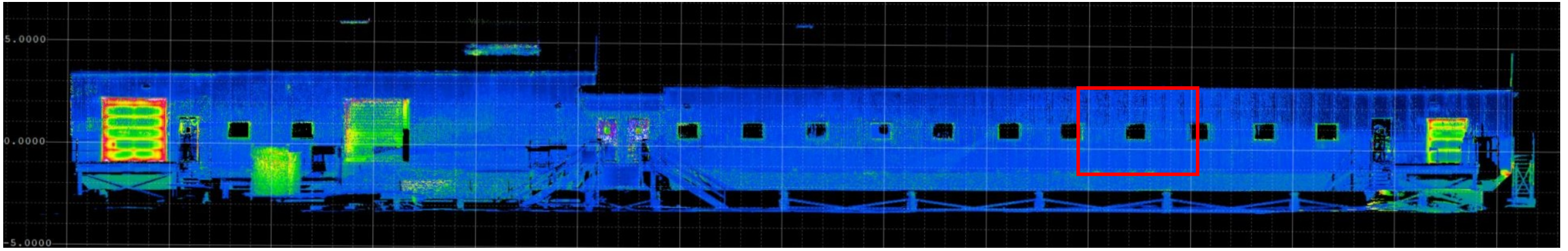
-15◦C



5◦C





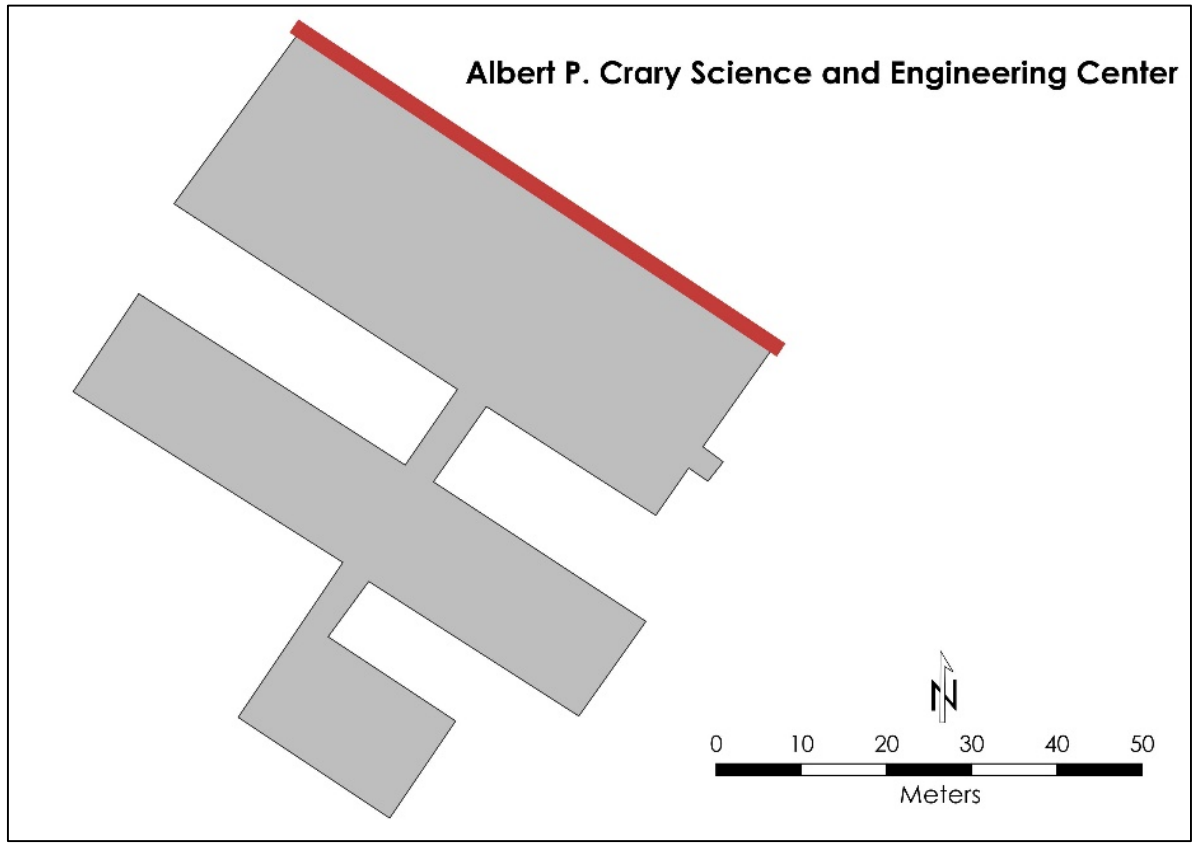


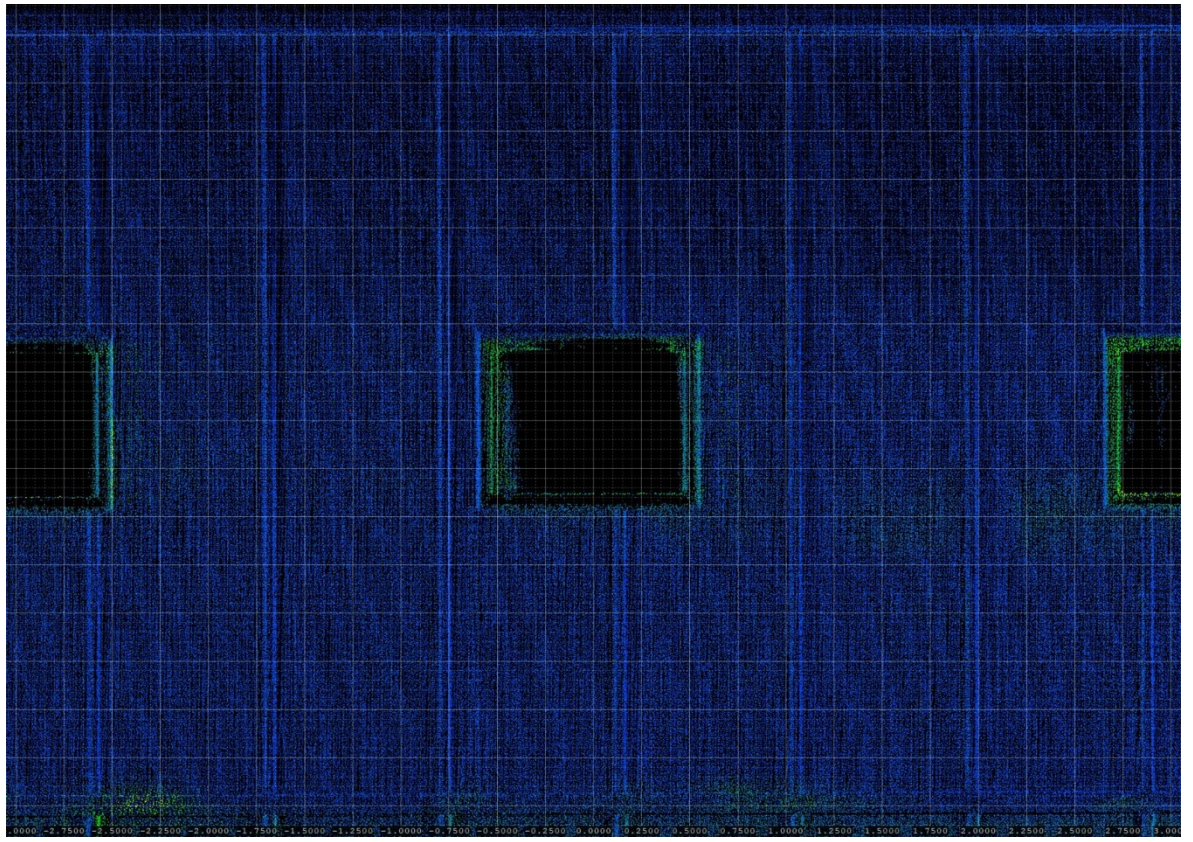
P1N-W-10

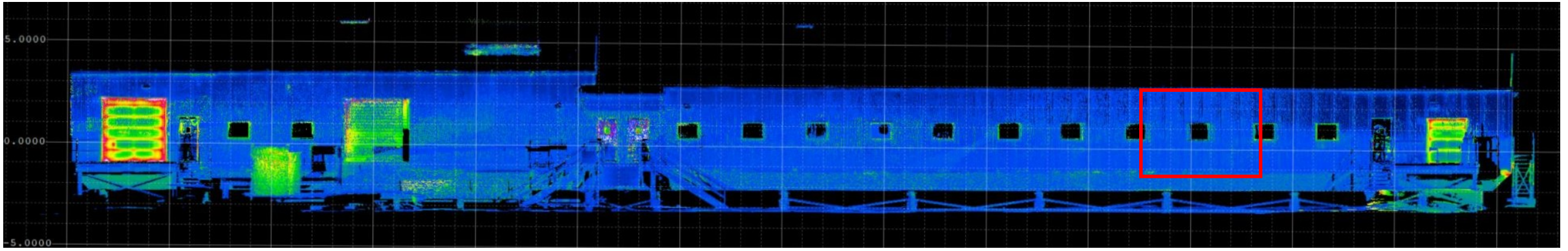
-15◦C



5◦C





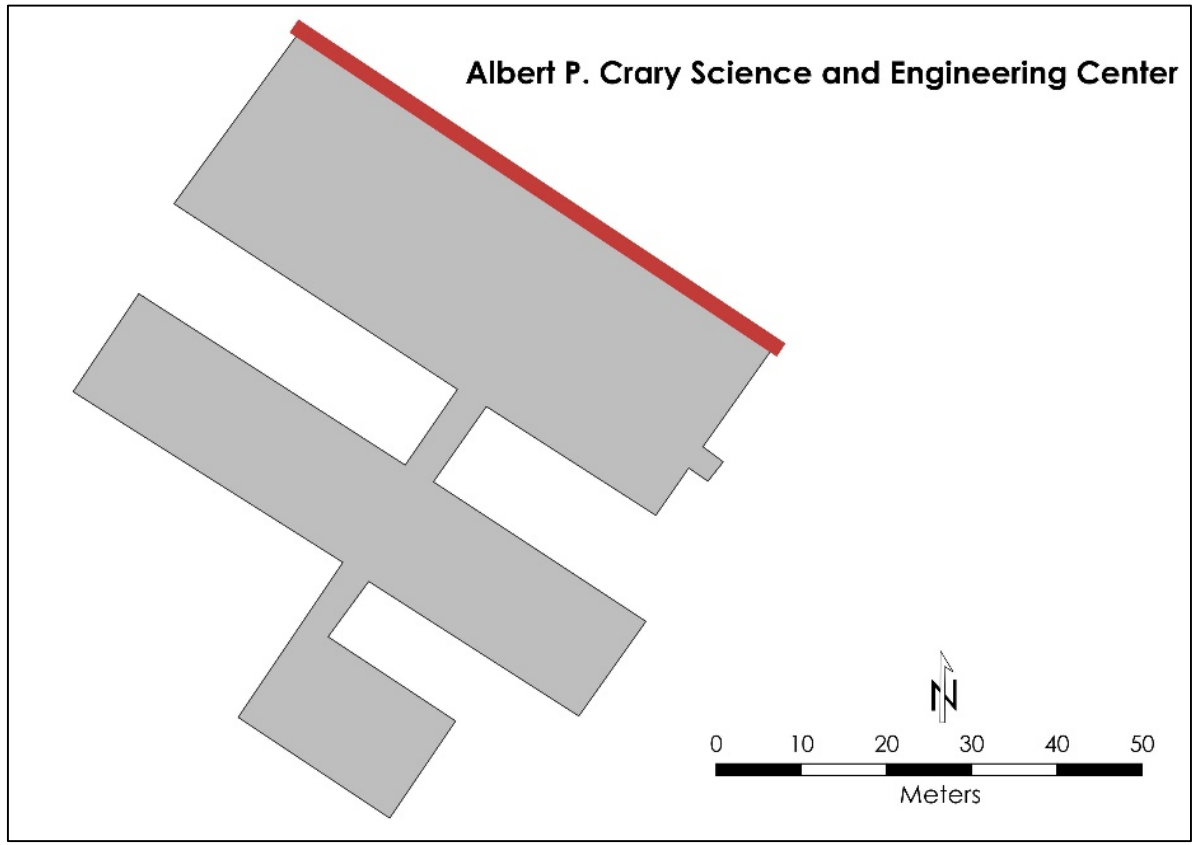


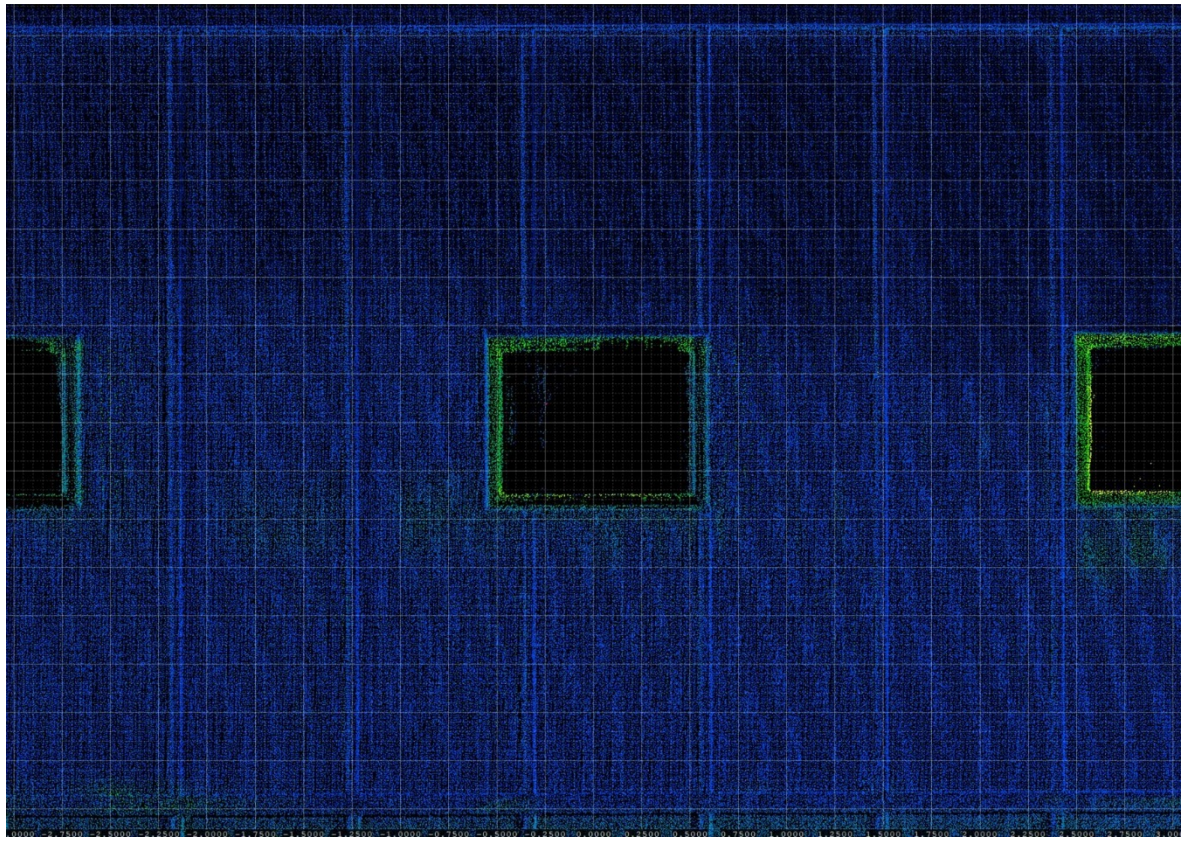
P1N-W-11

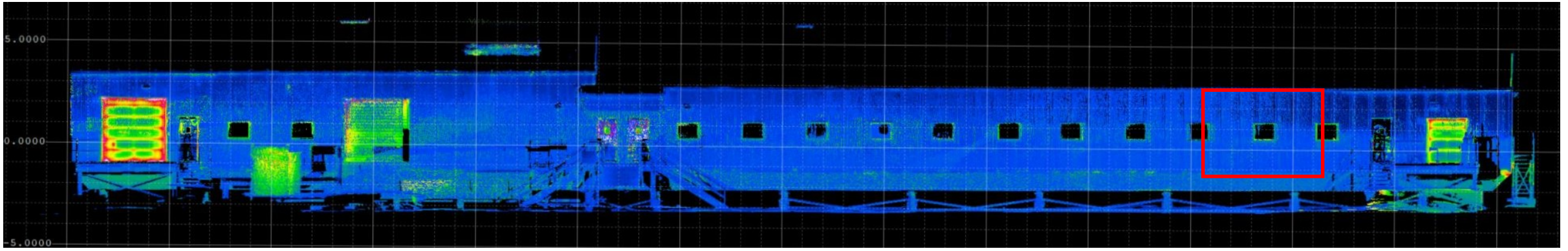
-15◦C



5◦C





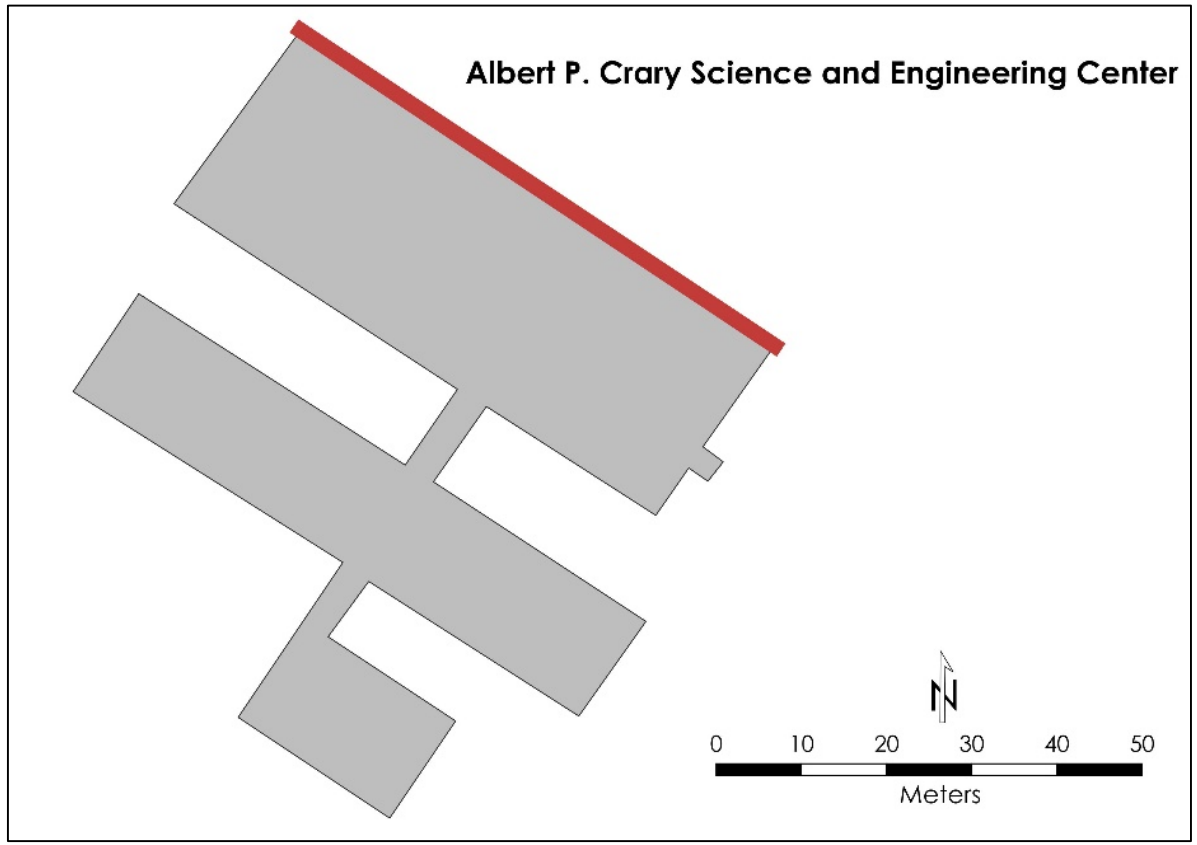


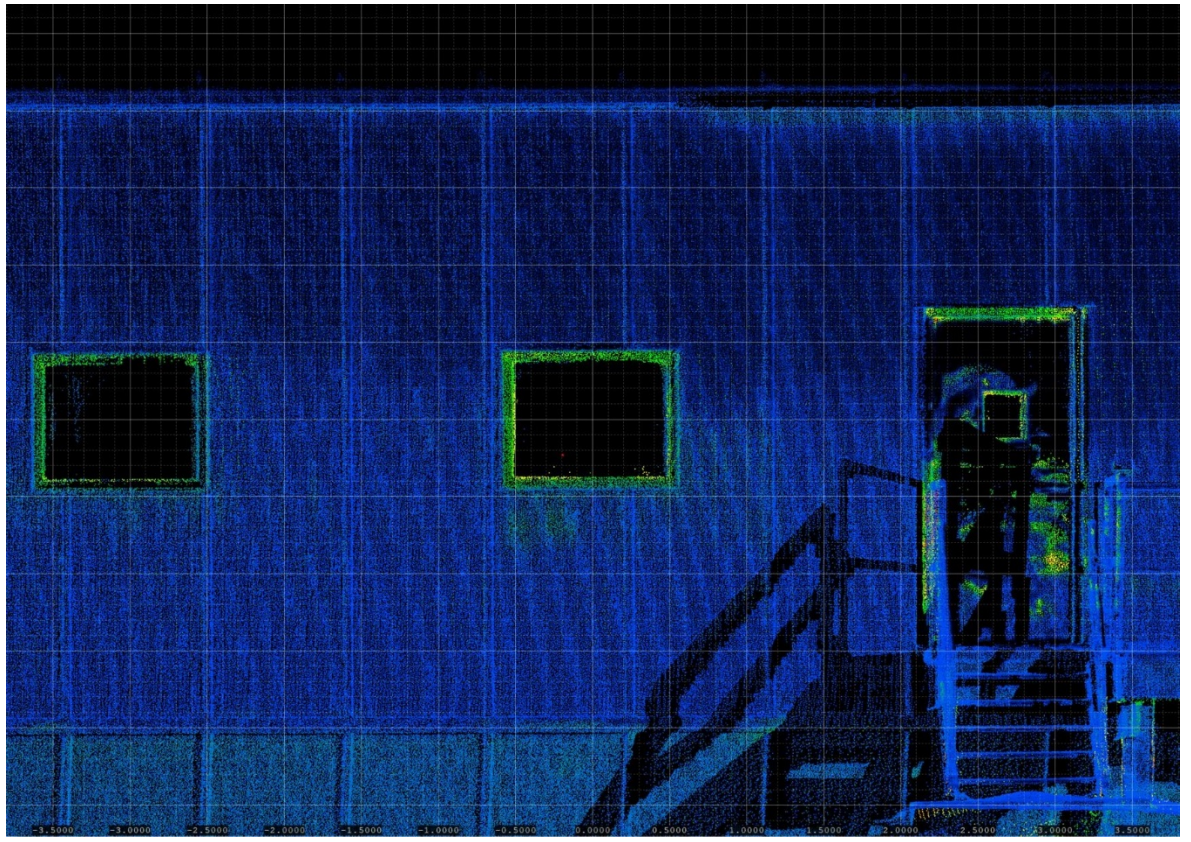
P1N-W-12

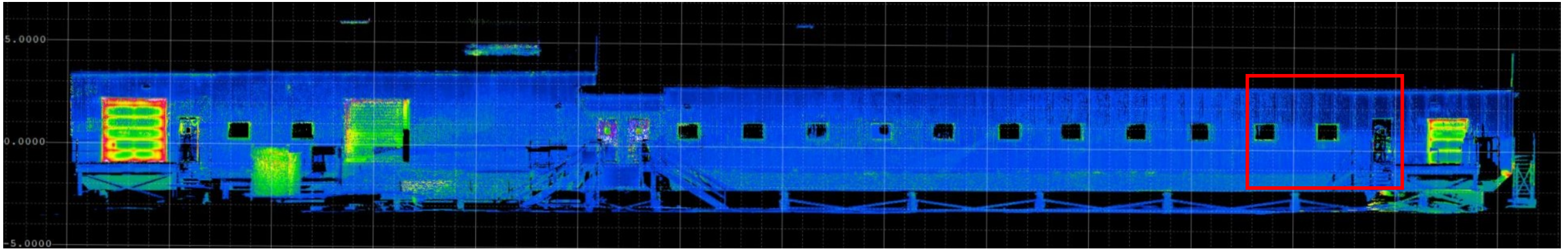
-15◦C



5◦C

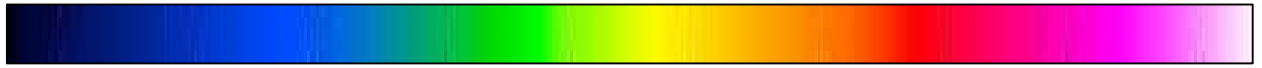




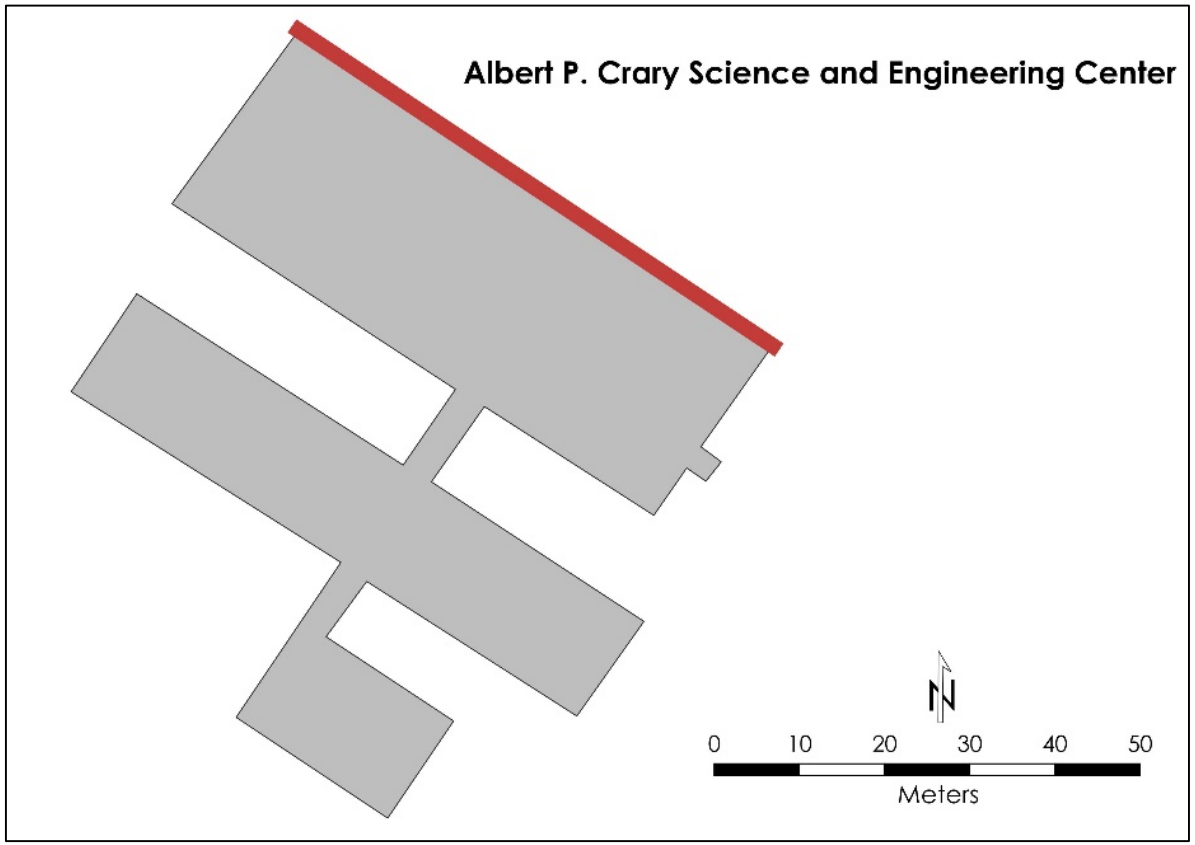


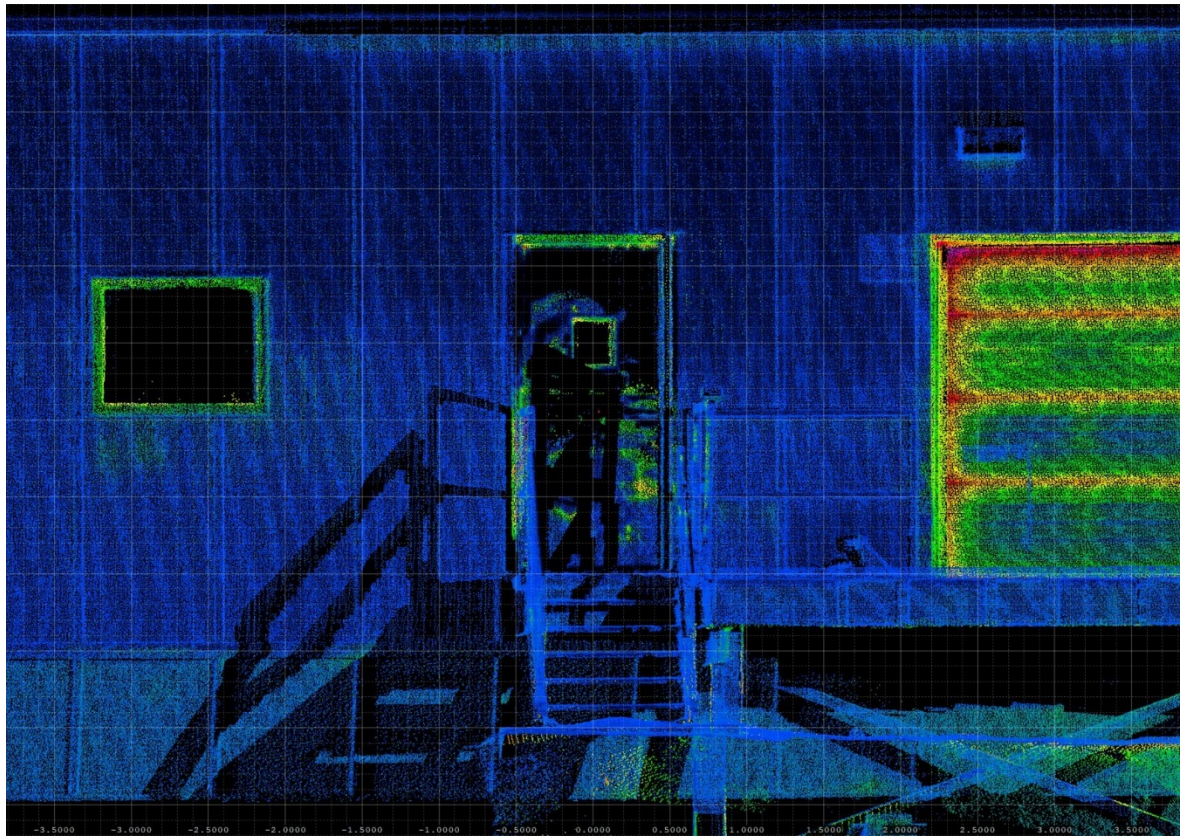
P1N-W-13

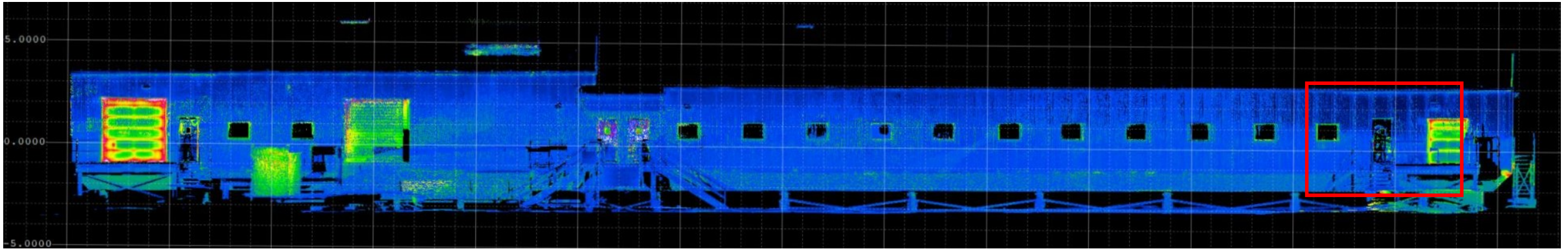
-15◦C



5◦C

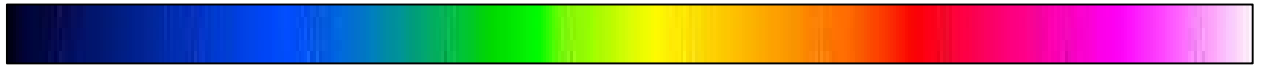




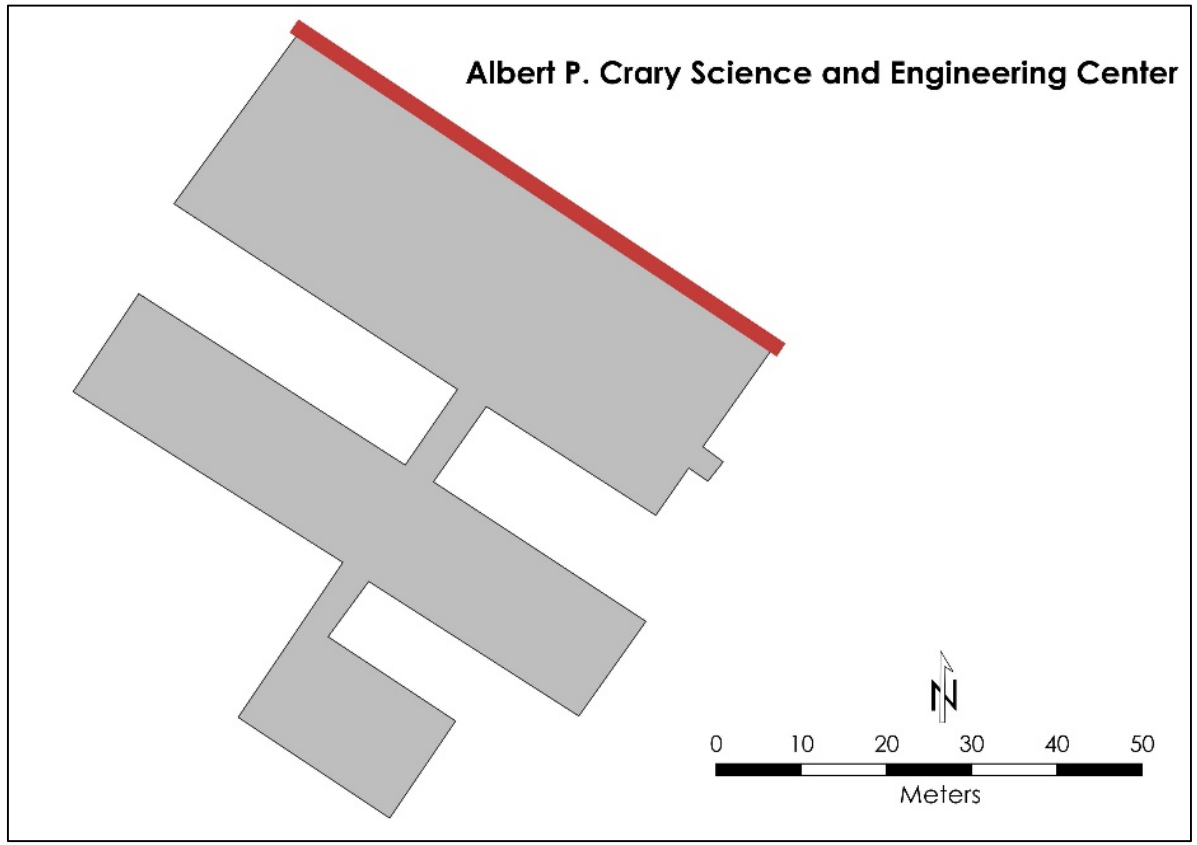


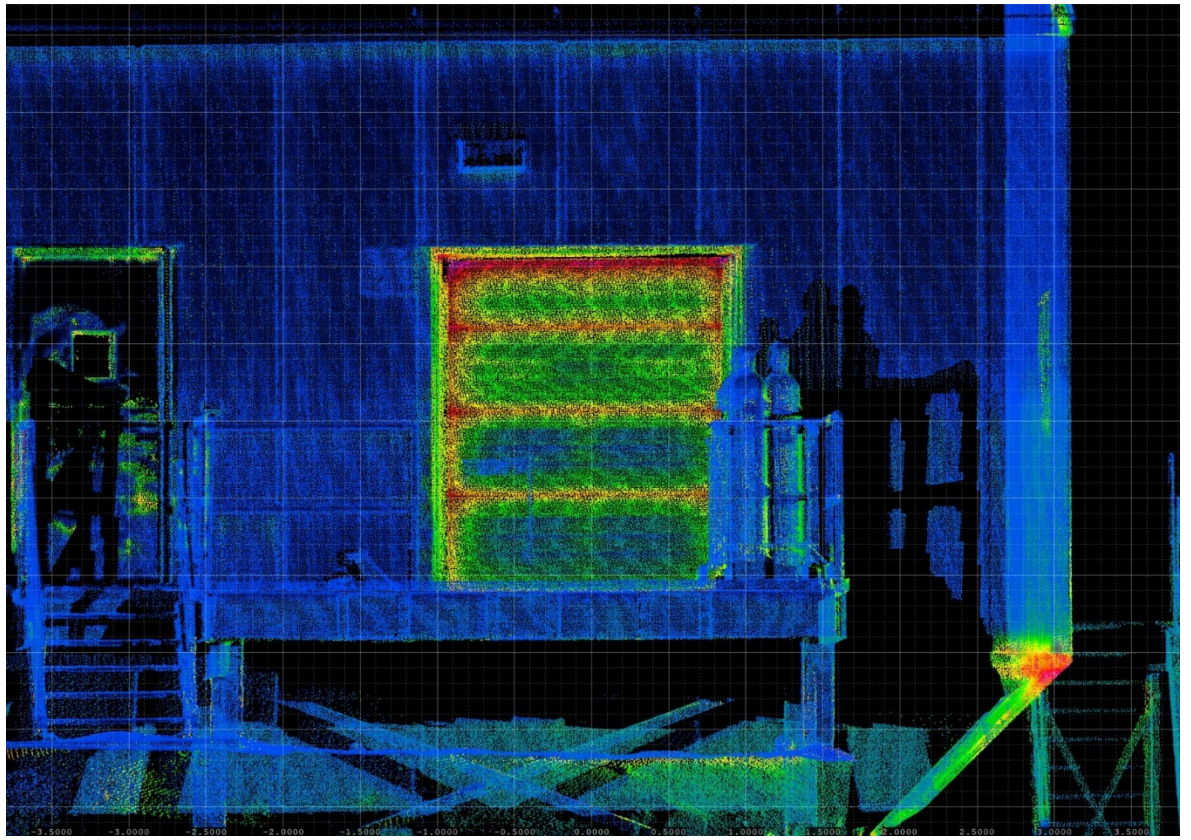
P1N-D-04

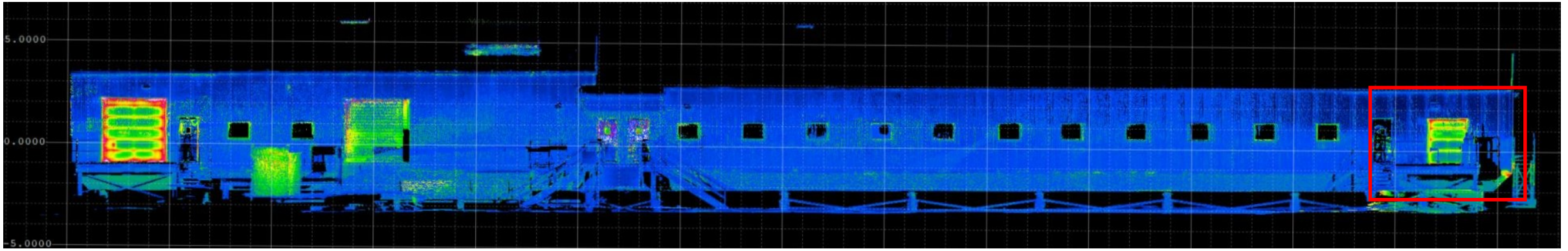
-15◦C



5◦C

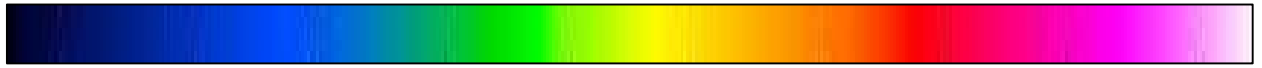




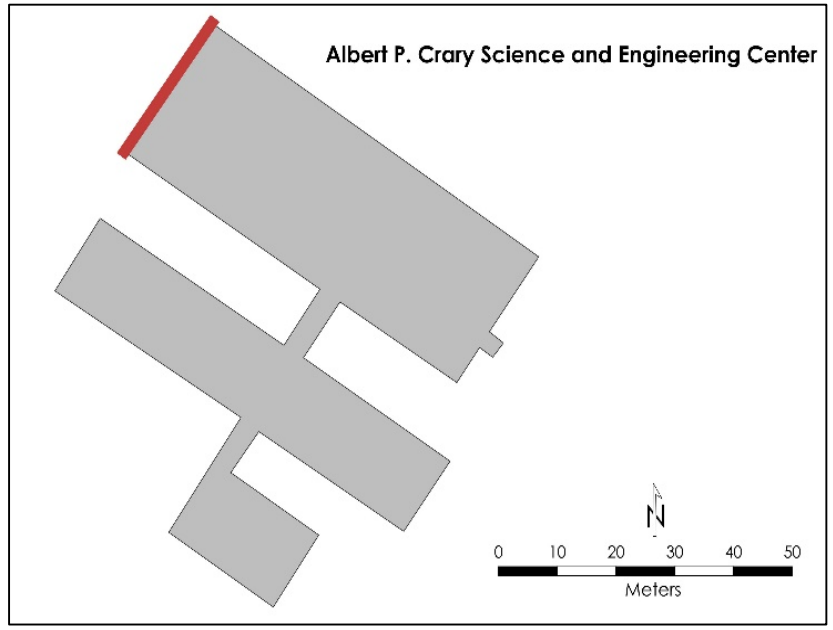


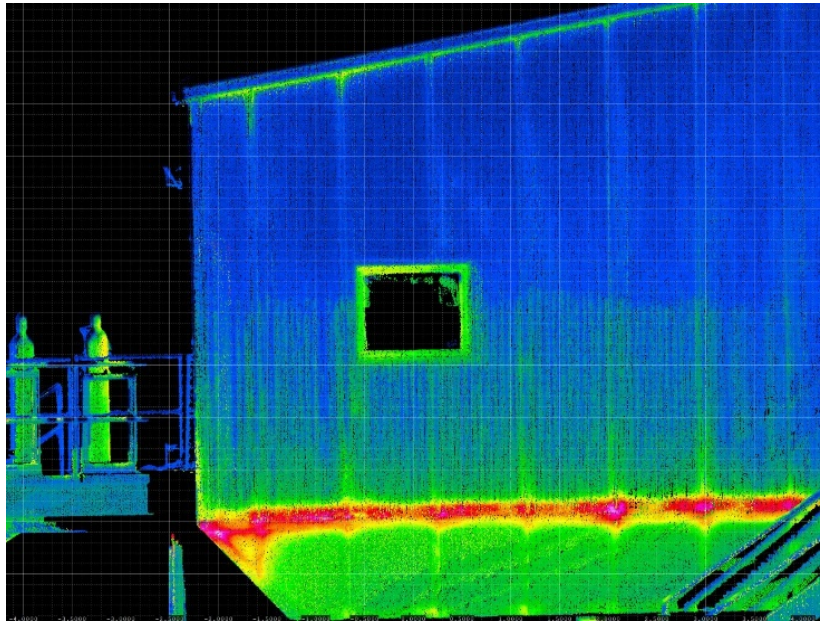
P1N-LD-03

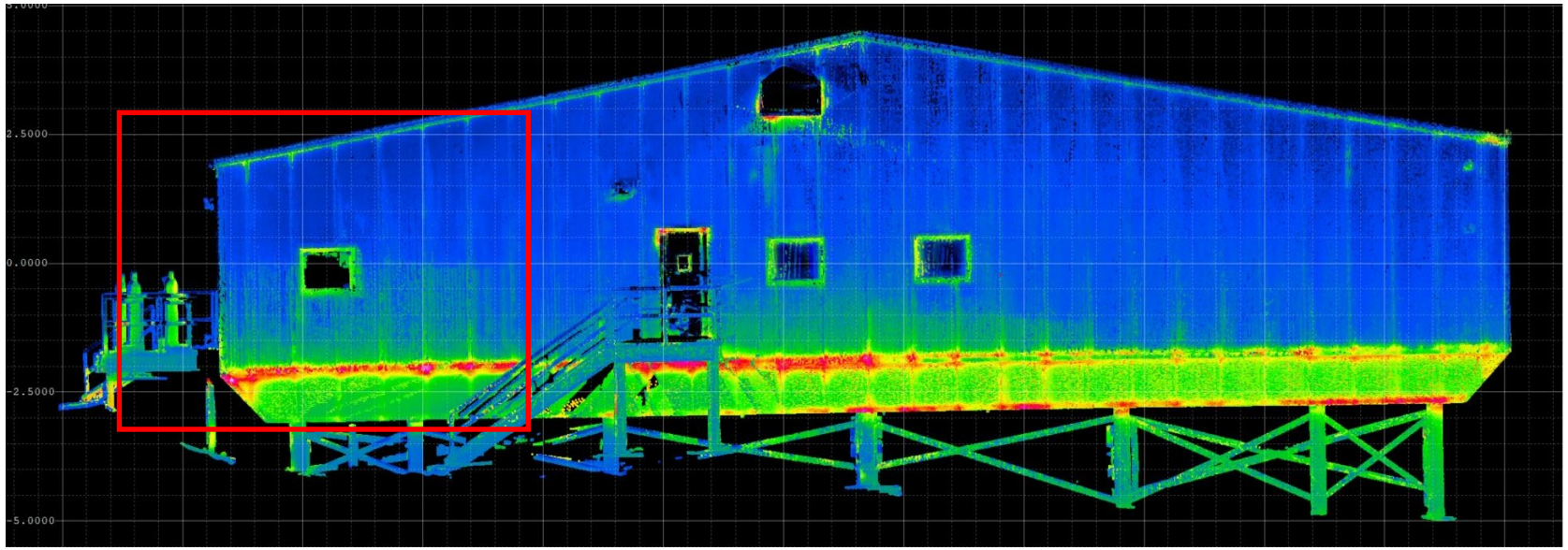
-15◦C



5◦C



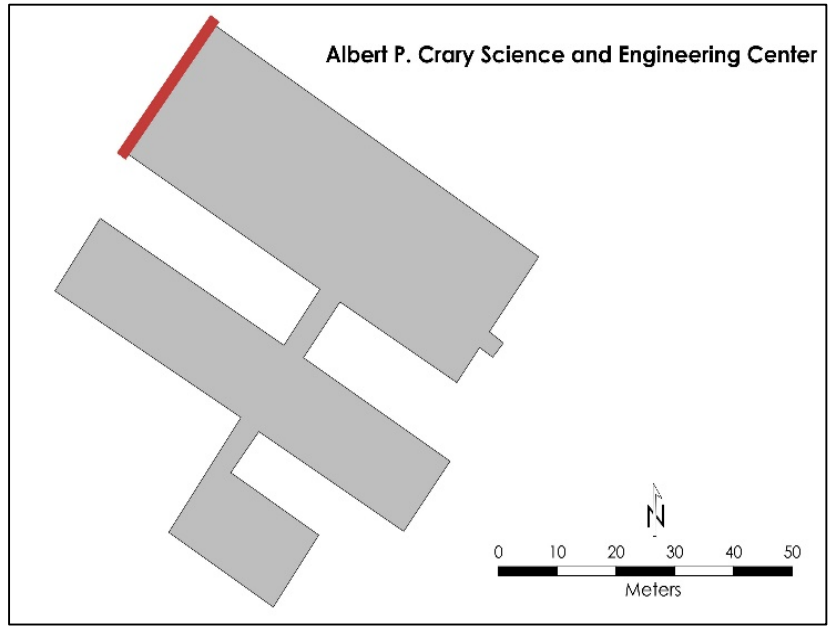


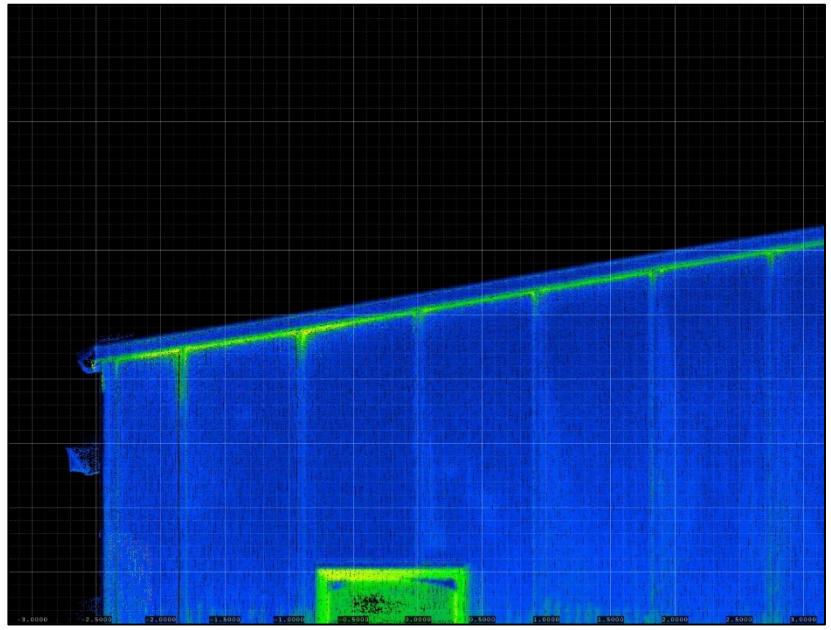


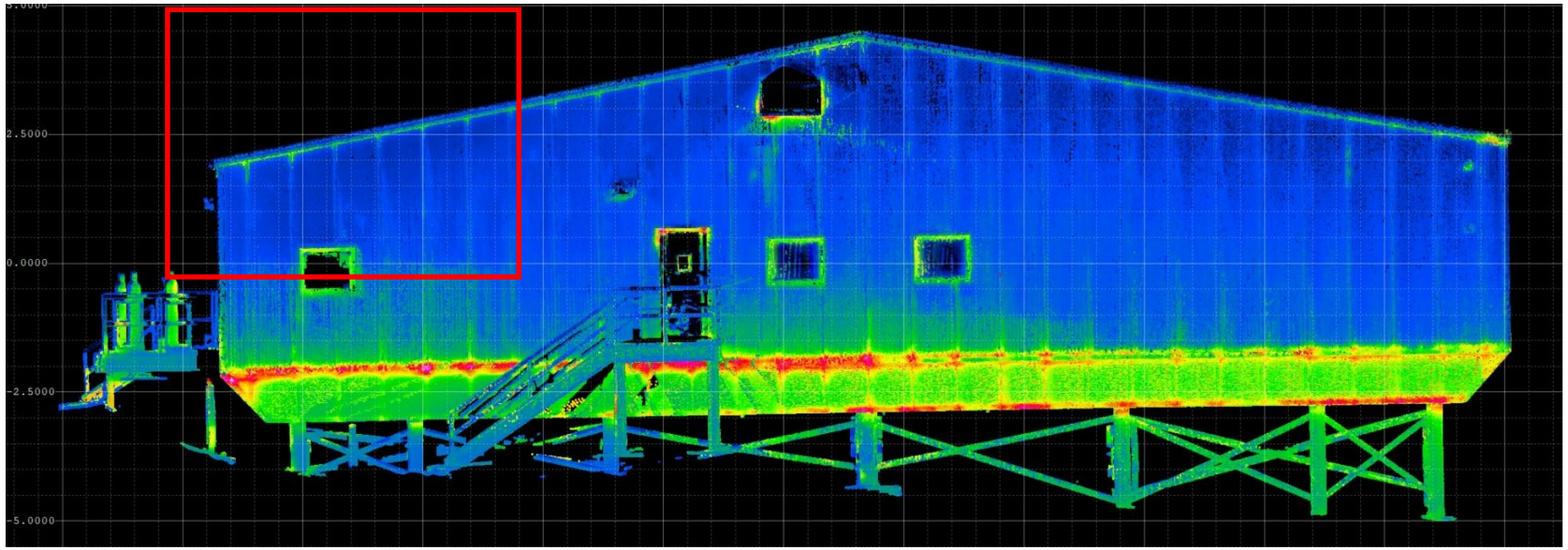
P1W-W-01

-15◦C

5◦C



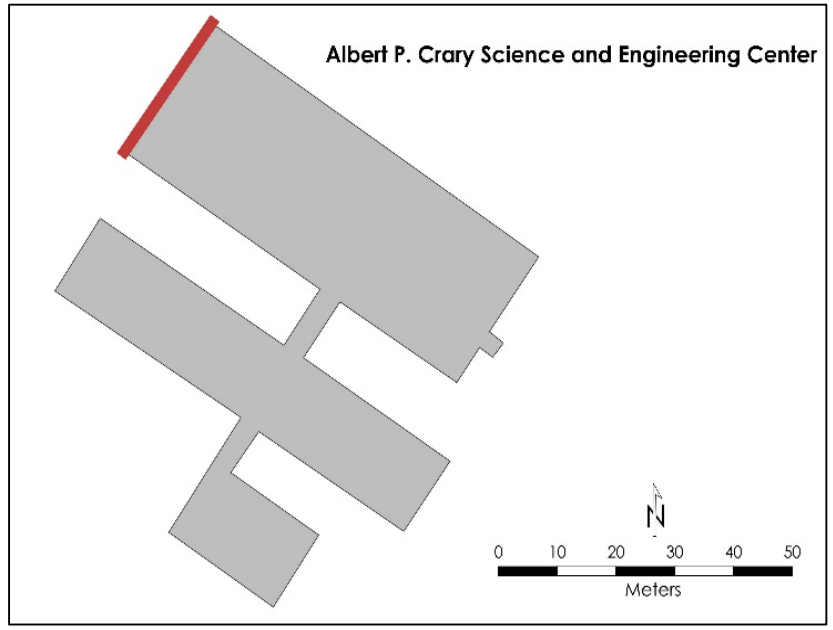


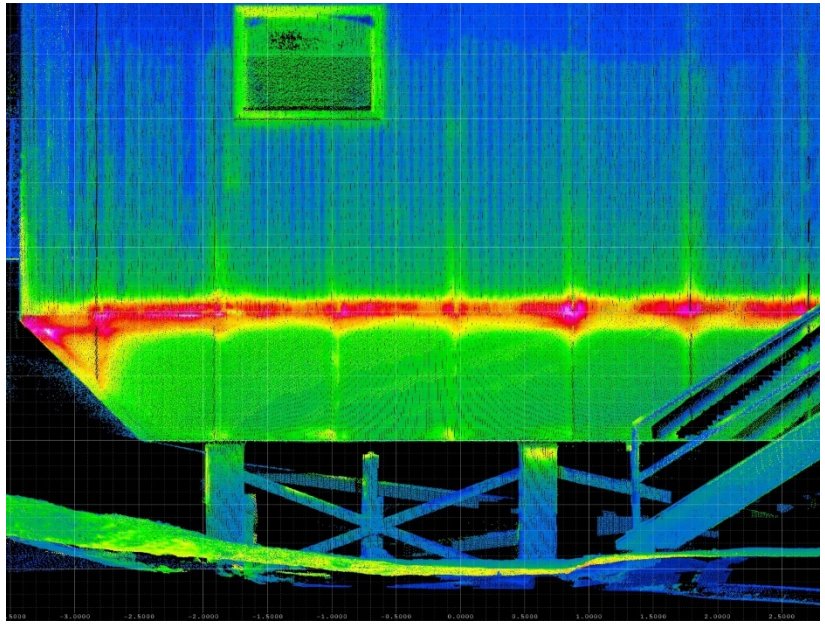


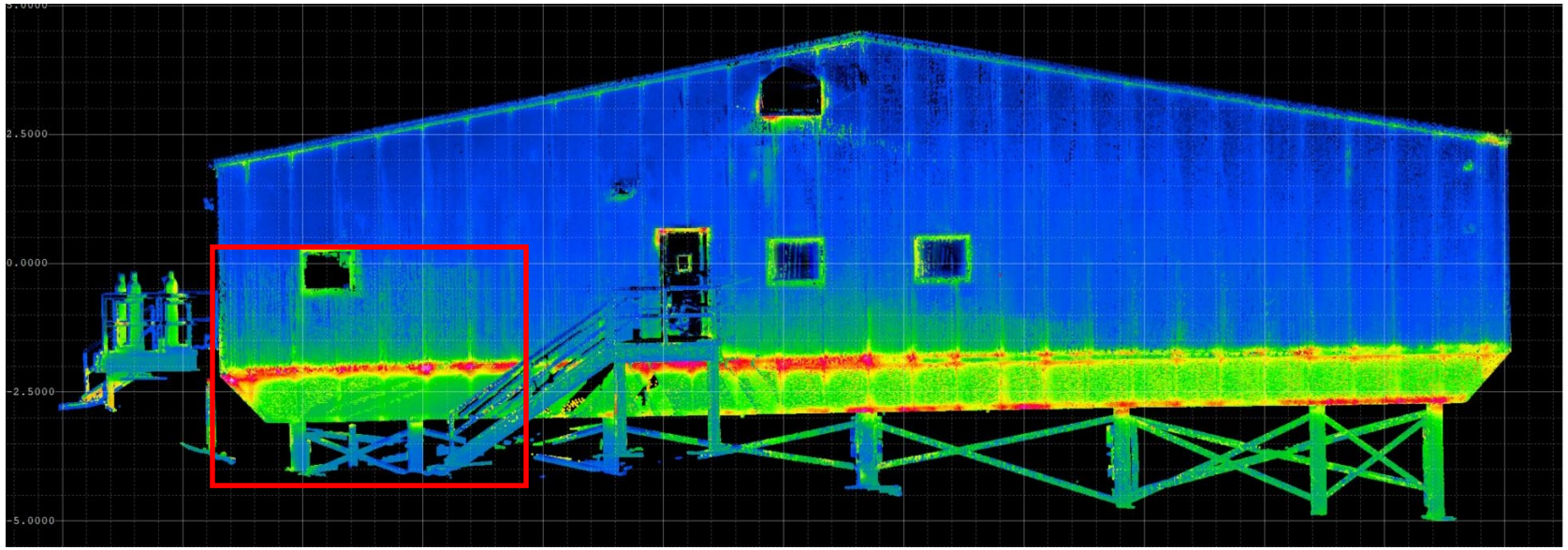
P1W-TA-01

-15◦C

5◦C



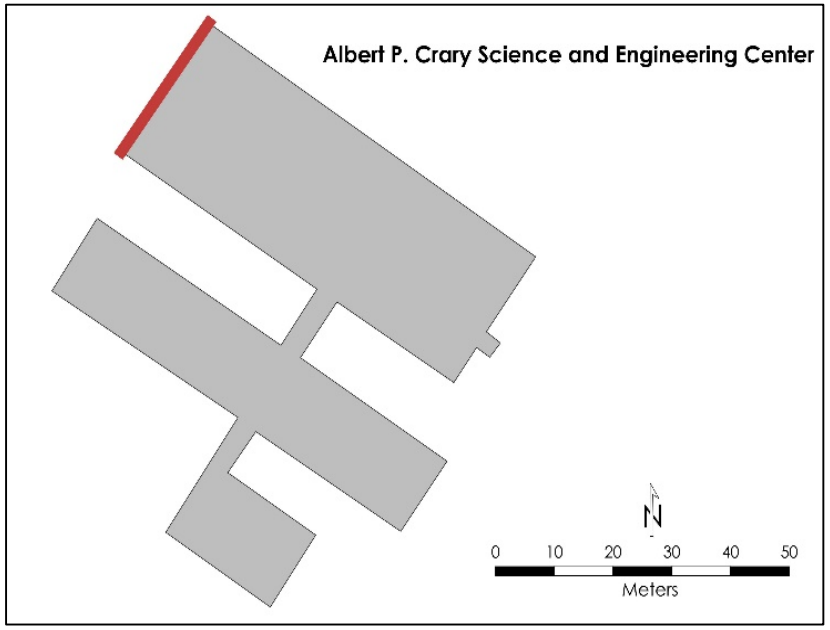


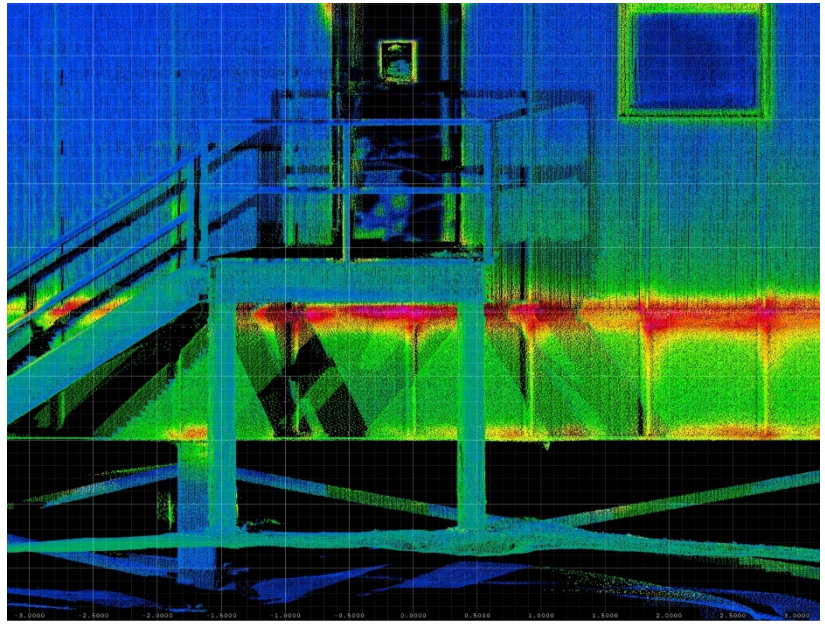


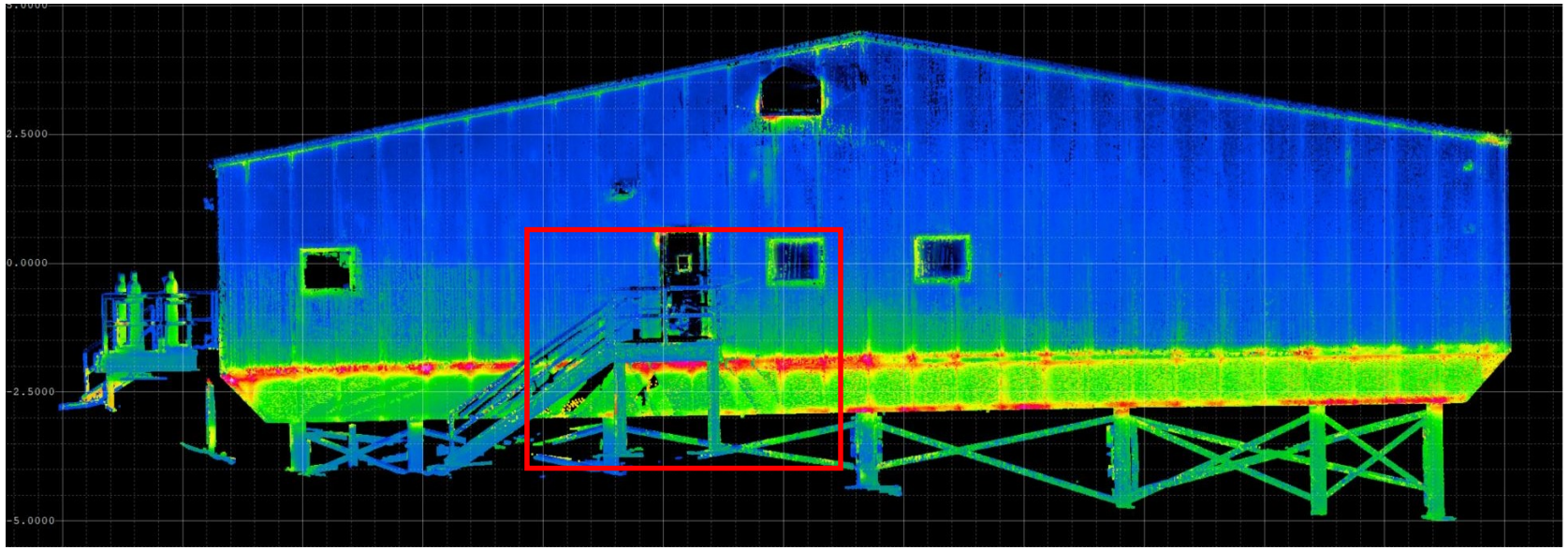
P1W-TA-02

-15◦C

5◦C



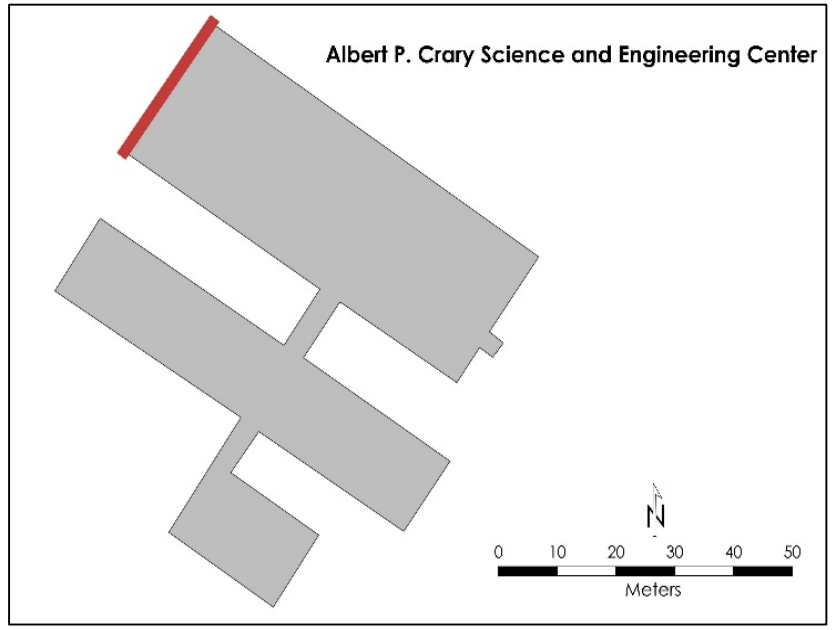


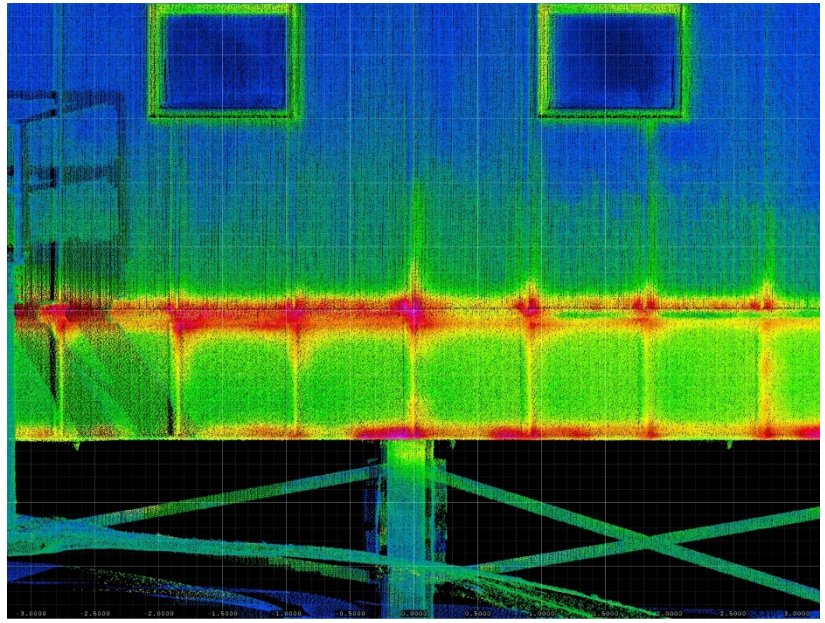


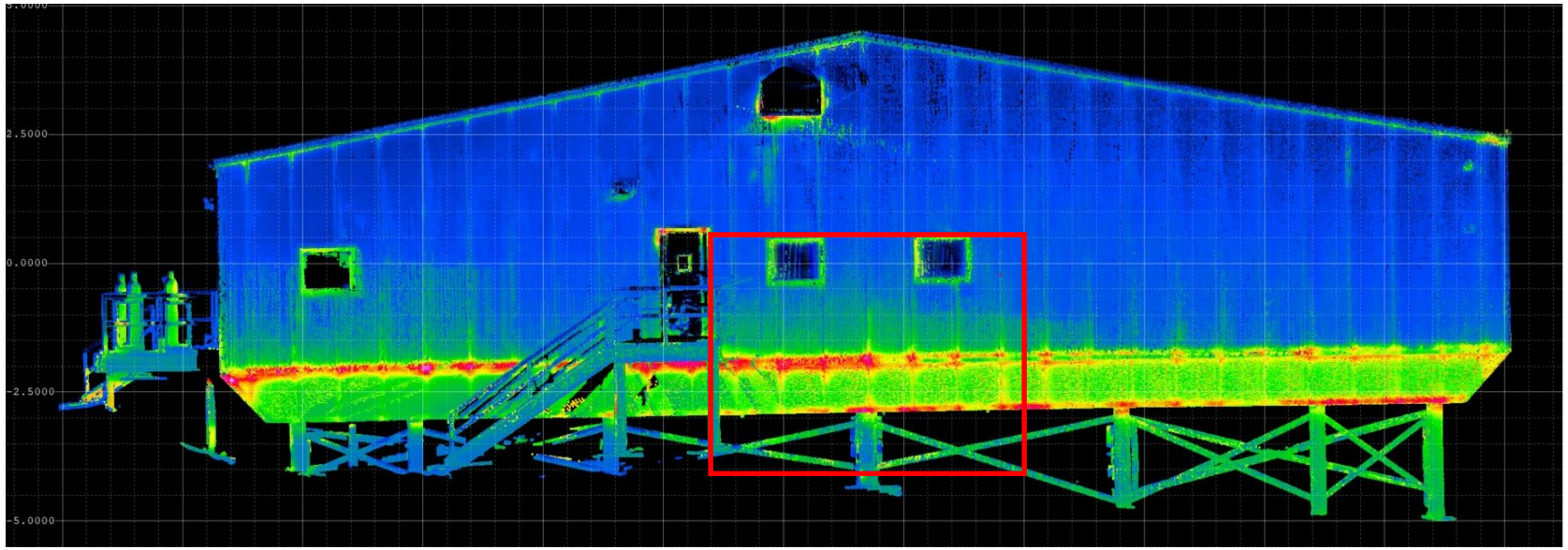
P1W-TA-03

-15◦C

5◦C



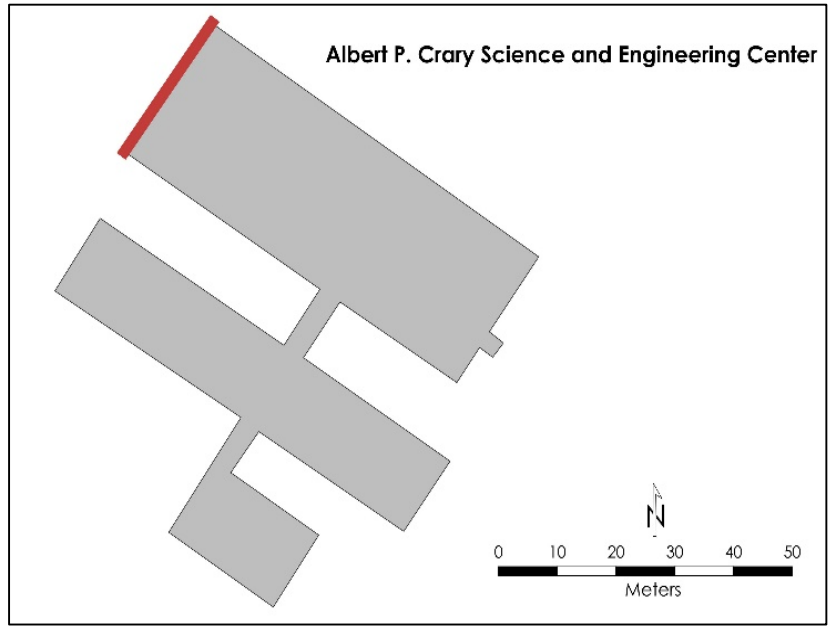


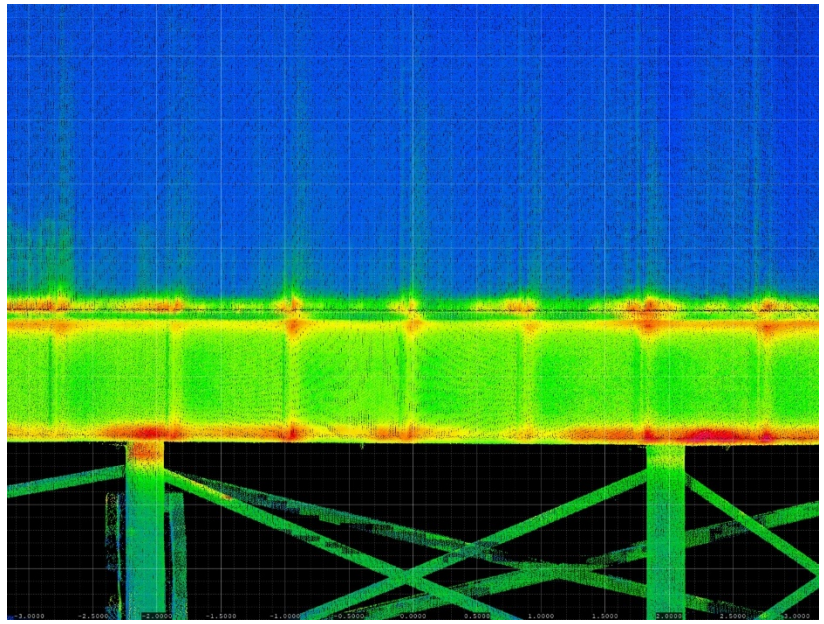


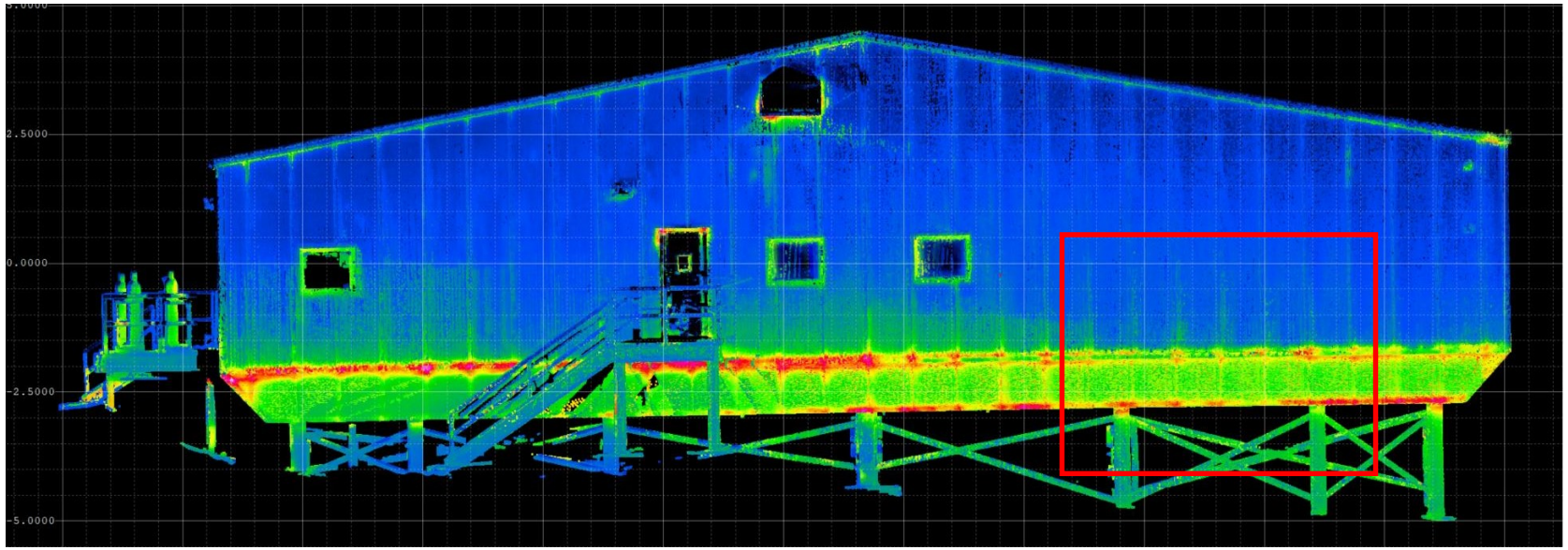
P1W-TA-03

-15◦C

5◦C



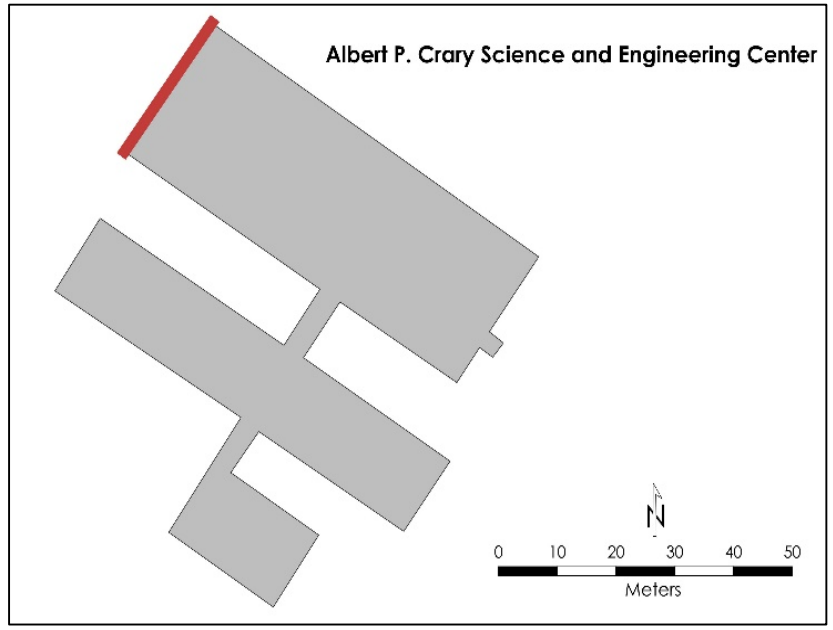


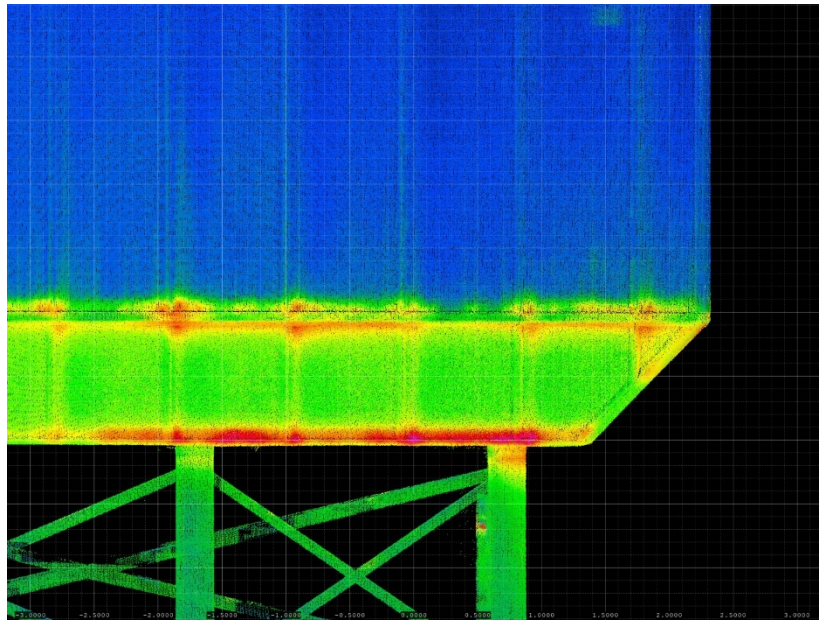


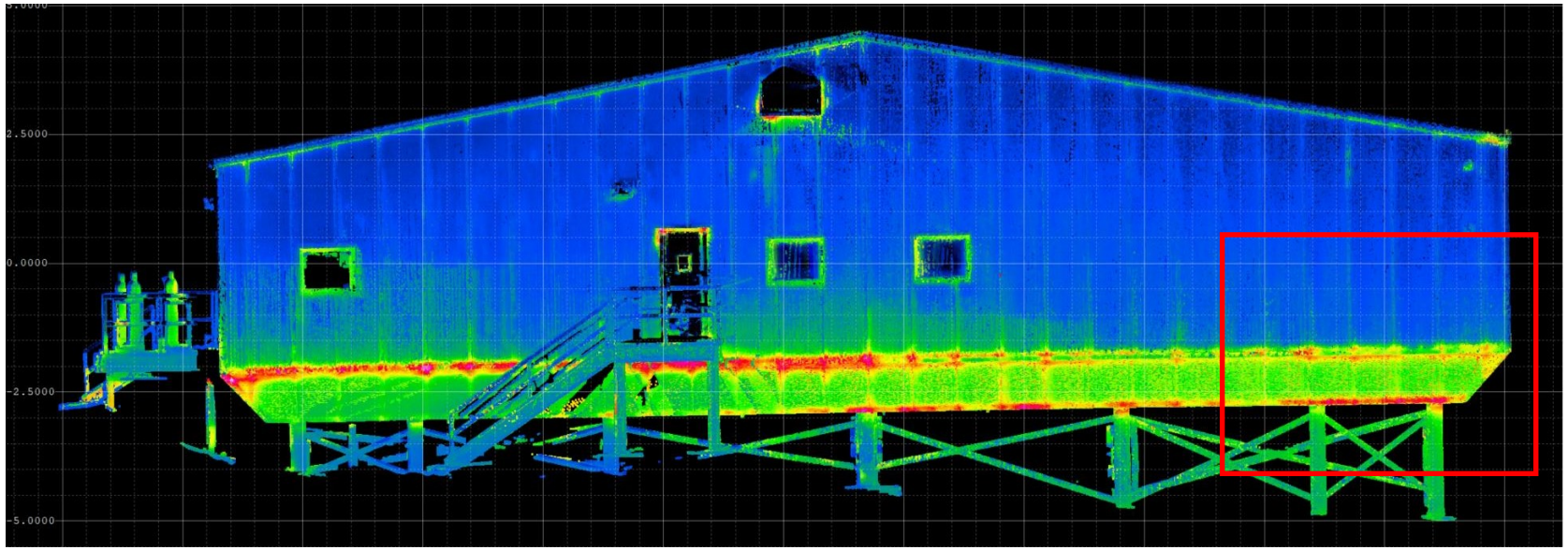
P1W-TA-04

-15◦C

5◦C





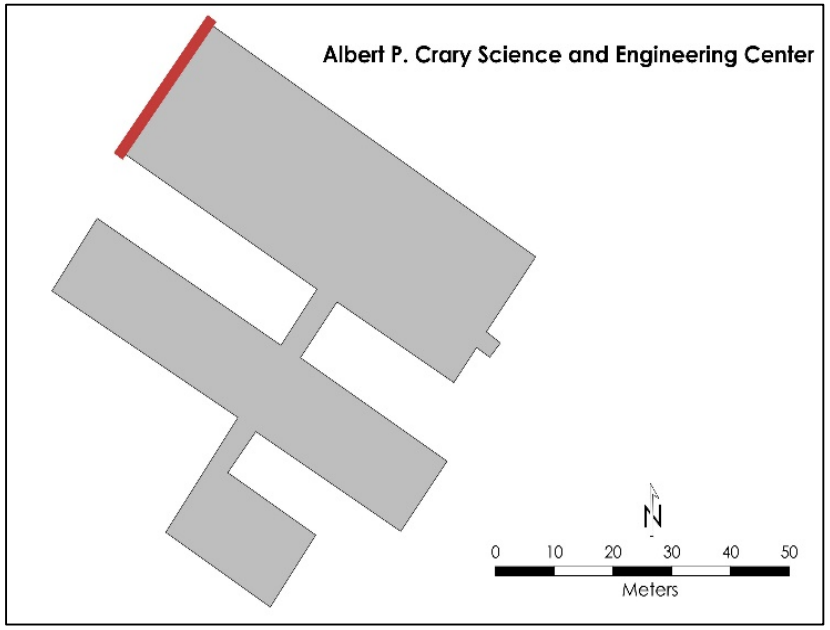


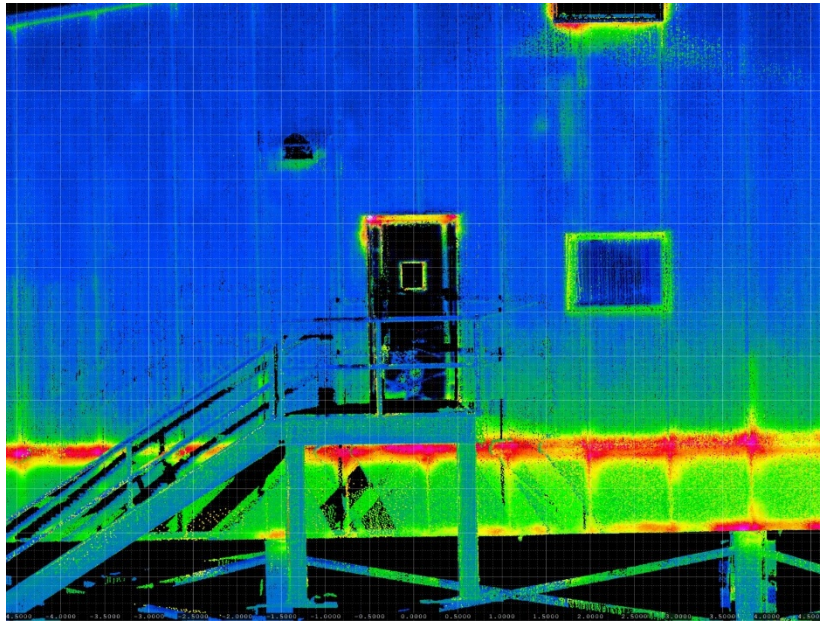
P1W-TA-05

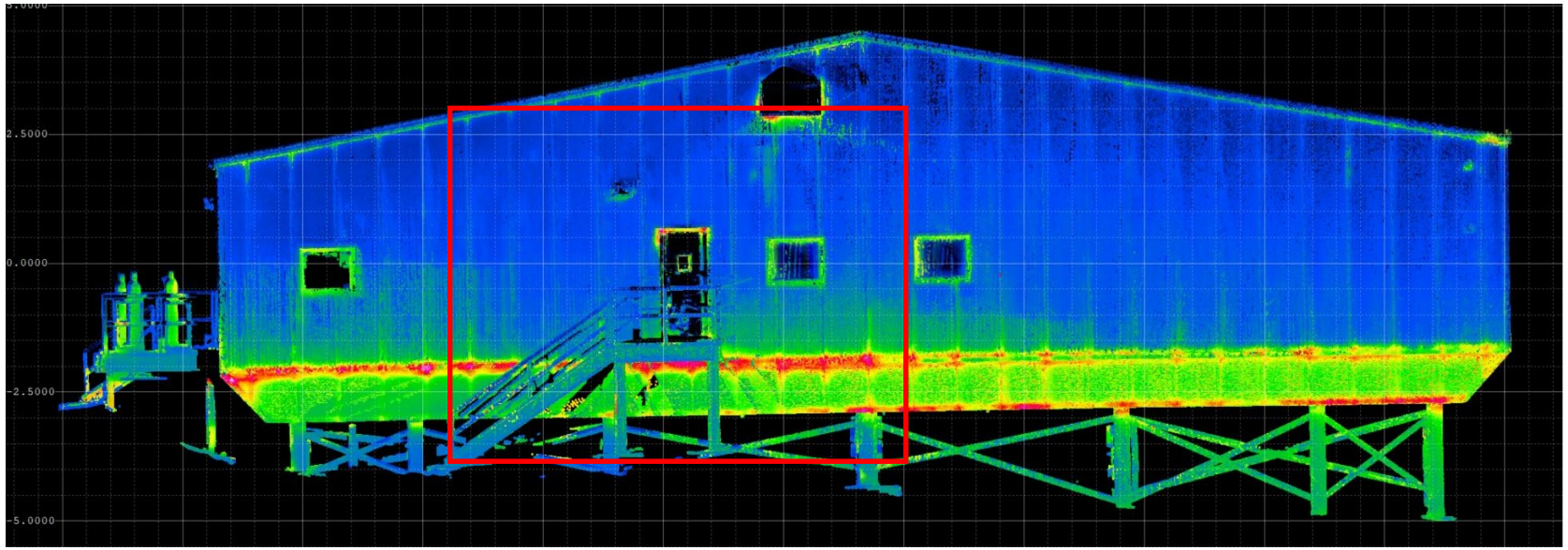
-15◦C



5◦C





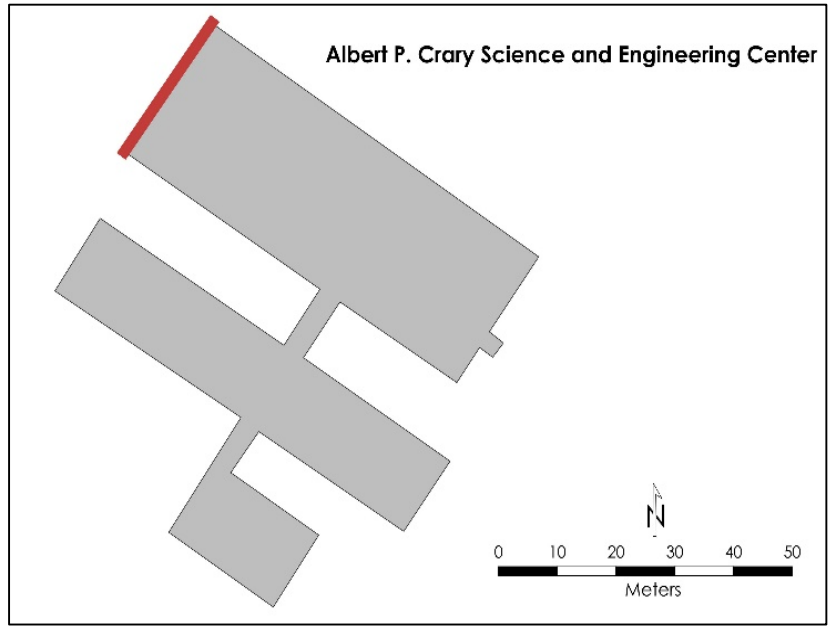


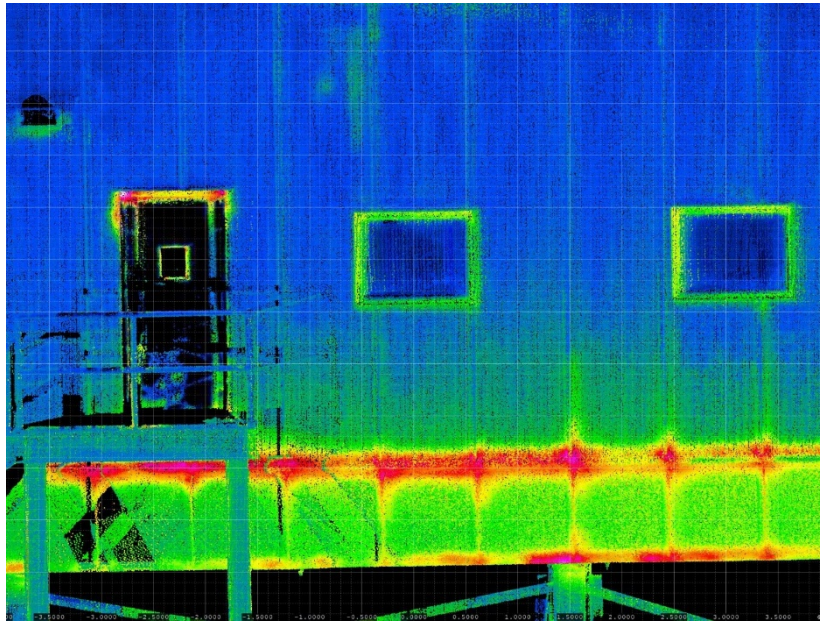
P1W-D-01

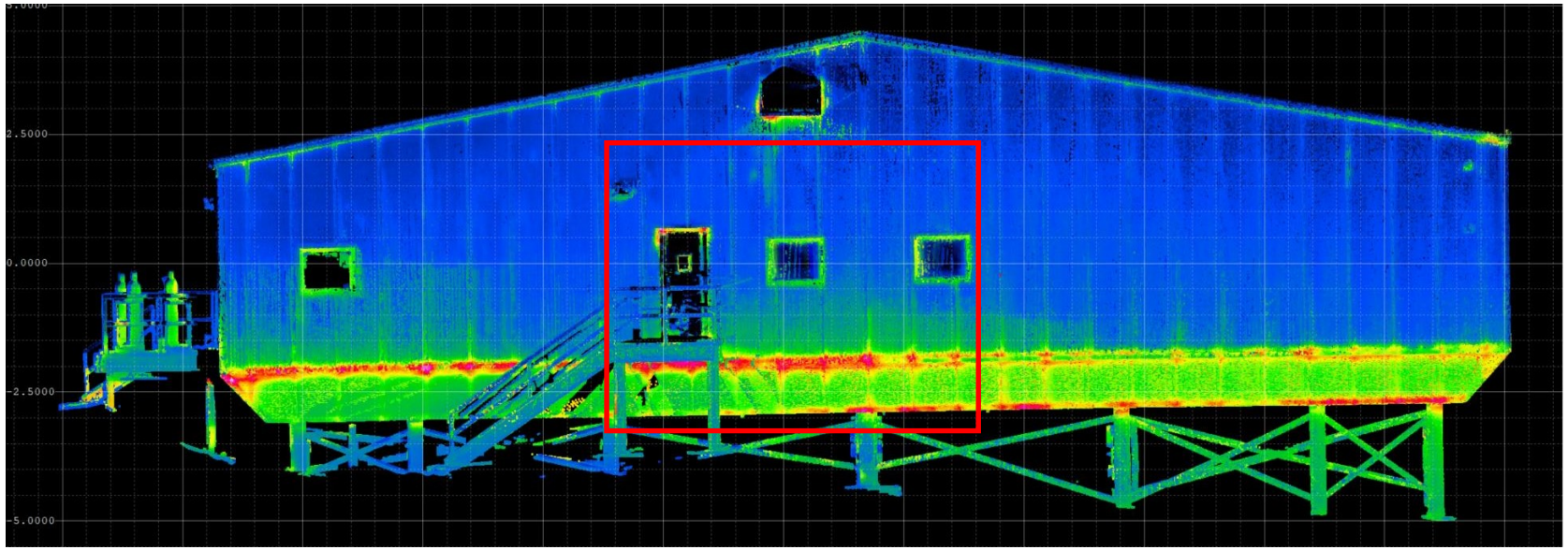
-15◦C



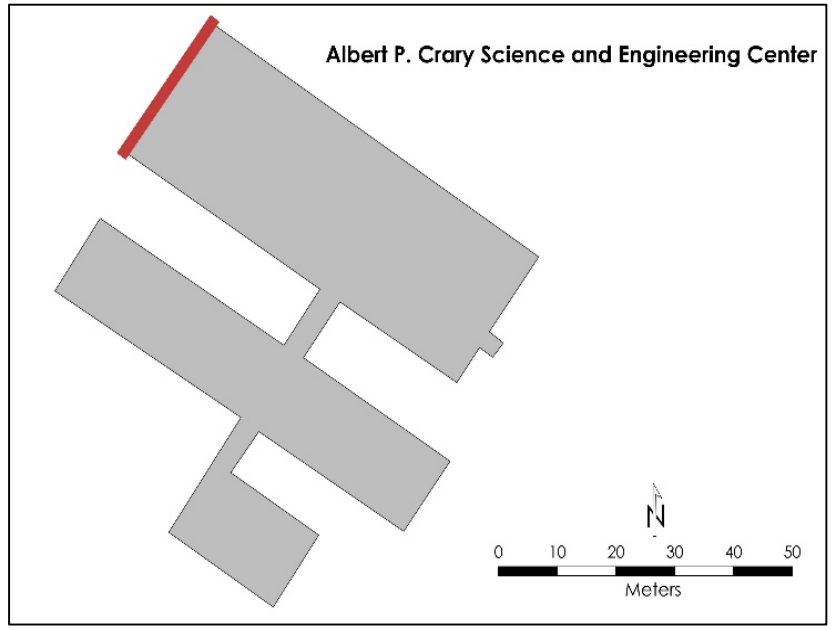
5◦C

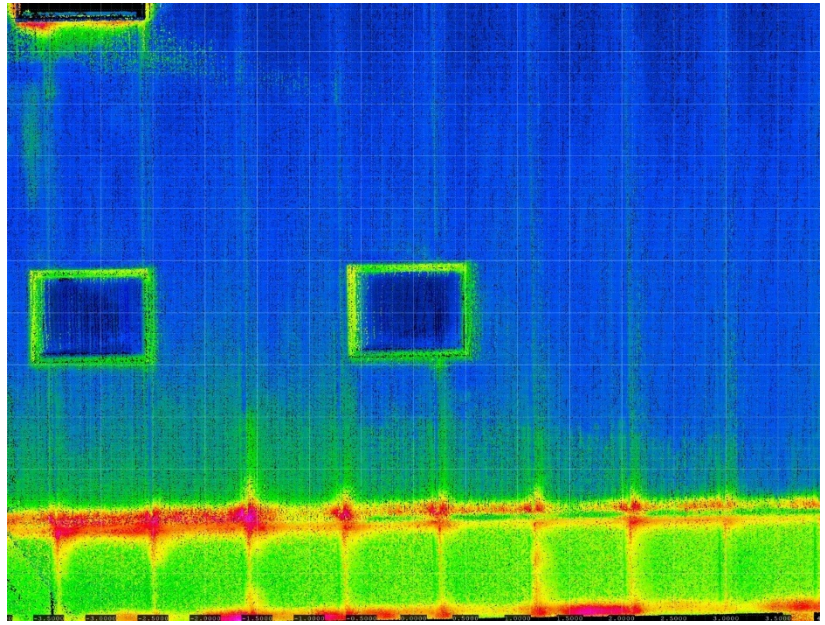


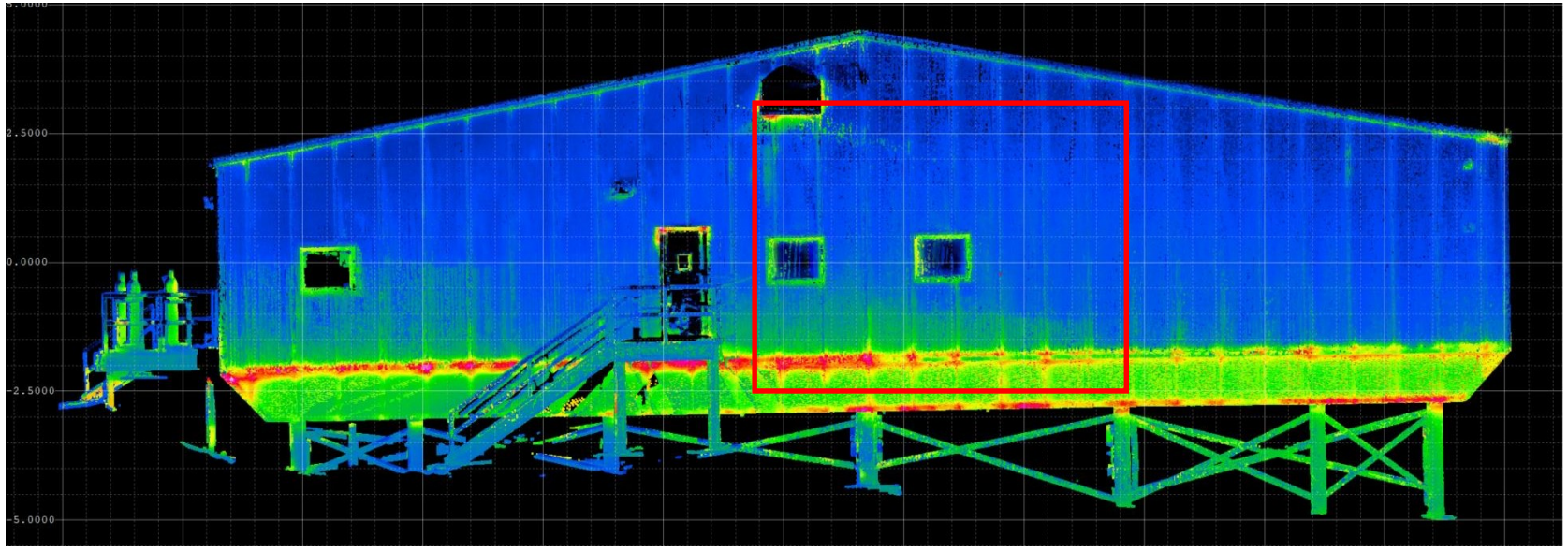




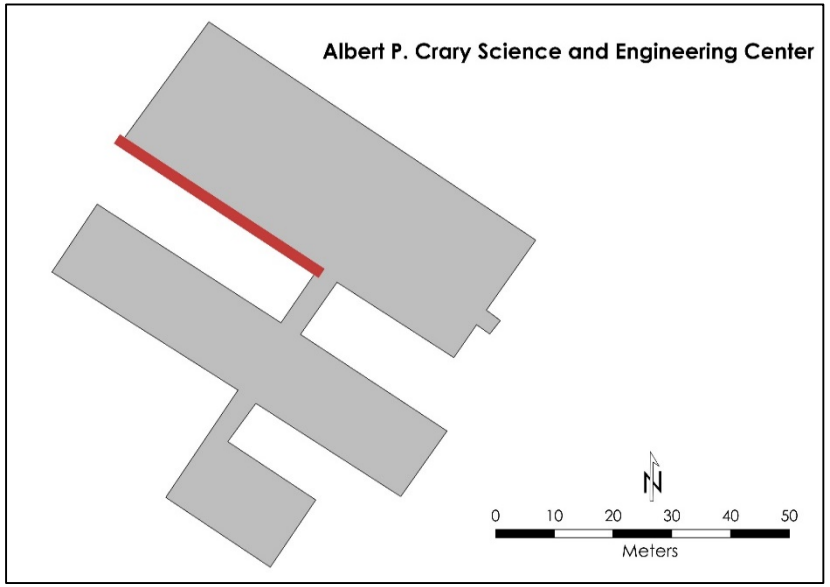
P1W-W-02 -15◦C 5◦C

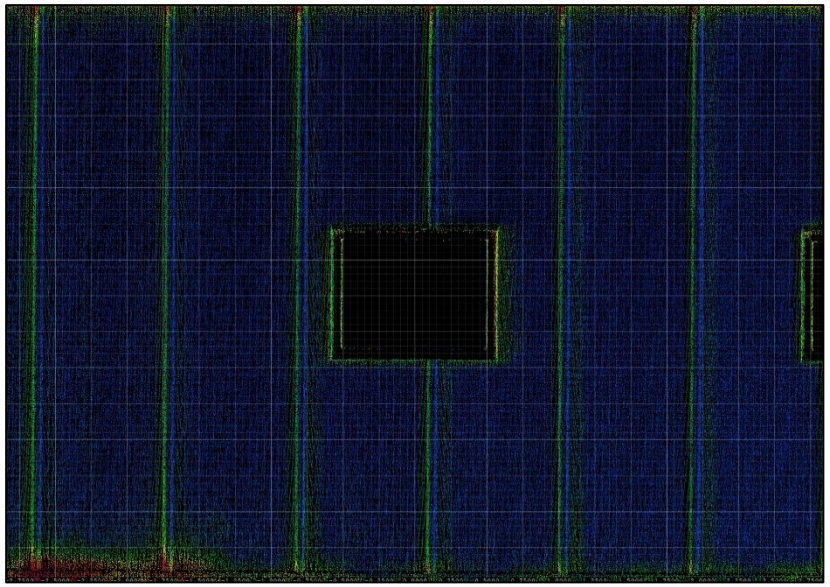


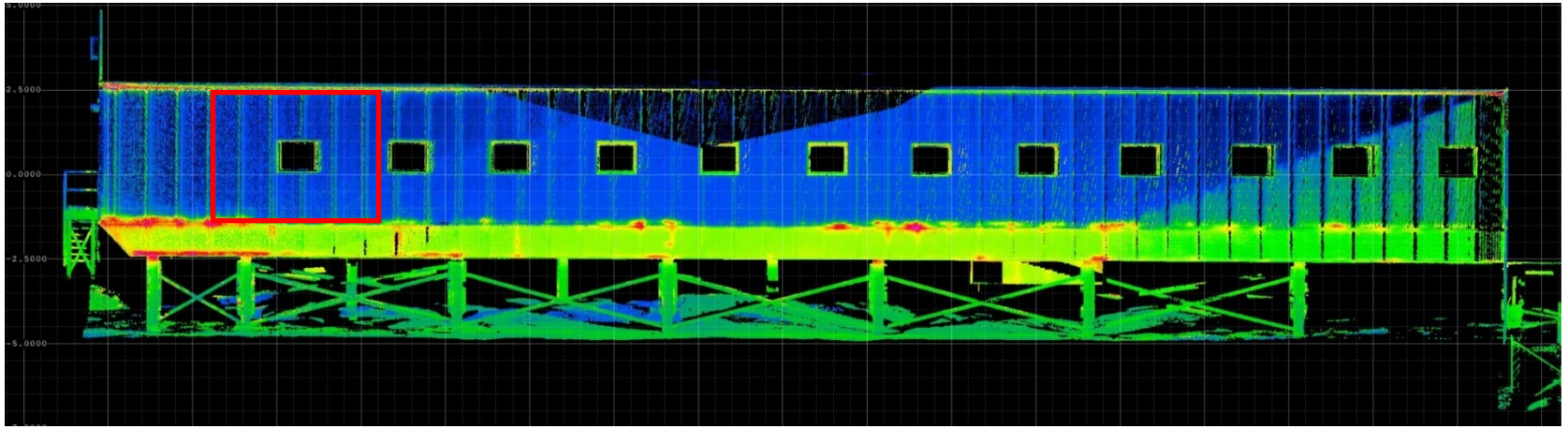




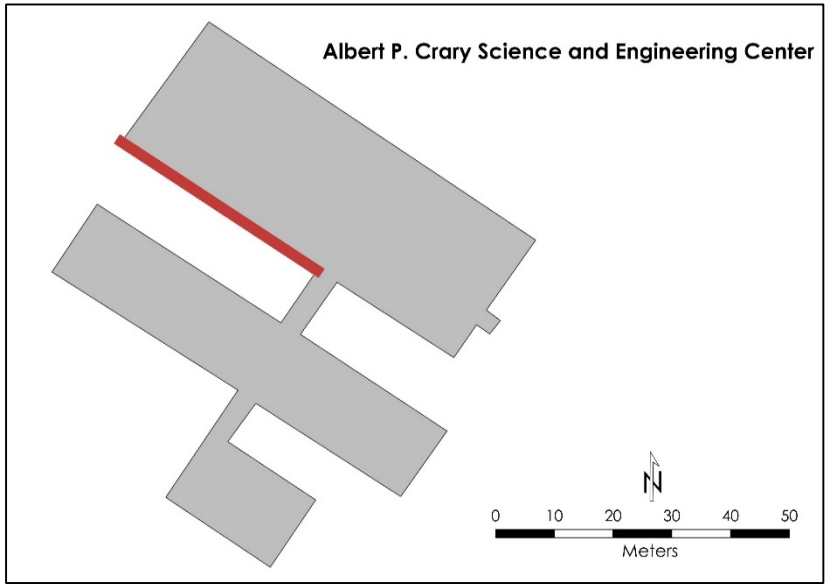
P1W-W-03 -15◦C 5◦C

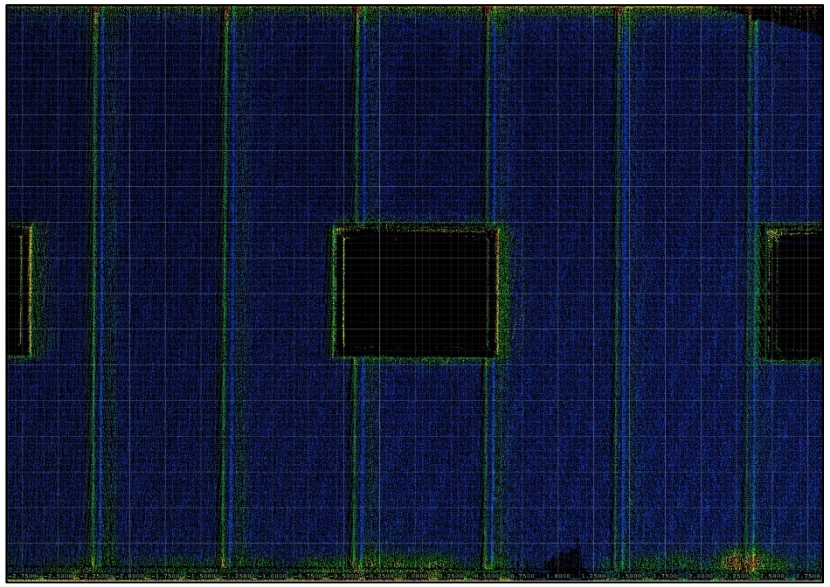


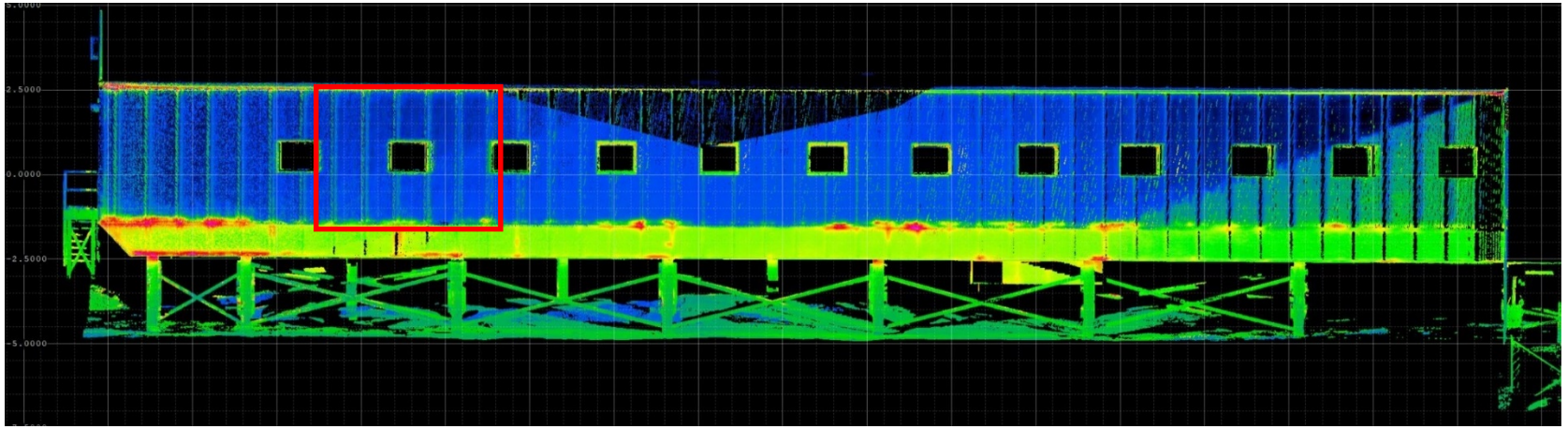




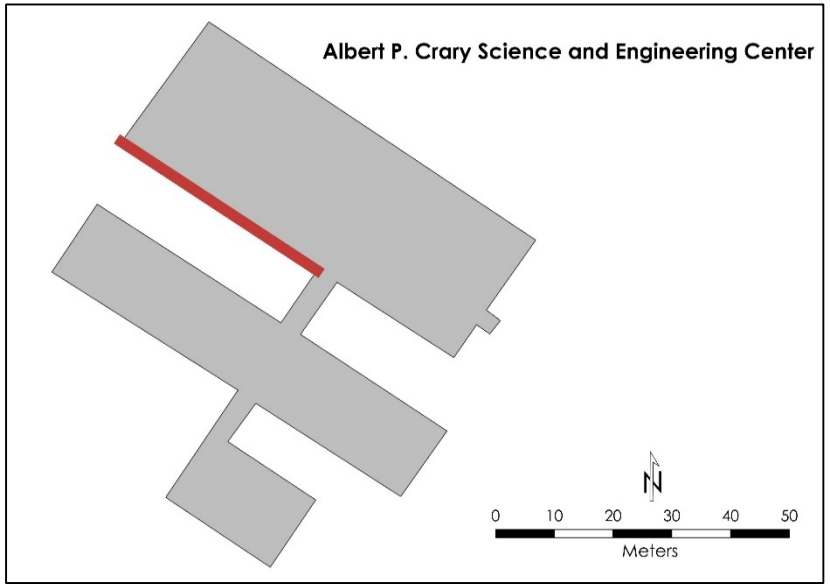
P1SW-W-01 -15◦C 5◦C

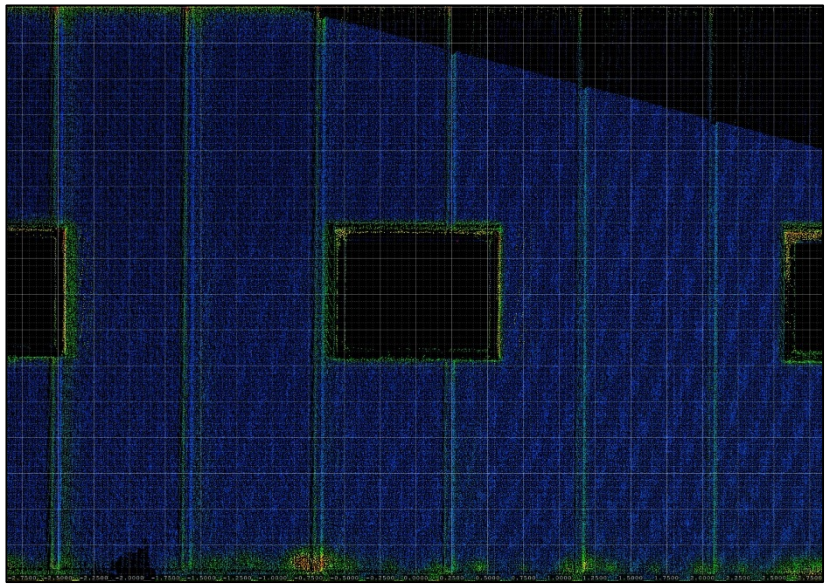


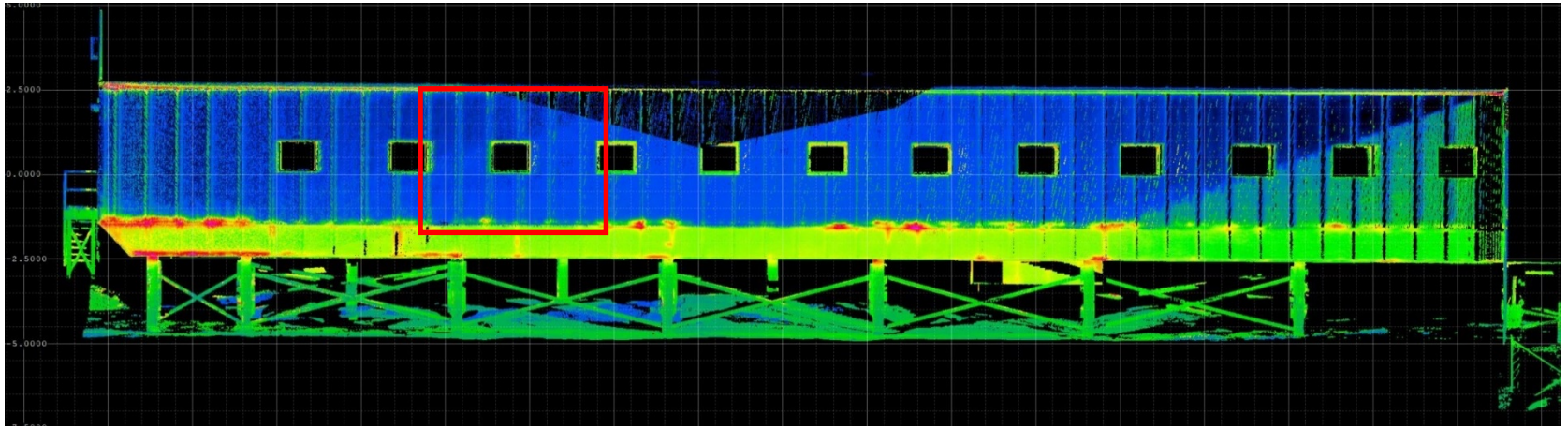




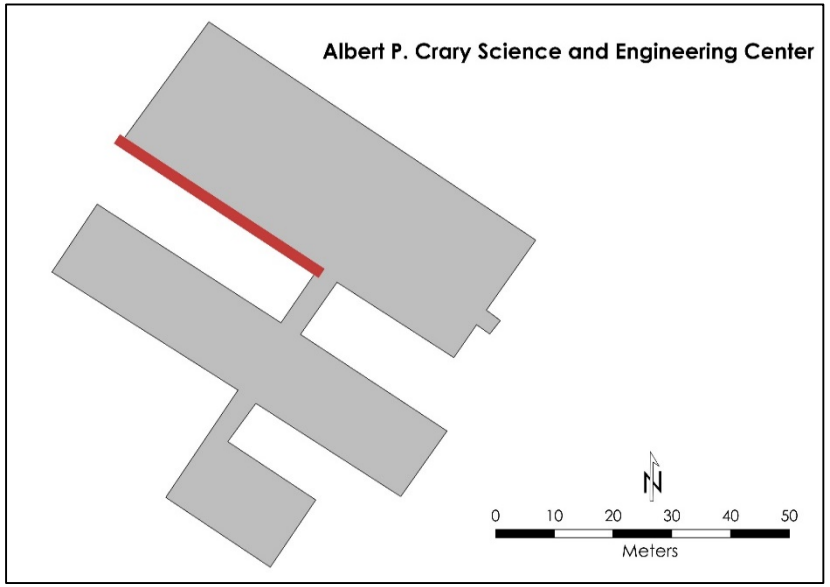
P1SW-W-02 -15◦C 5◦C

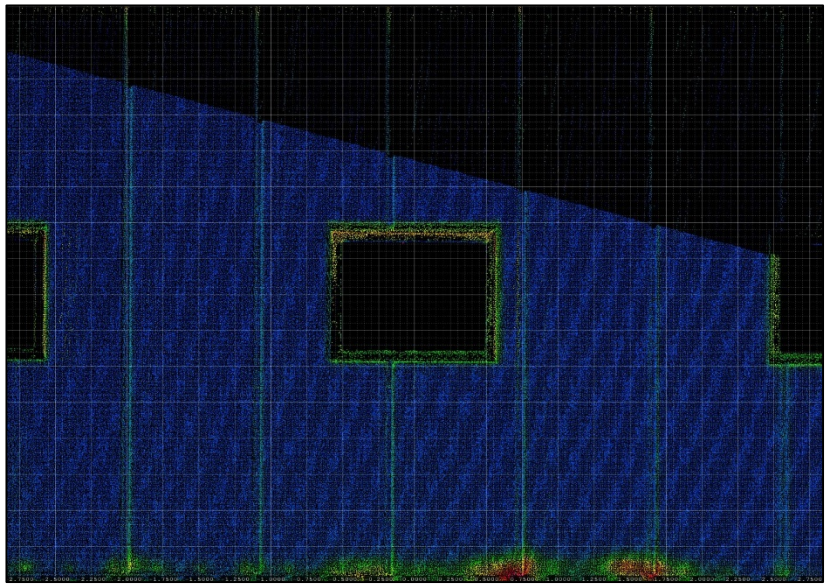


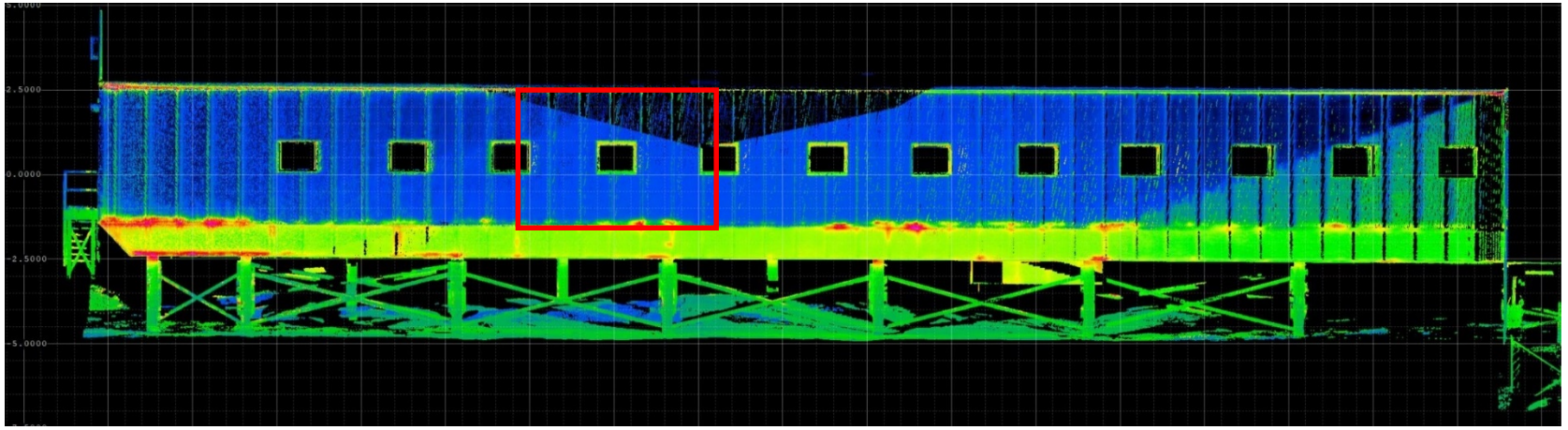




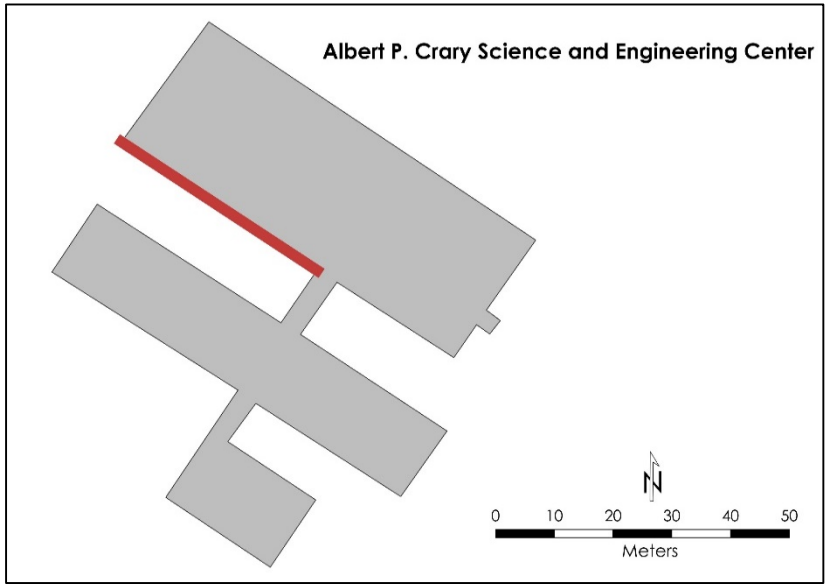
P1SW-W-03 -15◦C 5◦C

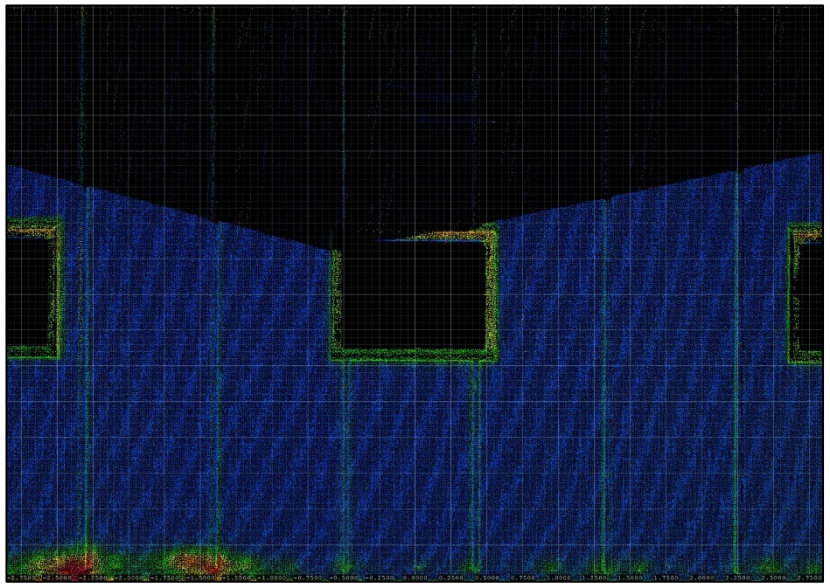


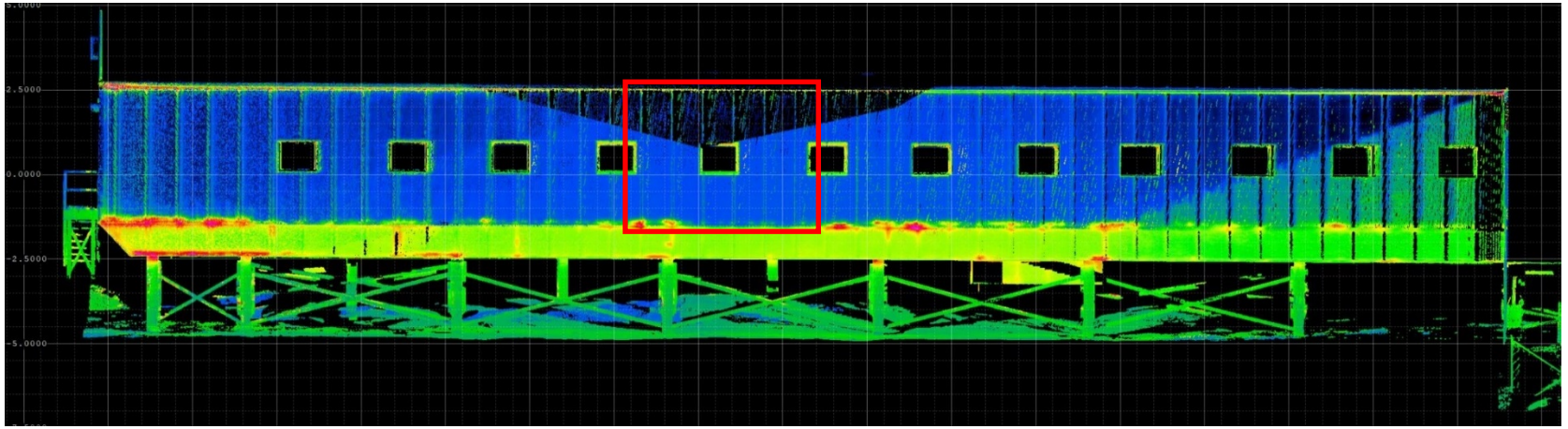




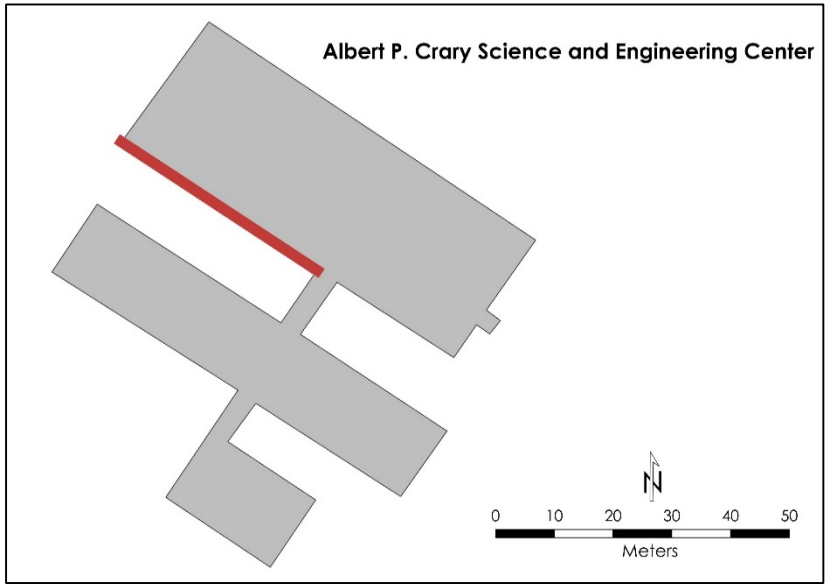
P1SW-W-04 -15◦C 5◦C

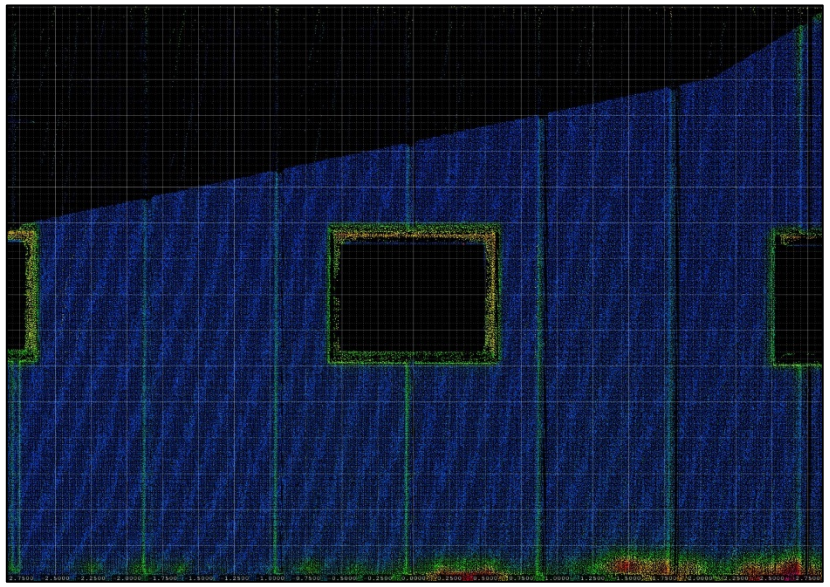


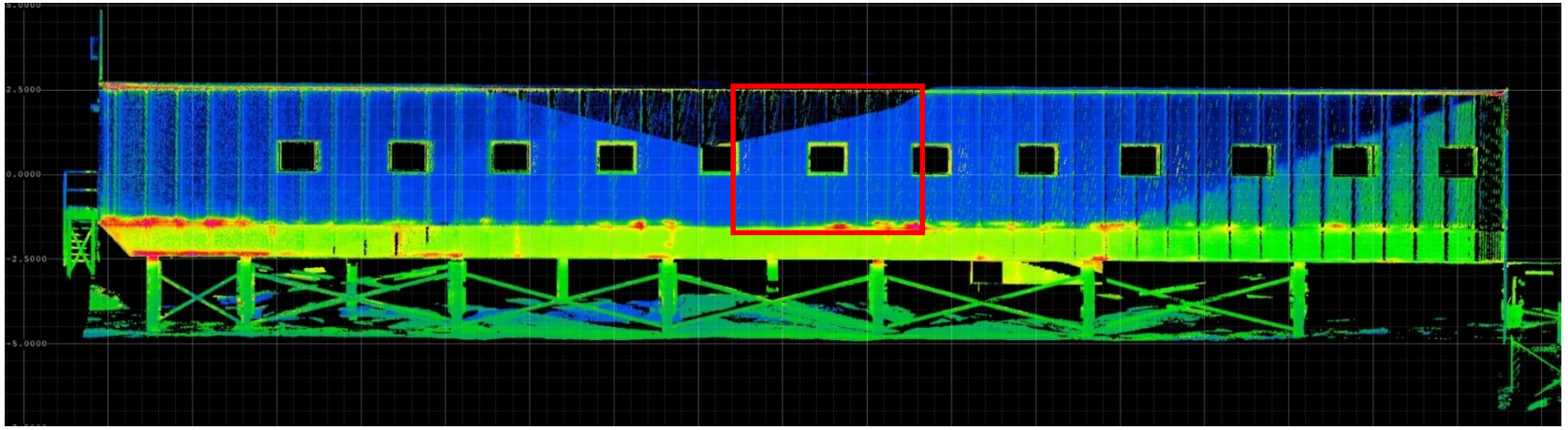




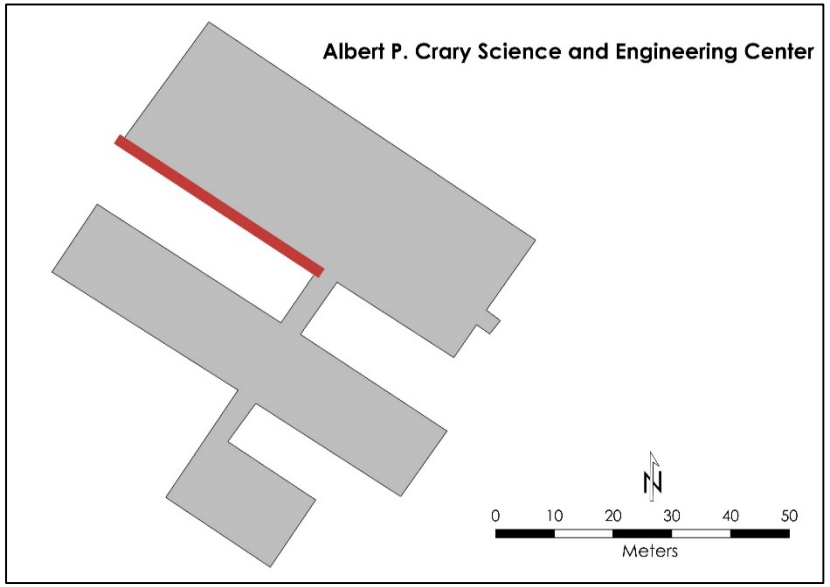
P1SW-W-05 -15◦C 5◦C

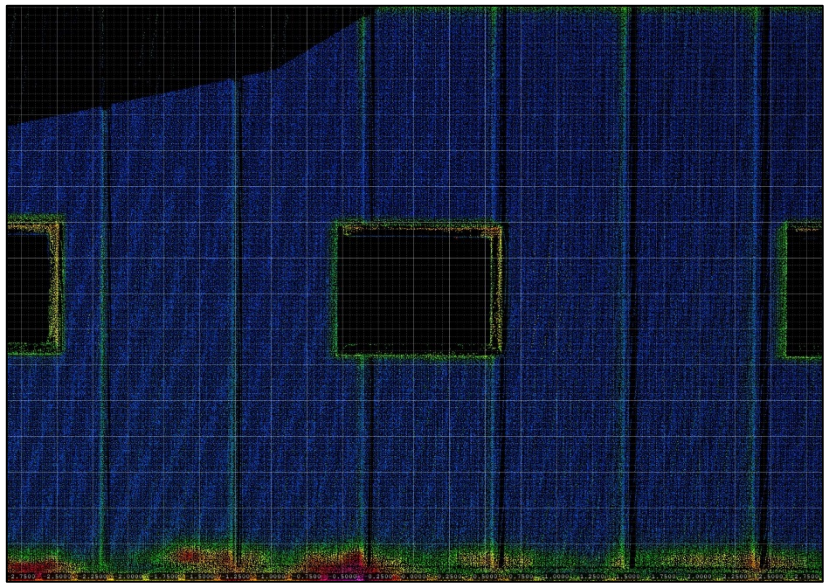


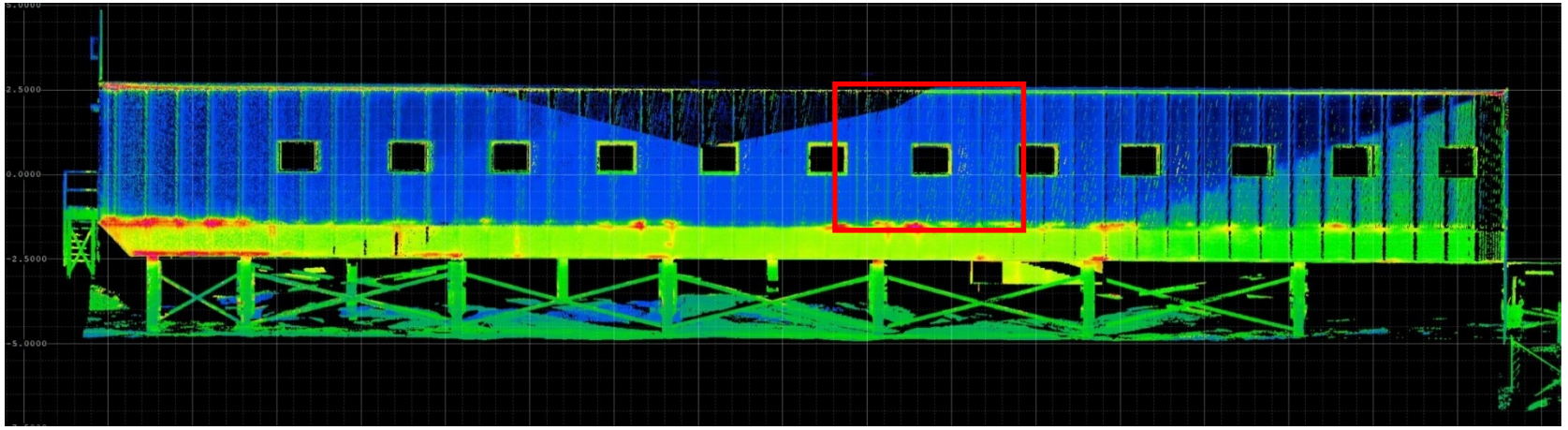




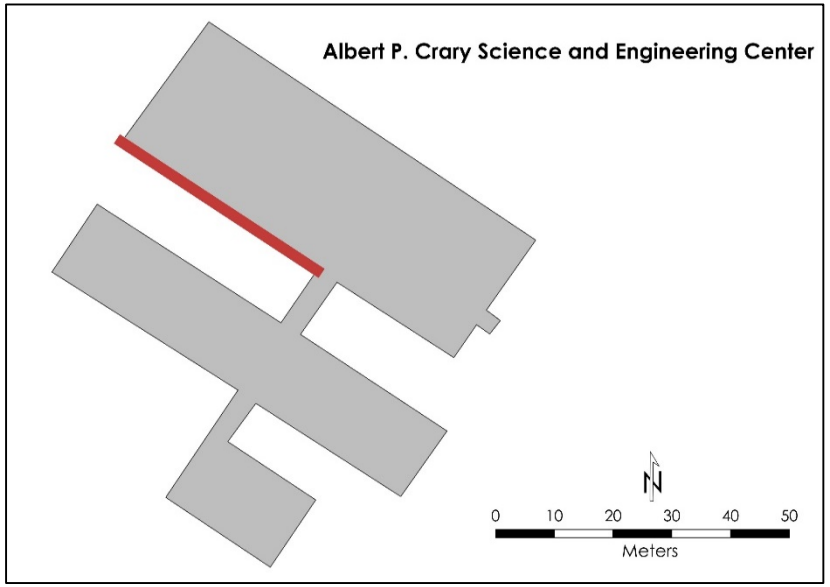
P1SW-W-06 -15◦C 5◦C

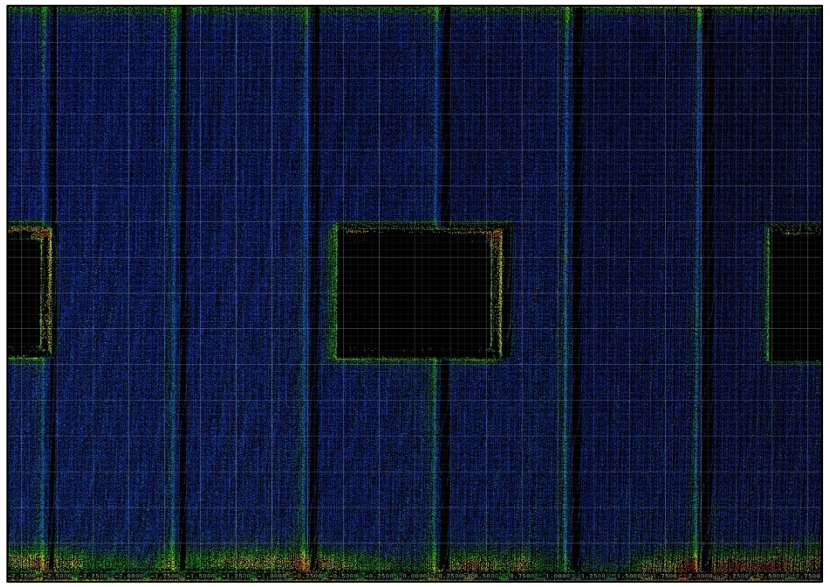


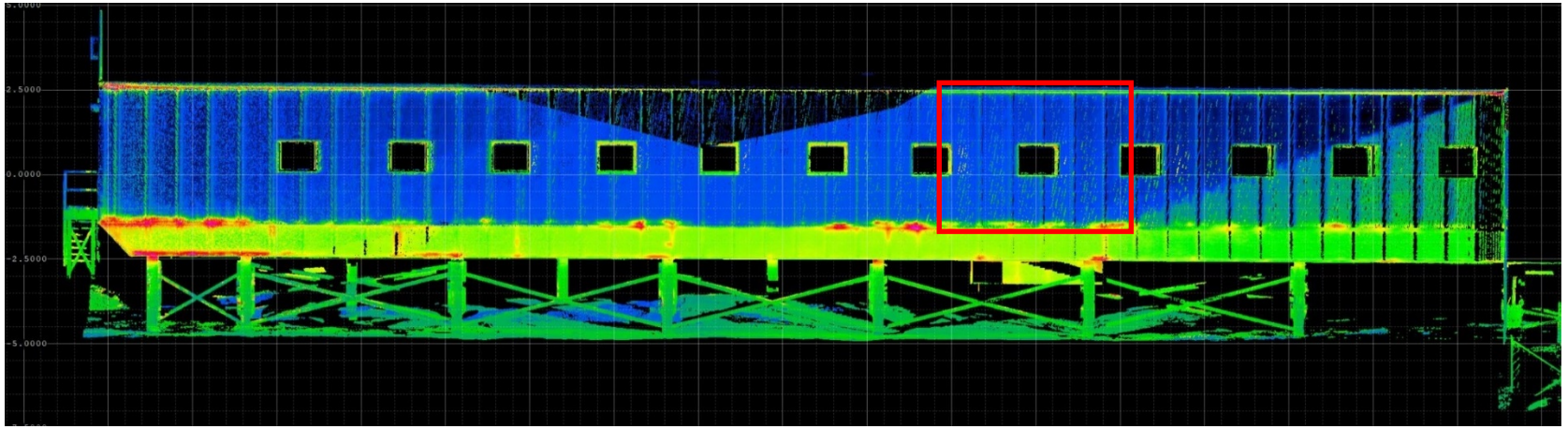




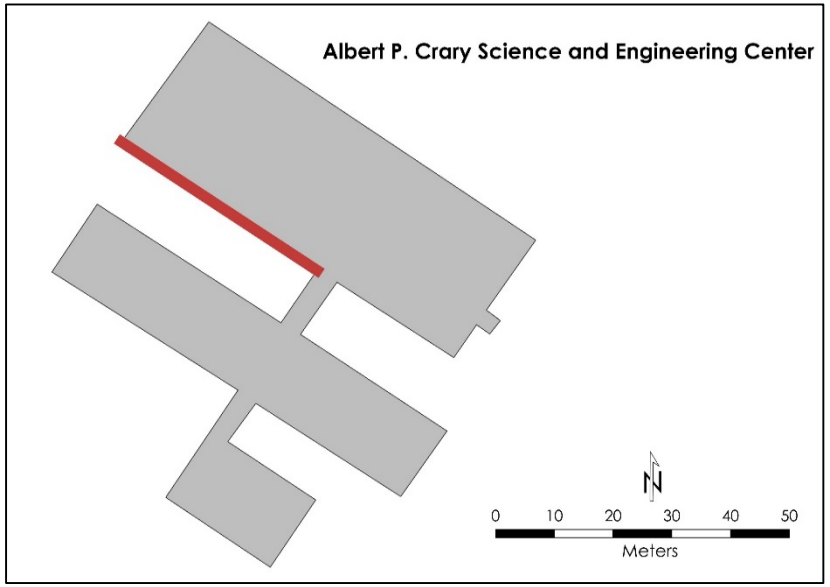
P1SW-W-07 -15◦C 5◦C

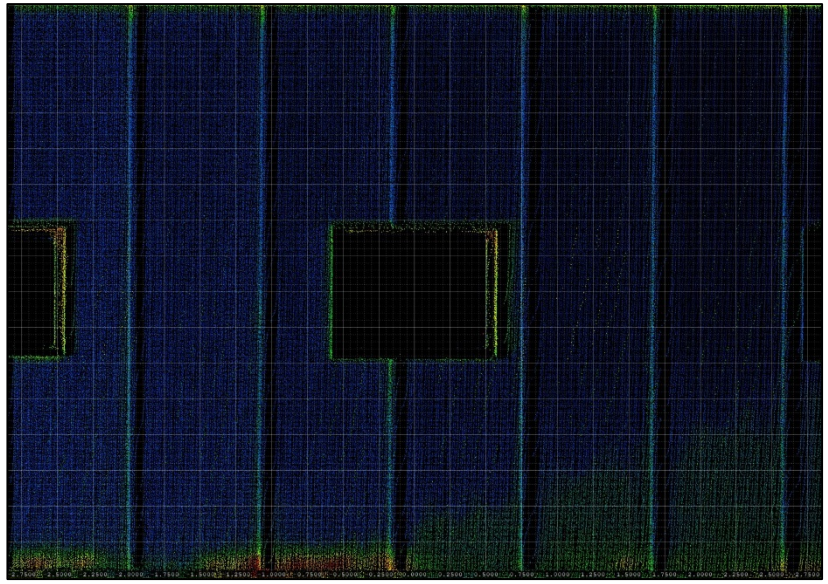


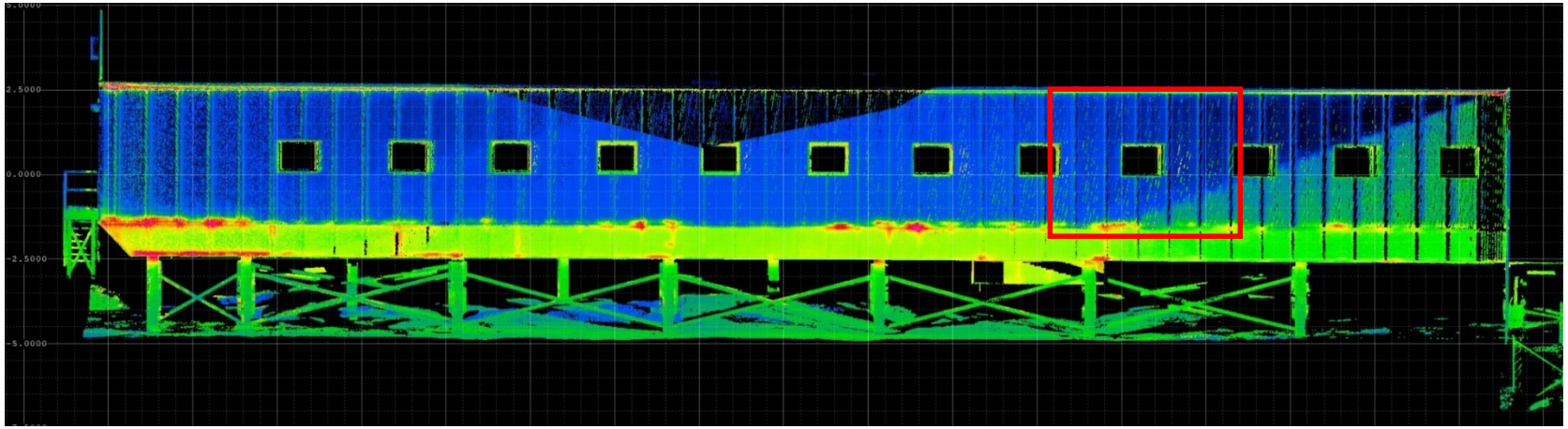




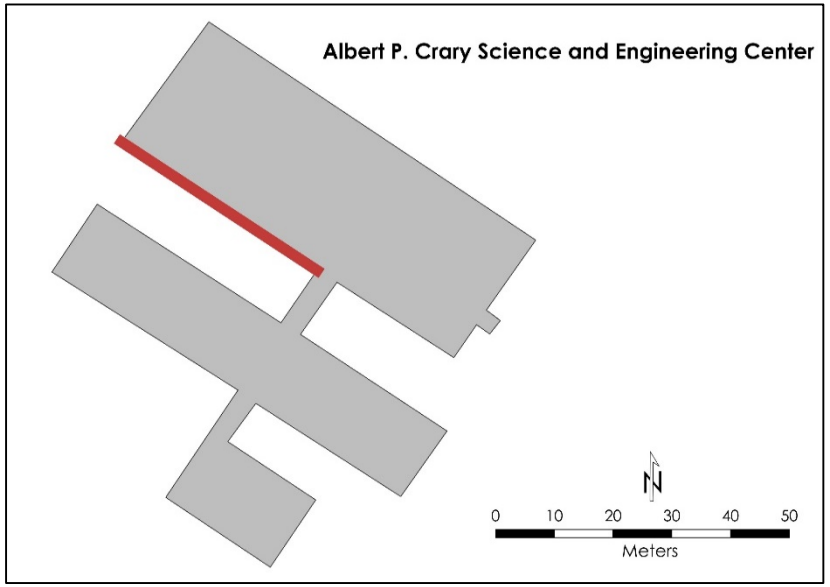
P1SW-W-08 -15◦C 5◦C

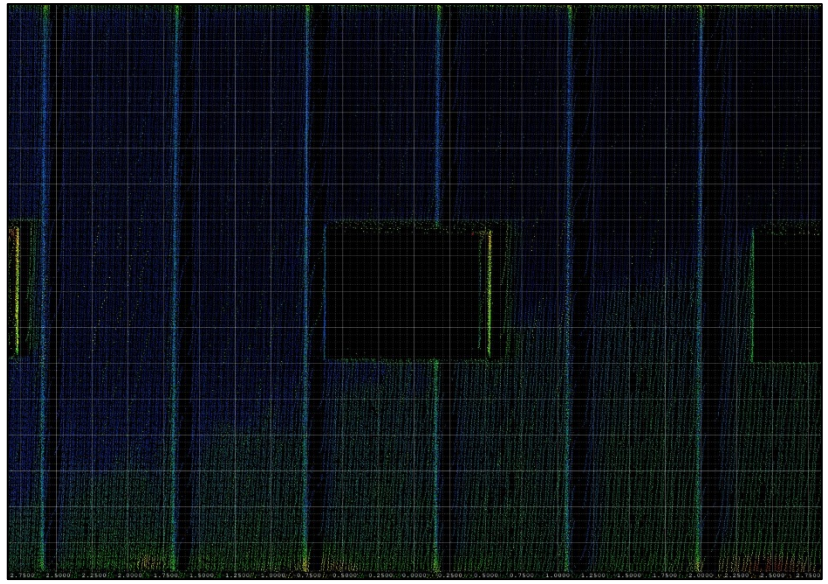


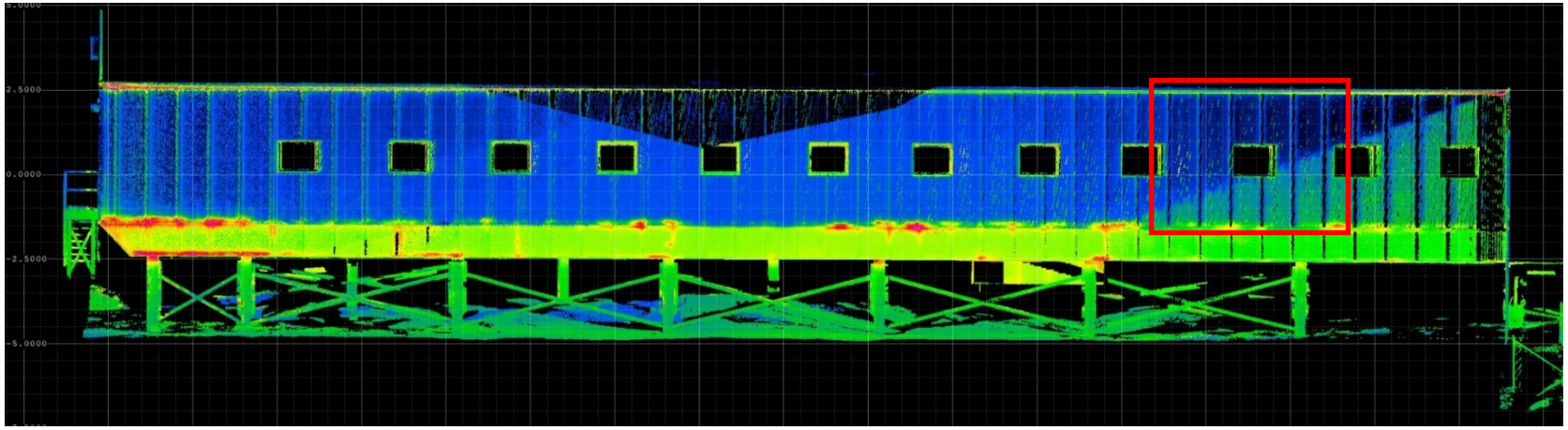




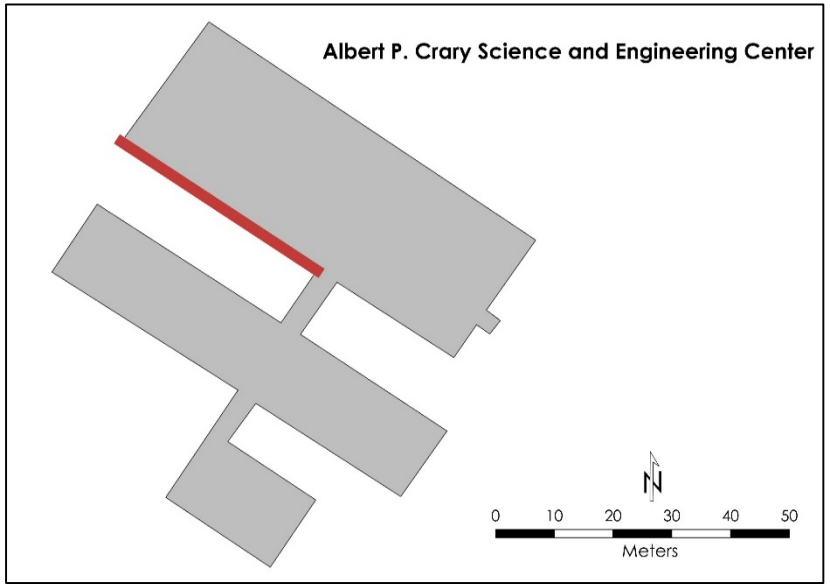
P1SW-W-09 -15◦C 5◦C

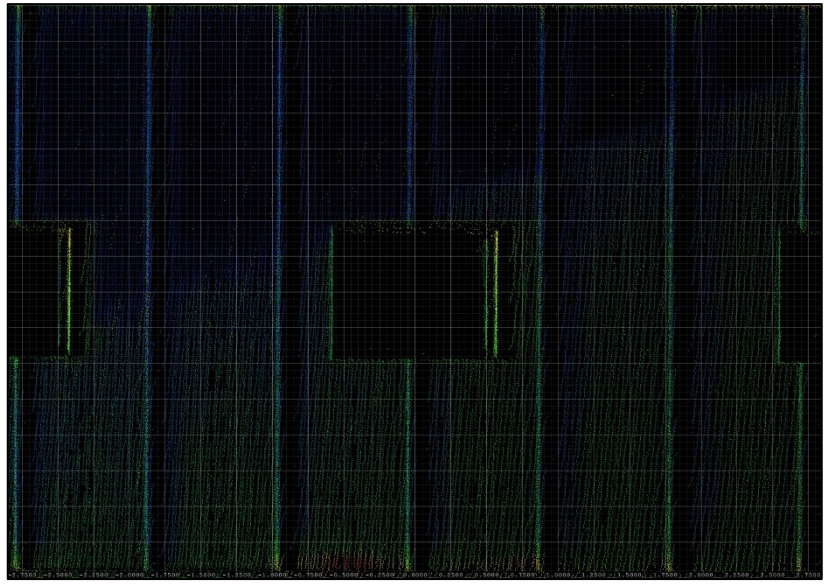


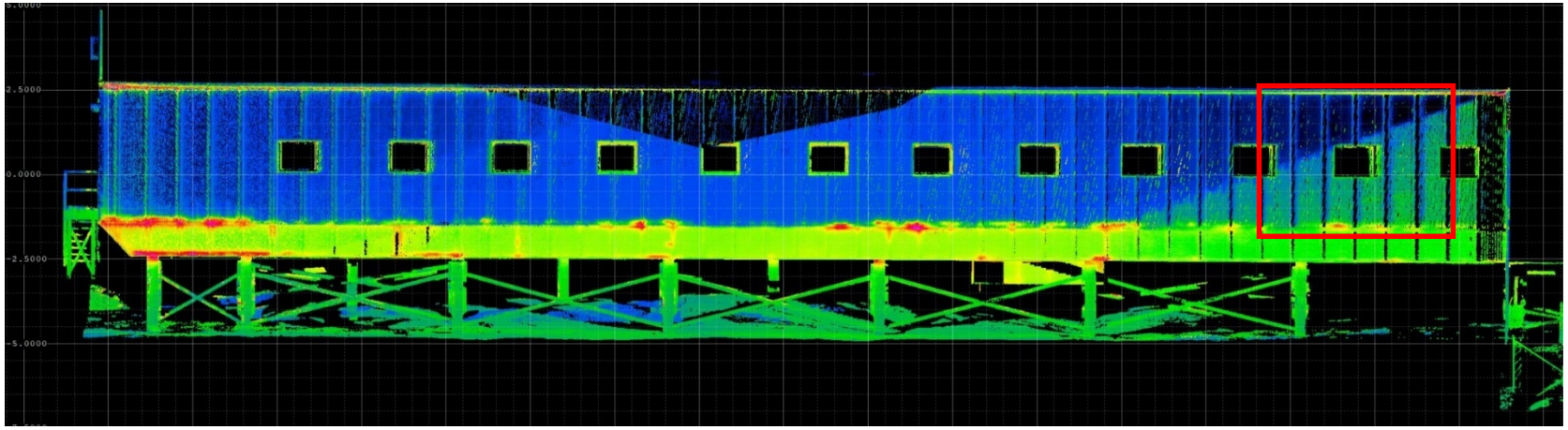




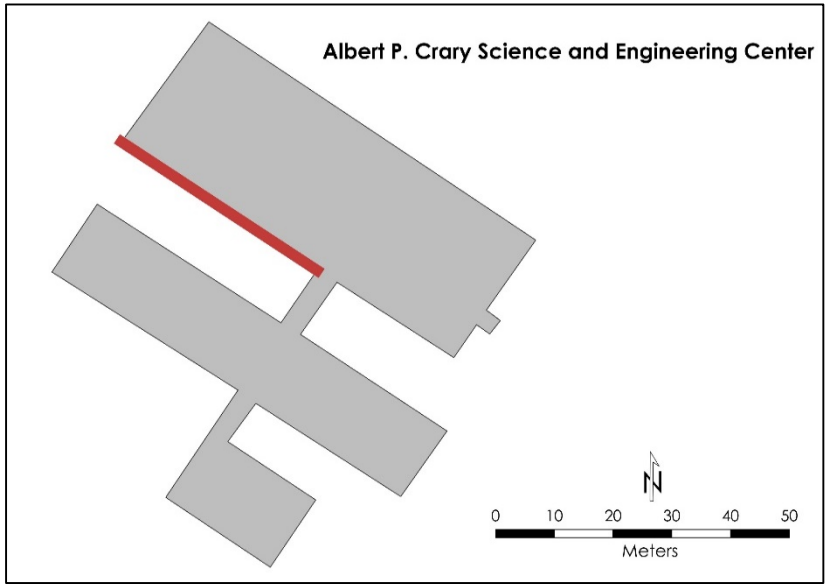
P1SW-W-10 -15◦C 5◦C

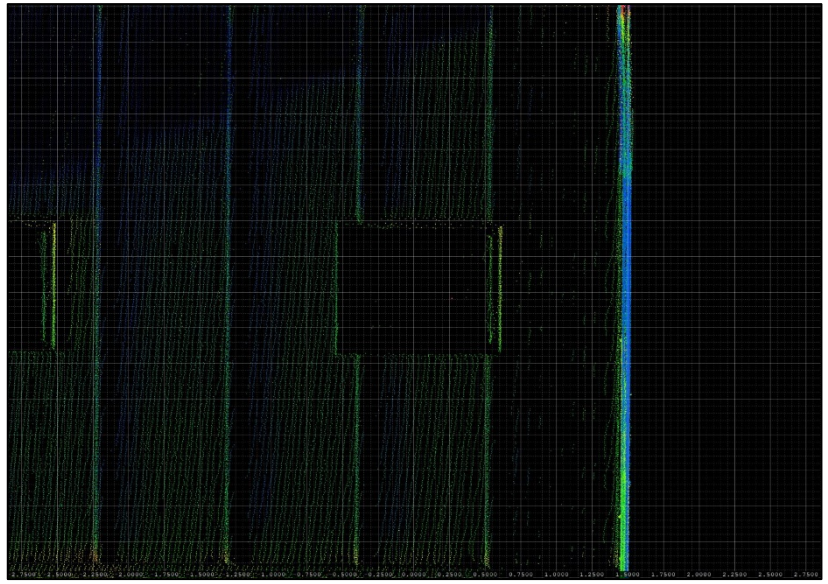


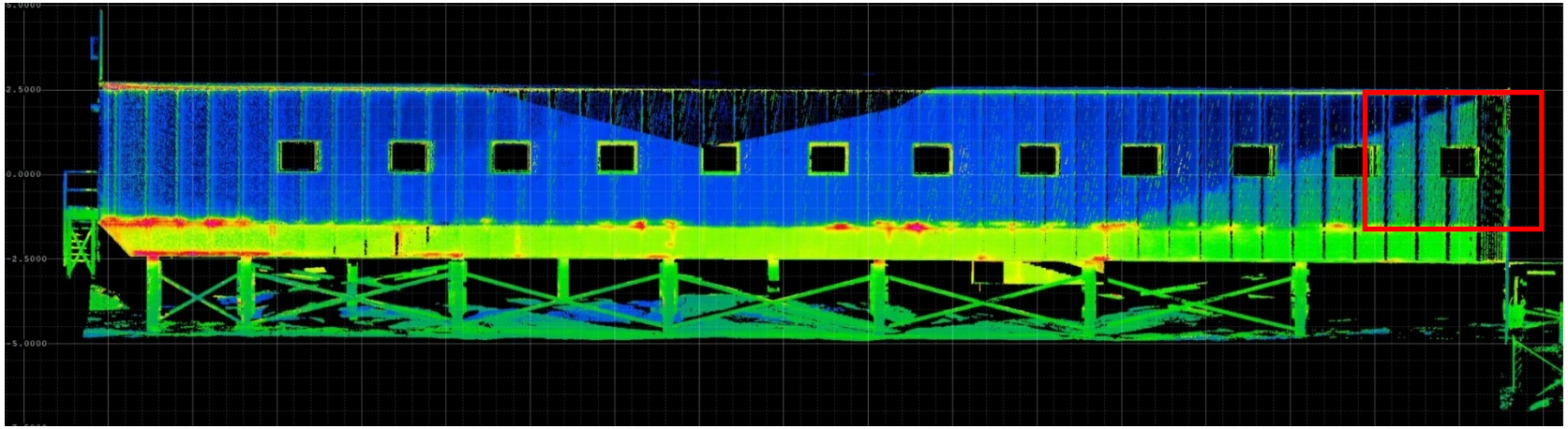




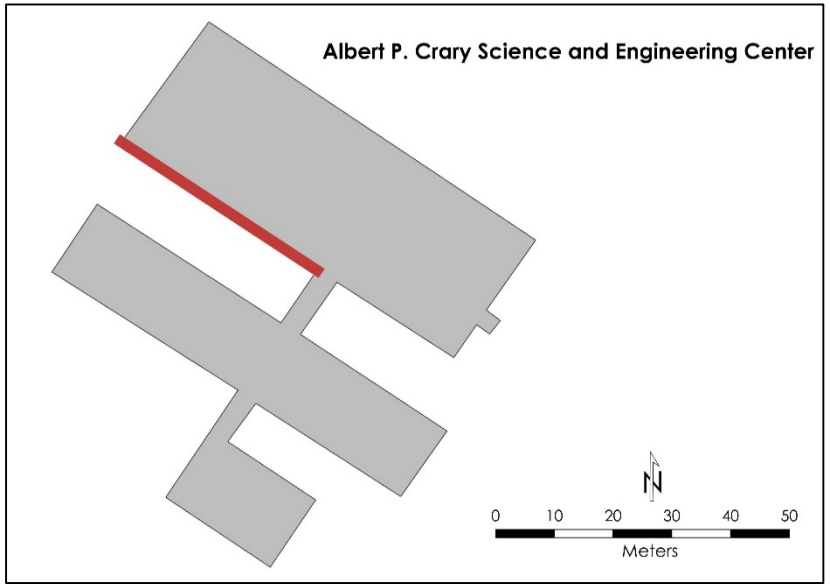
P1SW-W-11 -15◦C 5◦C

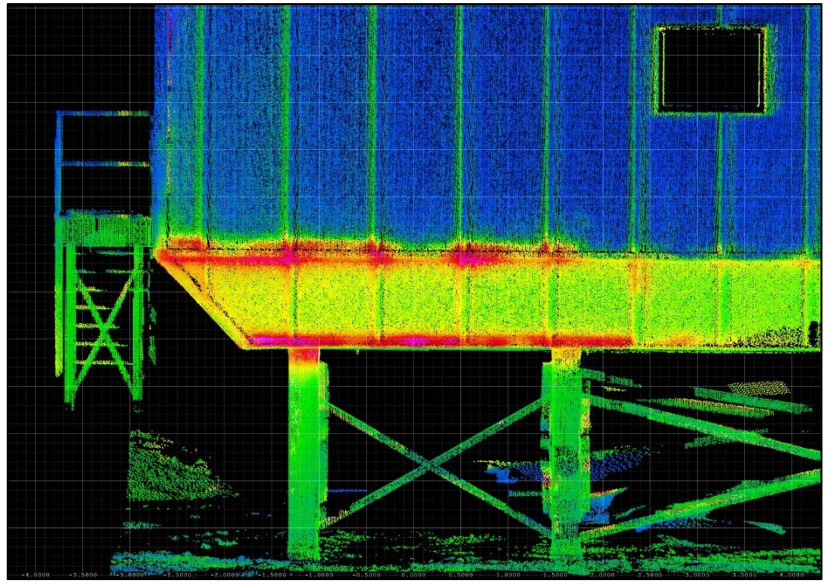


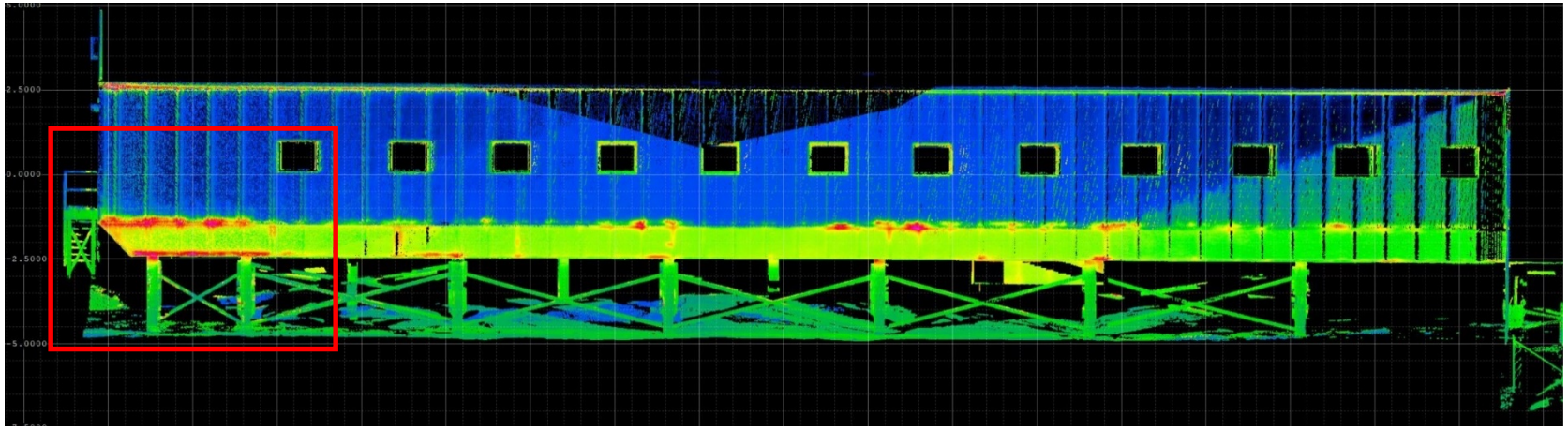




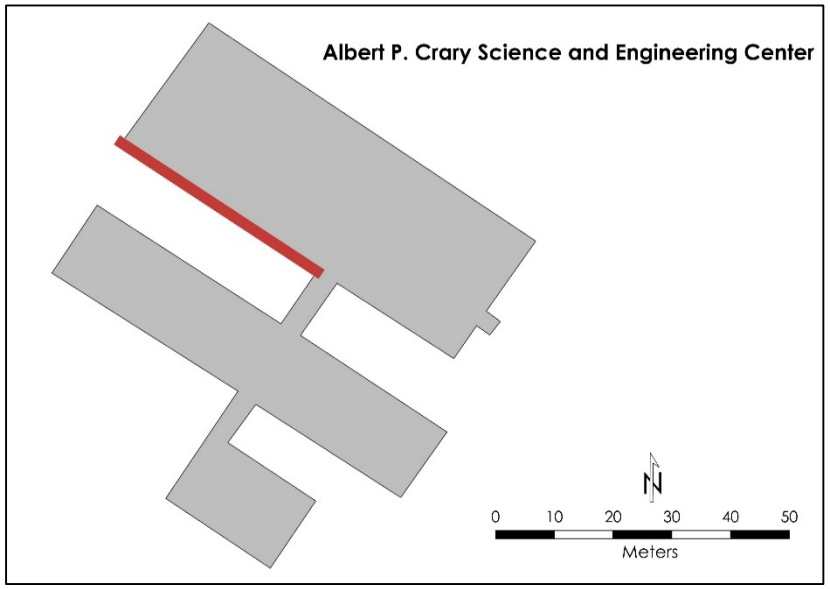
P1SW-W-12 -15◦C 5◦C

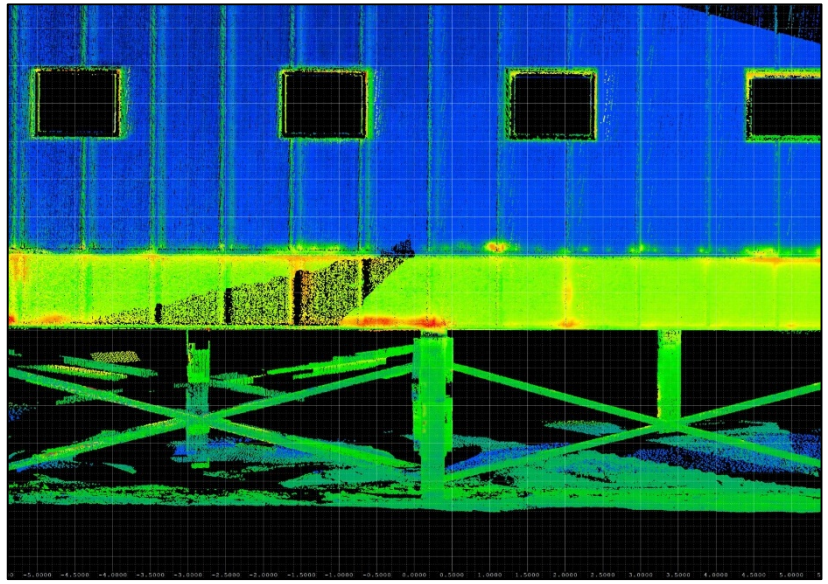


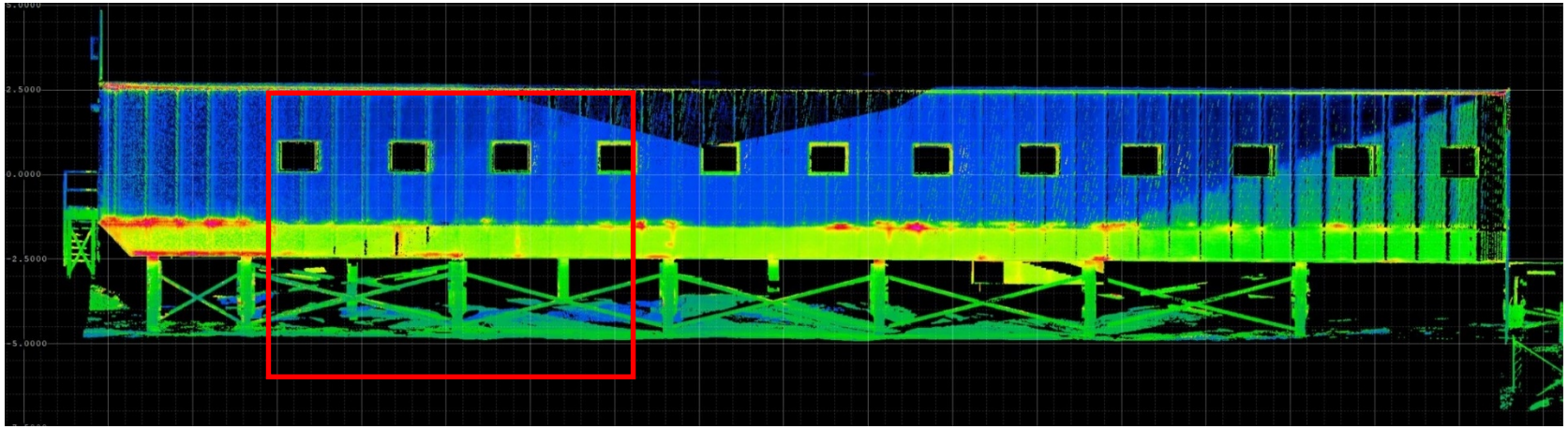




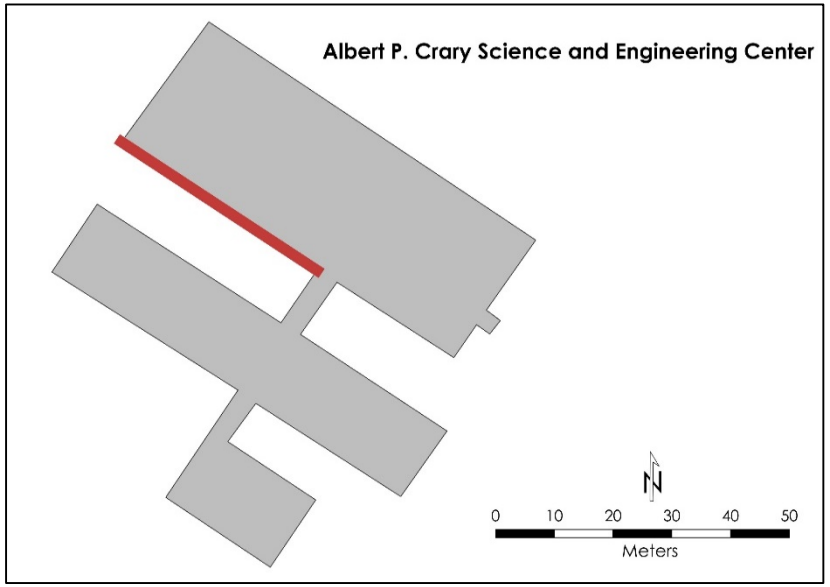
P1SW-TA-01 -15◦C 5◦C

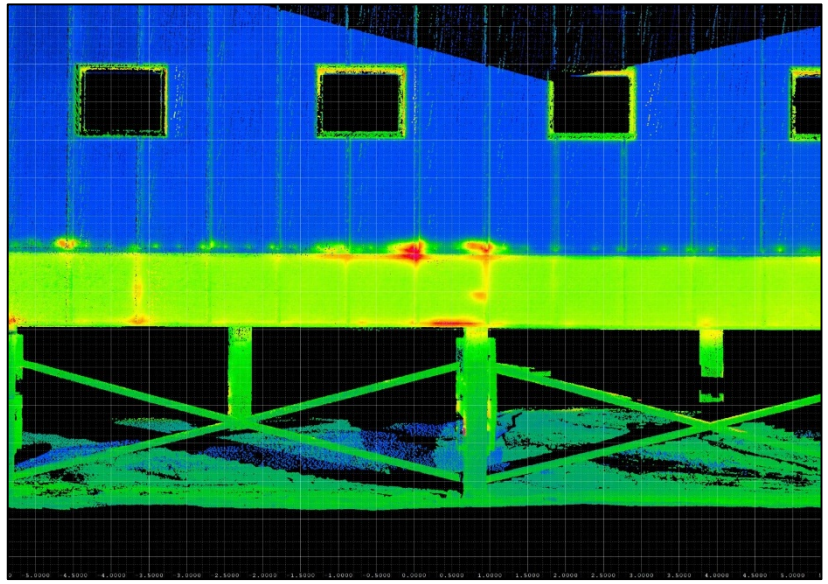


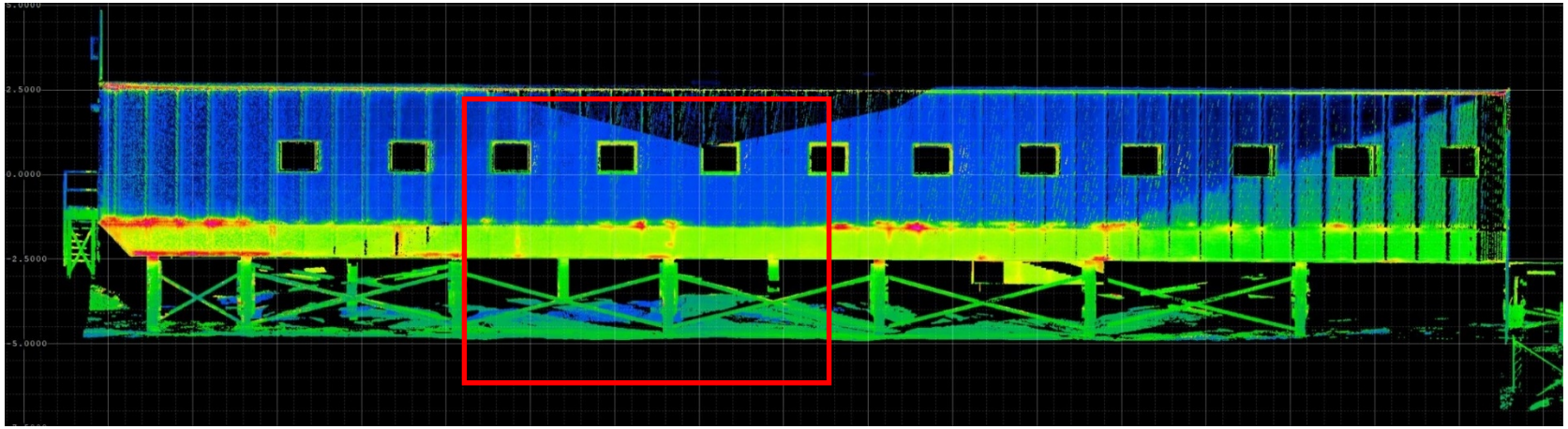




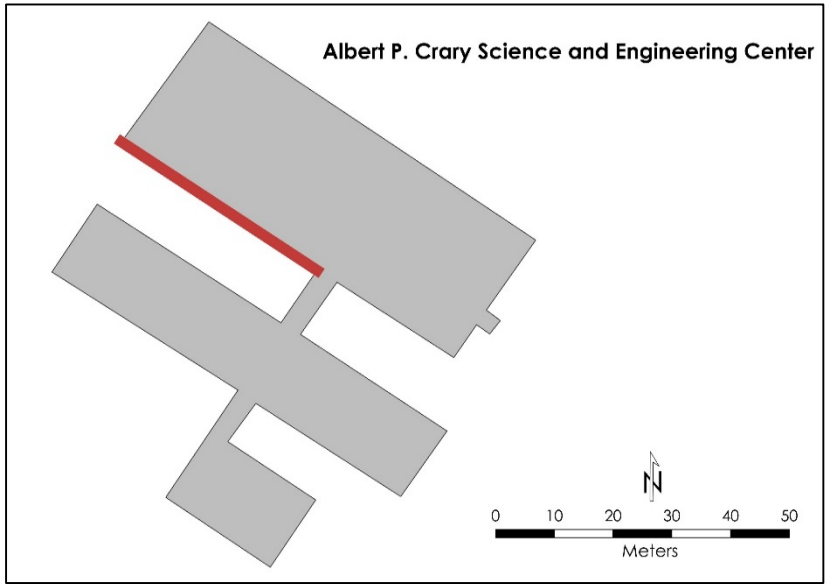
P1SW-TA-02 -15◦C 5◦C

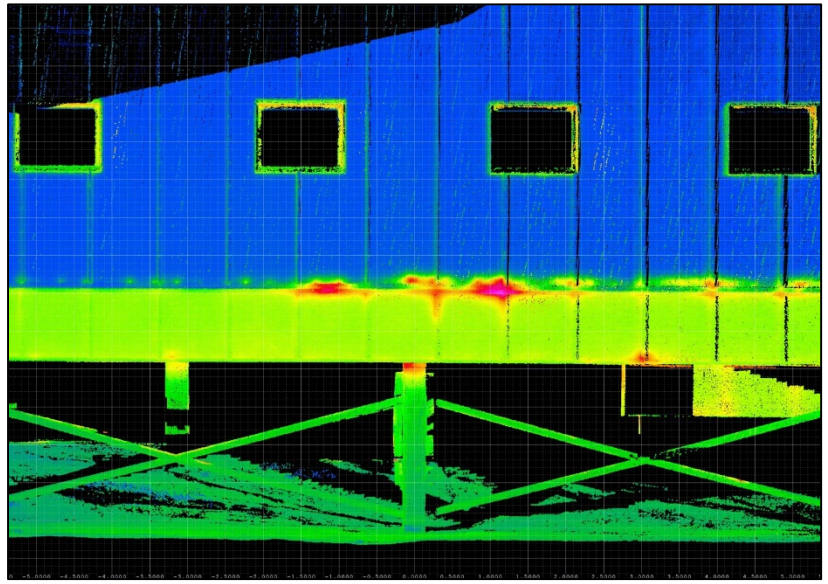


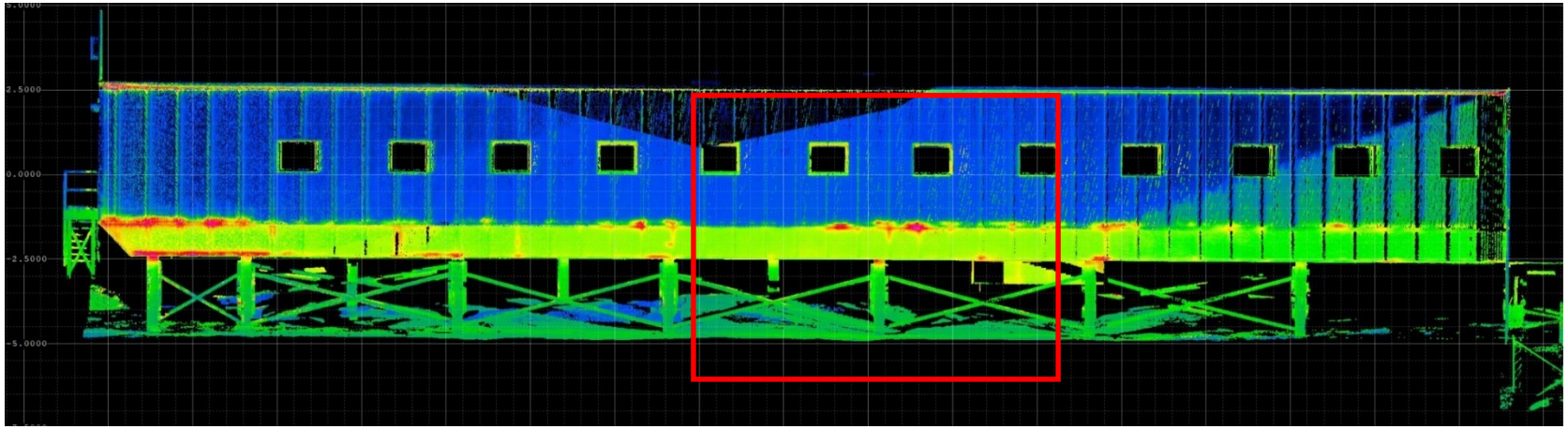




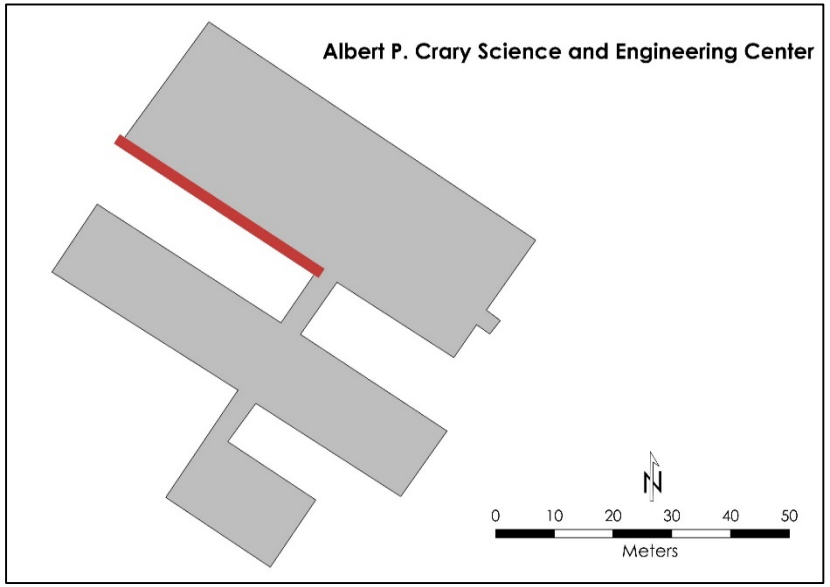
P1SW-TA-03 -15◦C 5◦C

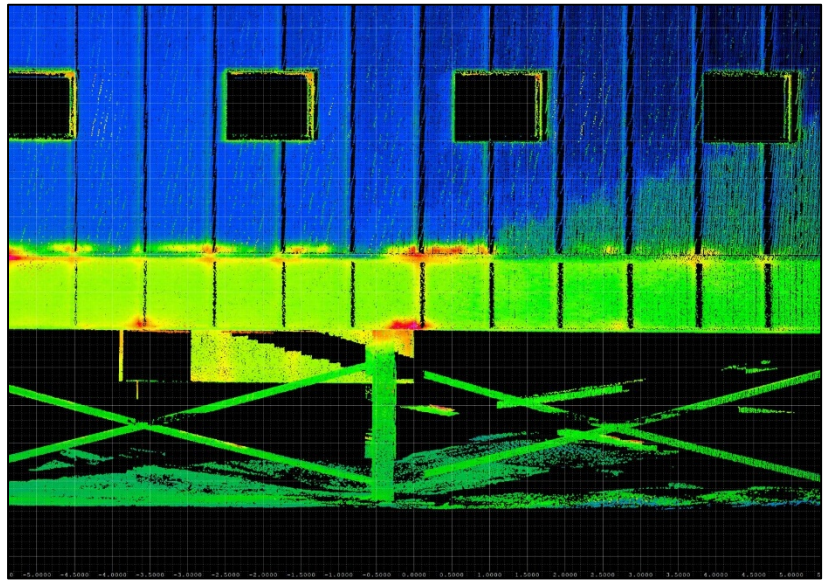


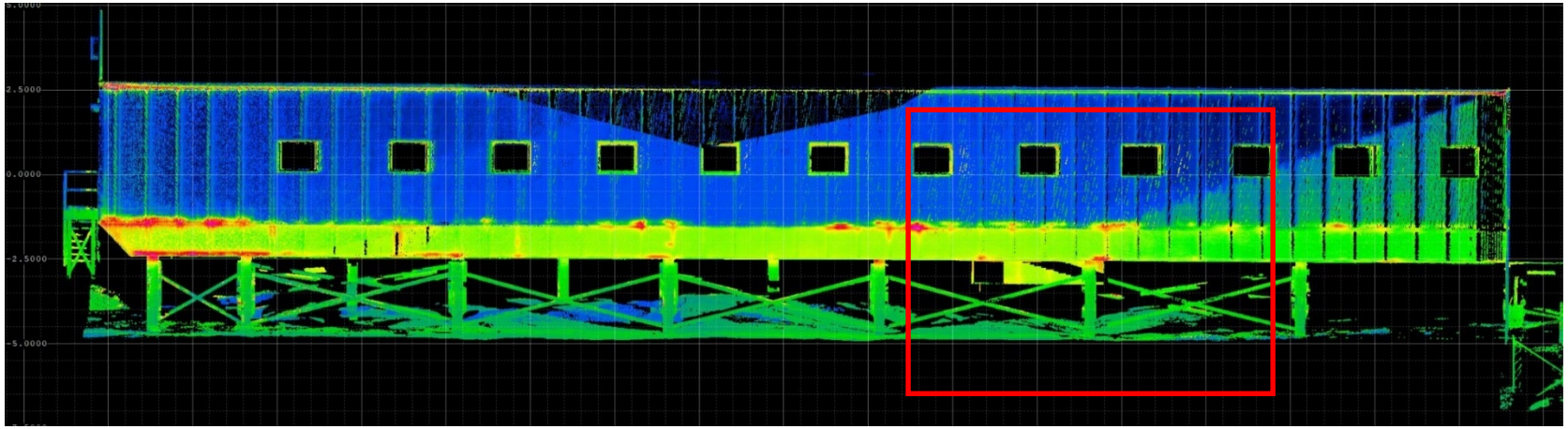




P1SW-TA-04 -15◦C 5◦C





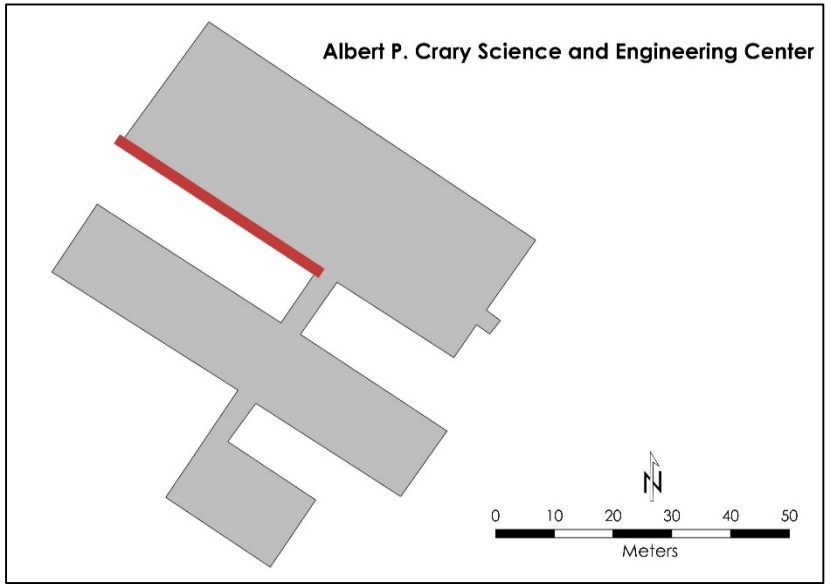


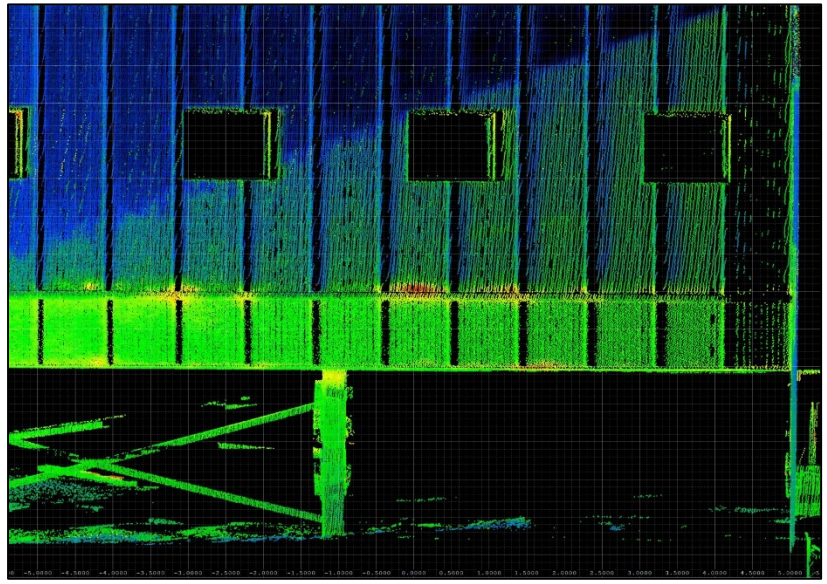
P1SW-TA-05

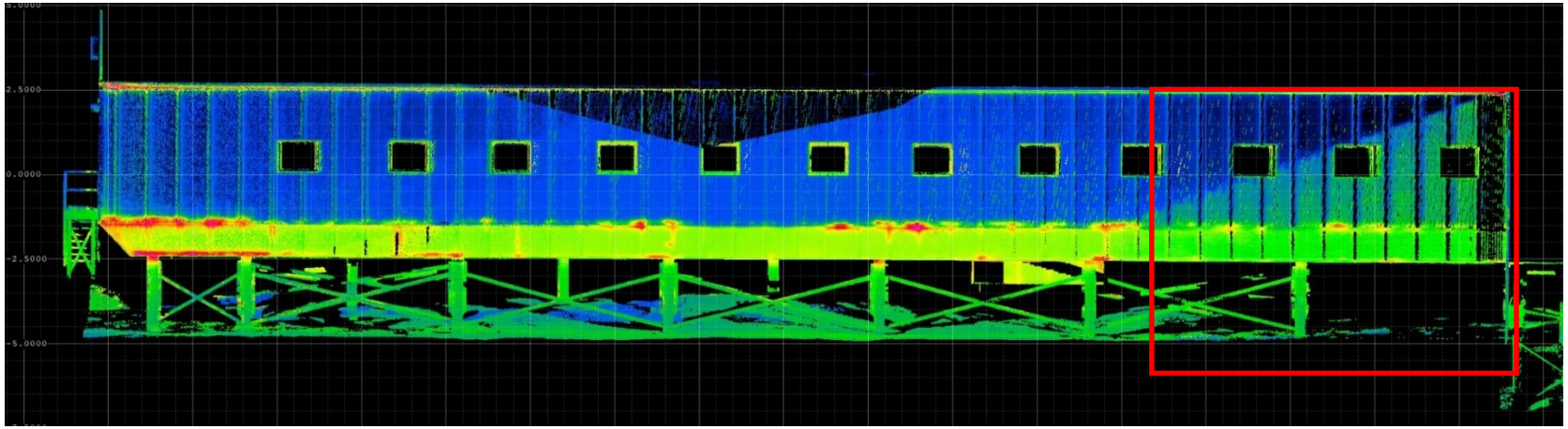
-15◦C



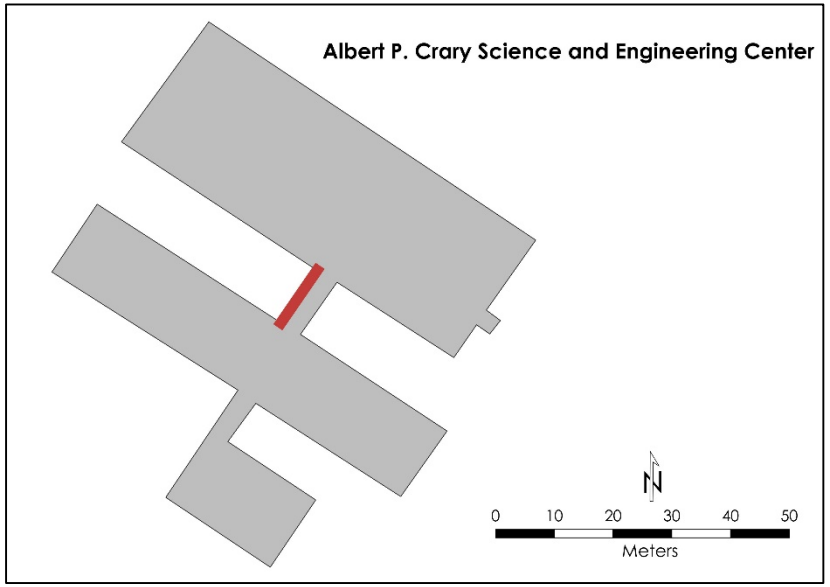
5◦C

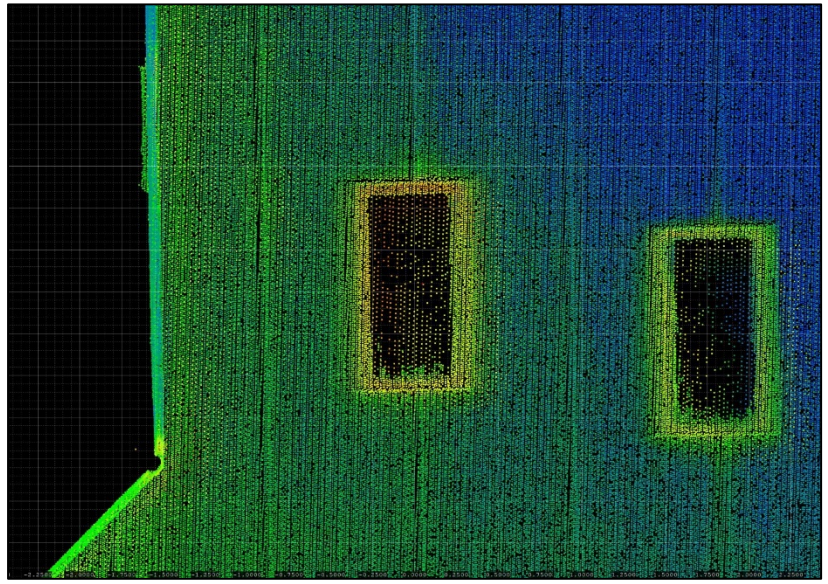


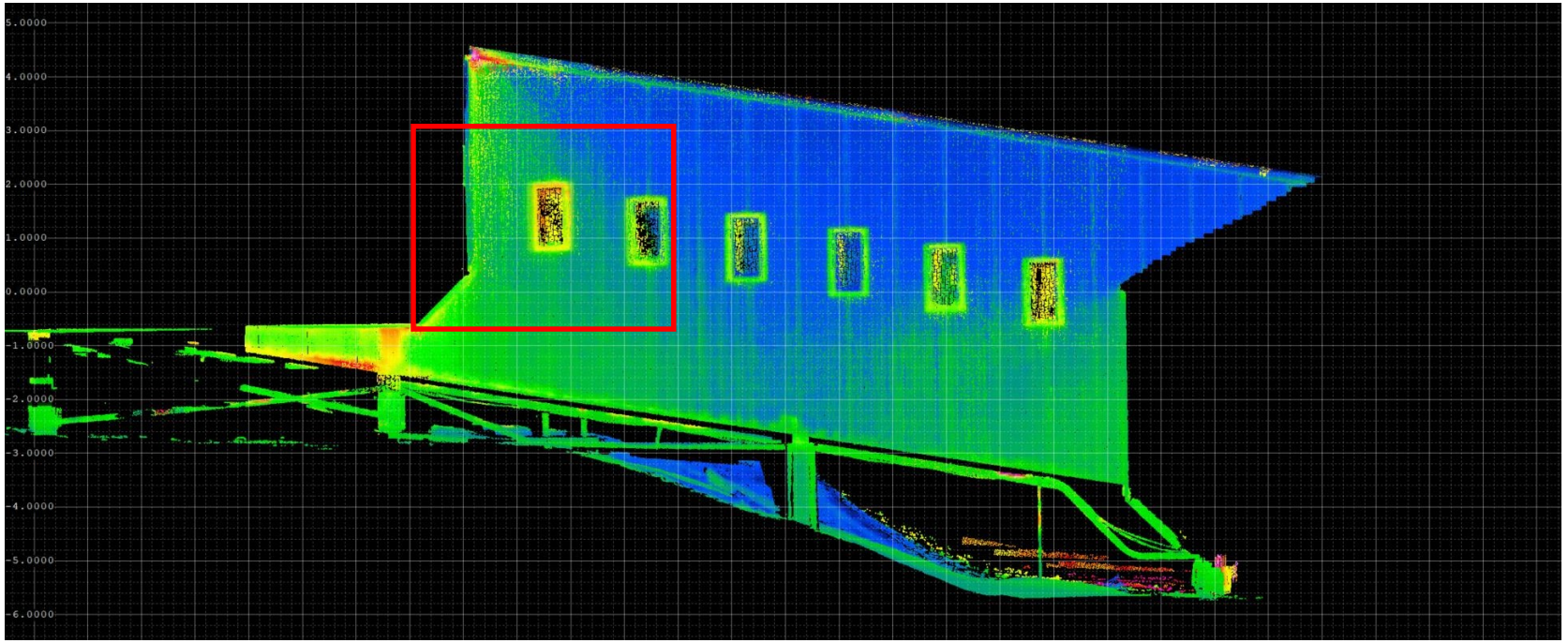




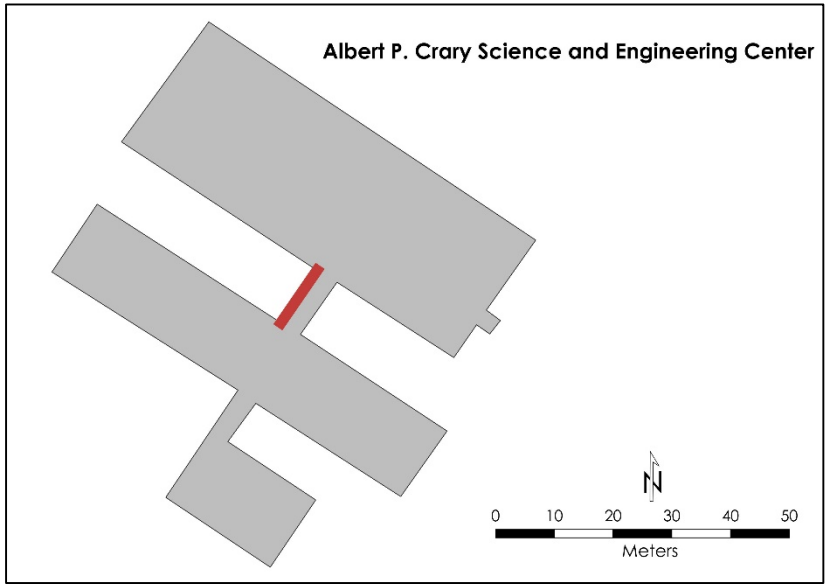
P1SW-TA-06 -15◦C 5◦C

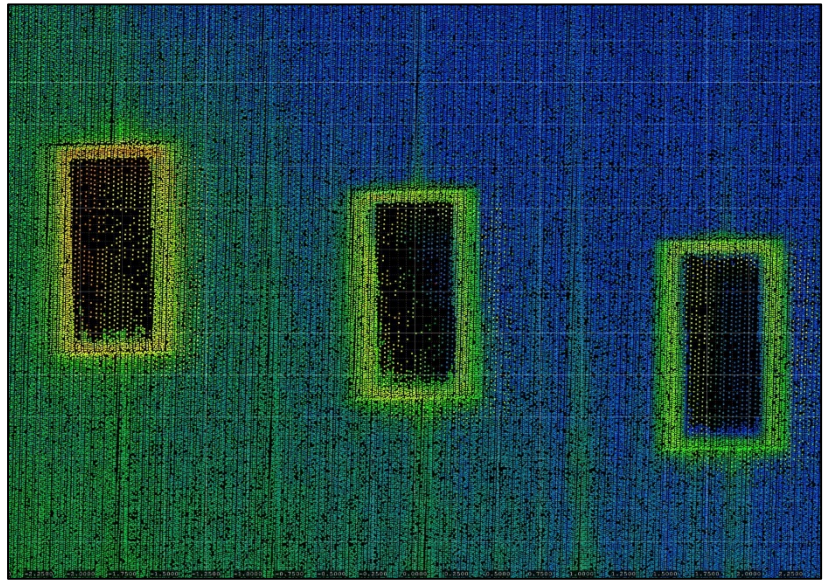


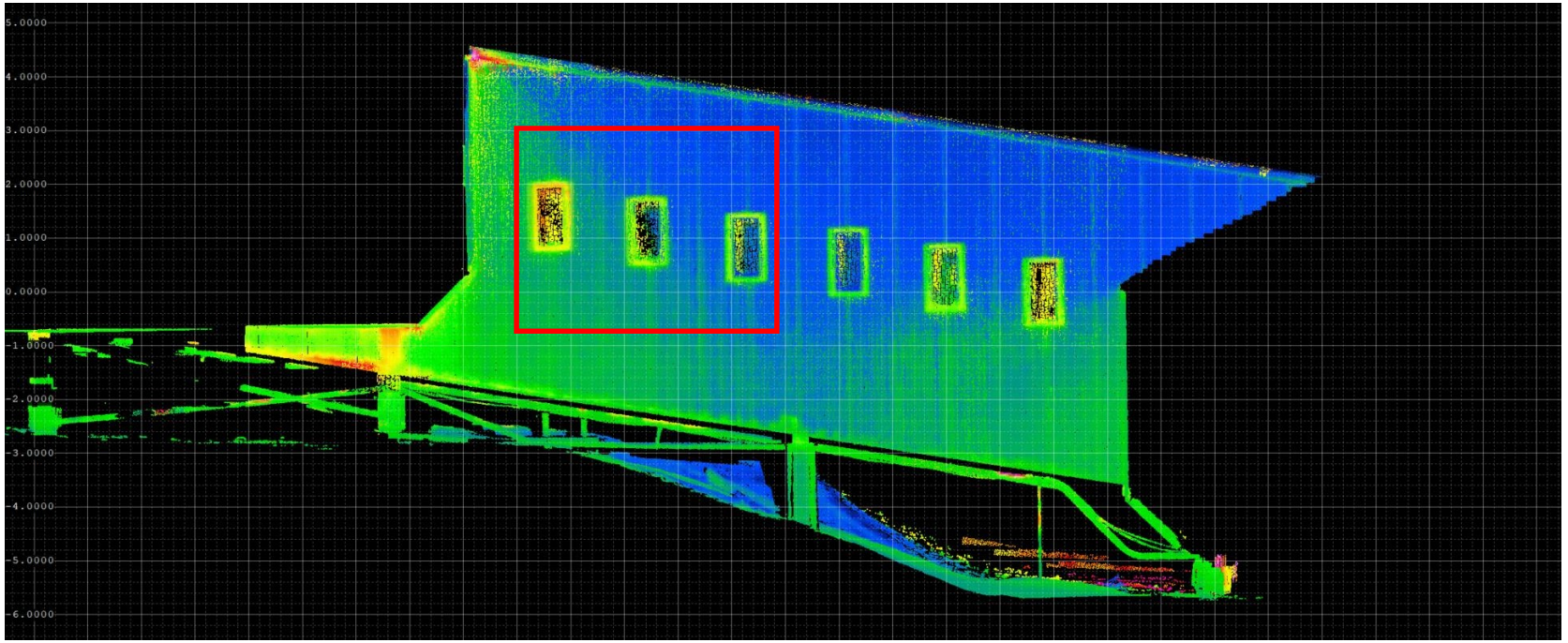




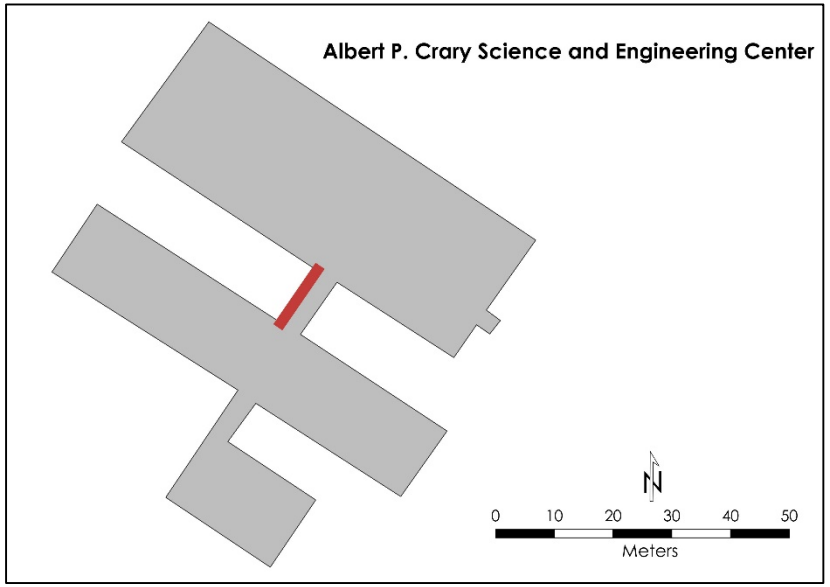
P2CW-W-01 -15◦C 5◦C

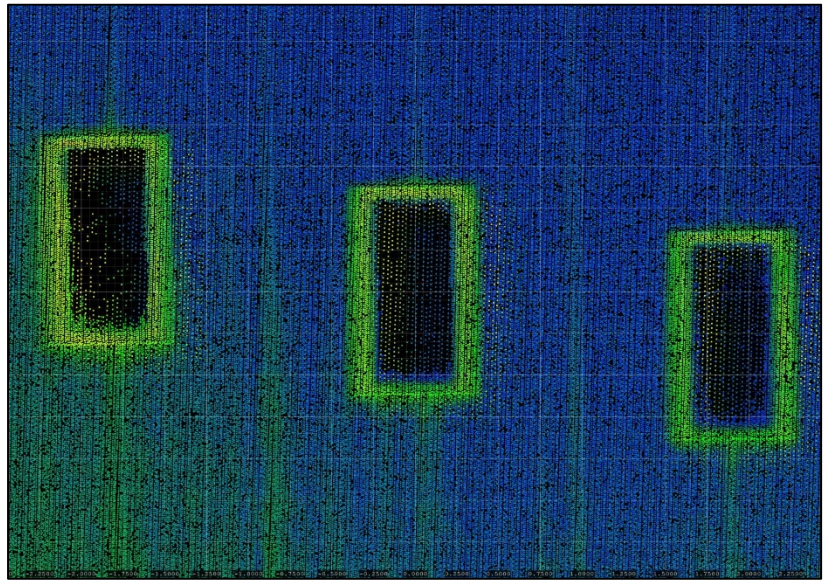


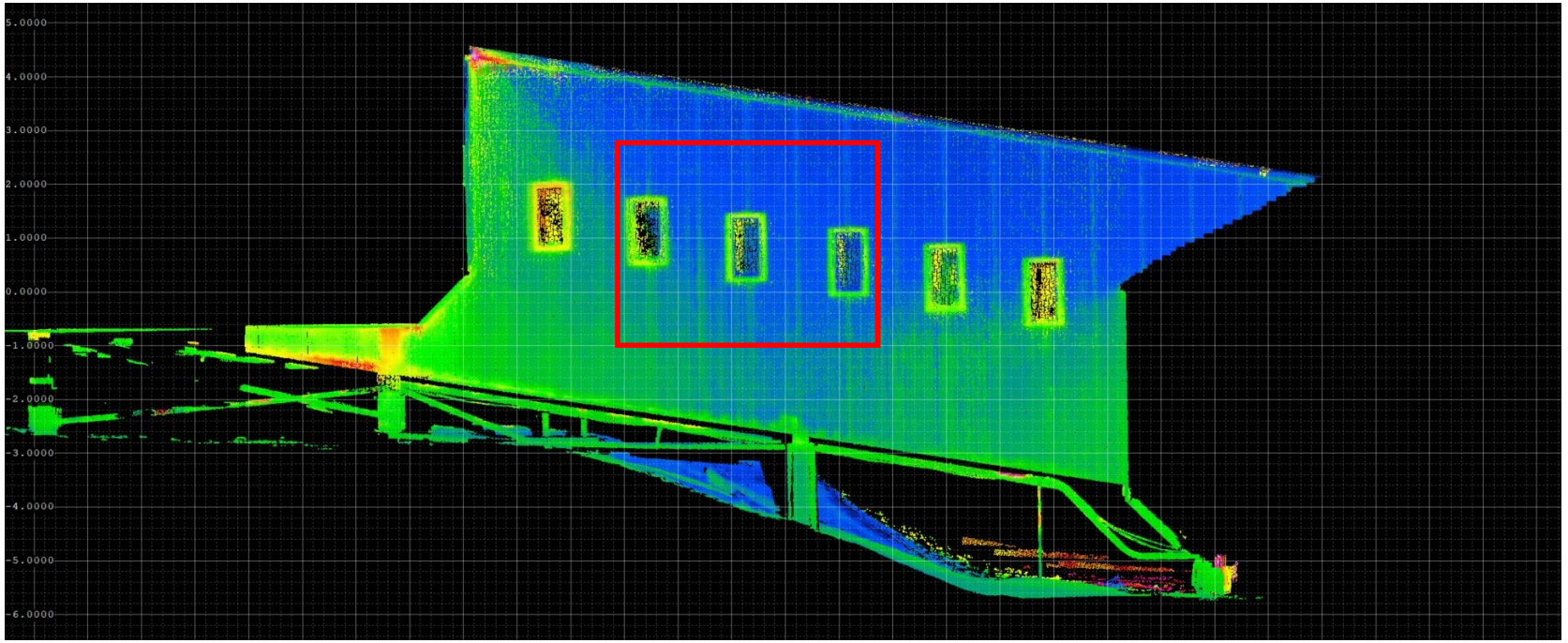




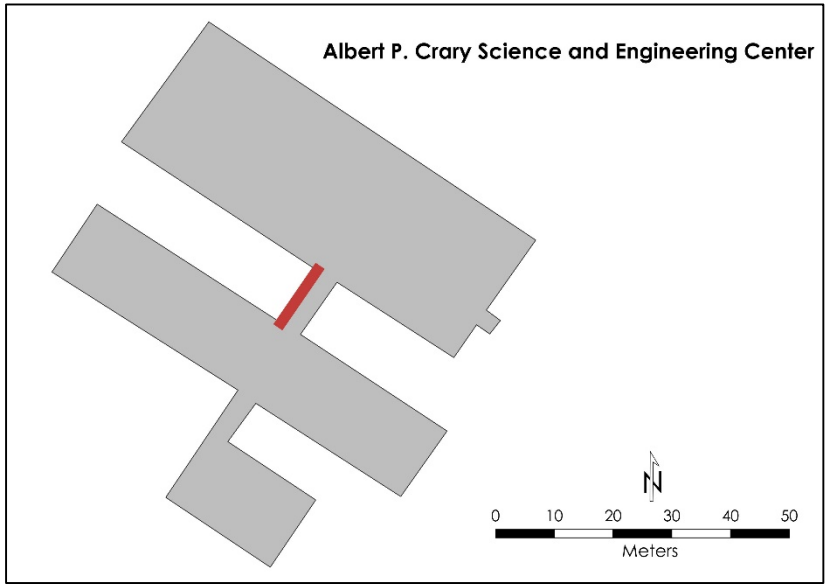
P2CW-W-02 -15◦C 5◦C

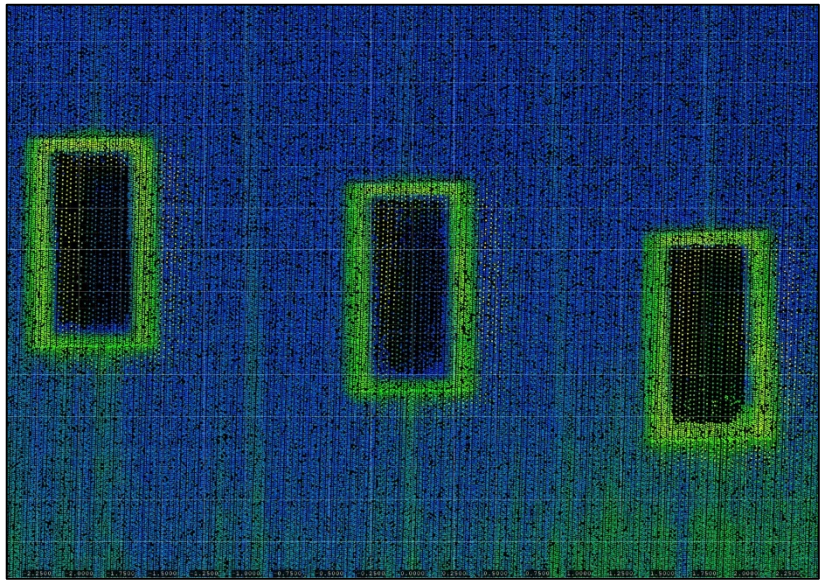


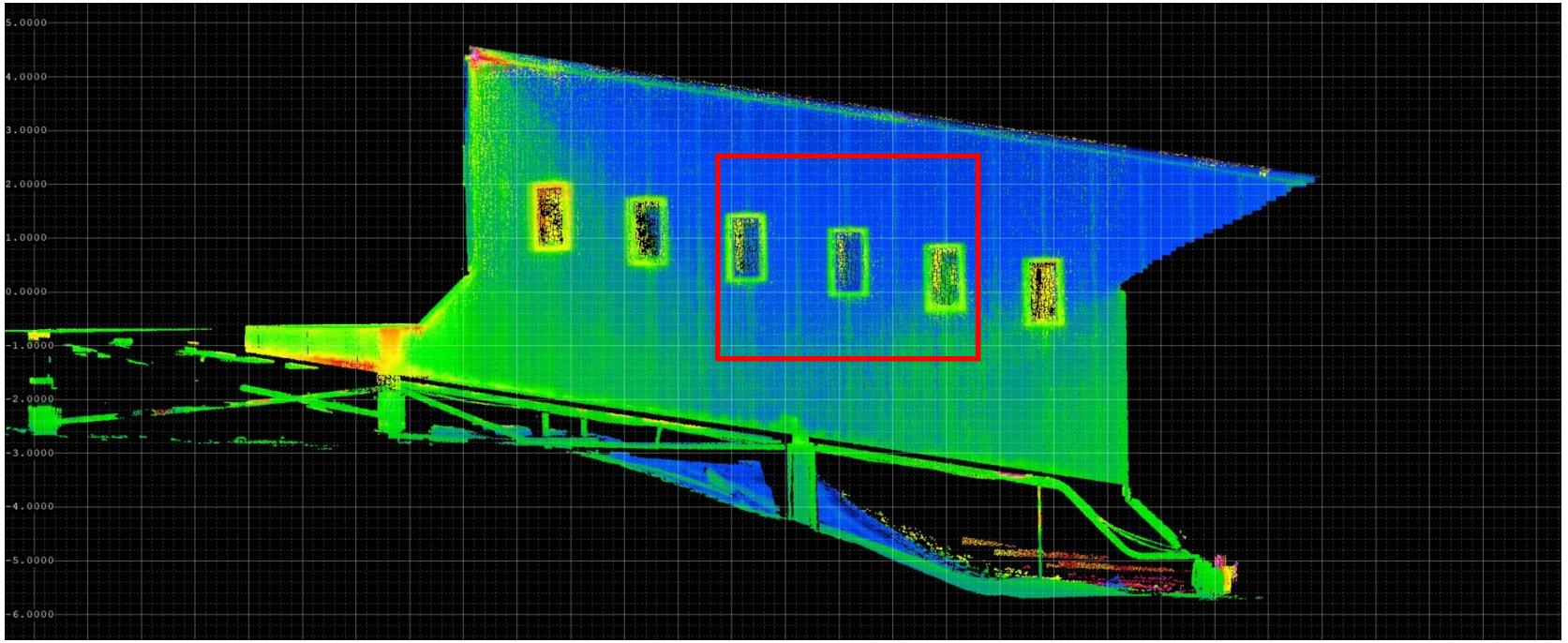




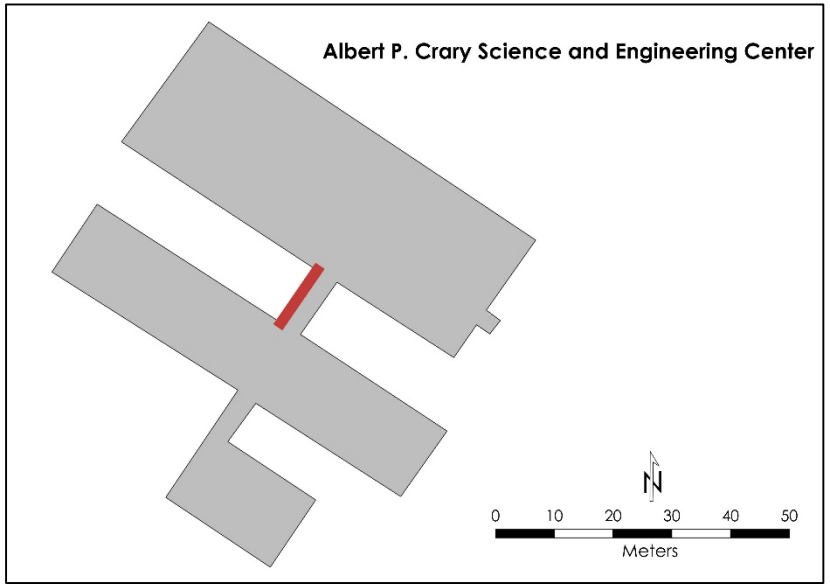
P2CW-W-03 -15◦C 5◦C

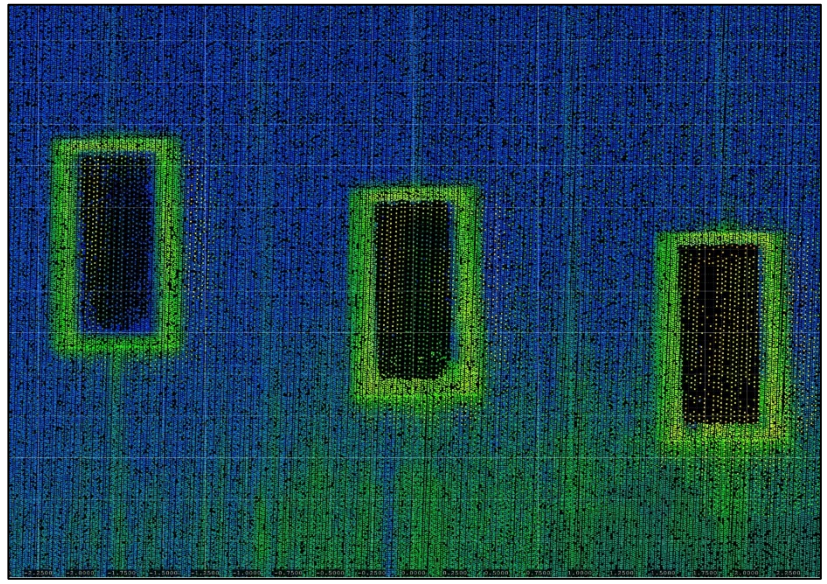


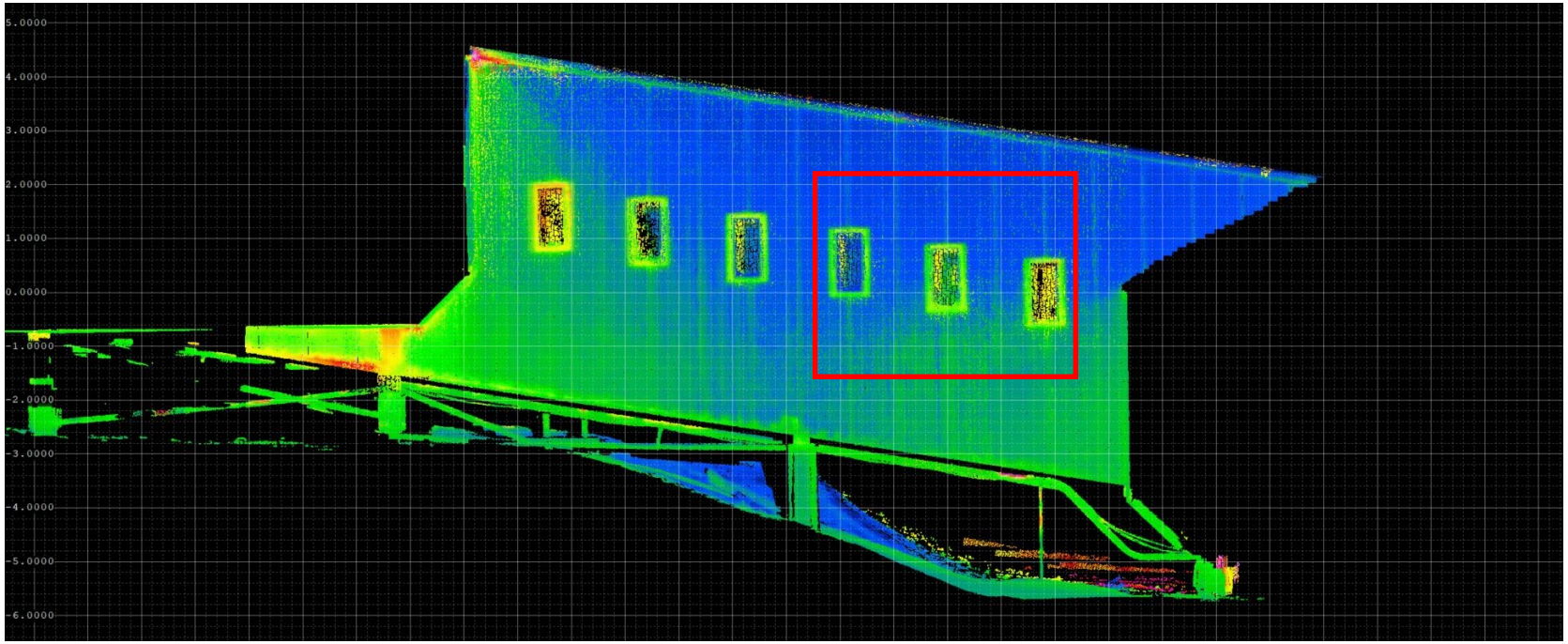




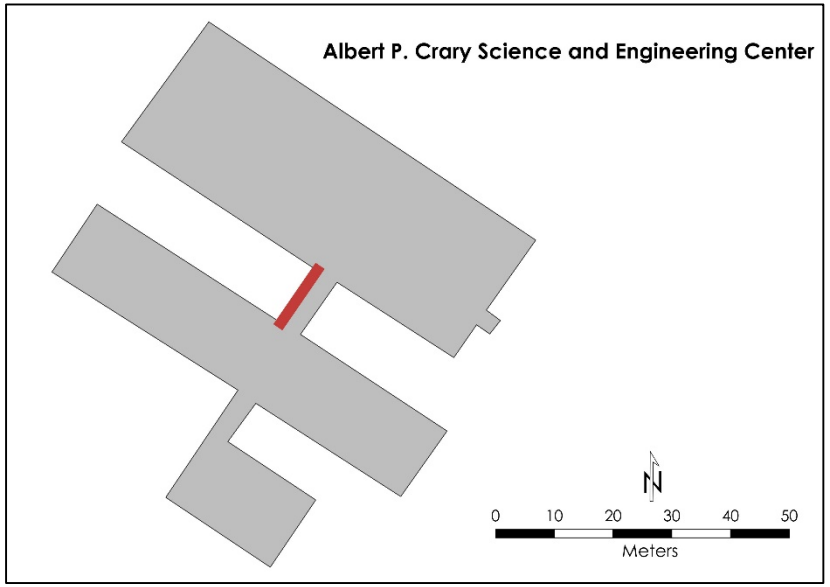
P2CW-W-04 -15◦C 5◦C

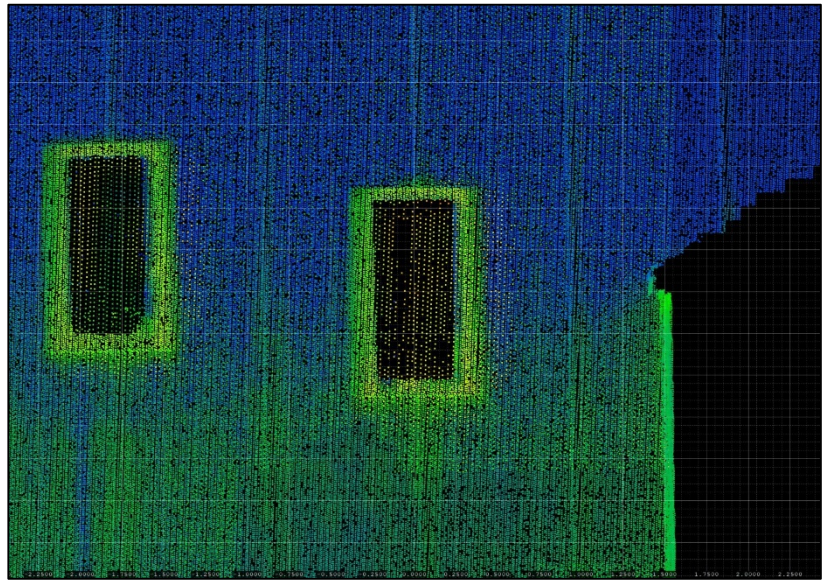


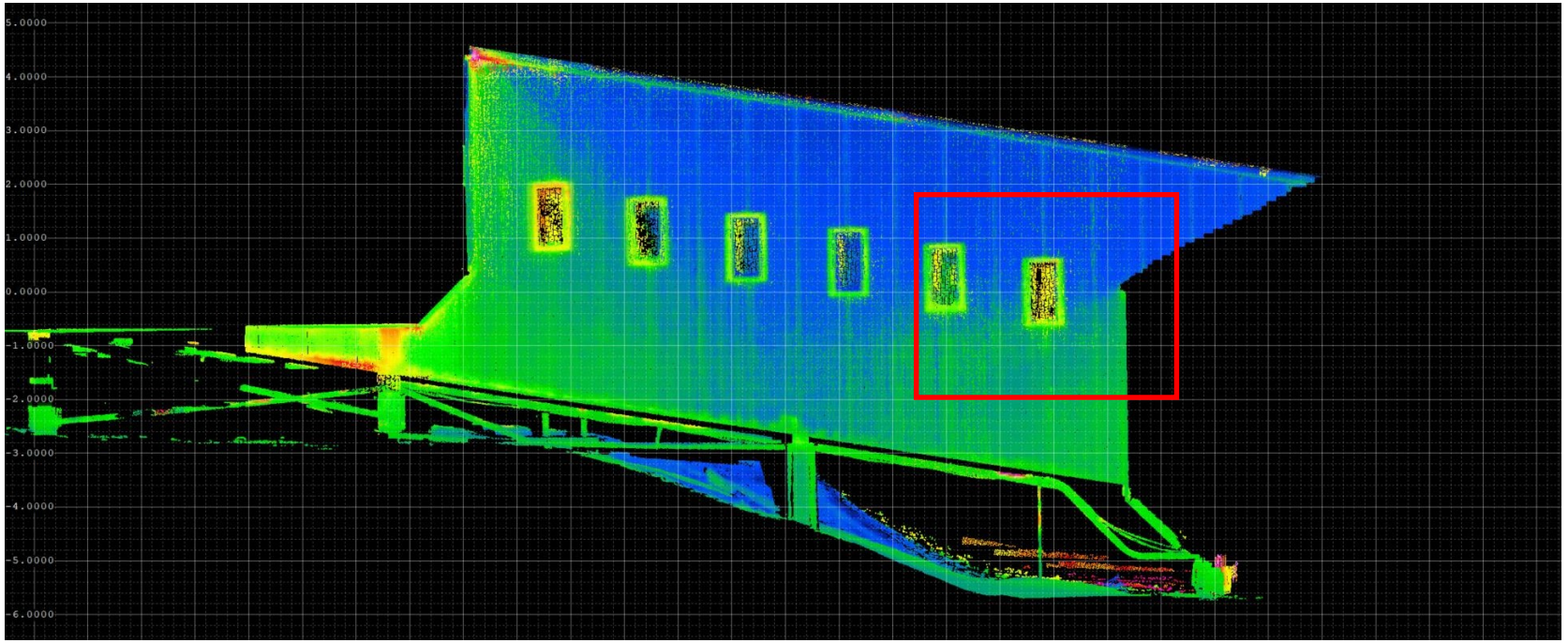




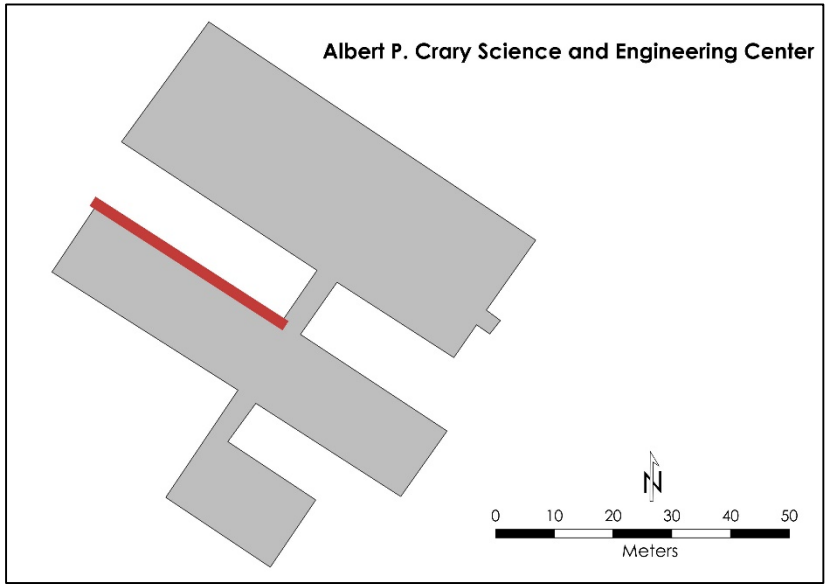
P2CW-W-05 -15◦C 5◦C

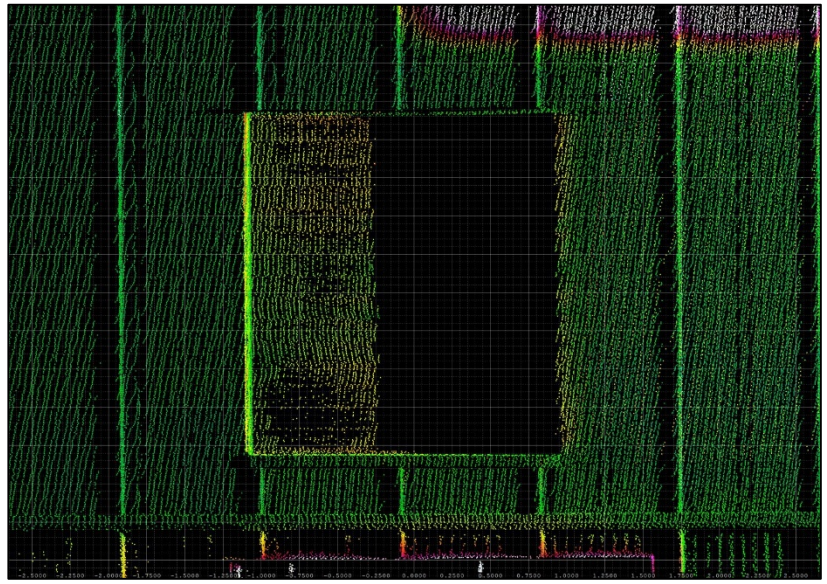


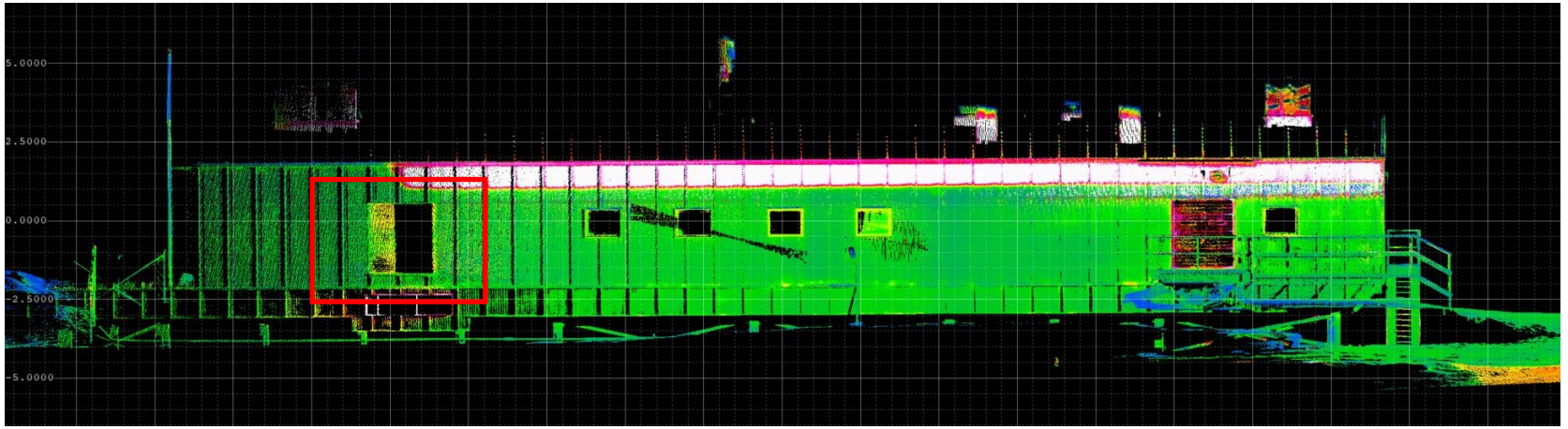




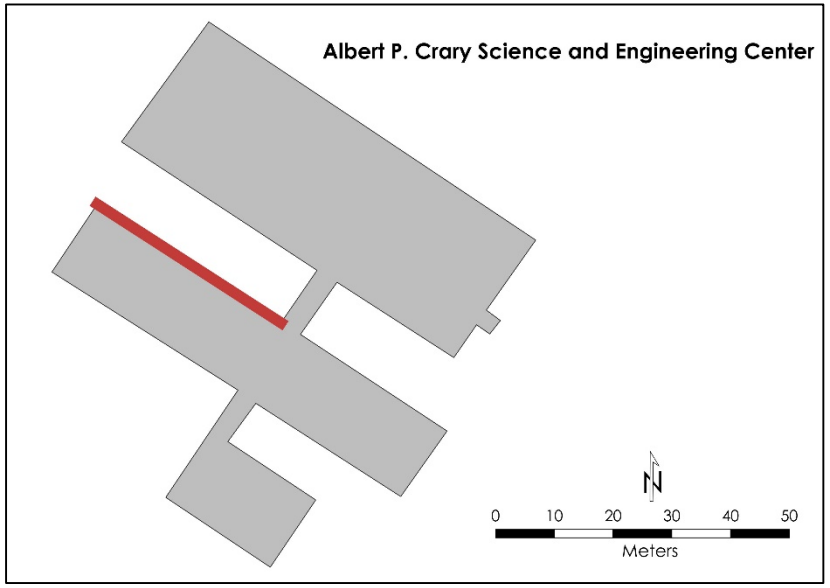
P2CW-W-06 -15◦C 5◦C

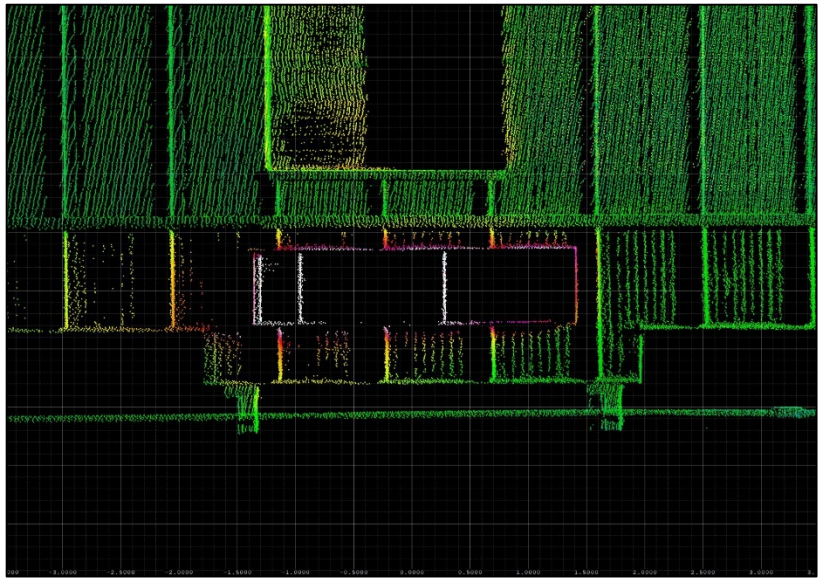


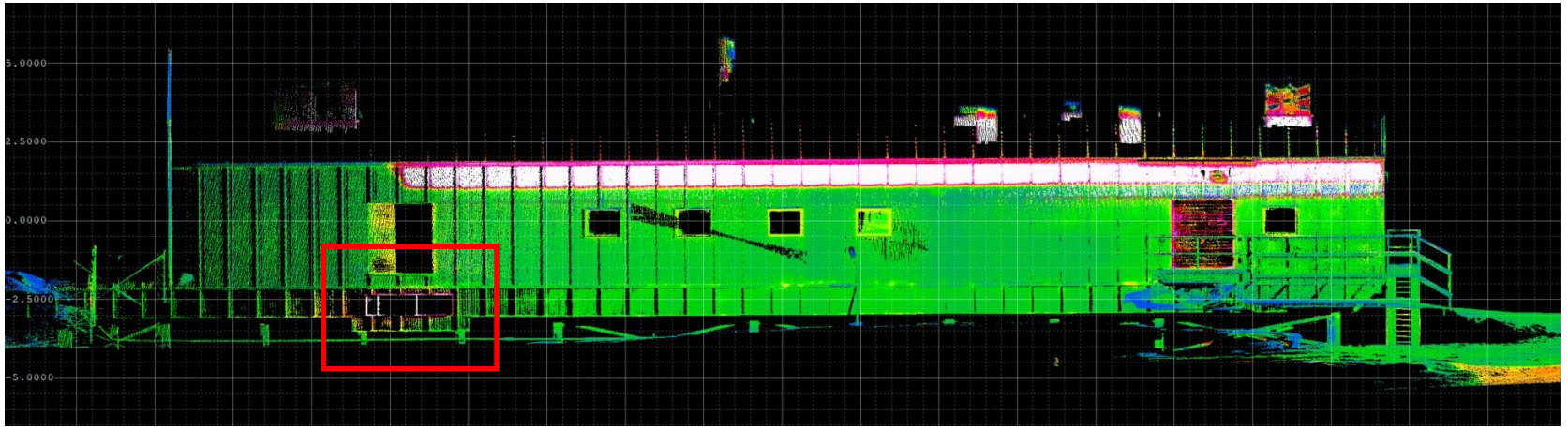




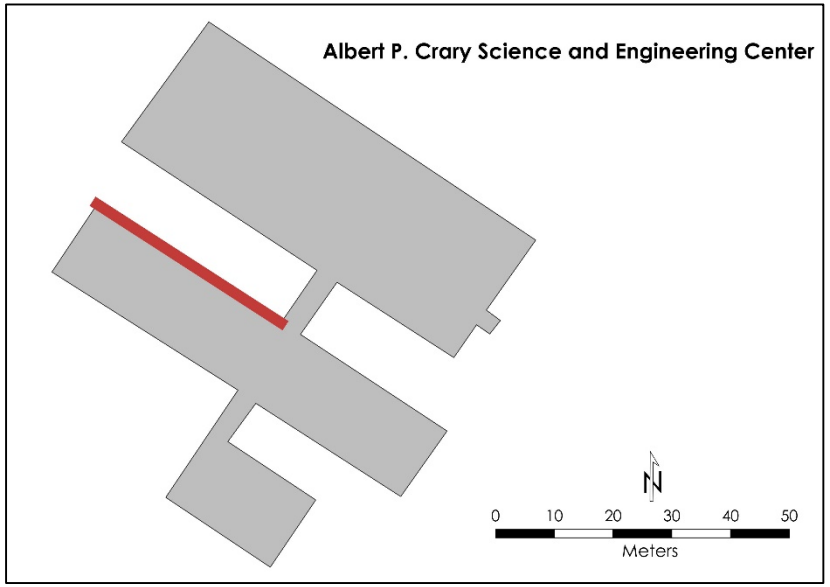
P2NW-LD-01 -15◦C 5◦C

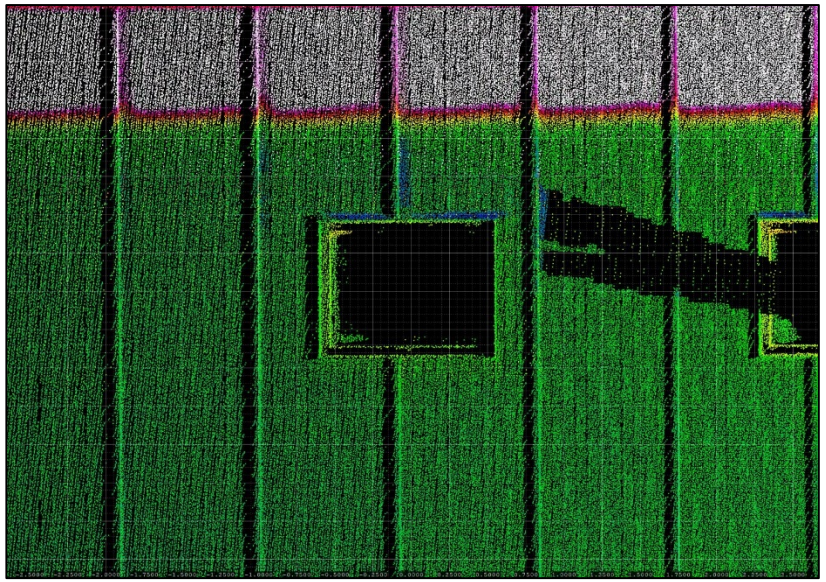


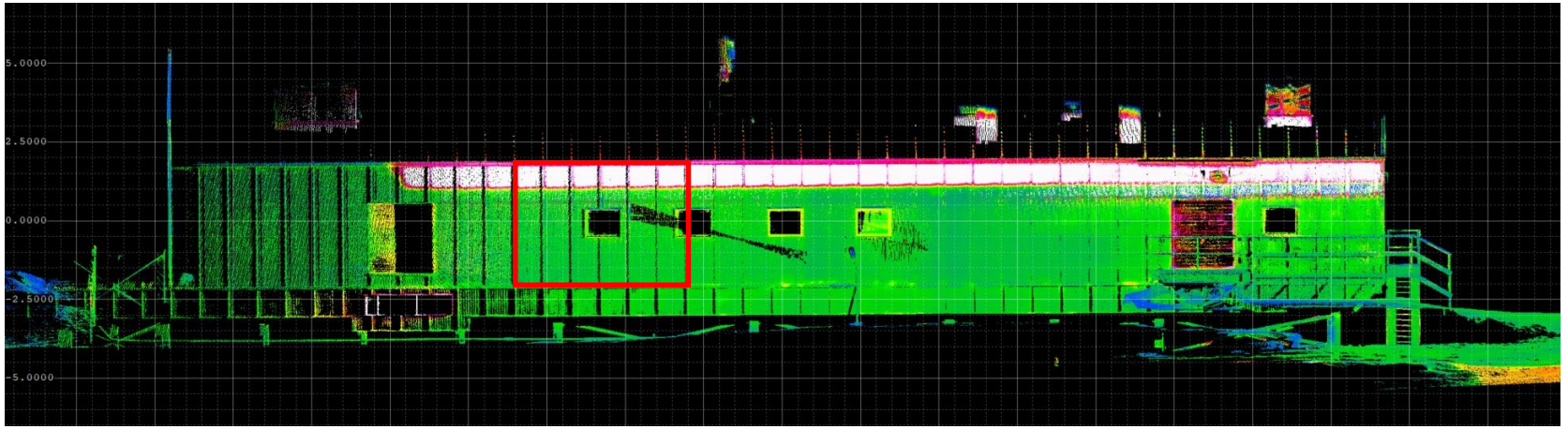




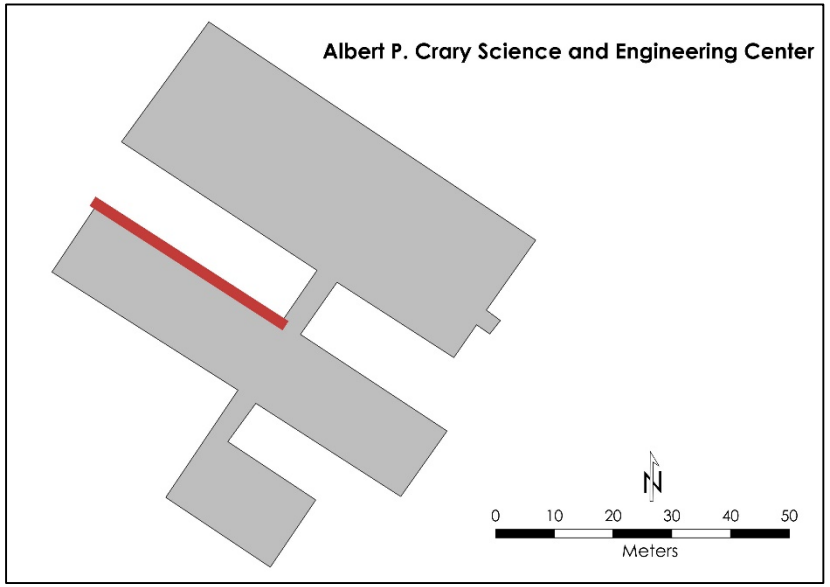
P2NW-V-01 -15◦C 5◦C

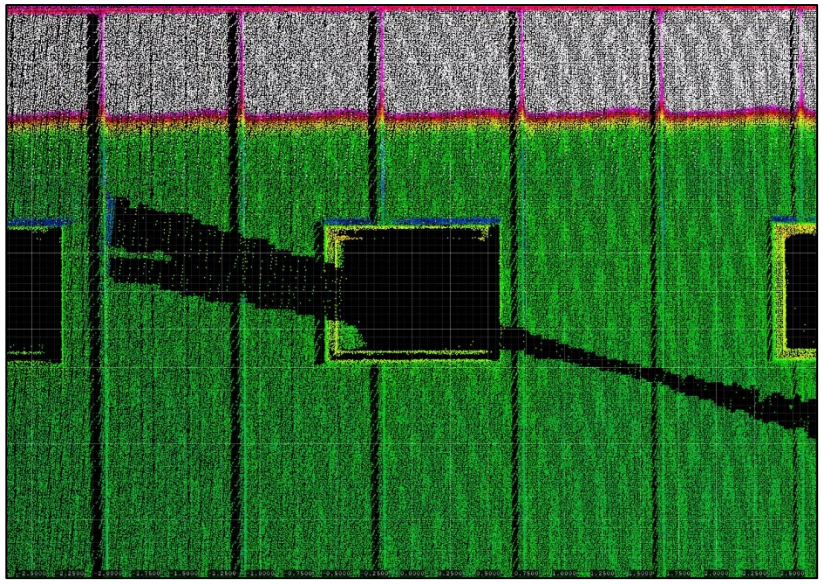


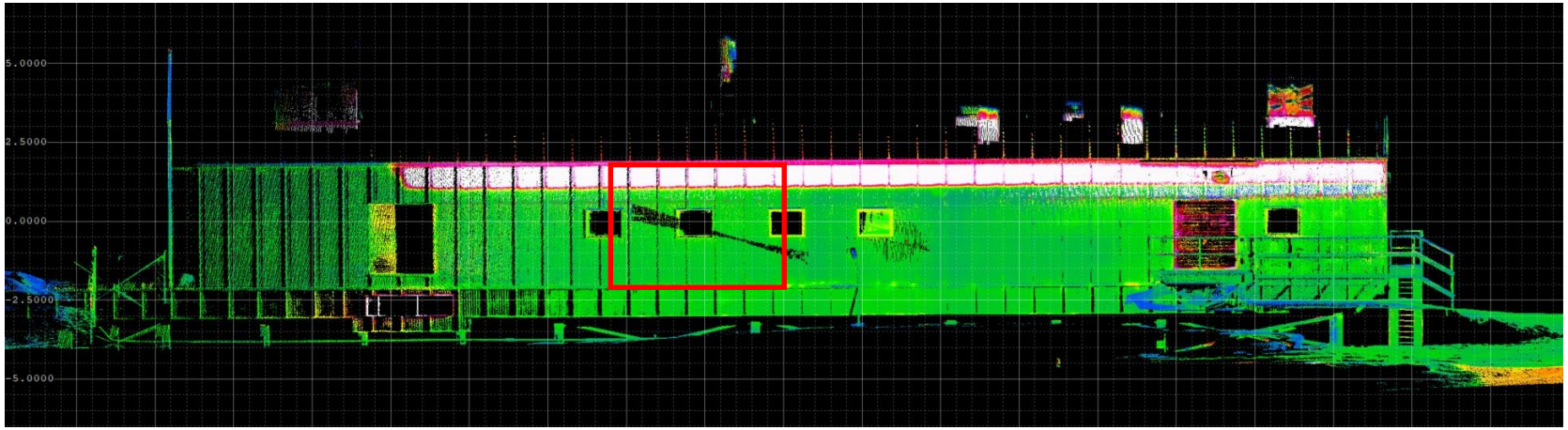




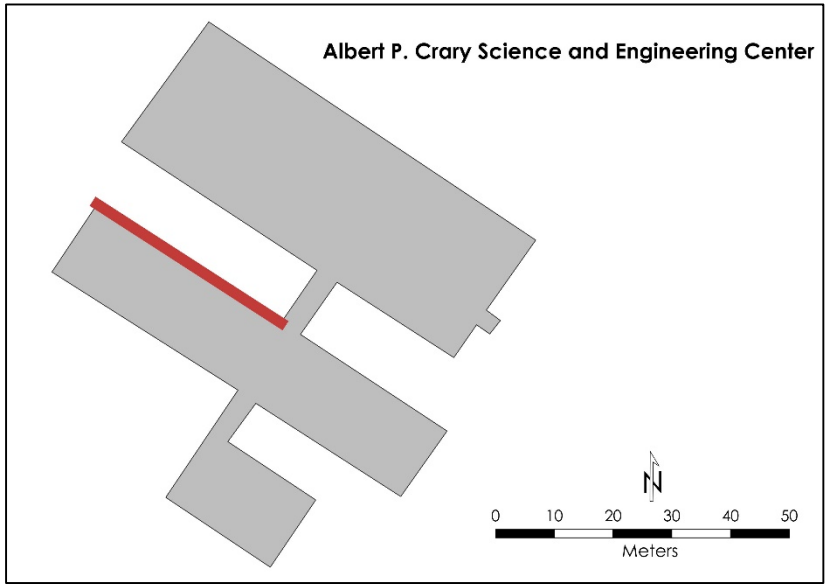
P2NW-W-01 -15◦C 5◦C

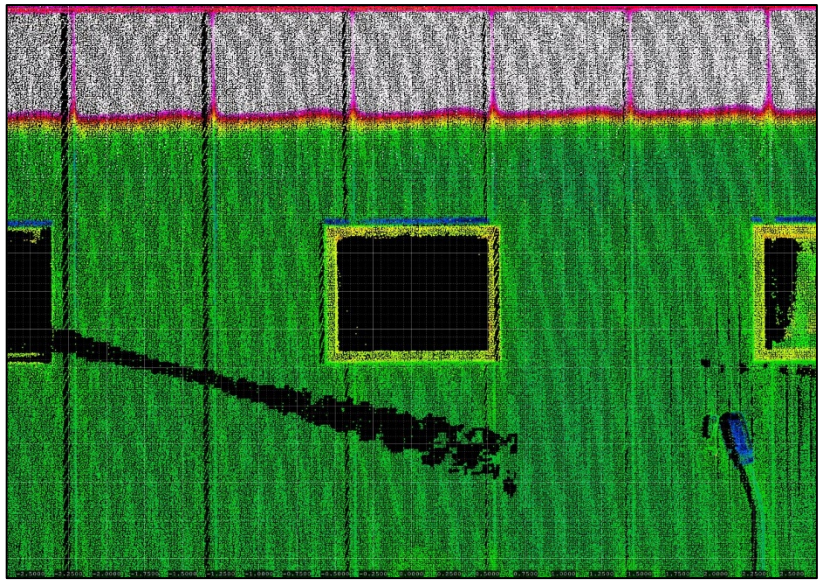


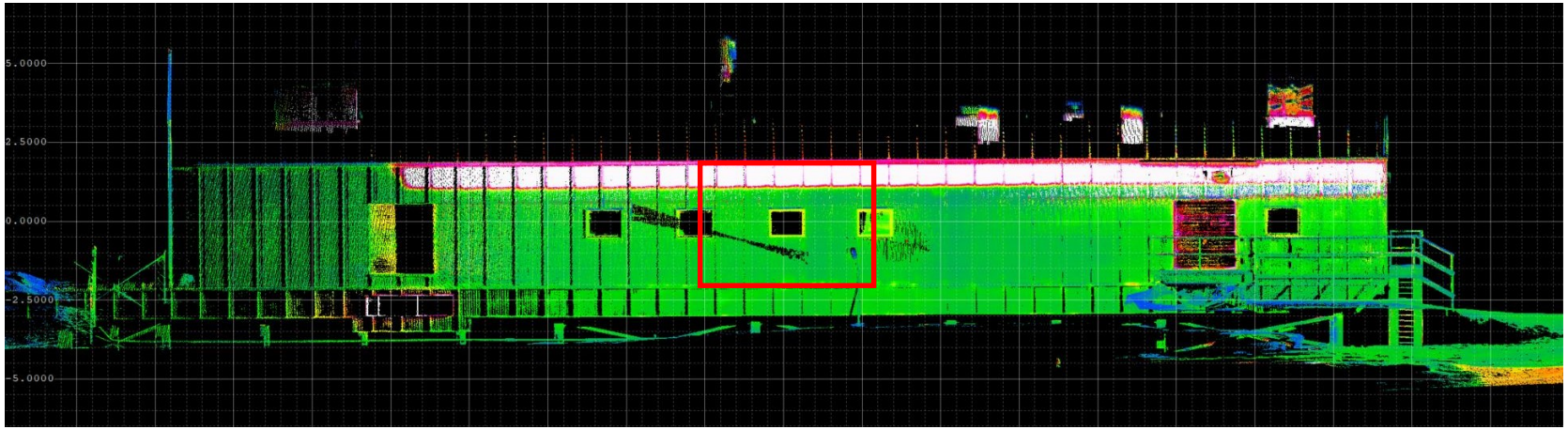




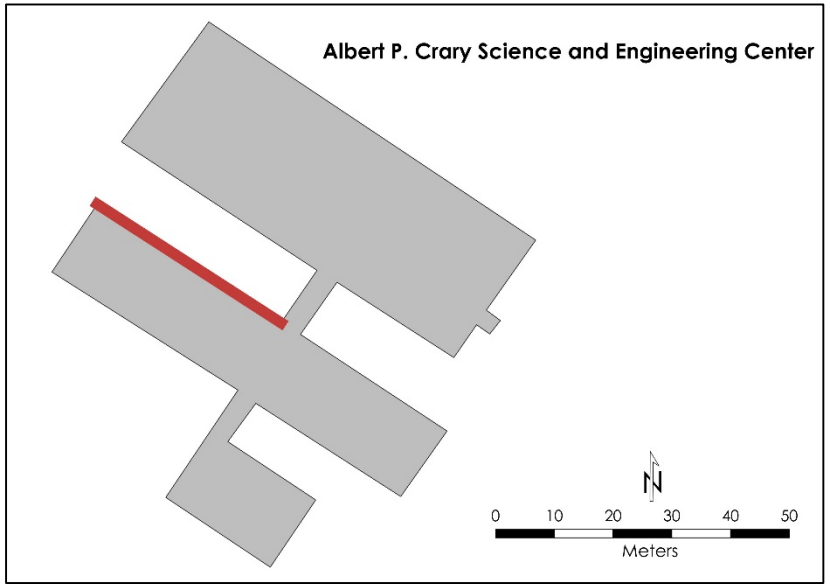
P2NW-W-02 -15◦C 5◦C

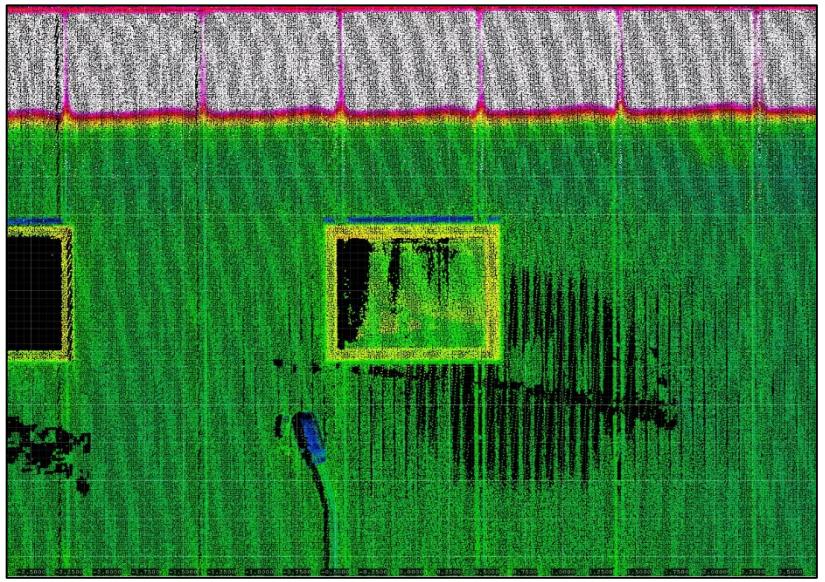


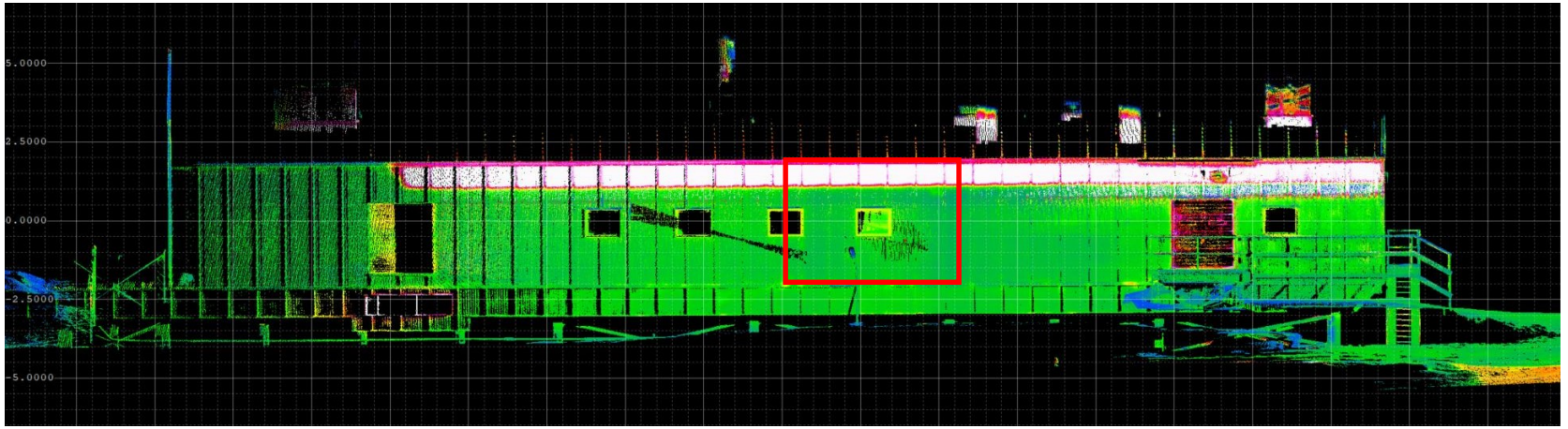




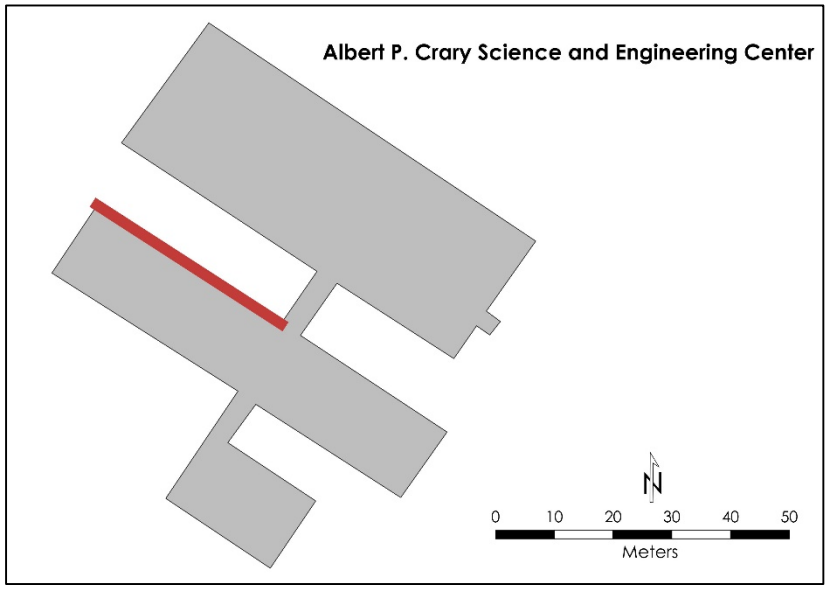
P2NW-W-03 -15◦C 5◦C

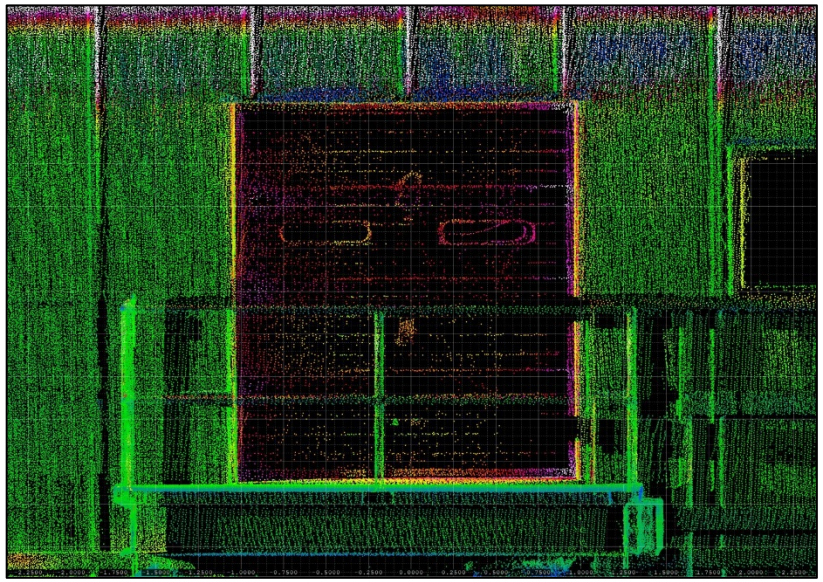


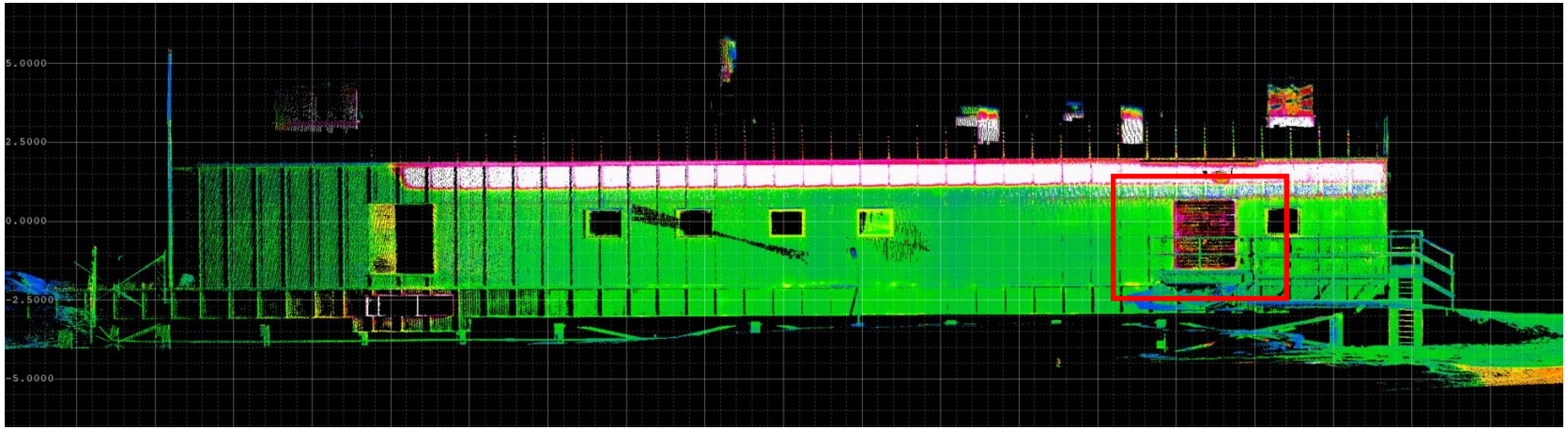




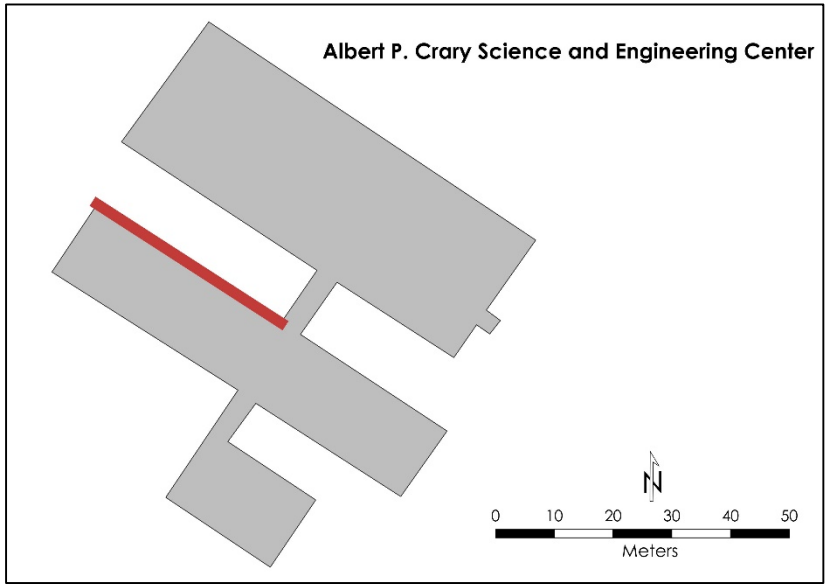
P2NW-W-04 -15◦C 5◦C

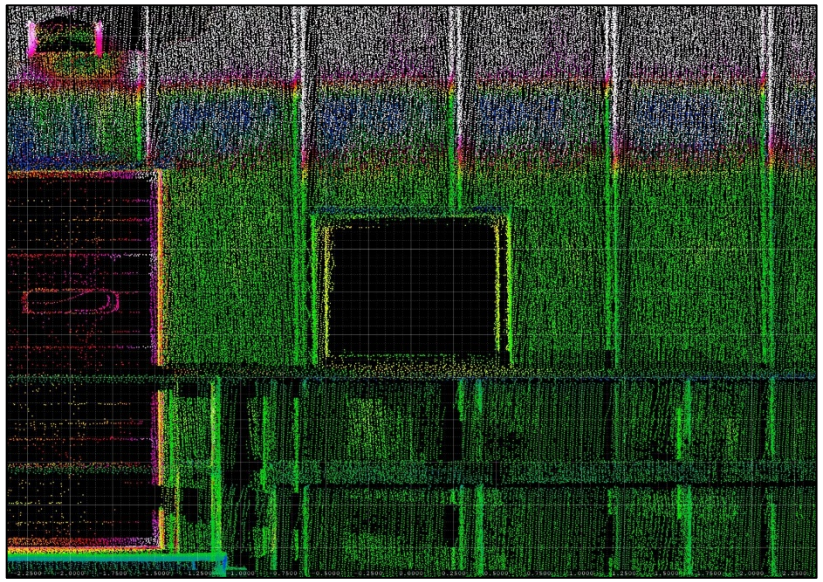


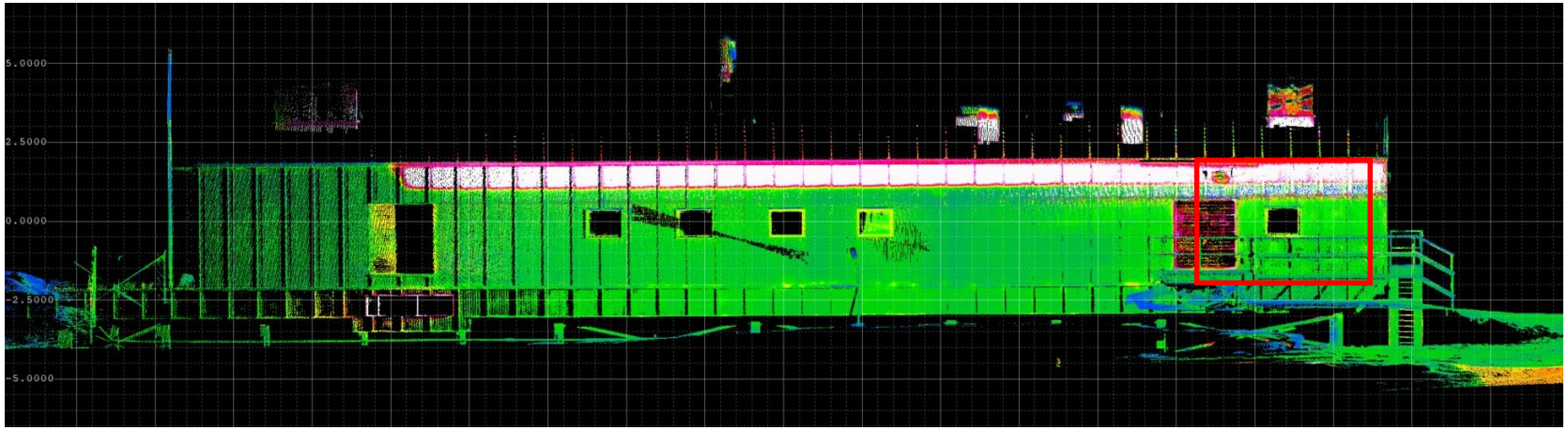




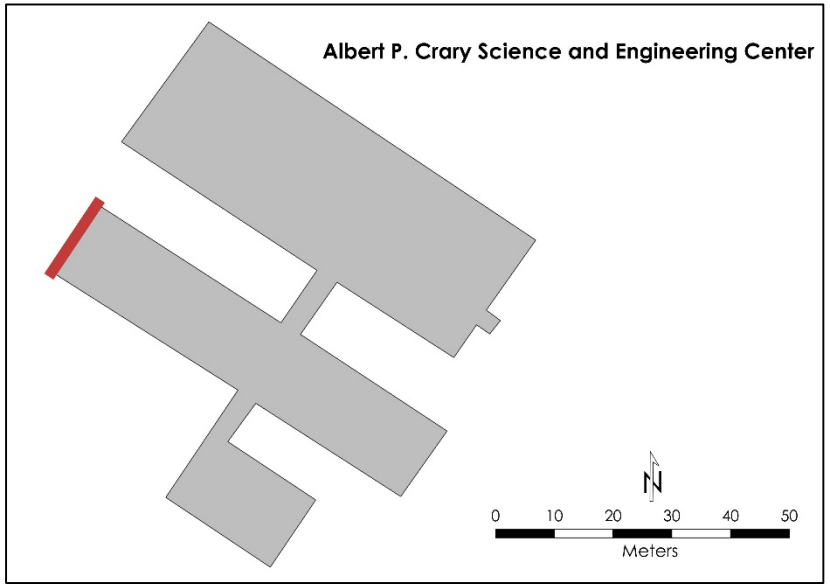
P2NW-LD-02 -15◦C 5◦C

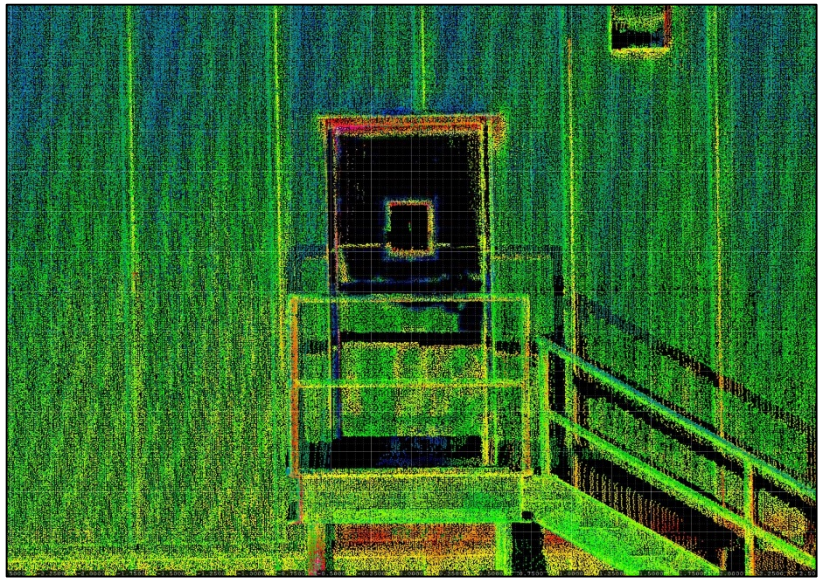


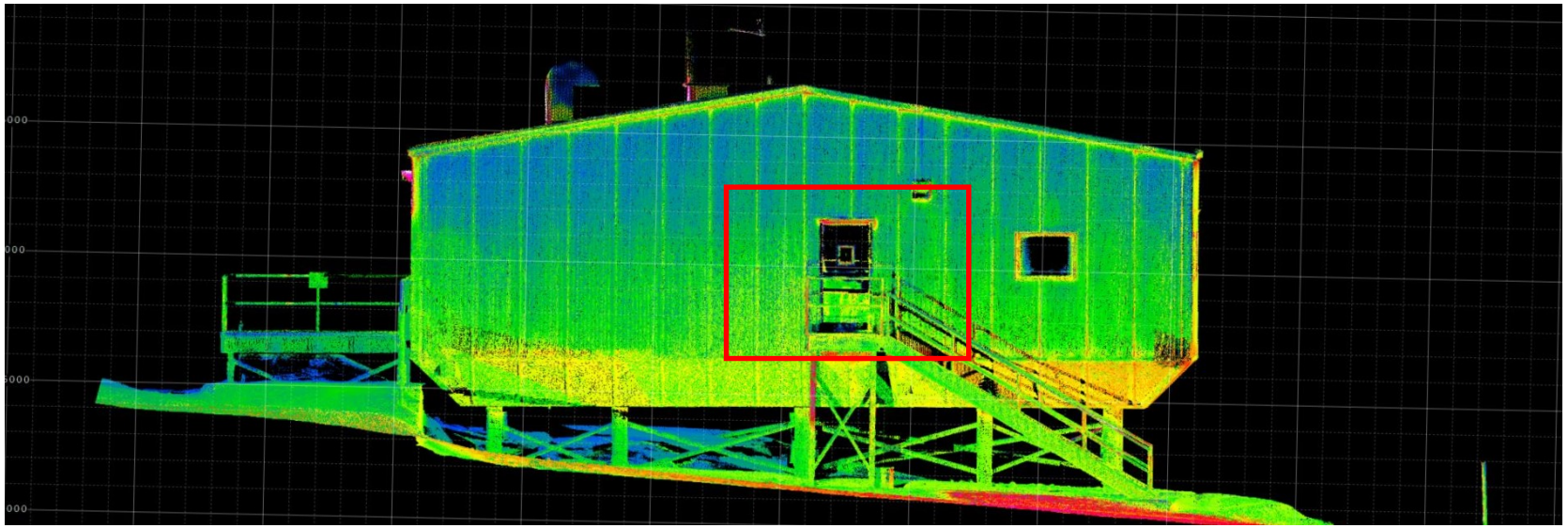




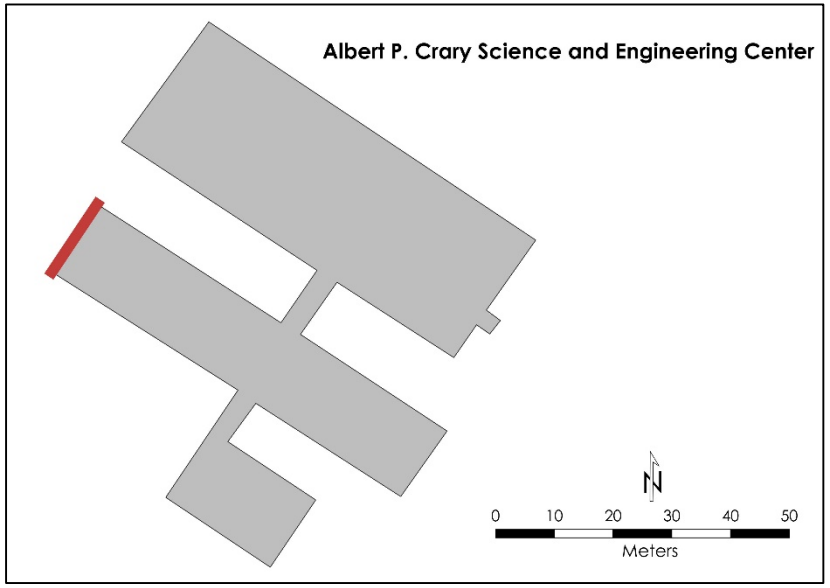
P2NW-W-05 -15◦C 5◦C

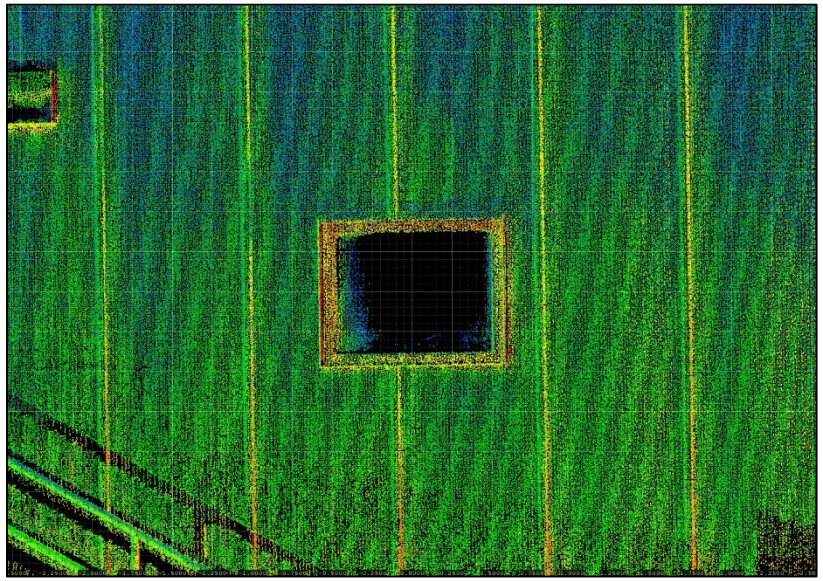


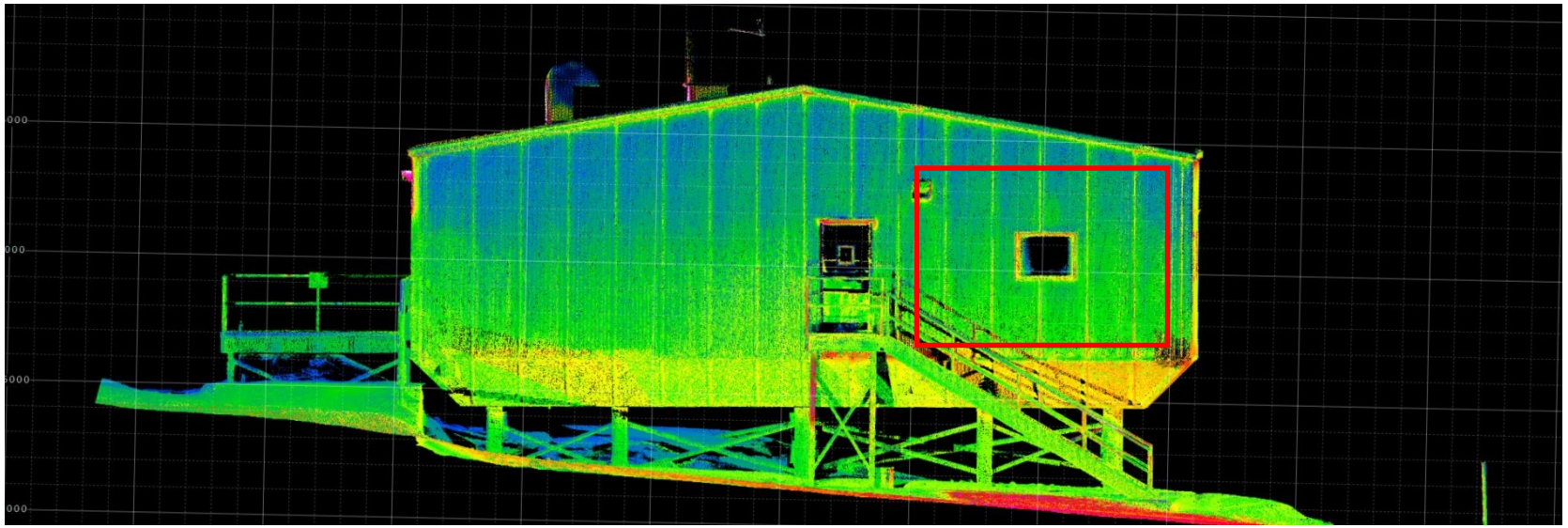




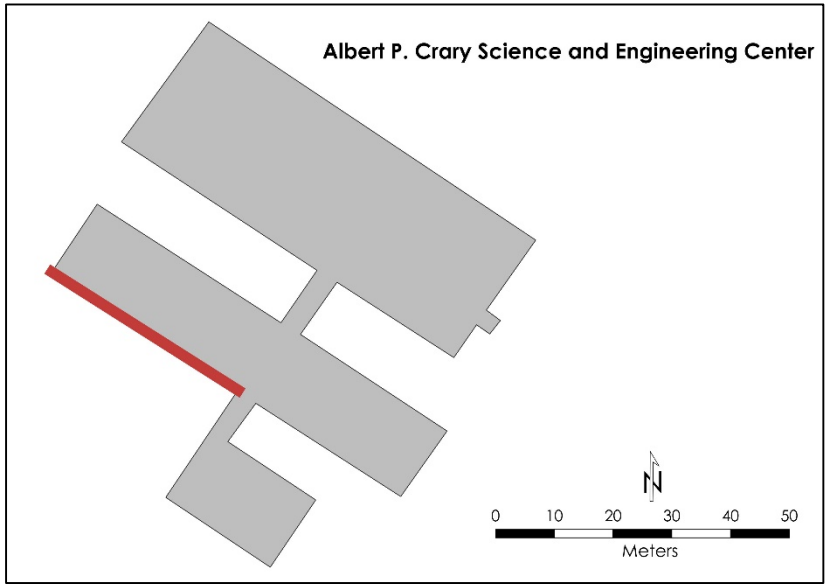
P2W-D-01 -15◦C 5◦C

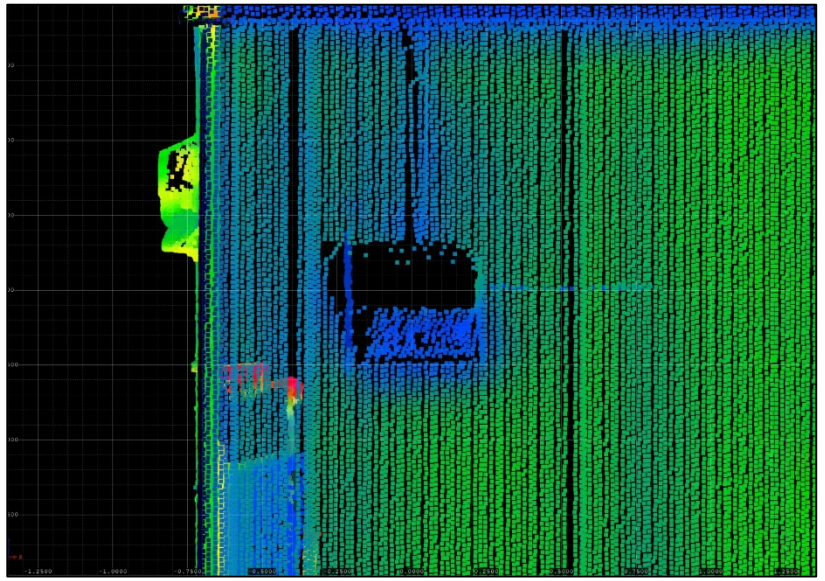


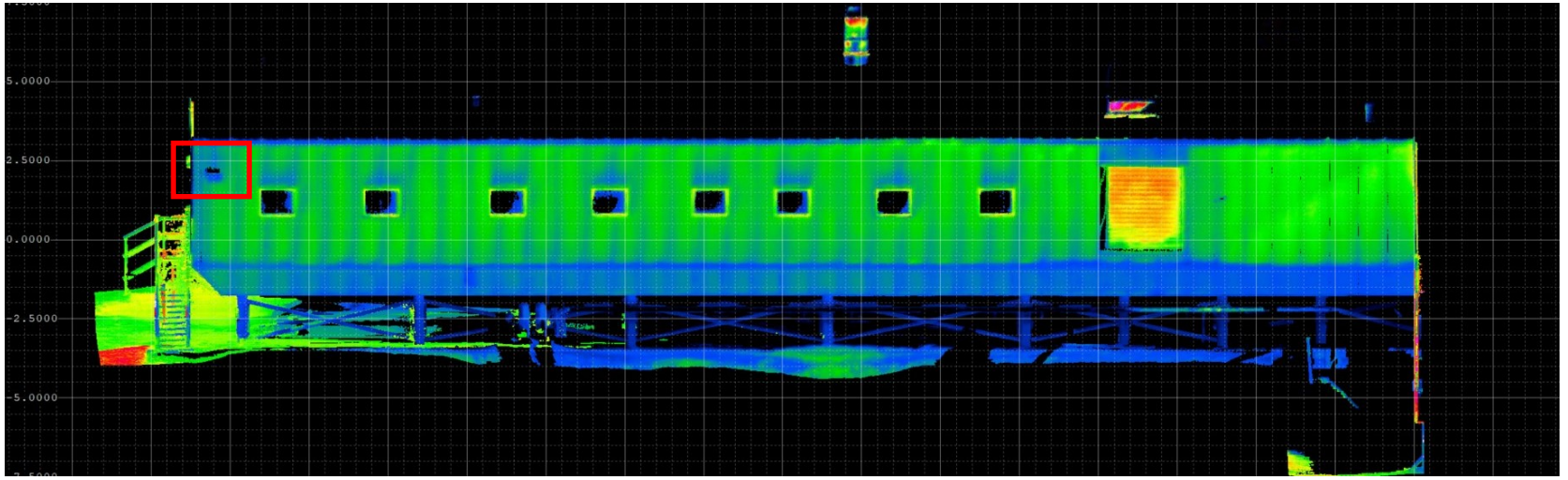




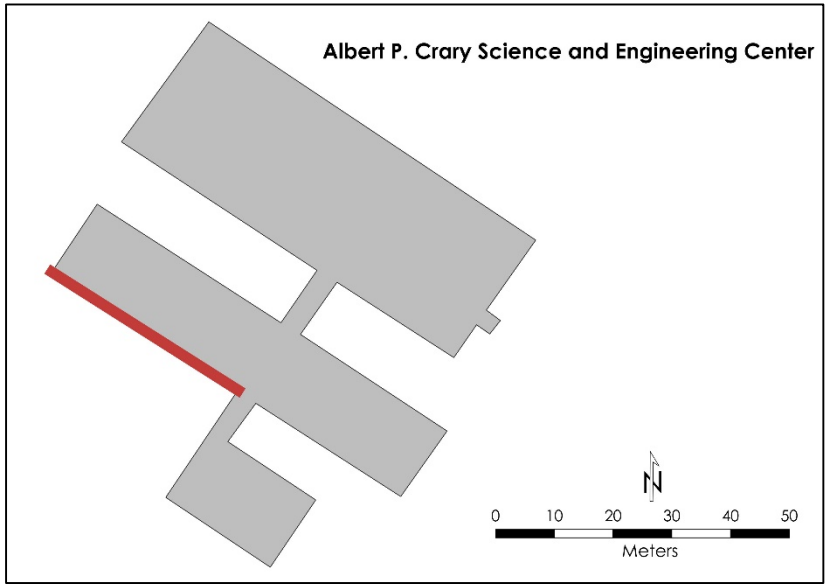
P2W-W-01 -15◦C 5◦C

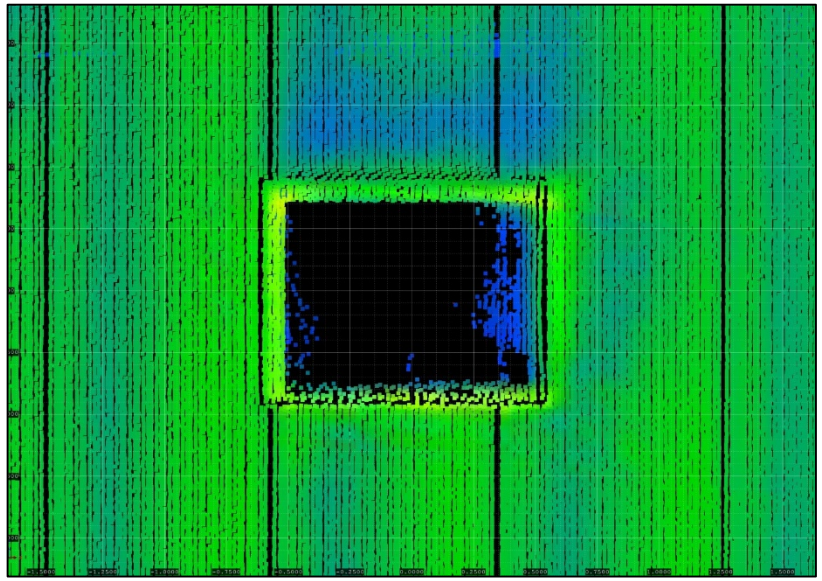


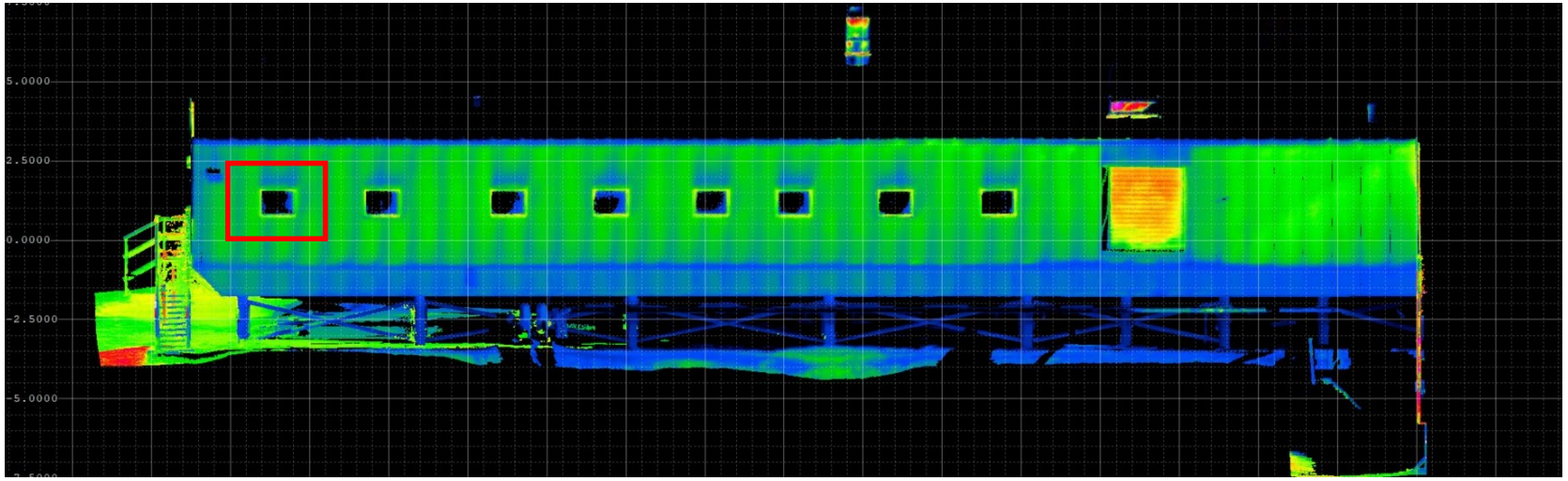




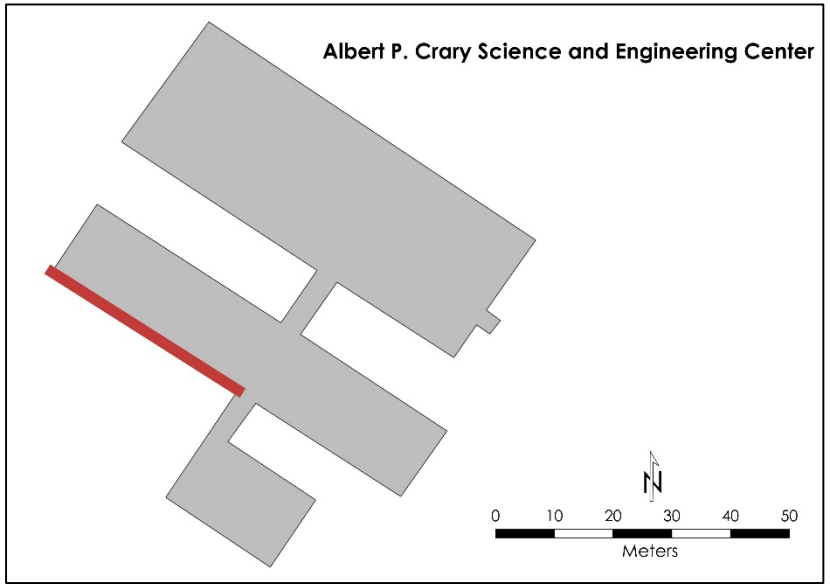
P2SW-V-01 -5◦C 20◦C

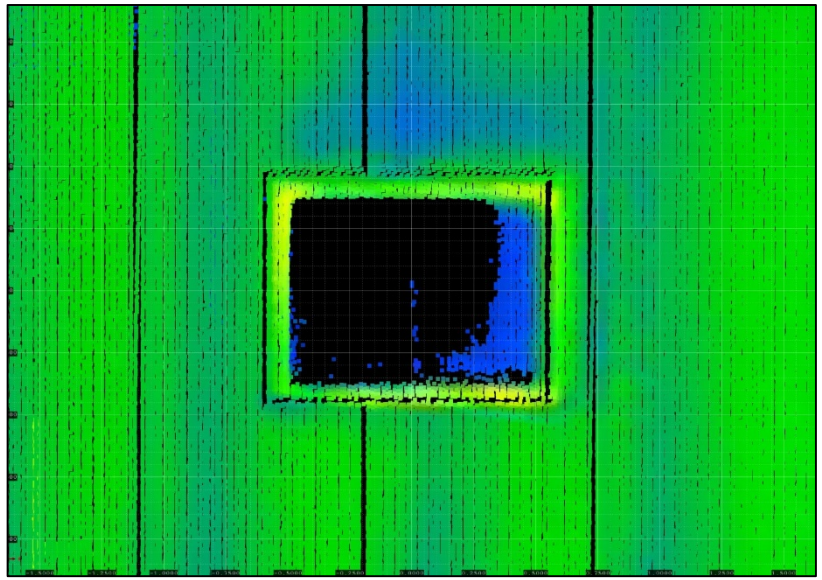


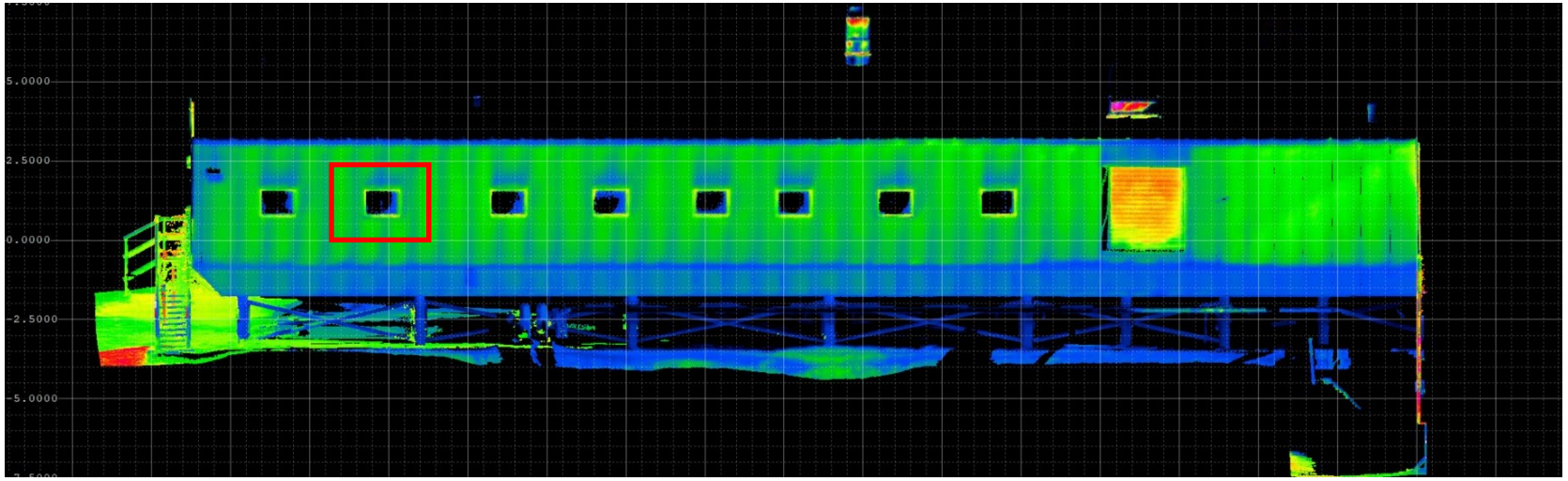




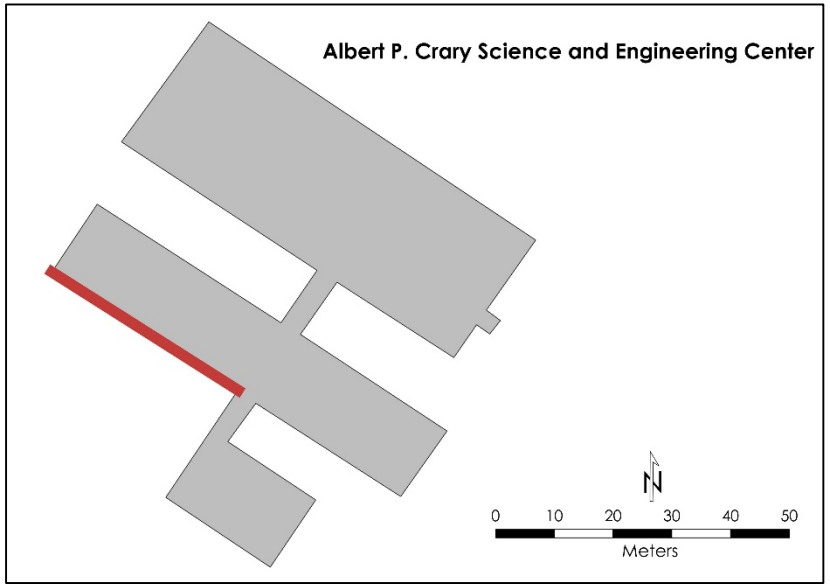
P2SW-W-01 -5◦C 20◦C

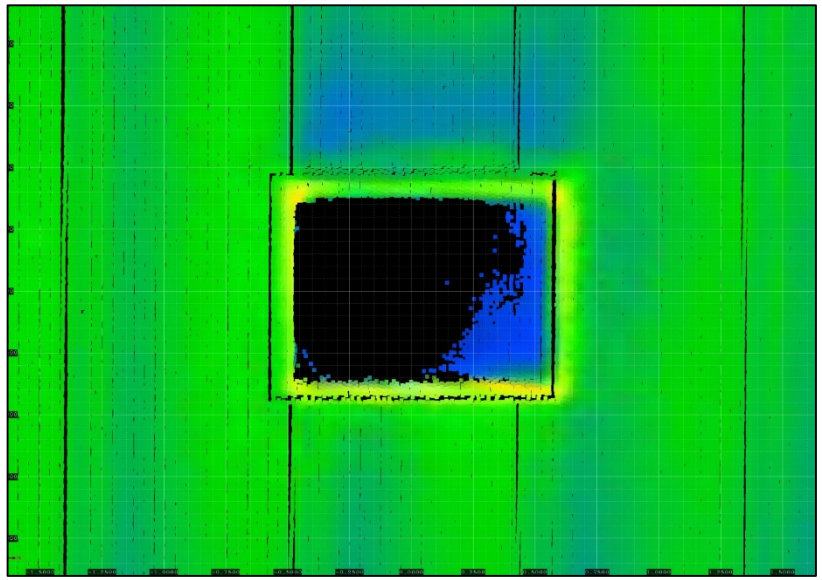


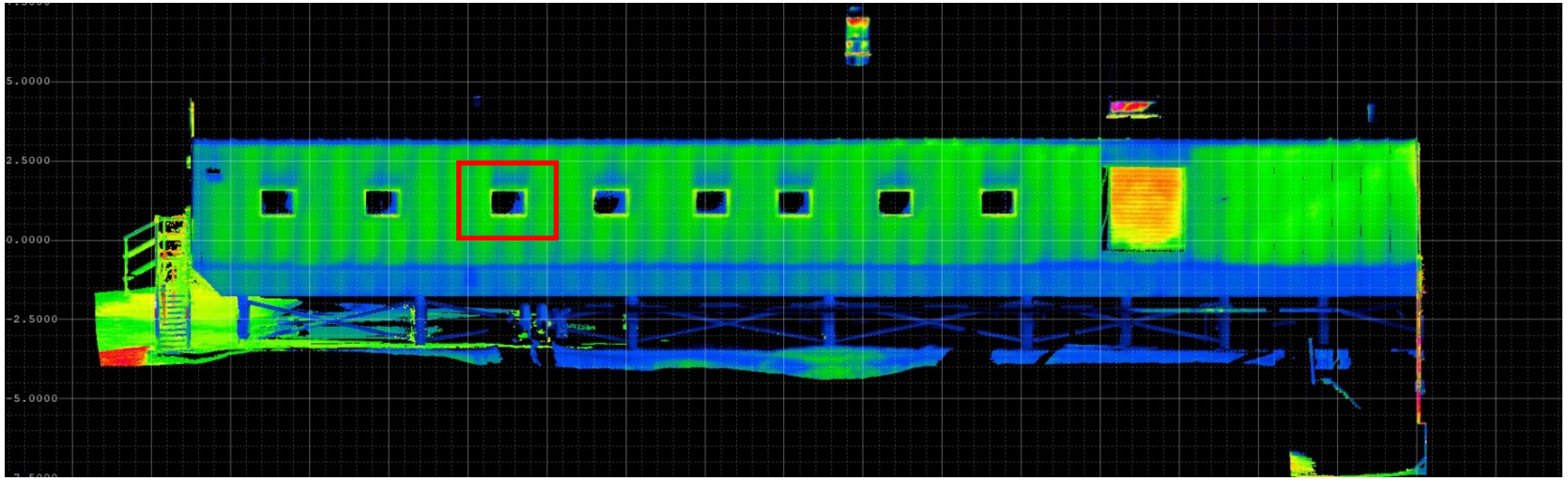




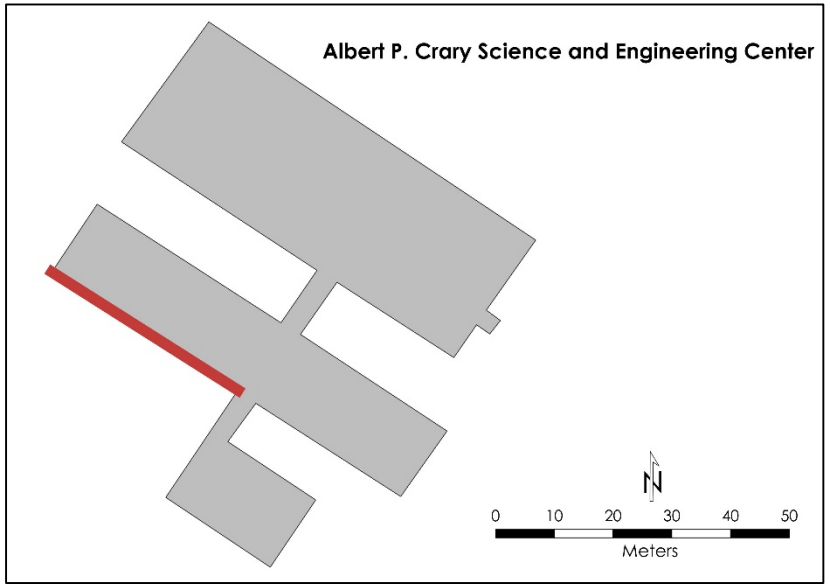
P2SW-W-02 -5◦C 20◦C

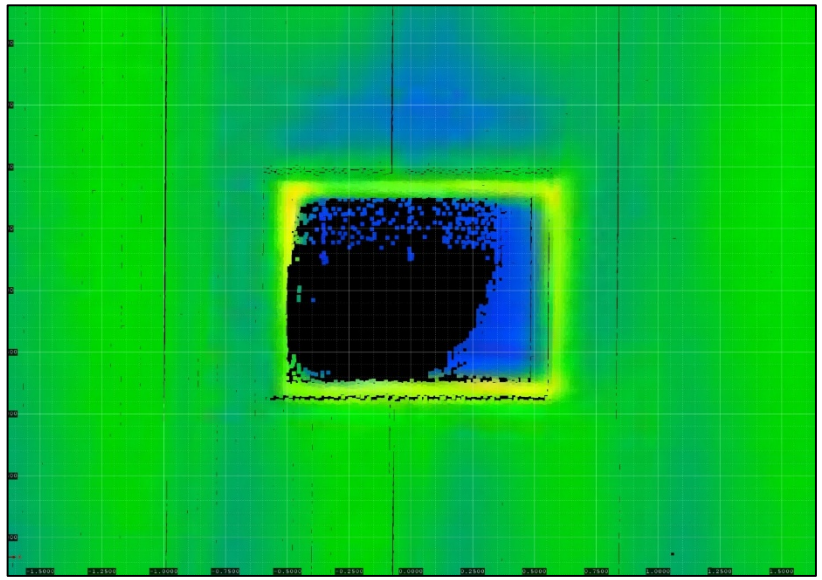


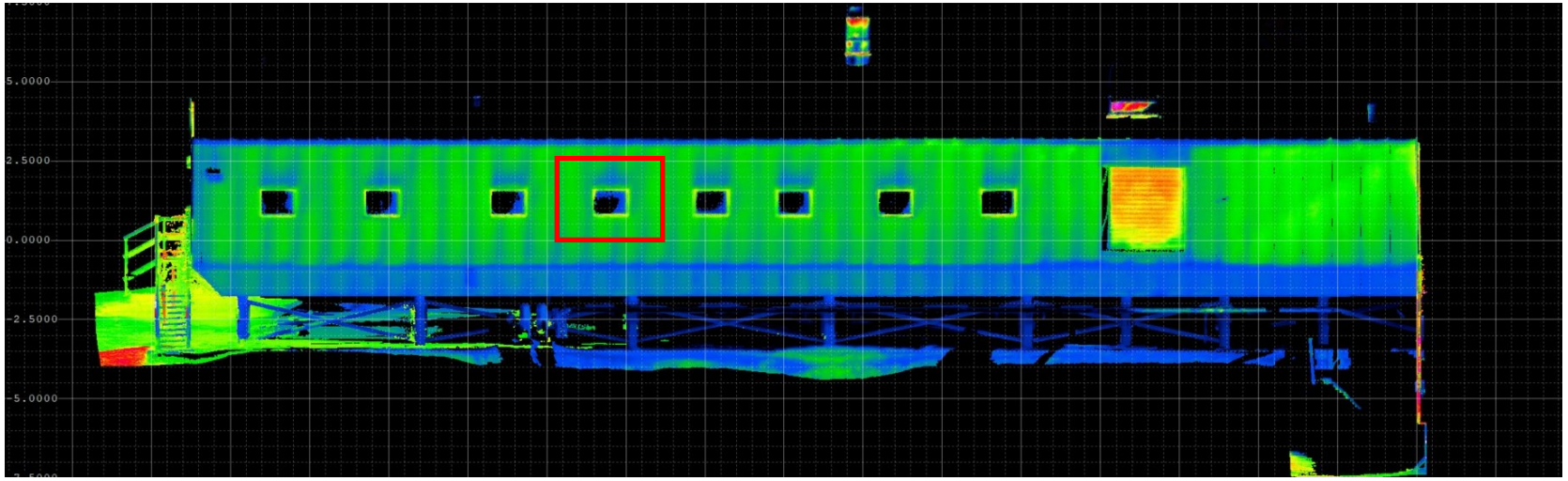




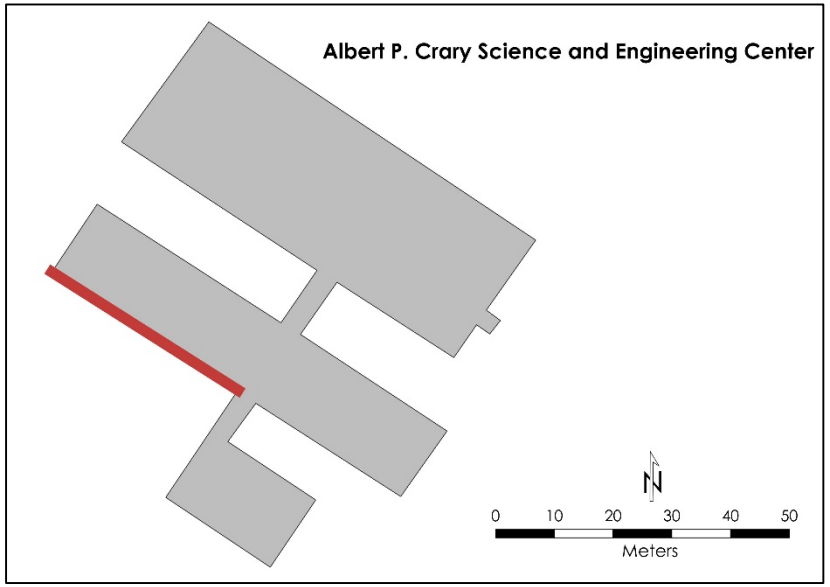
P2SW-W-03 -5◦C 20◦C

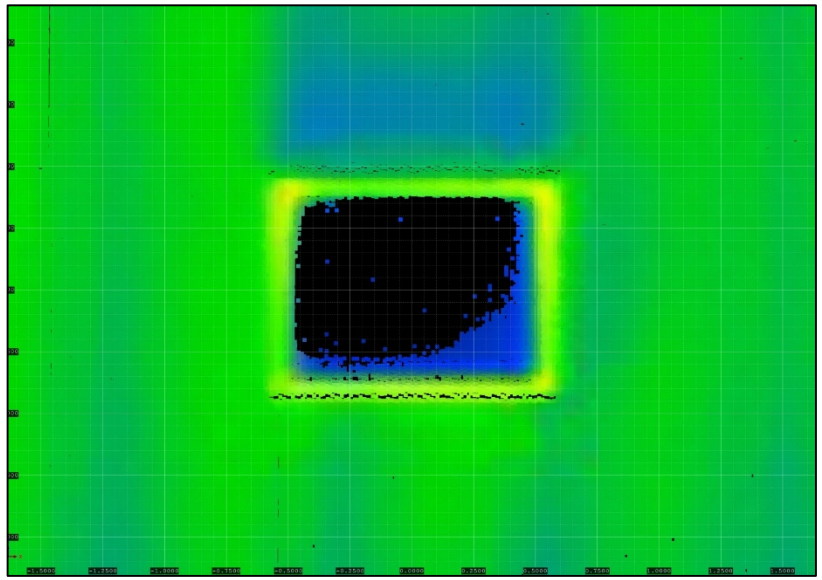


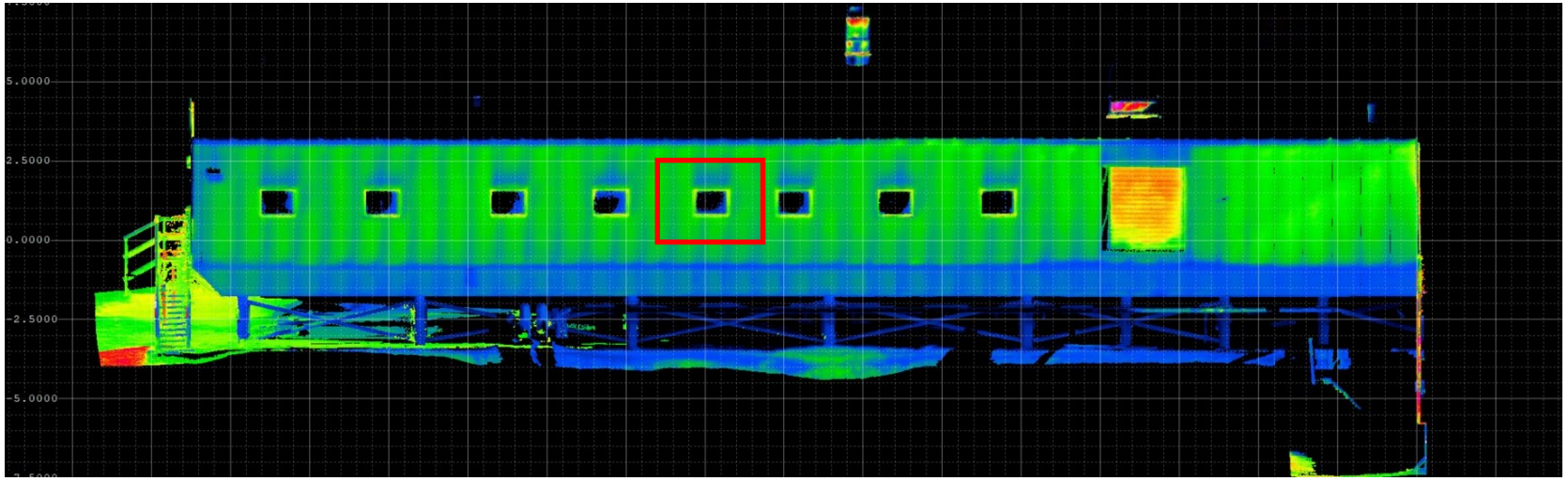




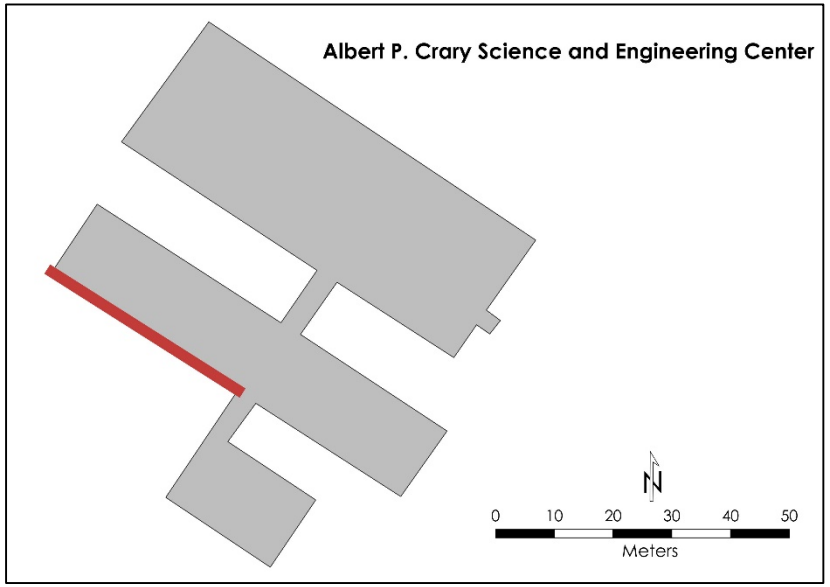
P2SW-W-04 -5◦C 20◦C

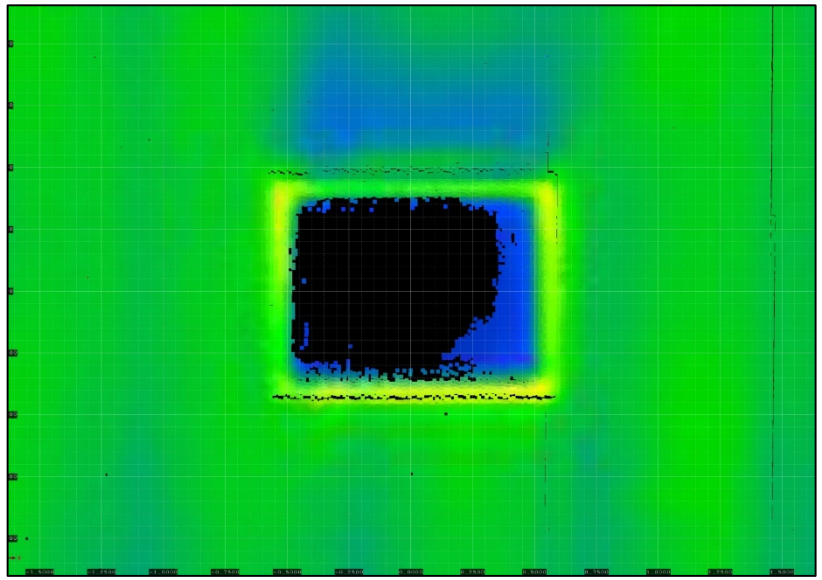


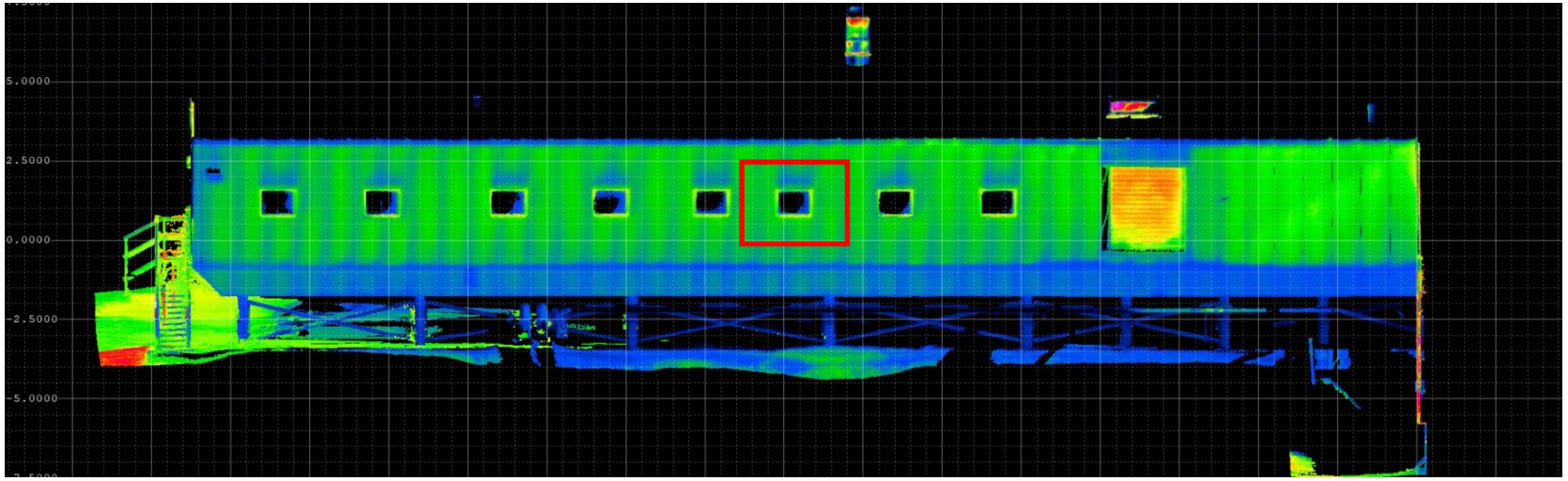




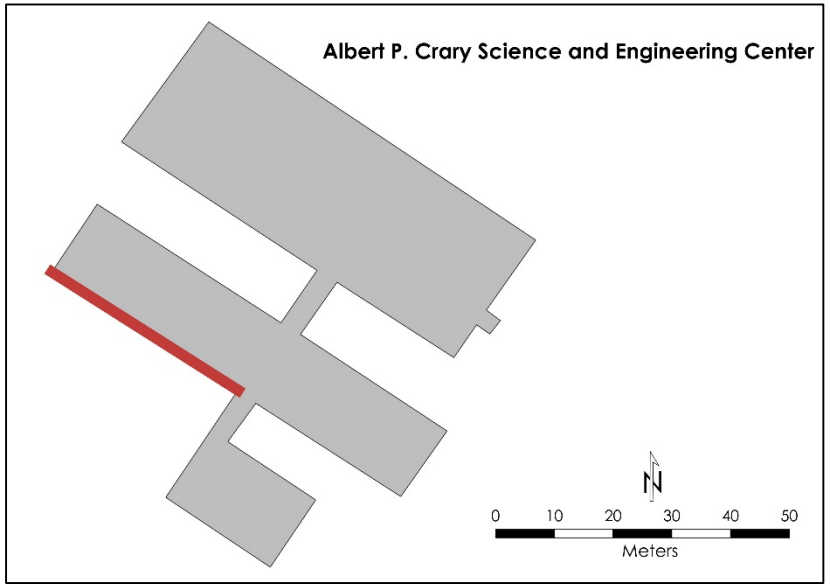
P2SW-W-05 -5◦C 20◦C

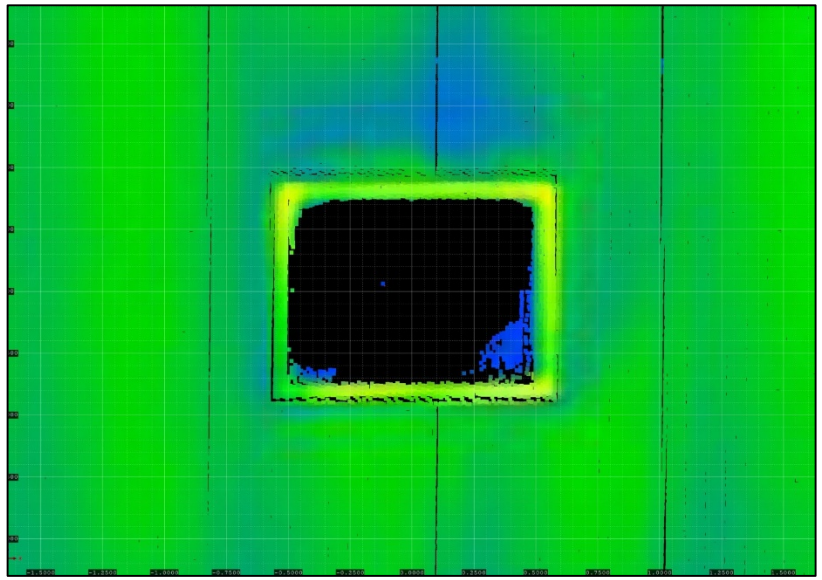


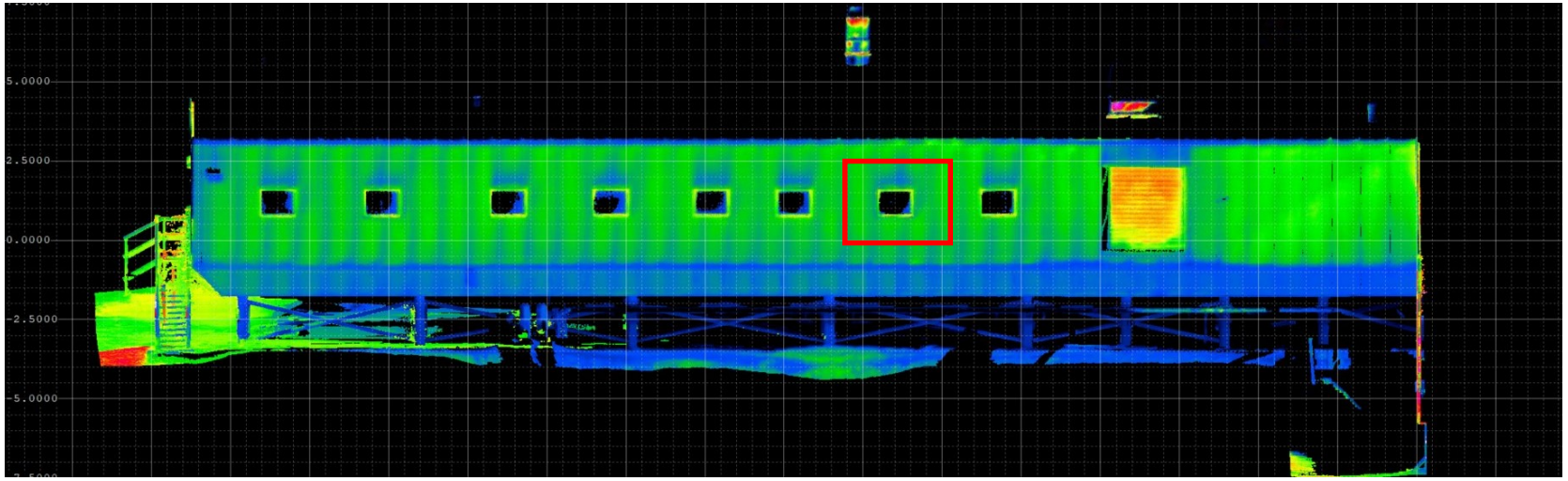




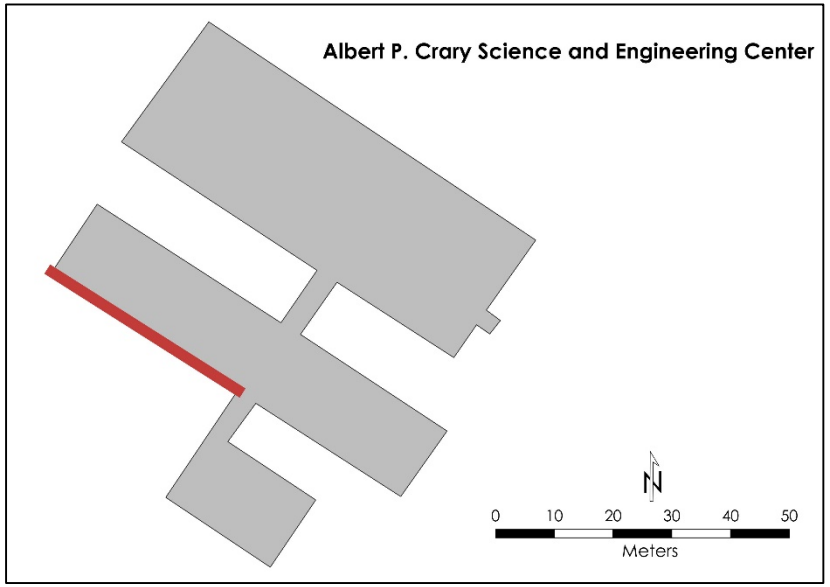
P2SW-W-06 -5◦C 20◦C

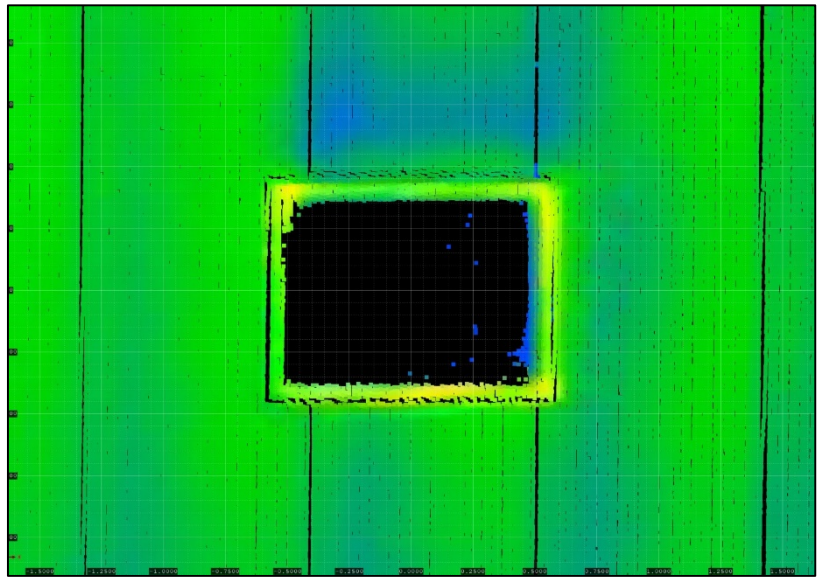


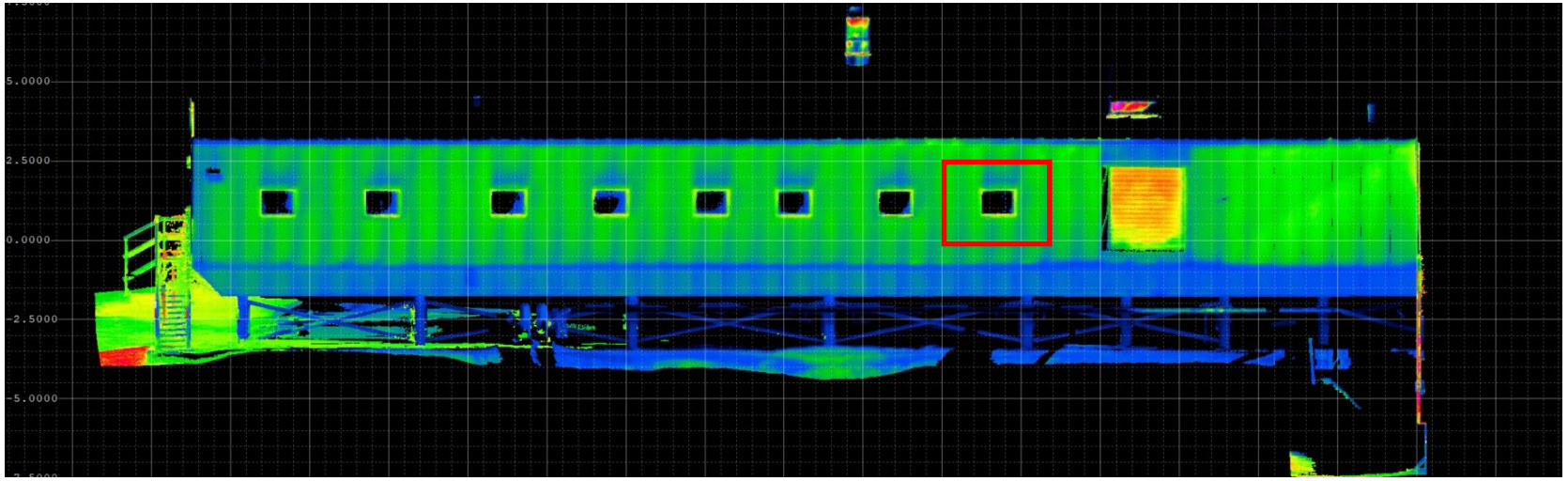




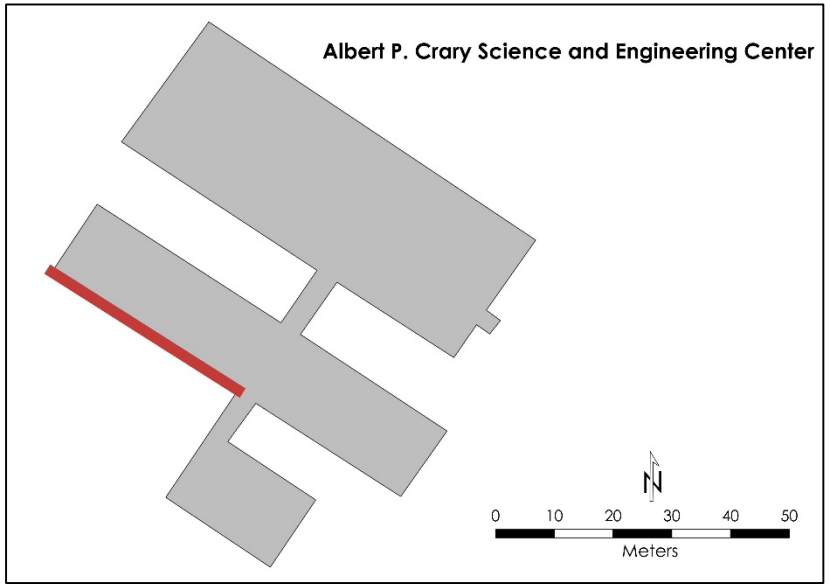
P2SW-W-07 -5◦C 20◦C

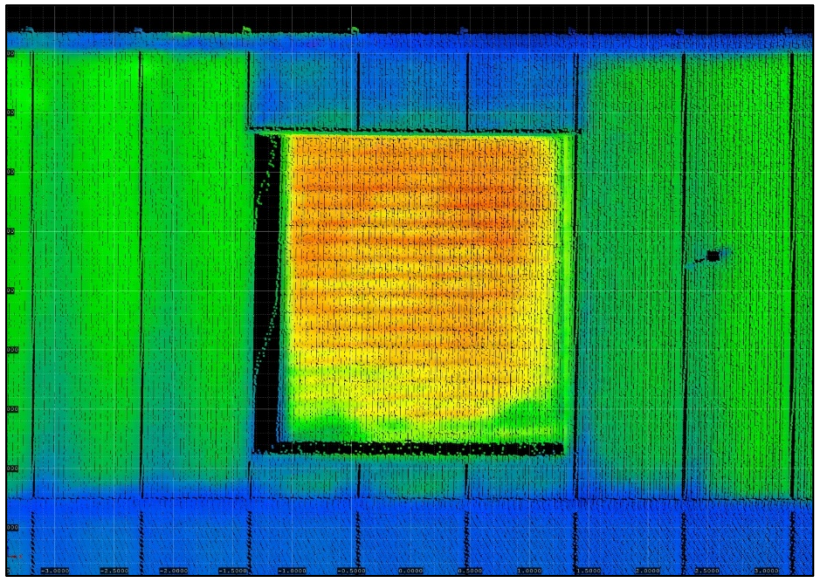


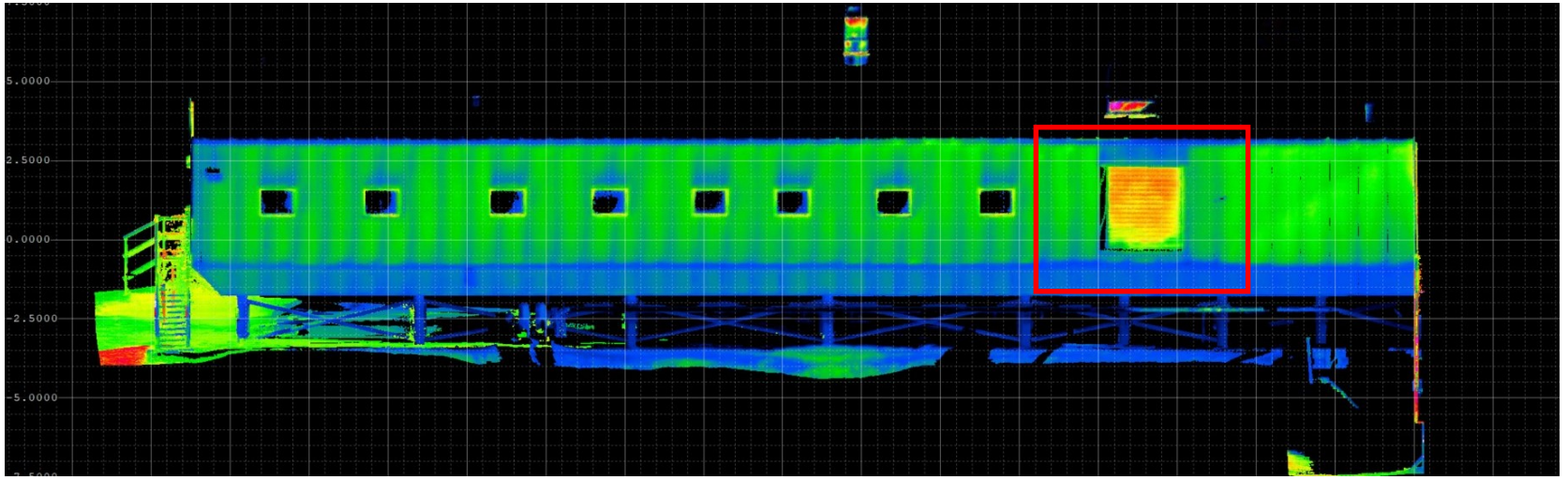




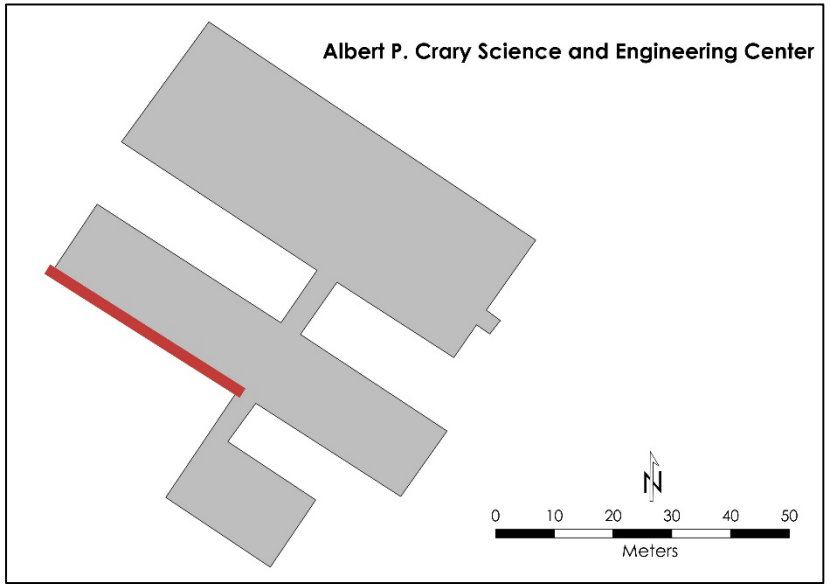
P2SW-W-08 -5◦C 20◦C

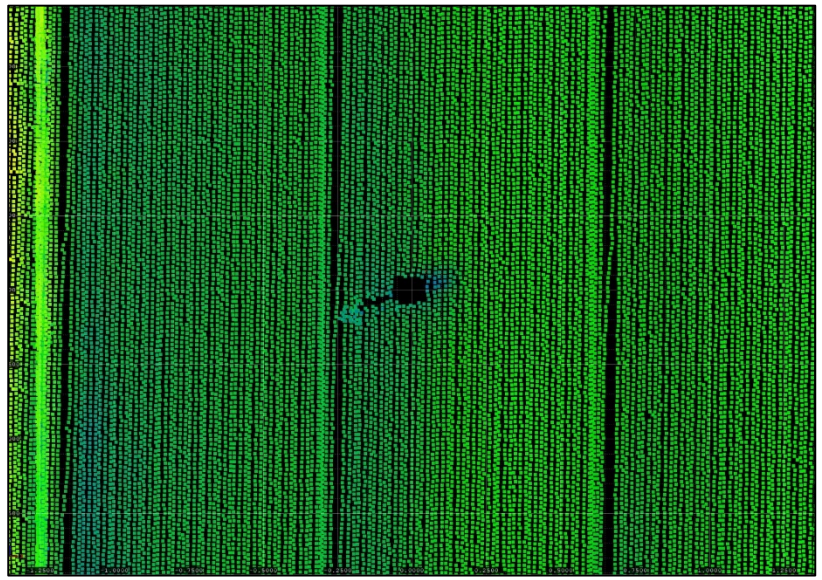


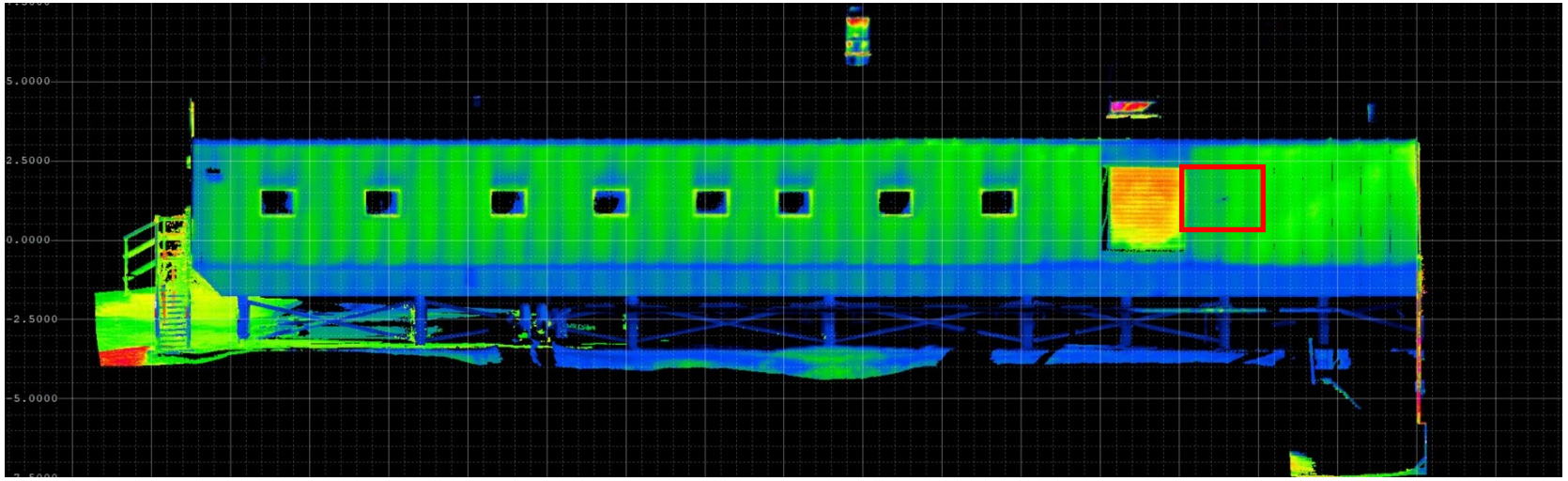




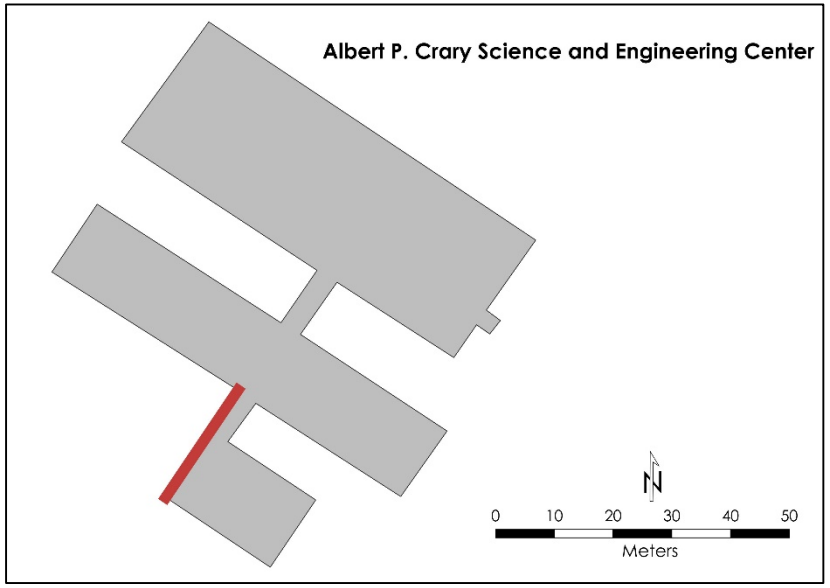
P2SW-LD-01 -5◦C 20◦C

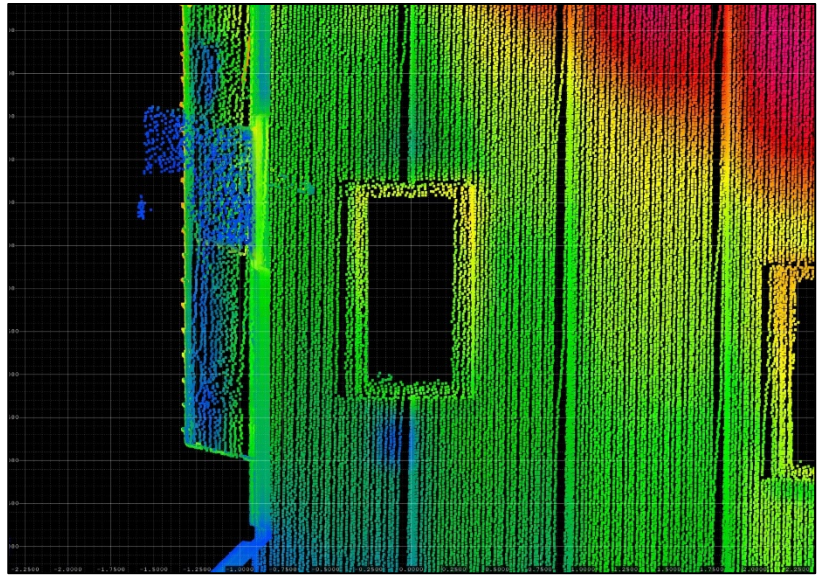


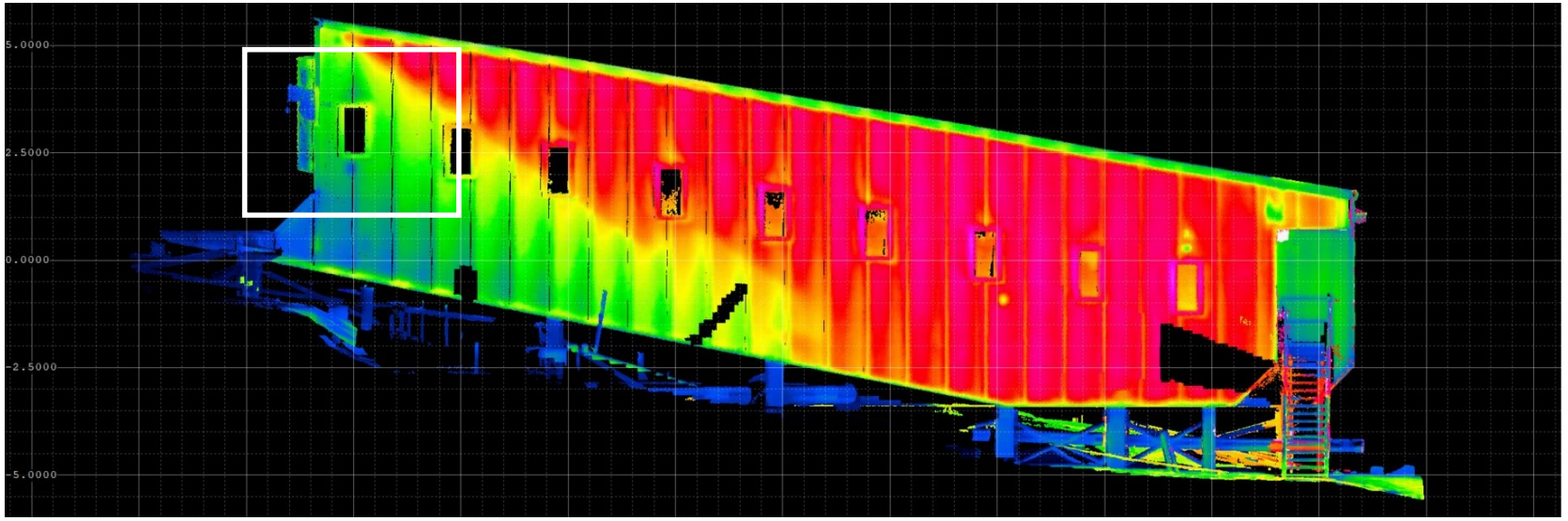




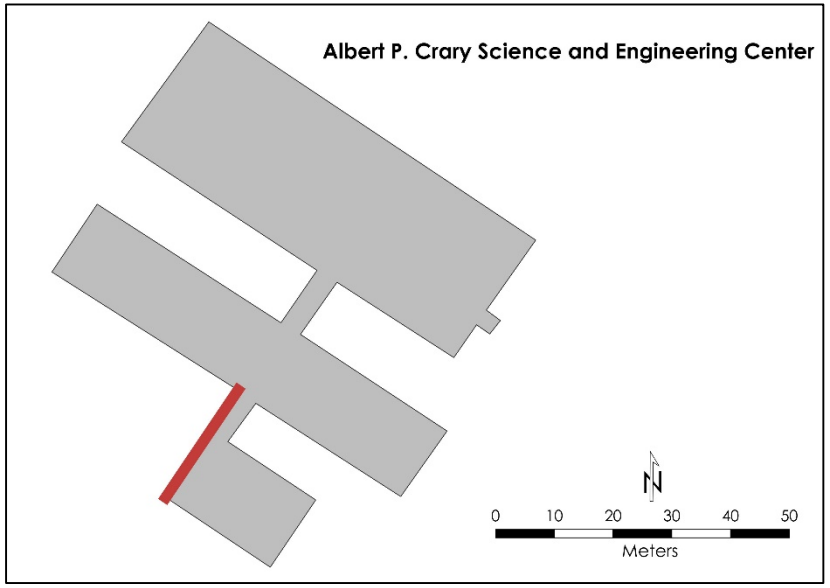
P2SW-V-02 -5◦C 20◦C

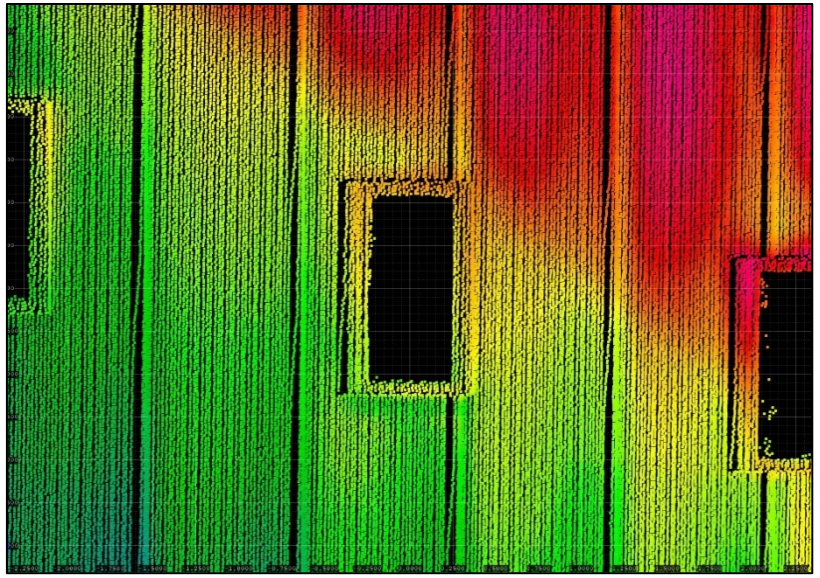


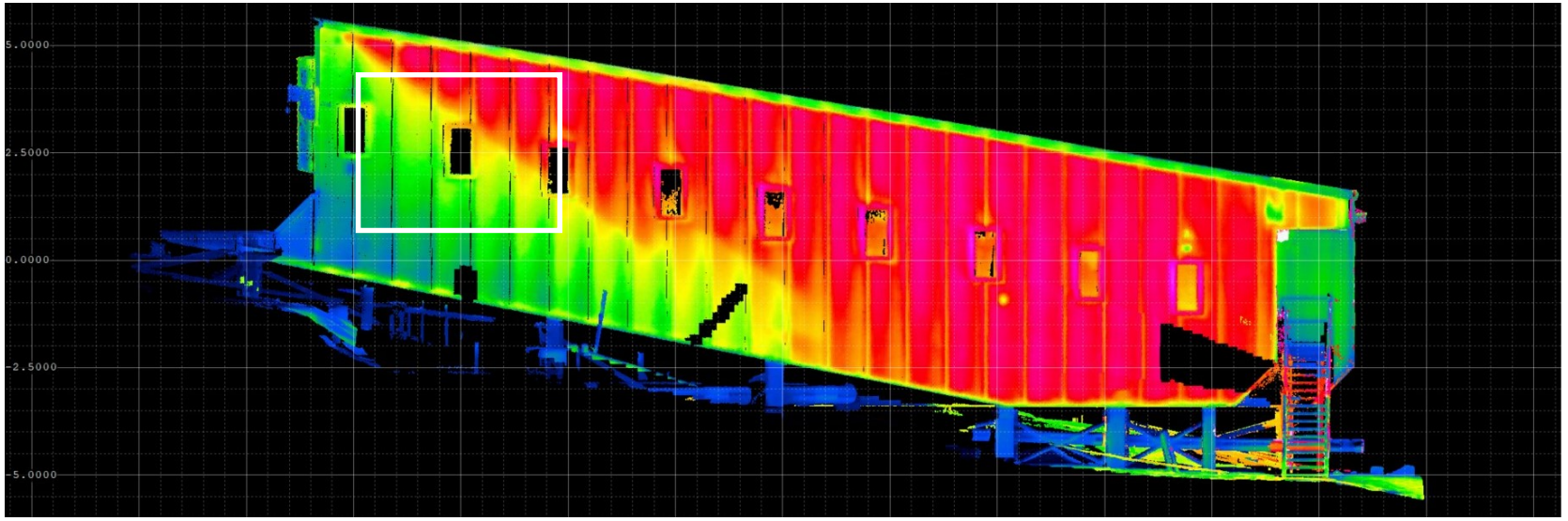




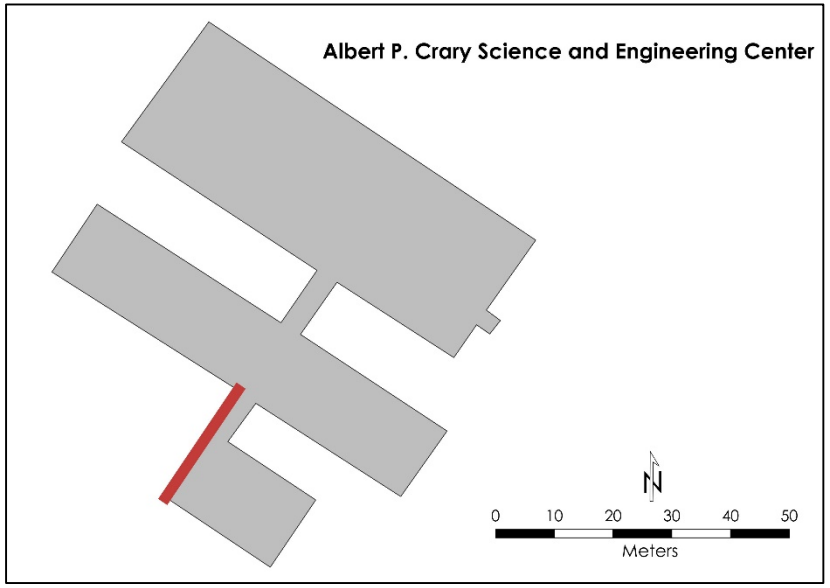
P3CW-W-01 -5◦C 20◦C

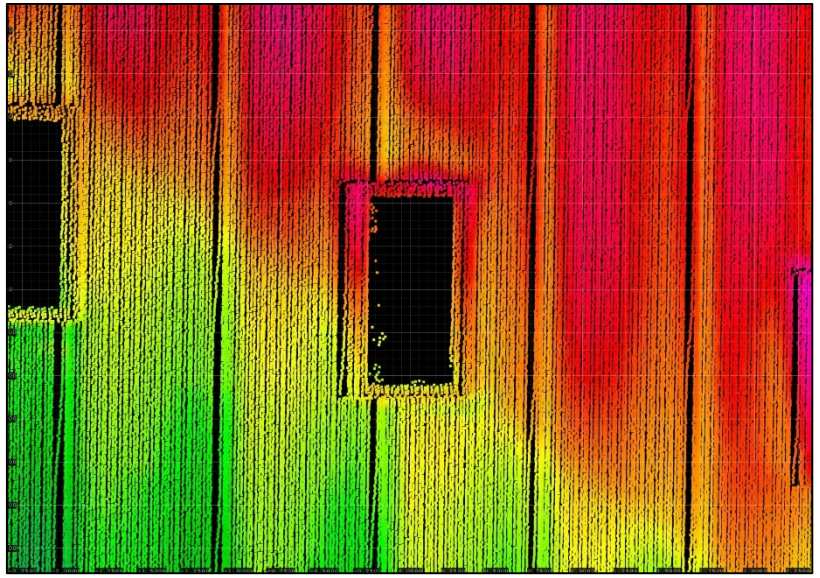


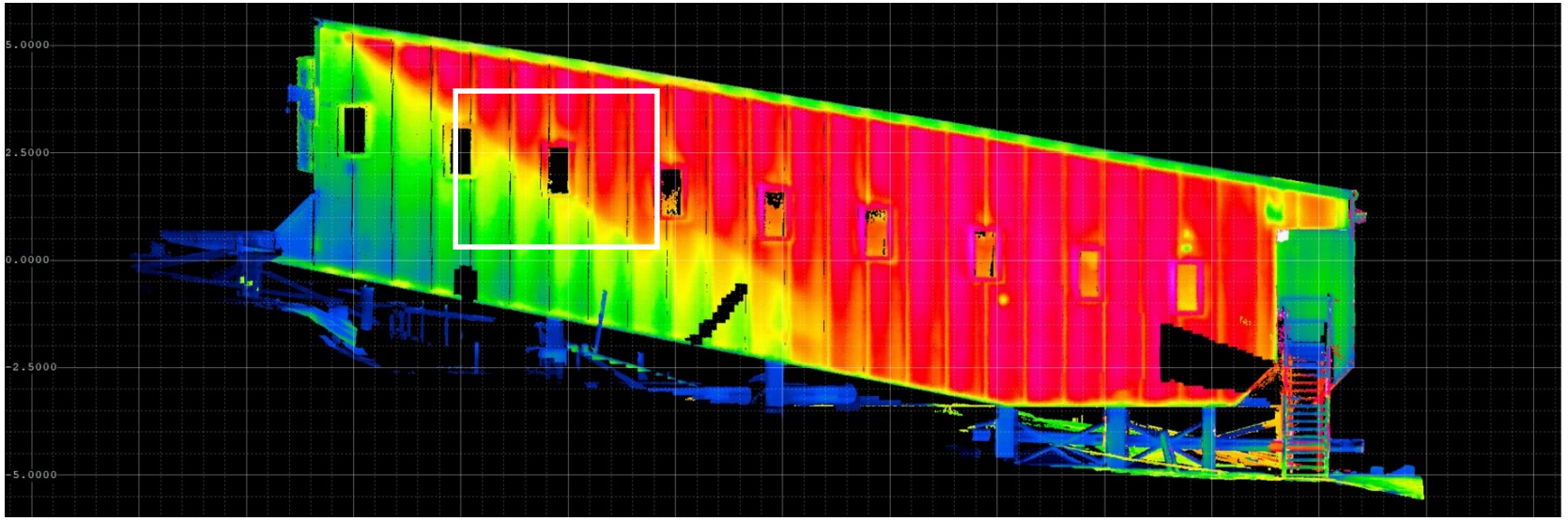




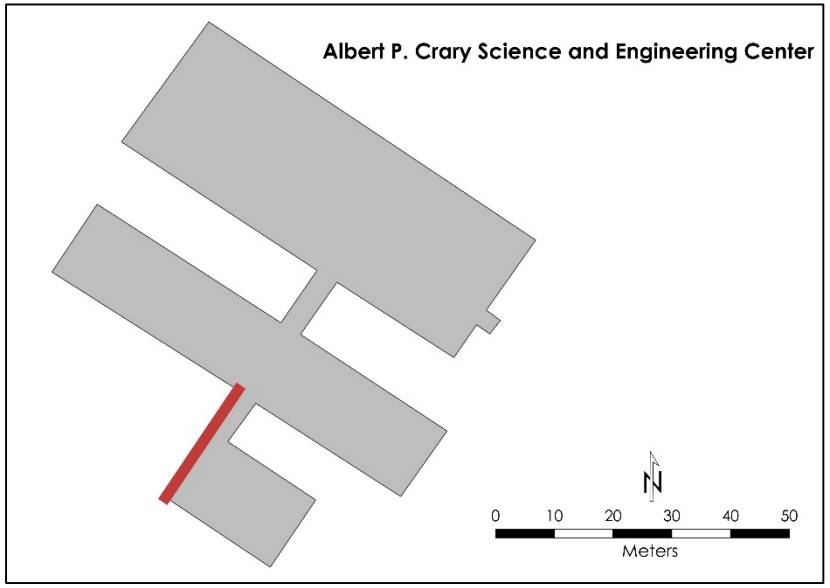
P3CW-W-02 -5◦C 20◦C

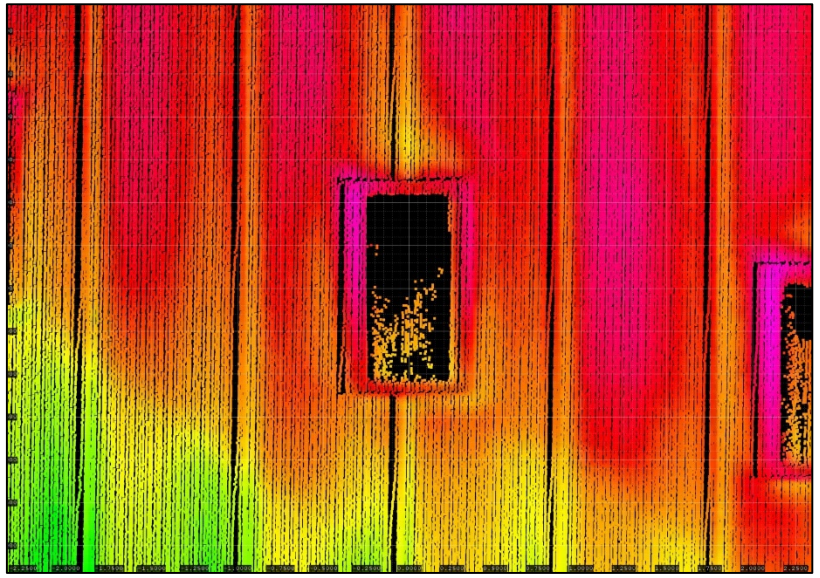


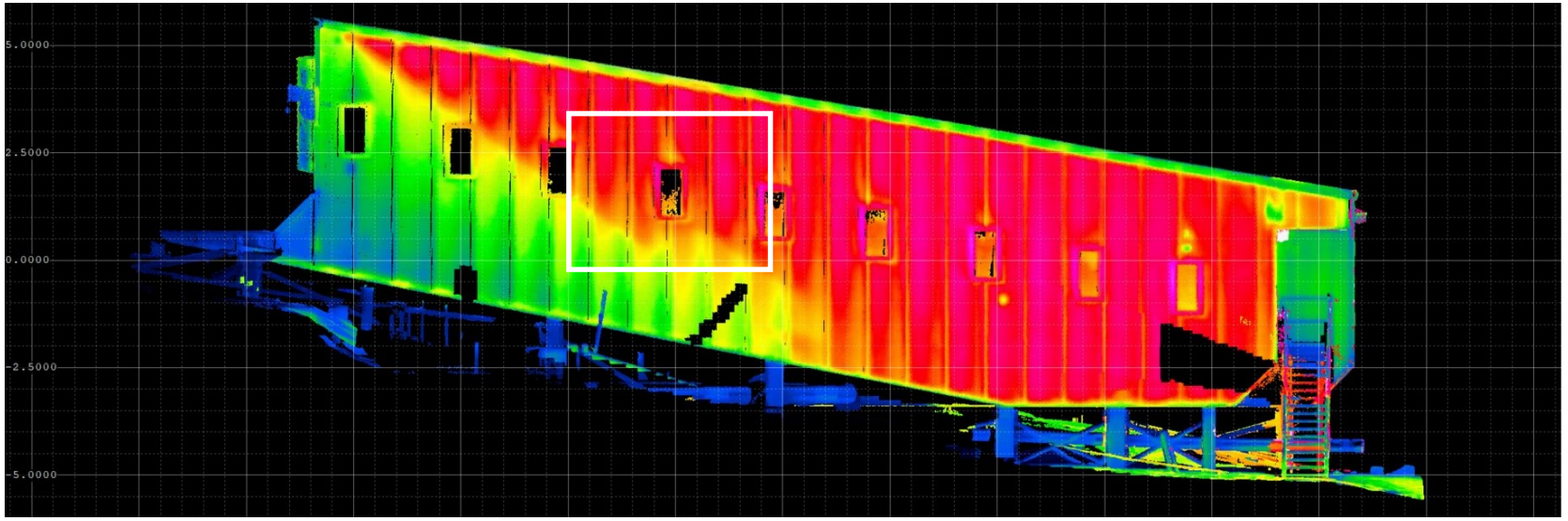




P3CW-W-03 -5◦C 20◦C





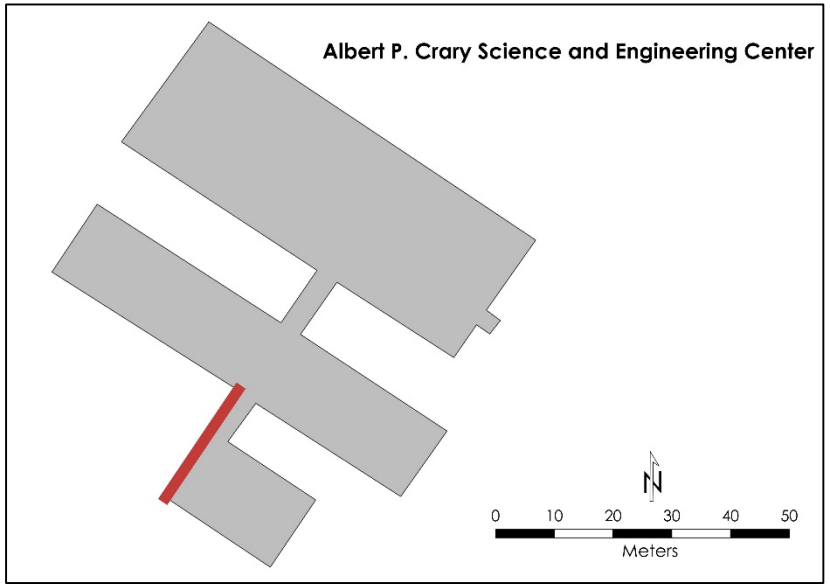


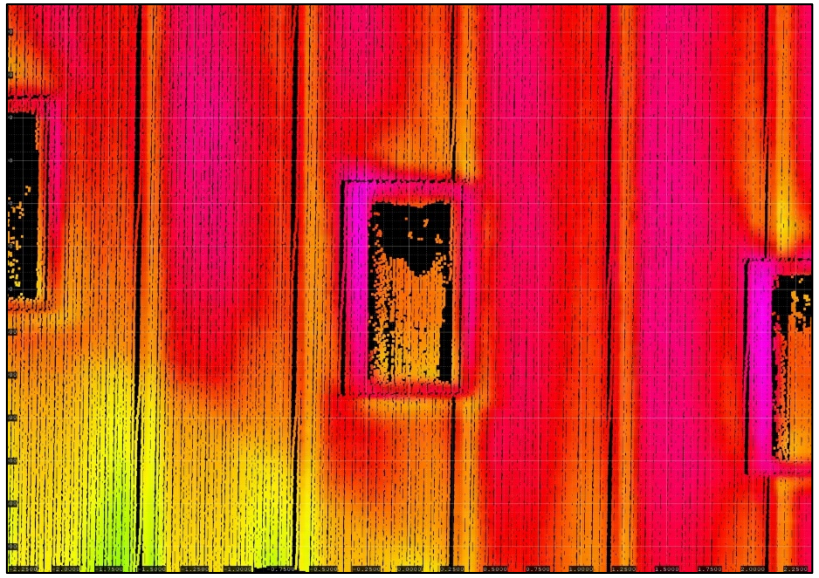
P3CW-W-04

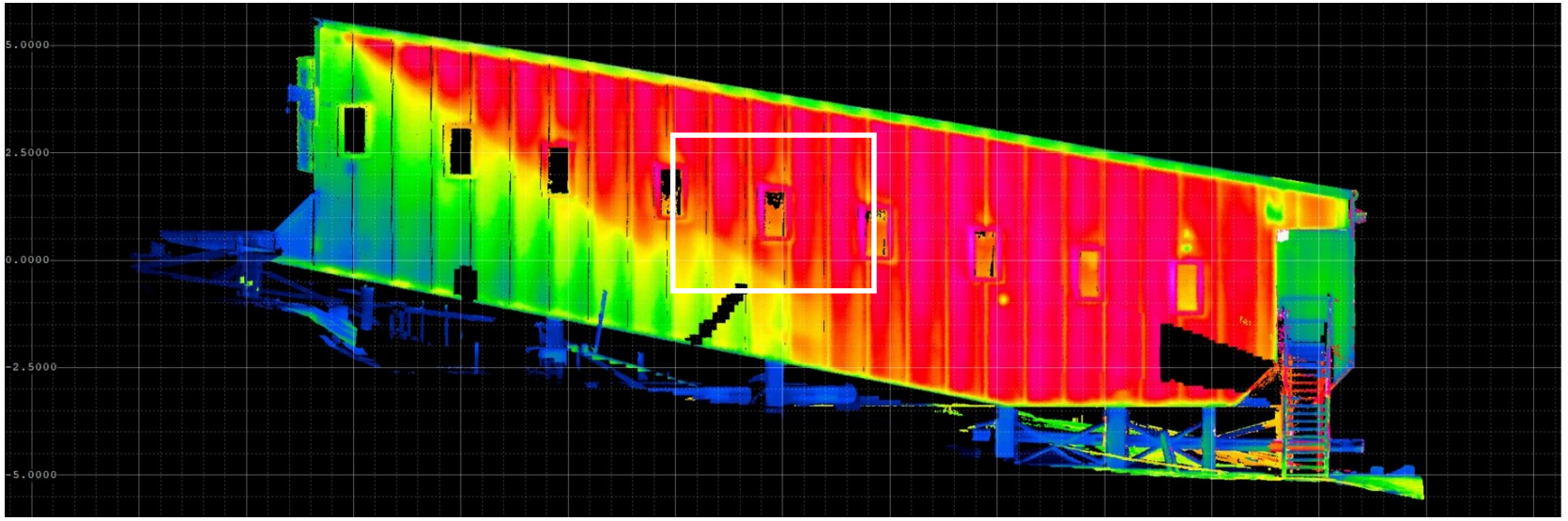
-5◦C



20◦C



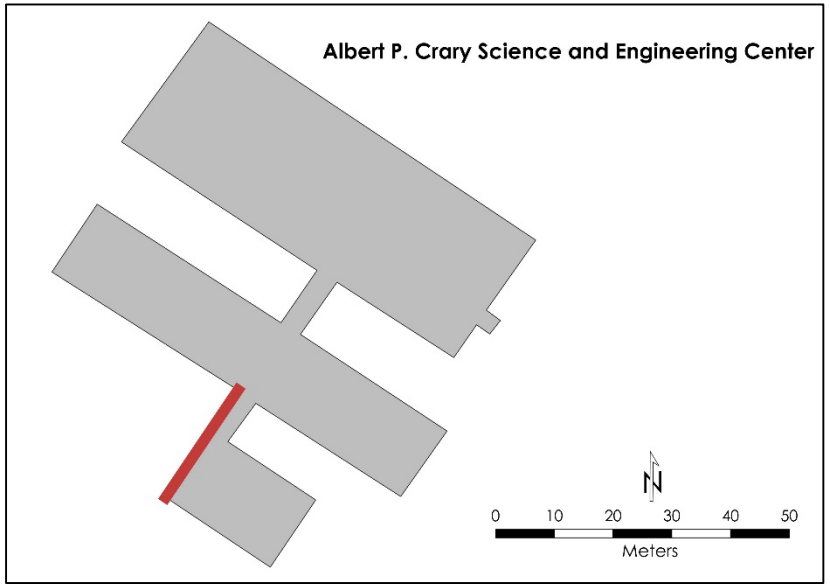


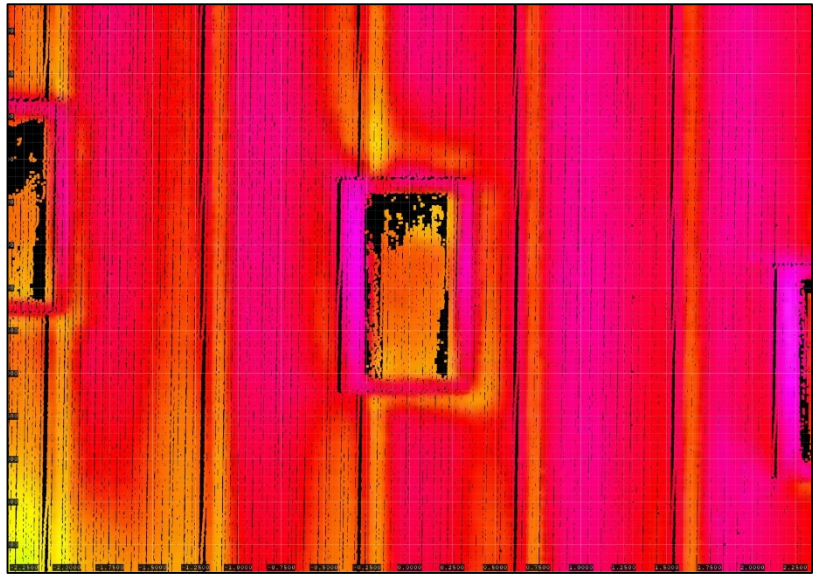


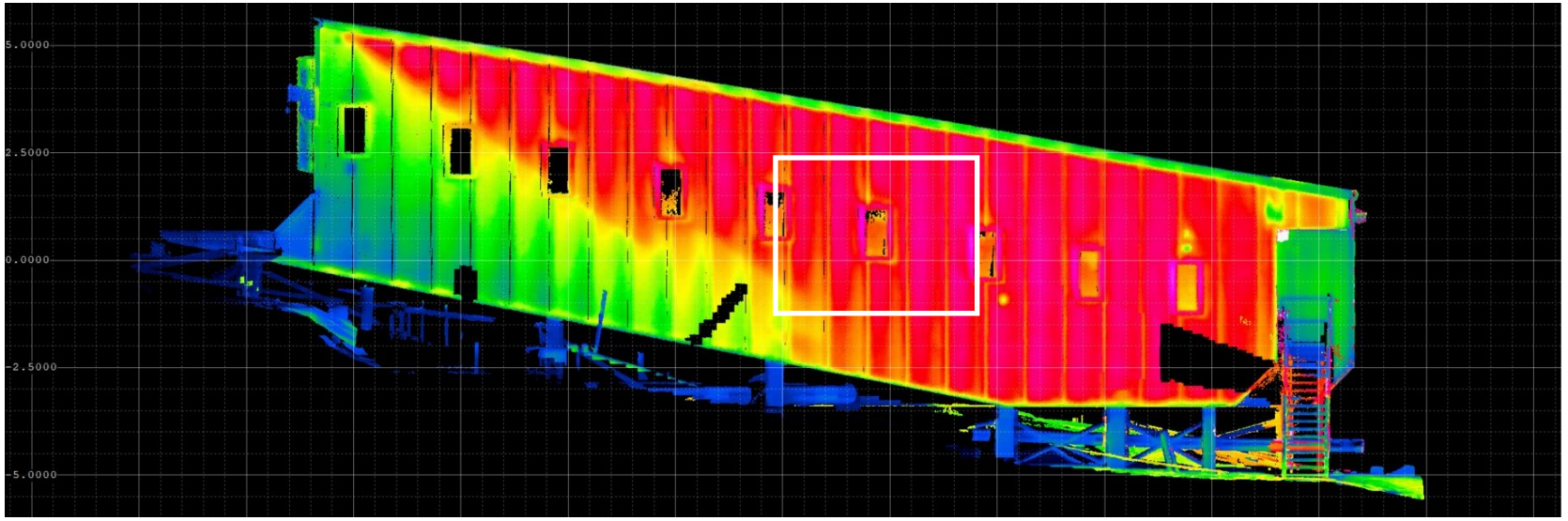
P3CW-W-05

-5◦C

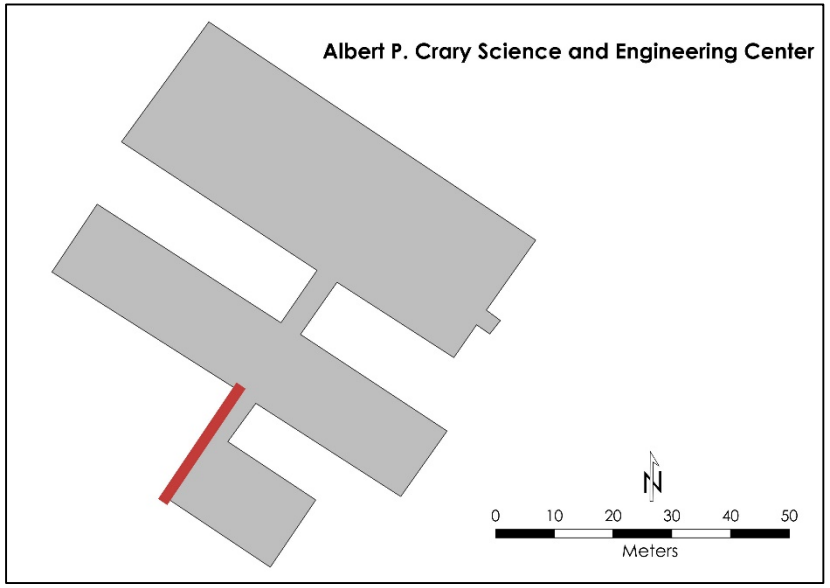
20◦C

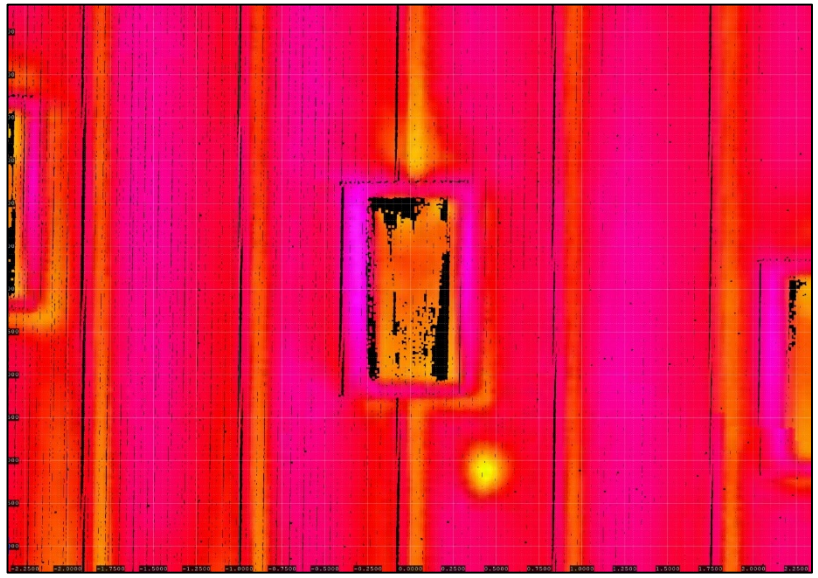


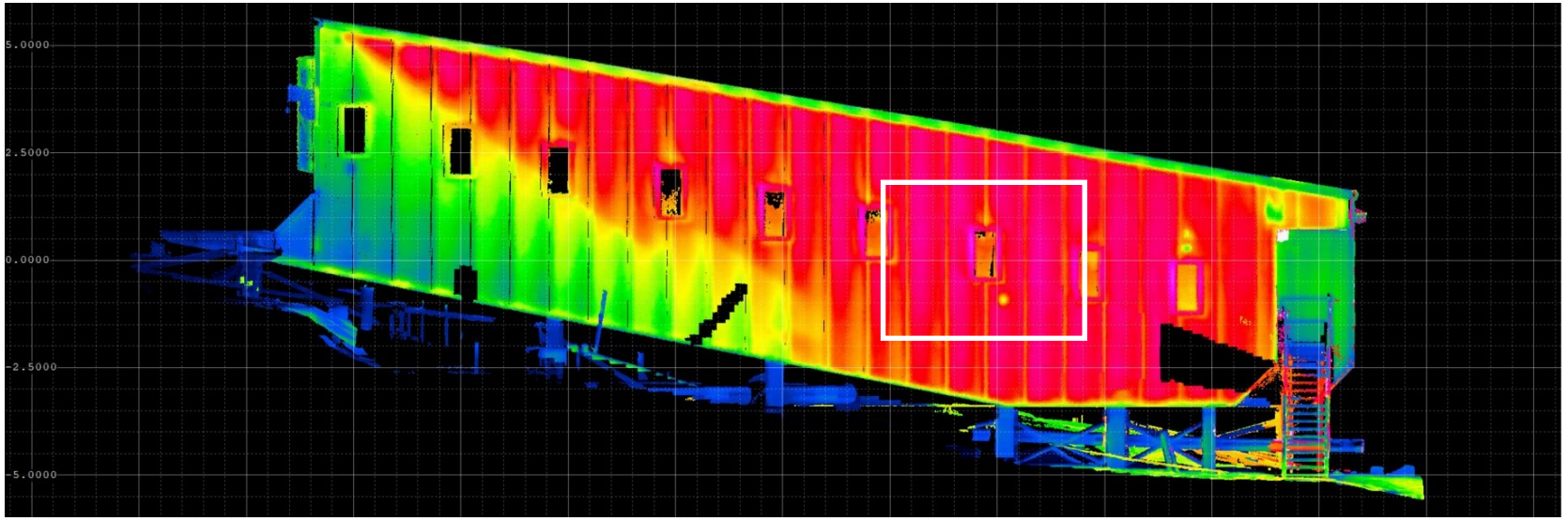




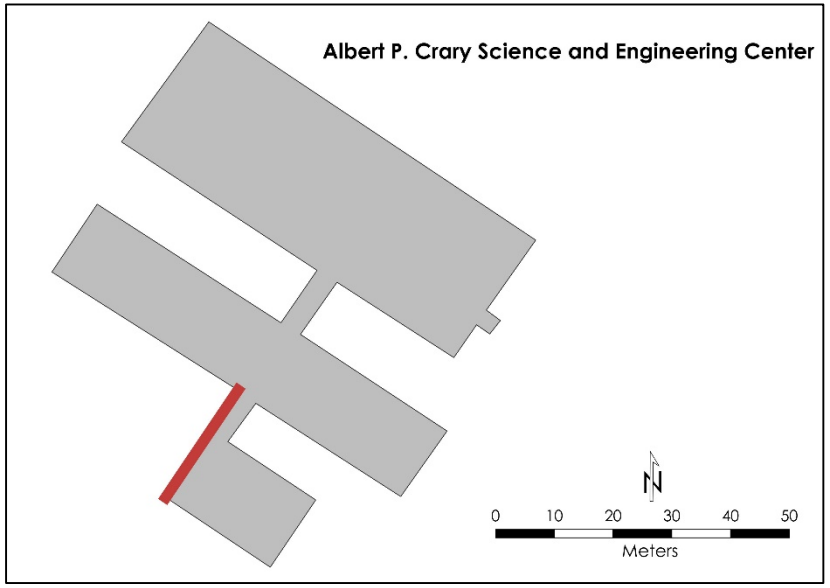
P3CW-W-06 -5◦C 20◦C

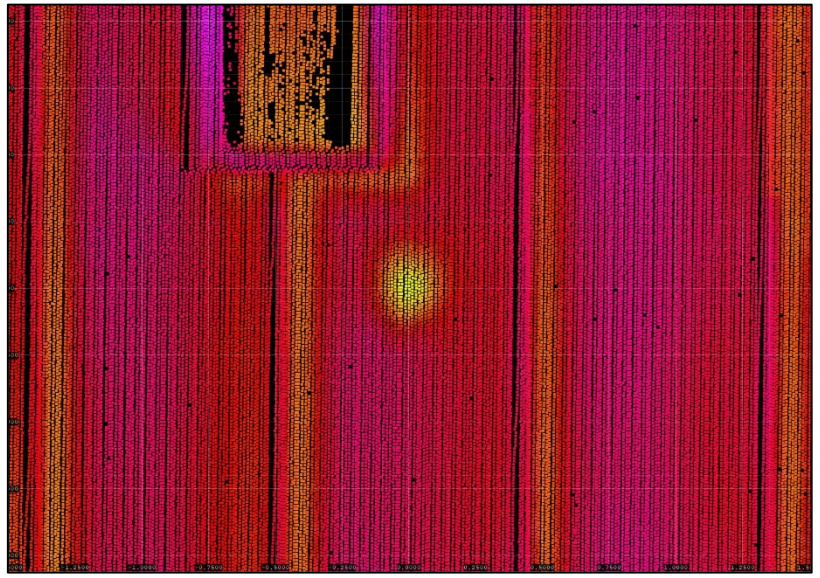


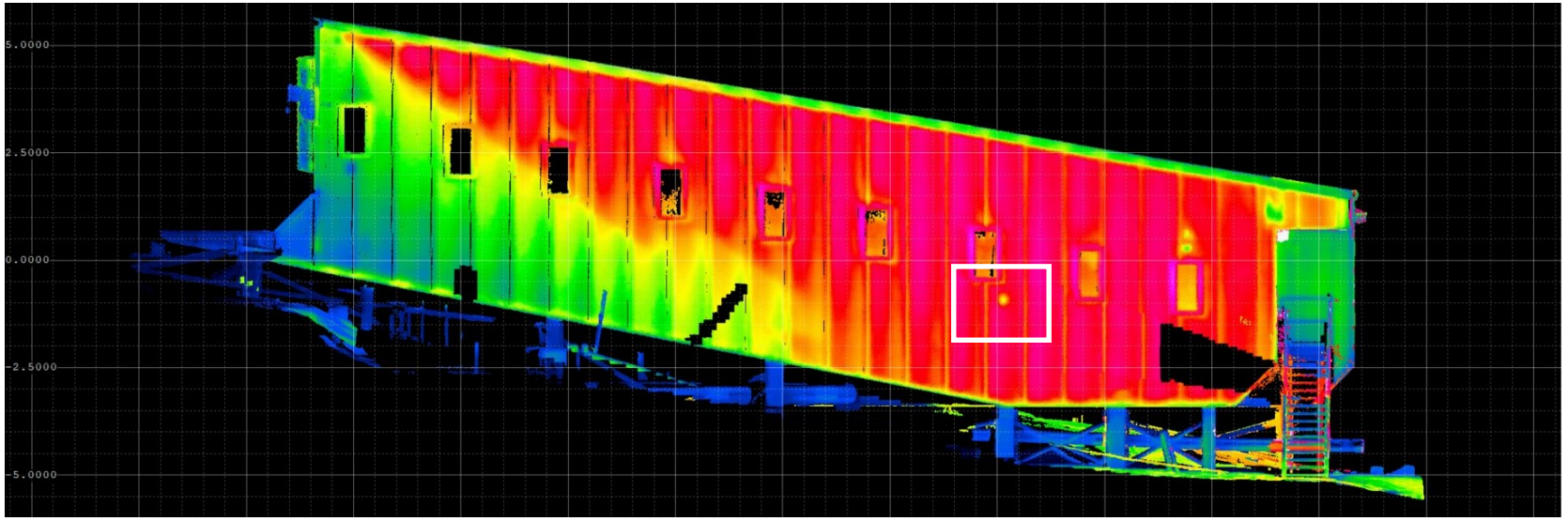




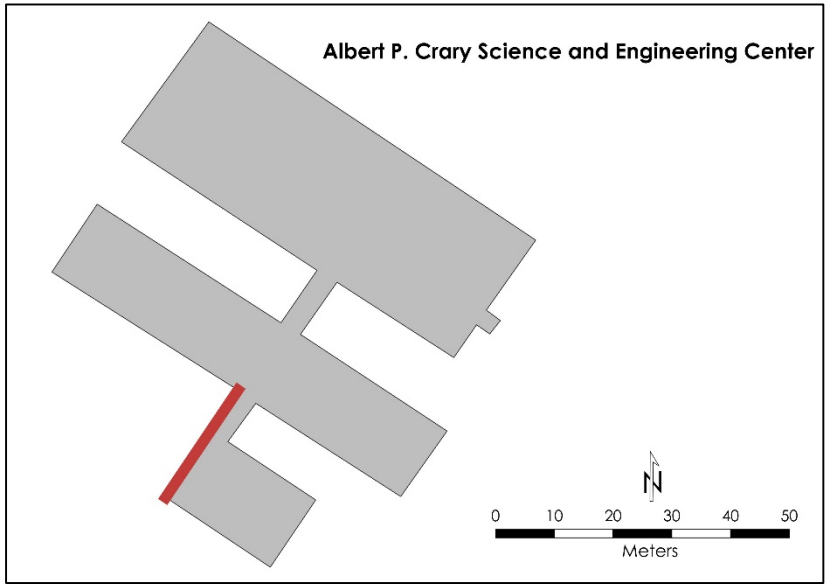
P3CW-W-07 -5◦C 20◦C

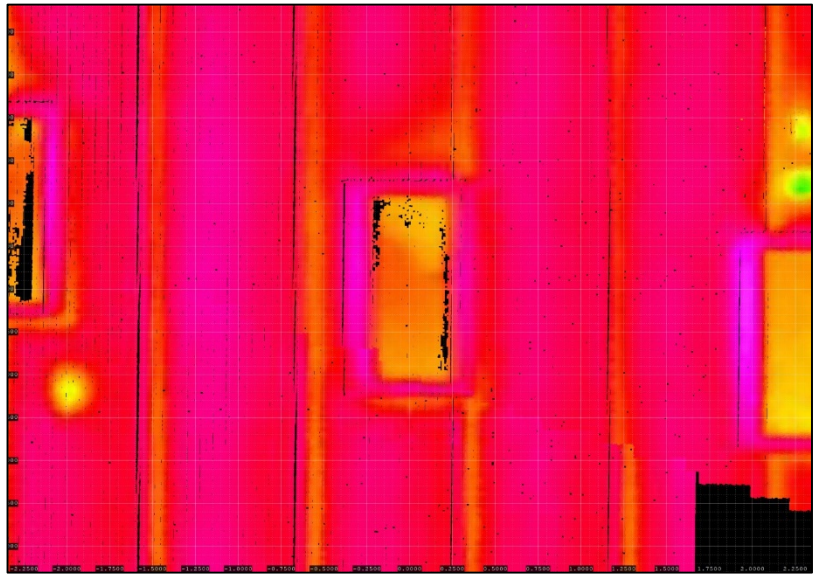


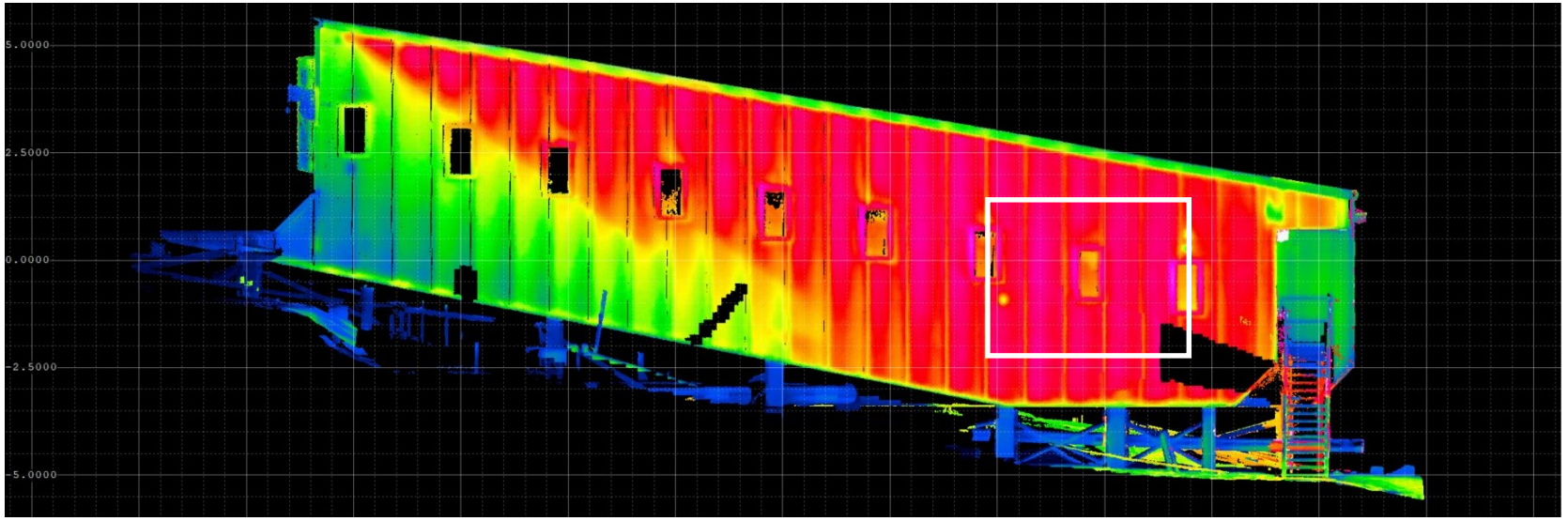




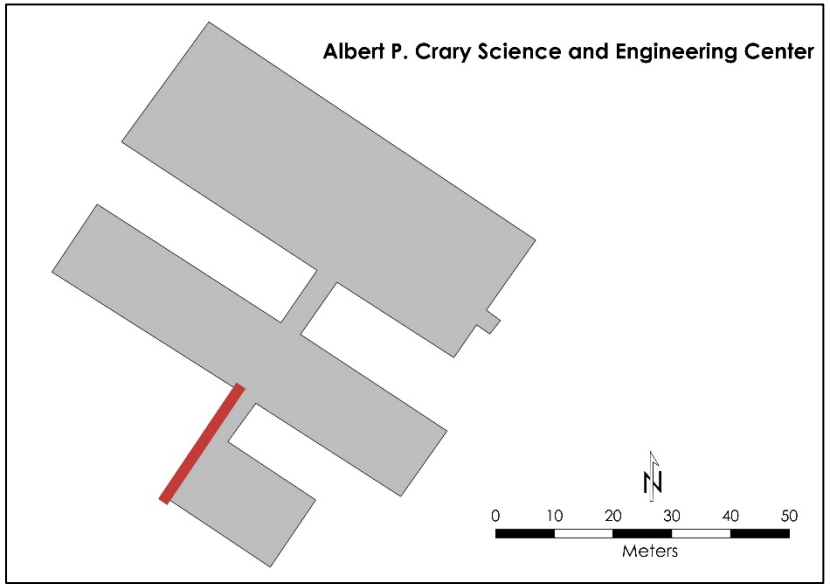
P3CW-TA-01 -5◦C 20◦C

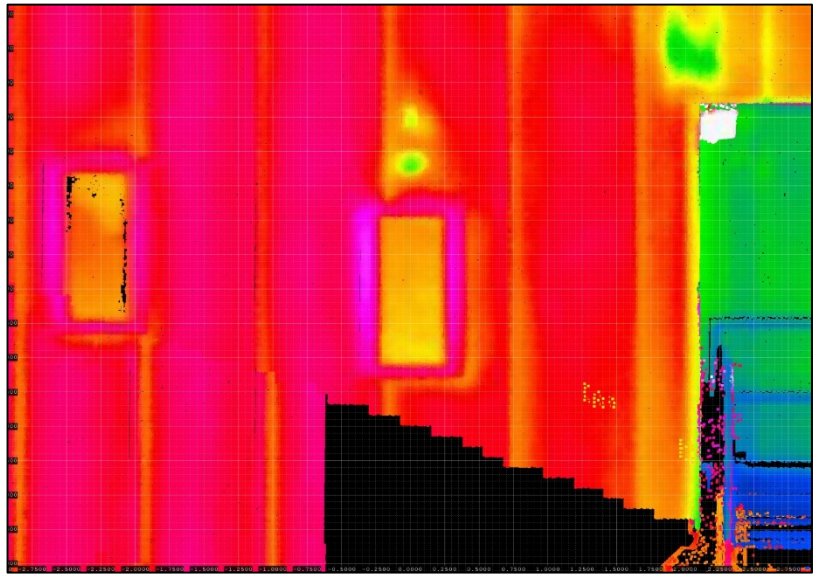


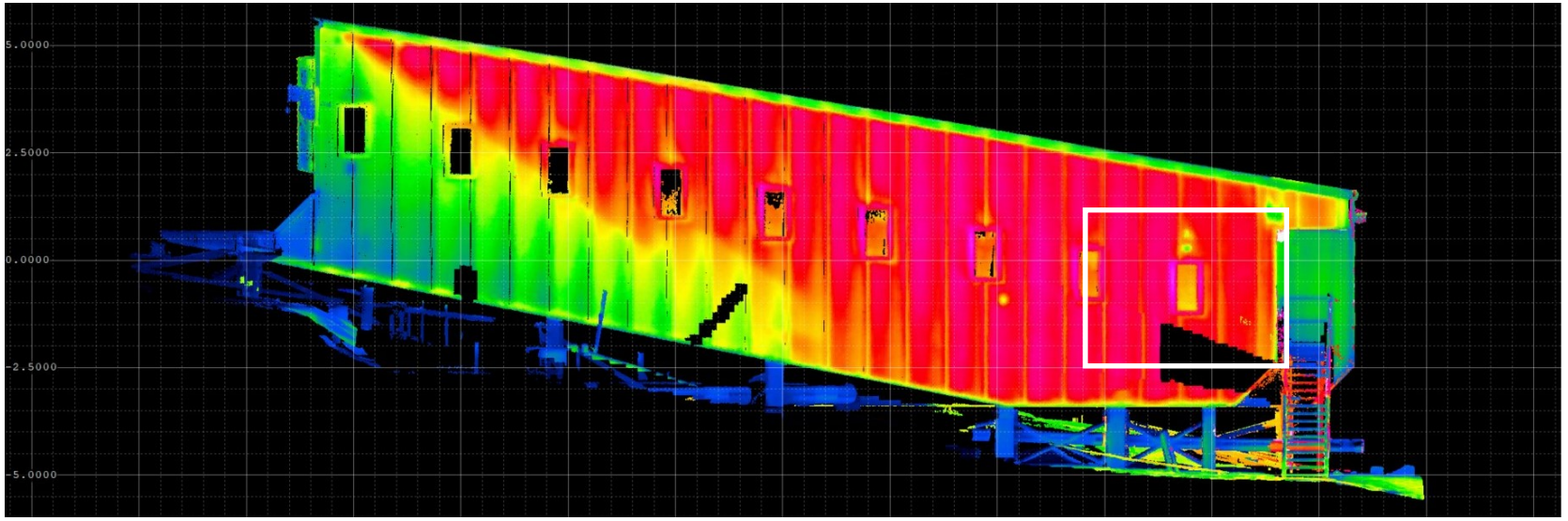




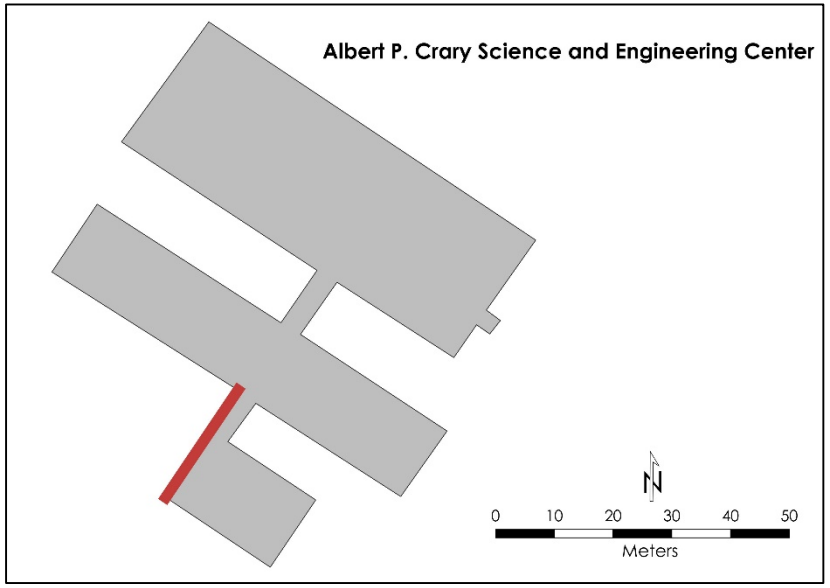
P3CW-W-08 -5◦C 20◦C

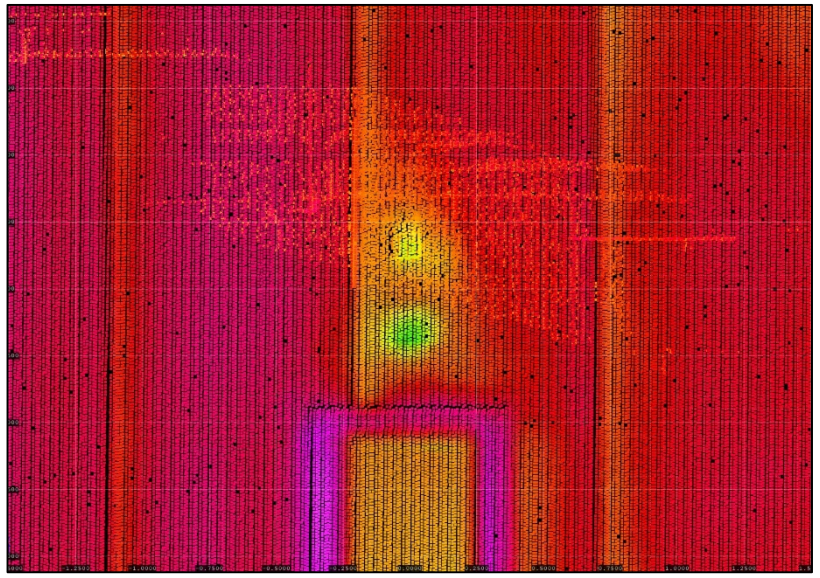


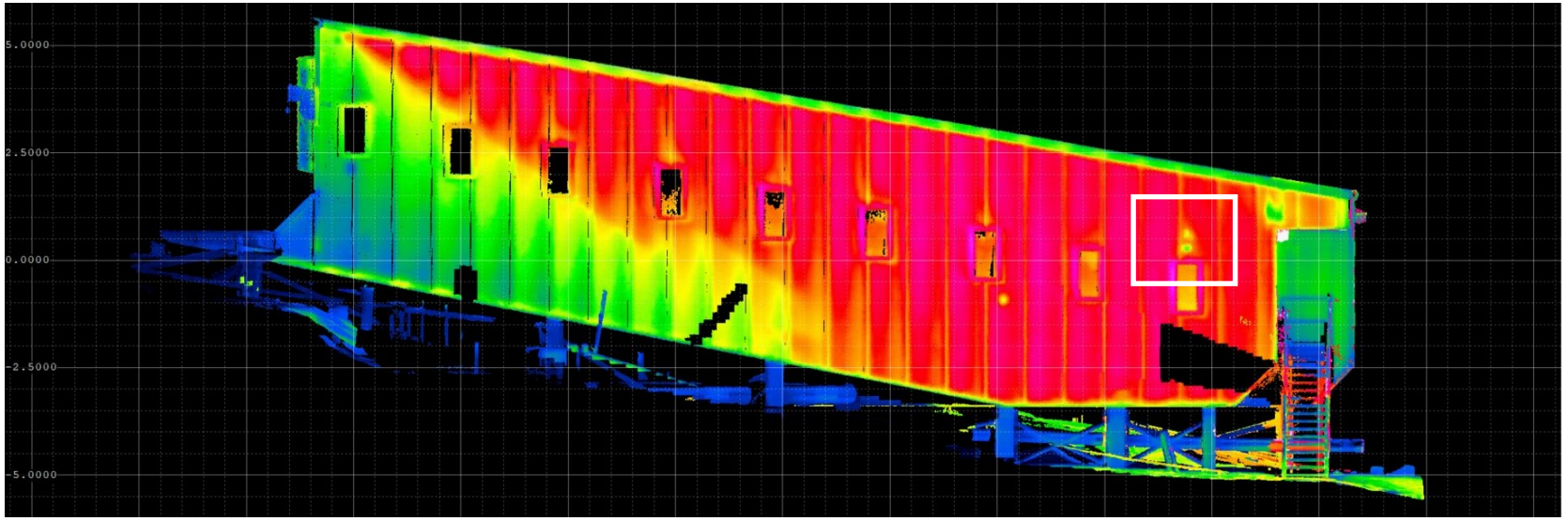




P3CW-W-09 -5◦C 20◦C





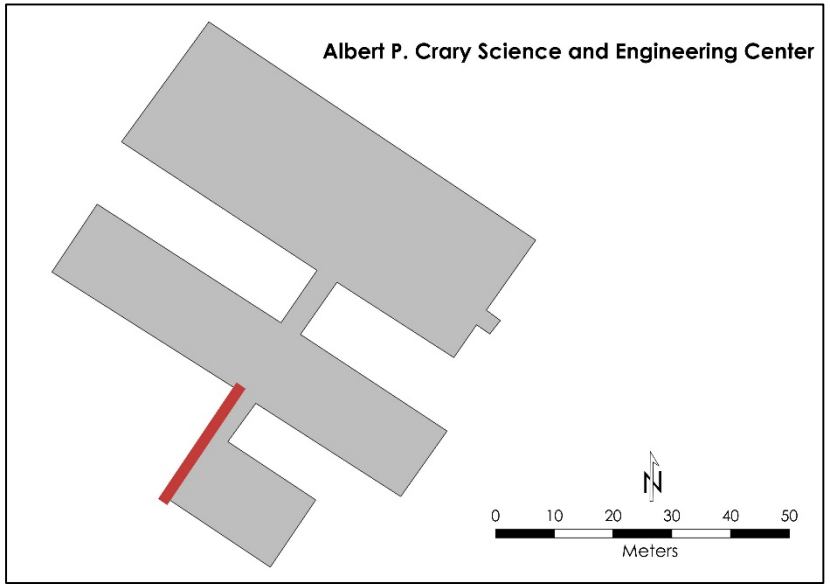


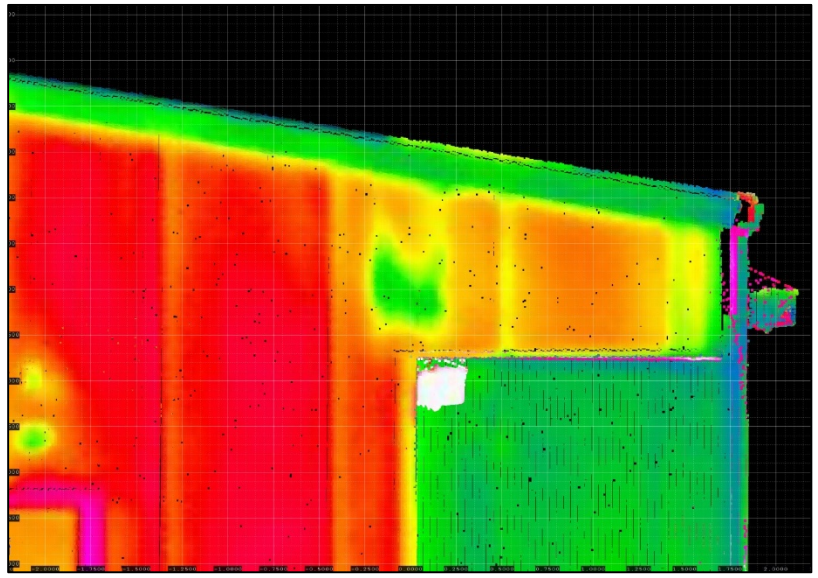
P3CW-TA-02

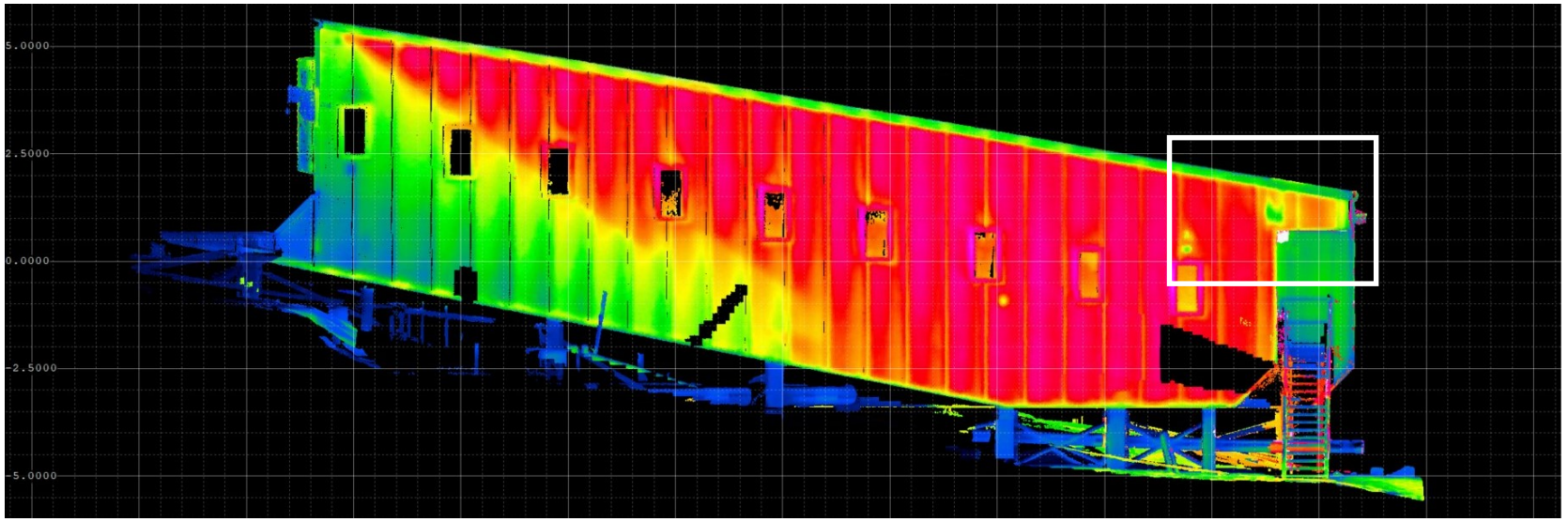
-5◦C



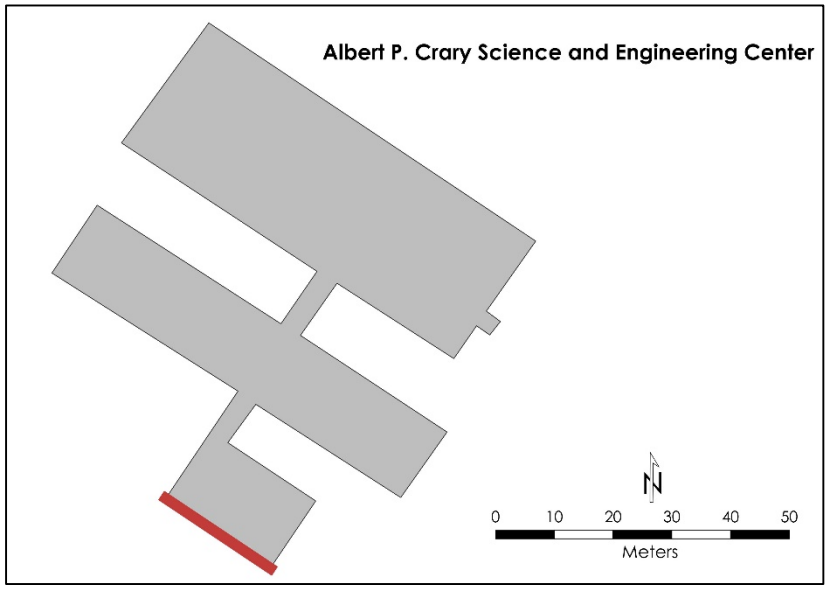
20◦C

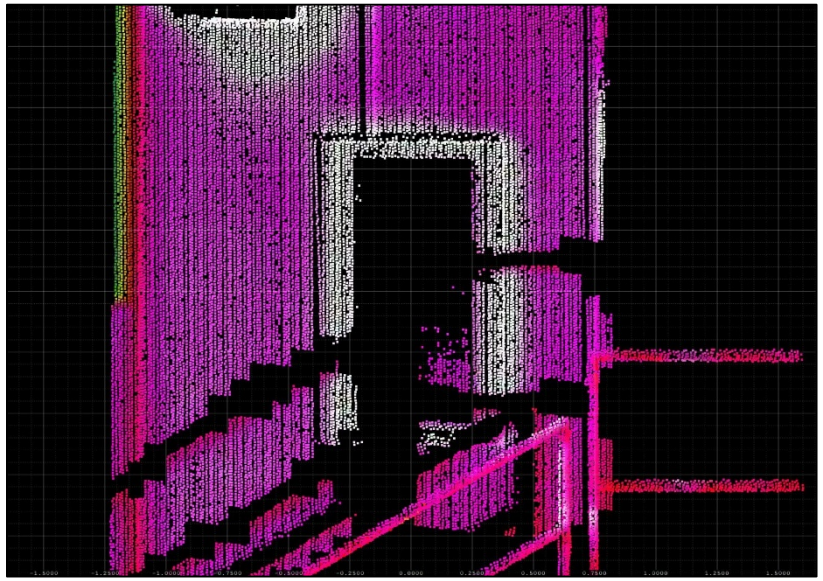


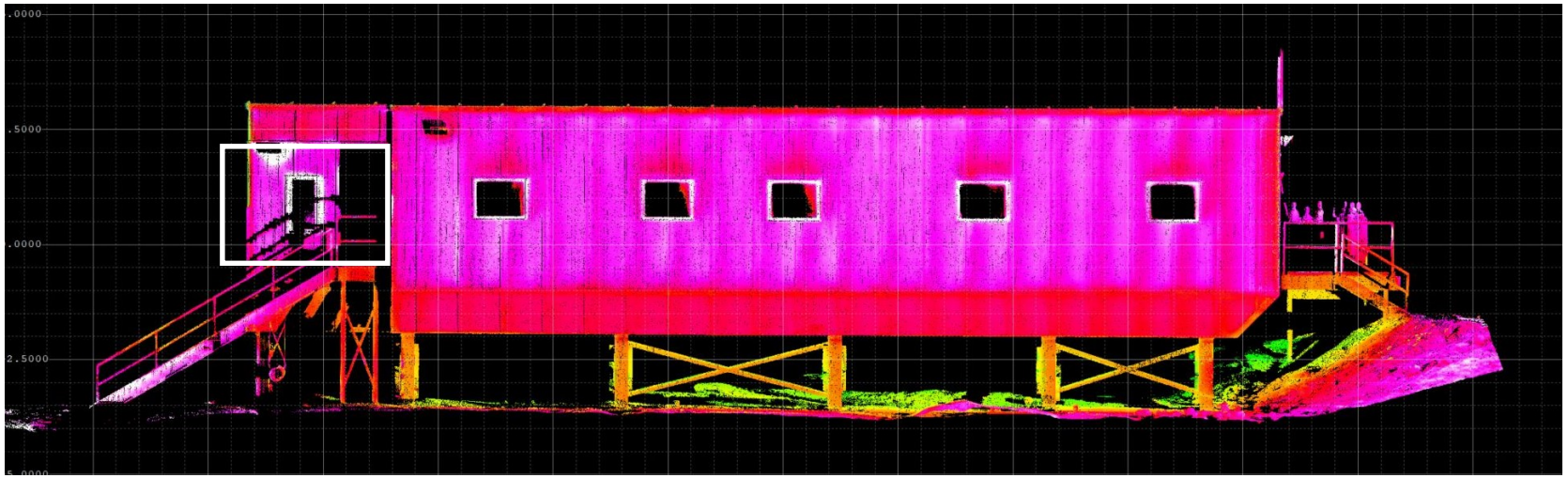




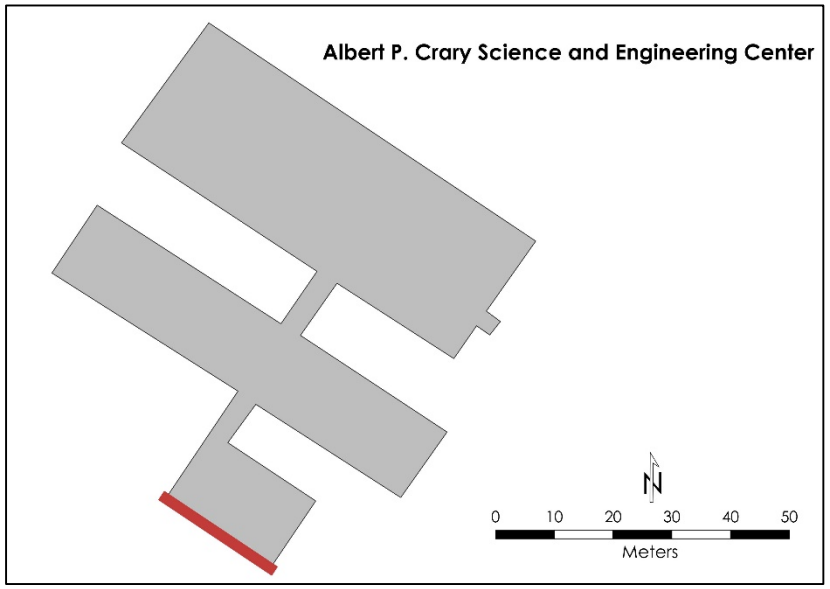
P3CW-TA-03 -5◦C 20◦C

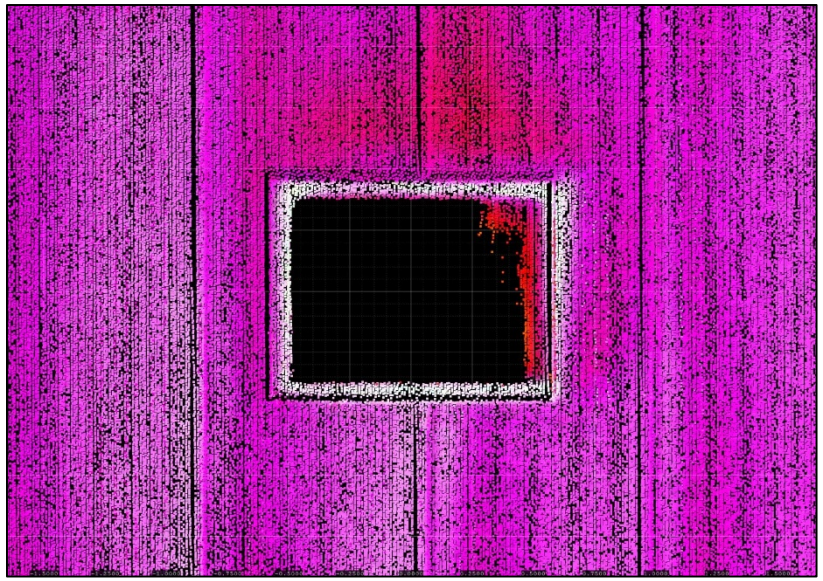


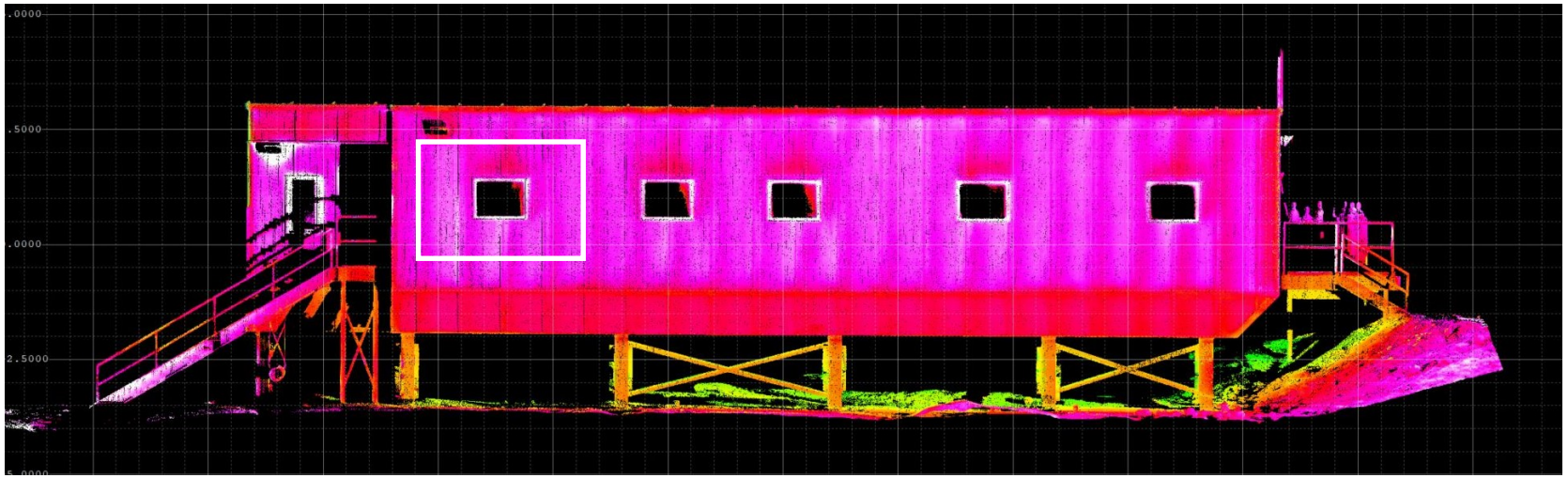




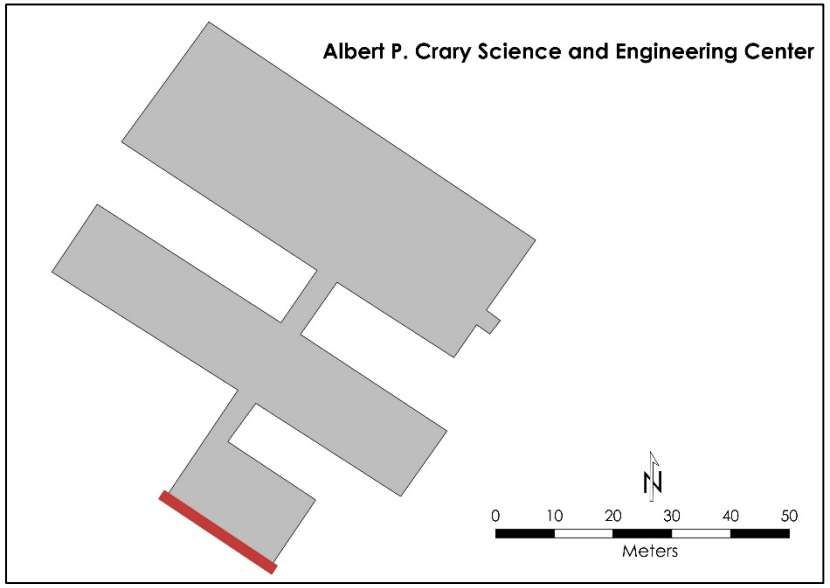
P3S-W-01 -15◦C 5◦C

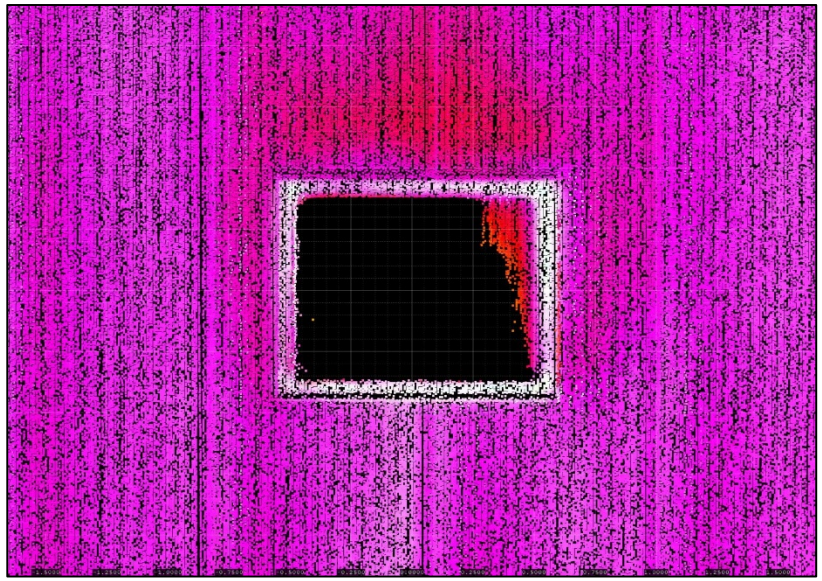


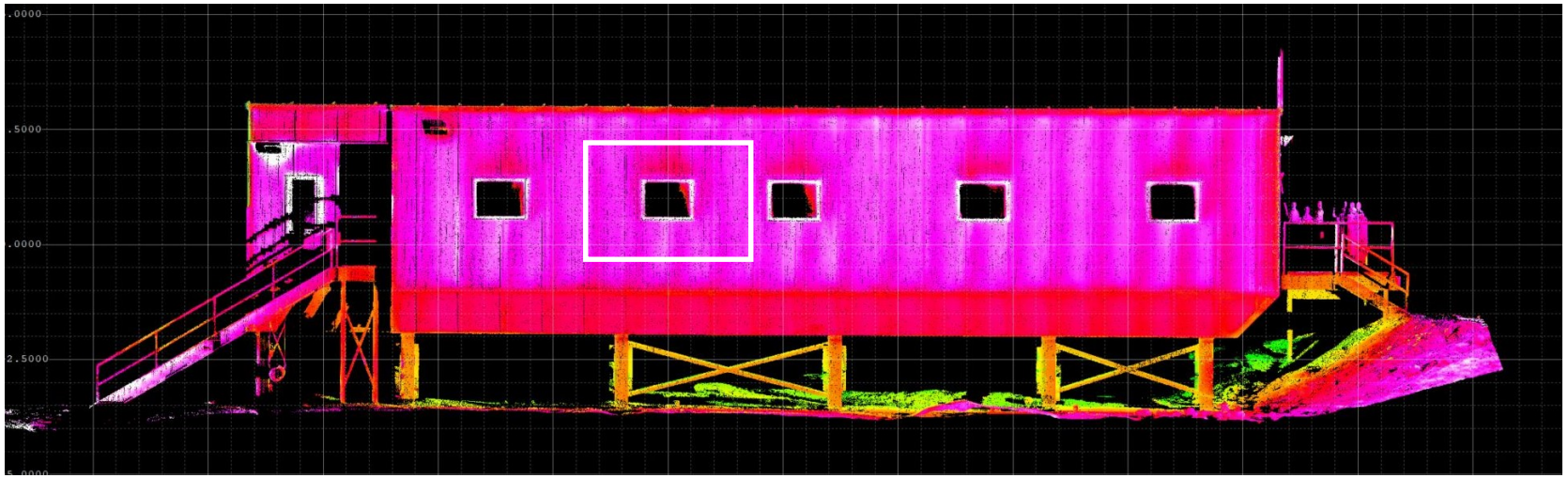




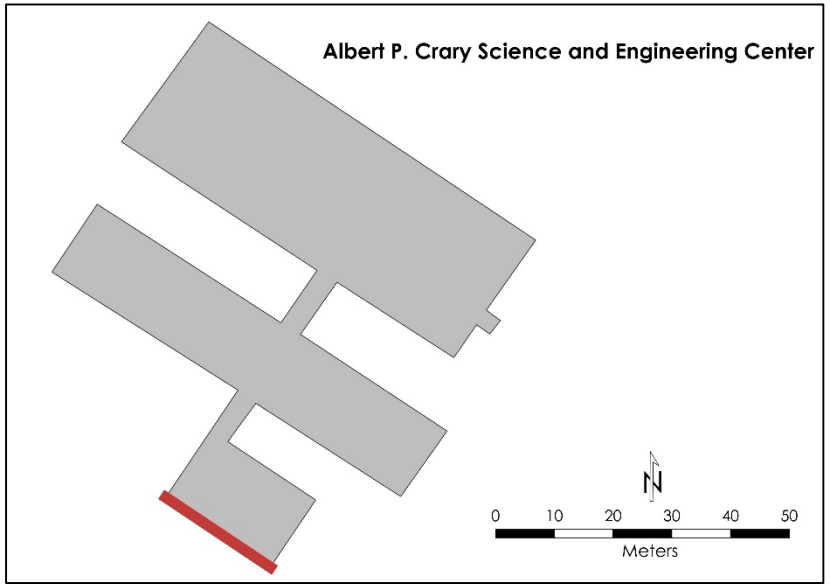
P3S-W-02 -15◦C 5◦C

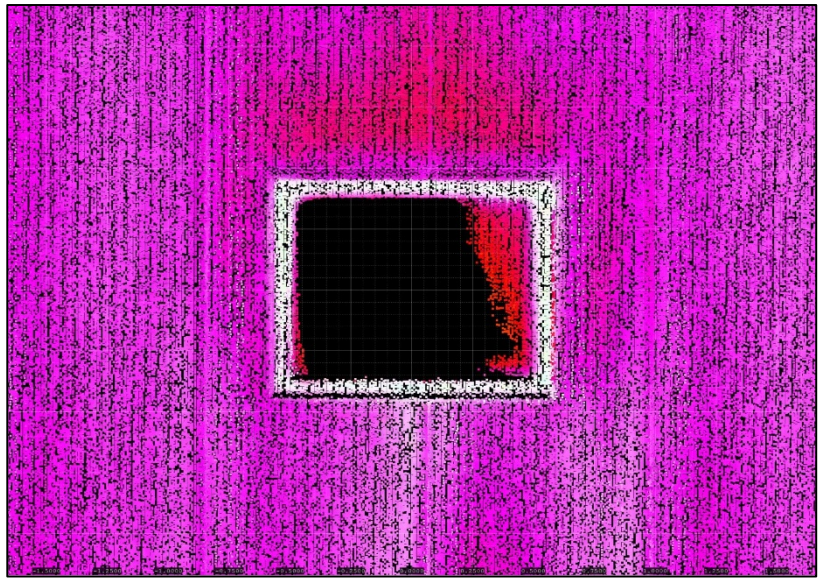


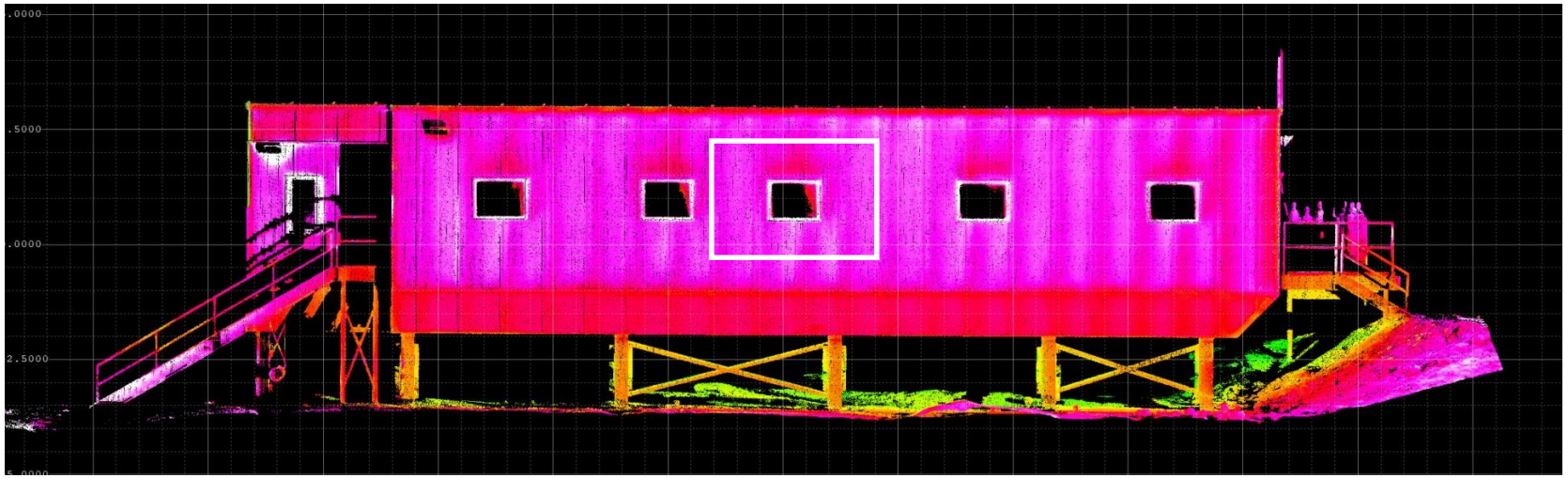




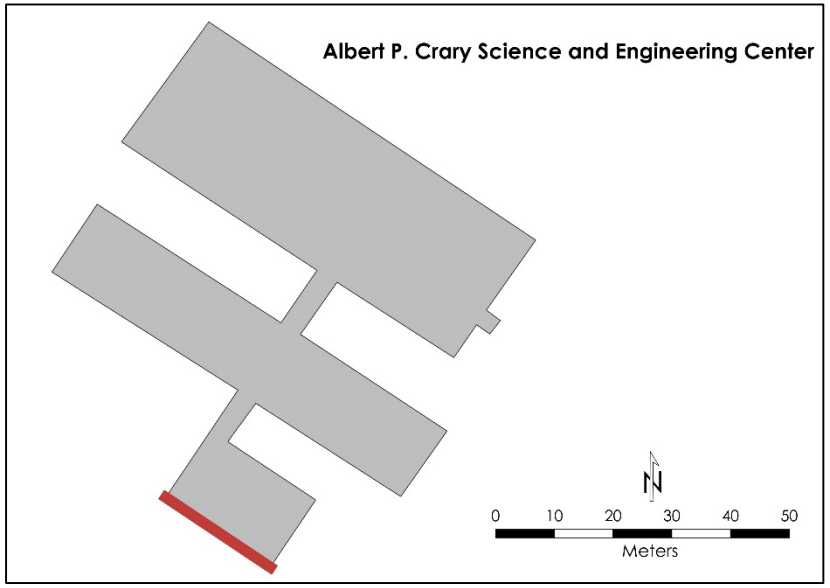
P3S-W-03 -15◦C 5◦C

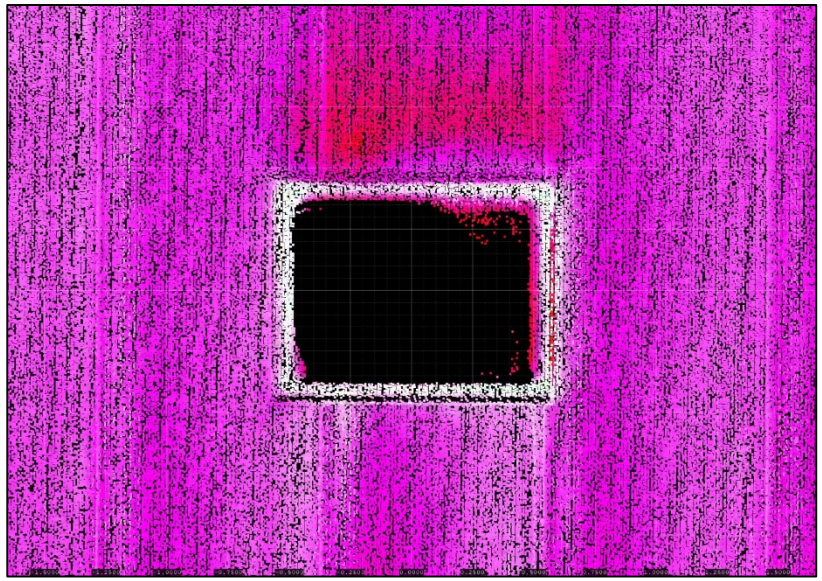


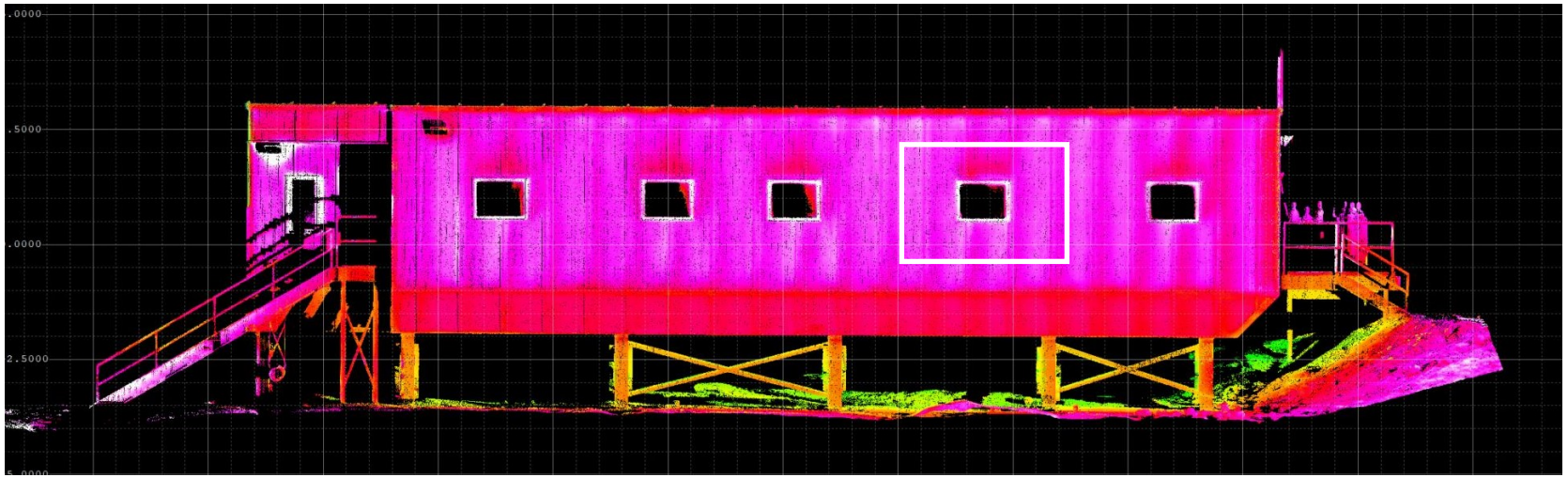




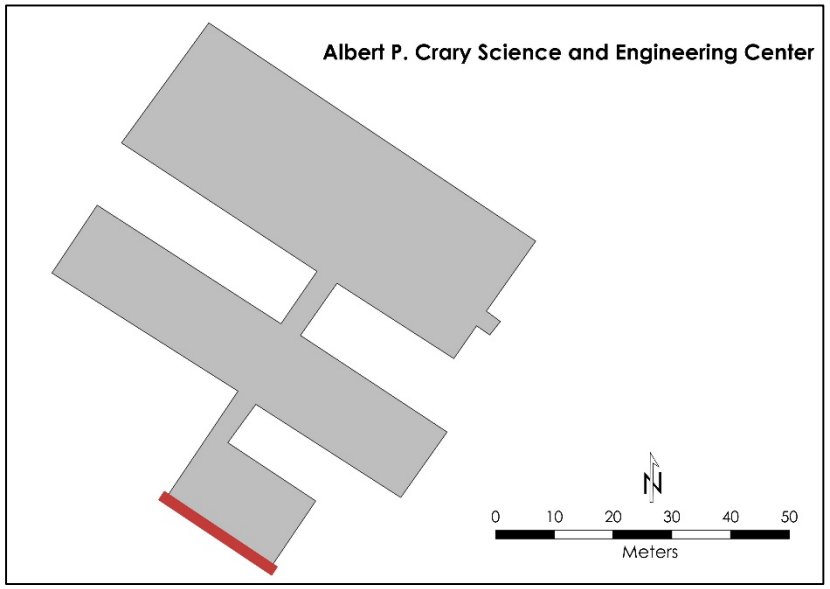
P3S-W-04 -15◦C 5◦C

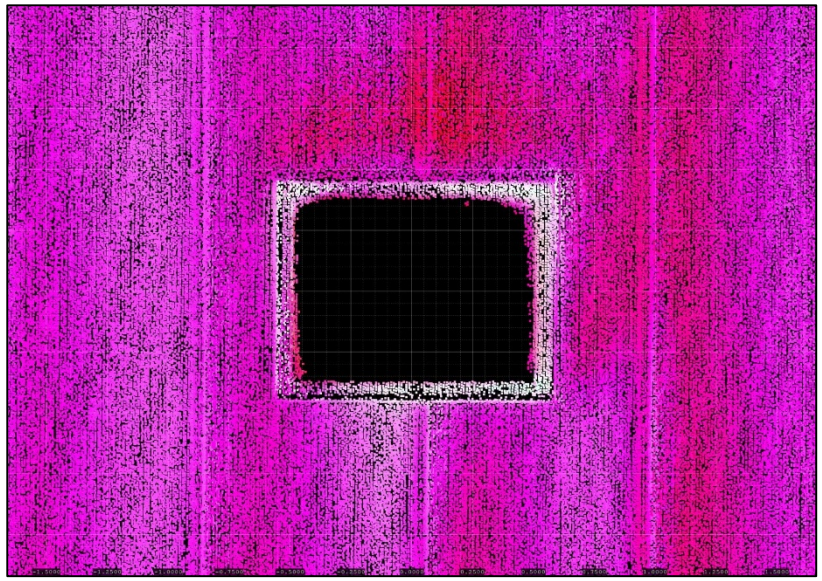


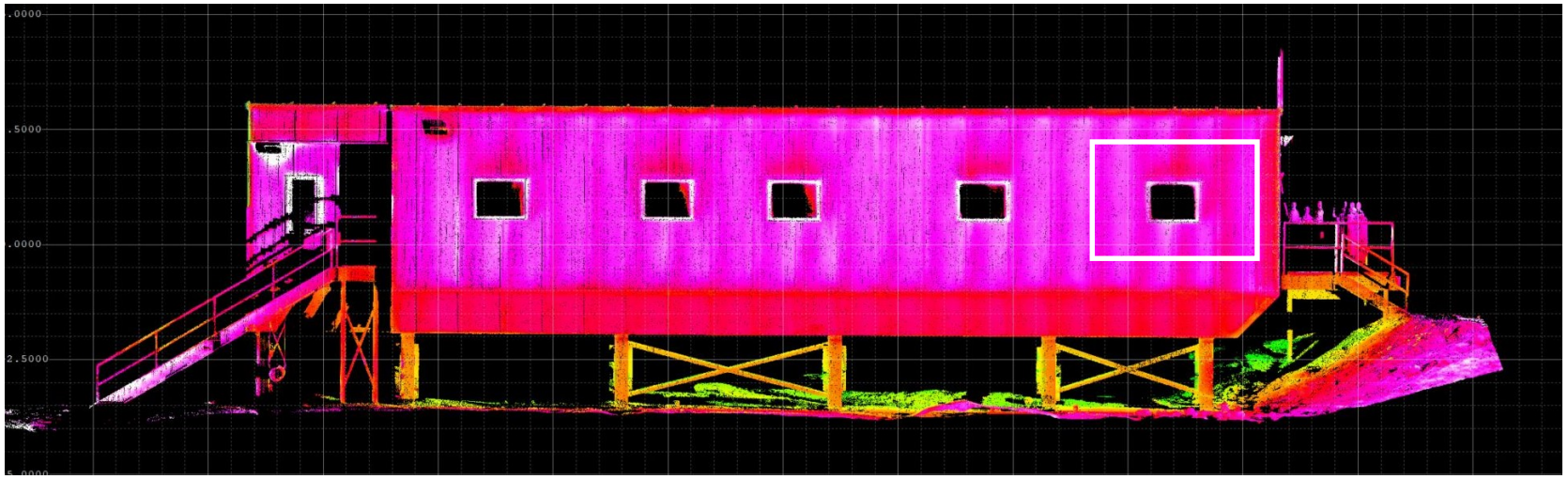




P3S-W-05 -15◦C 5◦C





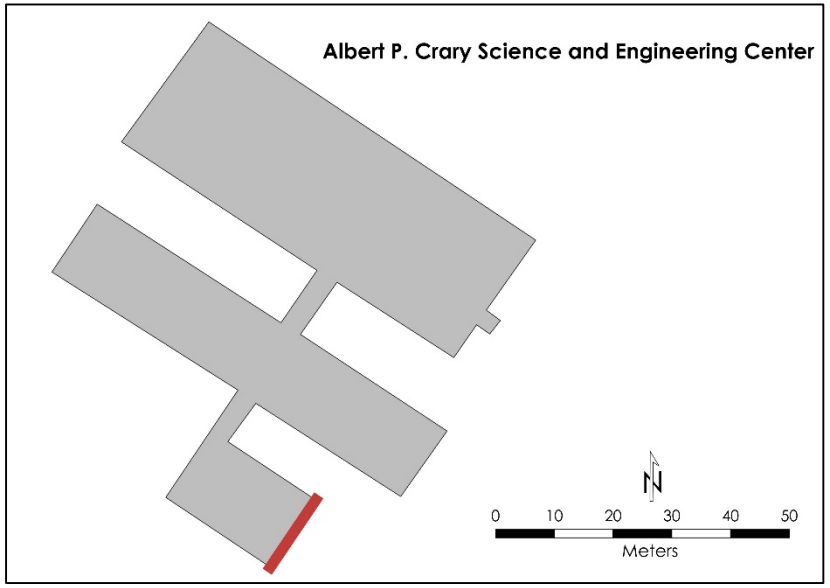


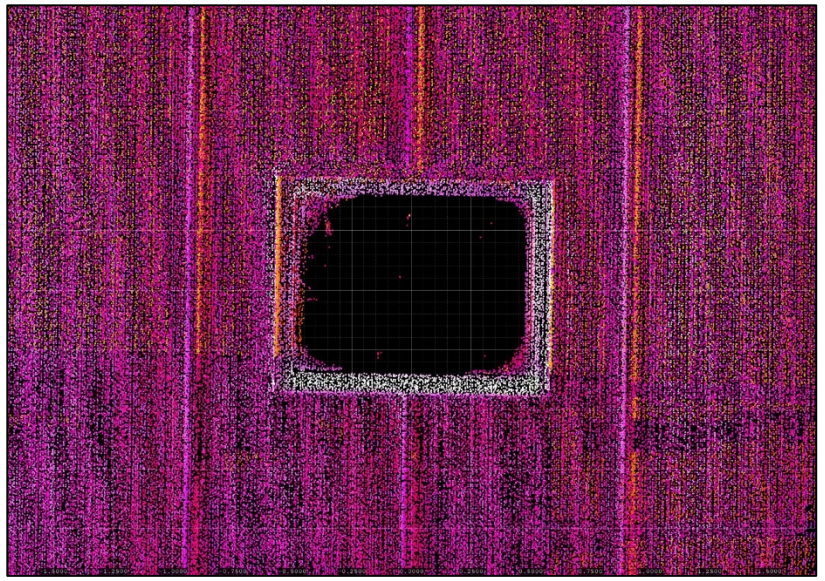
P3S-W-06

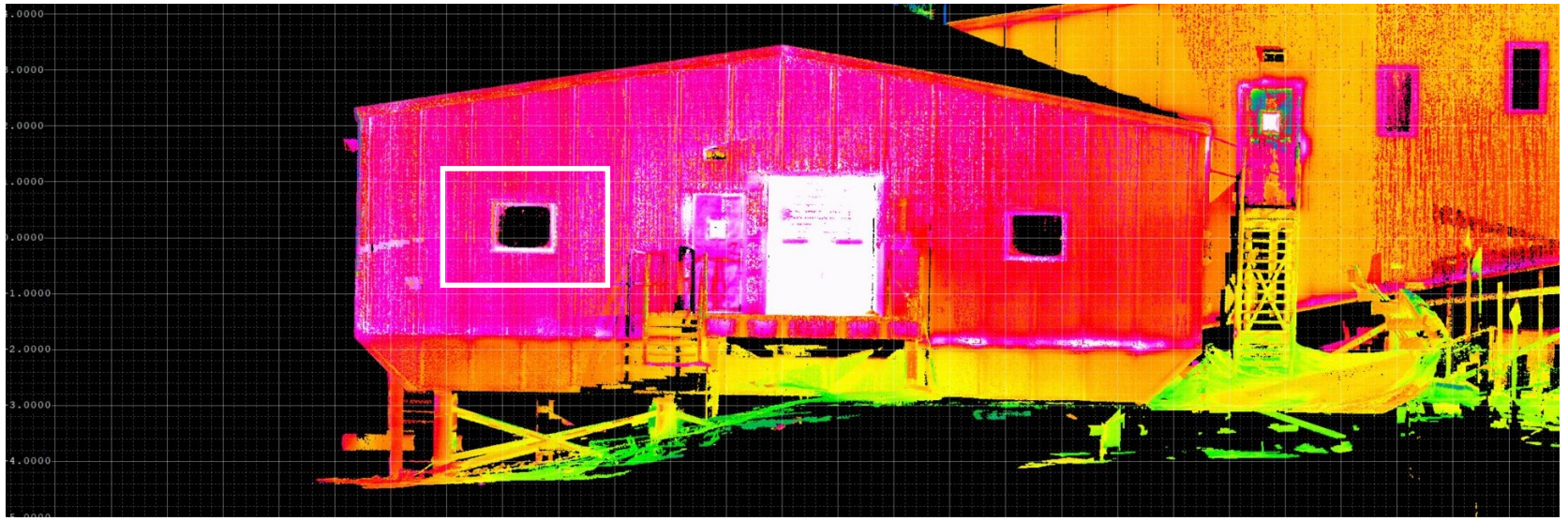
-15◦C



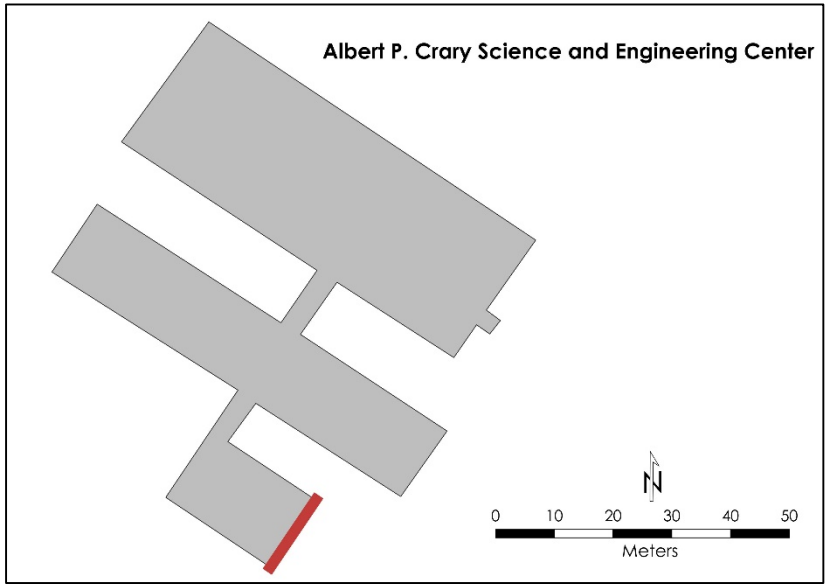
5◦C

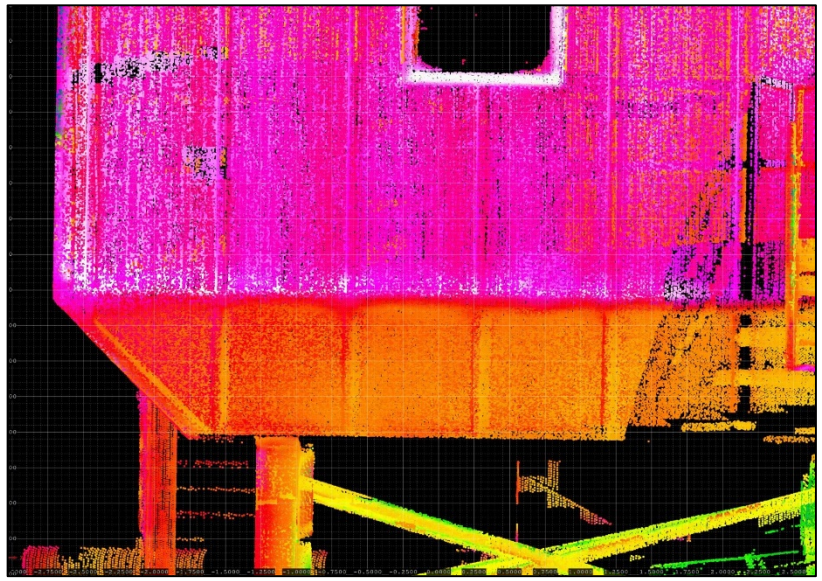


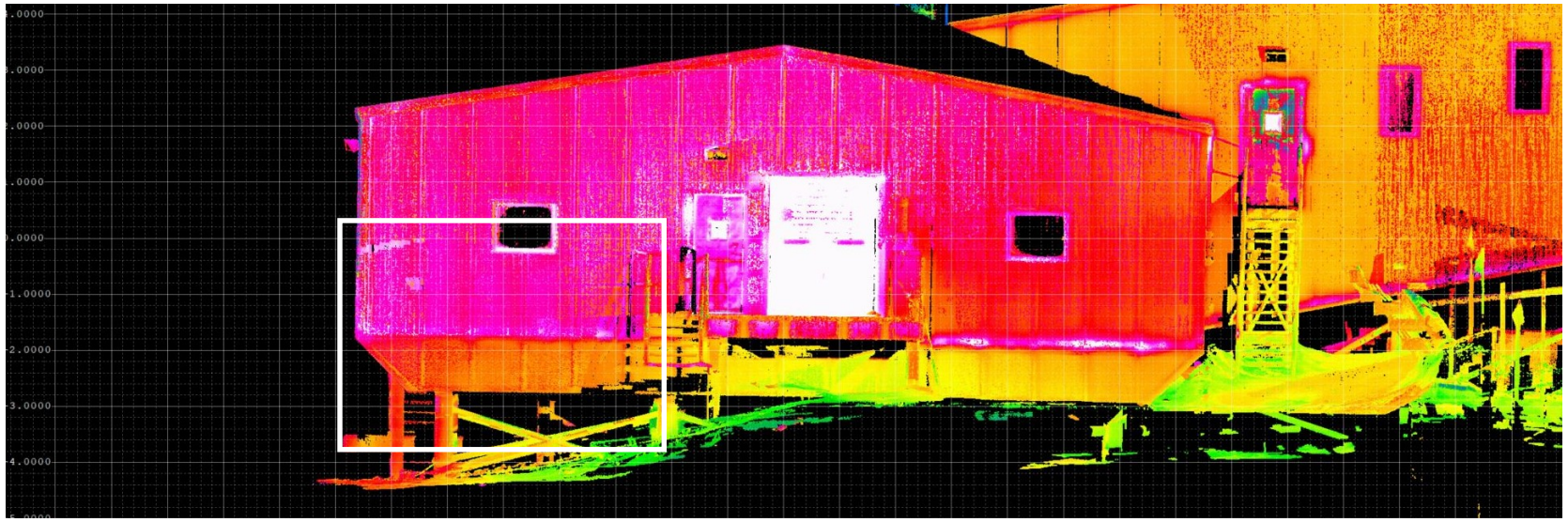




P3E-W-01 -15◦C 5◦C





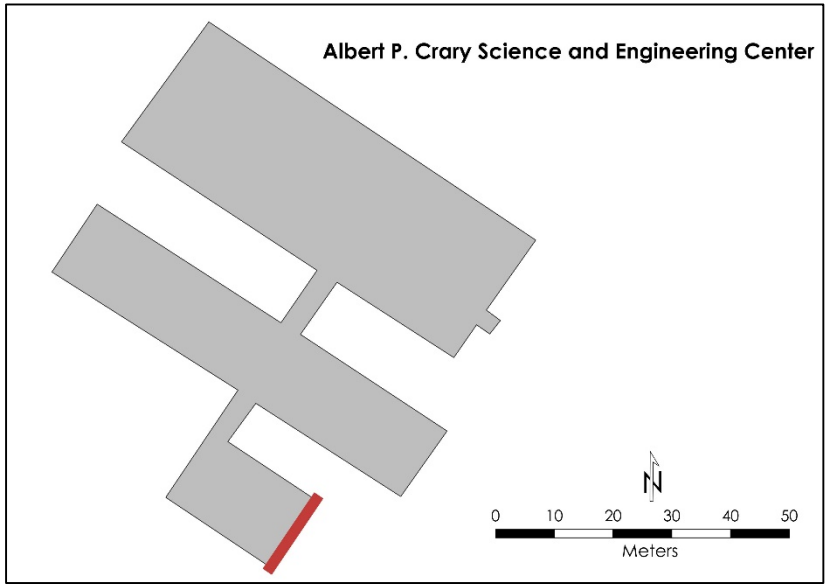


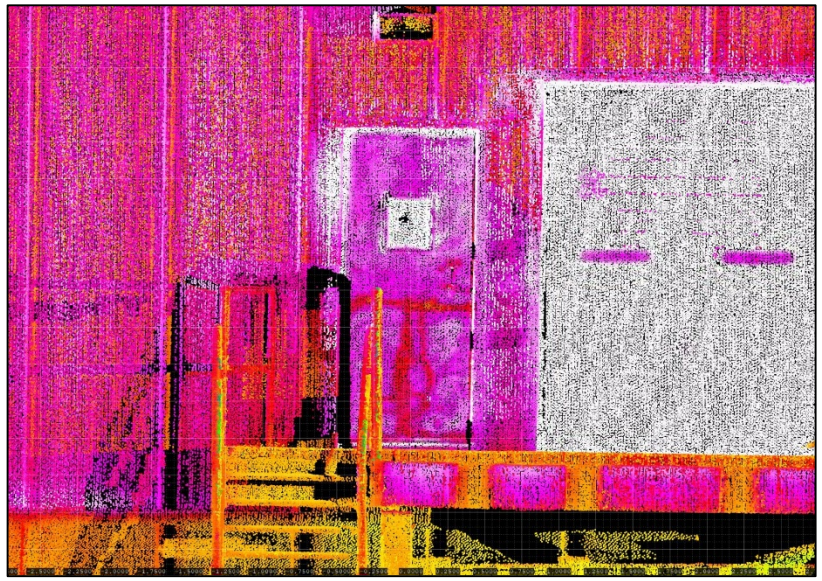
P3E-TA-01

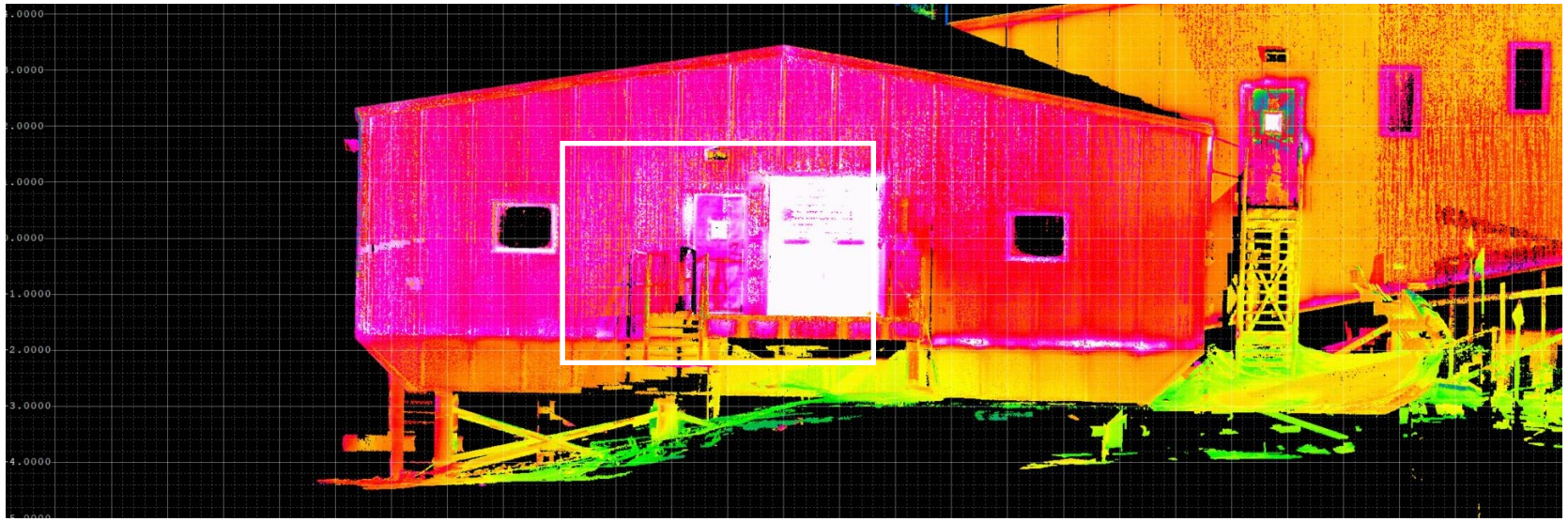
-15◦C



5◦C





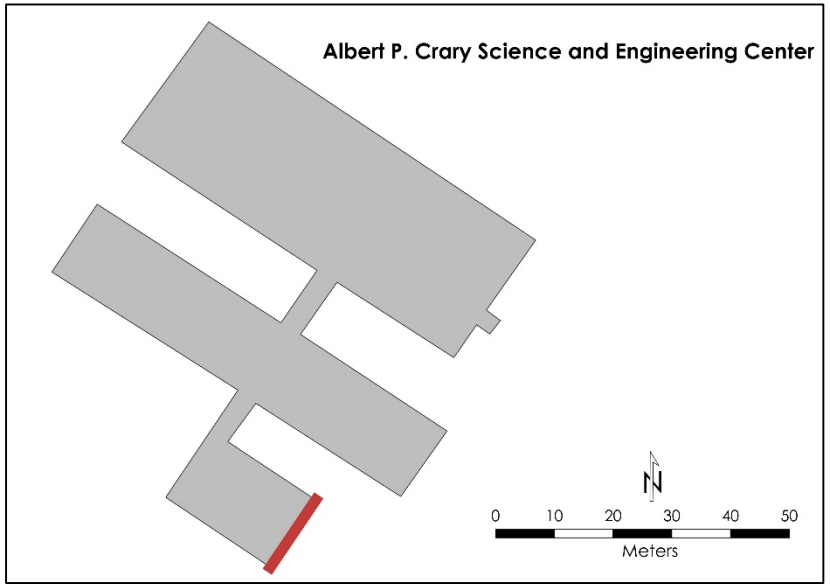


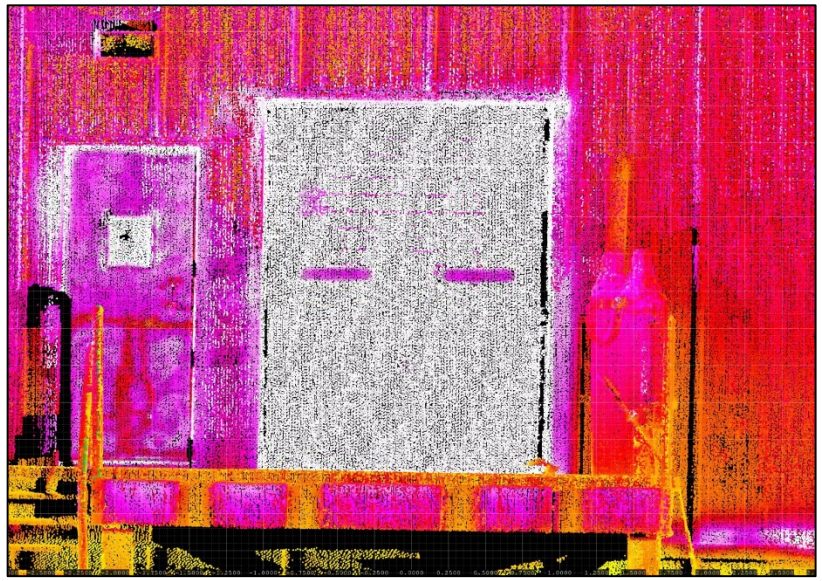
P3E-D-01

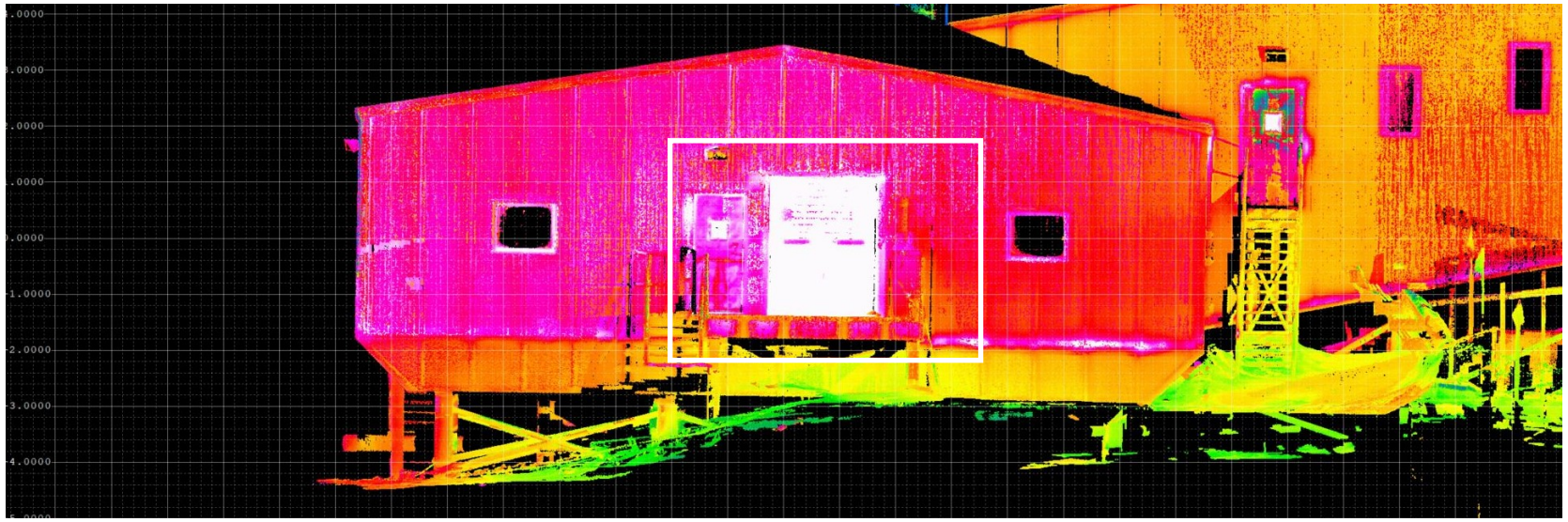
-15◦C



5◦C



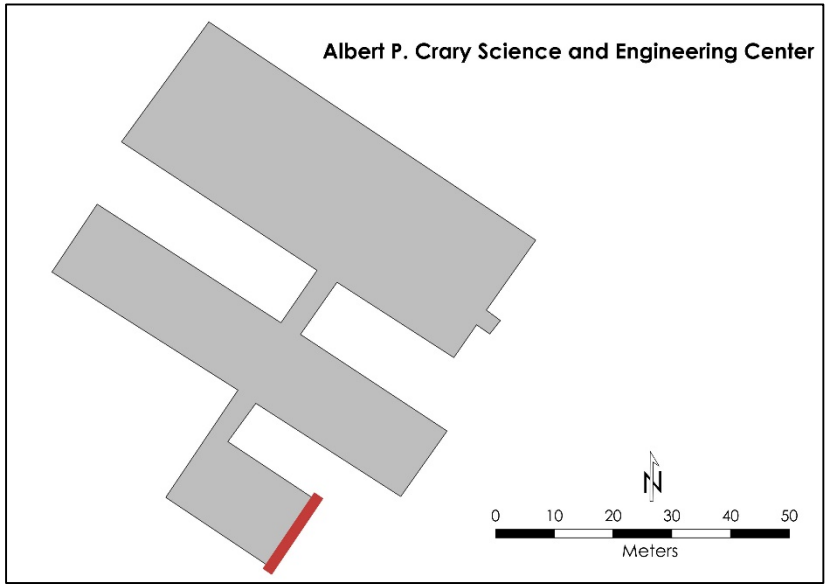


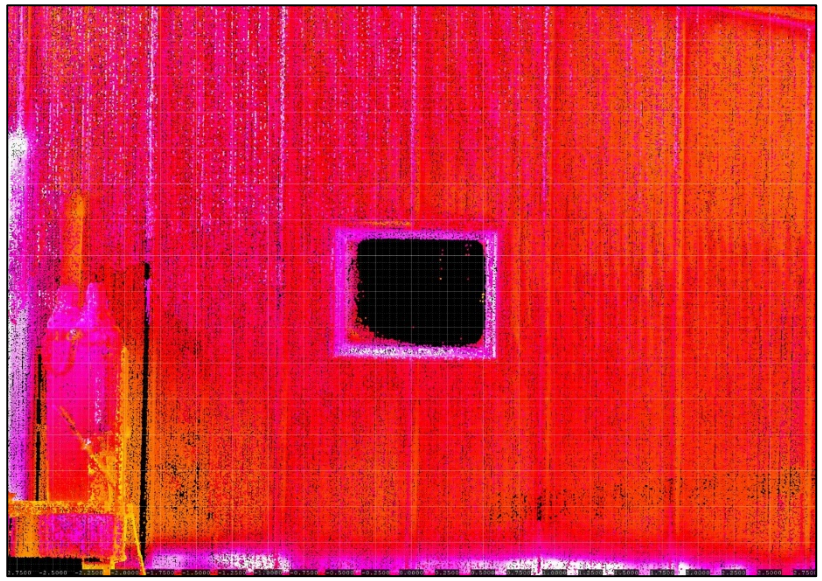


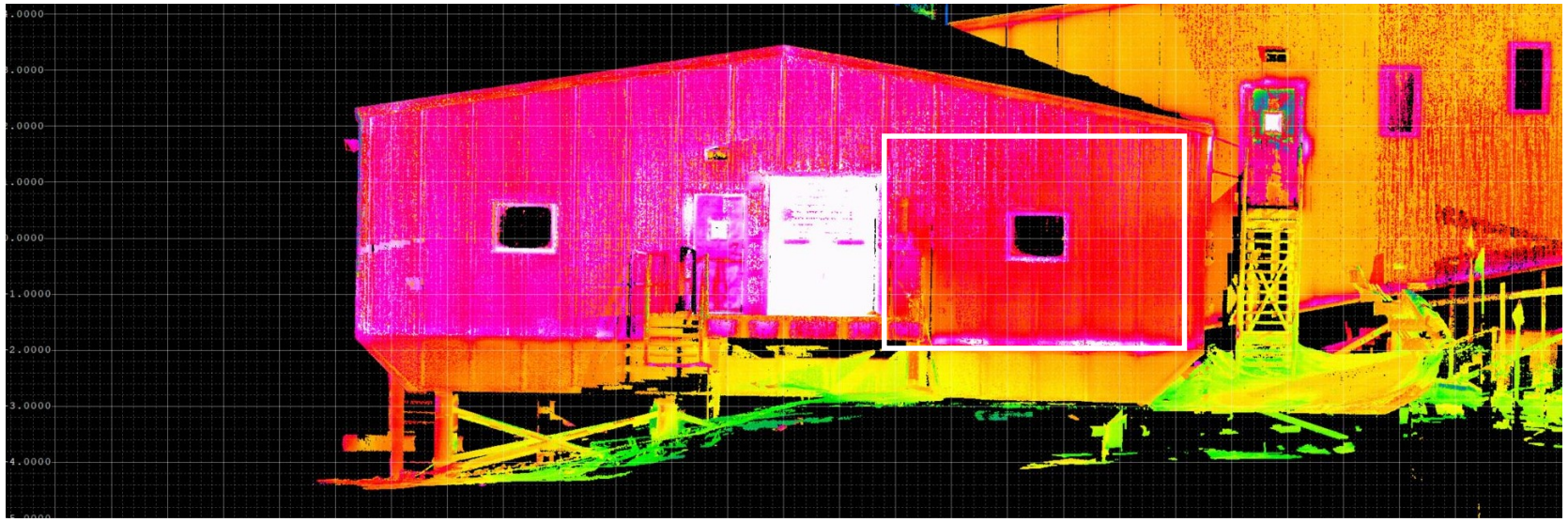
P3E-LD-01

-15◦C

5◦C





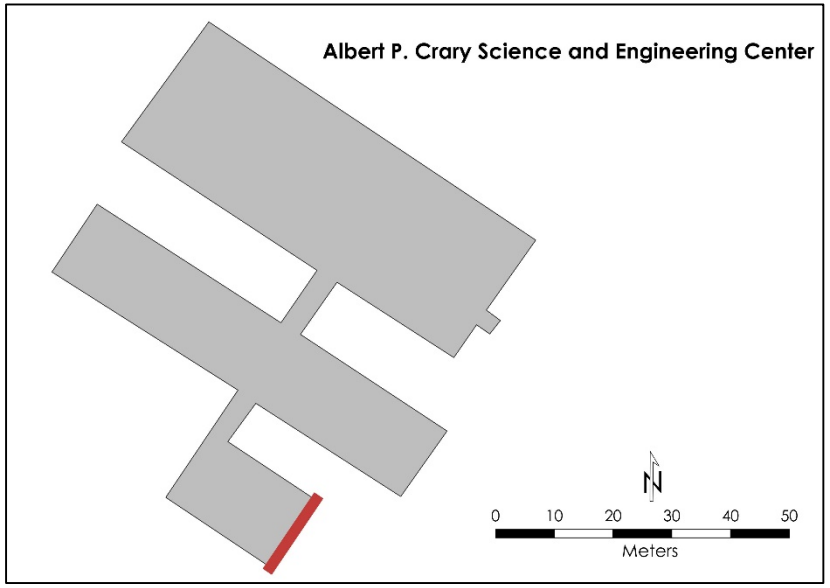


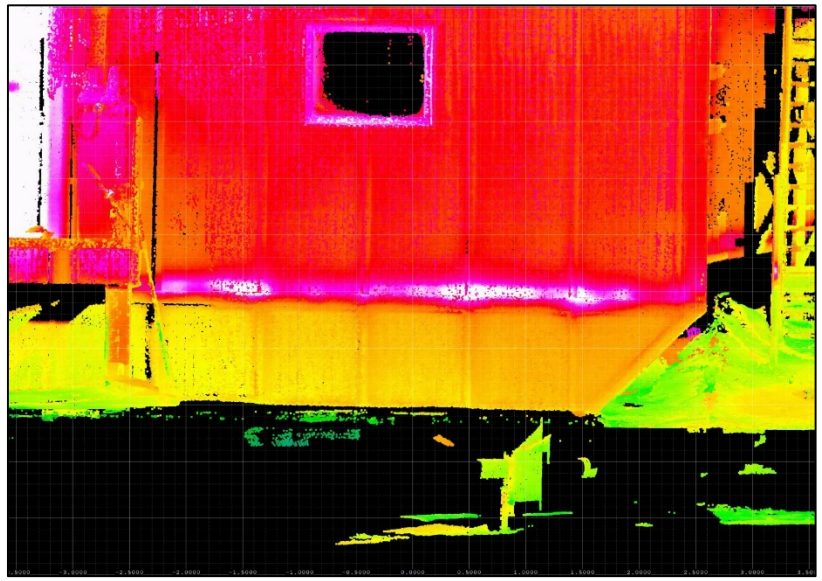
P3E-W-02

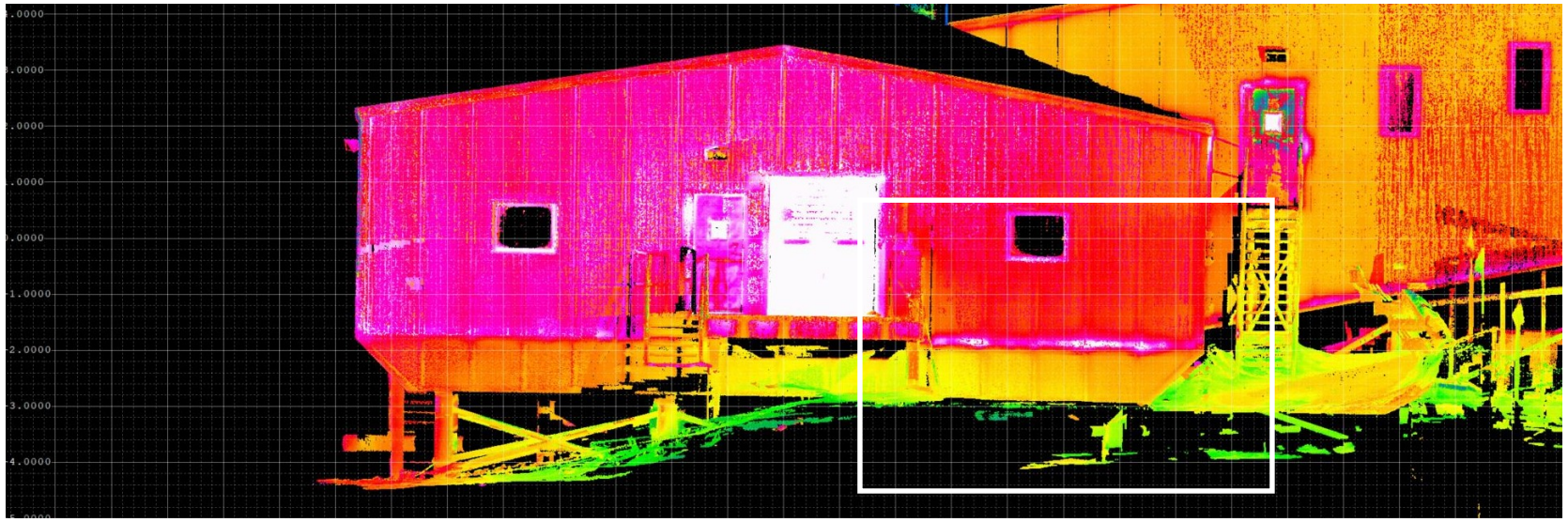
-15◦C



5◦C



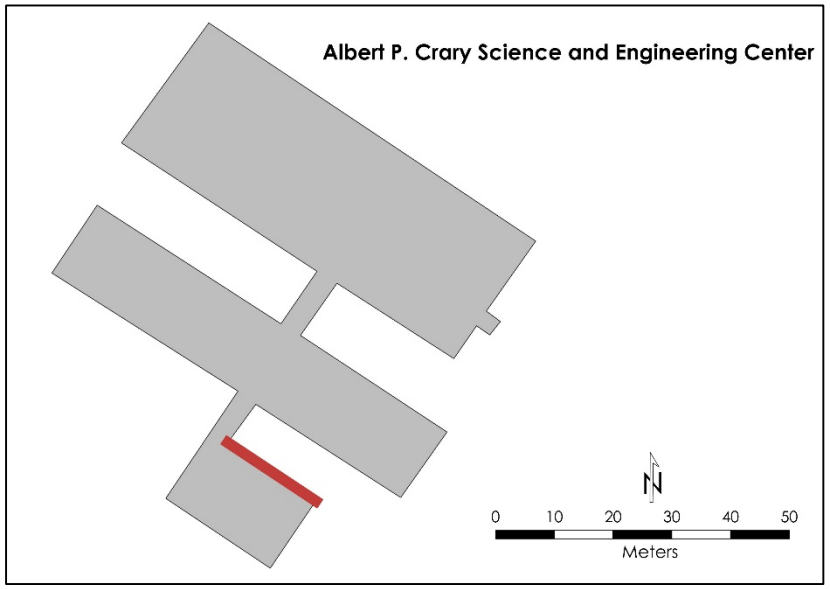


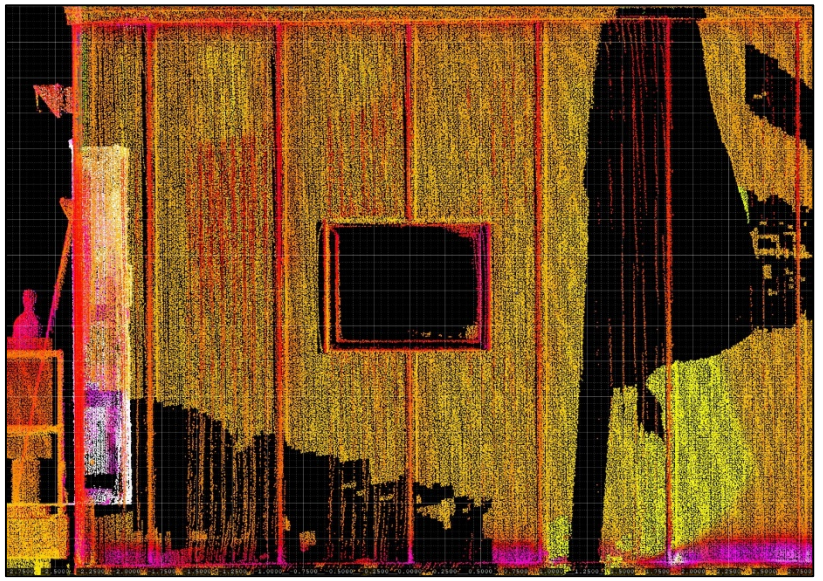


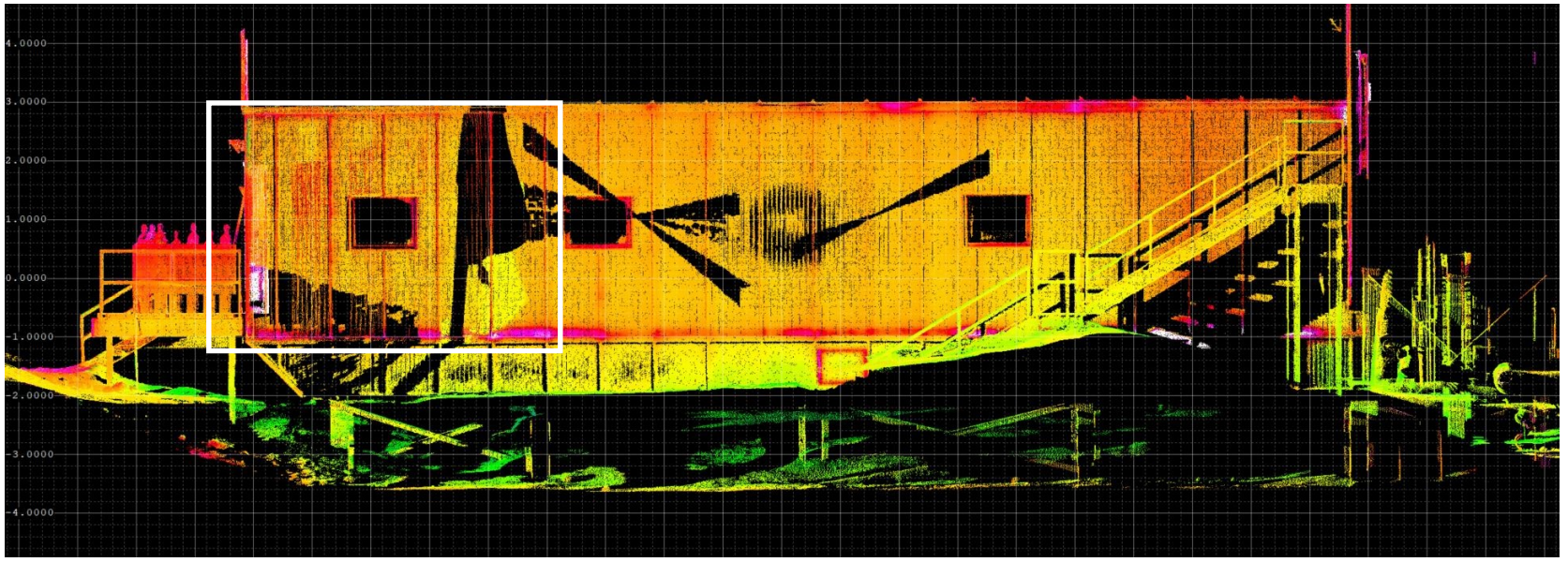
P3E-TA-02

-15◦C

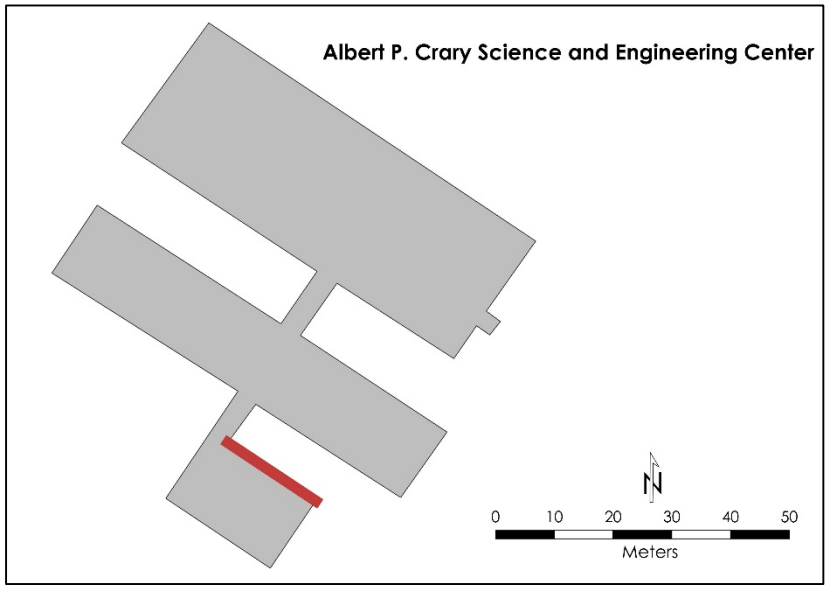
5◦C

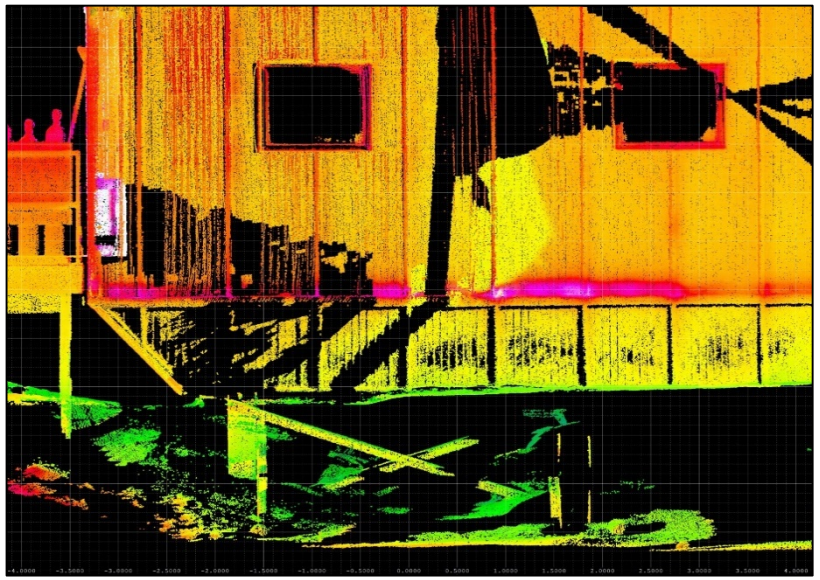


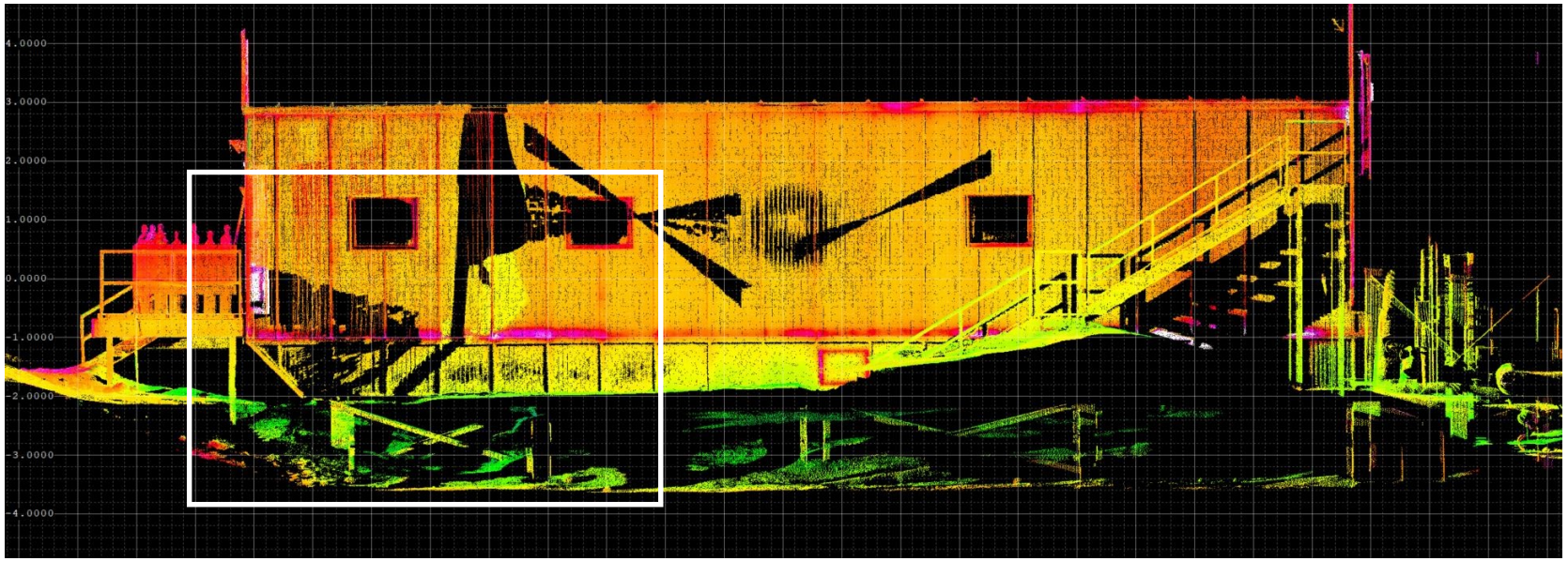




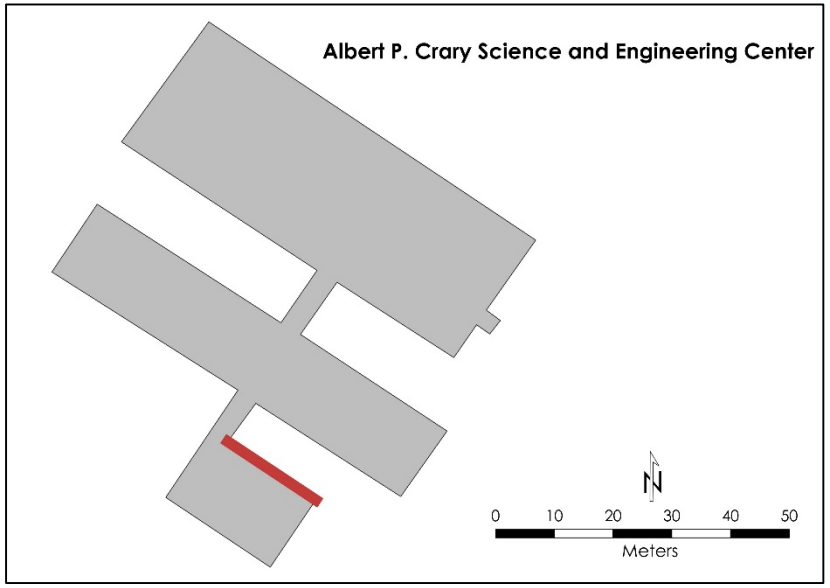
P3N-W-01 -15◦C 5◦C

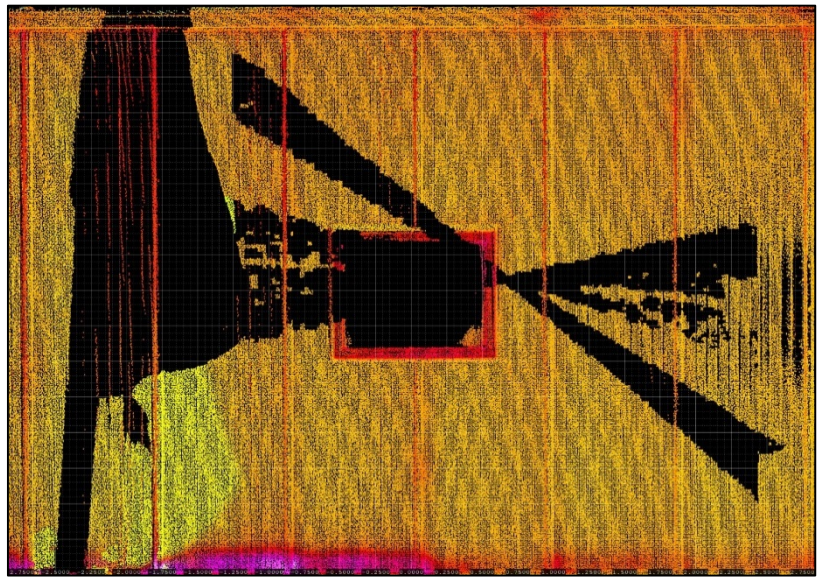


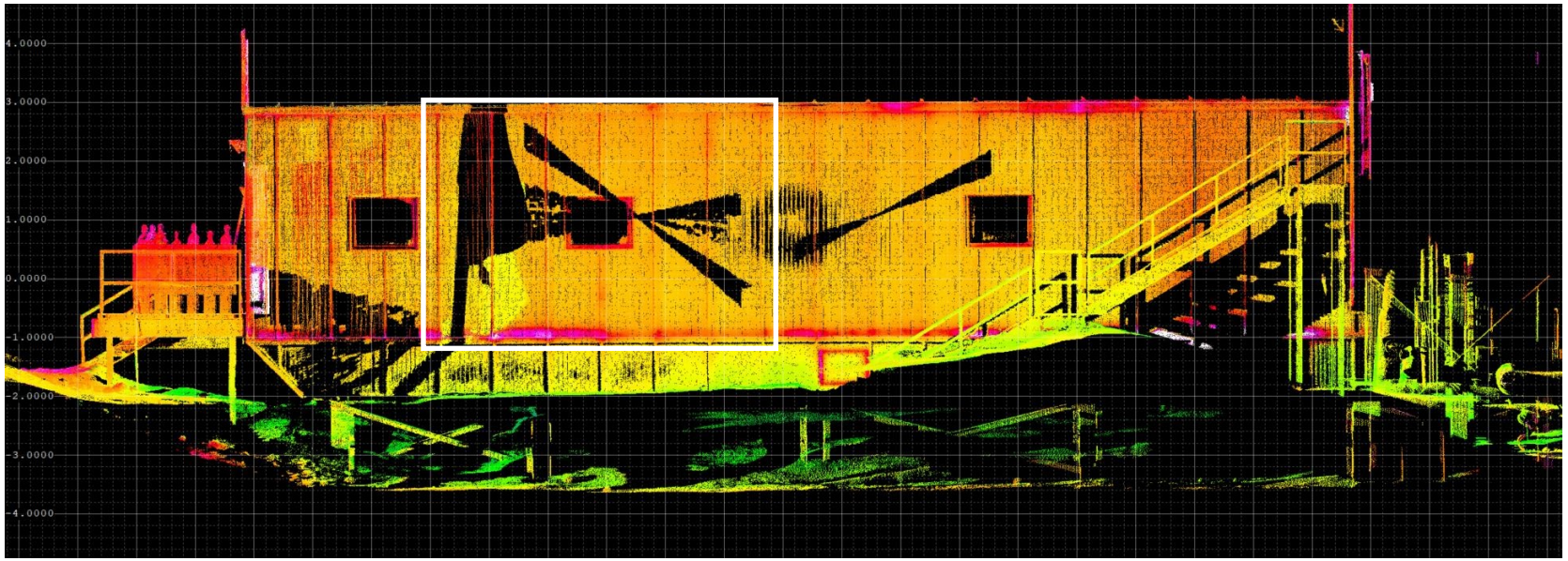




P3N-TA-01 -15◦C 5◦C



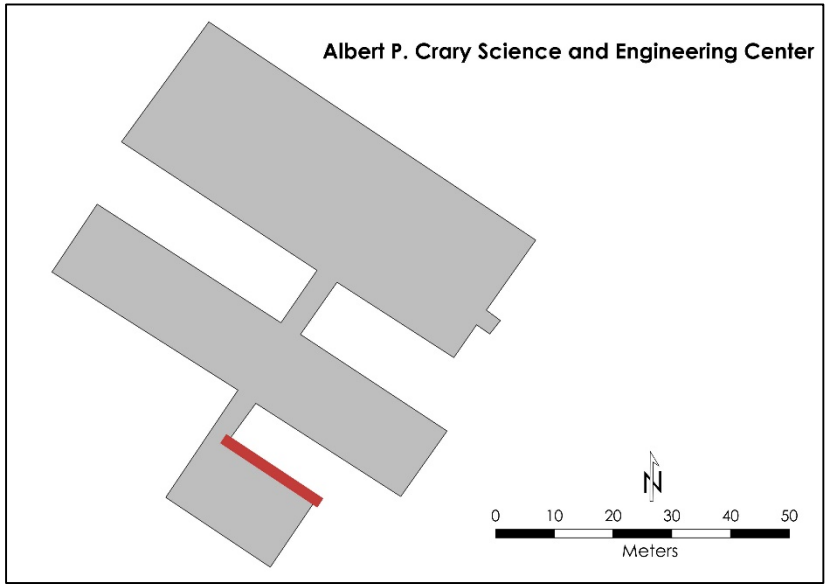


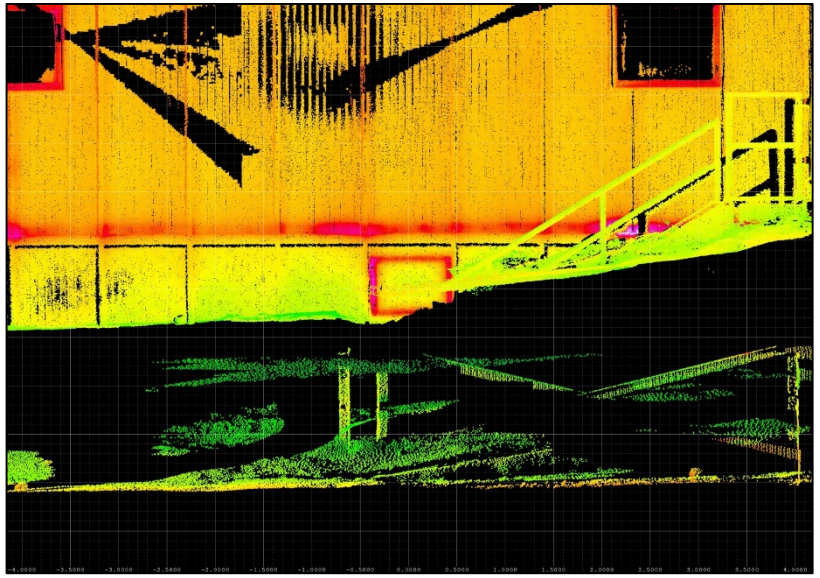


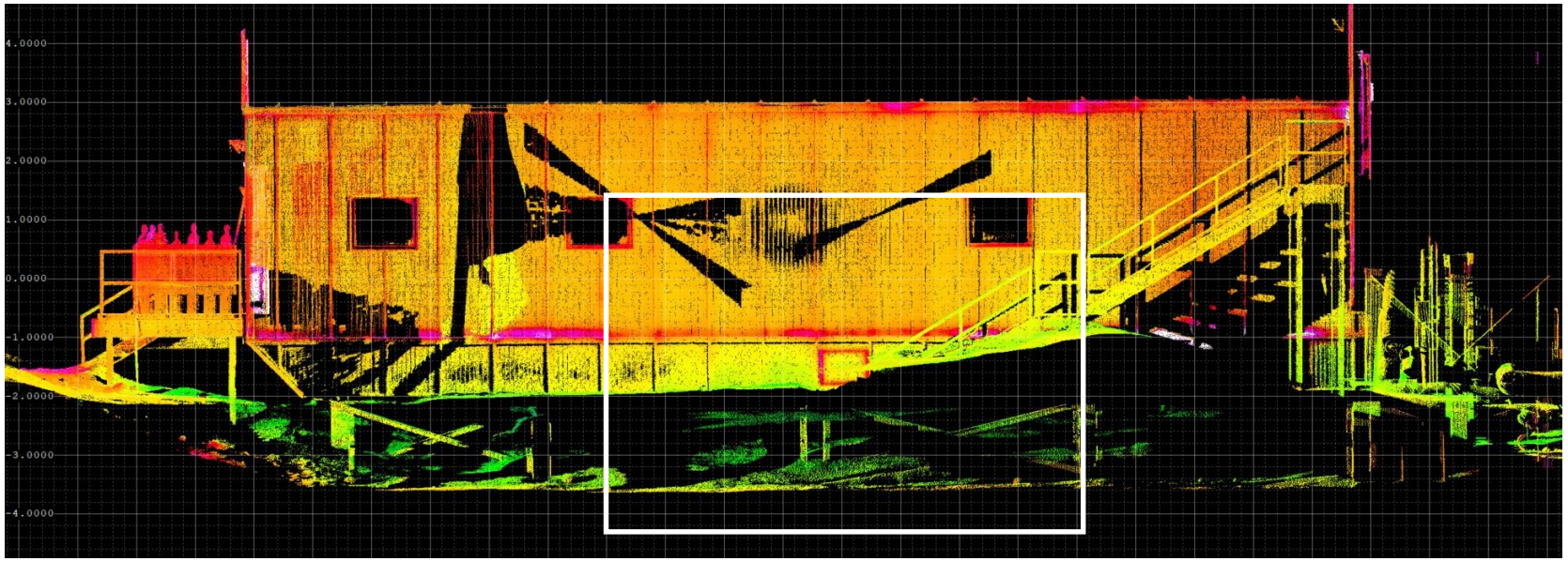
P3N-W-02

-15◦C

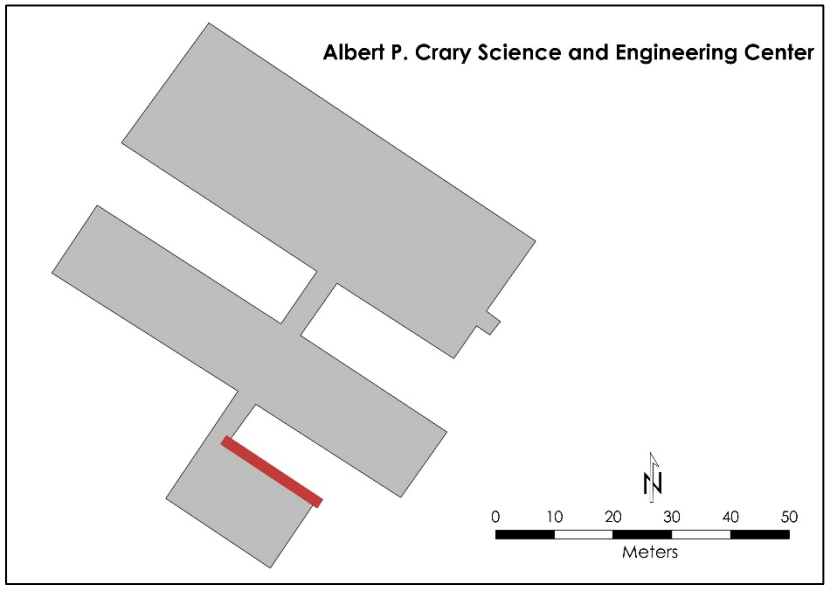
5◦C

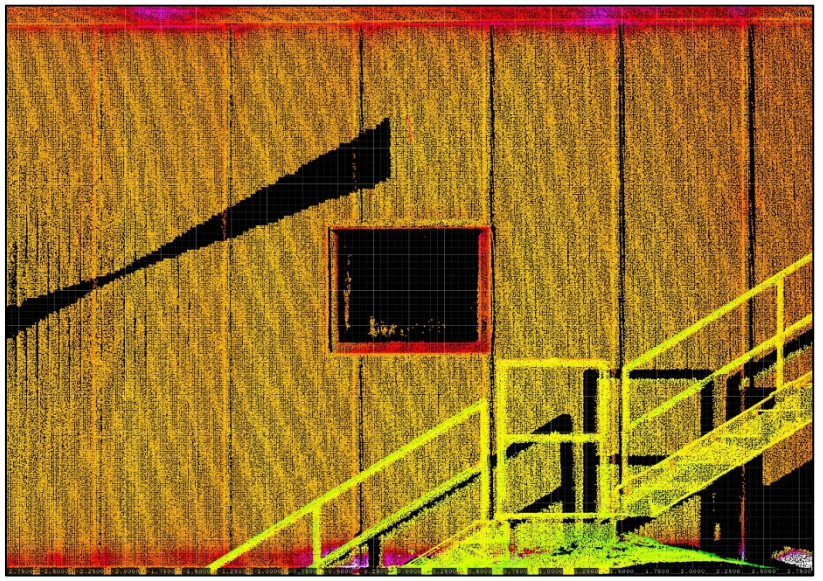


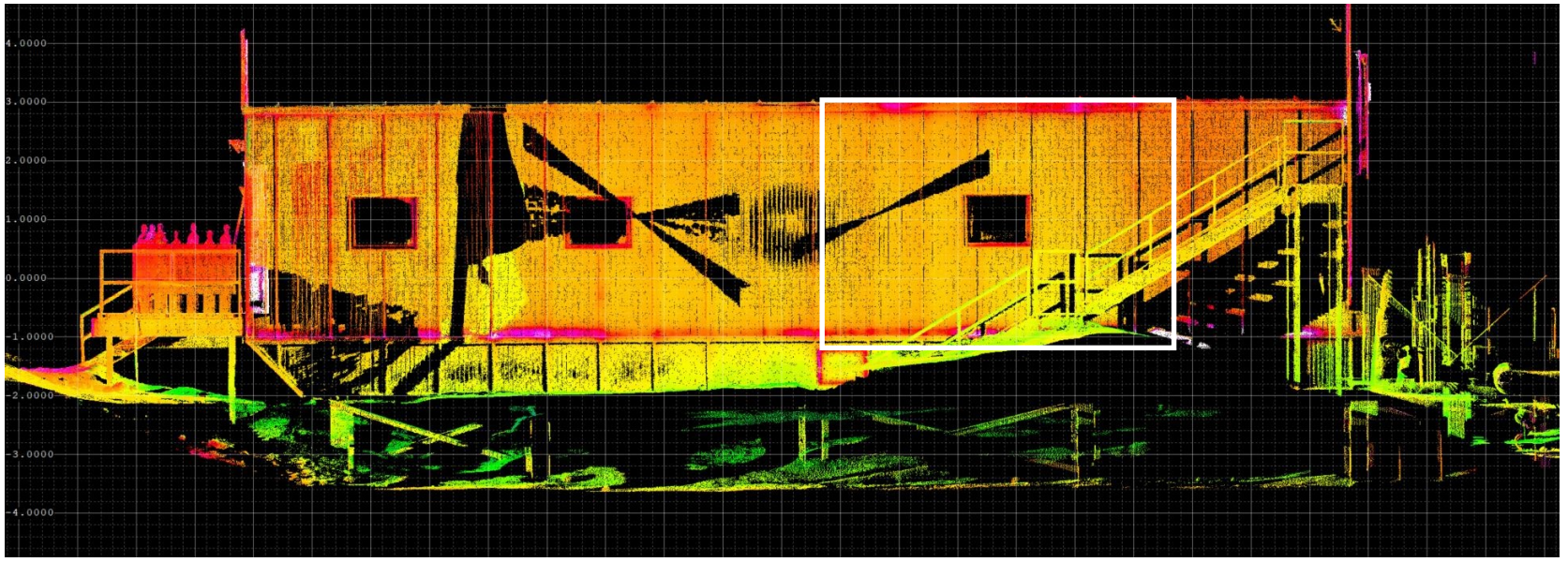




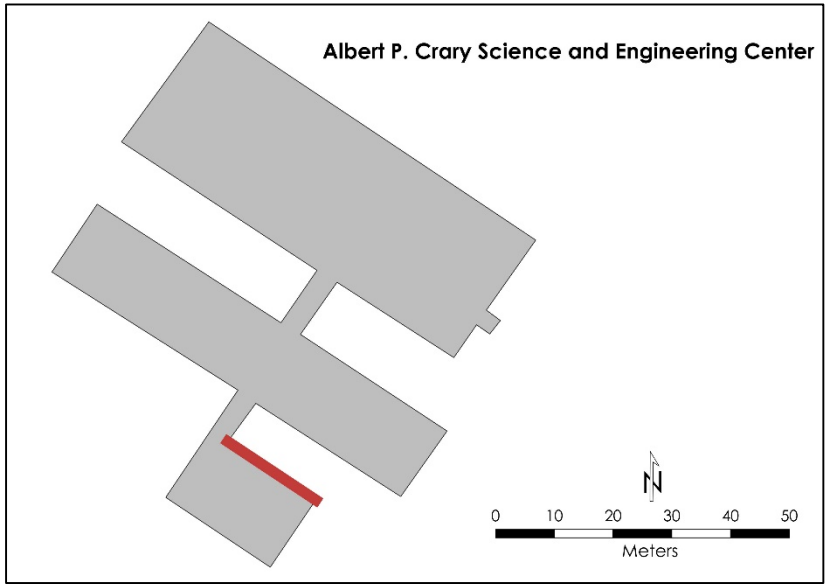
P3N-TA-02 -15◦C 5◦C

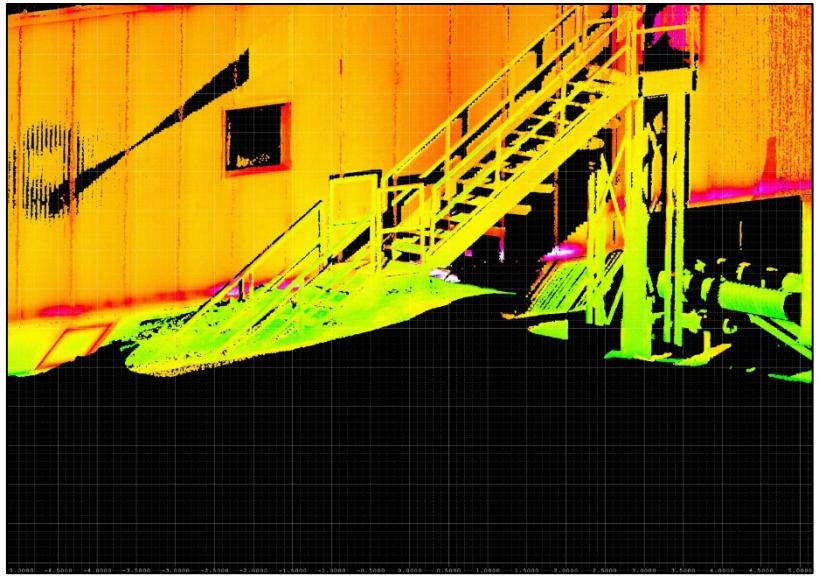


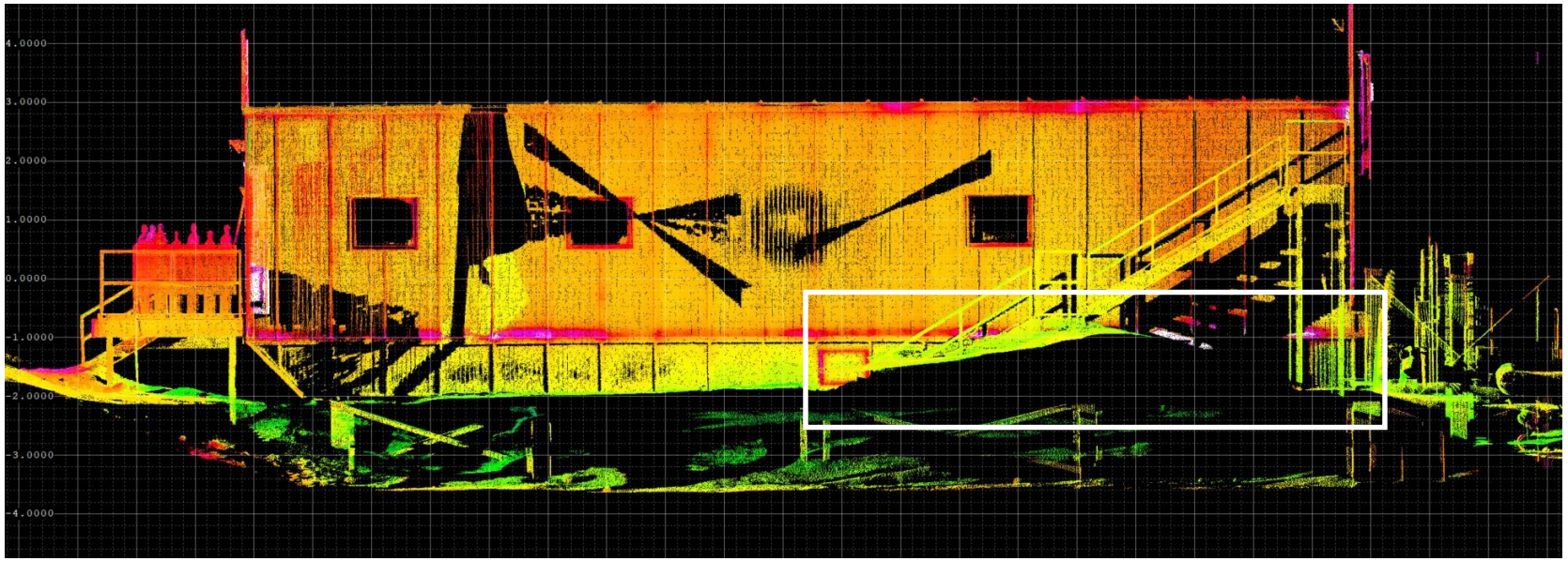




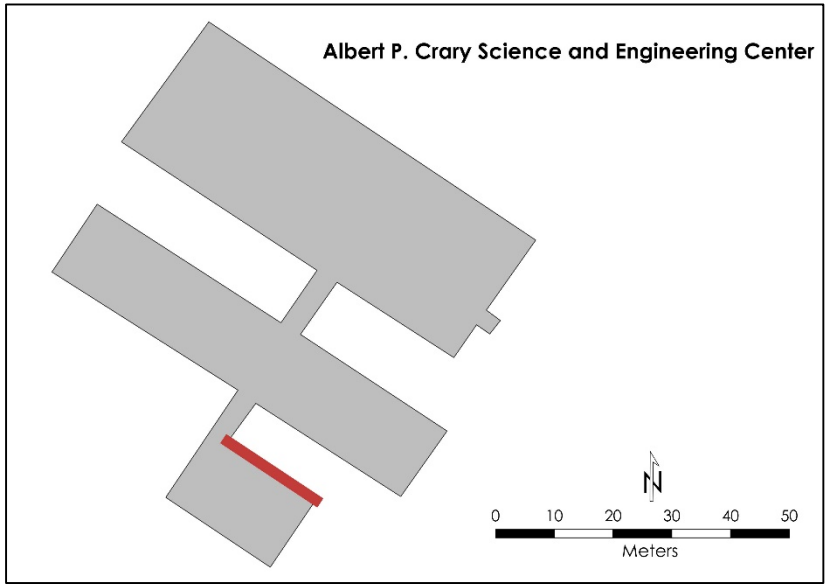
P3N-W-03 -15◦C 5◦C

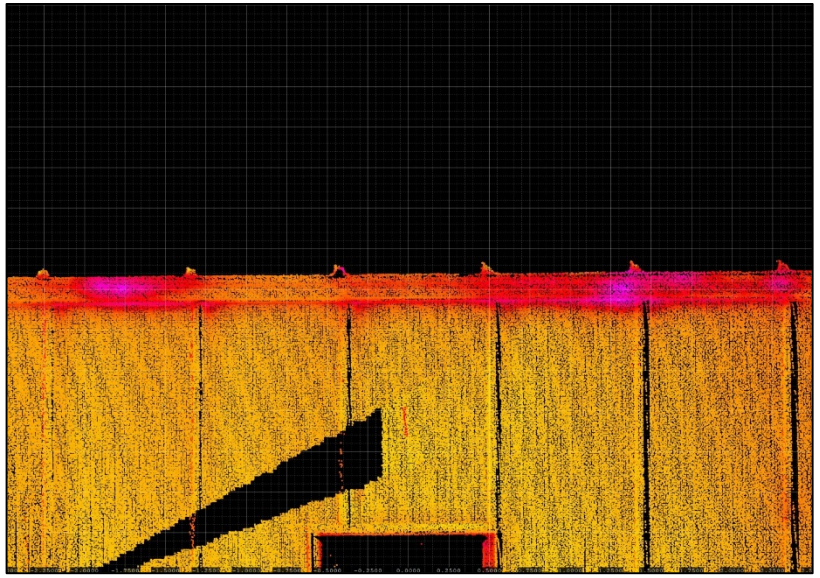


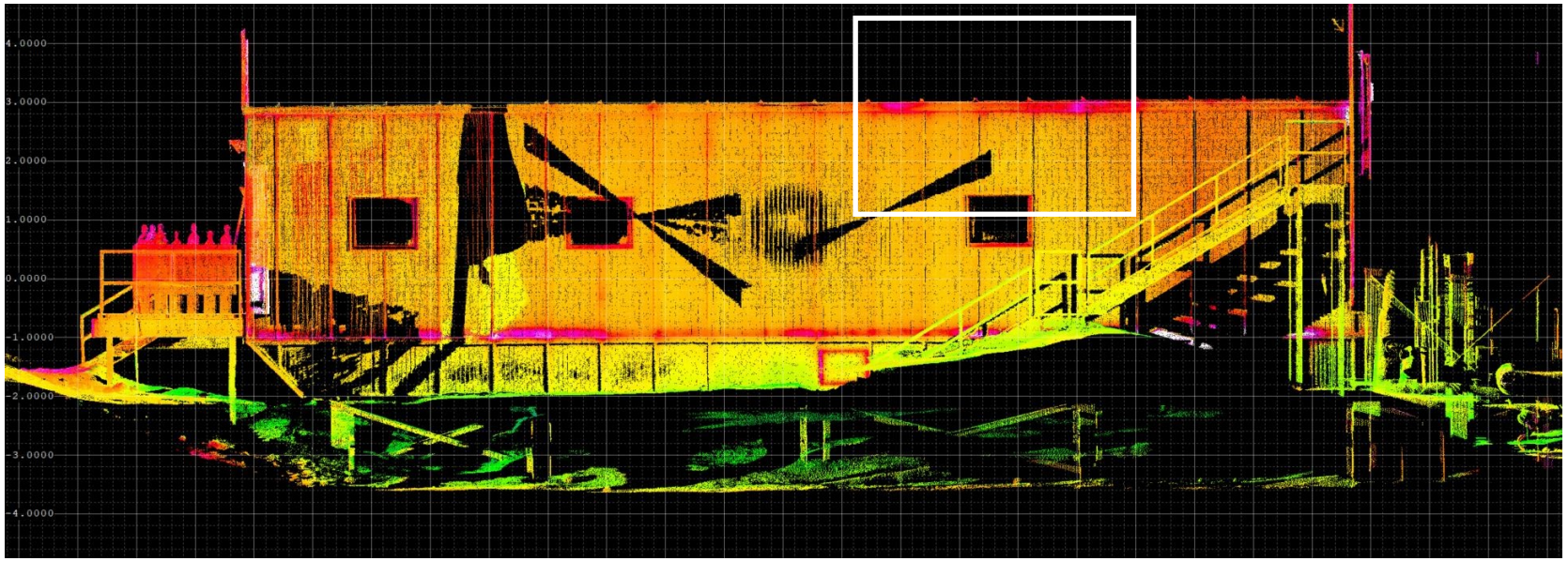




P3N-TA-03 -15◦C 5◦C





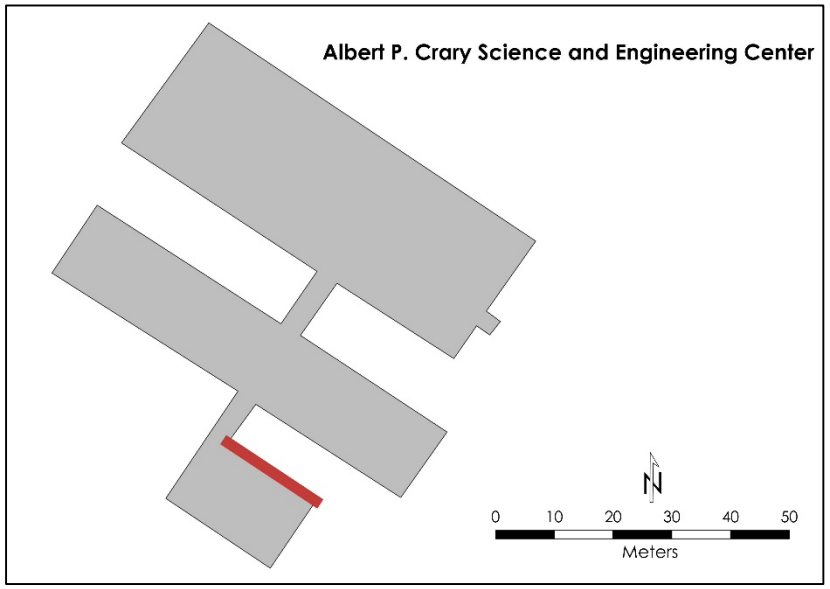


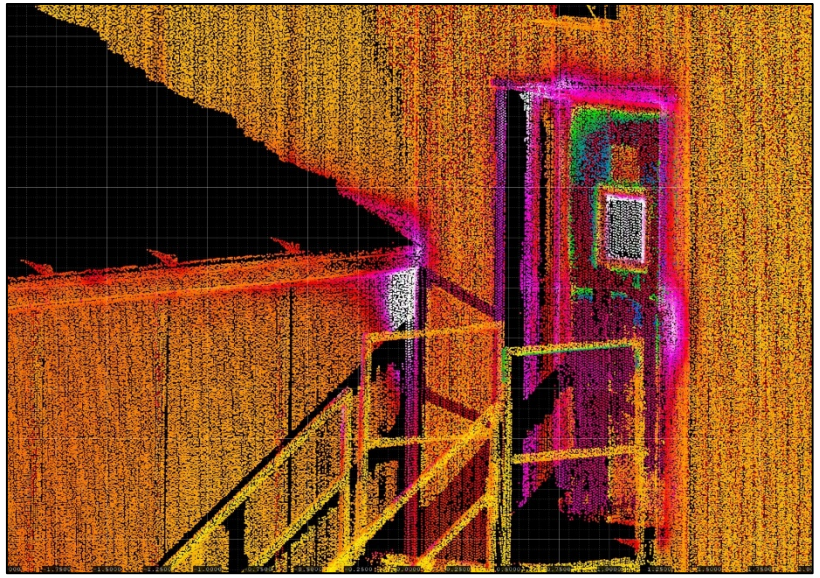
P3N-TA-04

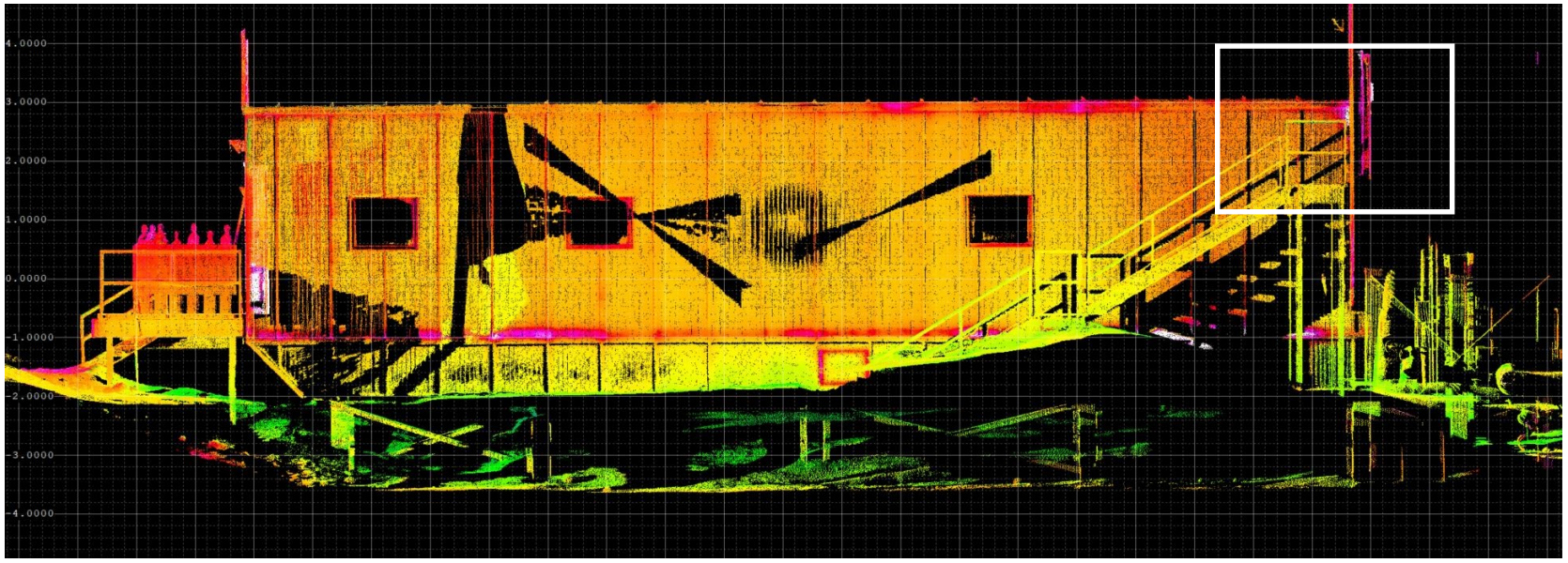
-15◦C



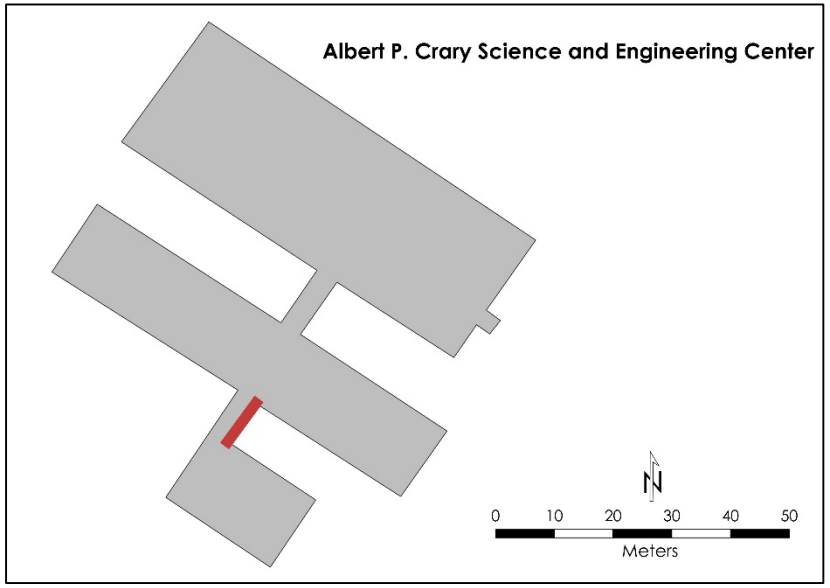
5◦C

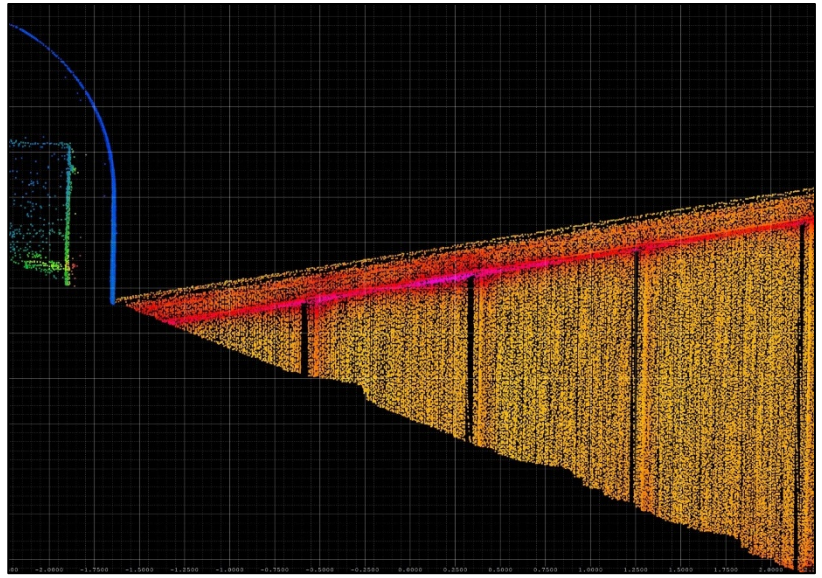


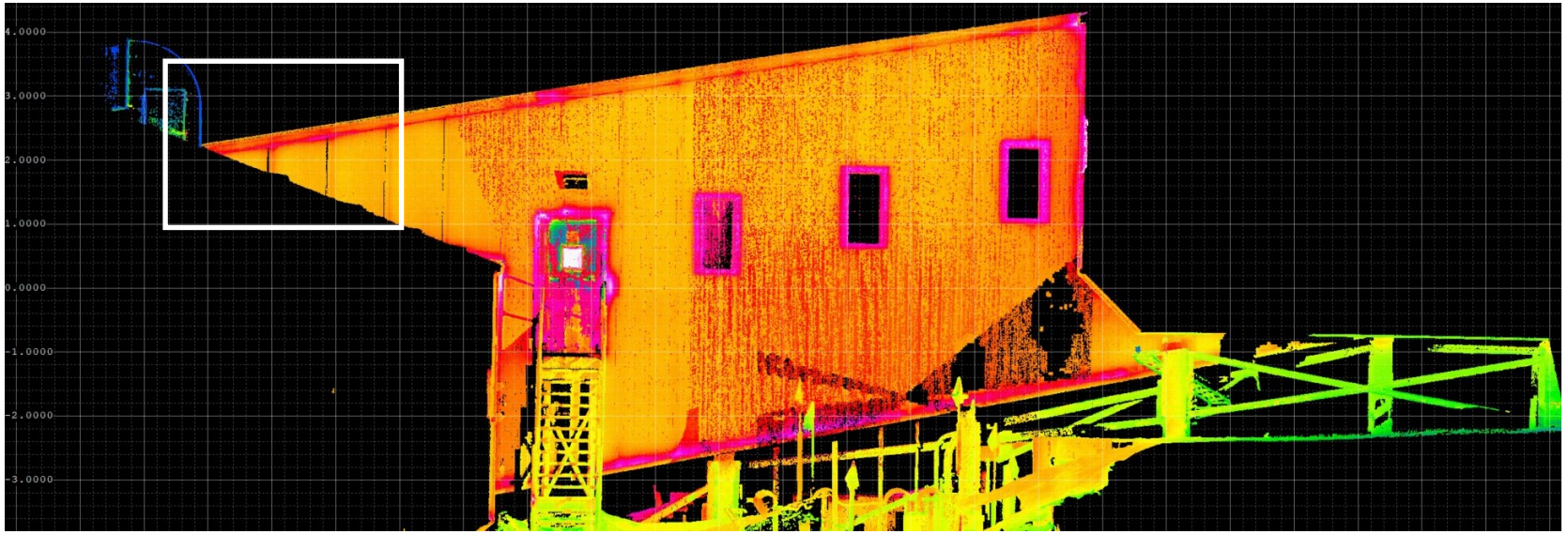




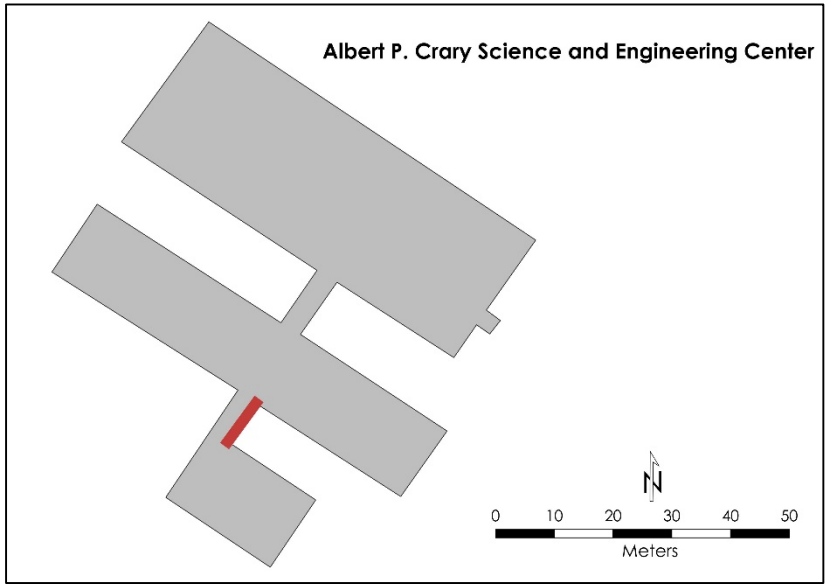
P3N-TA-05 -15◦C 5◦C

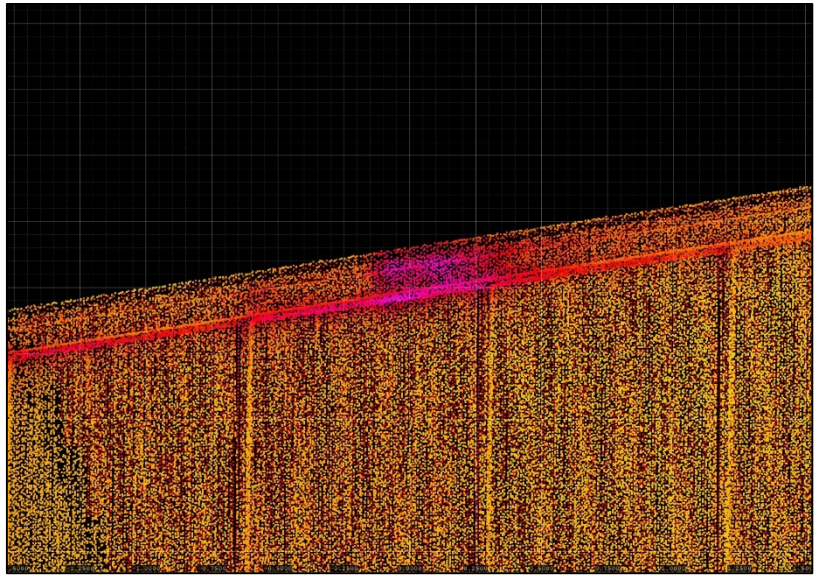


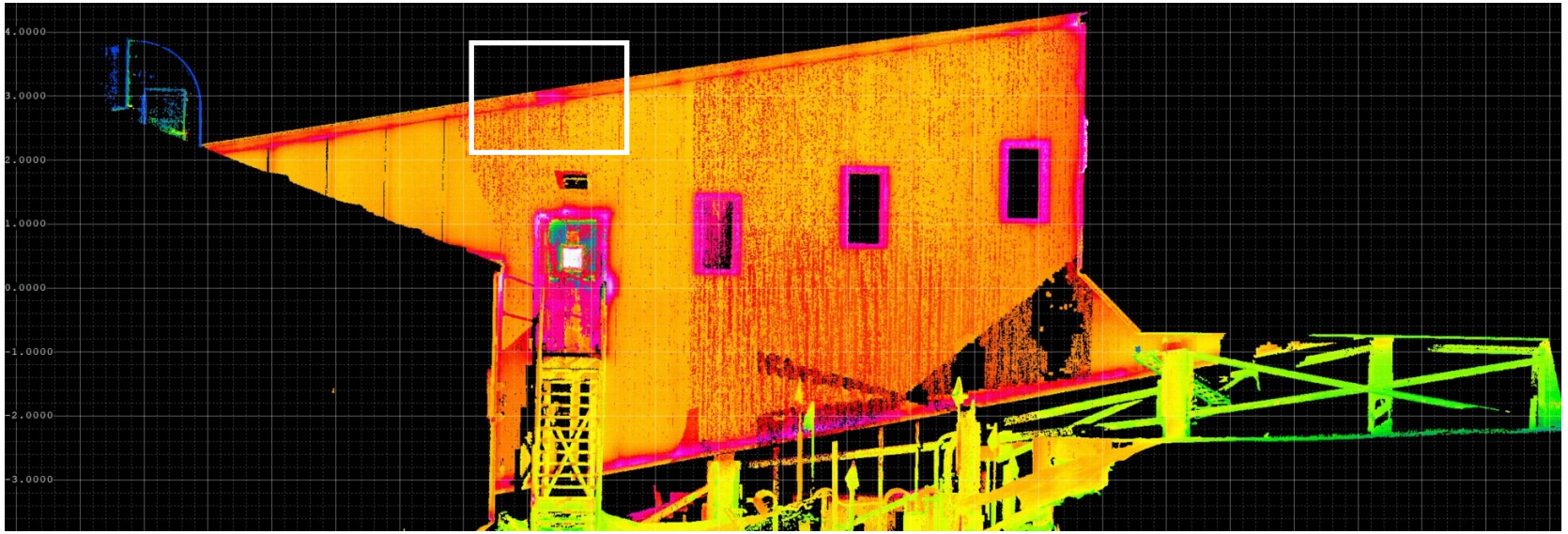




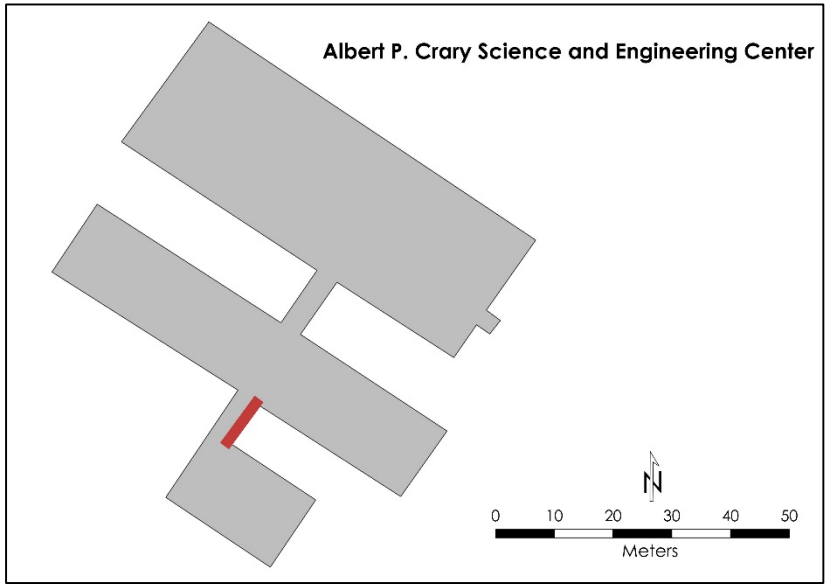
P3CE-TA-01 -15◦C 5◦C

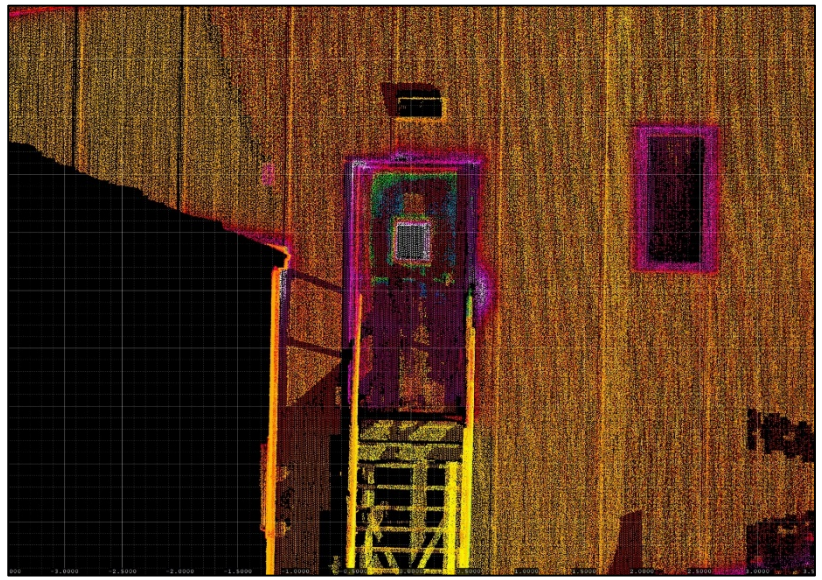


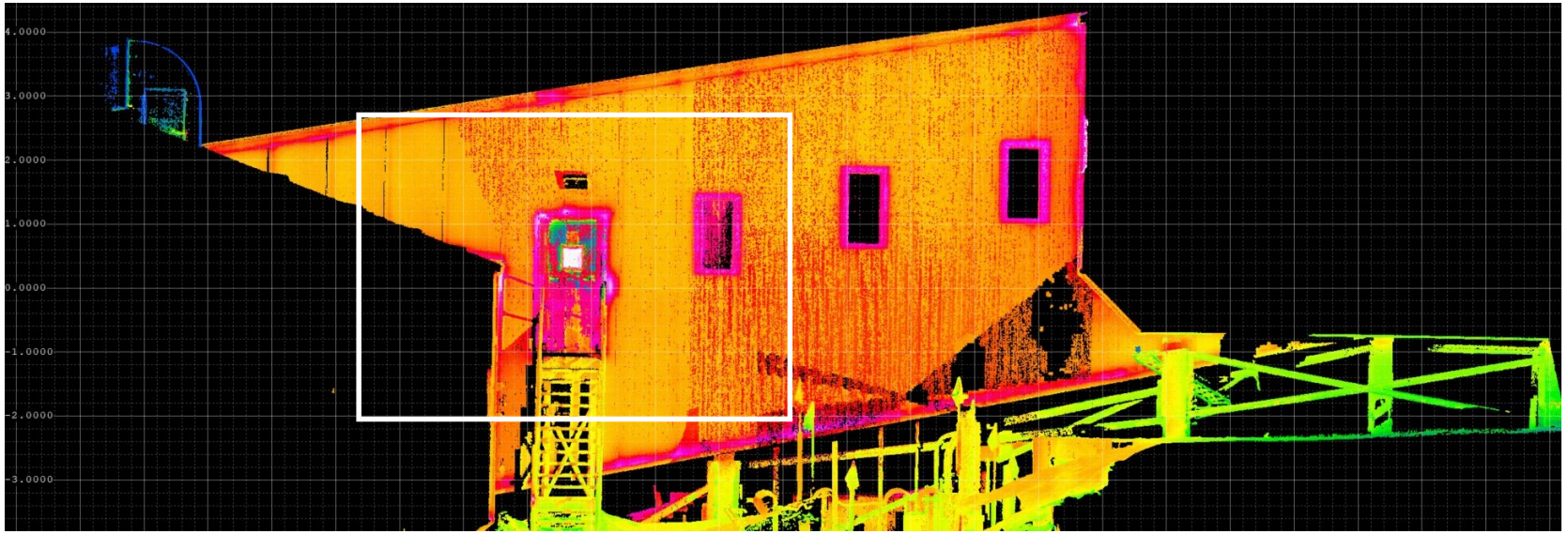




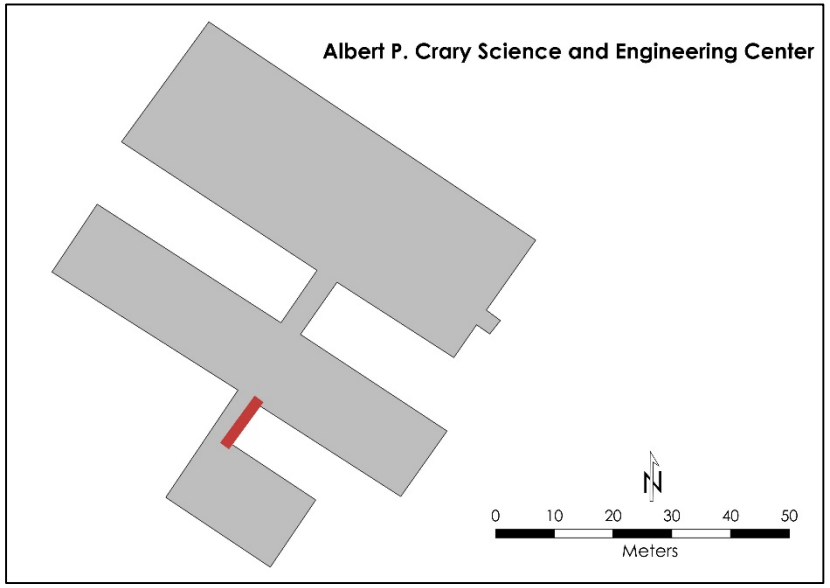
P3CE-TA-02 -15◦C 5◦C

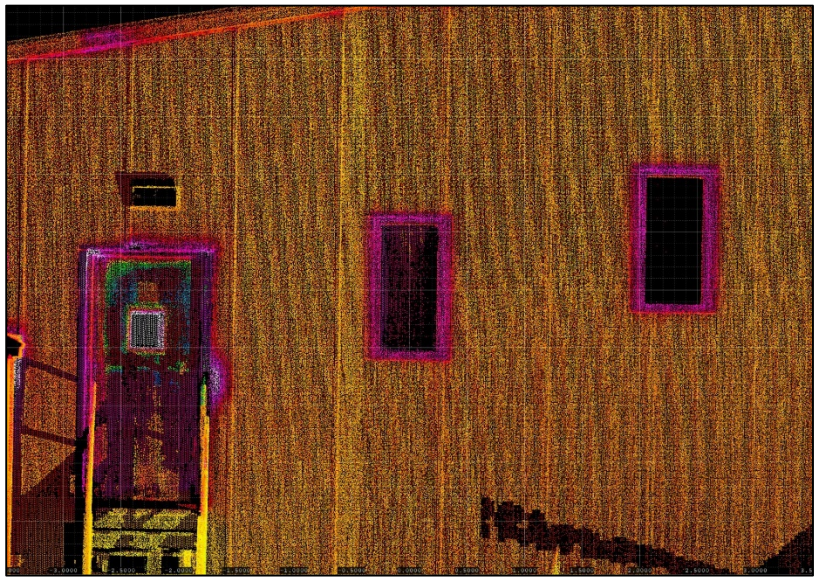


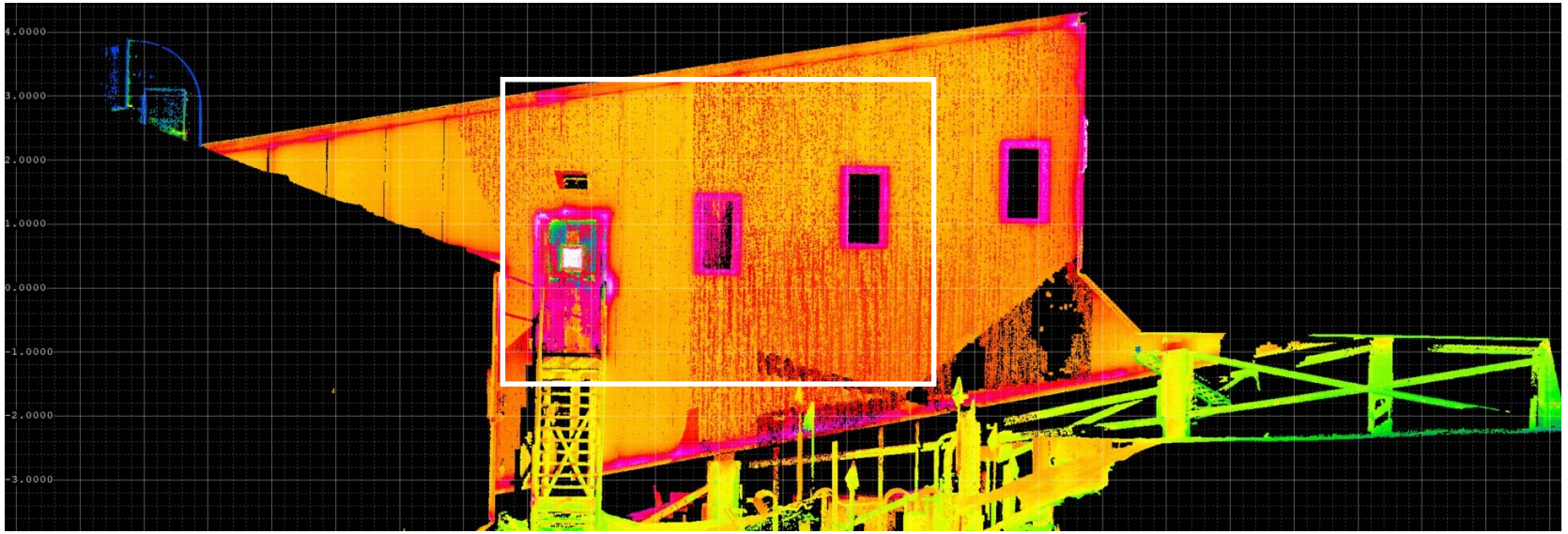




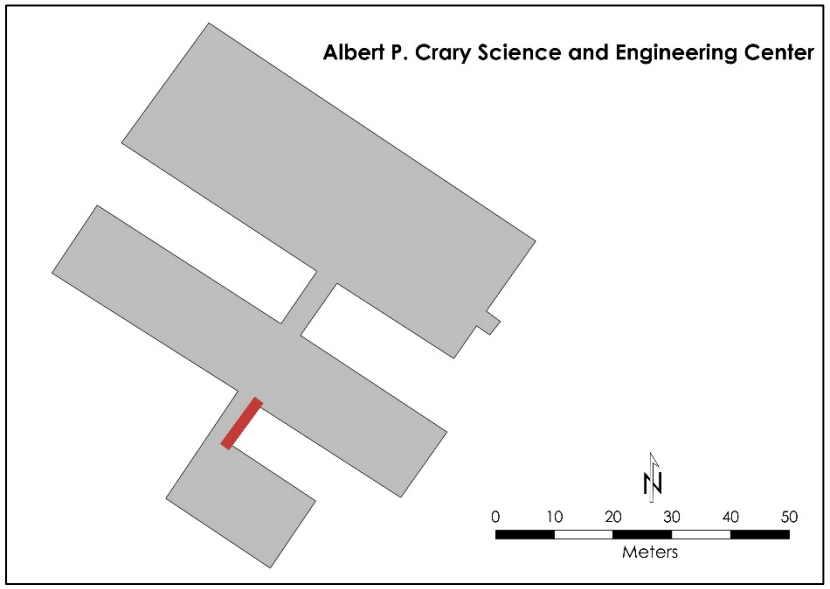
P3CE-D-01 -15◦C 5◦C

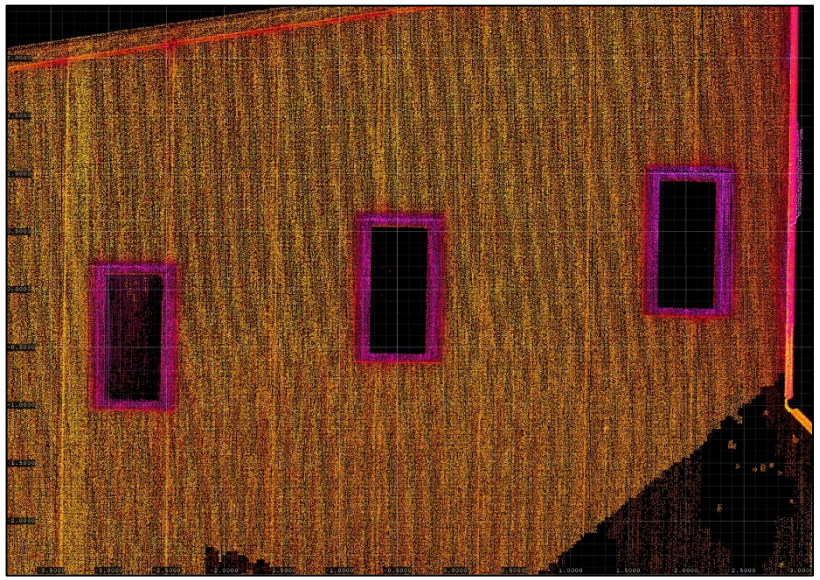


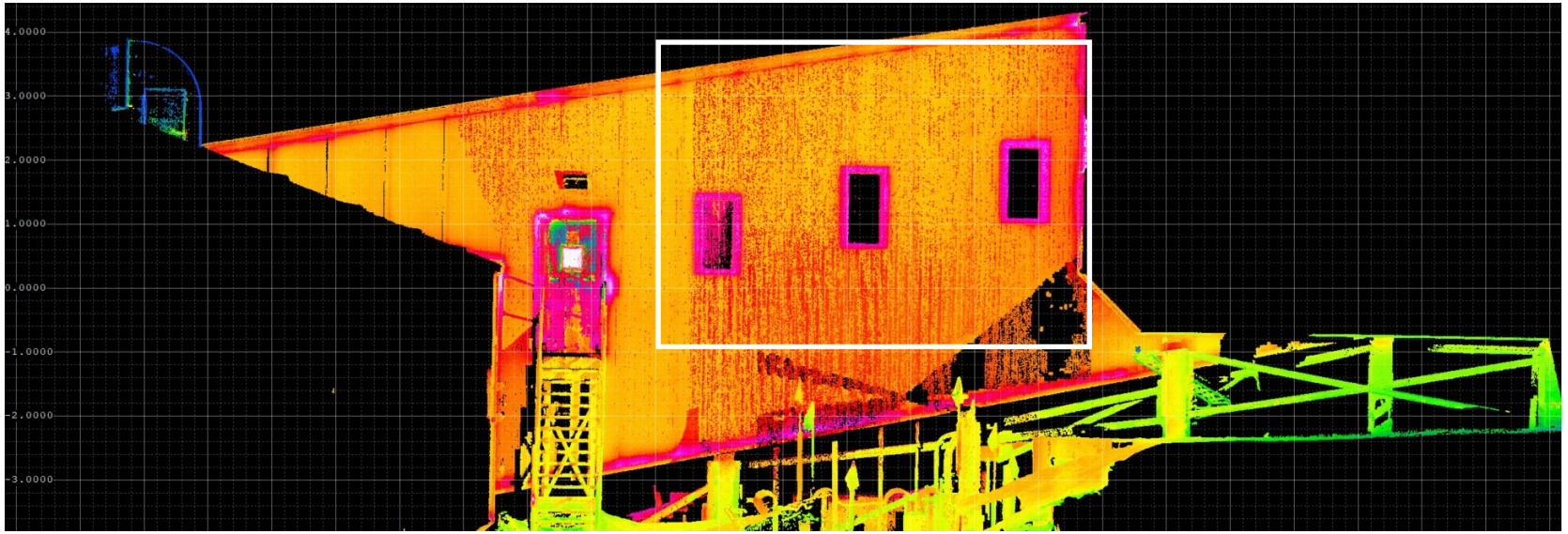




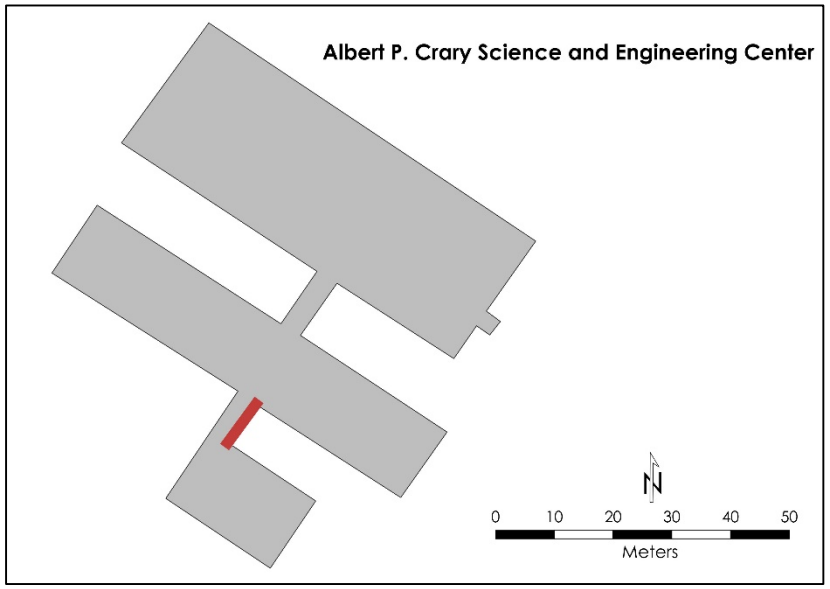
P3CE-W-01 -15◦C 5◦C

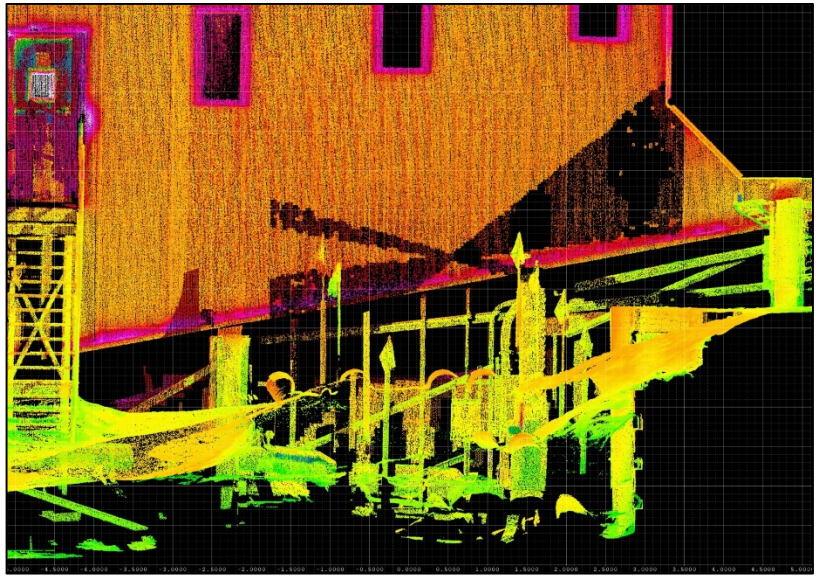


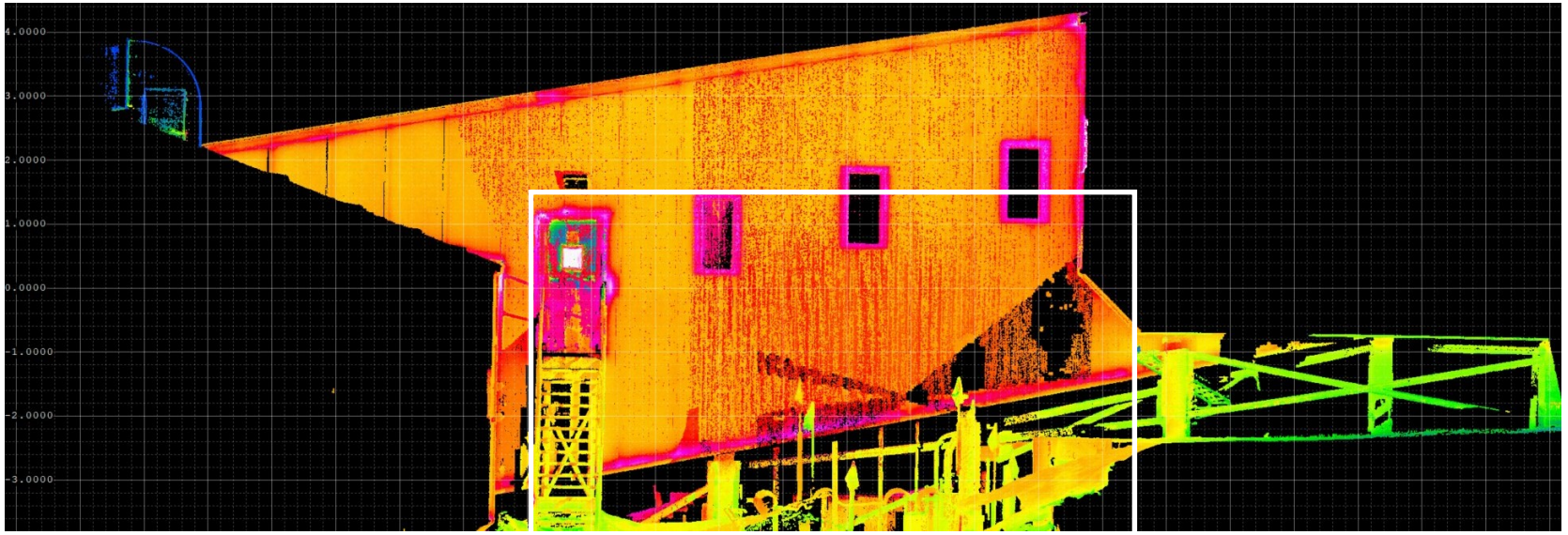




P3CE-W-02 -15◦C 5◦C





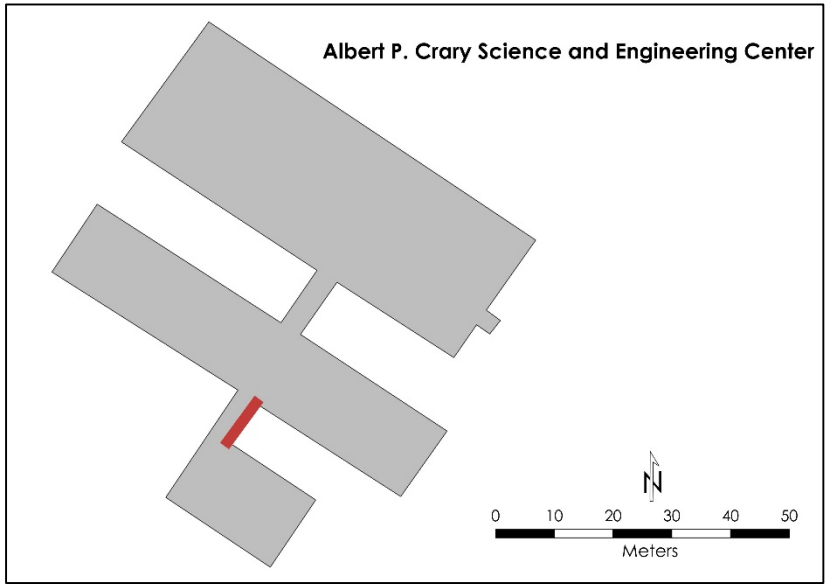


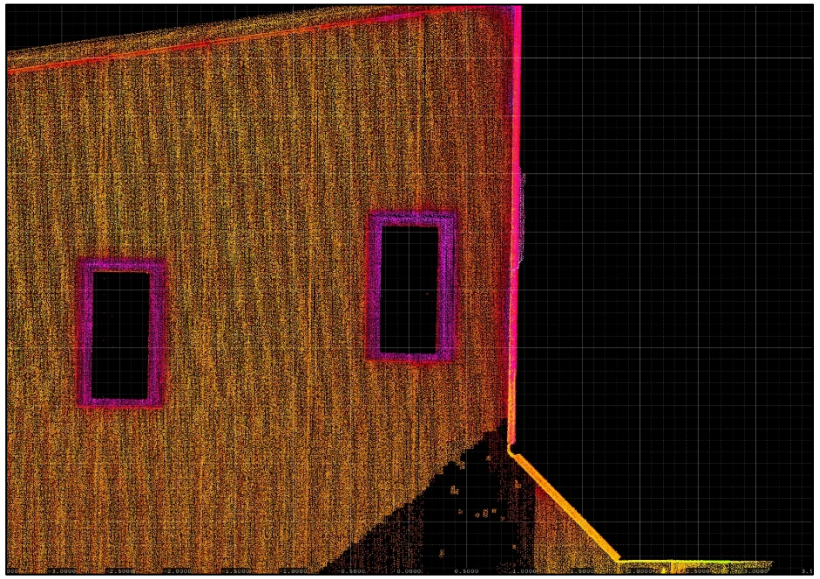
P3CE-TA-03

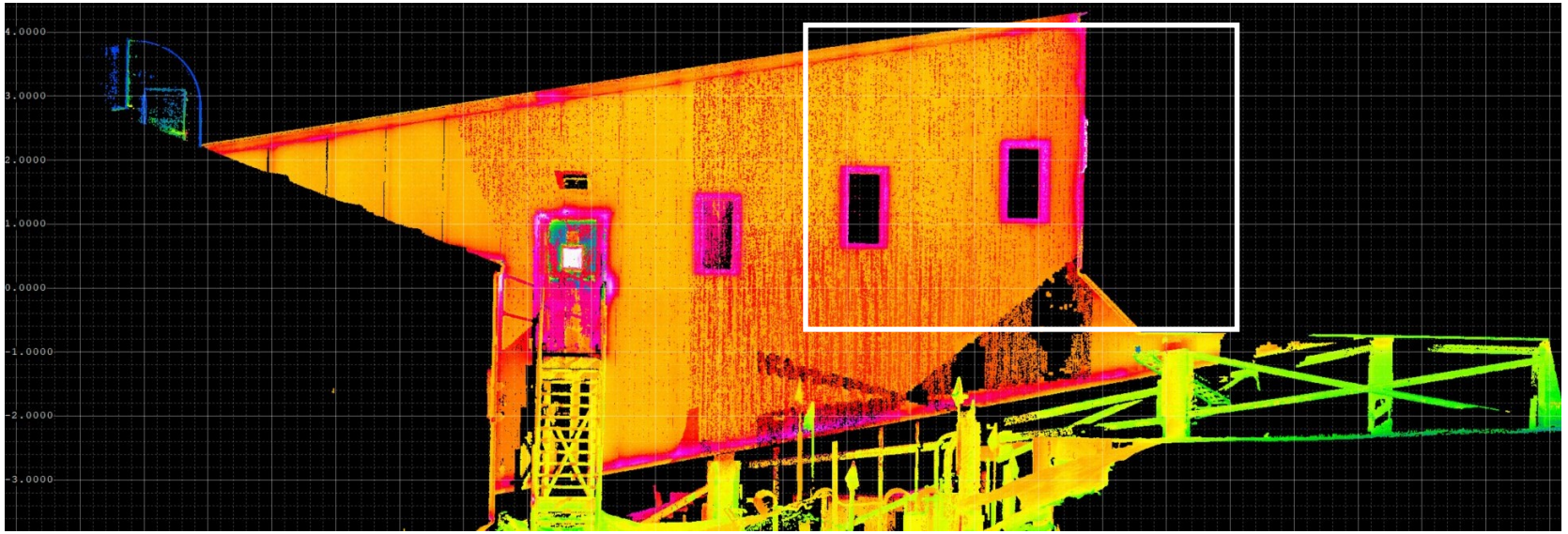
-15◦C



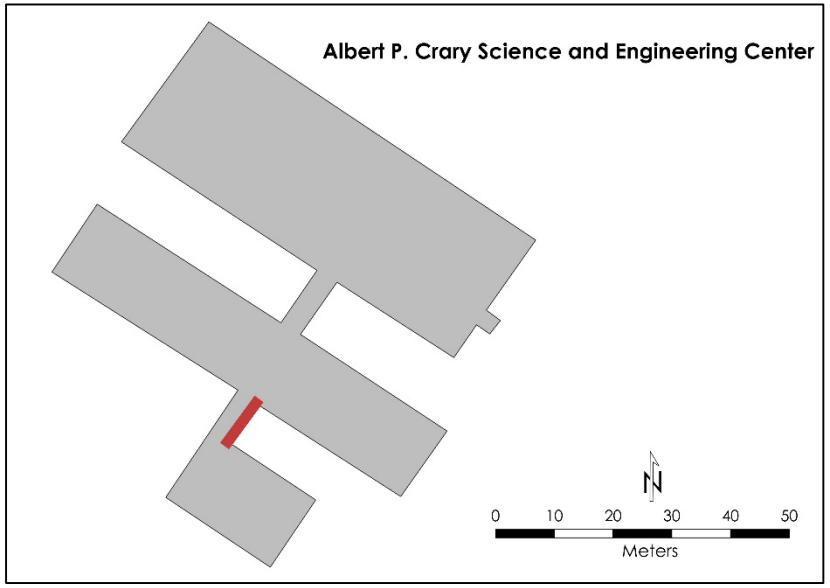
5◦C

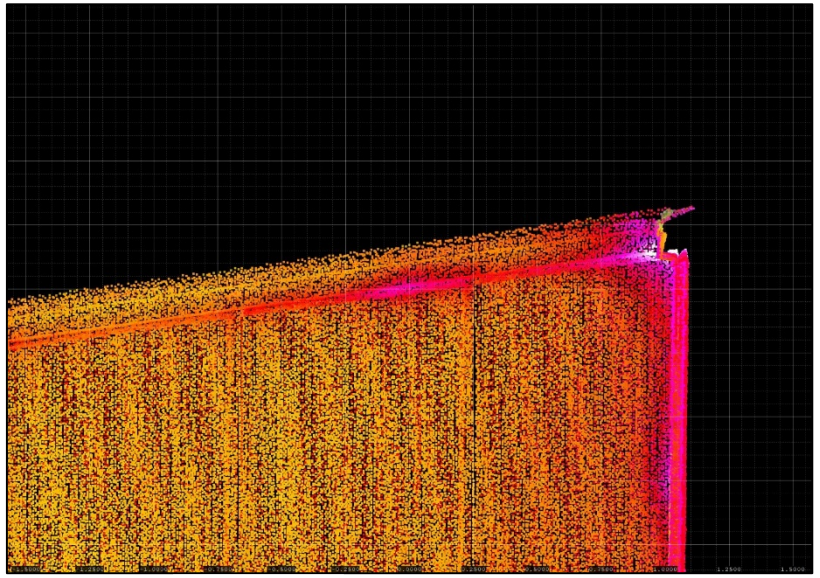


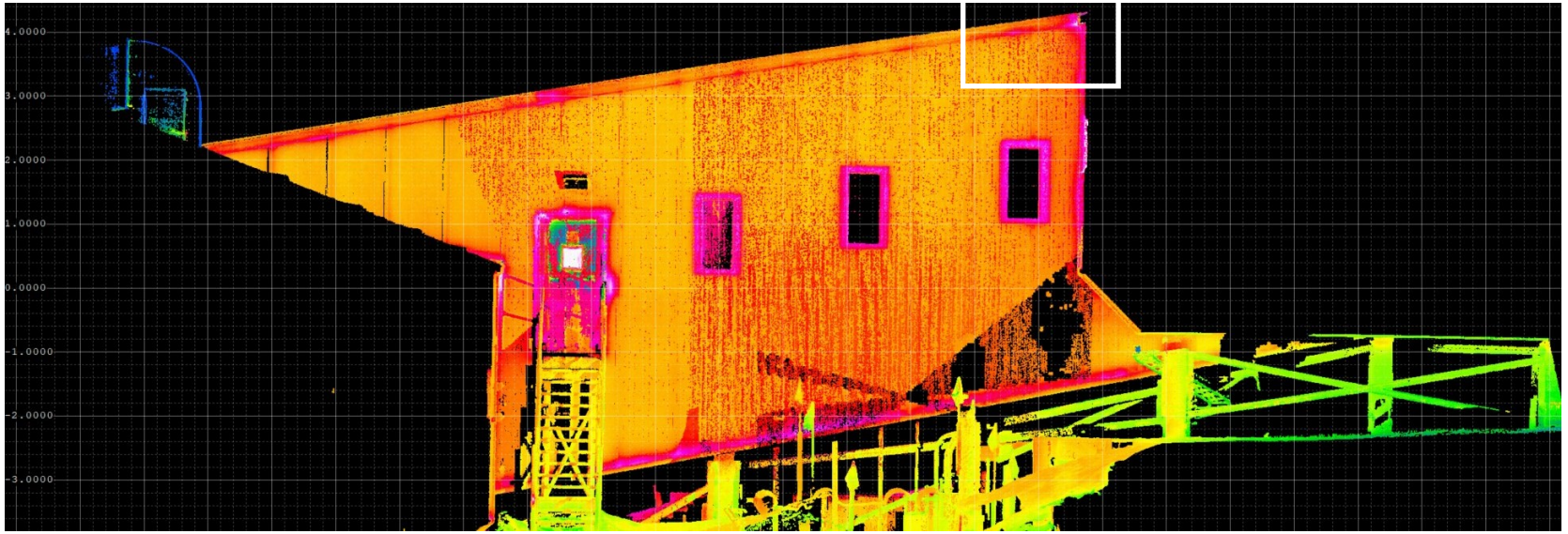




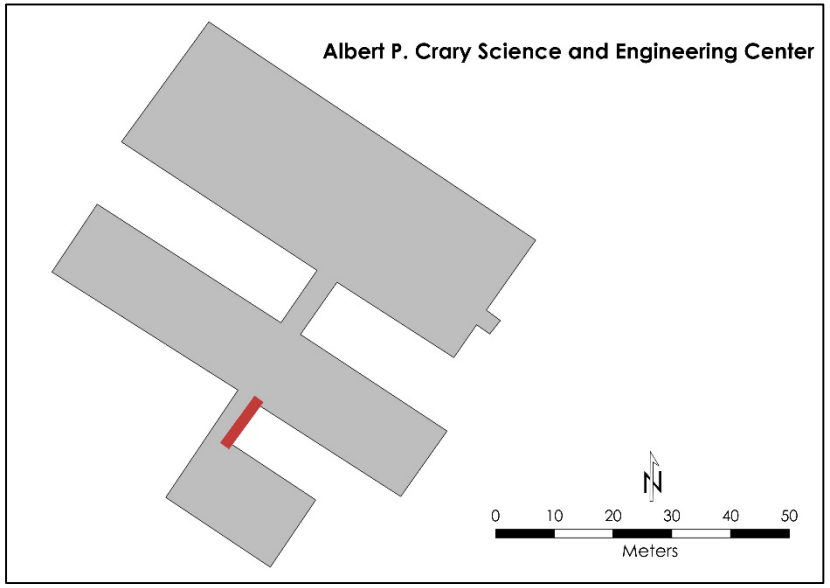
P3CE-W-03 -15◦C 5◦C

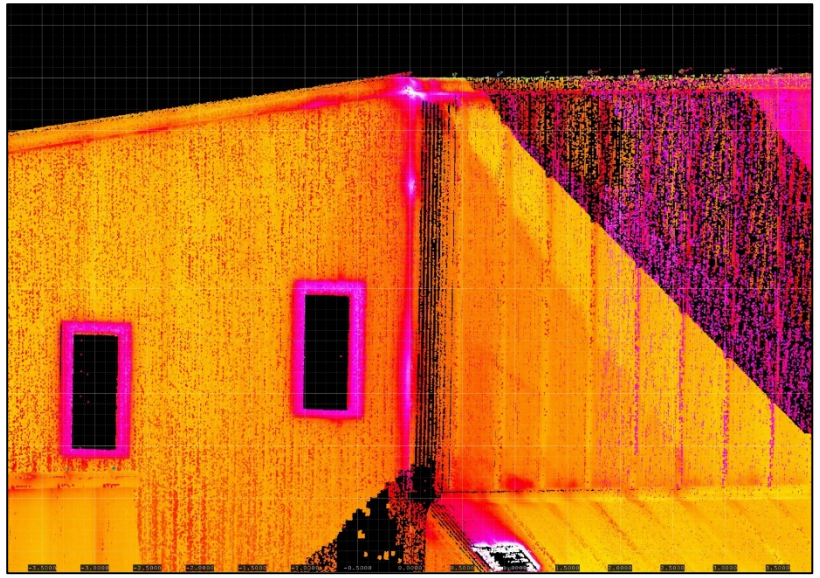


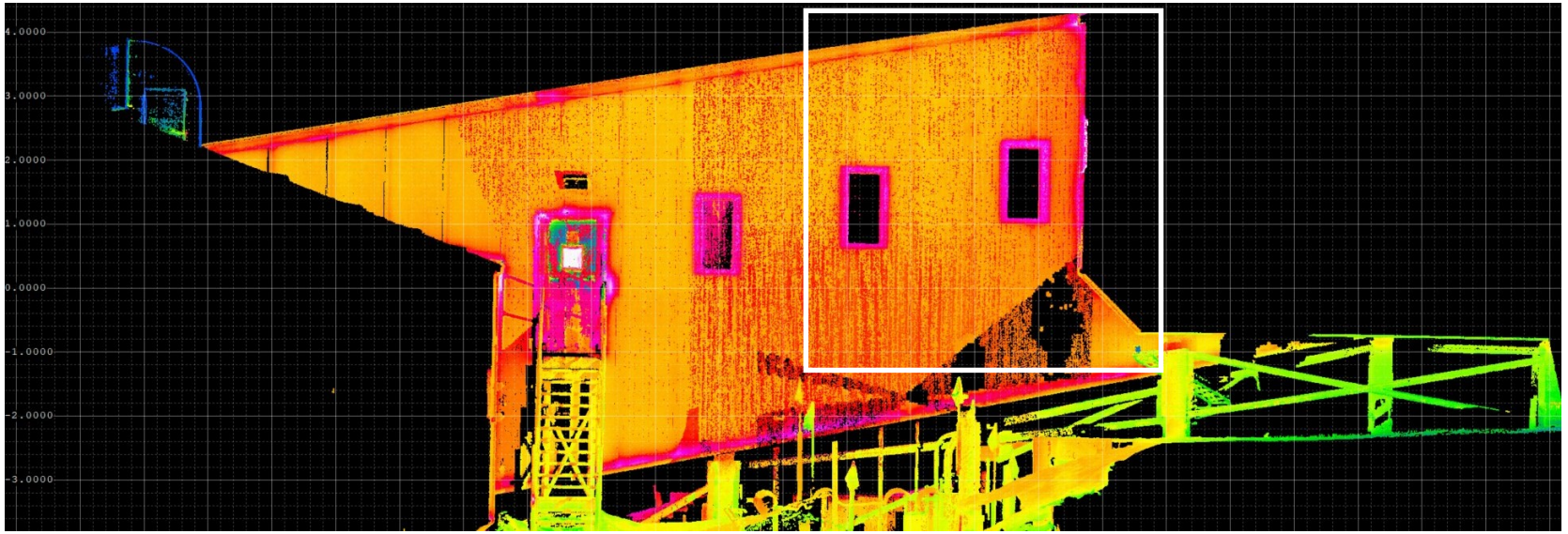




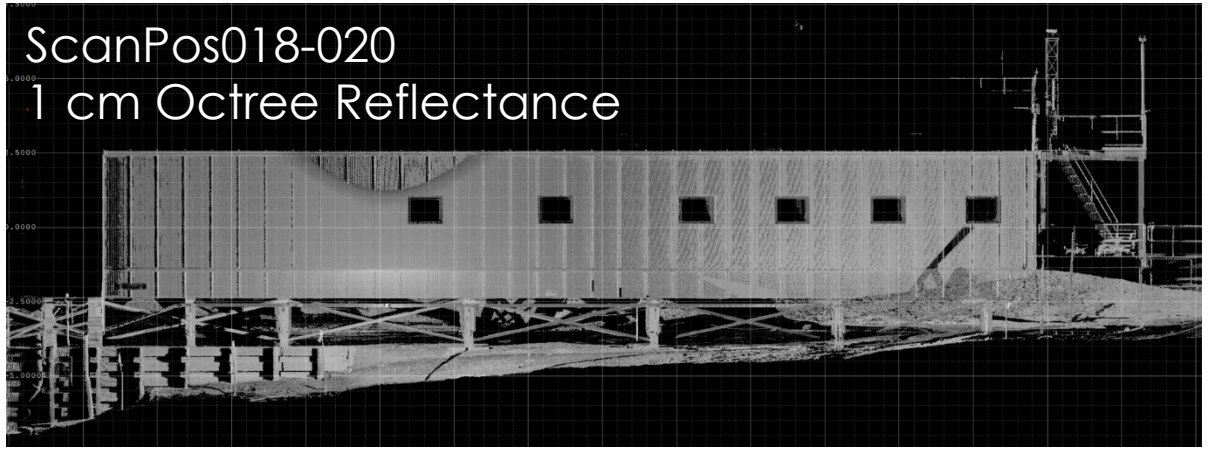
P3CE-TA-04 -15◦C 5◦C



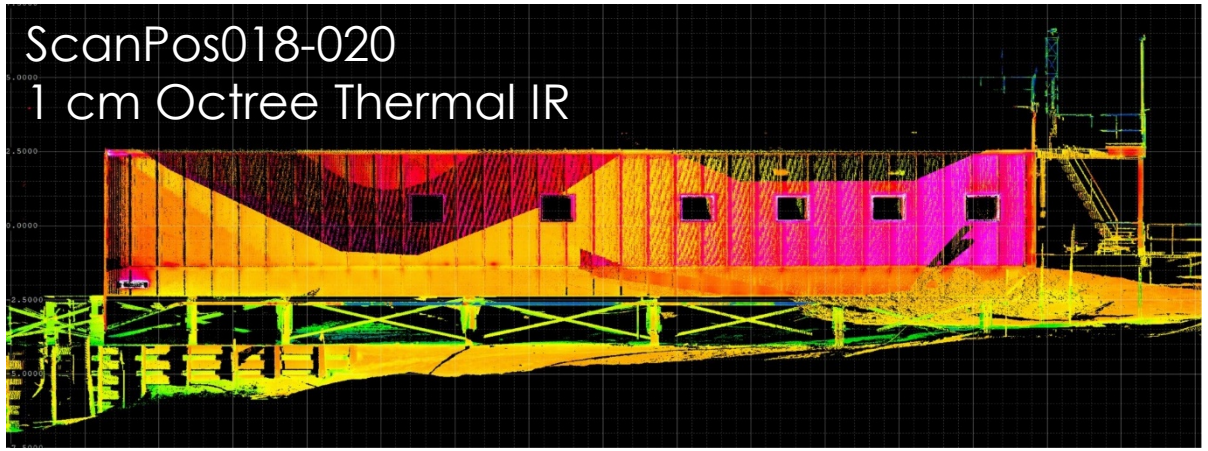


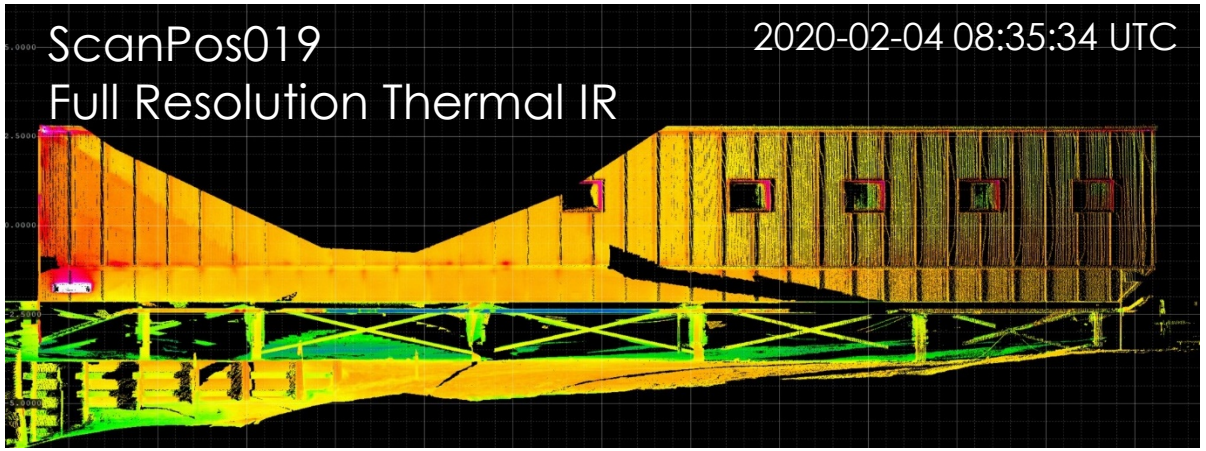


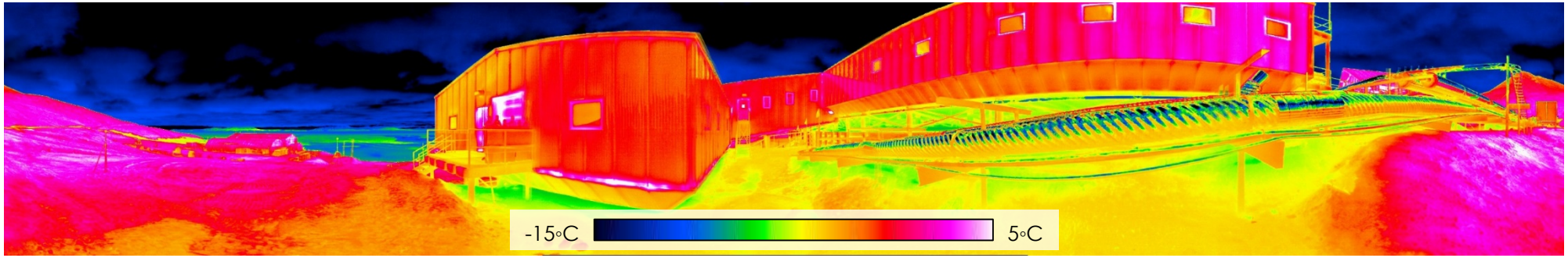
P3CE-TA-05 -15◦C 5◦C



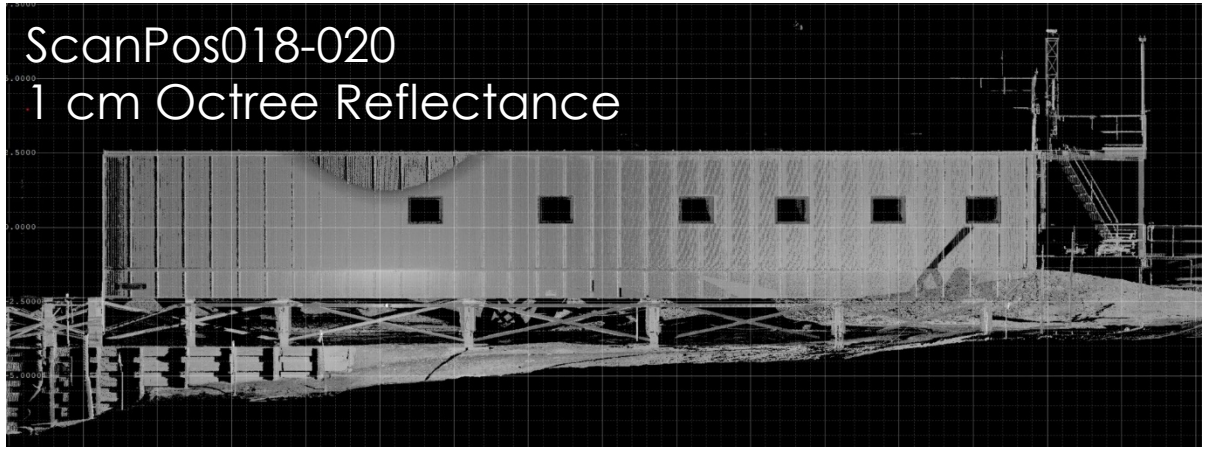




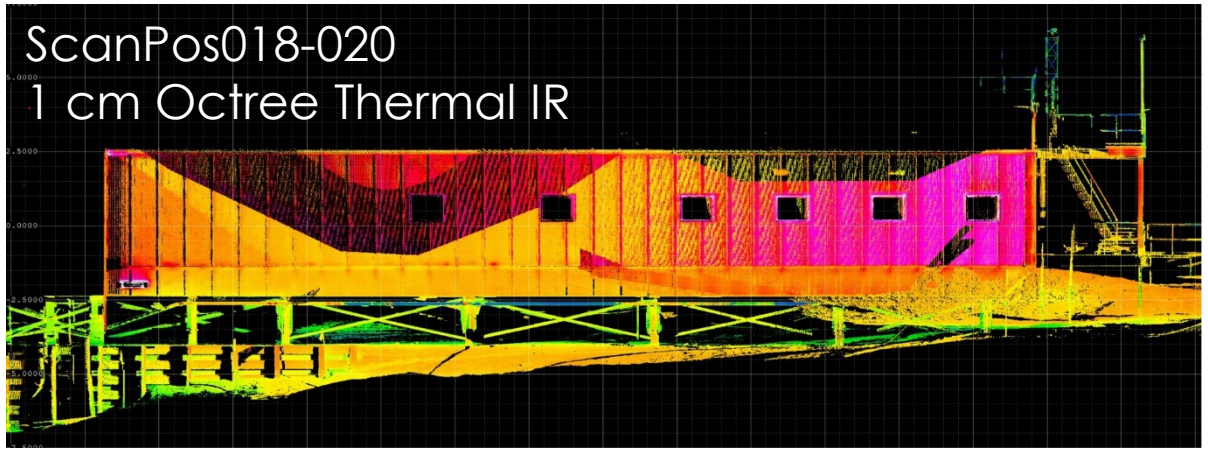


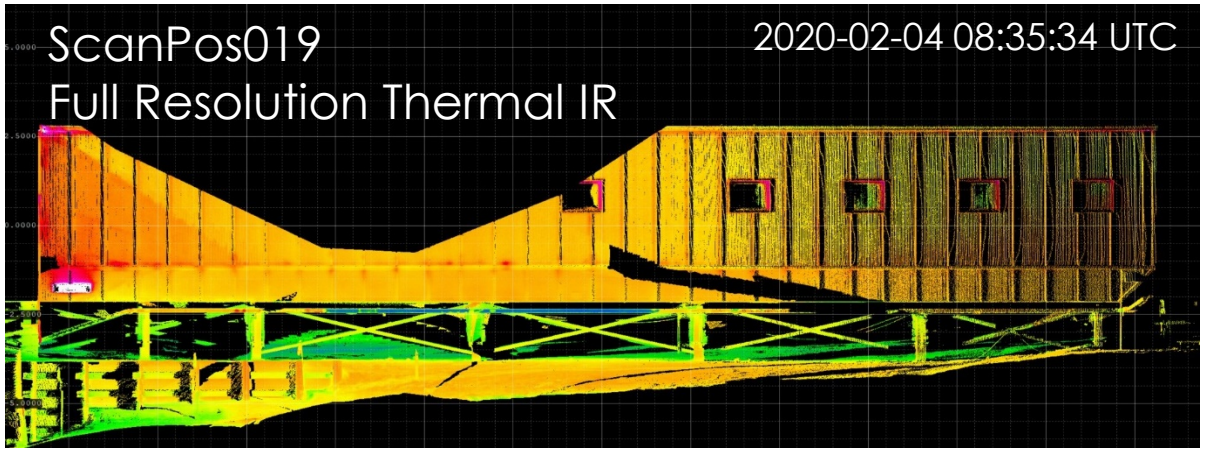


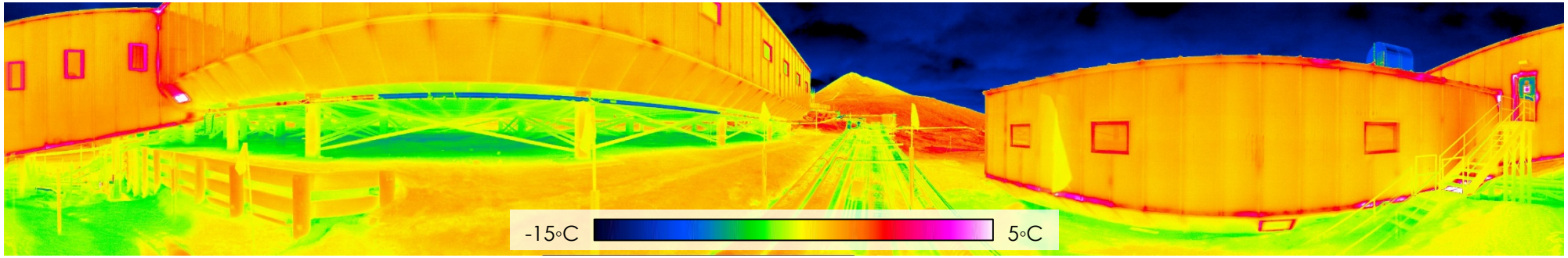
ScanPos018 – TIR Panorama



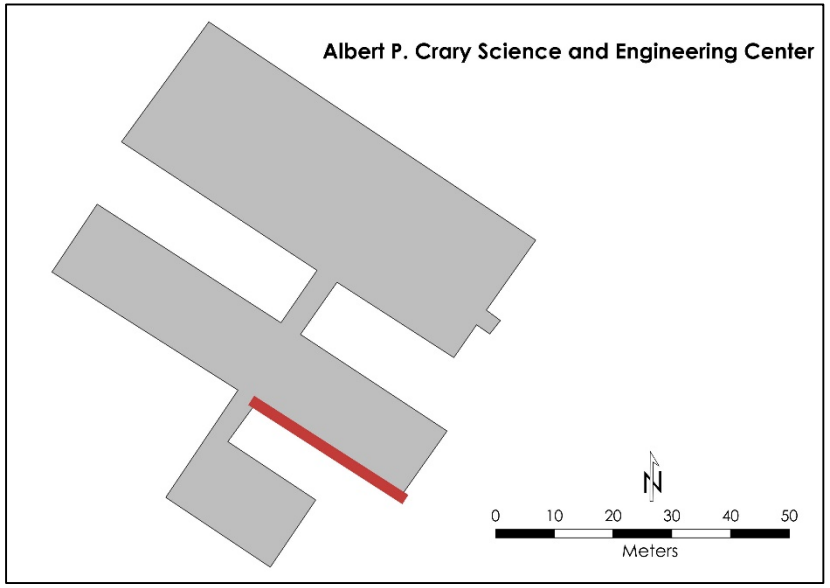


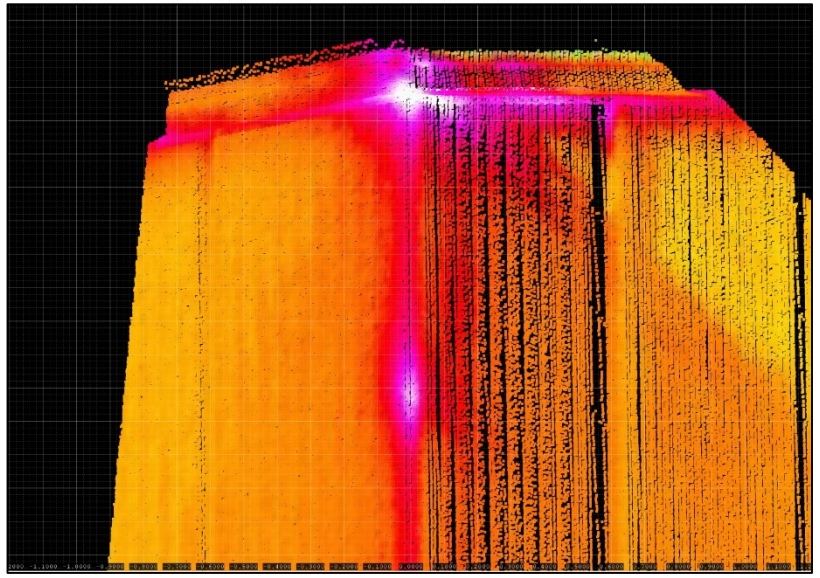


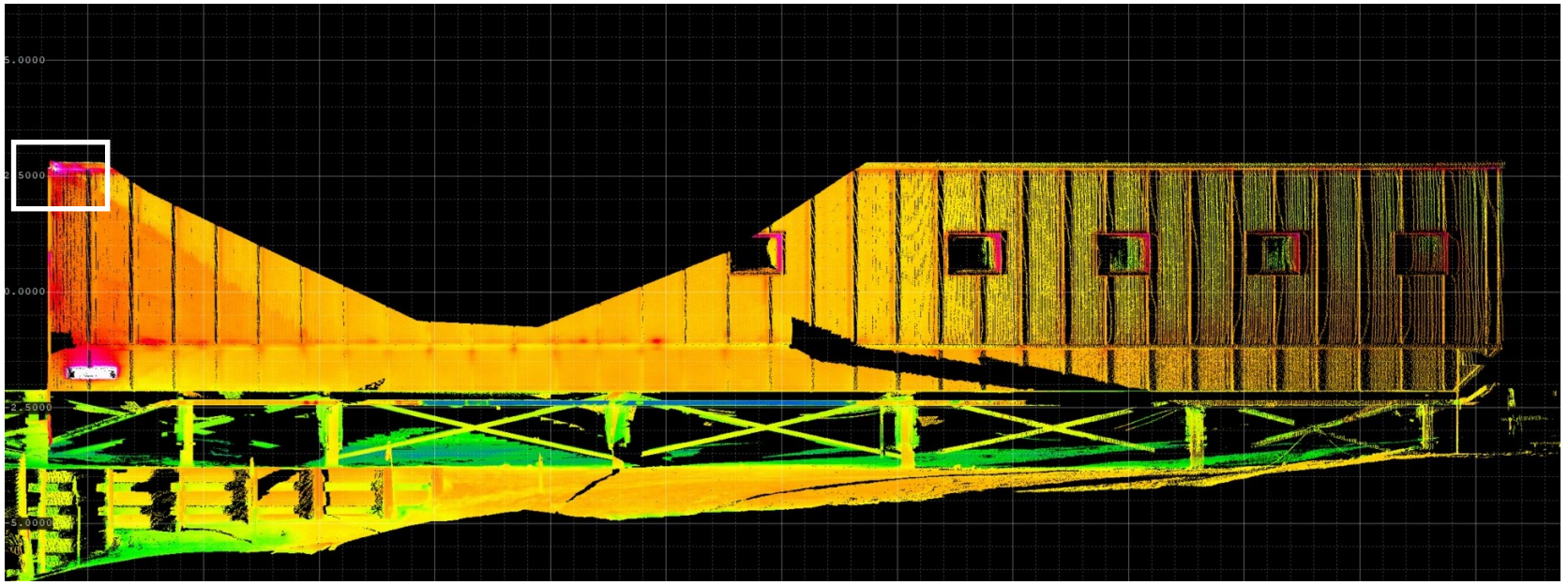




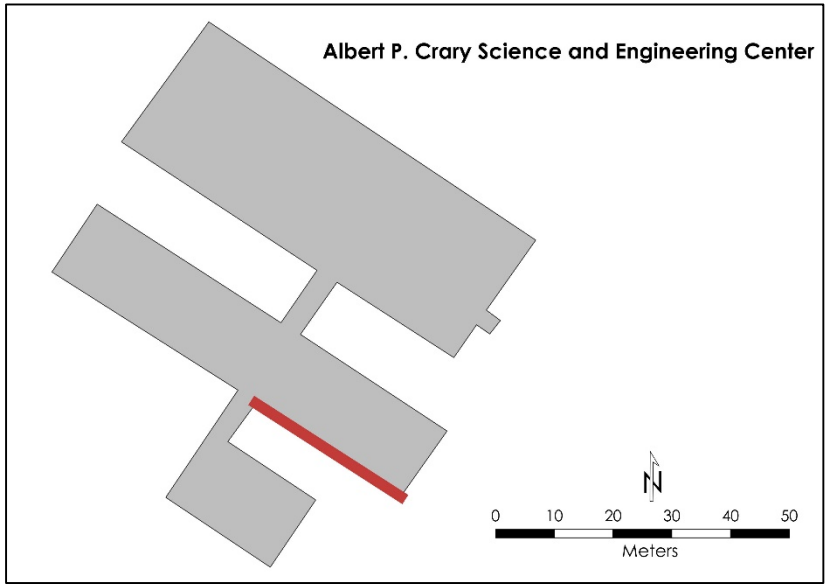
ScanPos019 – TIR Panorama

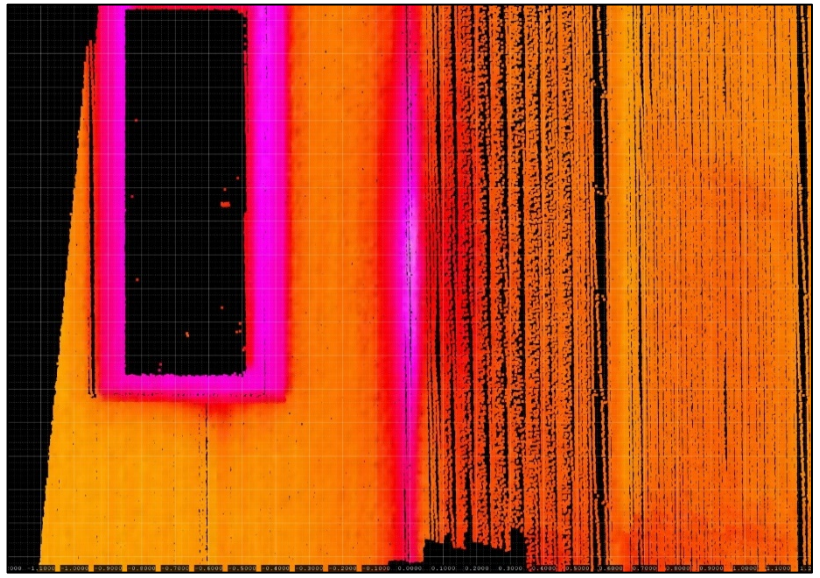


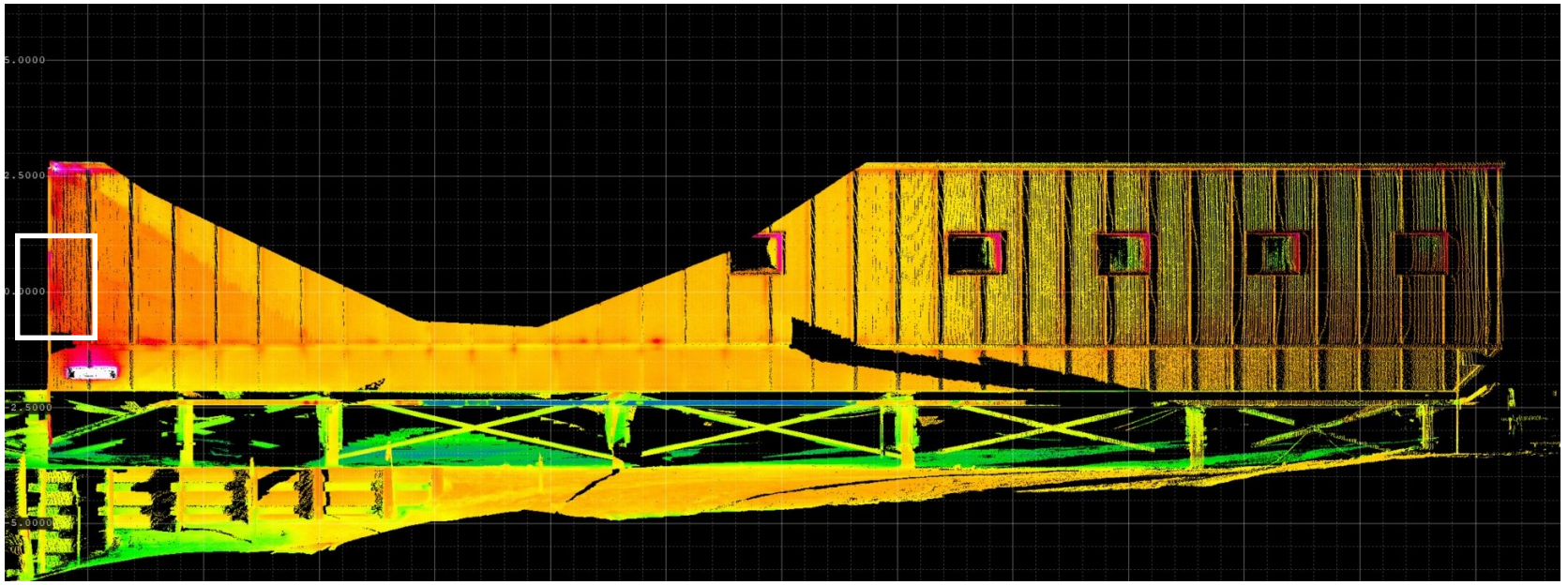




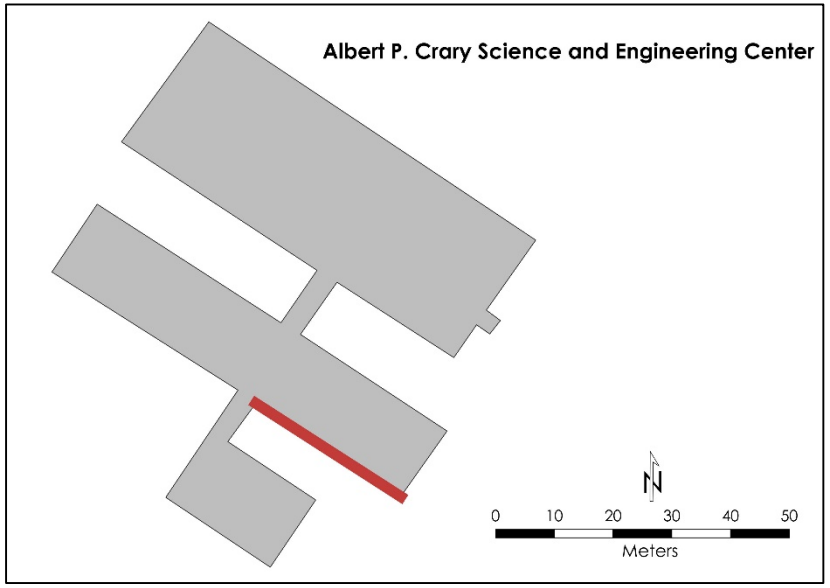
P2SE-TA-01 -15◦C 5◦C

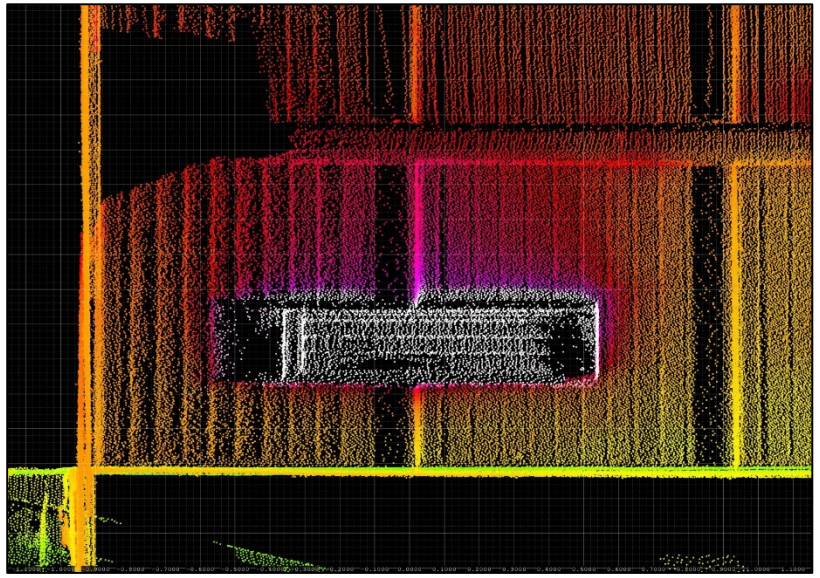


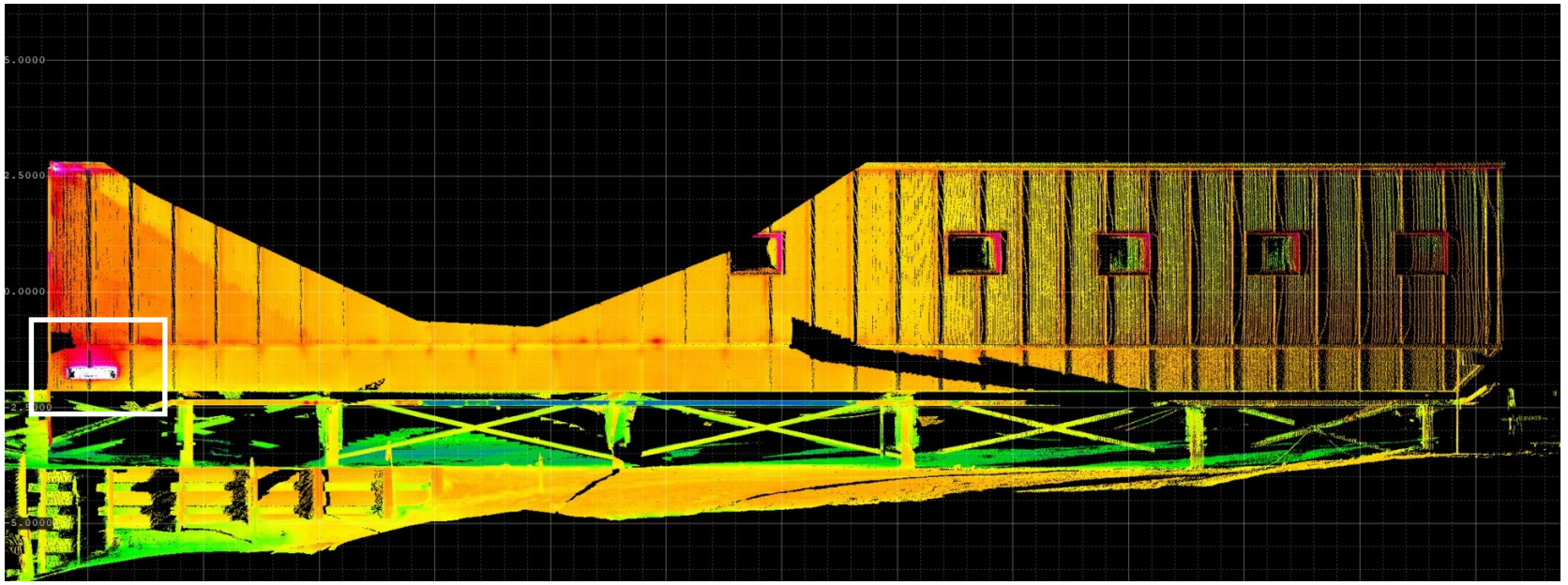




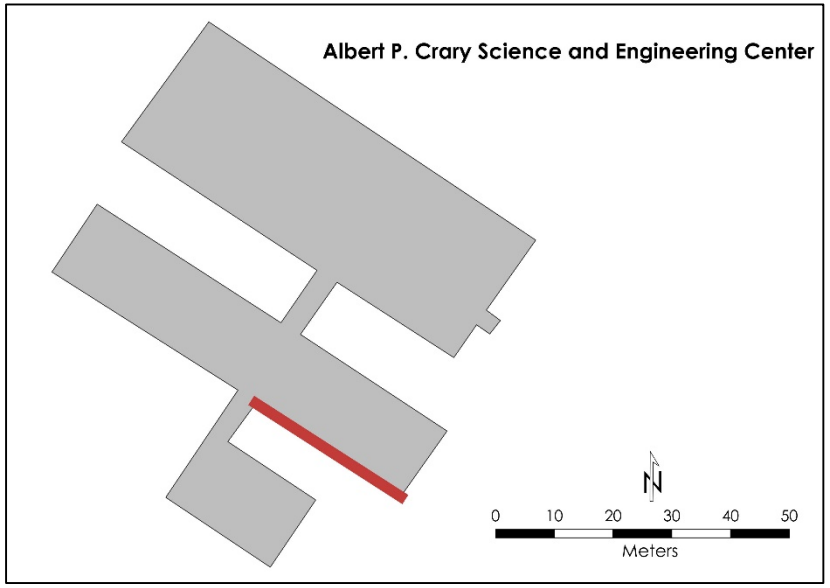
P2SE-TA-02 -15◦C 5◦C

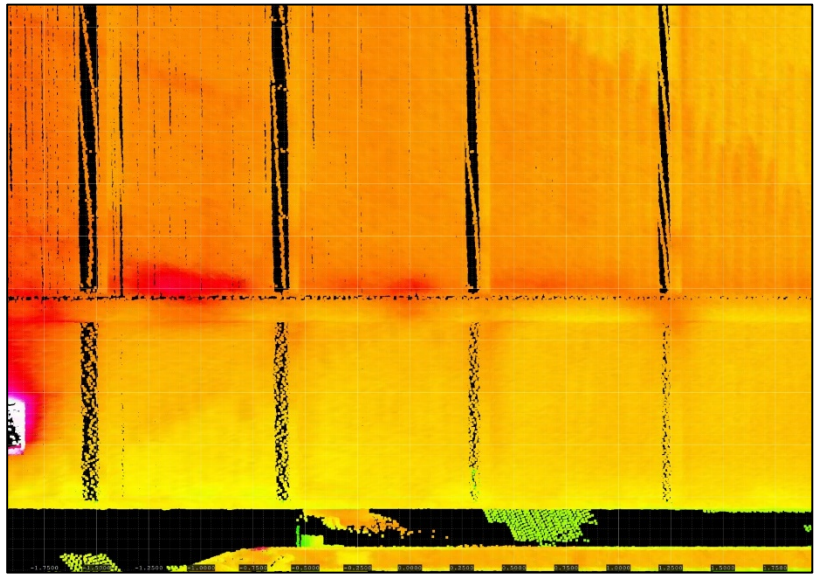


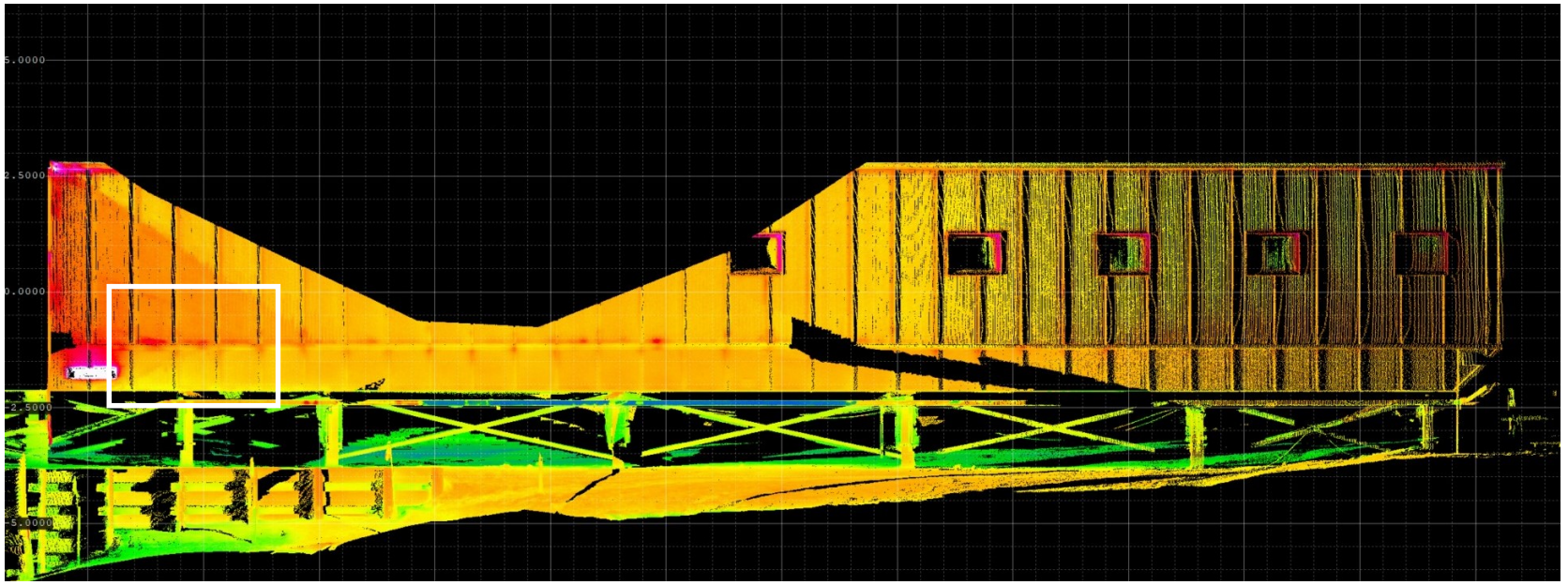




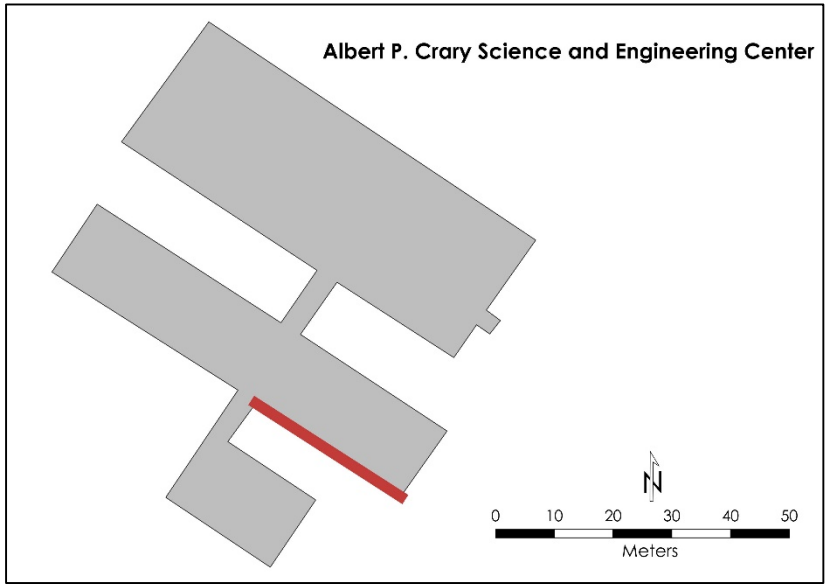
P2SE-V-01 -15◦C 5◦C

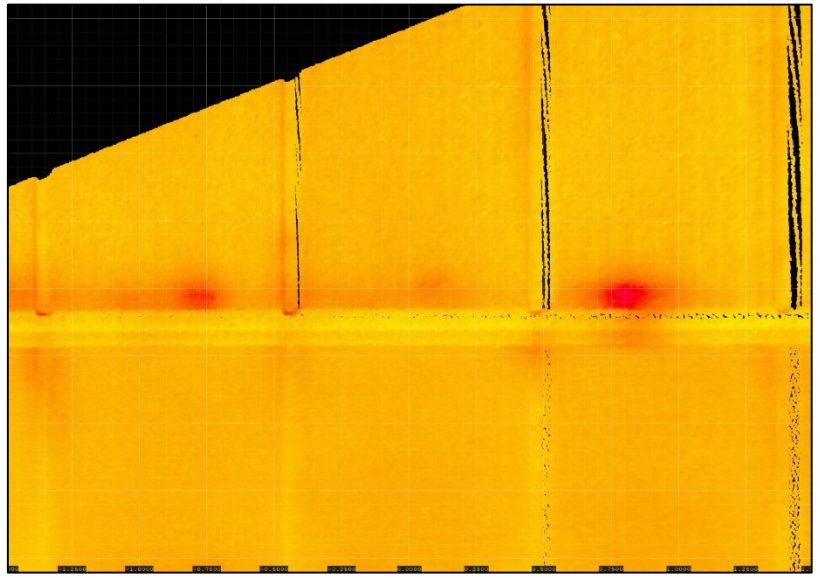


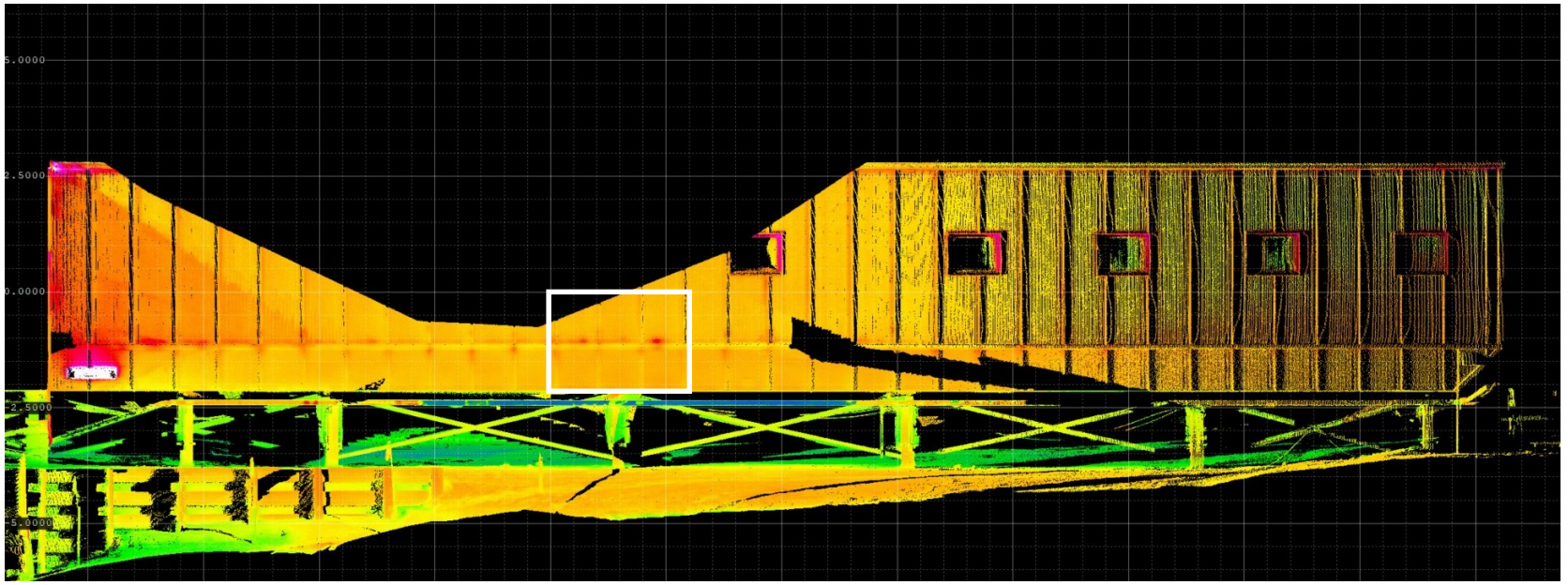




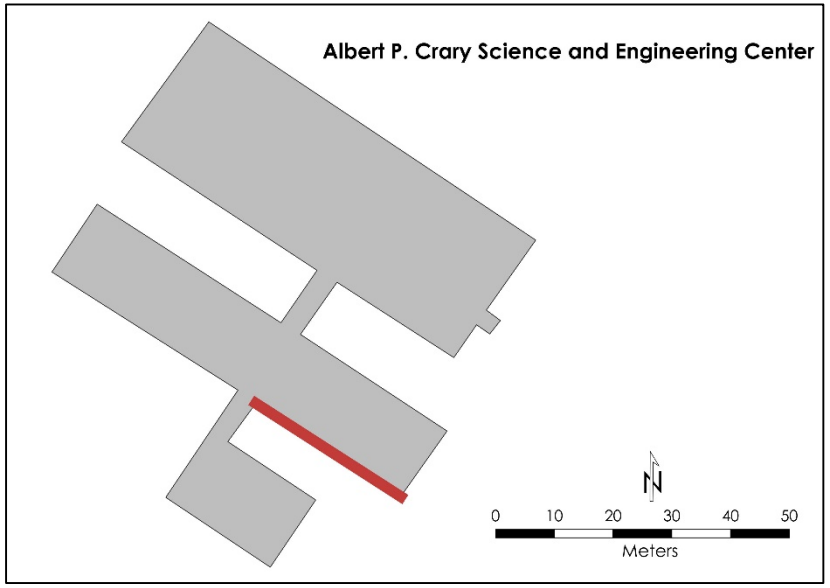
P2SE-TA-03 -15◦C 5◦C

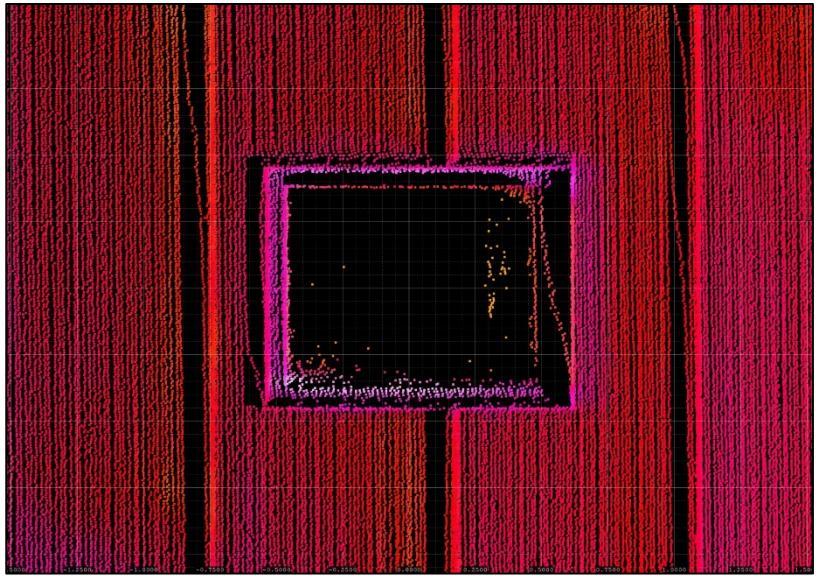


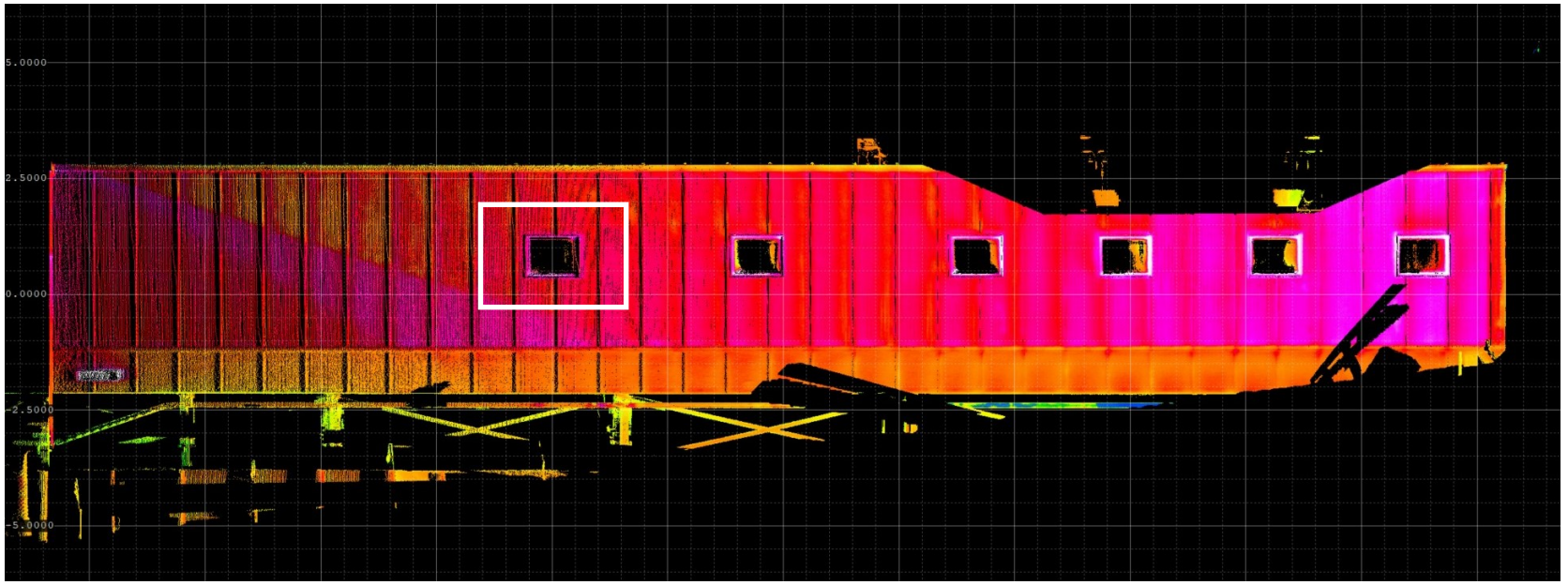




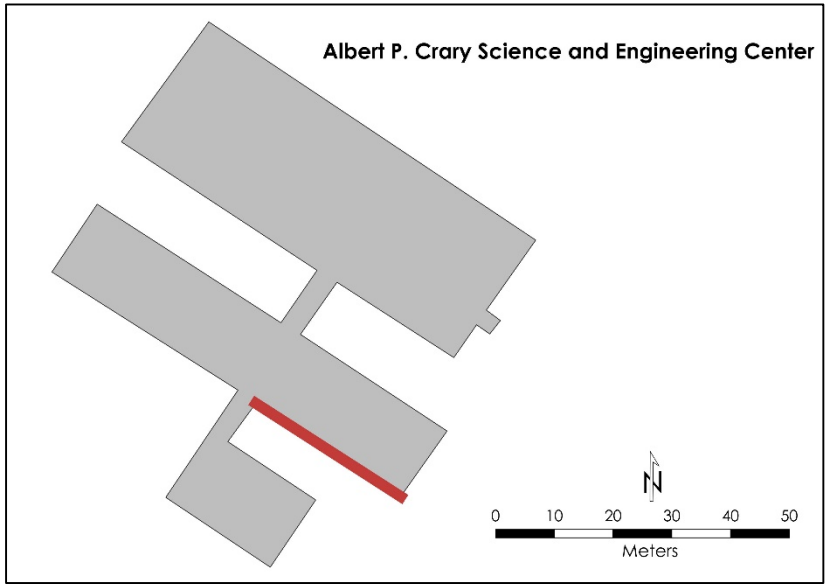
P2SE-TA-04 -15◦C 5◦C

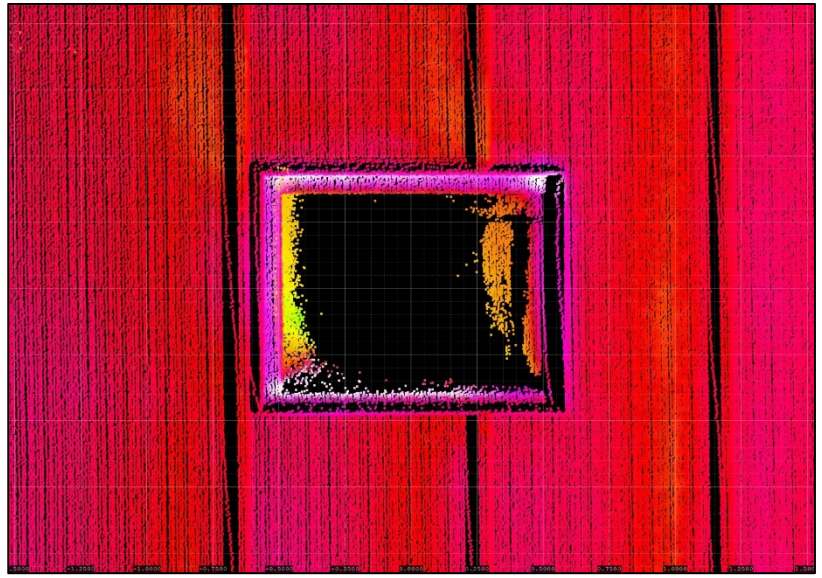


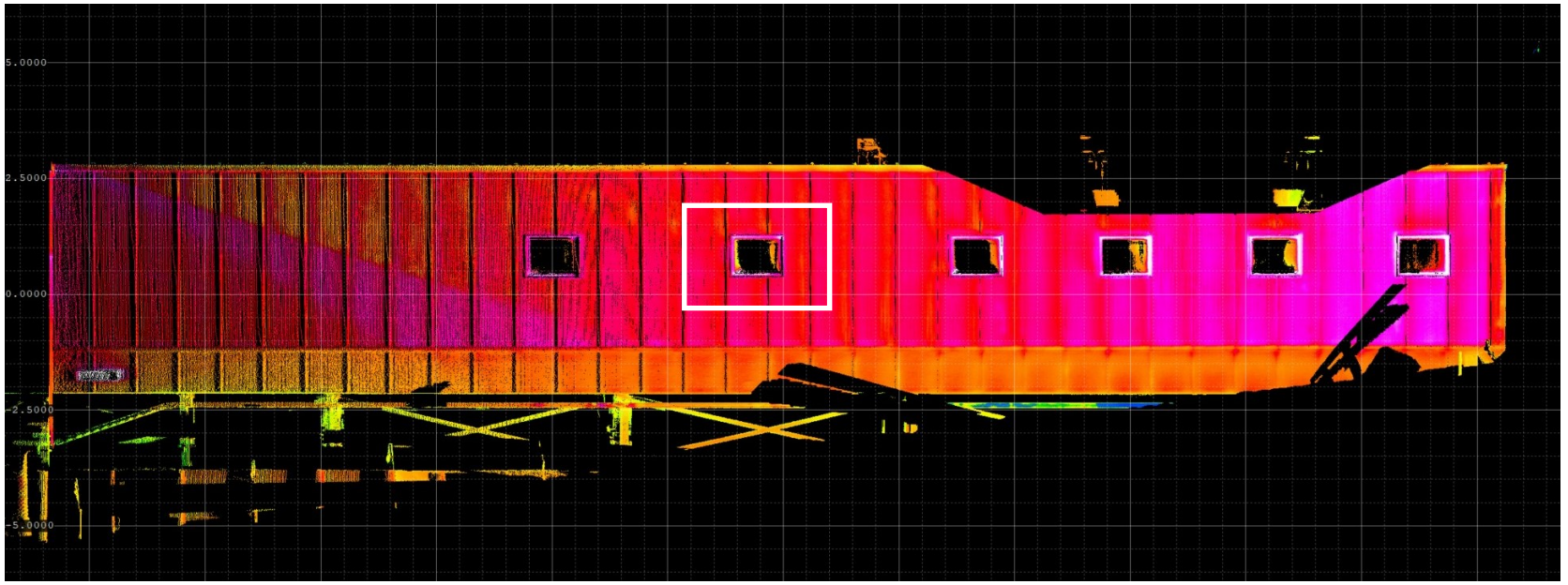




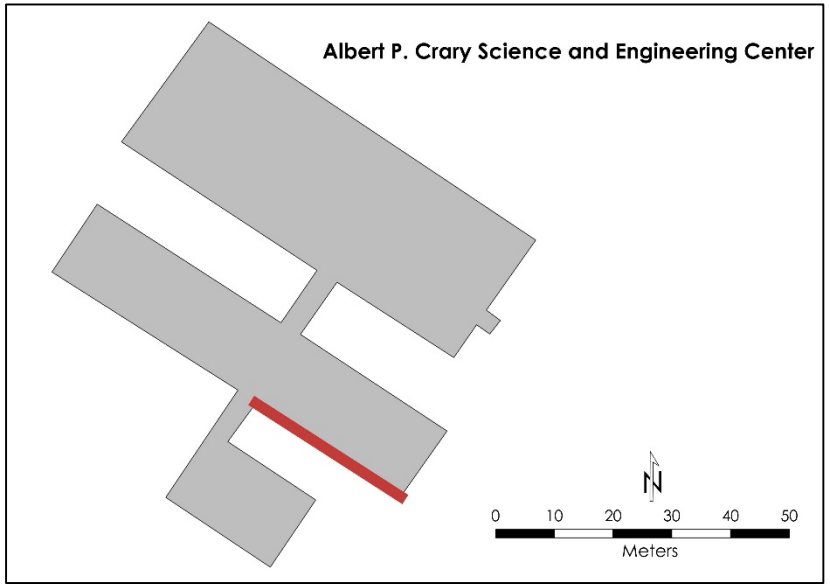
P2SE-W-01 -15◦C 5◦C

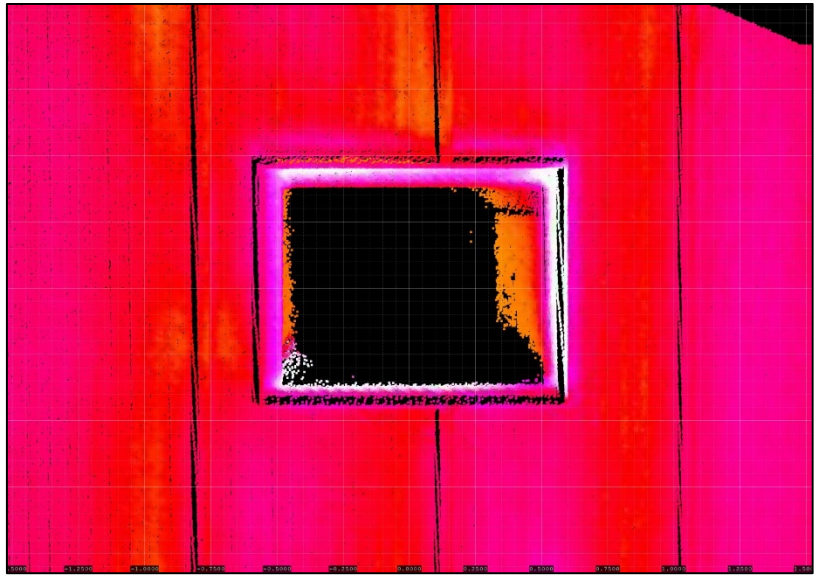


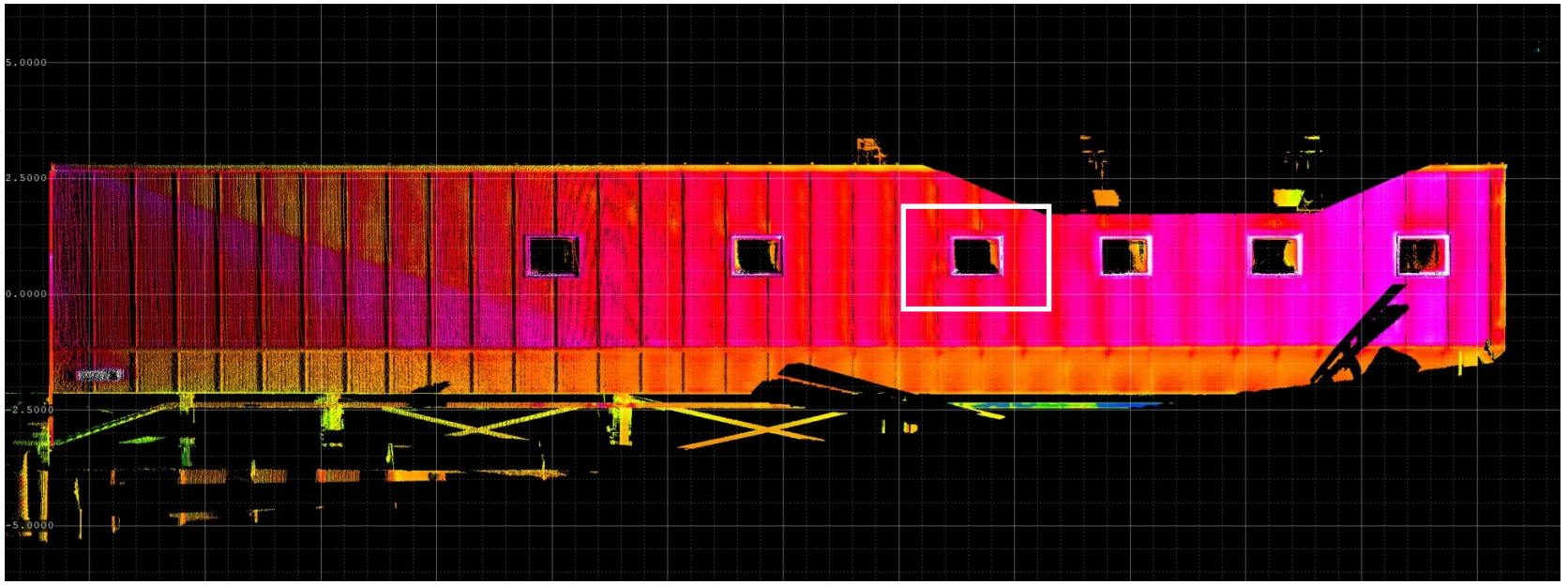




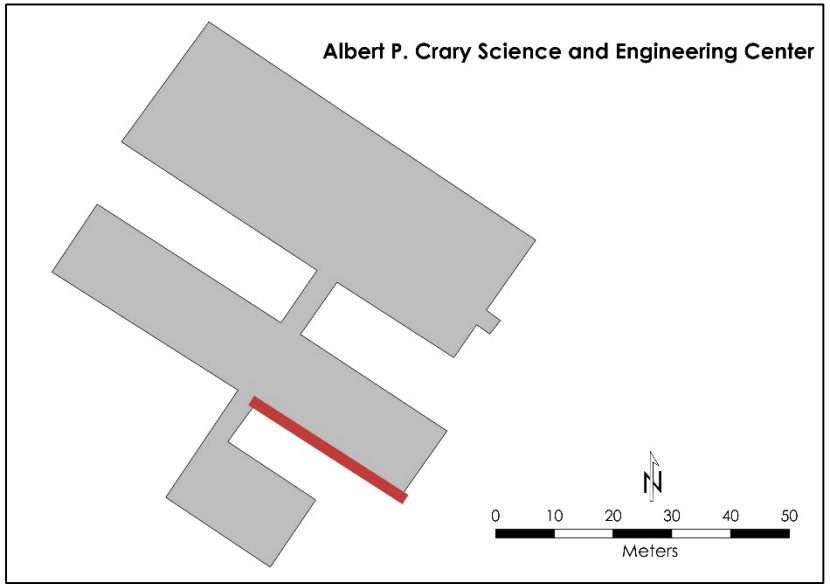
P2SE-W-02 -15◦C 5◦C

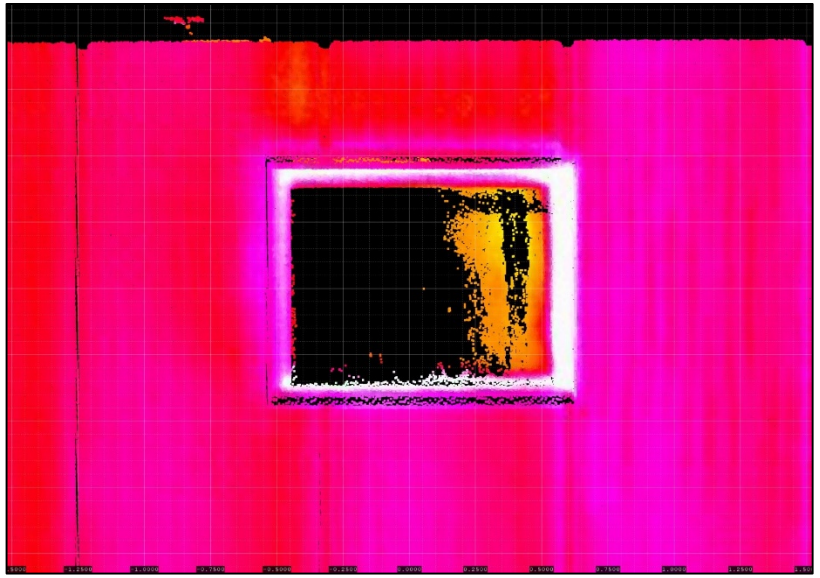


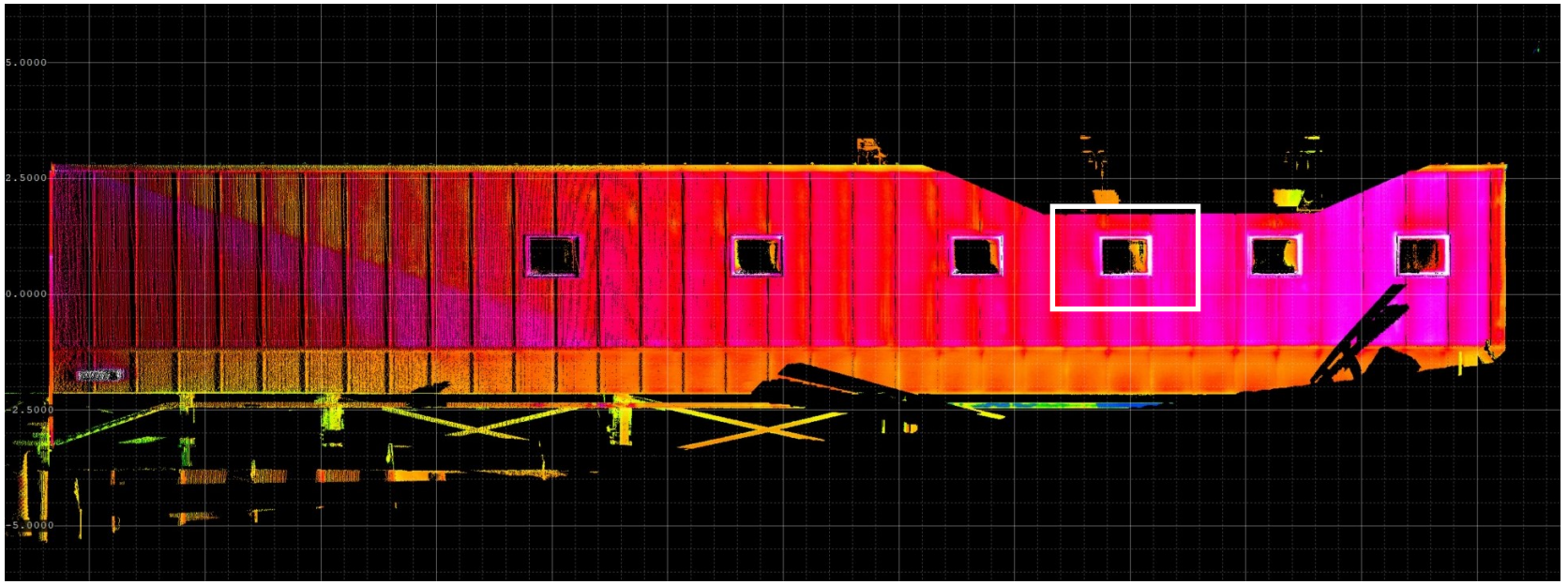




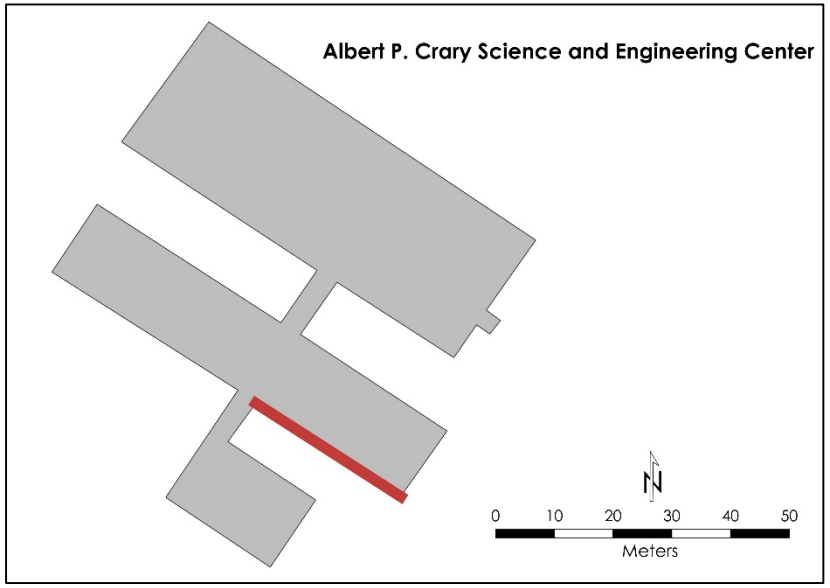
P2SE-W-03 -15◦C 5◦C

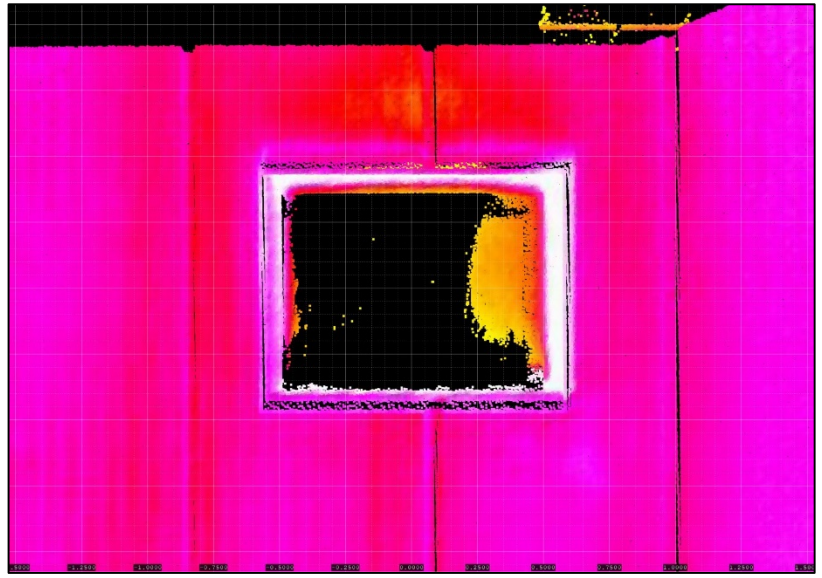


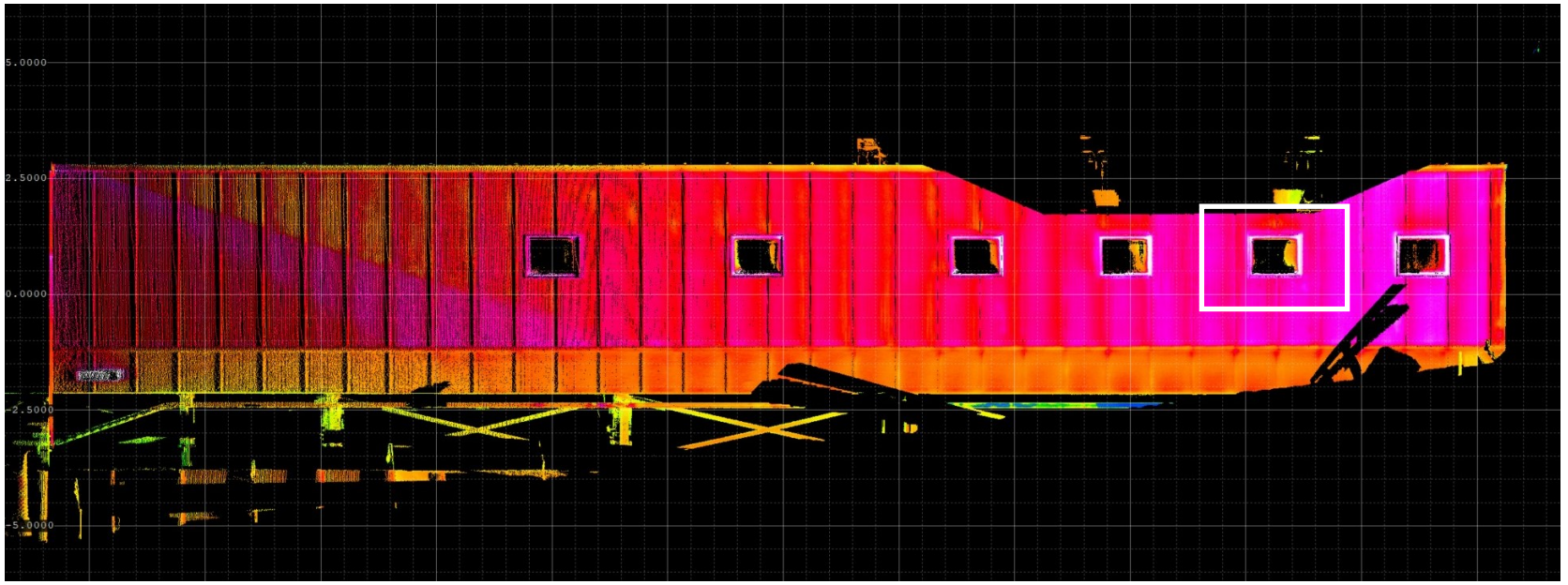




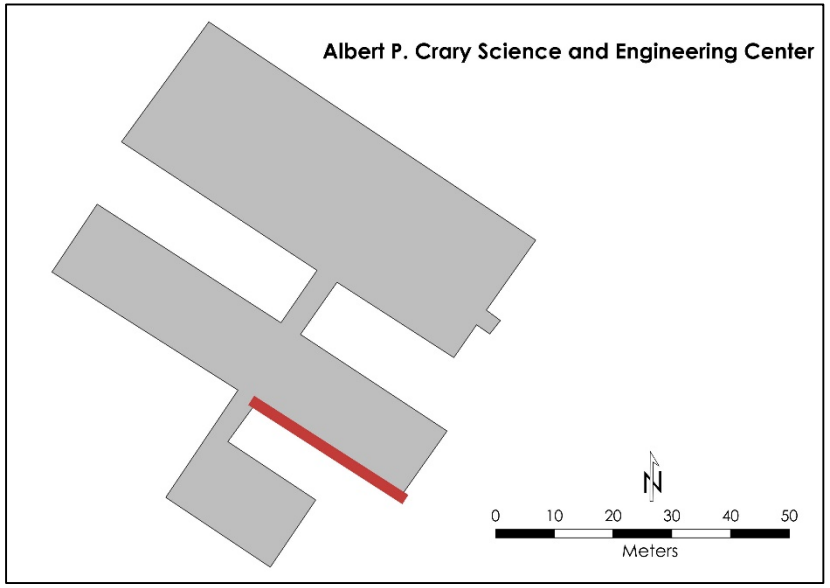
P2SE-W-04 -15◦C 5◦C

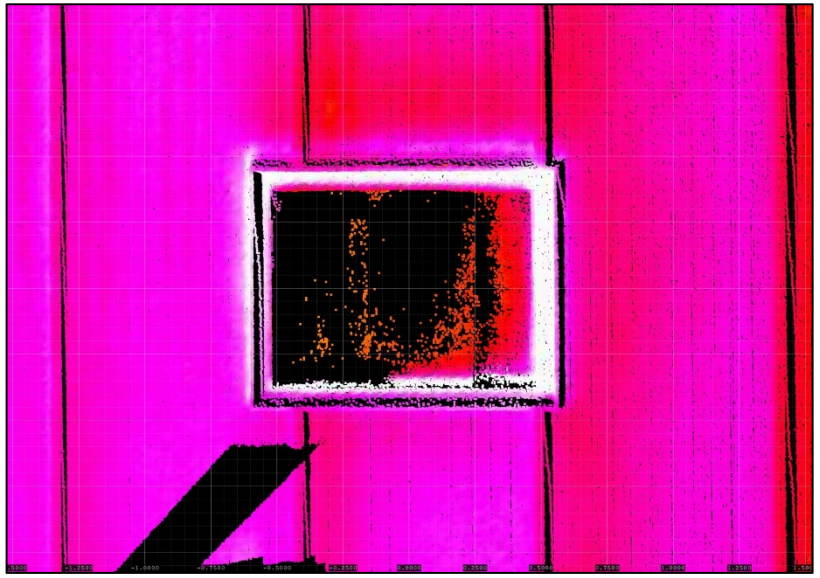


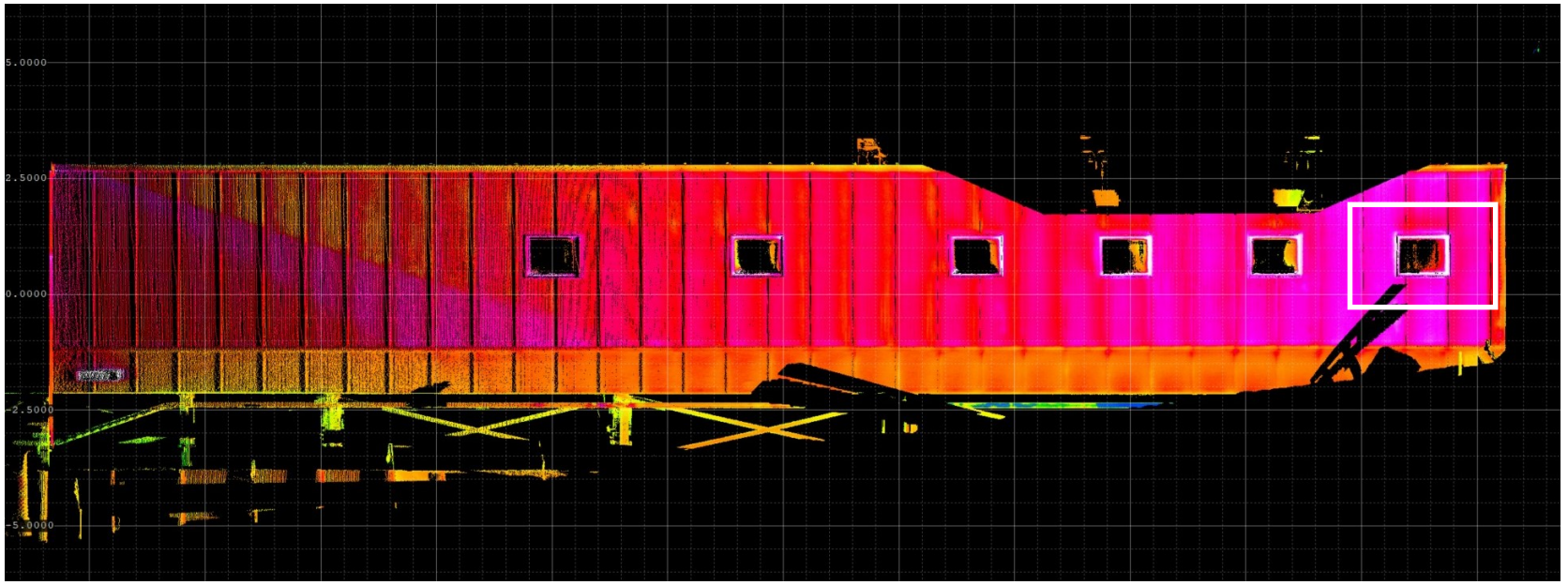




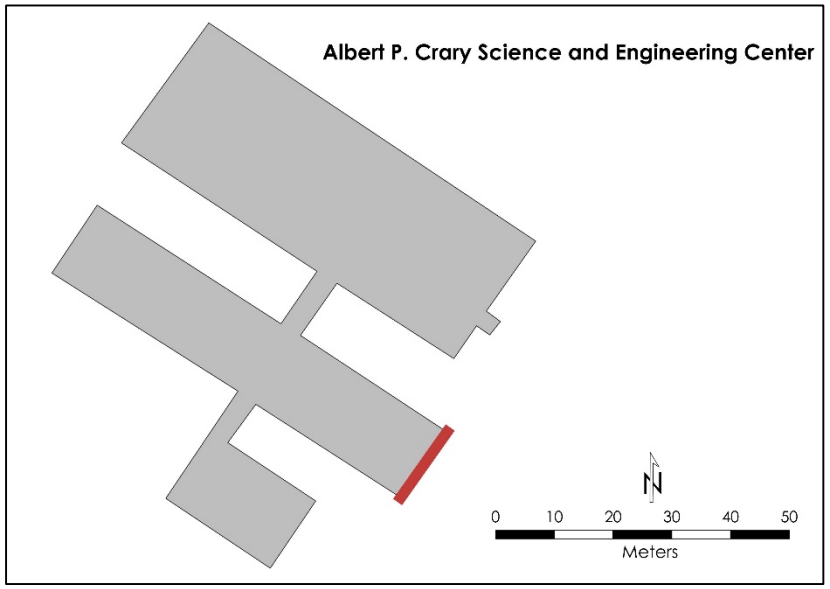
P2SE-W-05 -15◦C 5◦C

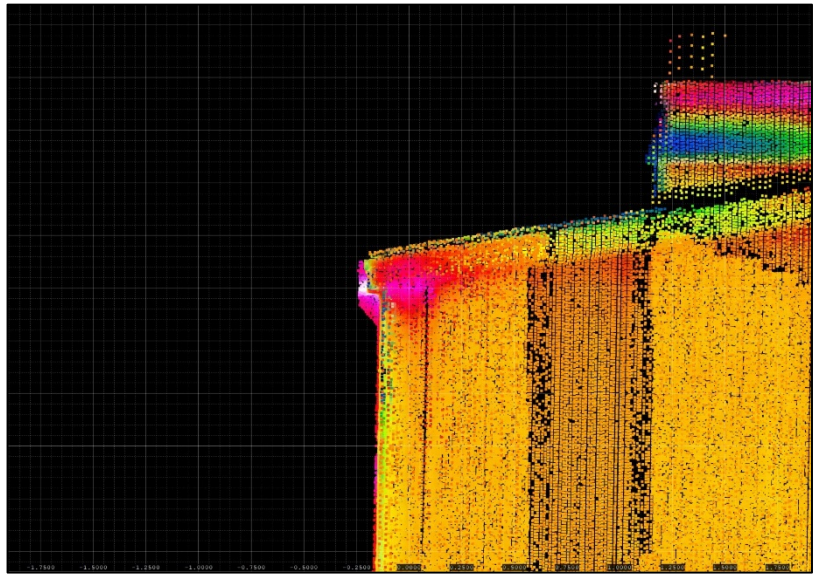


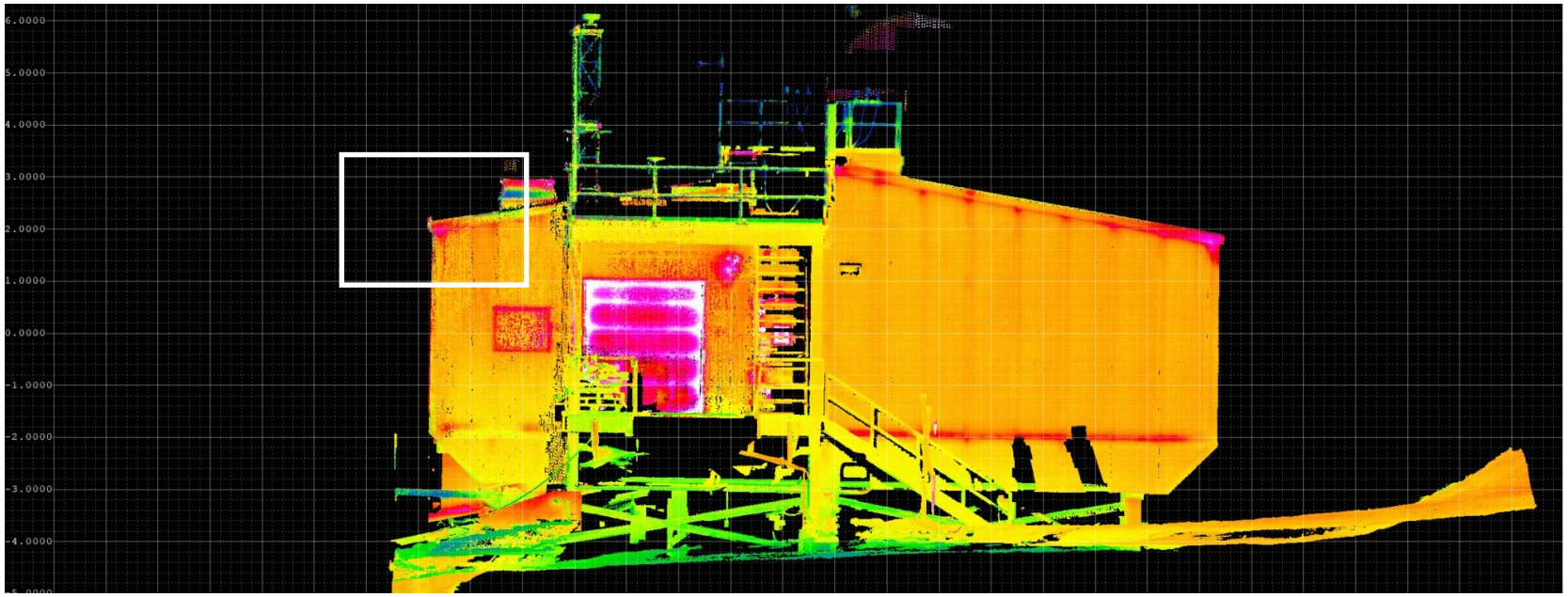




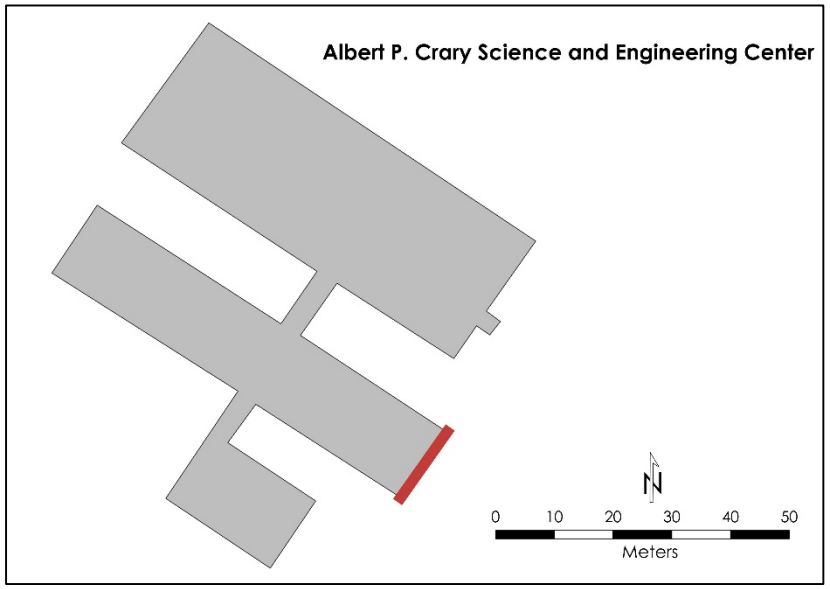
P2SE-W-06 -15◦C 5◦C

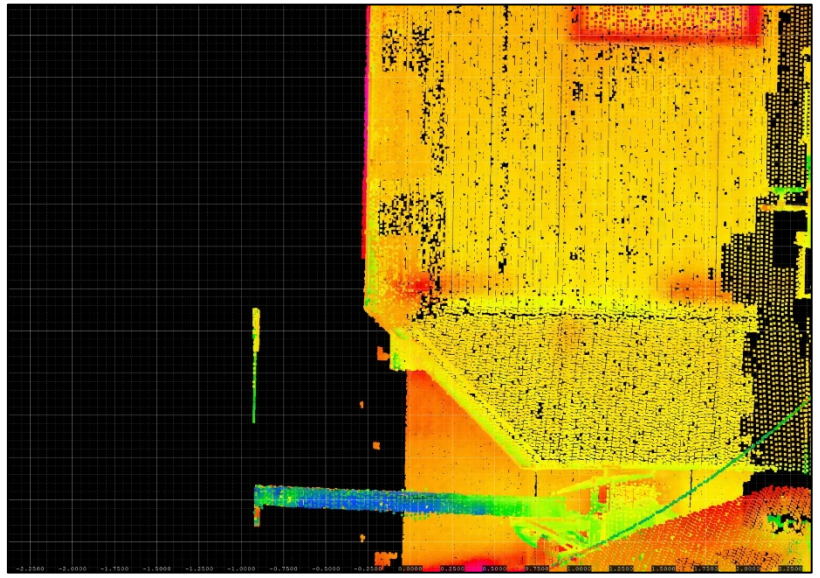


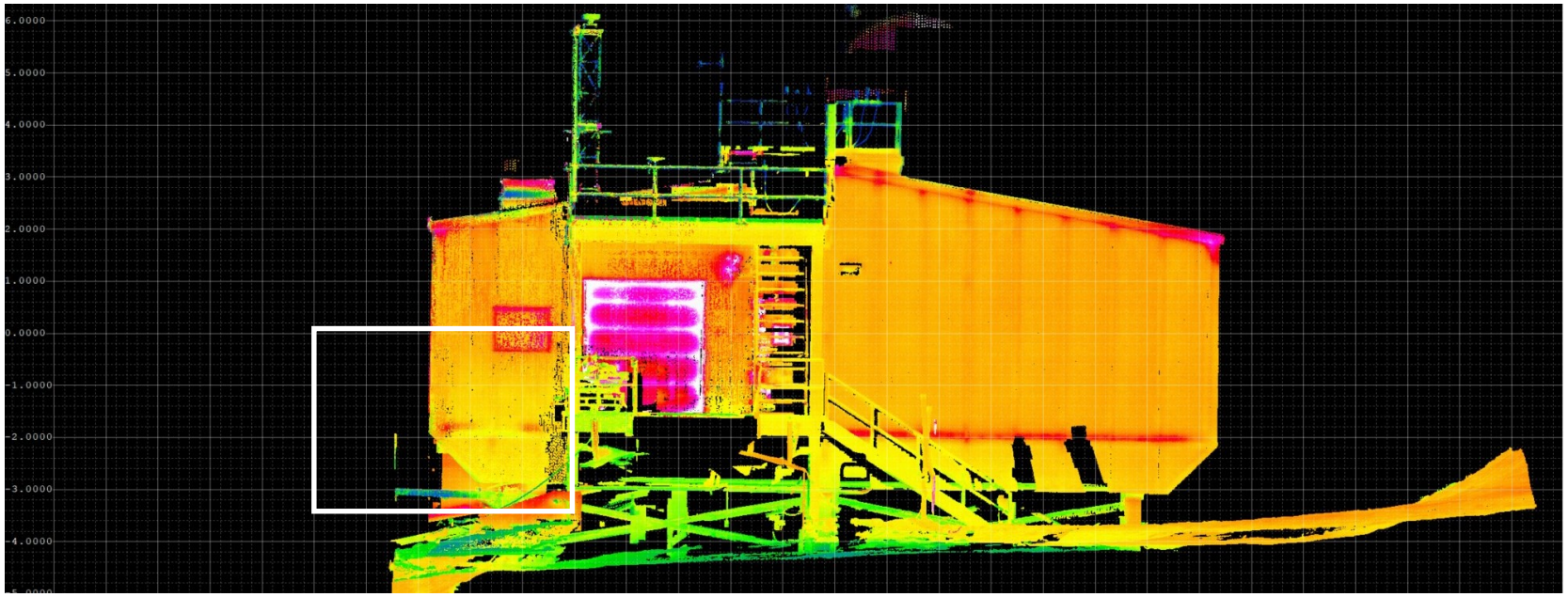




P2E-TA-01 -15◦C 5◦C





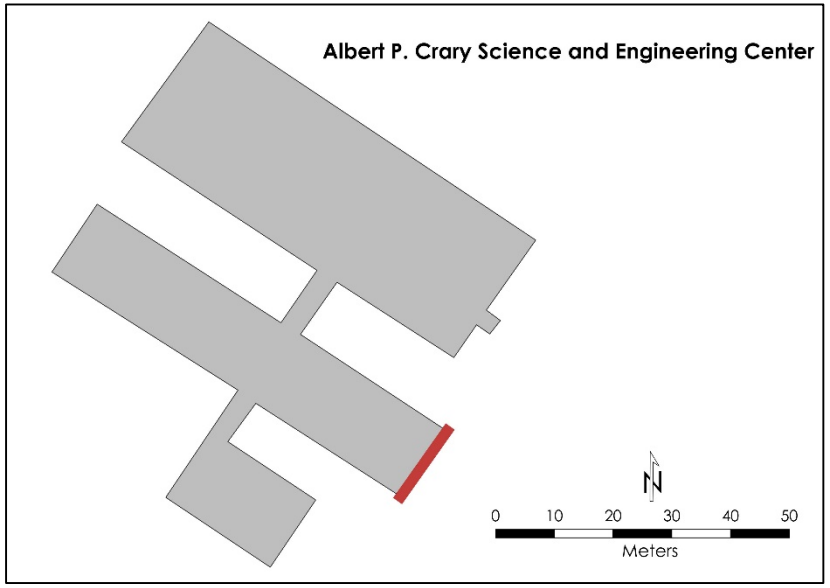


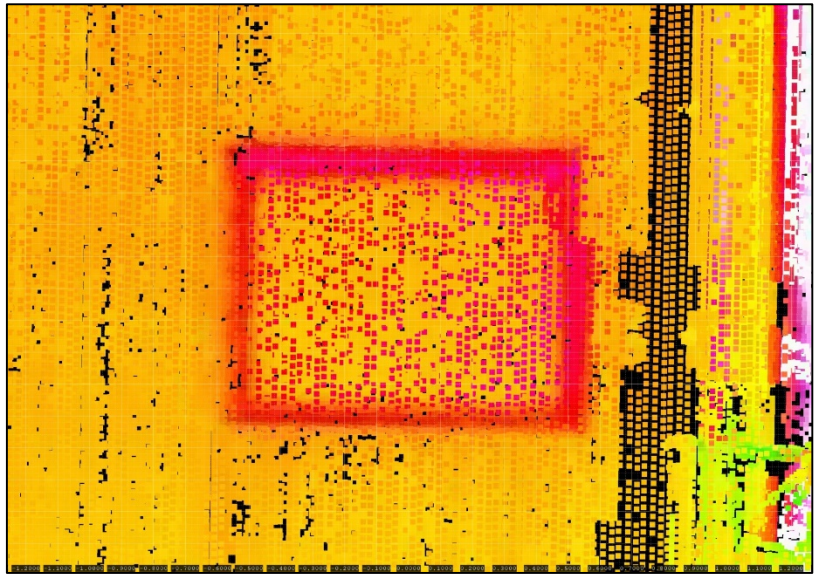
P2E-TA-02

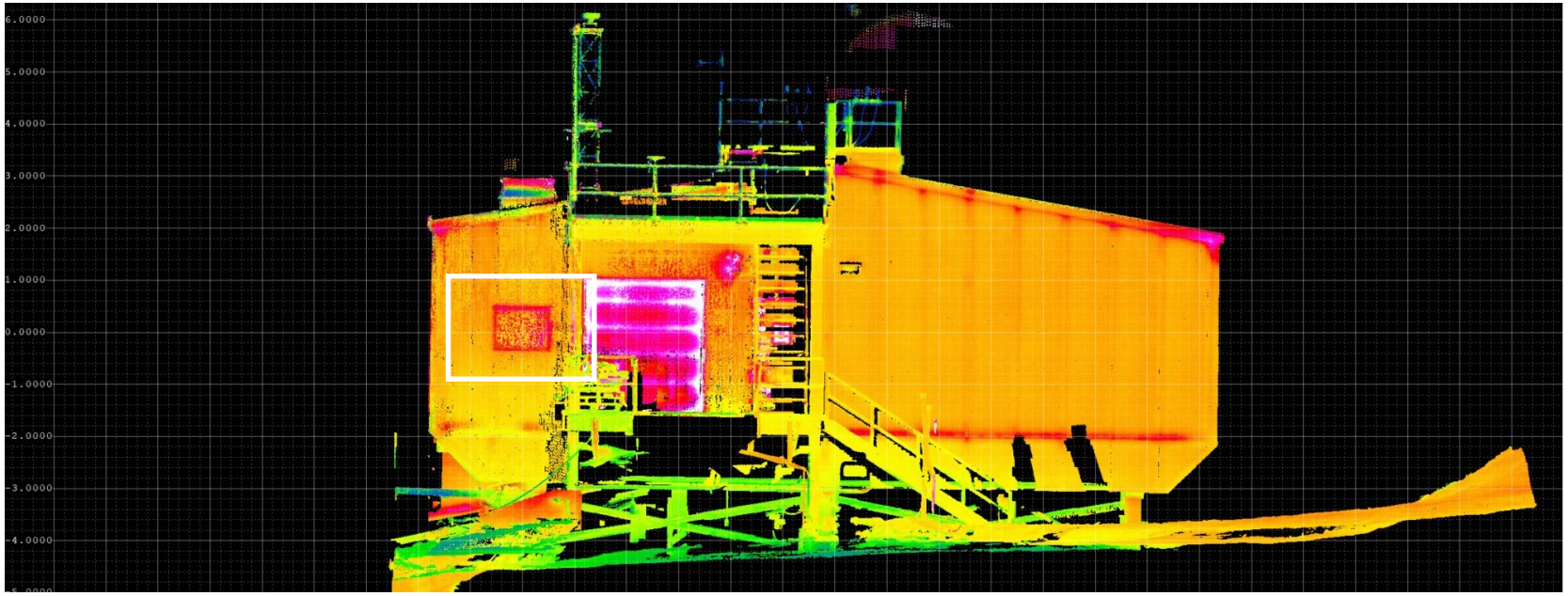
-15◦C



5◦C





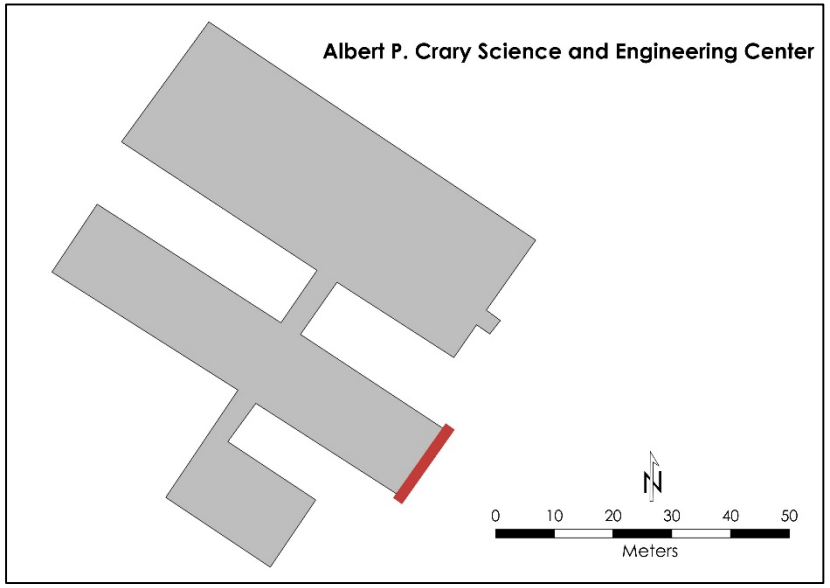


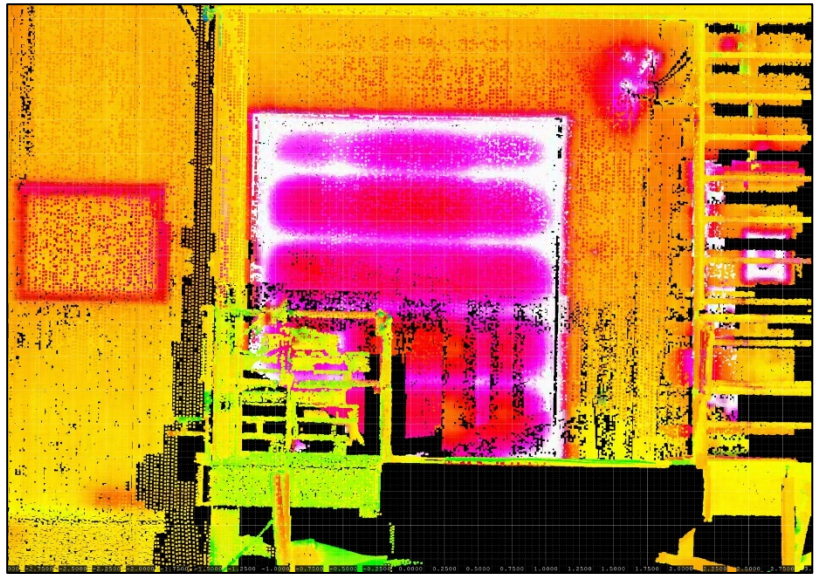
P2E-W-01

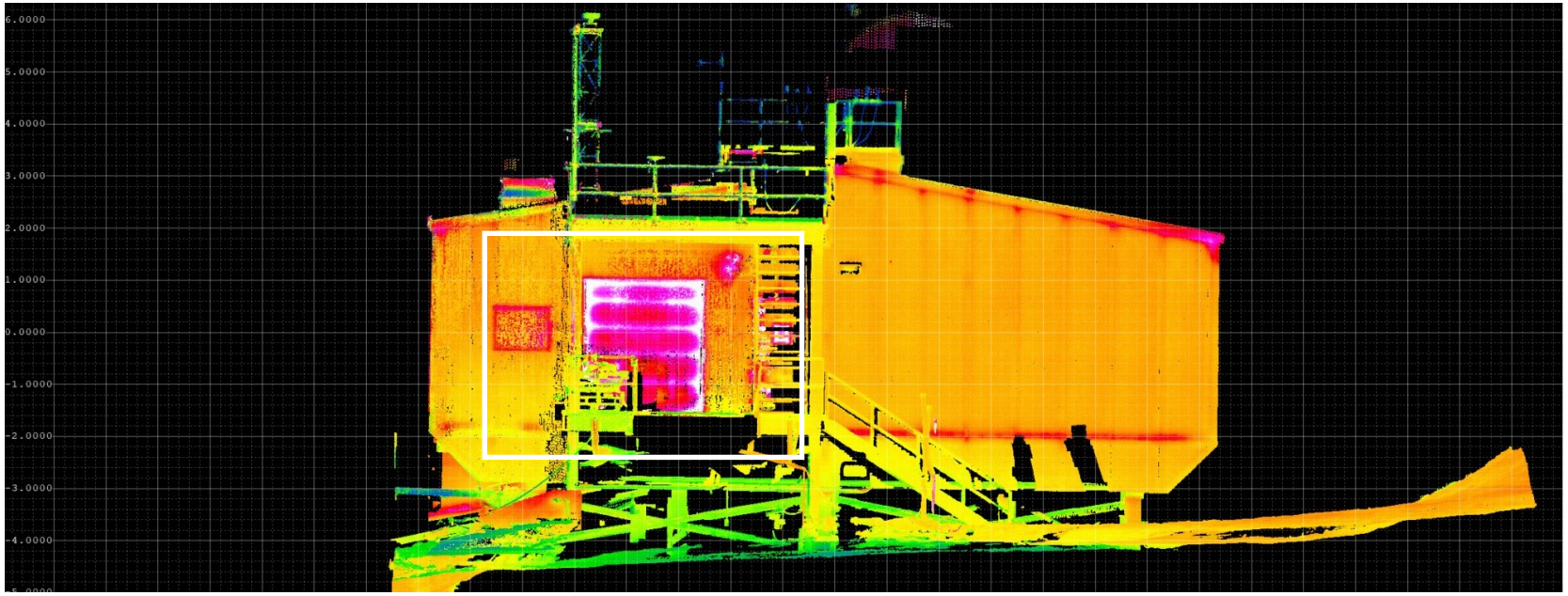
-15◦C



5◦C





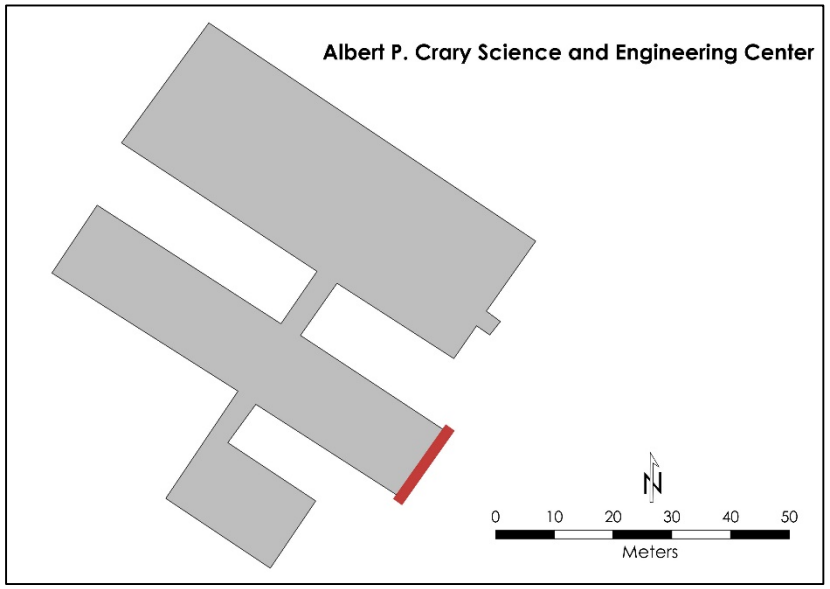


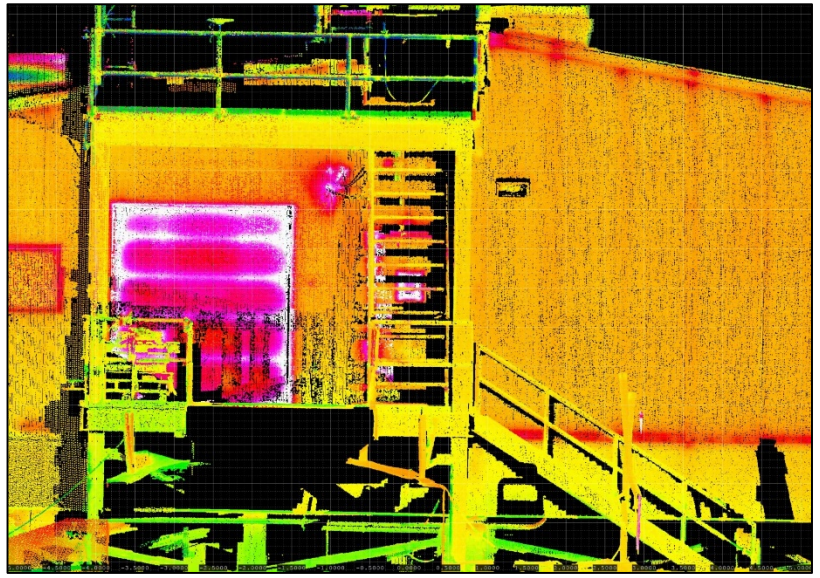
P2E-LD-01

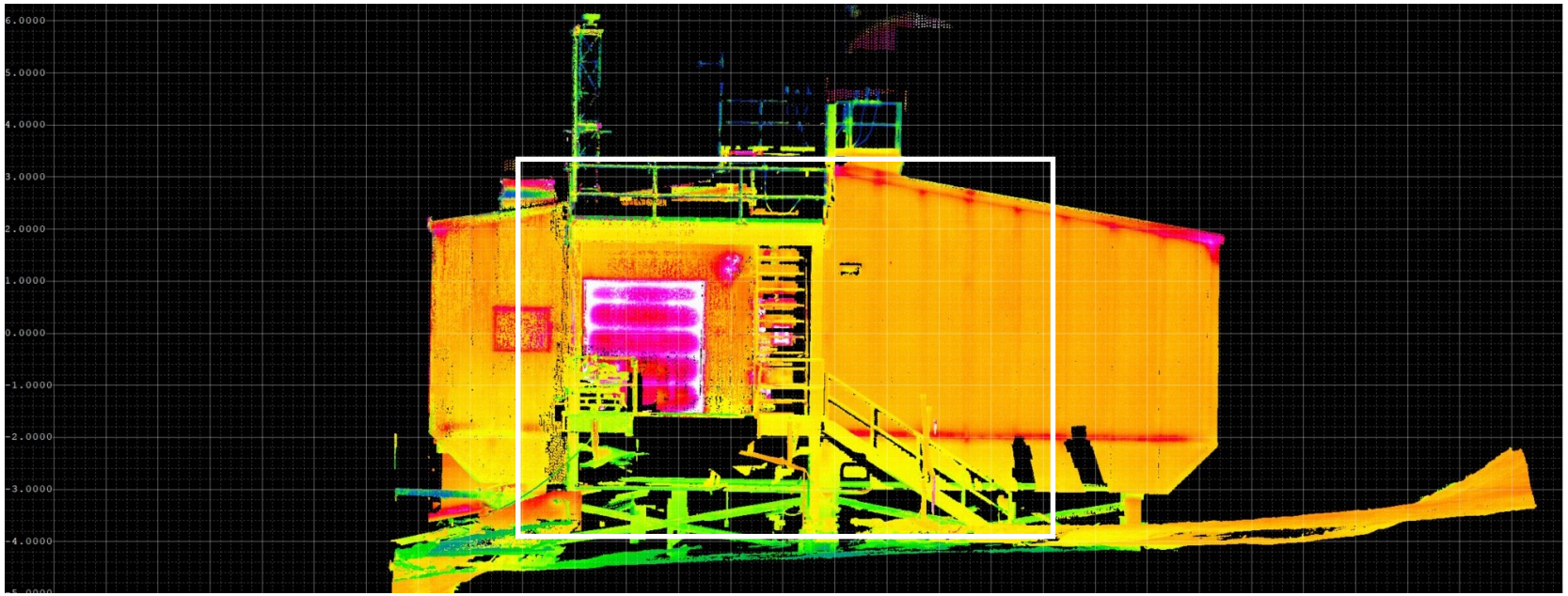
-15◦C



5◦C





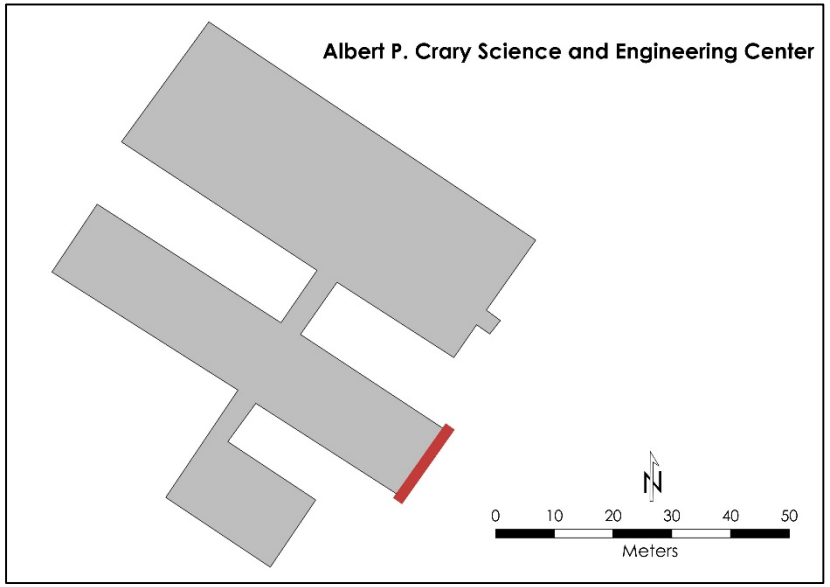


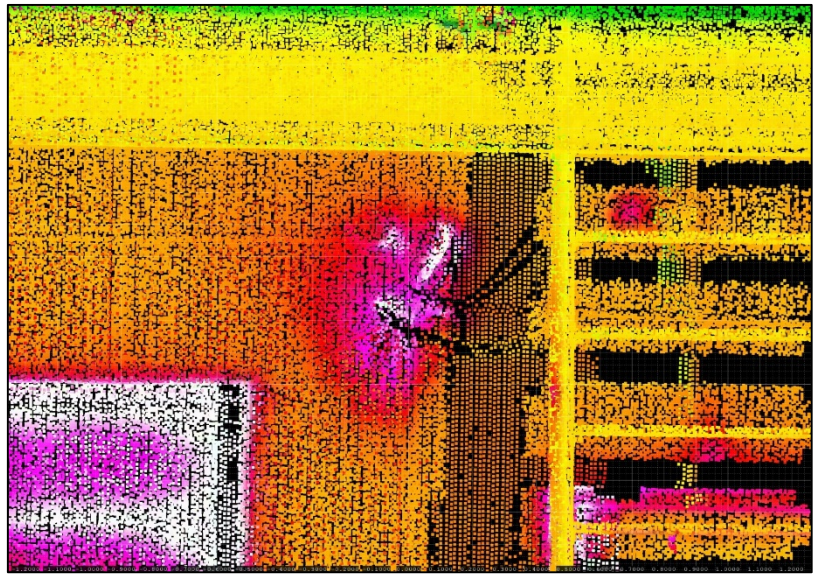
P2E-D-01

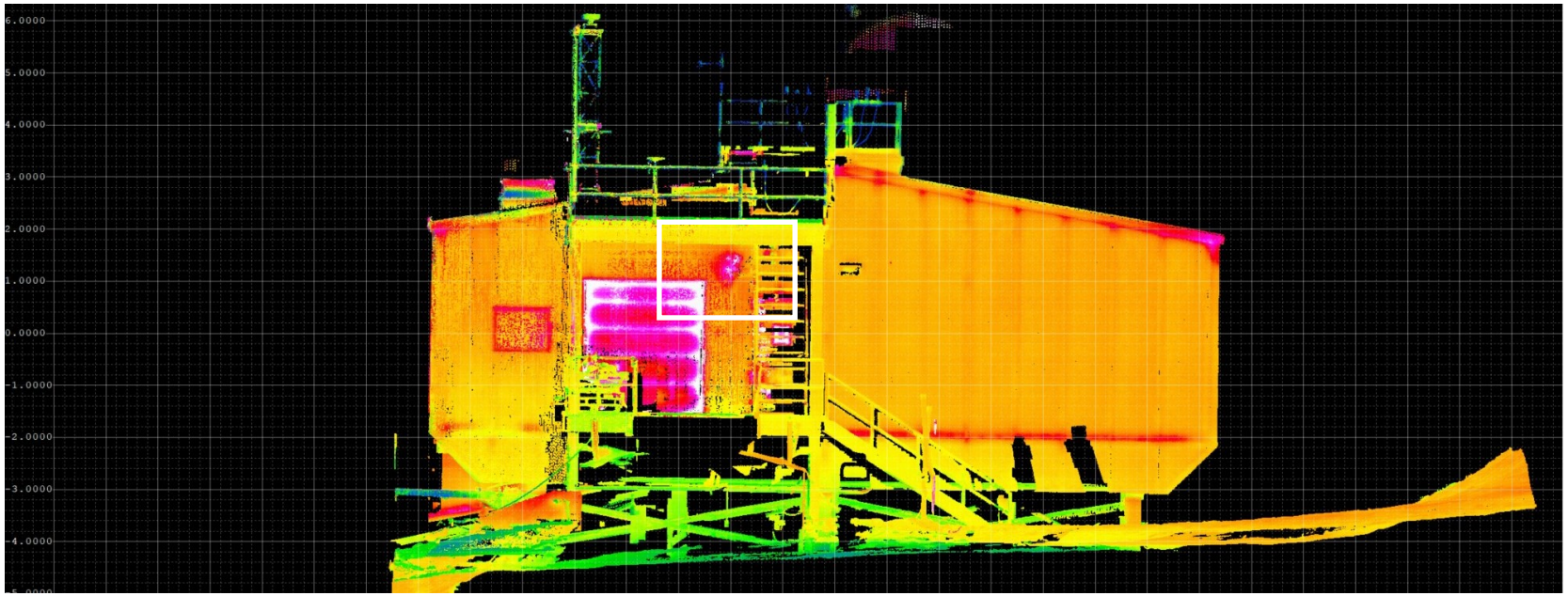
-15◦C



5◦C





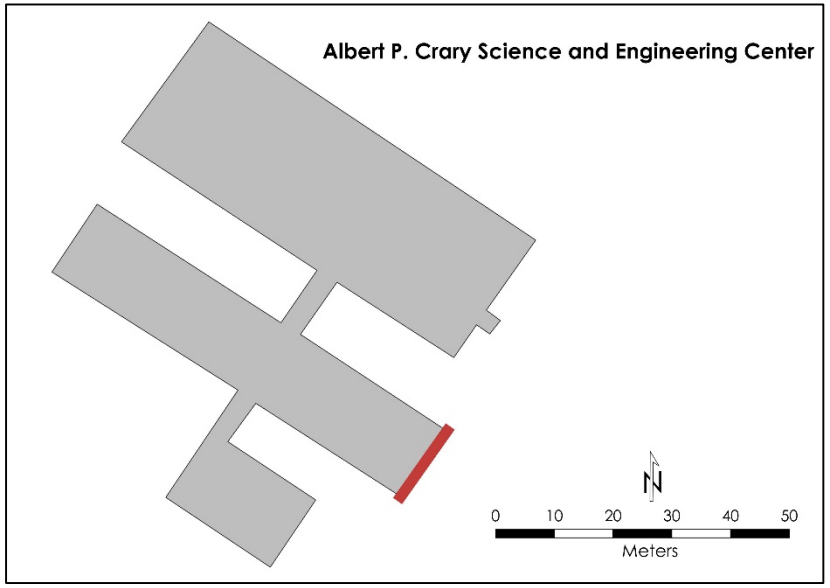


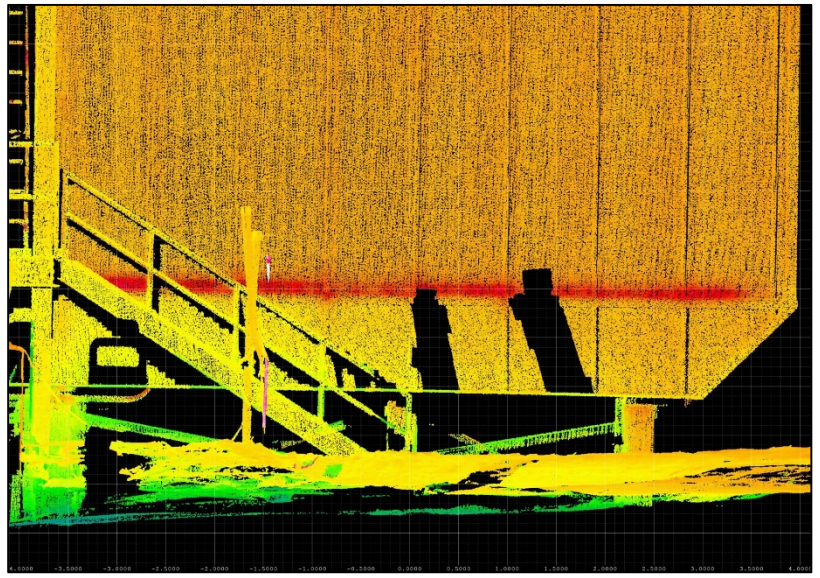
P2E-TA-03

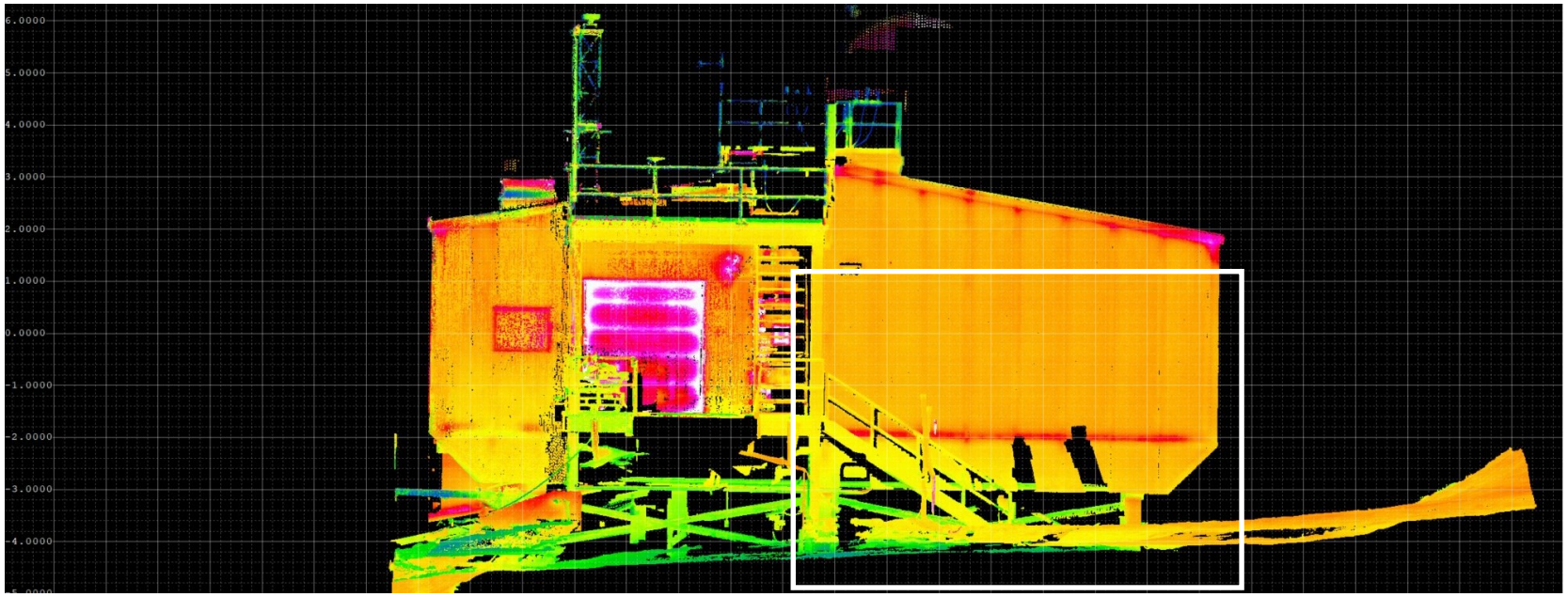
-15◦C



5◦C





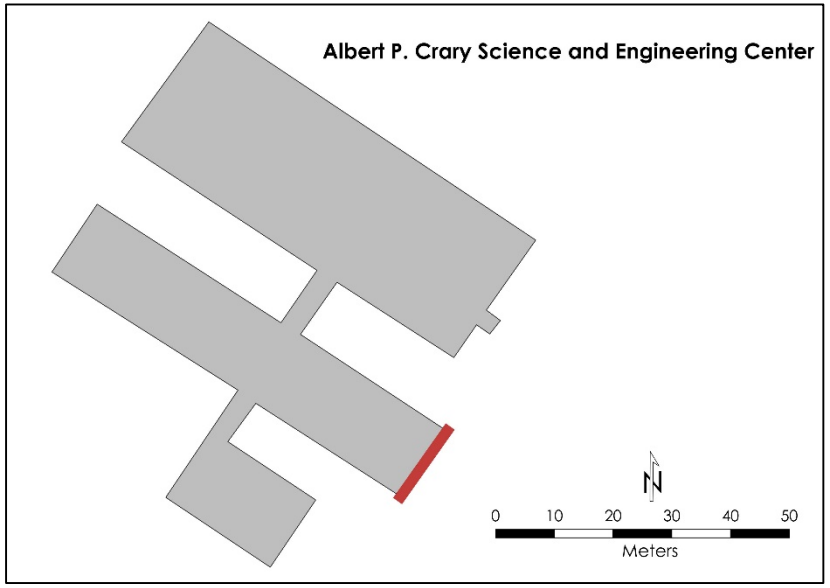


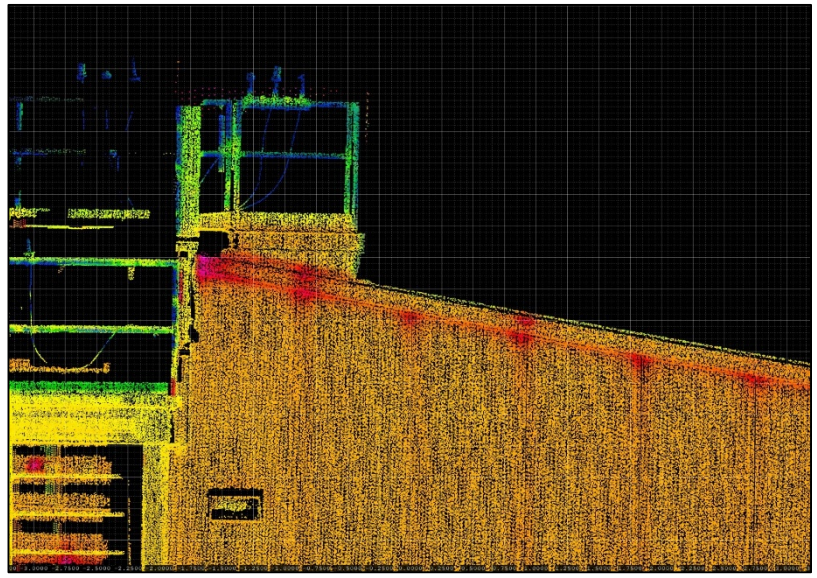
P2E-TA-04

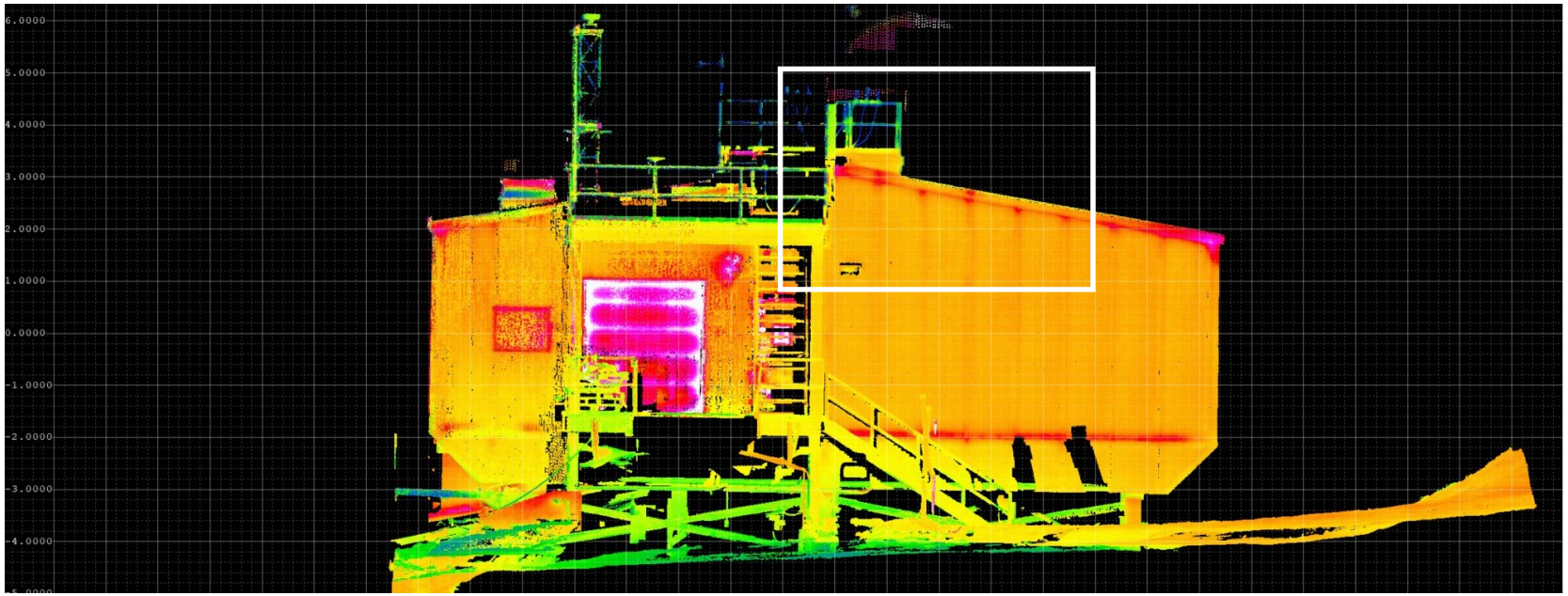
-15◦C



5◦C





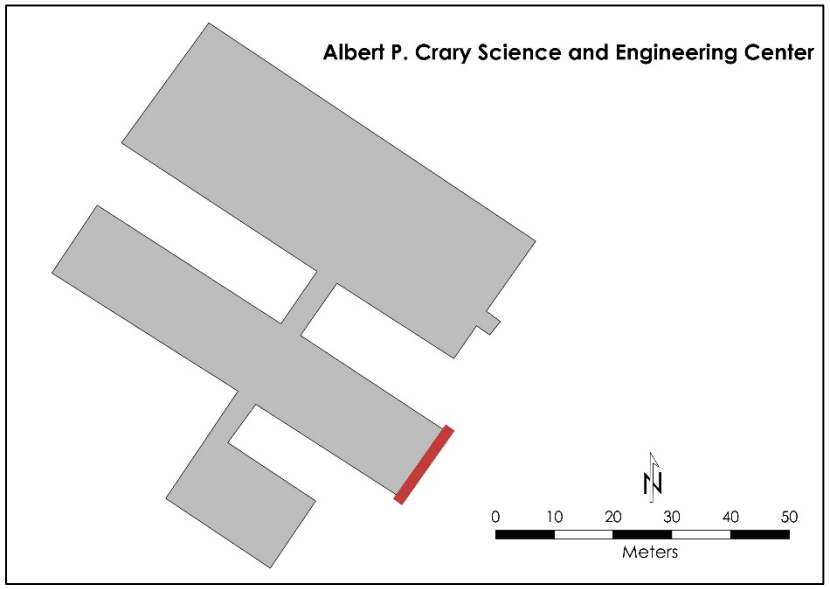


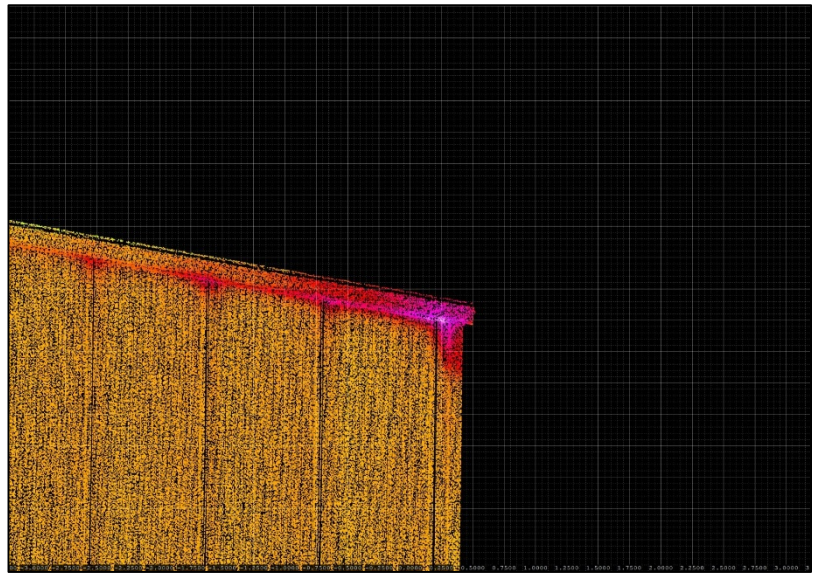
P2E-TA-05

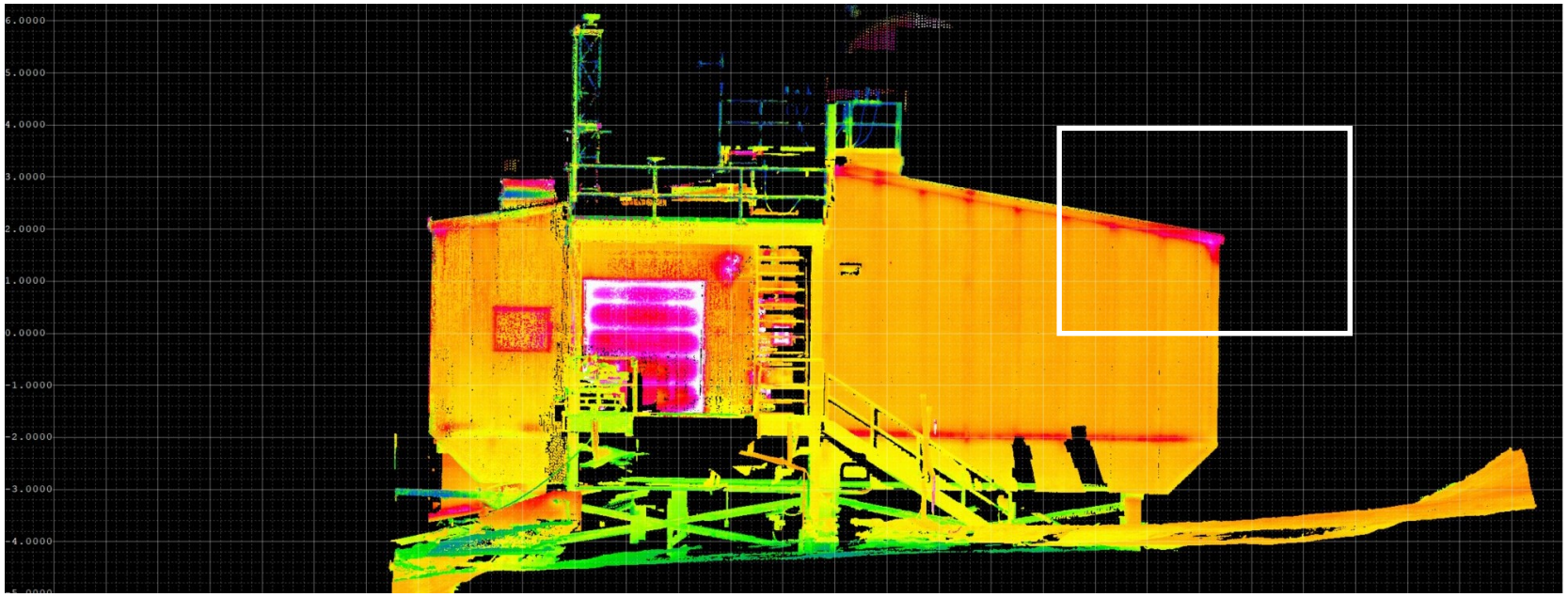
-15◦C



5◦C



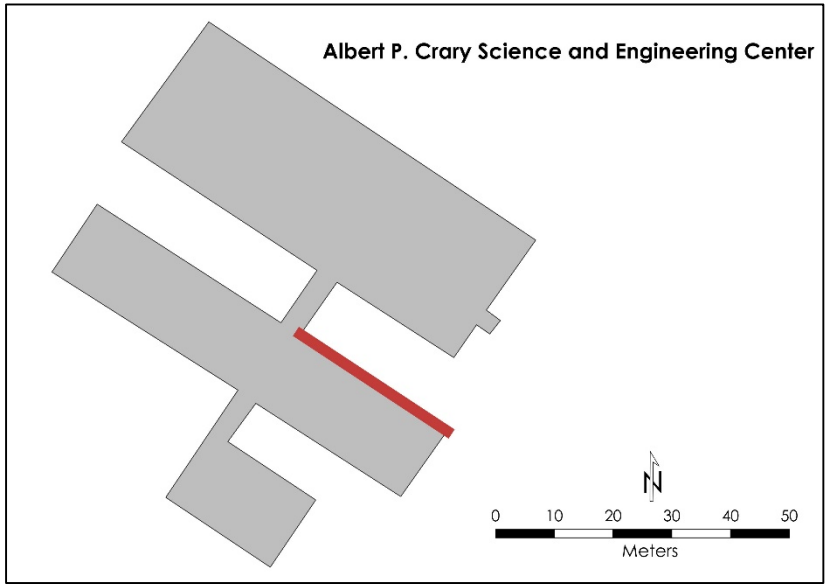


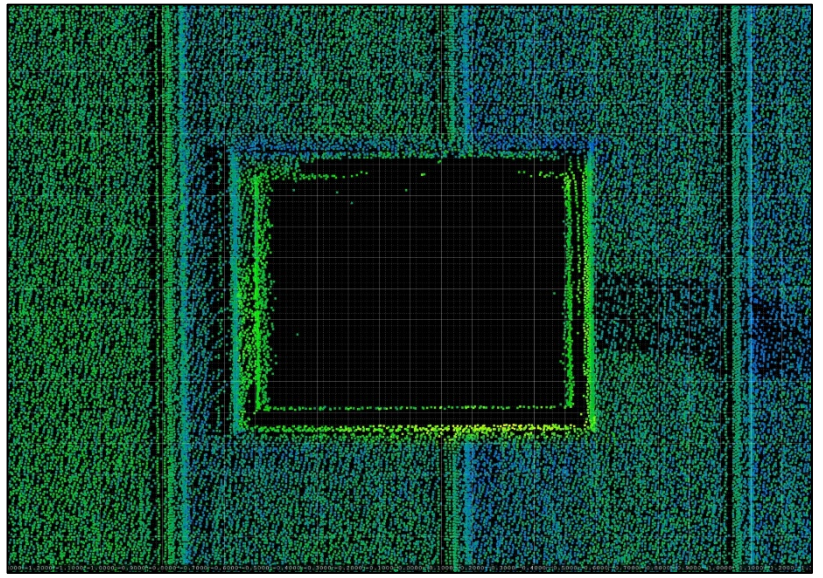


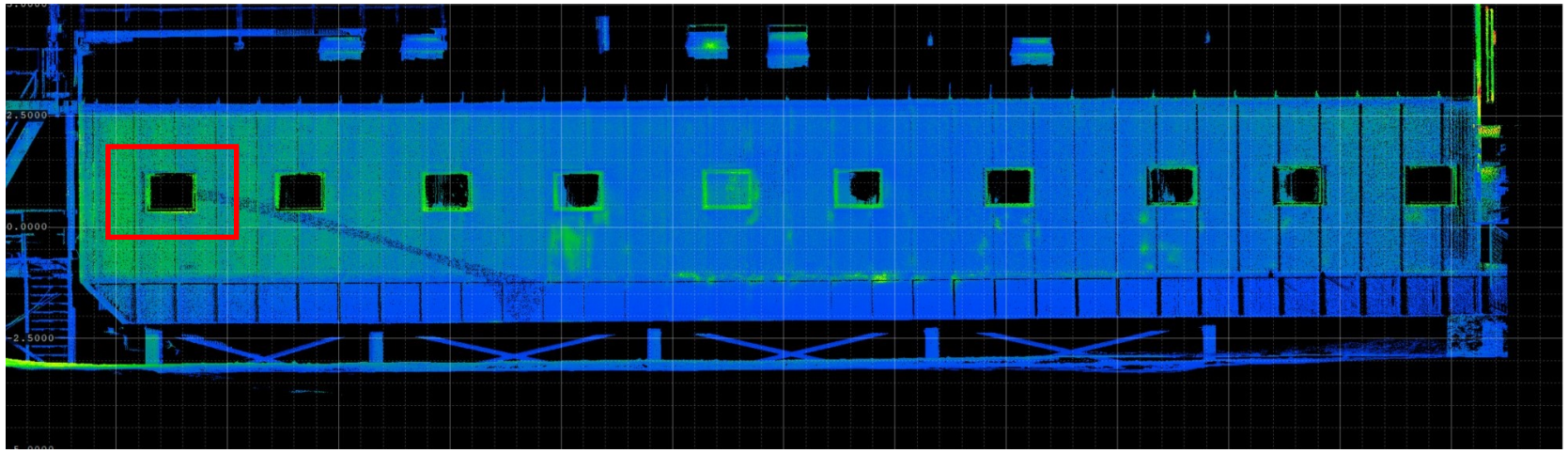
P2E-TA-06

-15◦C

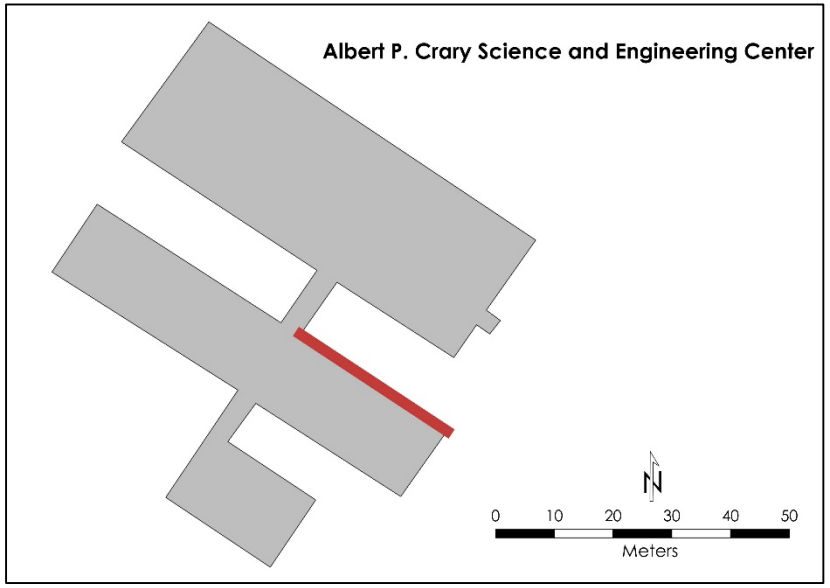
5◦C

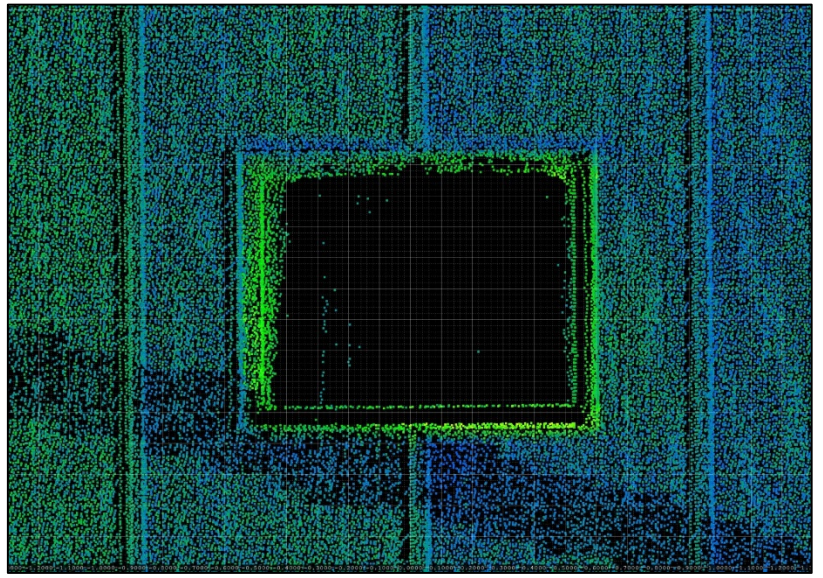


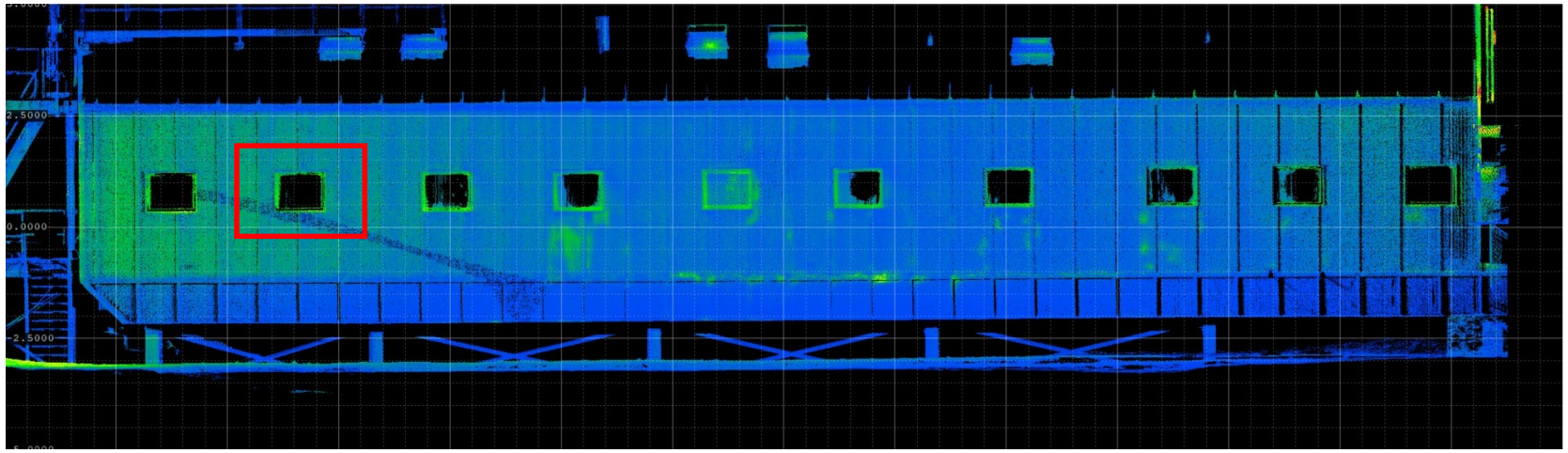




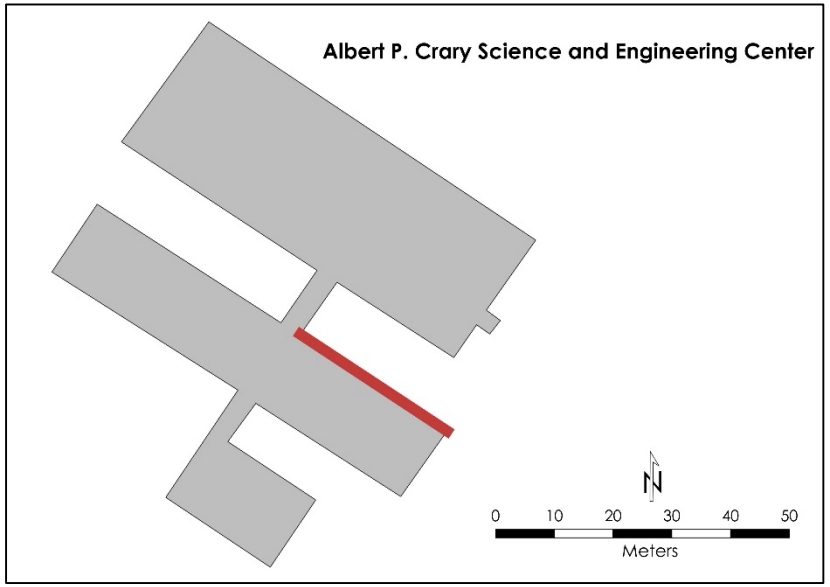
P2NE-W-01 -15◦C 5◦C

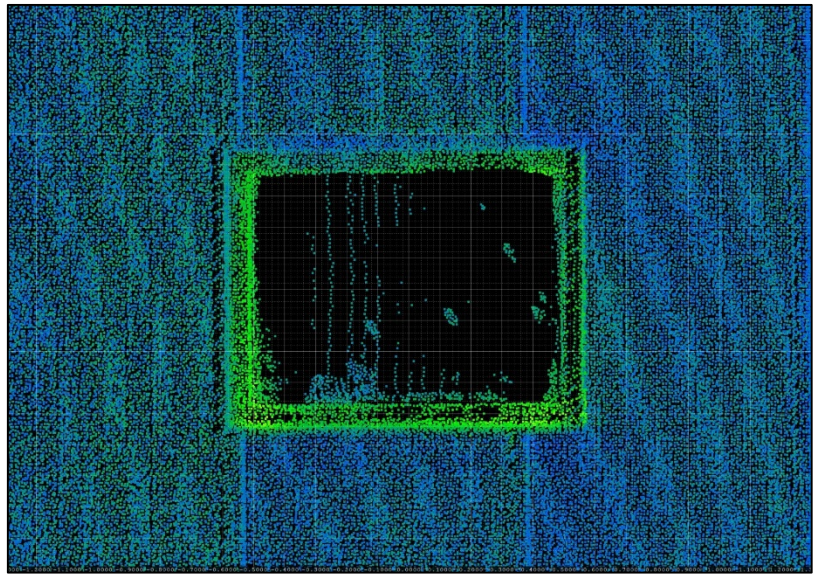


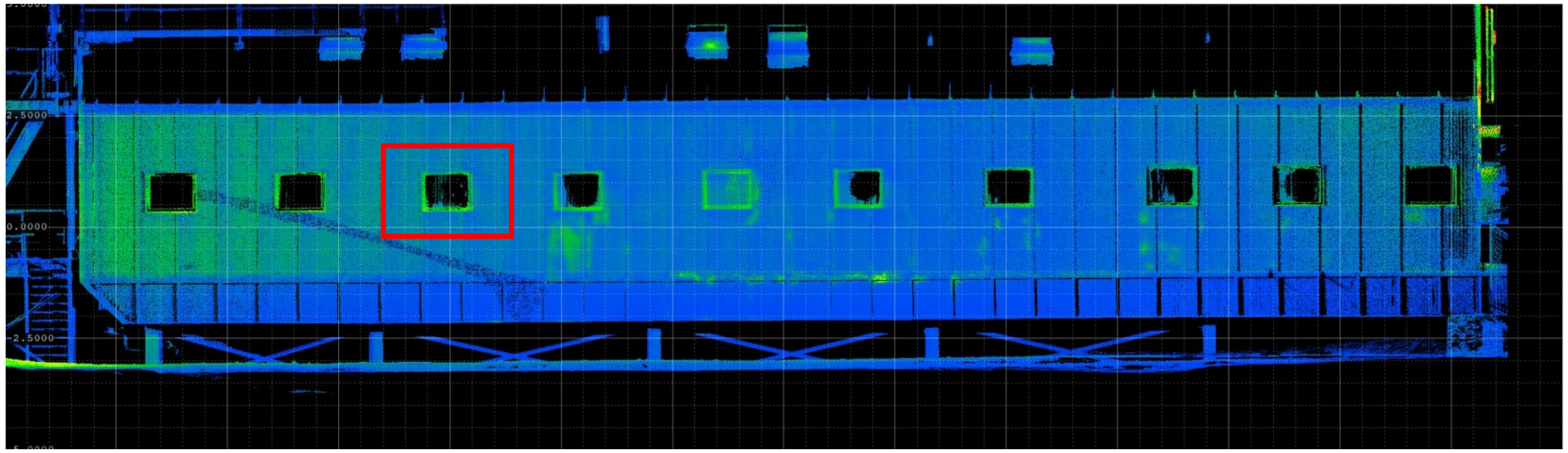




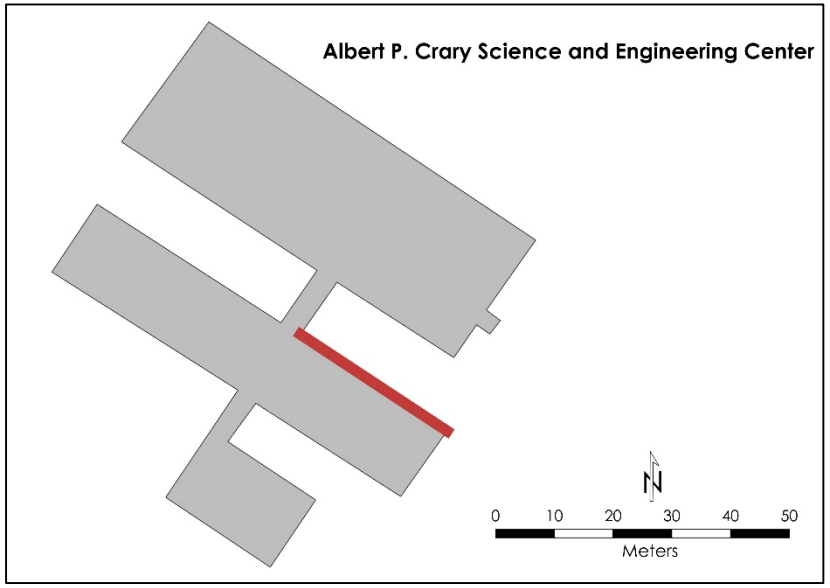
P2NE-W-02 -15◦C 5◦C

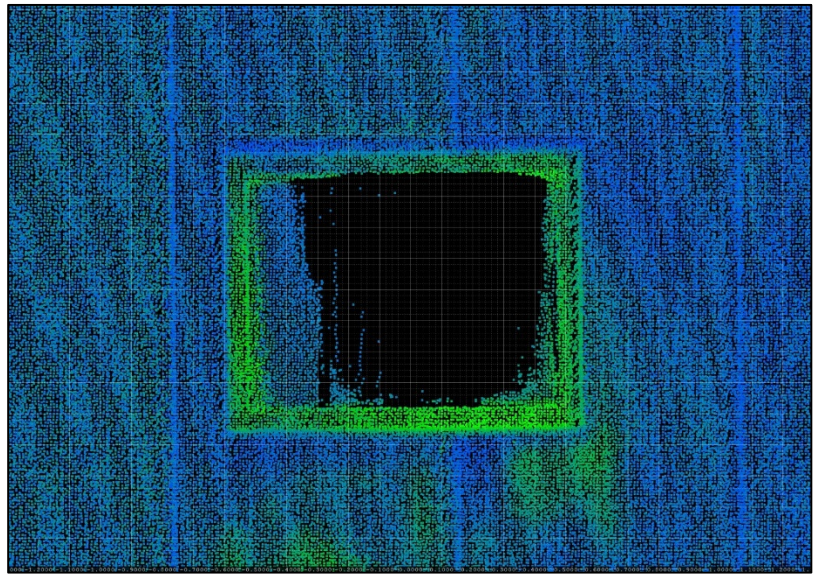


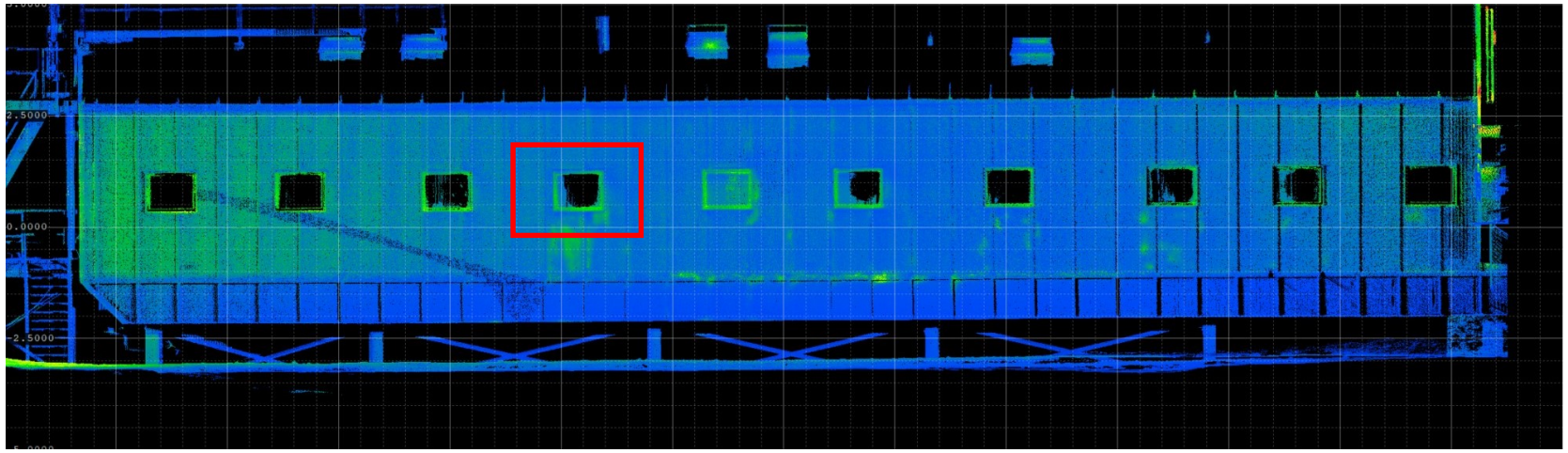




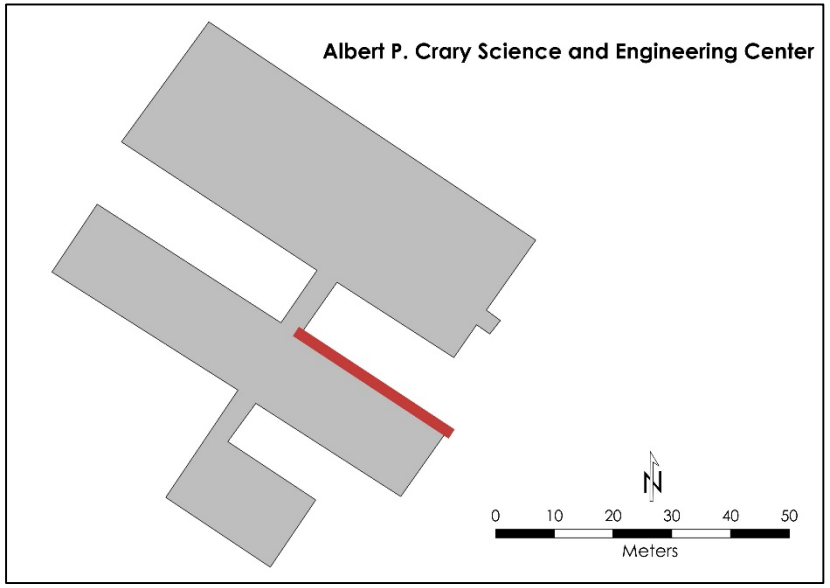
P2NE-W-03 -15◦C 5◦C

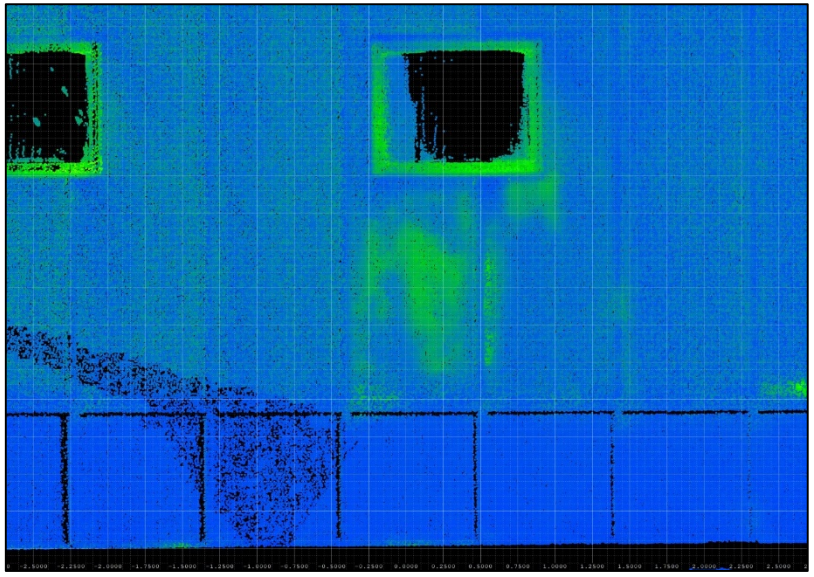


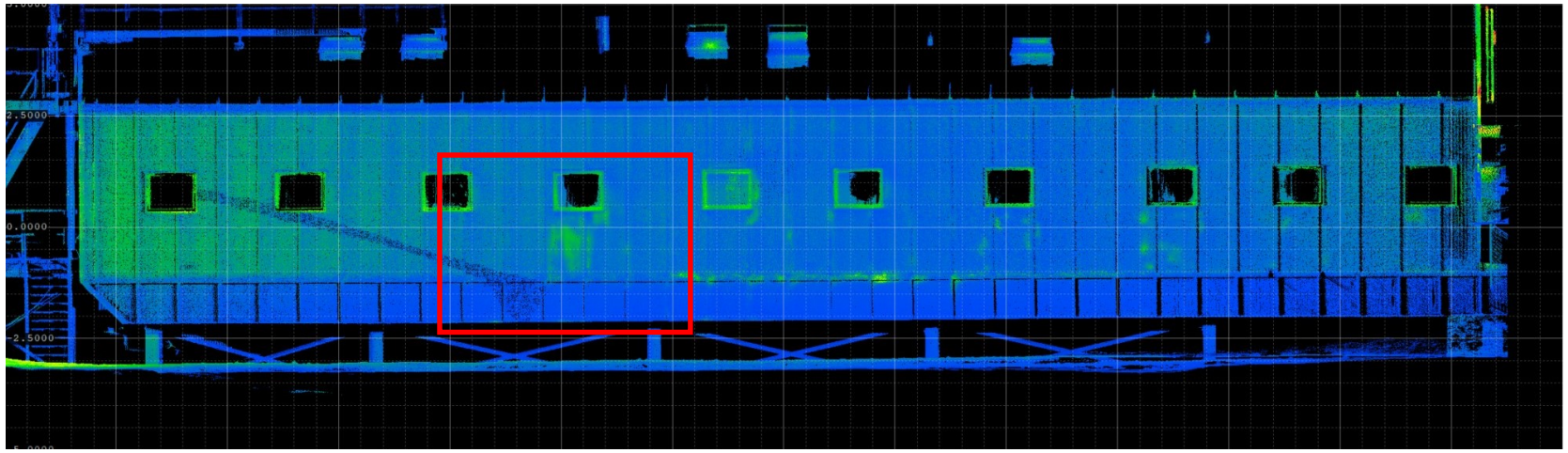




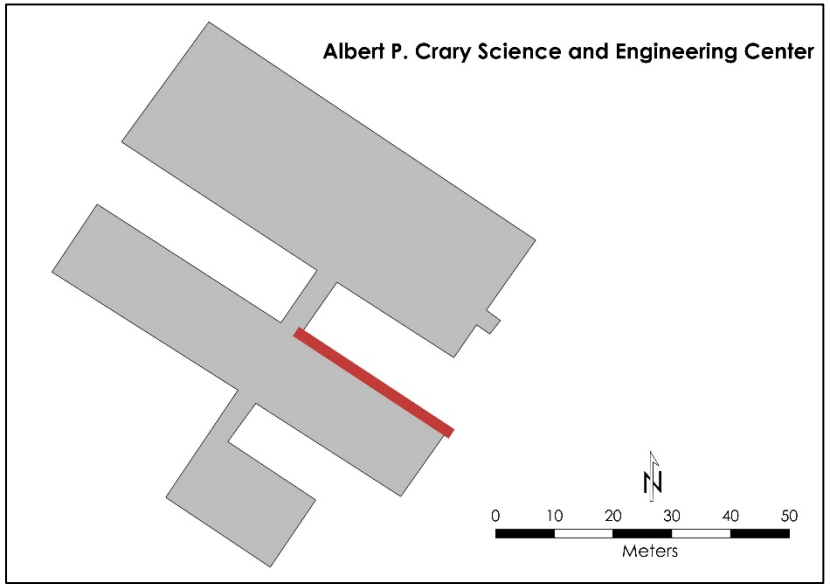
P2NE-W-04 -15◦C 5◦C

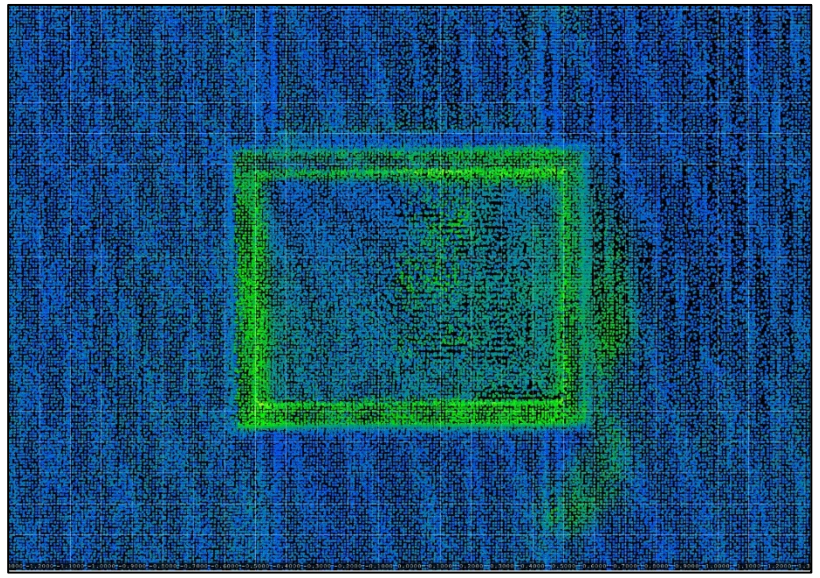


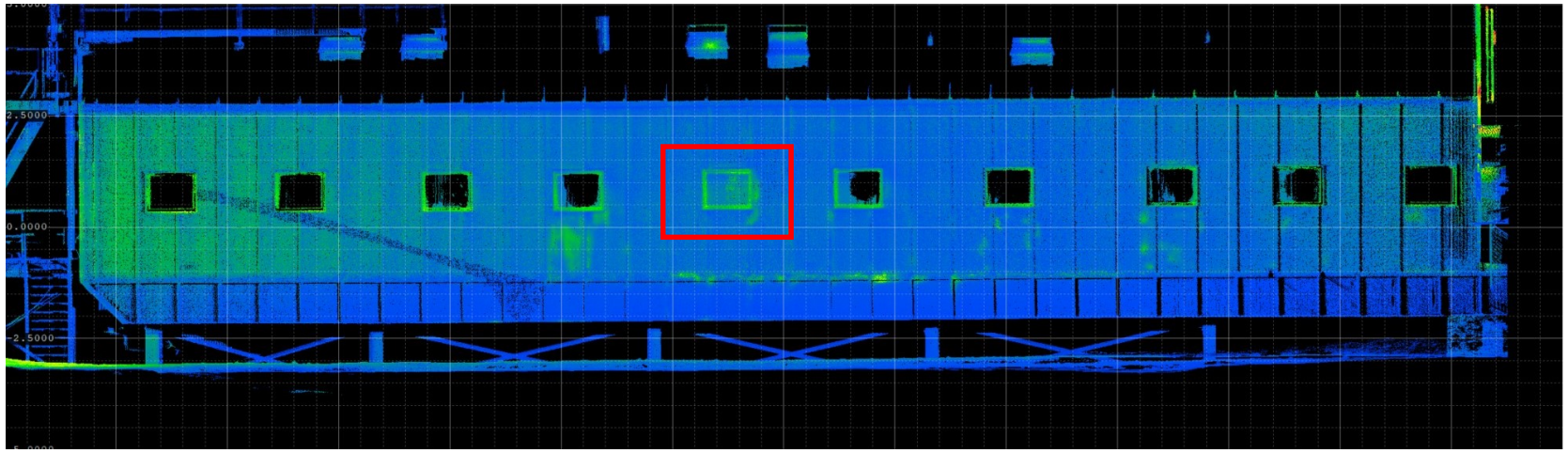




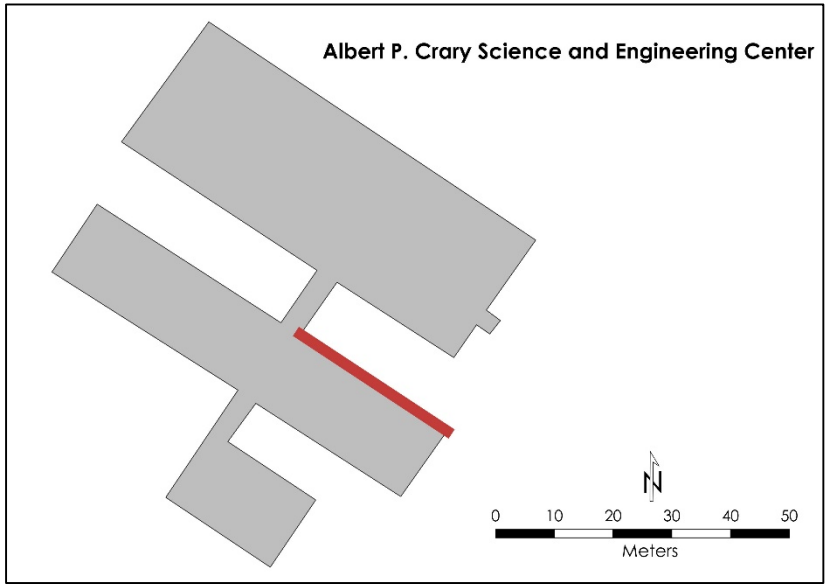
P2NE-TA-01 -15◦C 5◦C

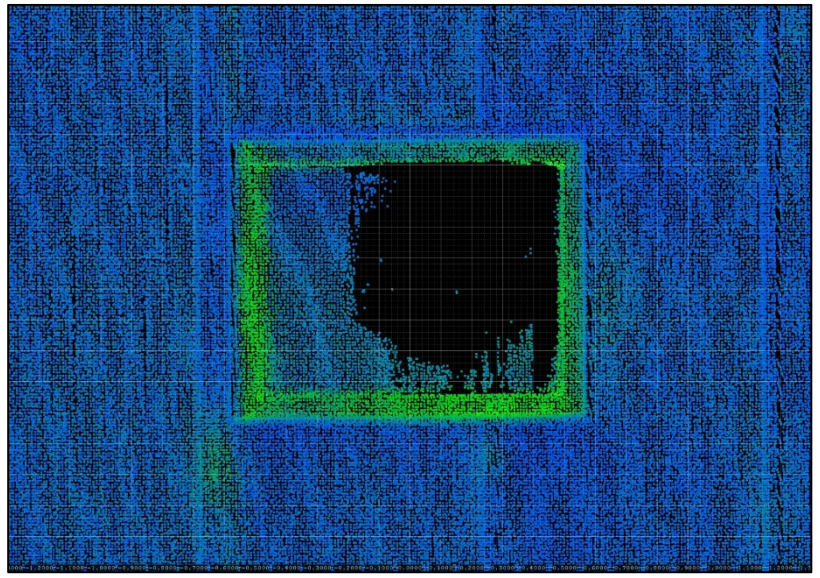


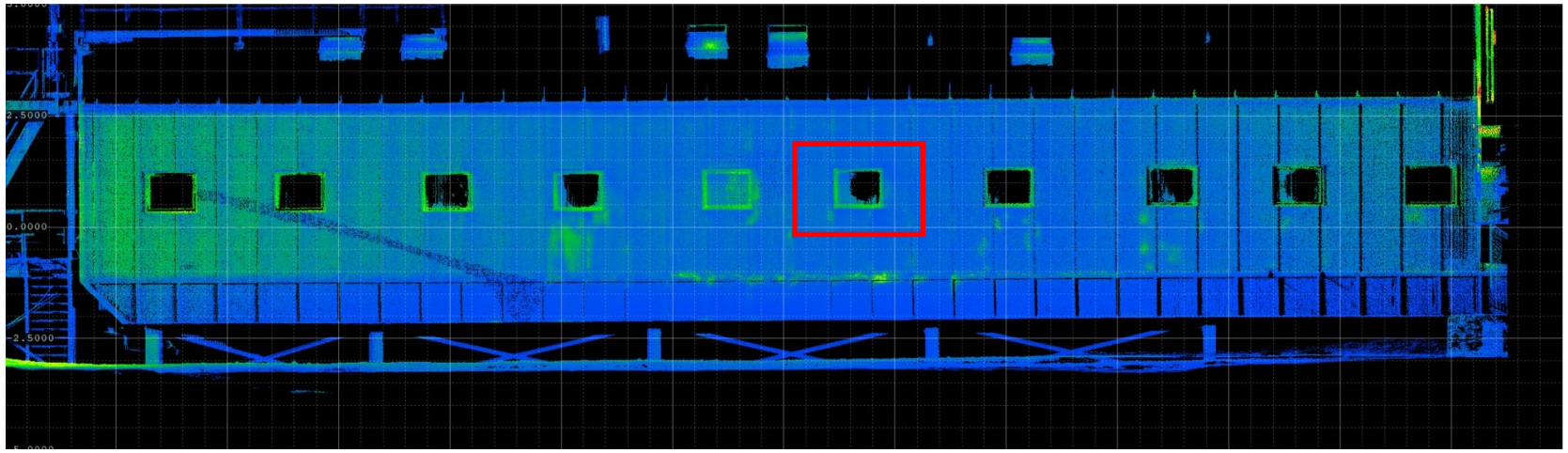




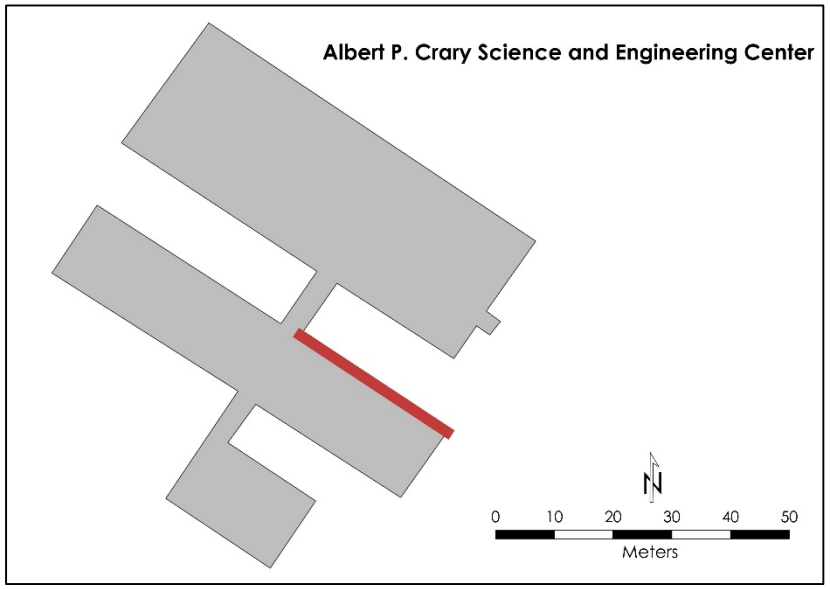
P2NE-W-05 -15◦C 5◦C

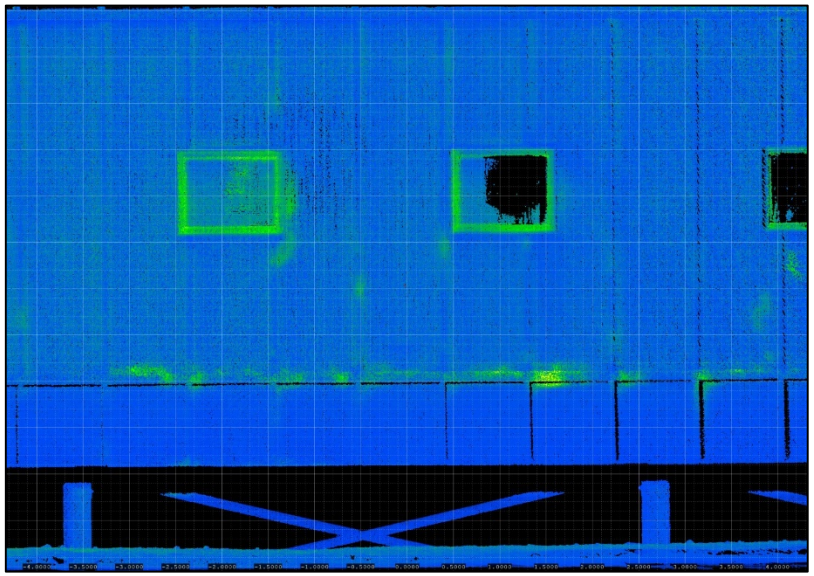


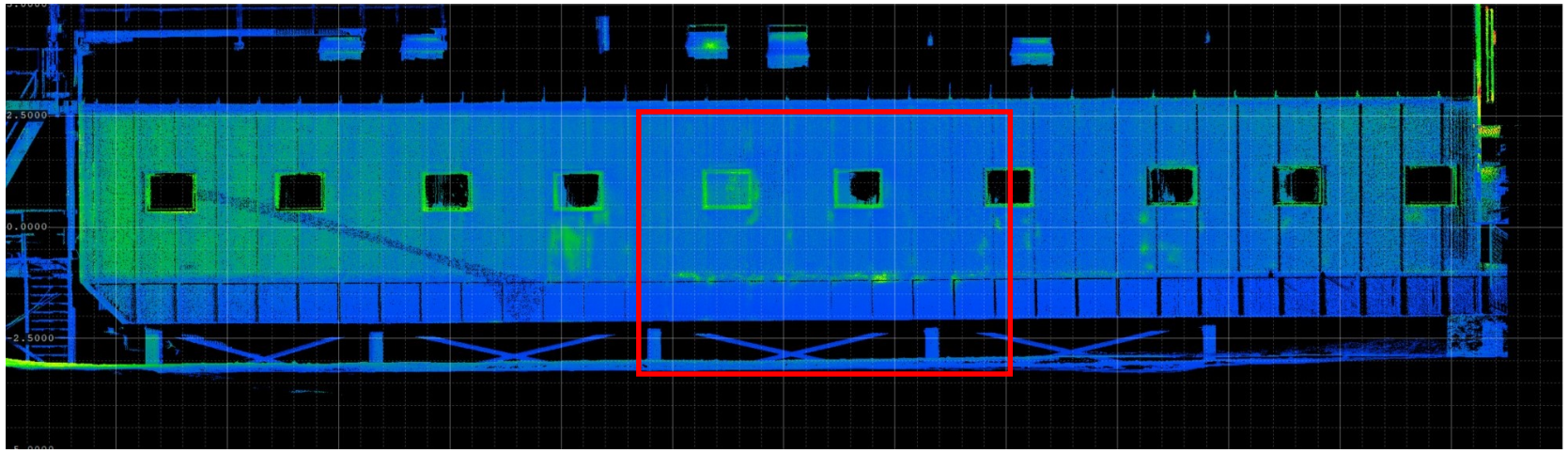




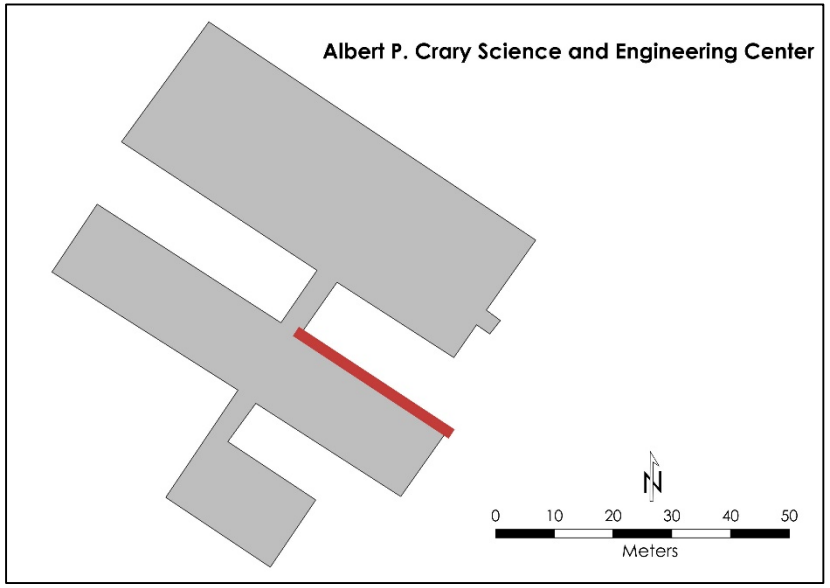
P2NE-W-06 -15◦C 5◦C

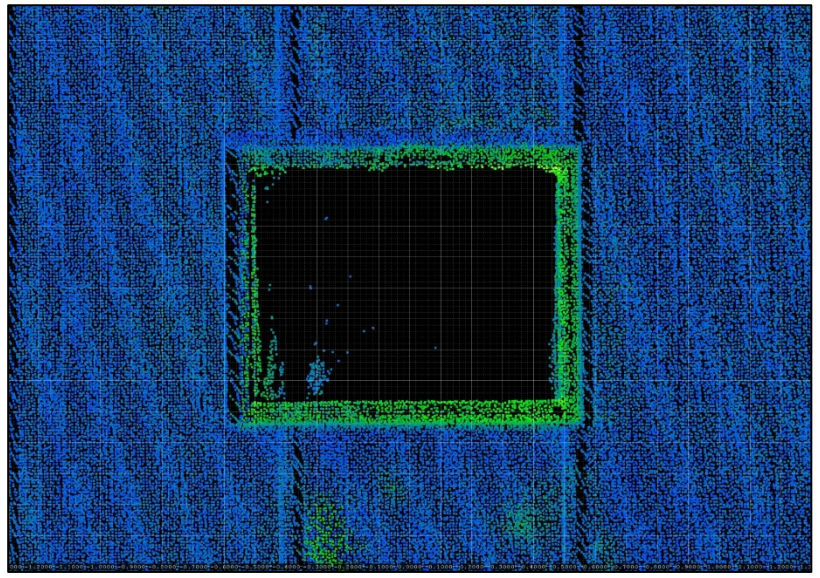


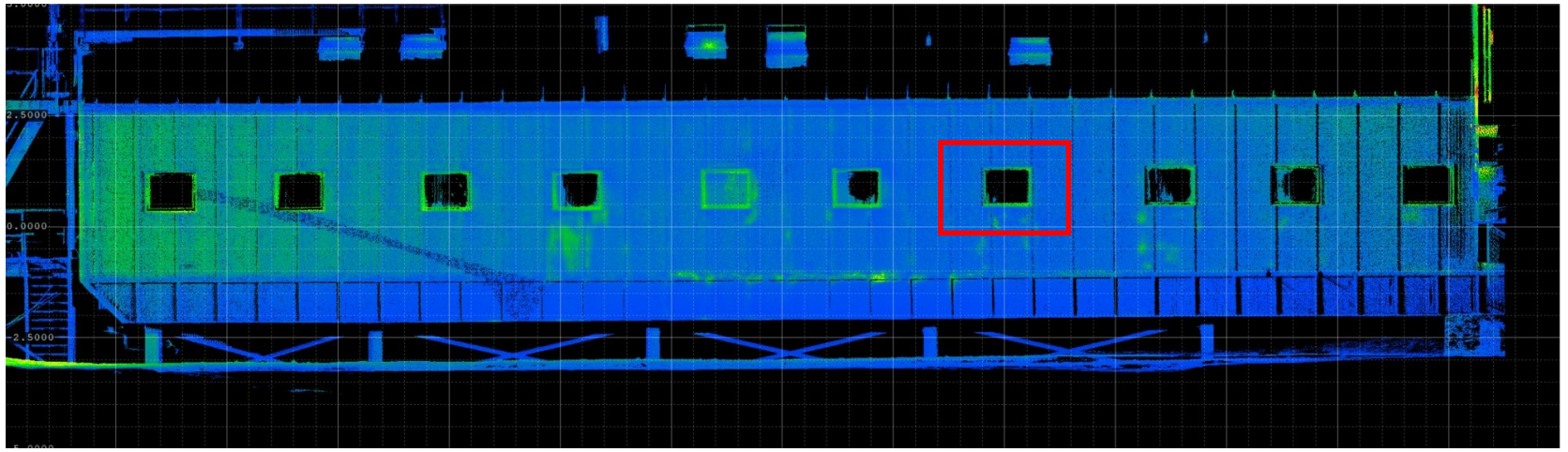




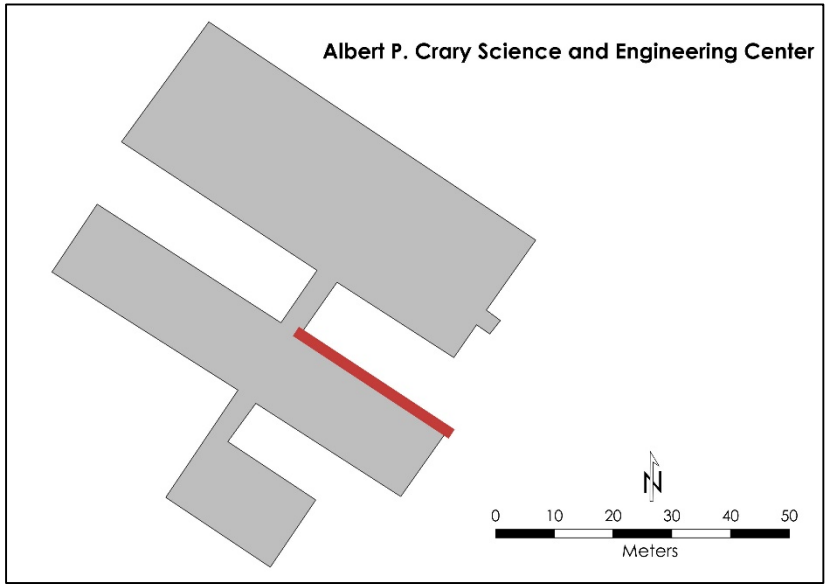
P2NE-TA-02 -15◦C 5◦C

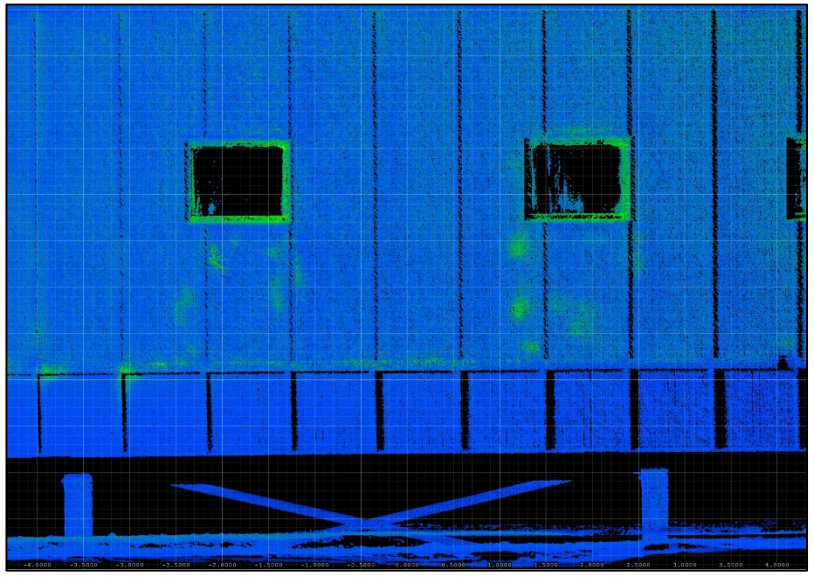


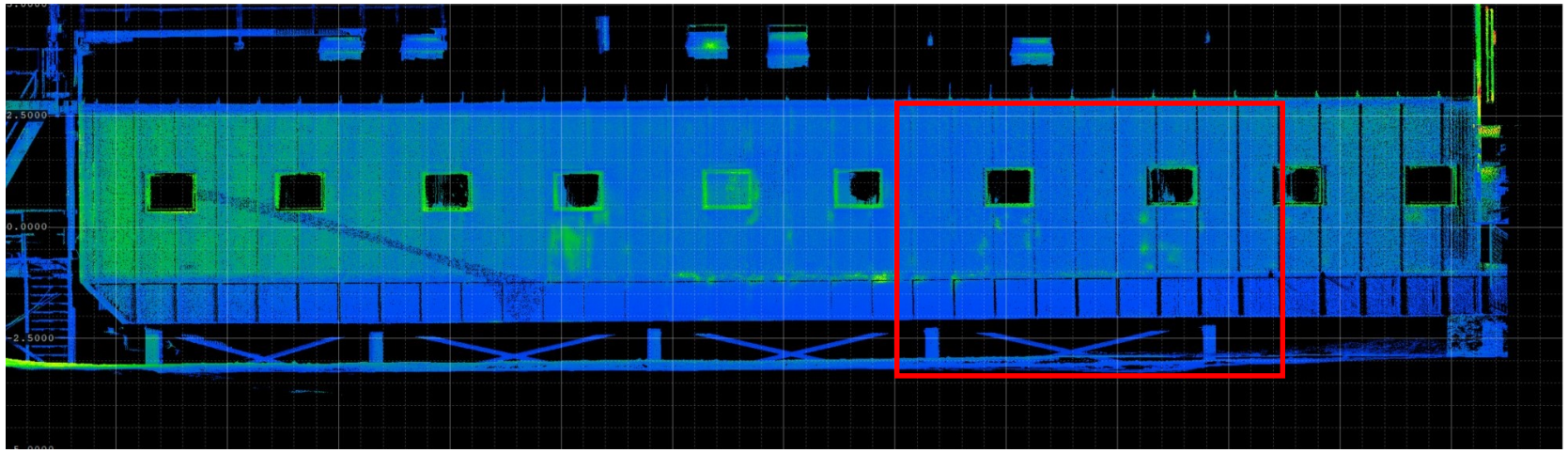




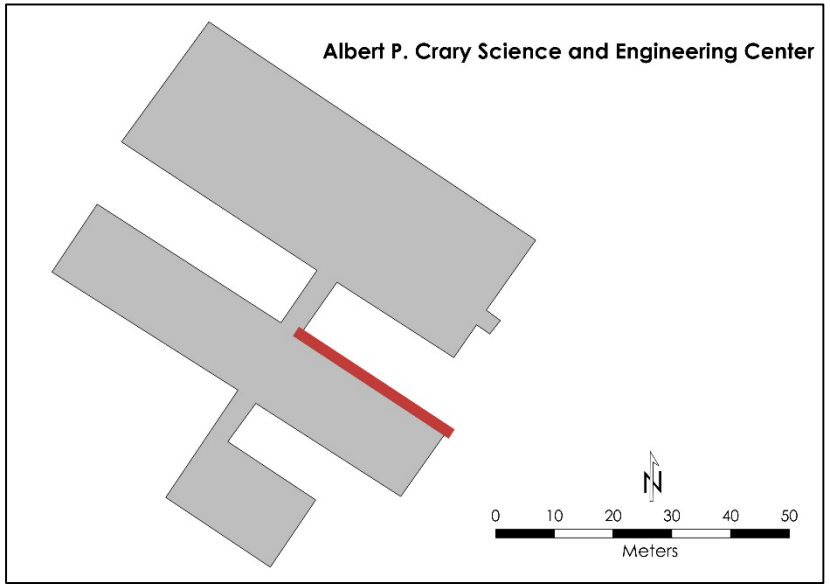
P2NE-W-07 -15◦C 5◦C

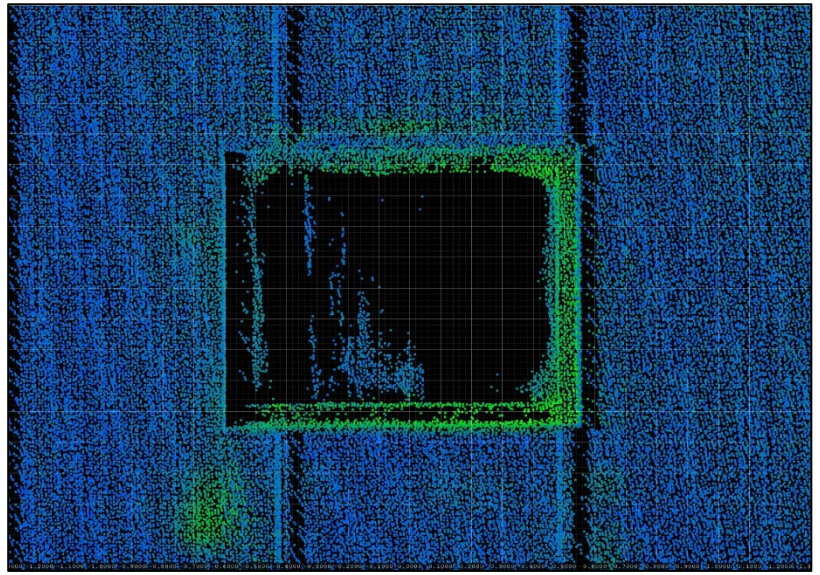


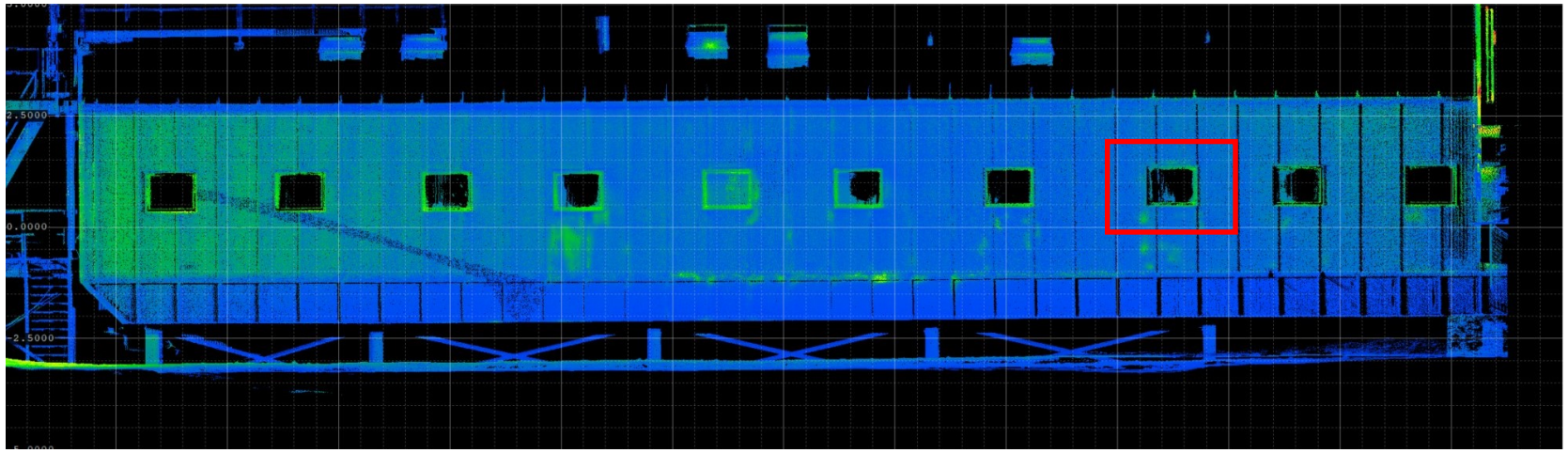




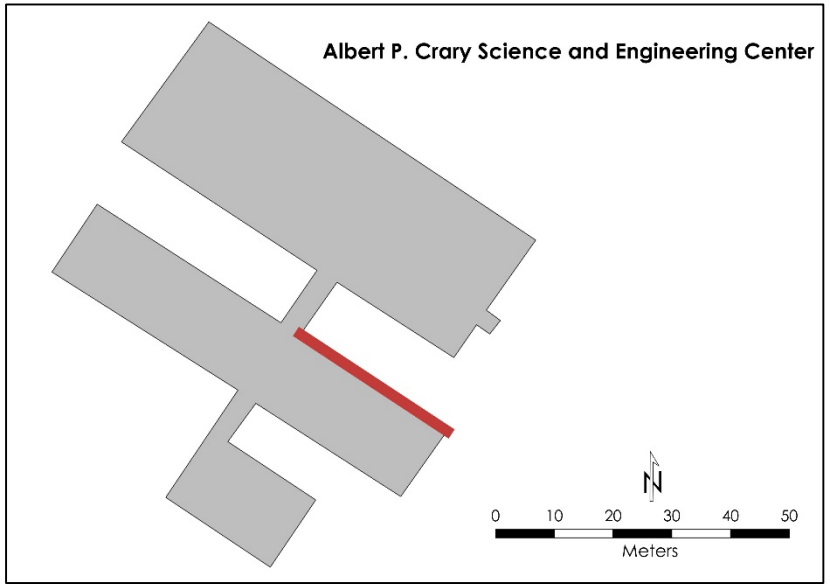
P2NE-TA-03 -15◦C 5◦C

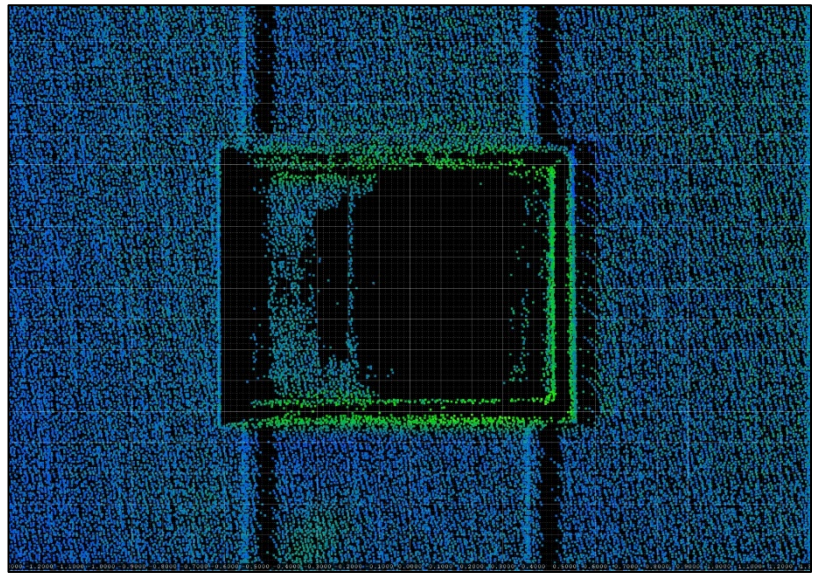


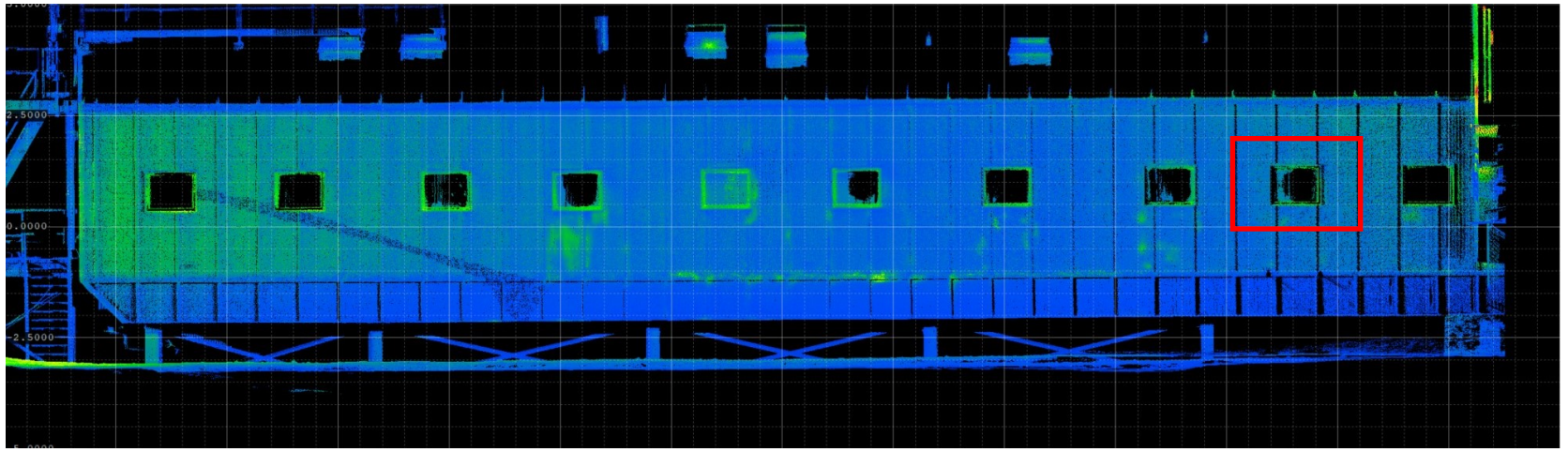




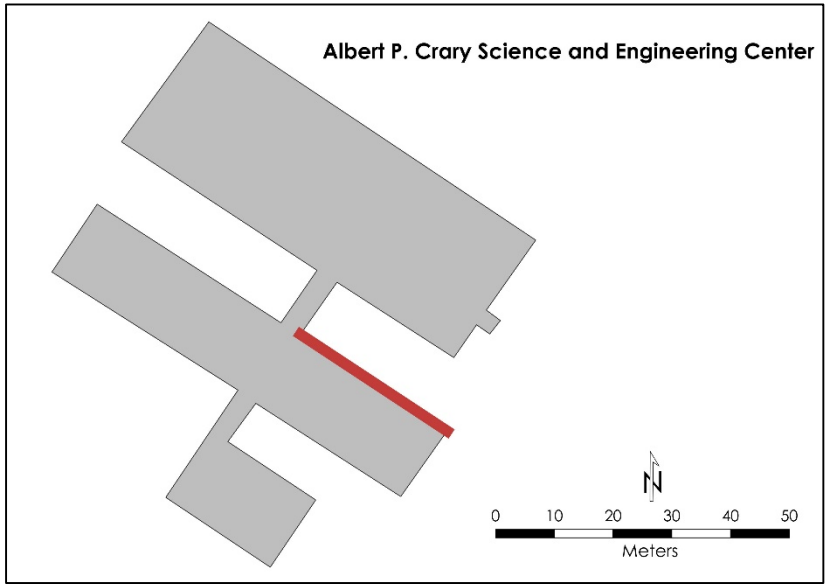
P2NE-W-08 -15◦C 5◦C

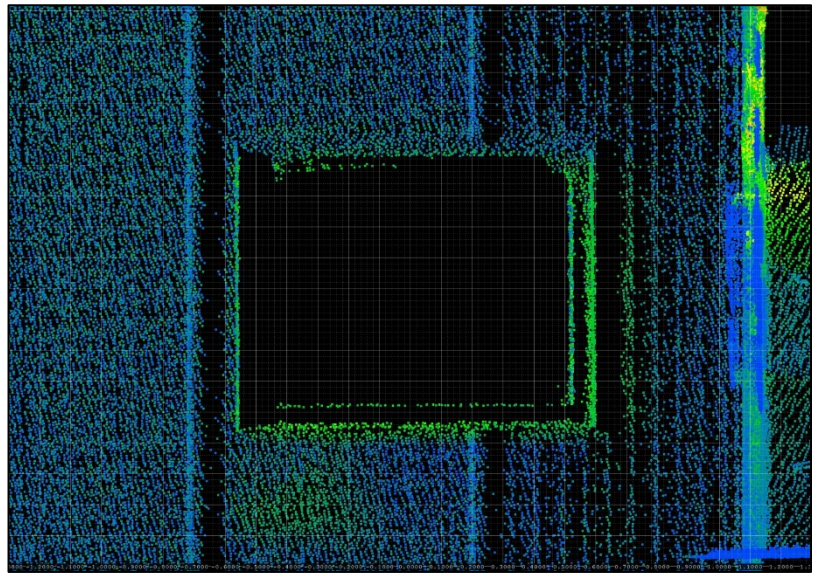


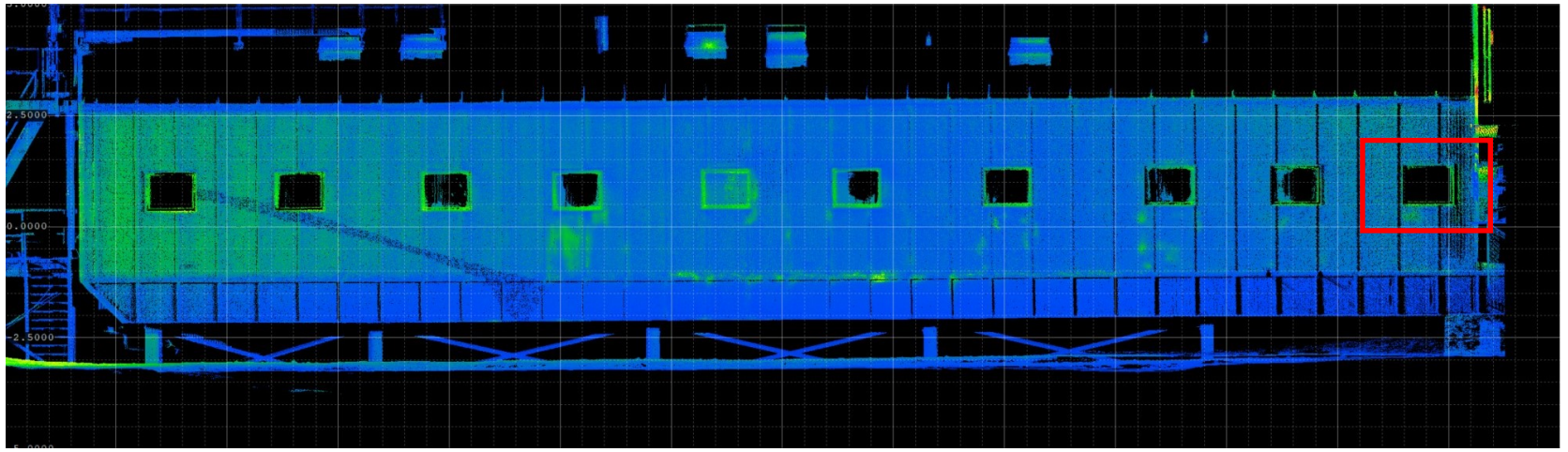




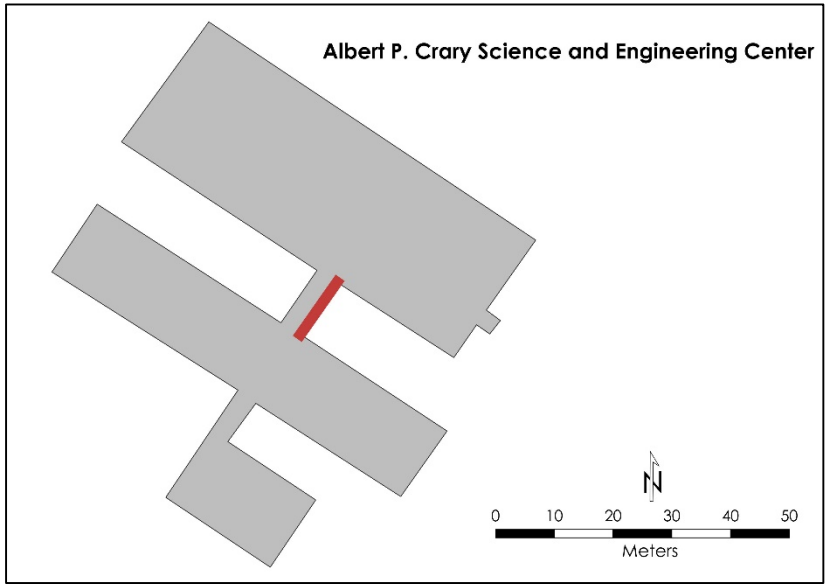
P2NE-W-09 -15◦C 5◦C

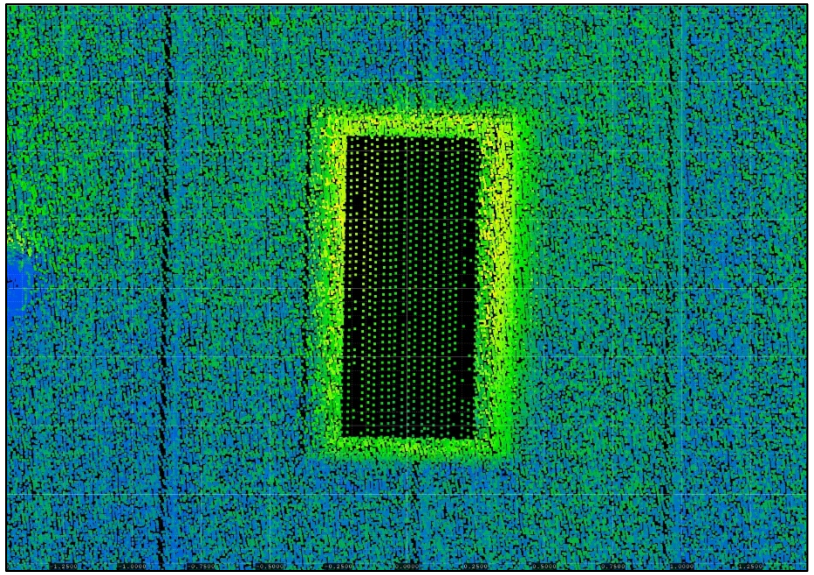


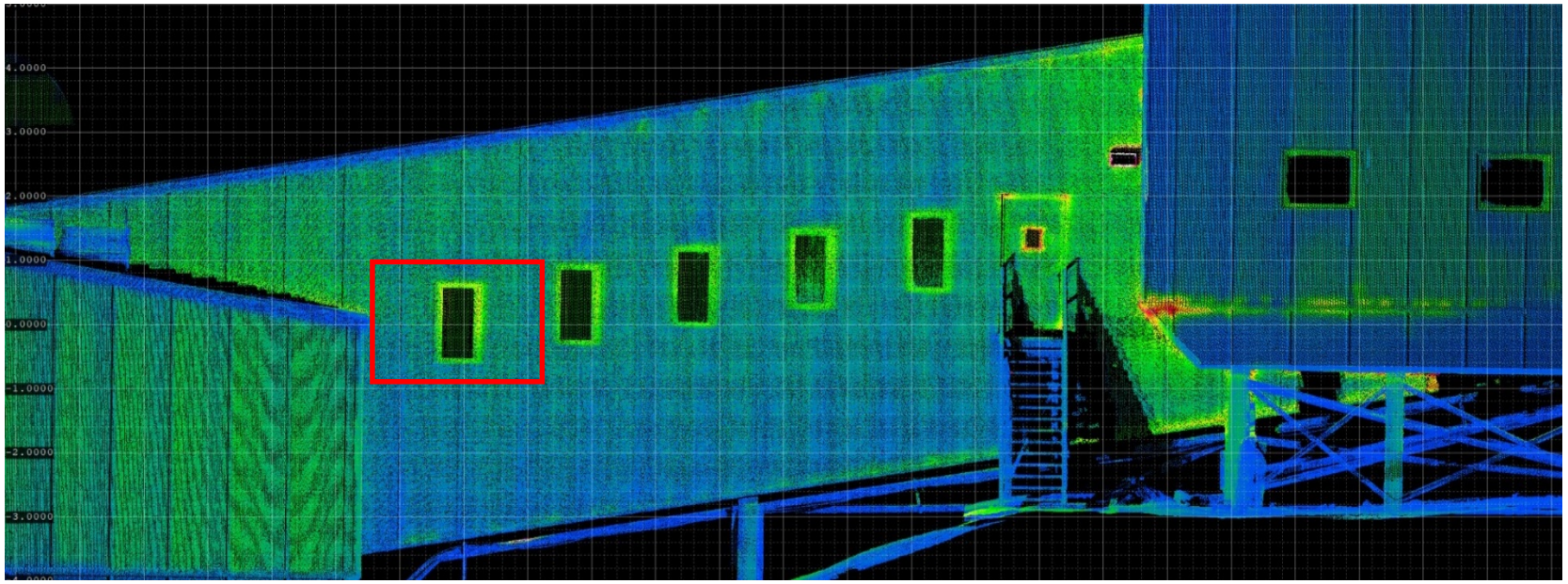




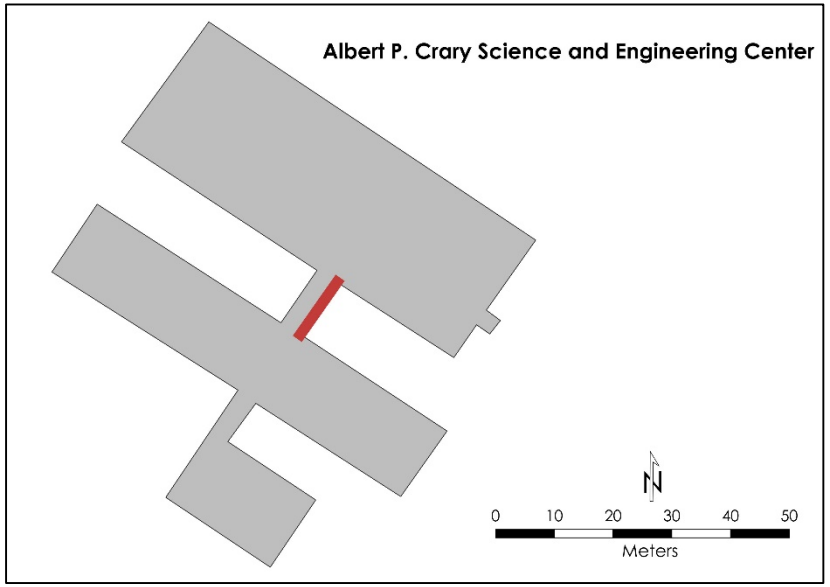
P2NE-W-10 -15◦C 5◦C

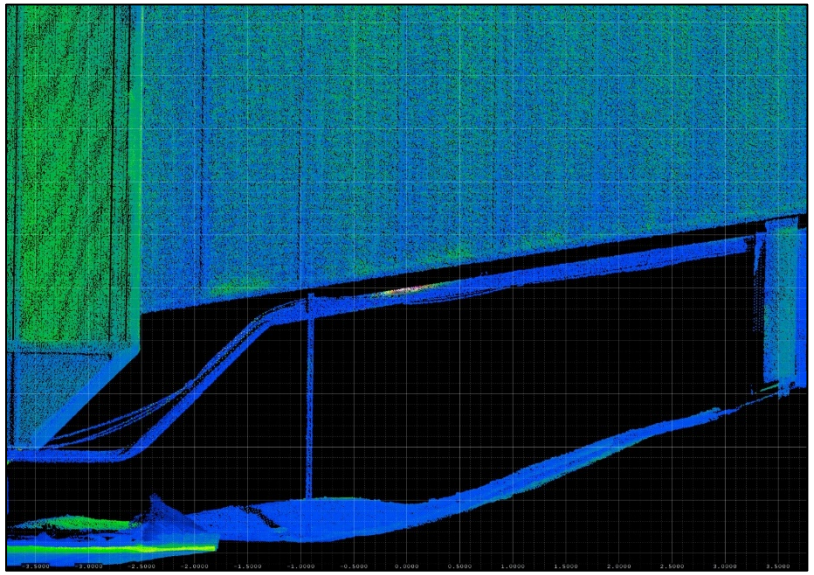


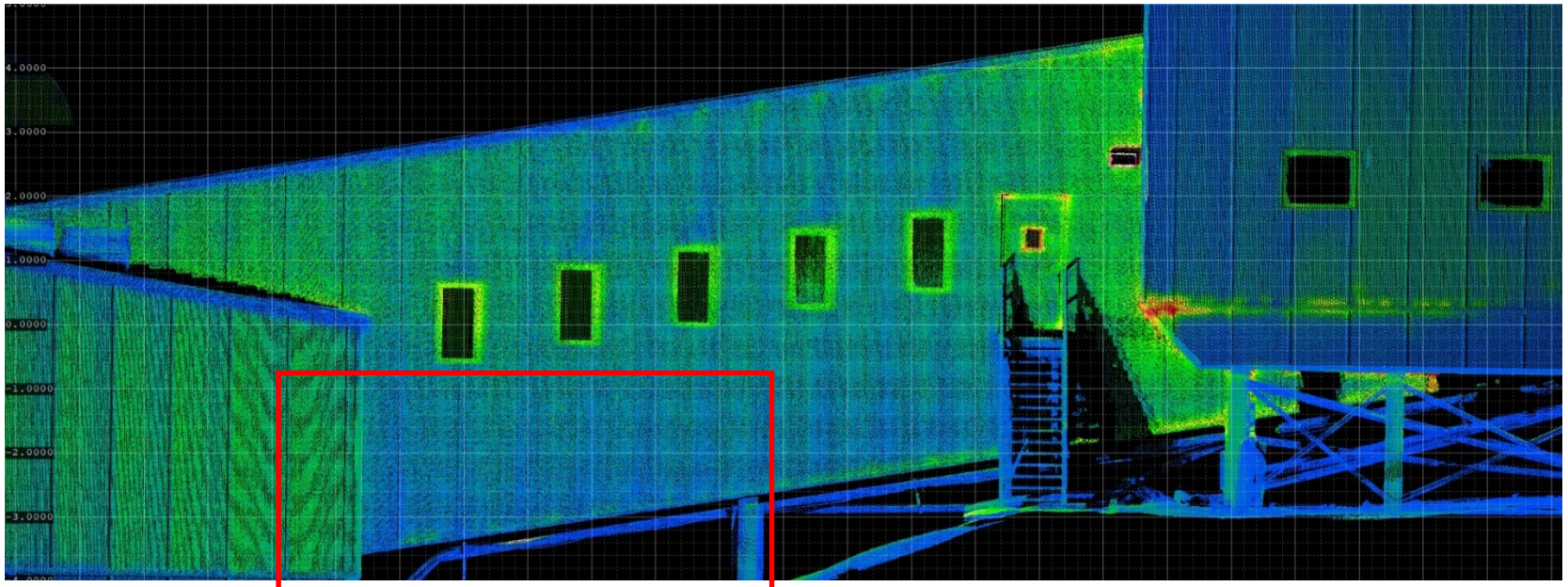




P2CE-W-01 -15◦C 5◦C





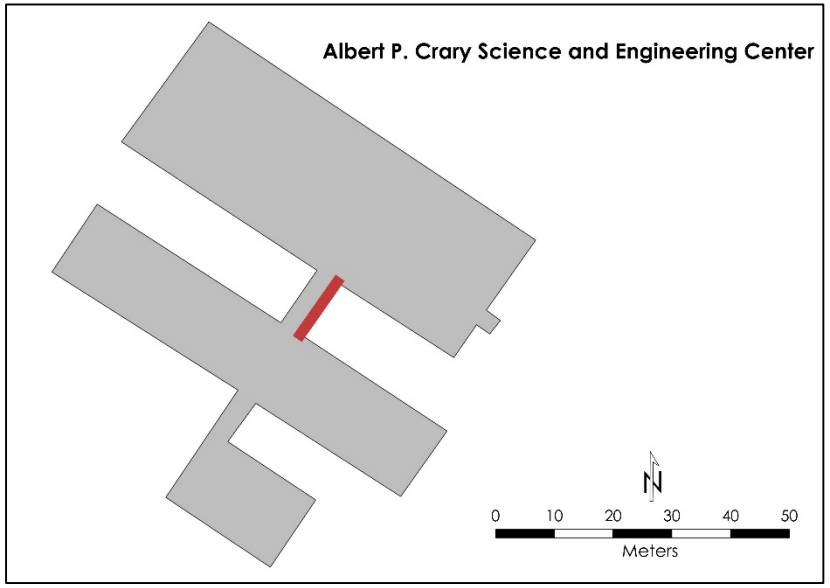


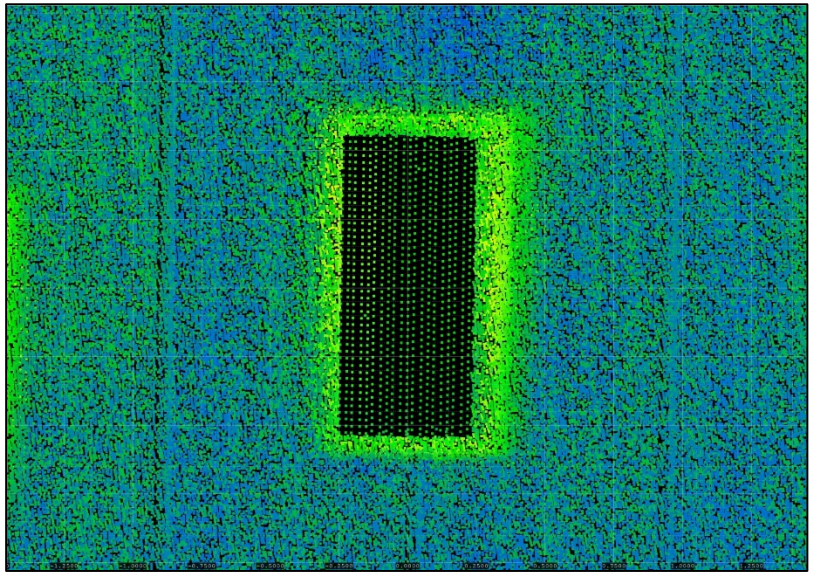
P2CE-TA-01

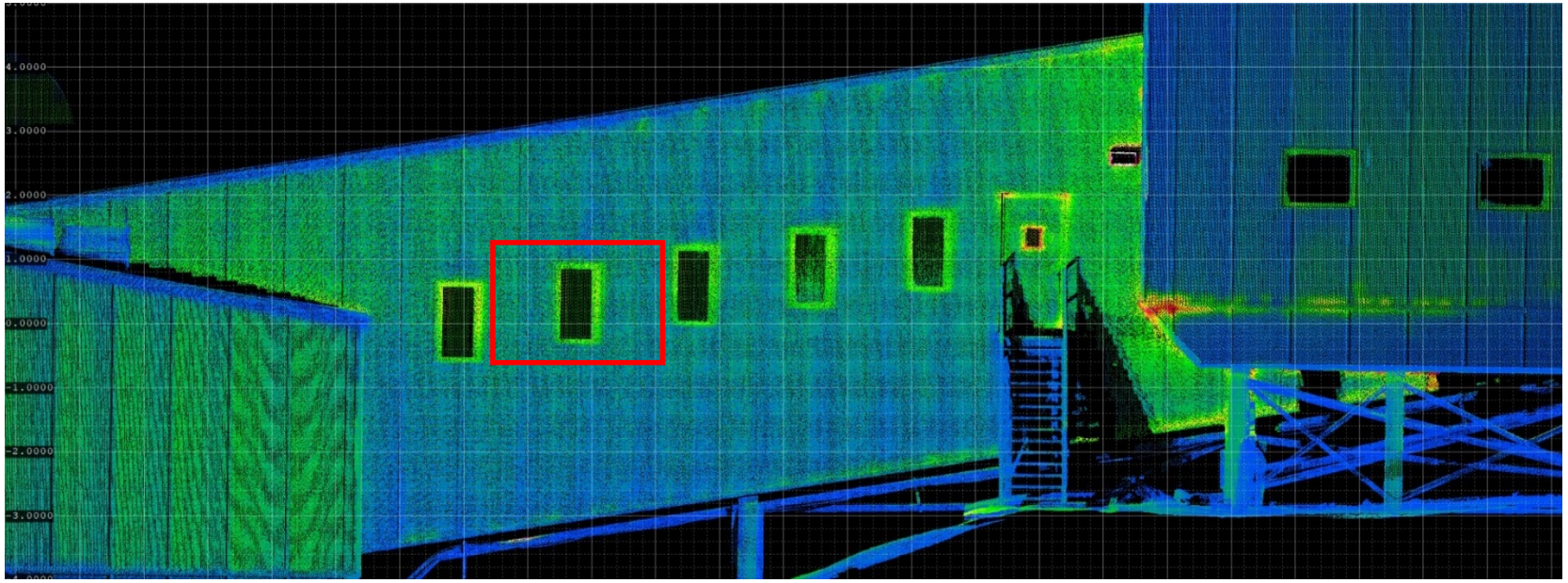
-15◦C



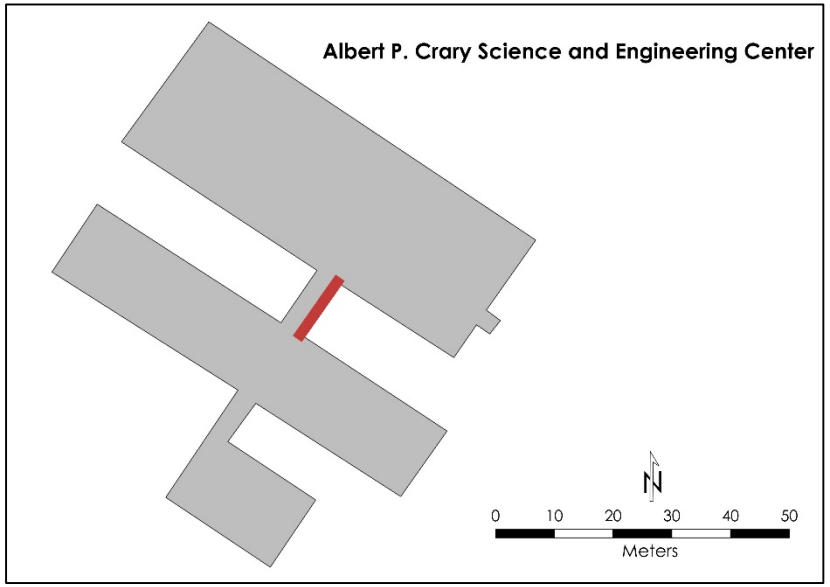
5◦C

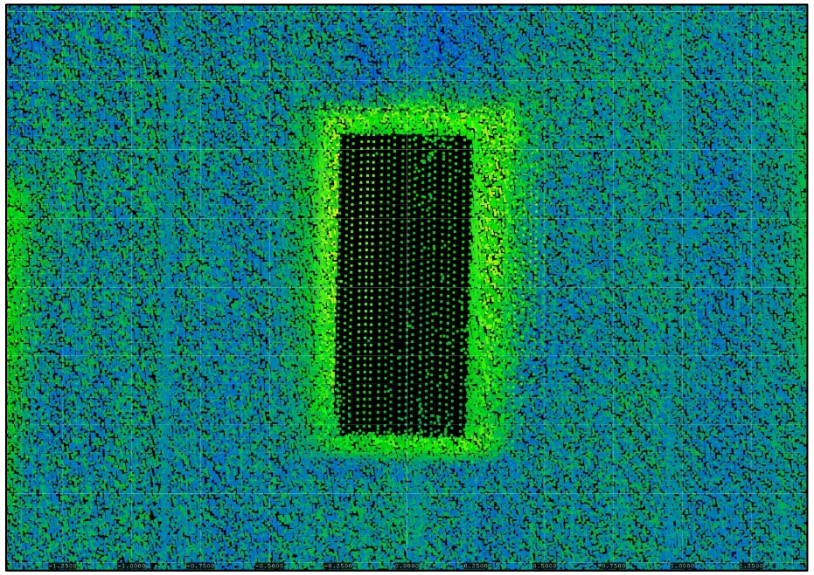


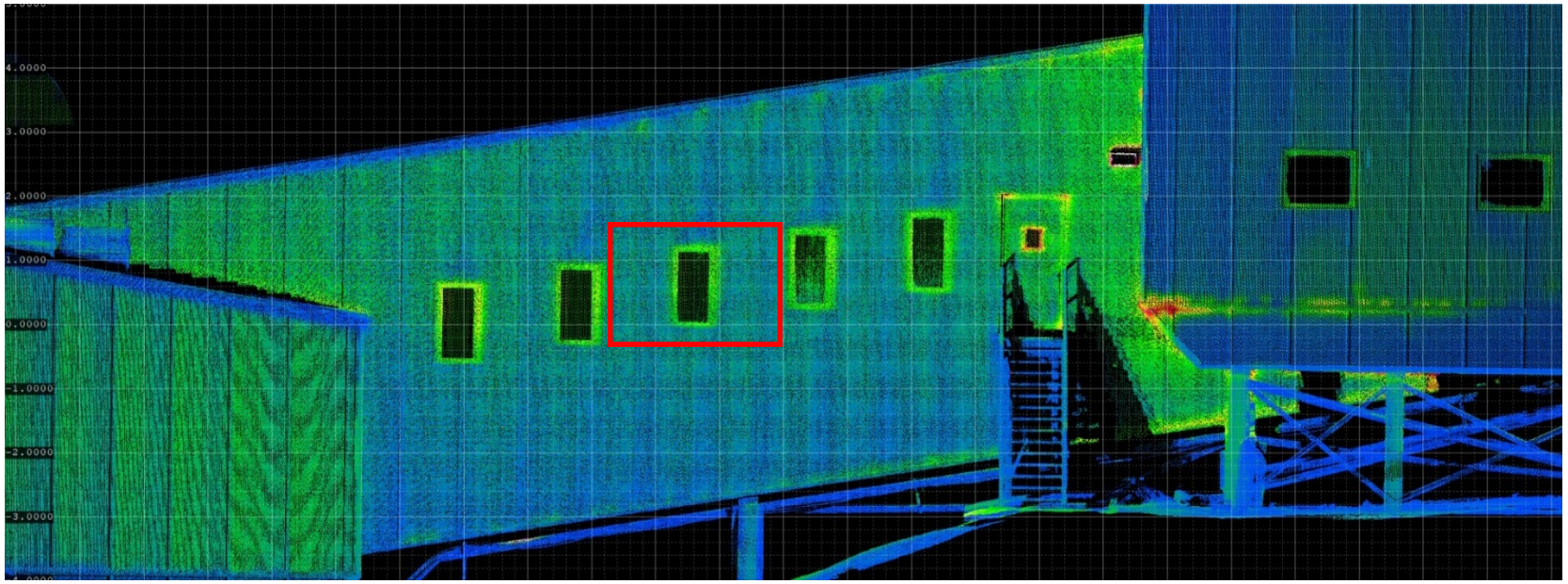




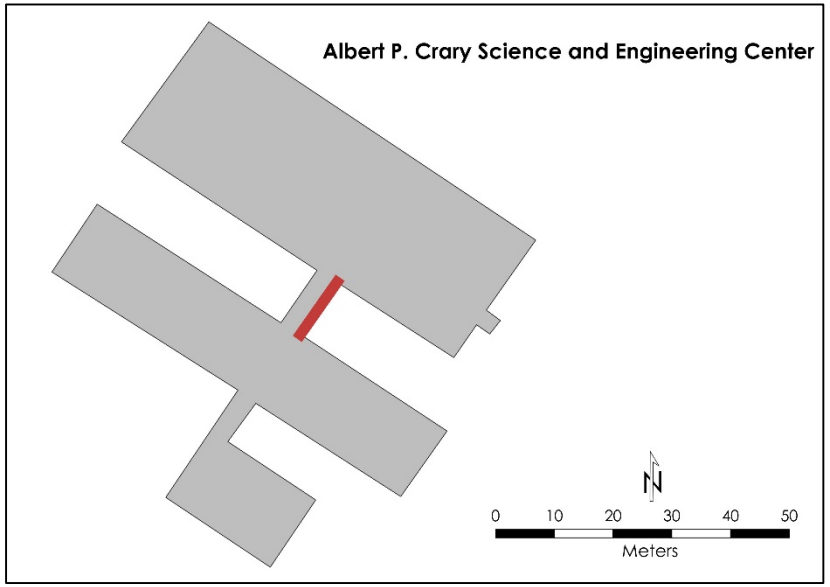
P2CE-W-02 -15◦C 5◦C

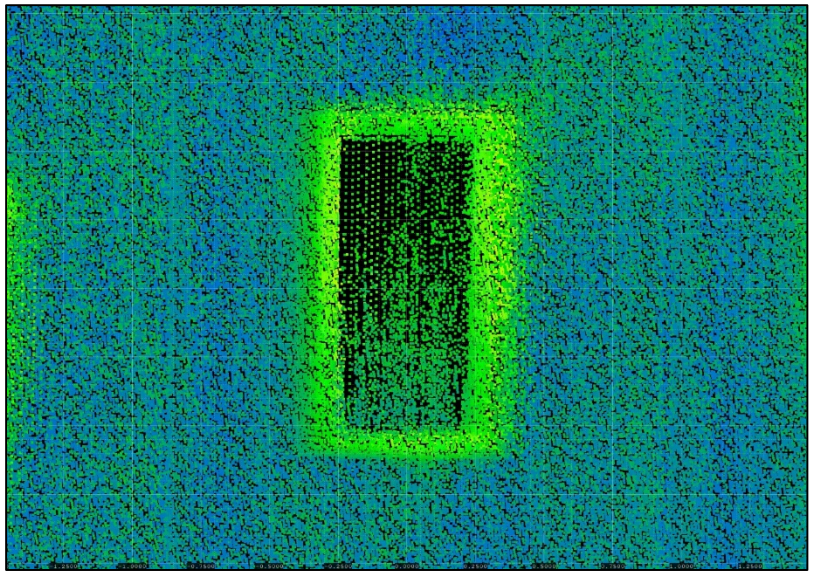


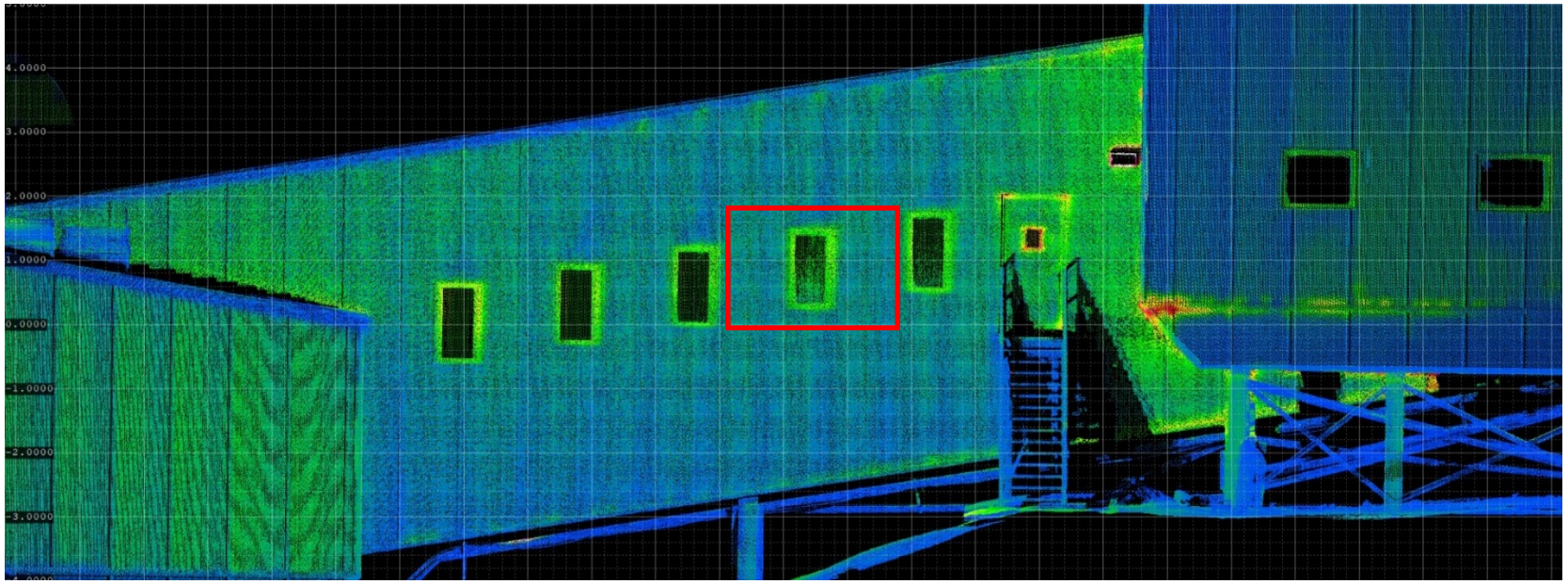




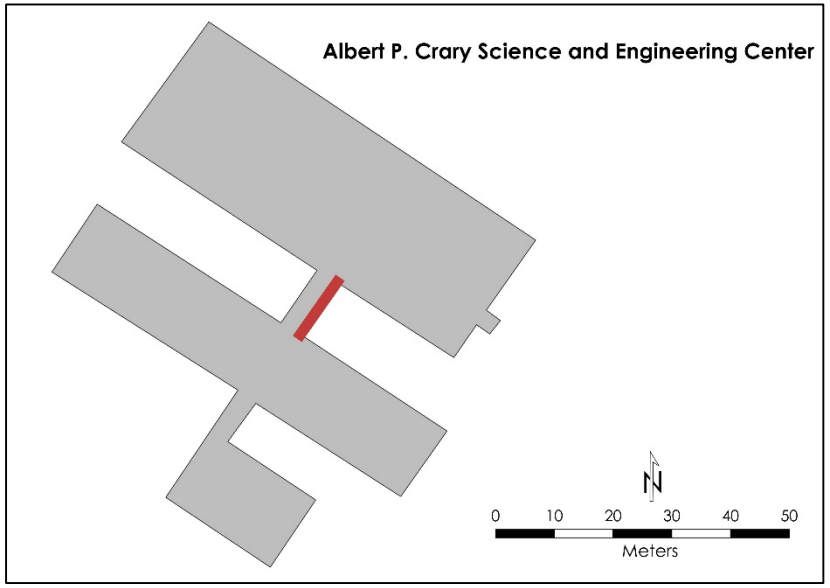
P2CE-W-03 -15◦C 5◦C

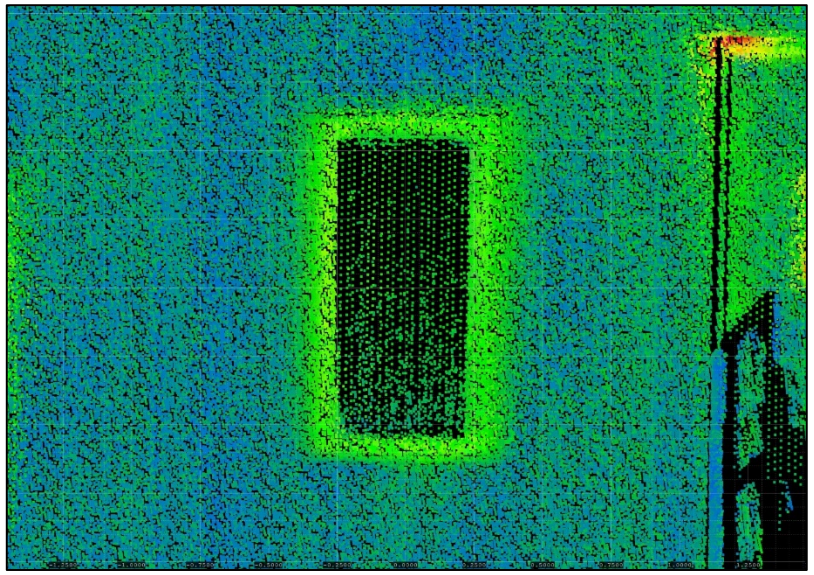


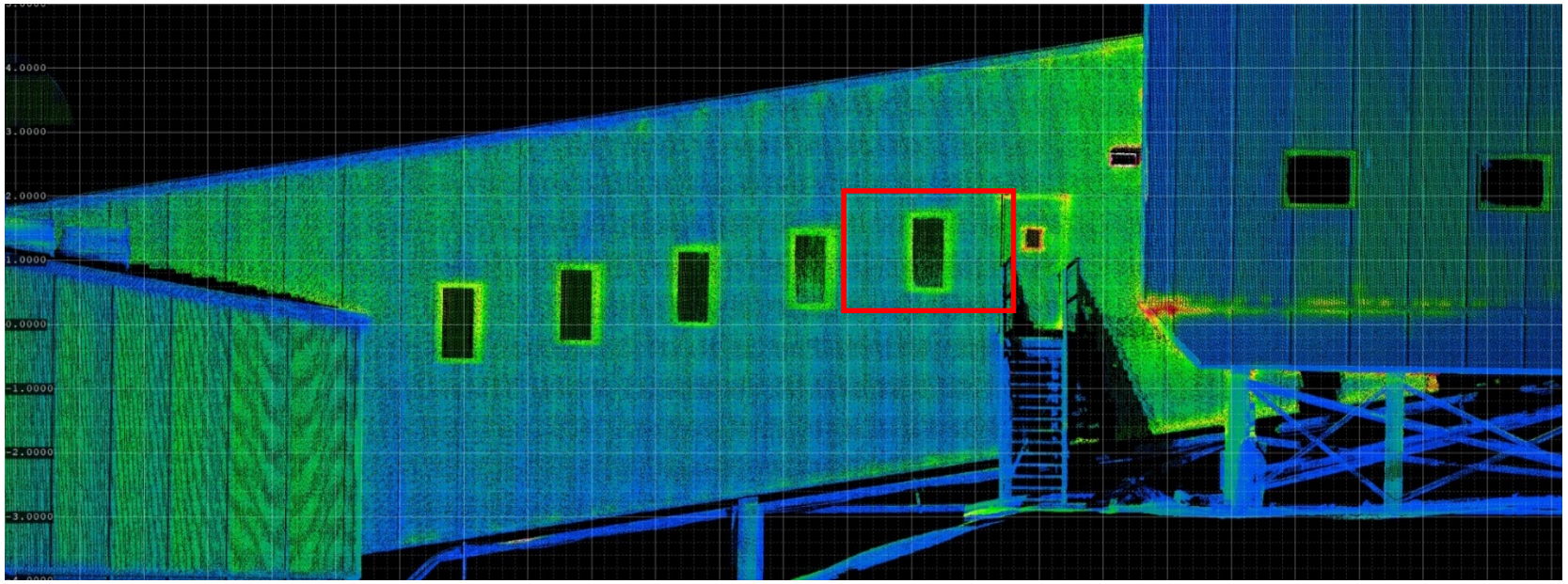




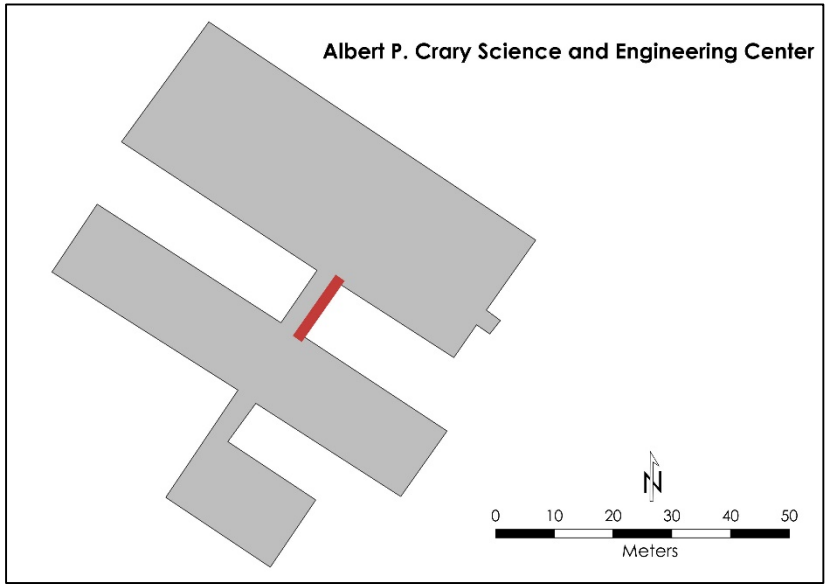
P2CE-W-04 -15◦C 5◦C

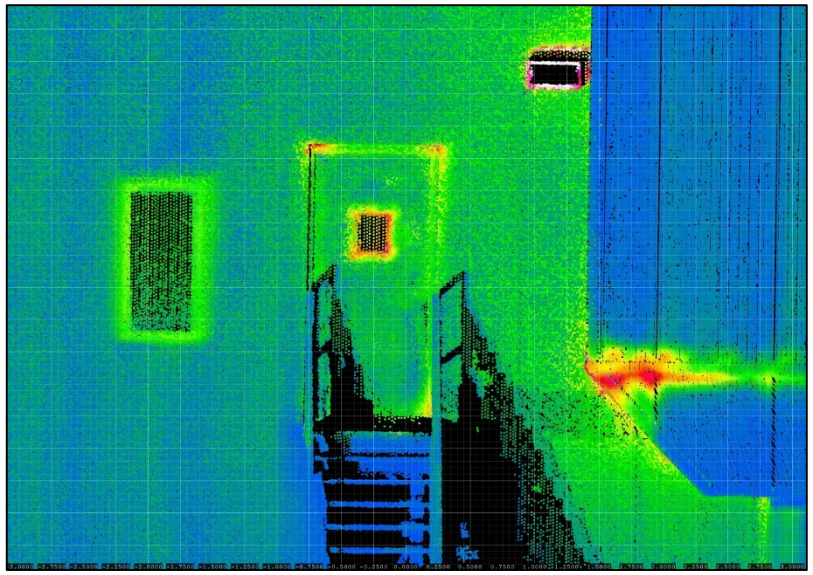


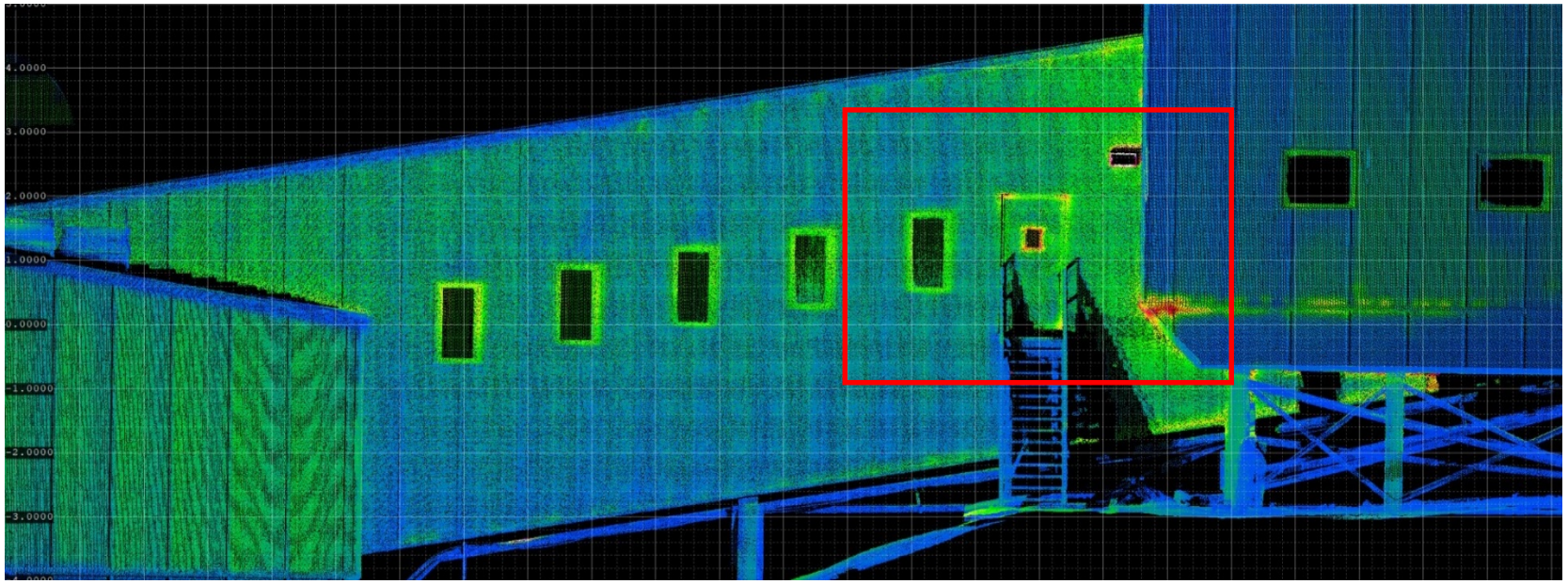




P2CE-W-05 -15◦C 5◦C





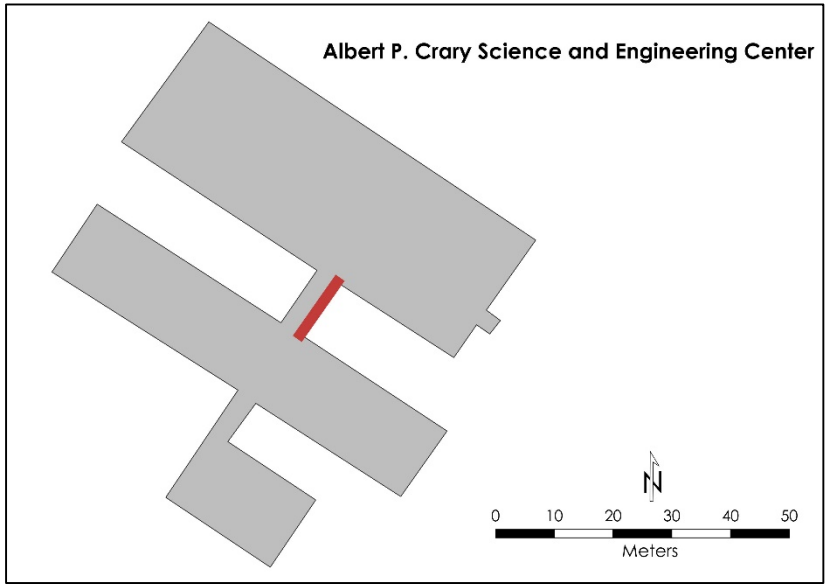


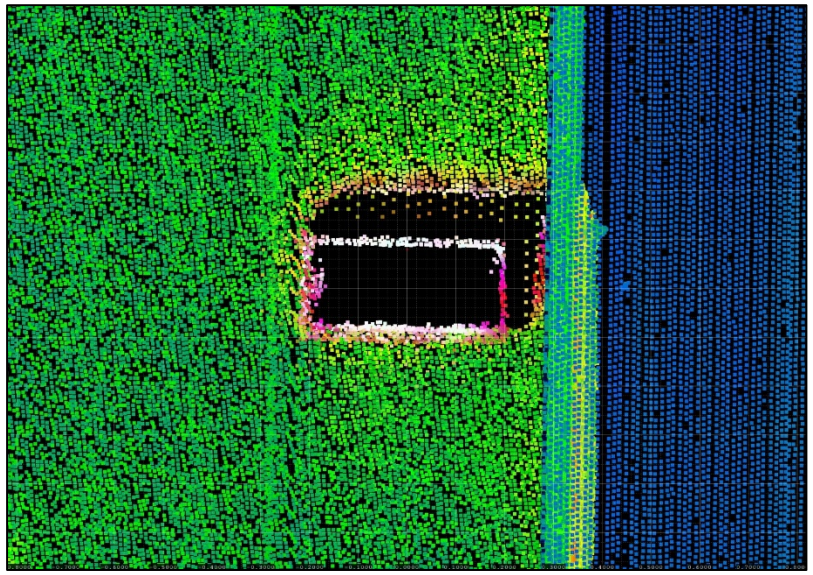
P2CE-D-01

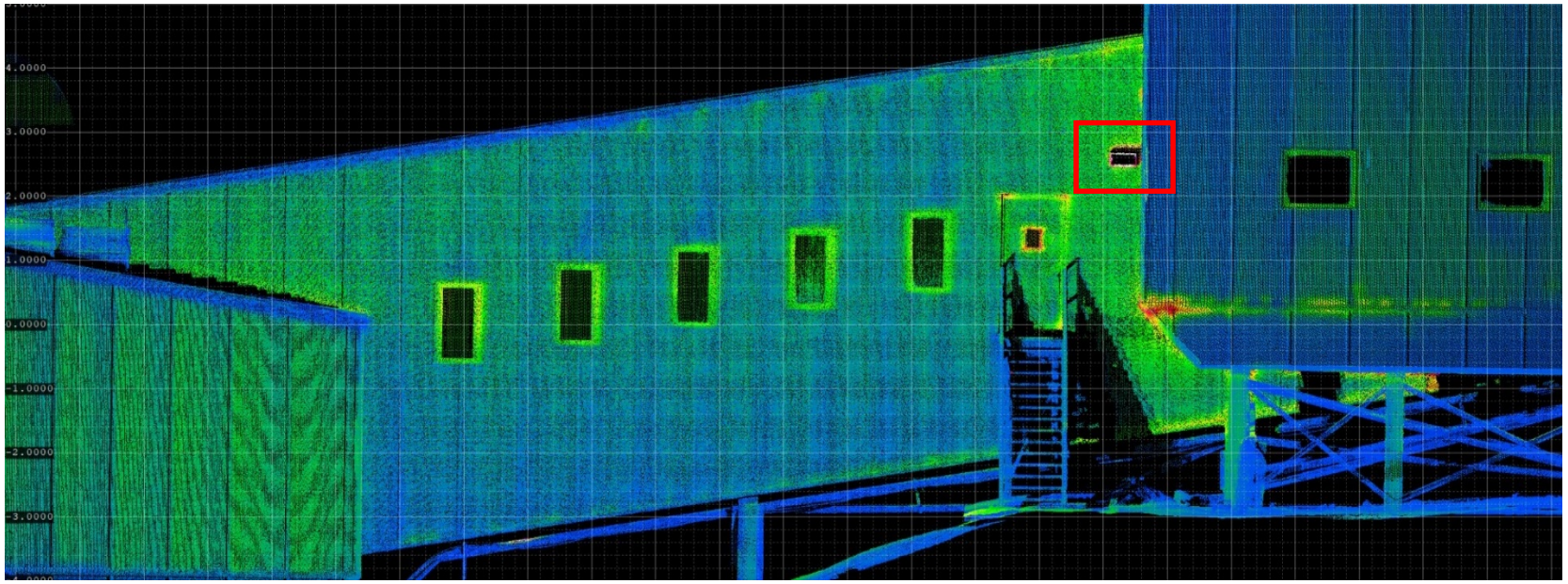
-15◦C



5◦C





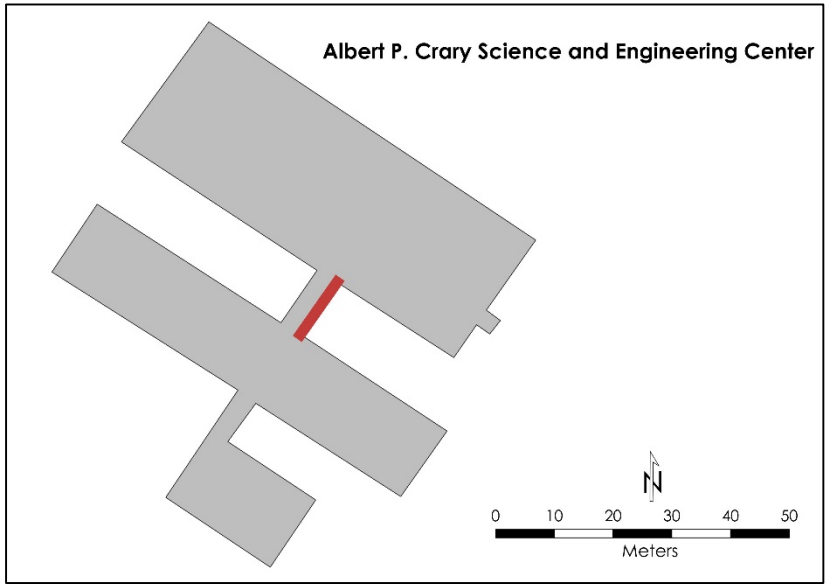


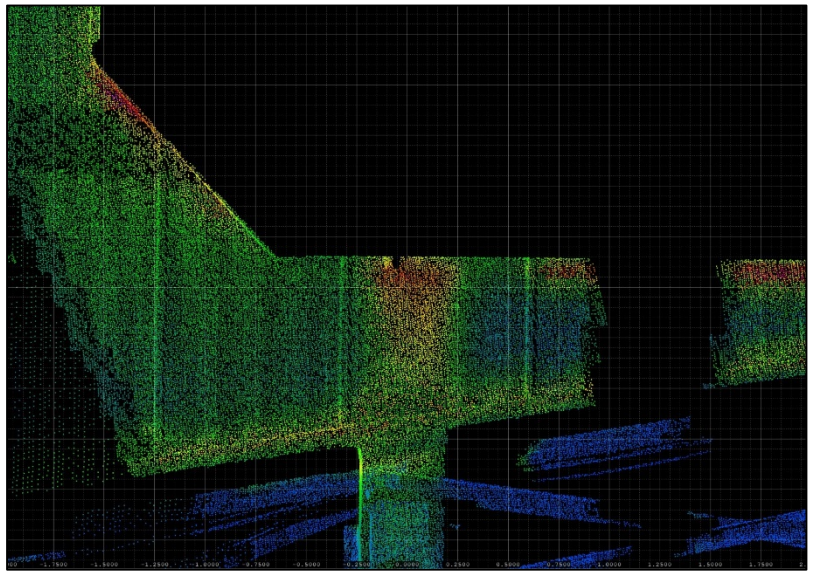
P2CE-V-01

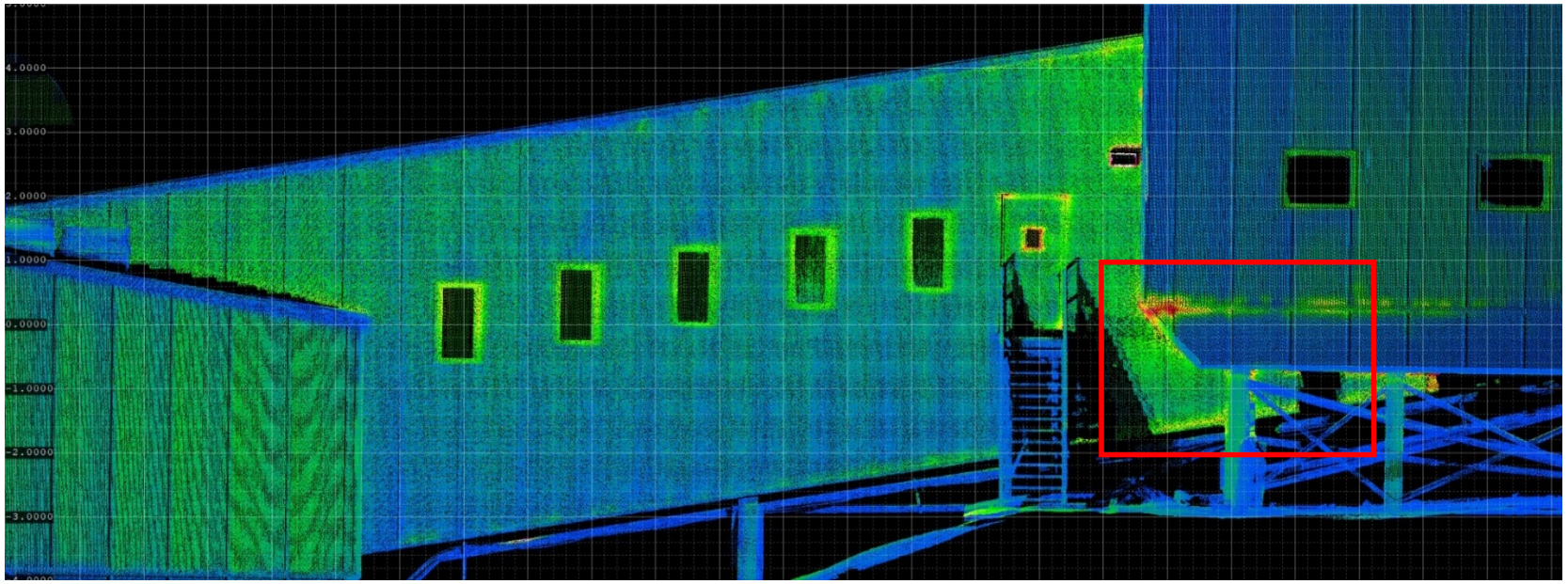
-15◦C



5◦C





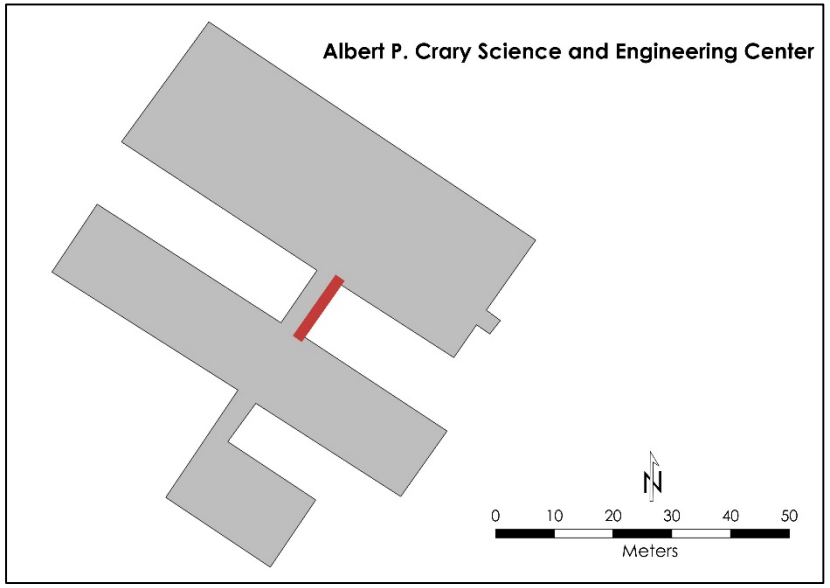


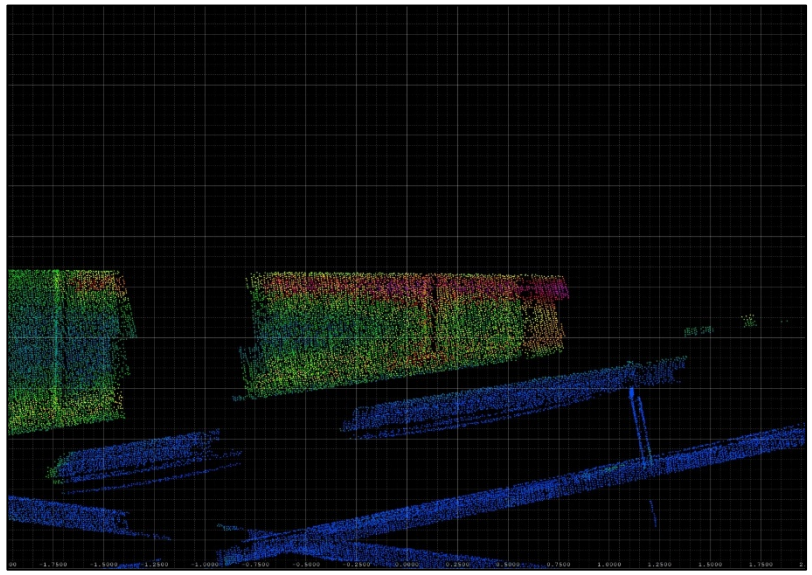
P2CE-TA-02

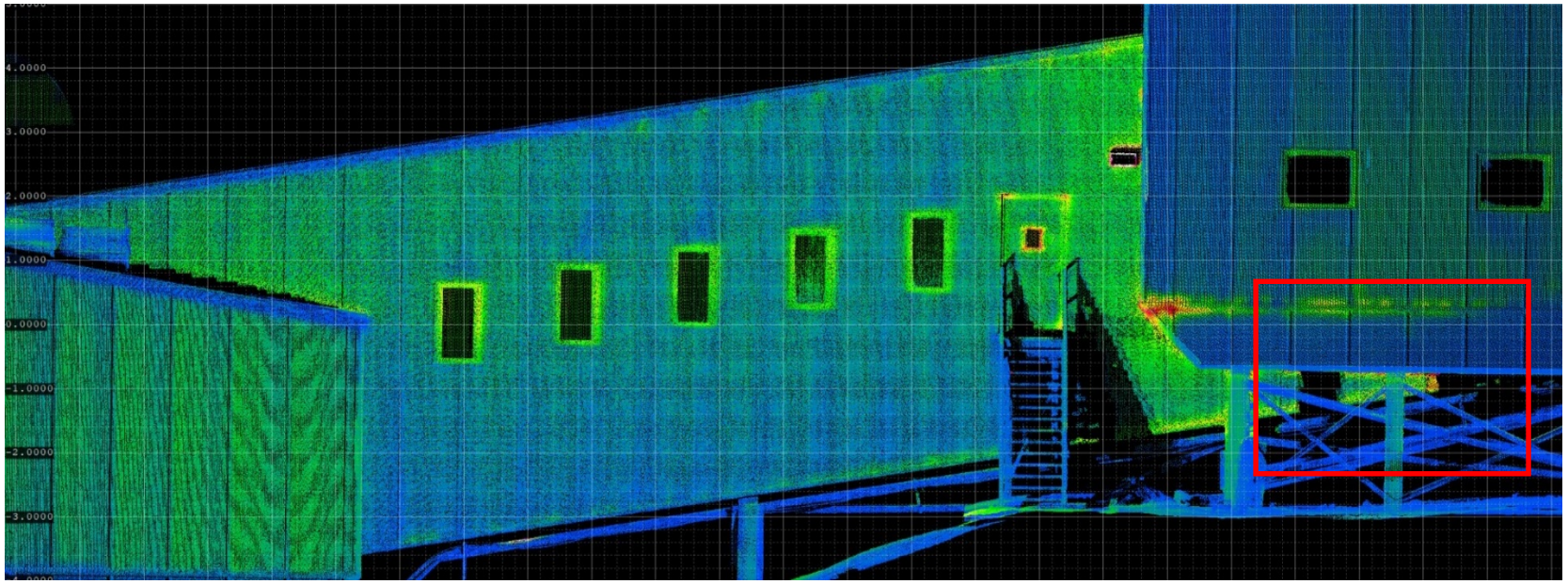
-15◦C



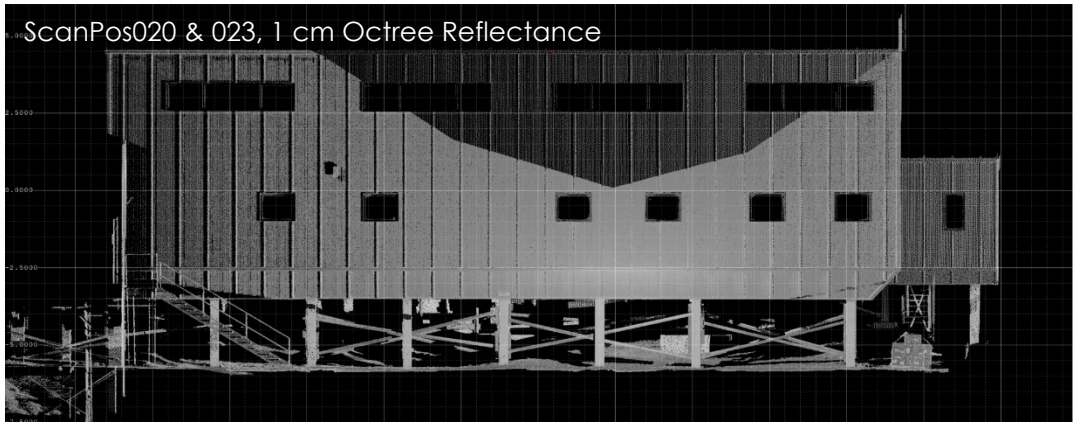
5◦C

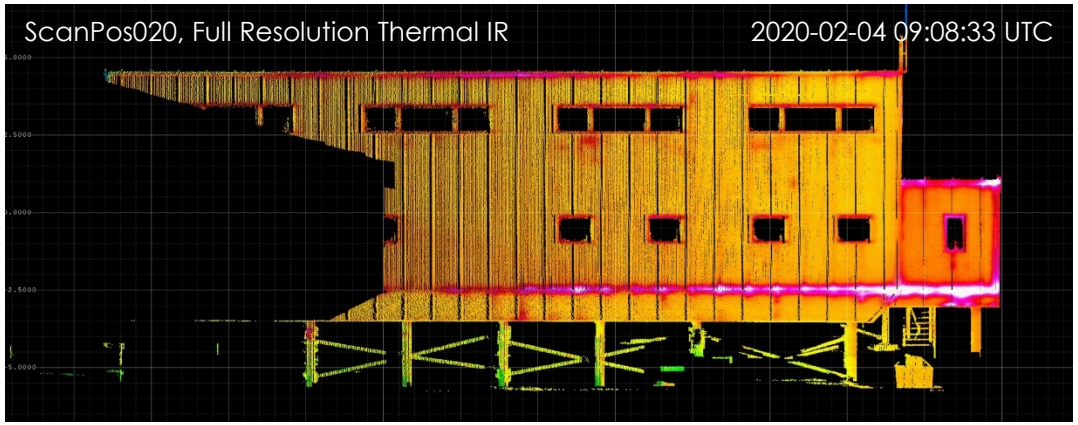


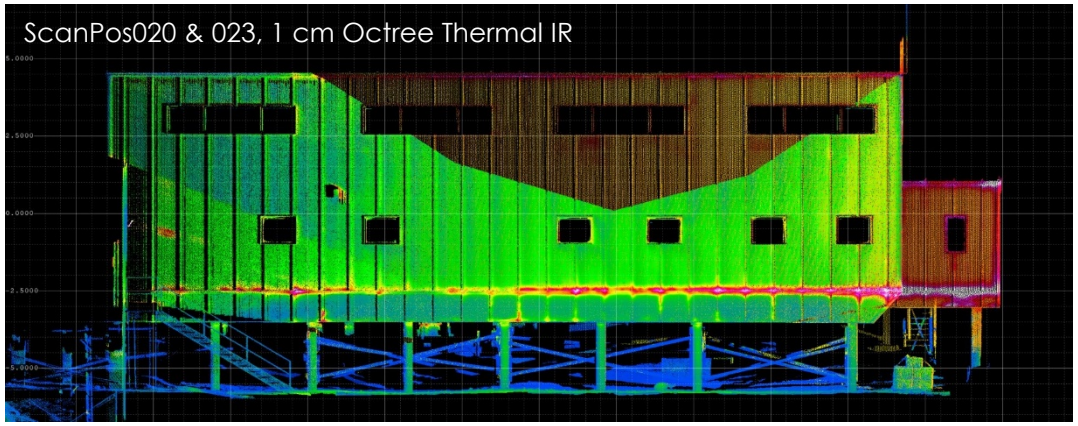


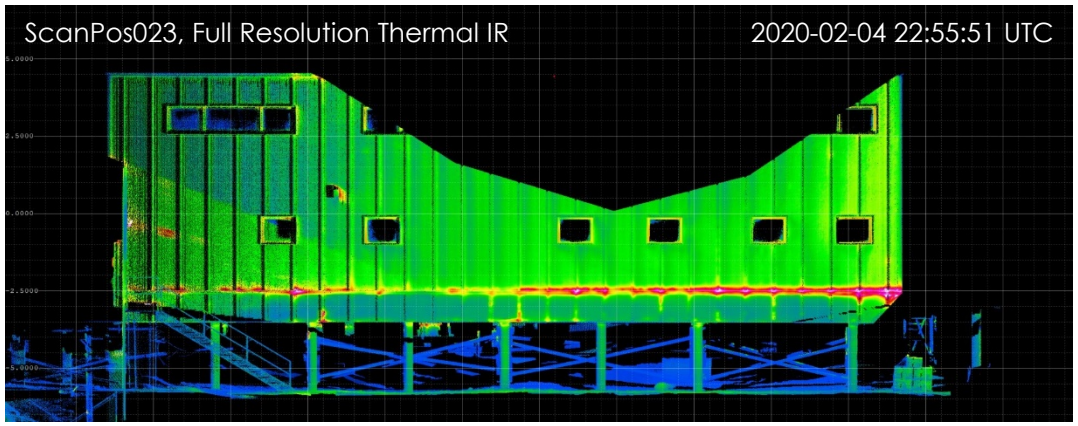


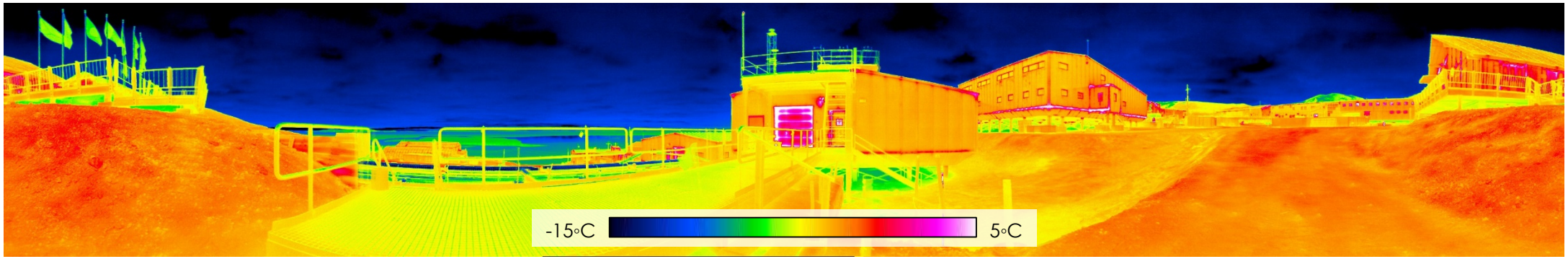
P2CE-TA-03 -15◦C 5◦C



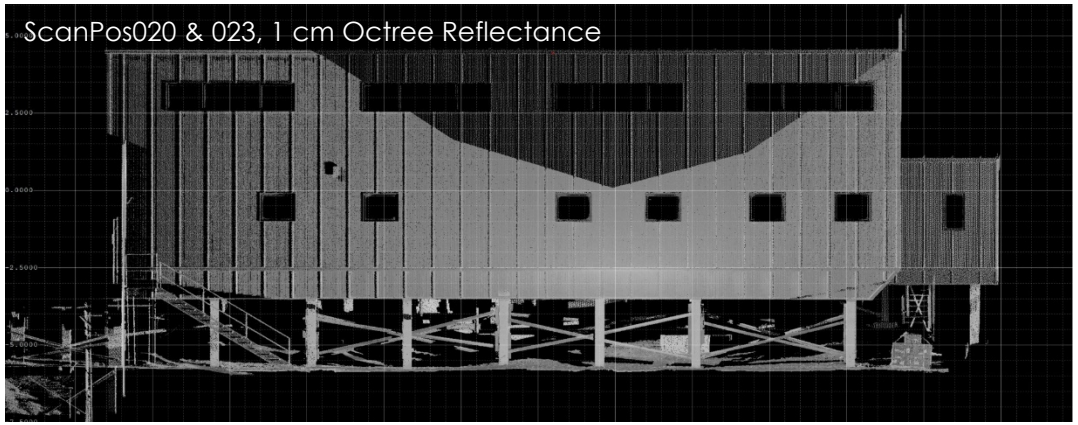


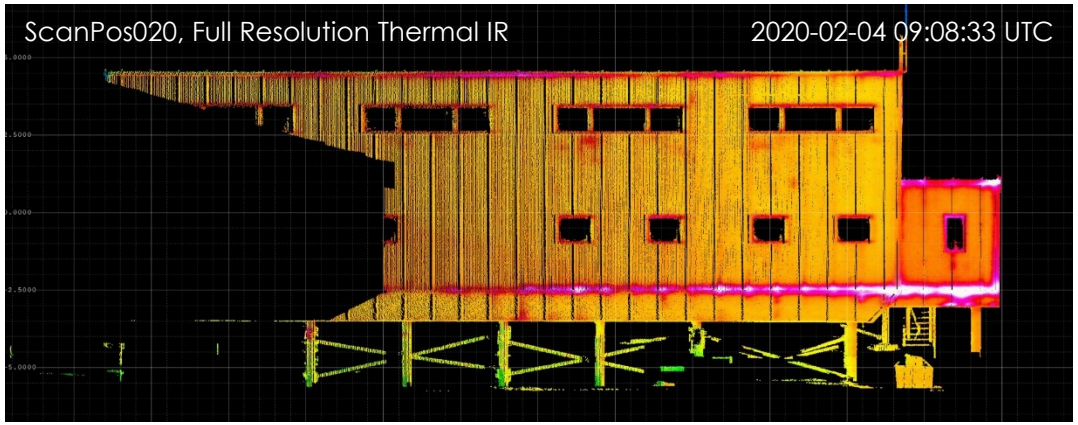


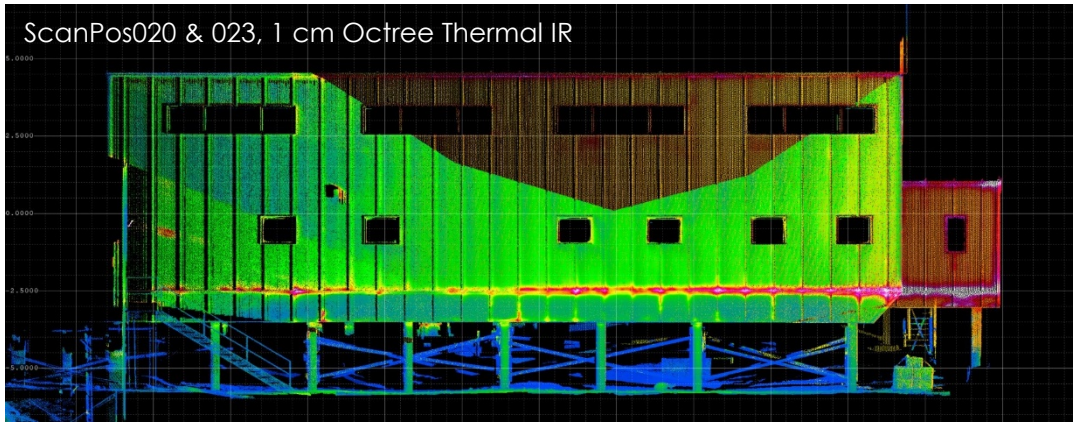


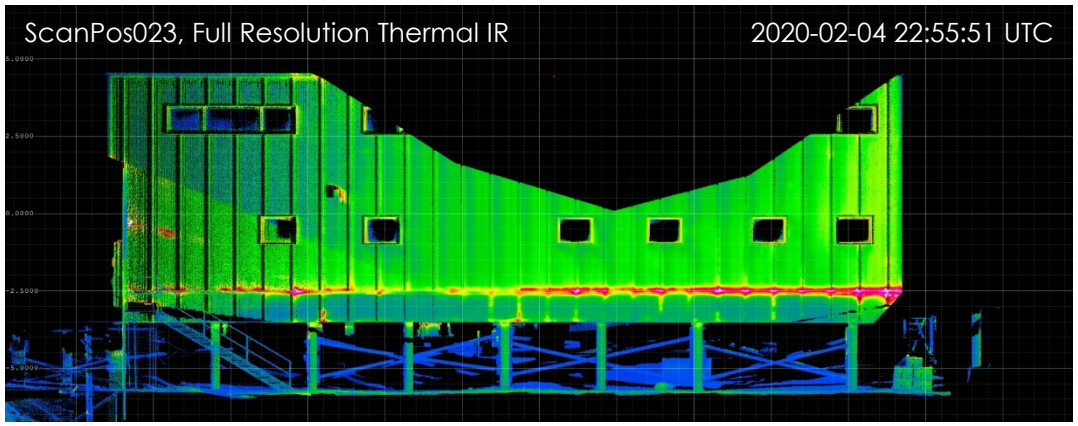


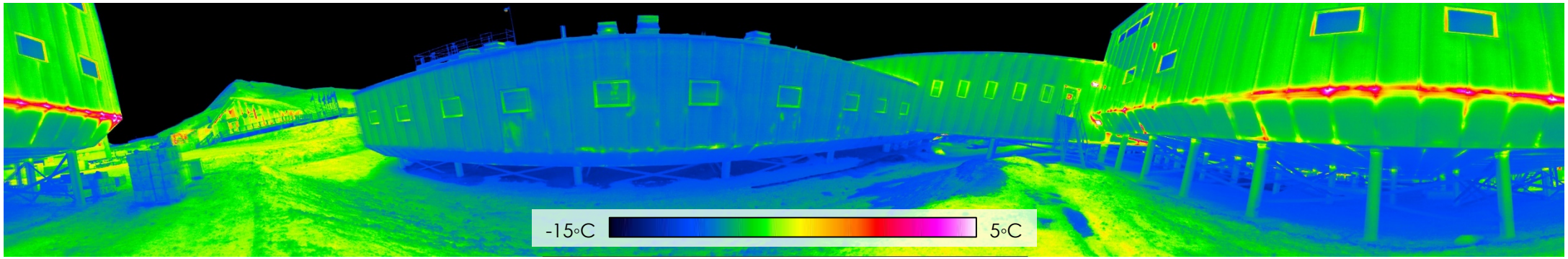
ScanPos020 – TIR Panorama



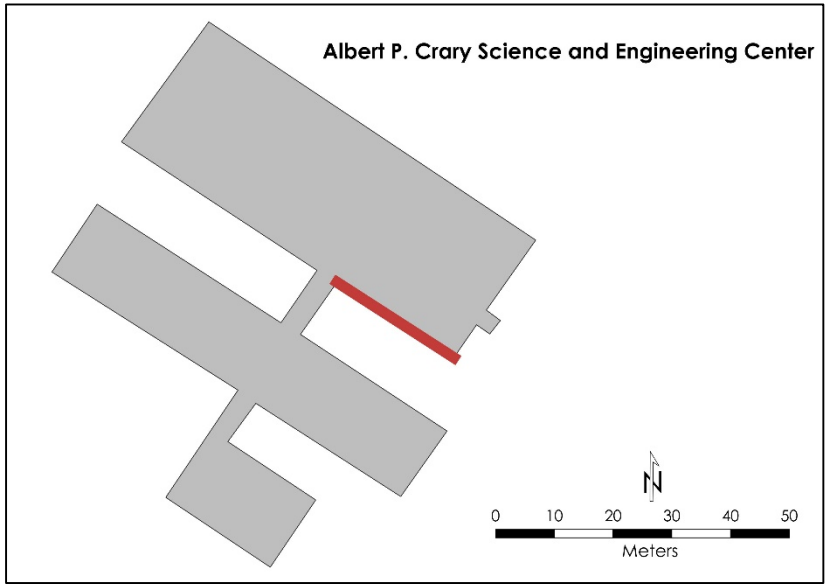


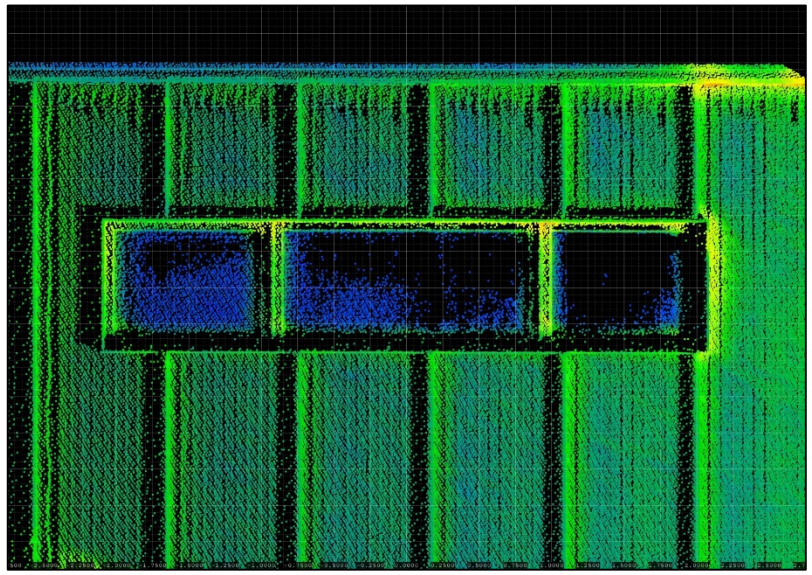


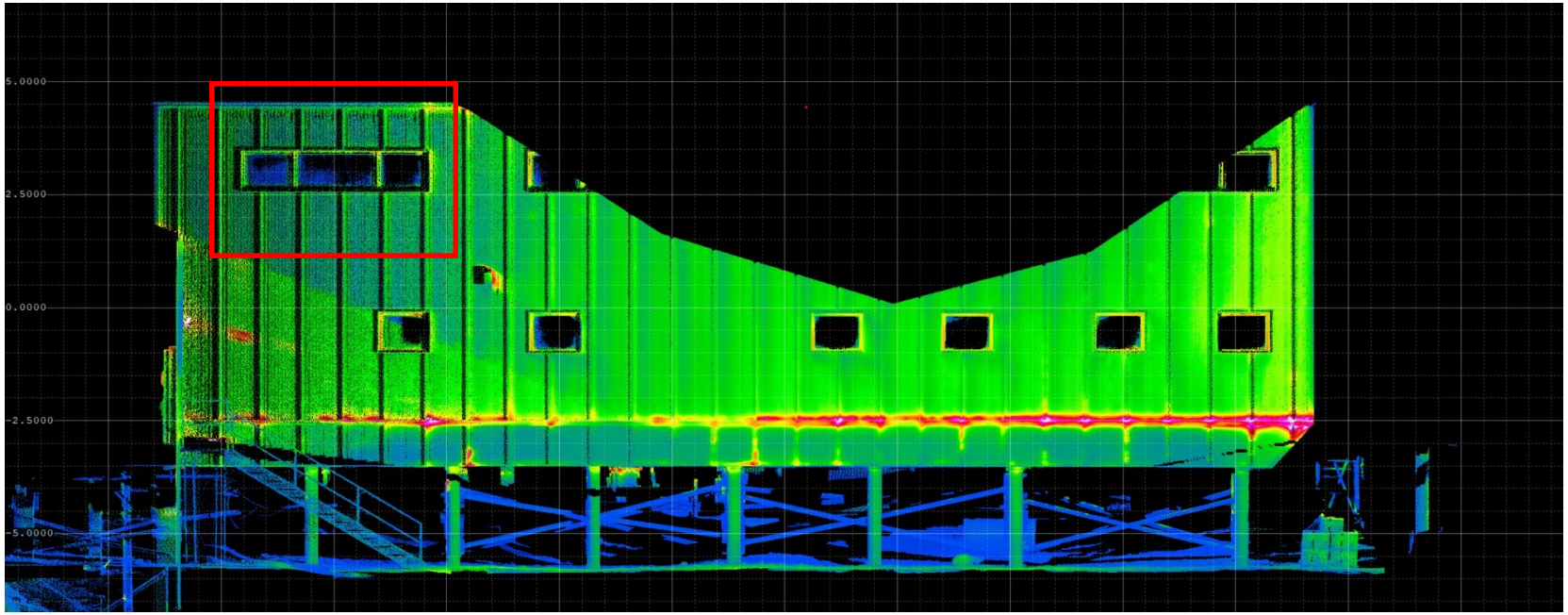




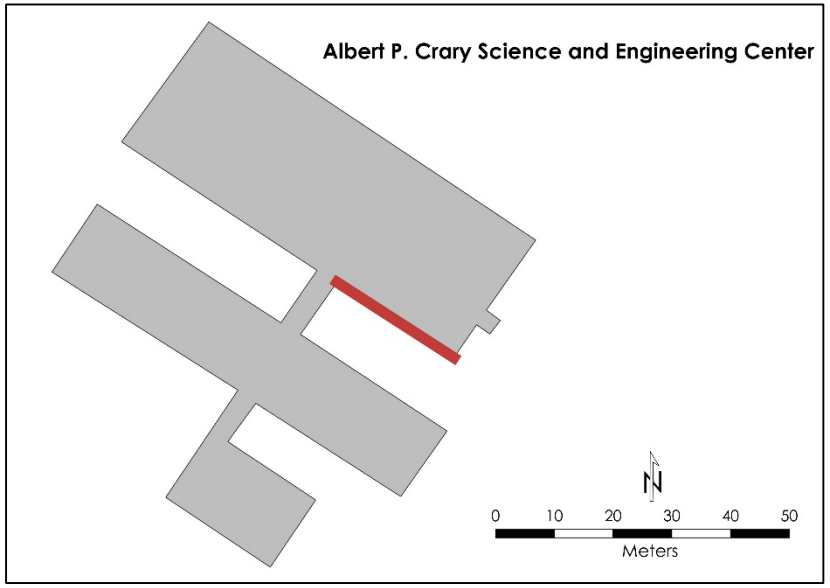
ScanPos023 – TIR Panorama

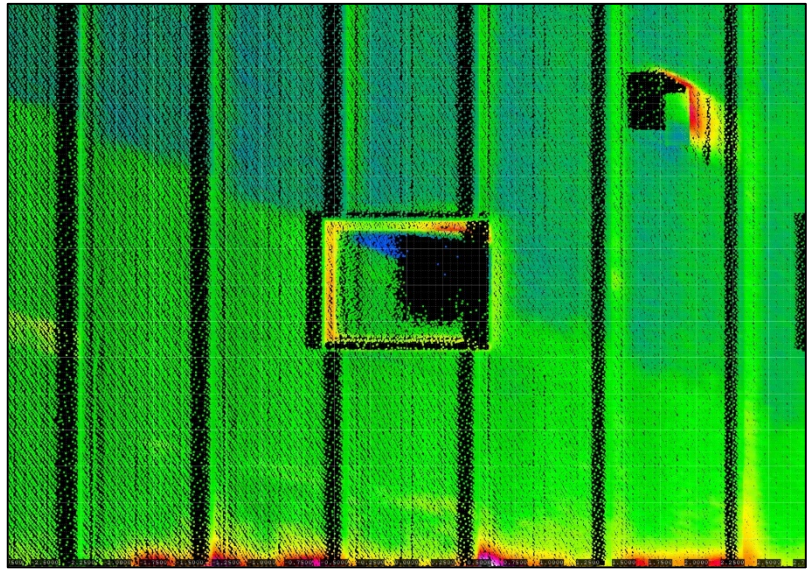


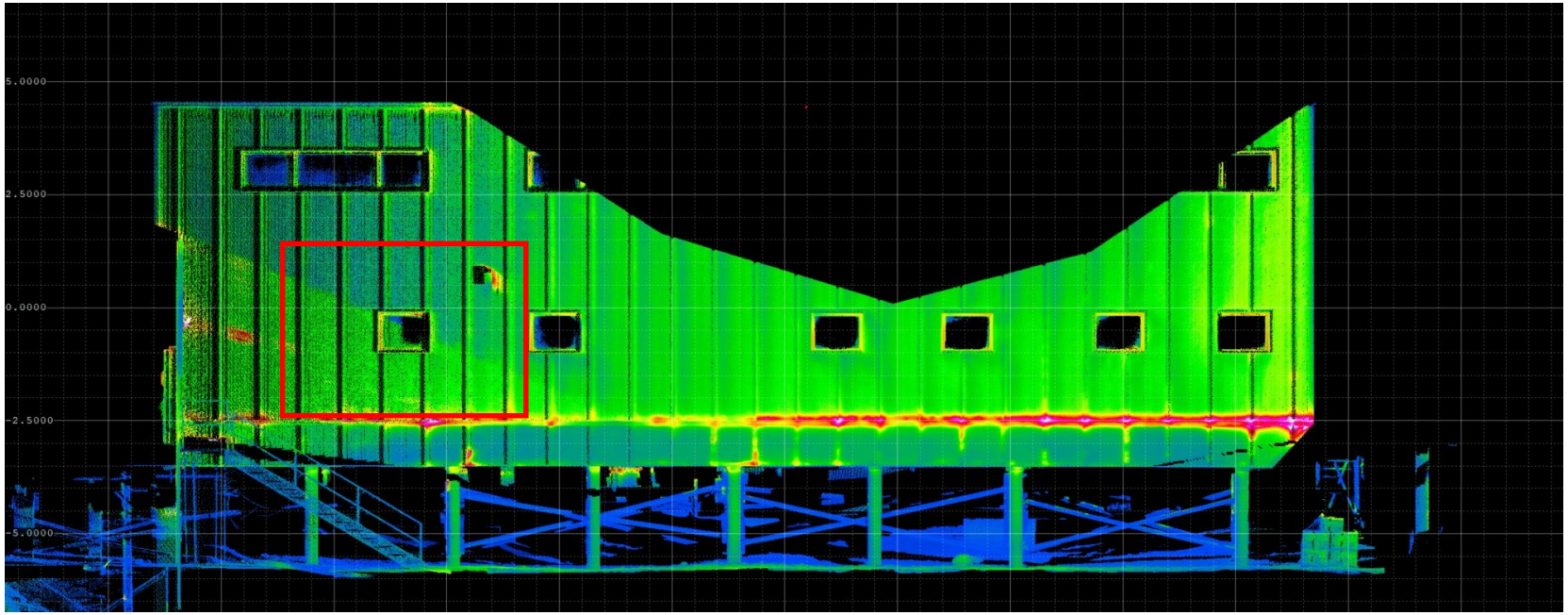




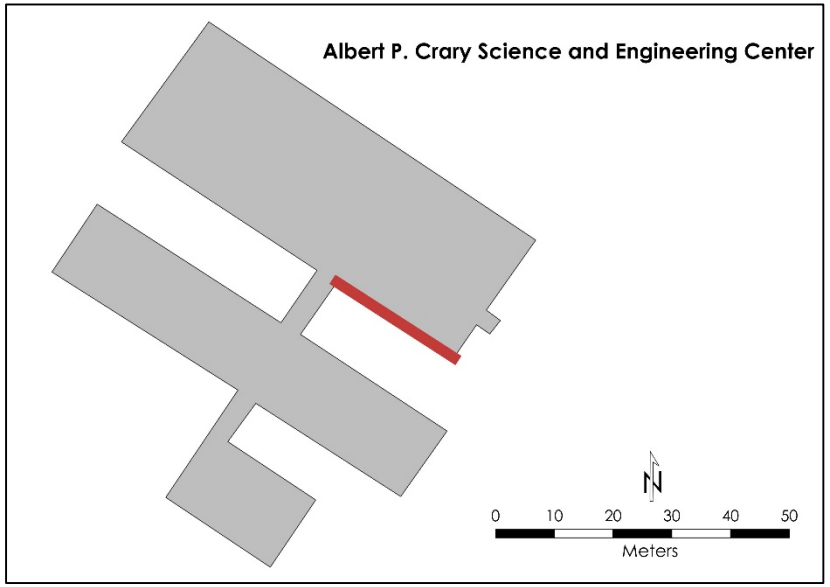
P1SE-W-01 -15◦C 5◦C

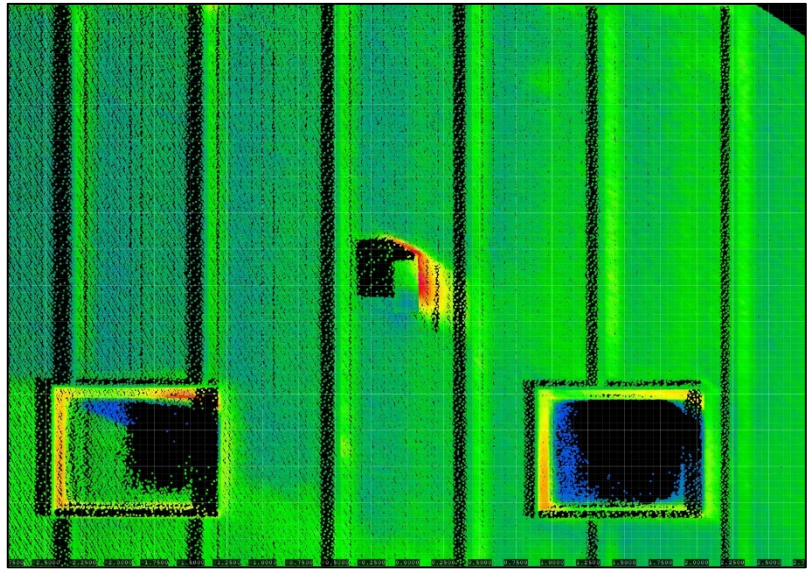


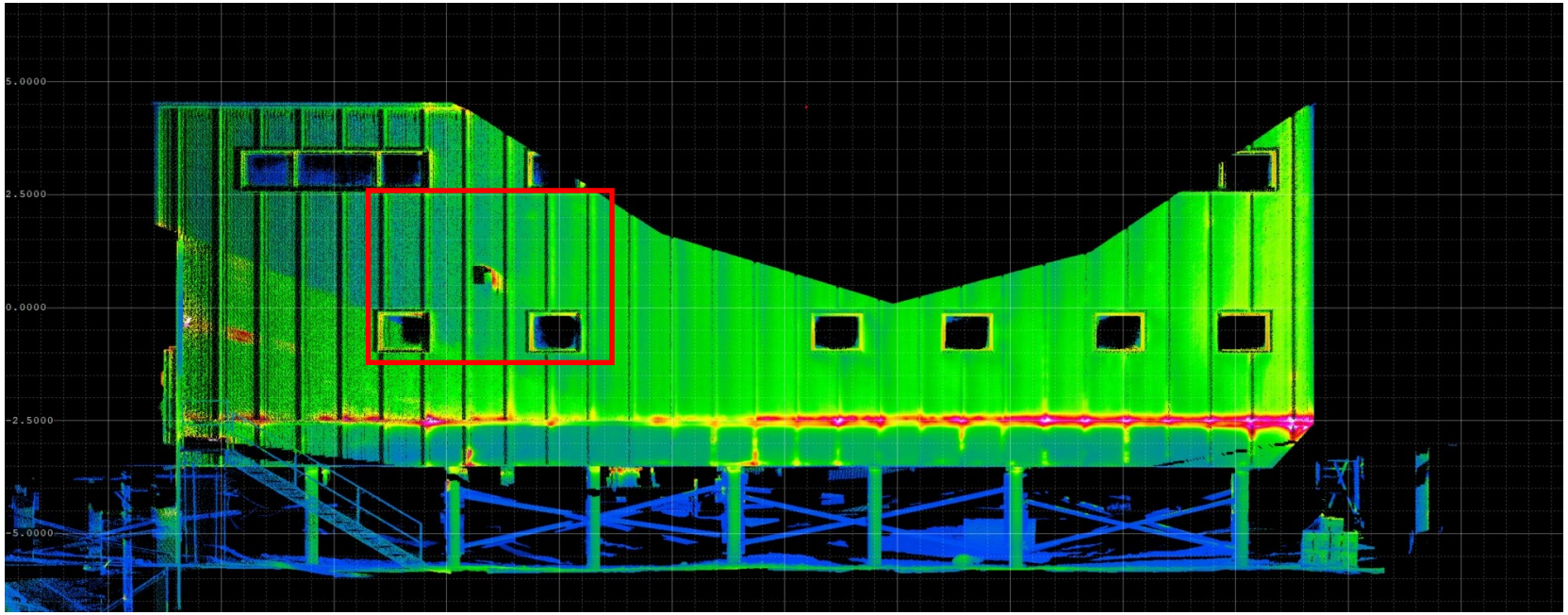




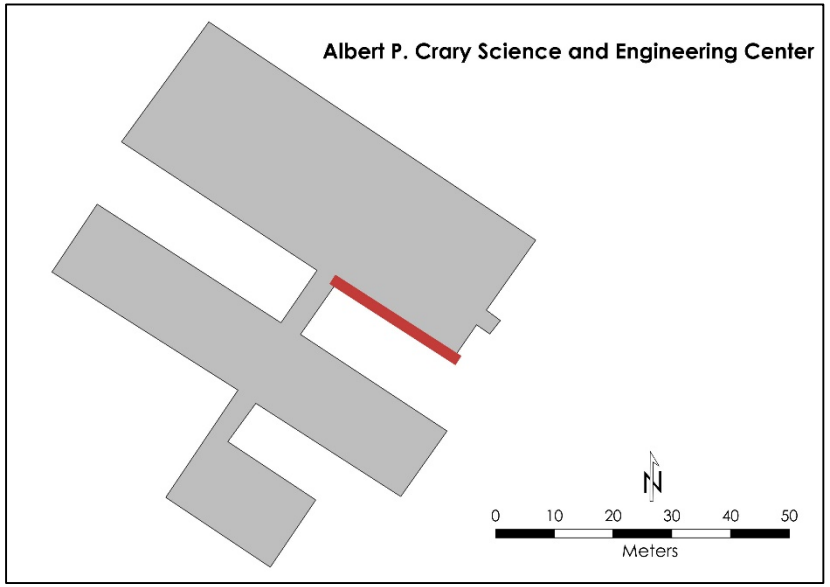
P1SE-W-02 -15◦C 5◦C

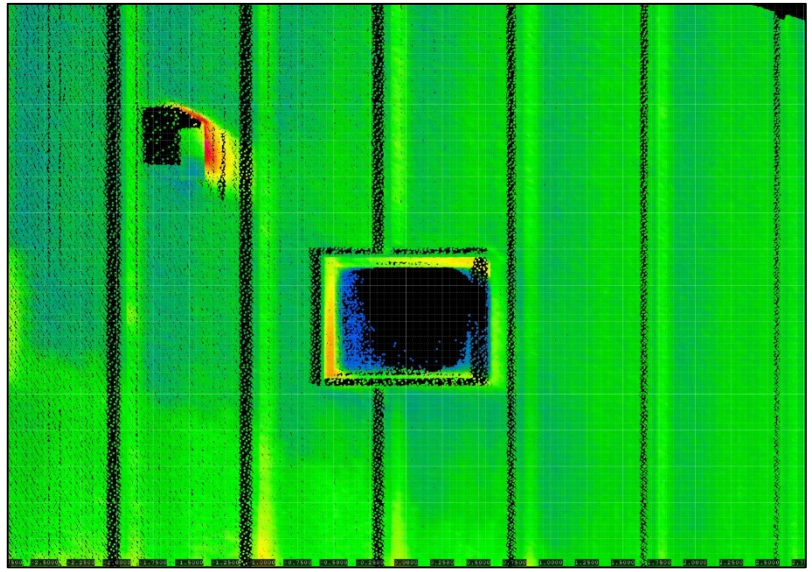


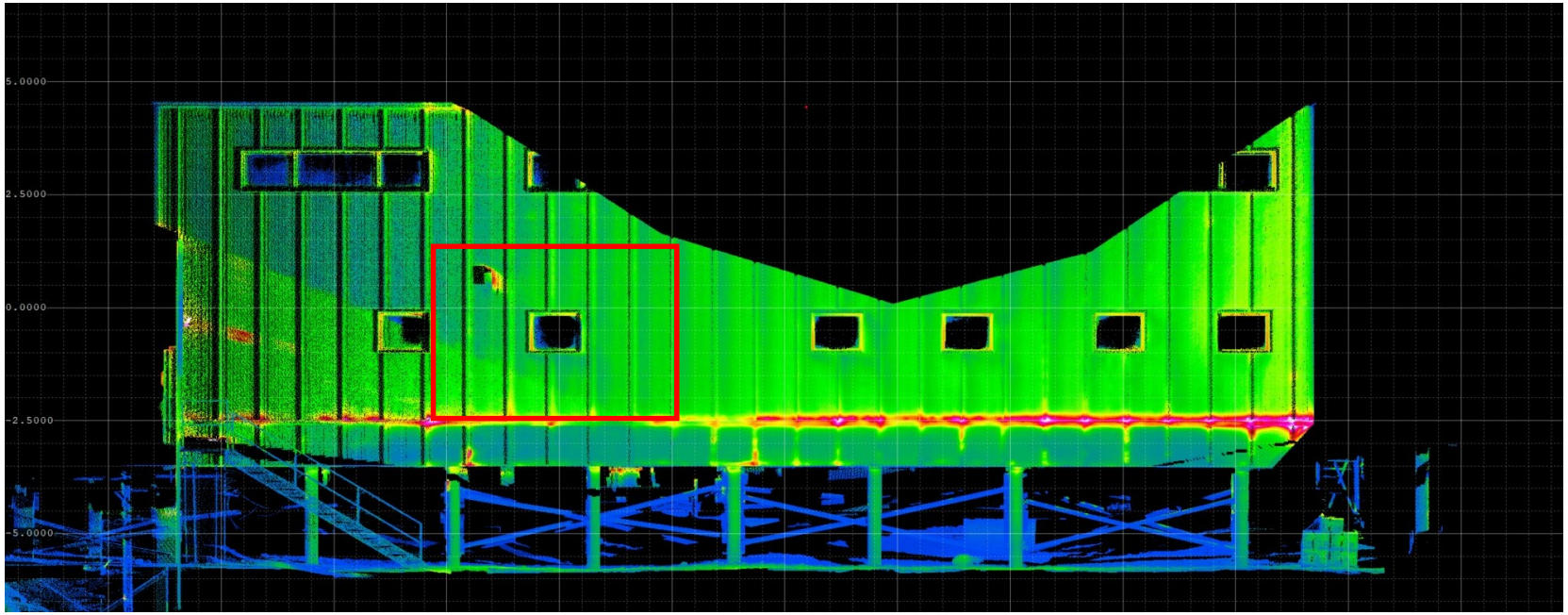




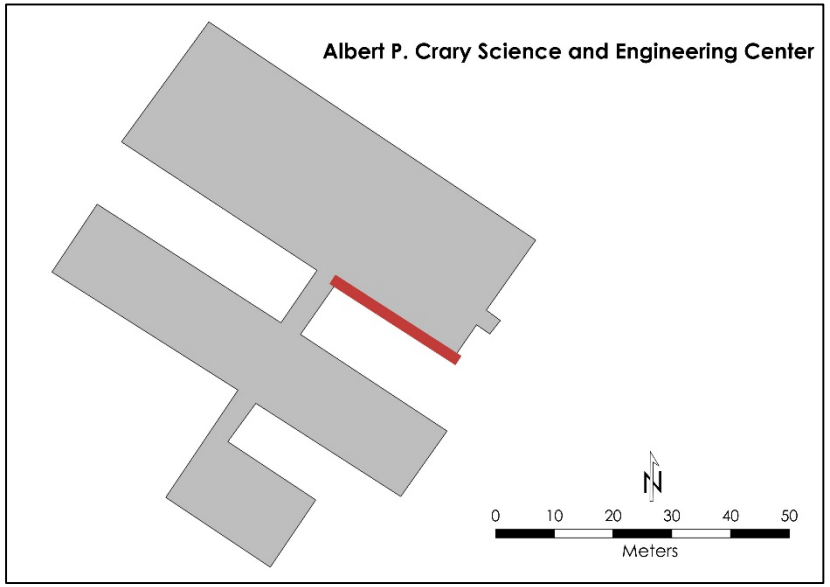
P1SE-V-01 -15◦C 5◦C

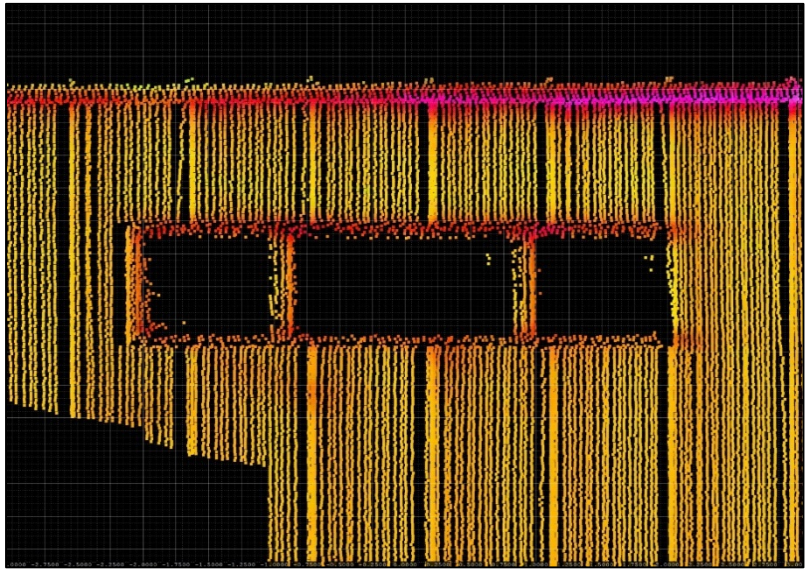


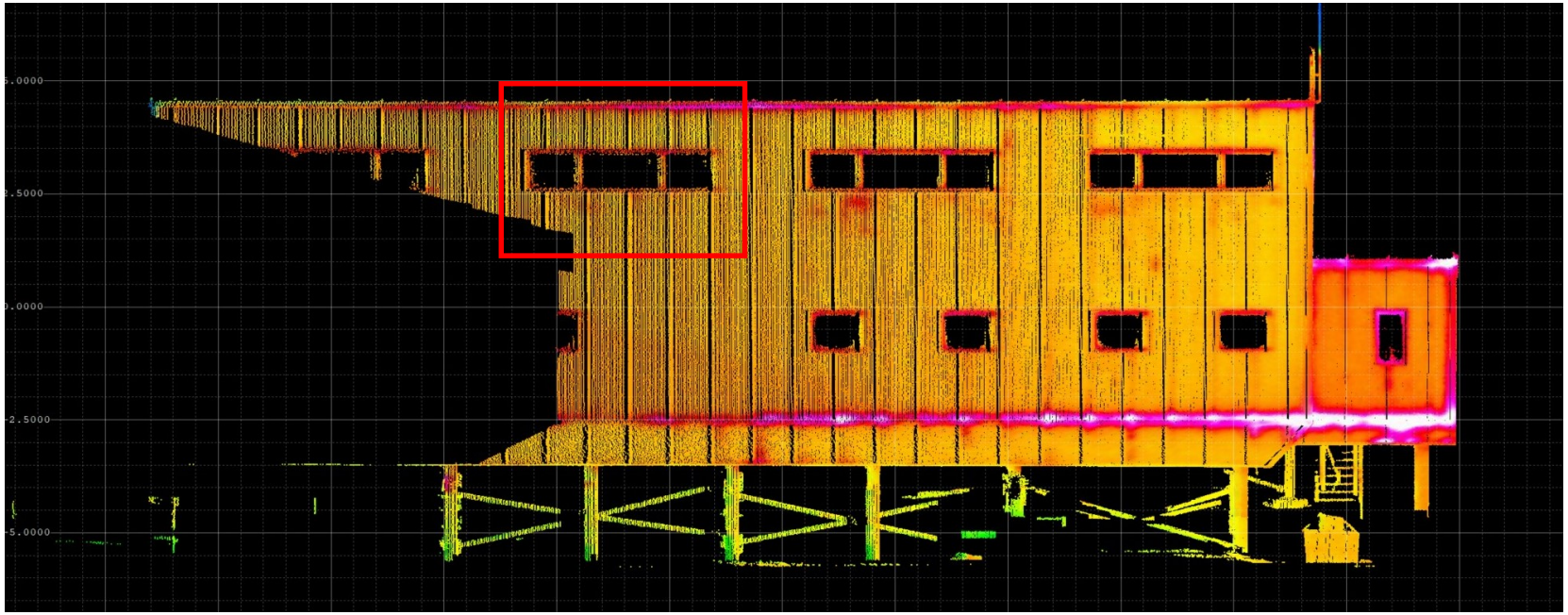




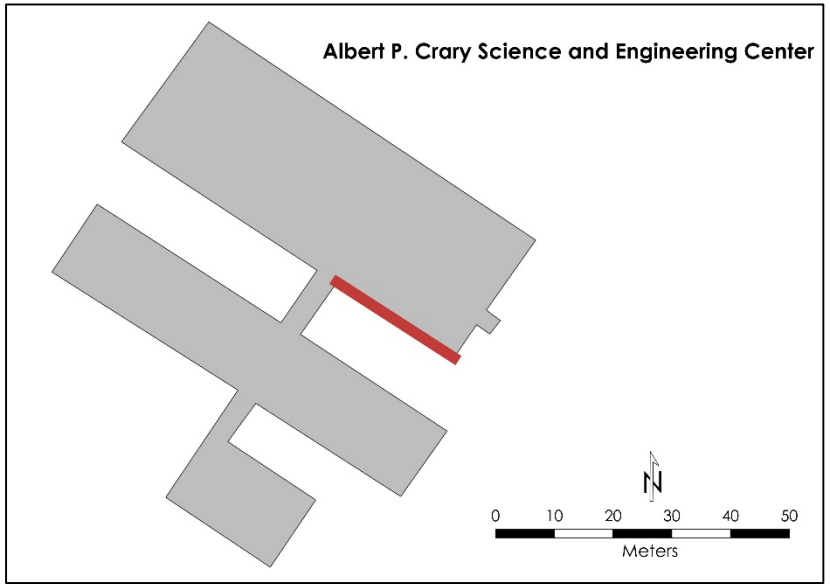
P1SE-W-03 -15◦C 5◦C

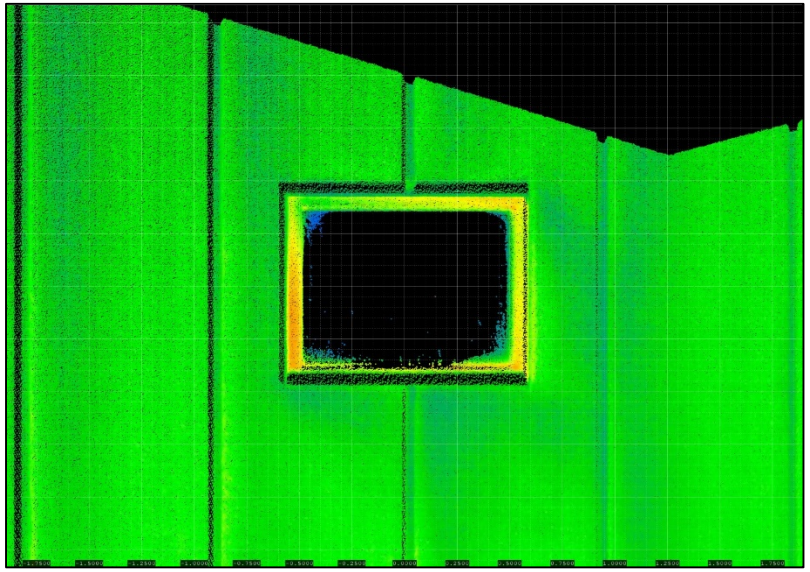


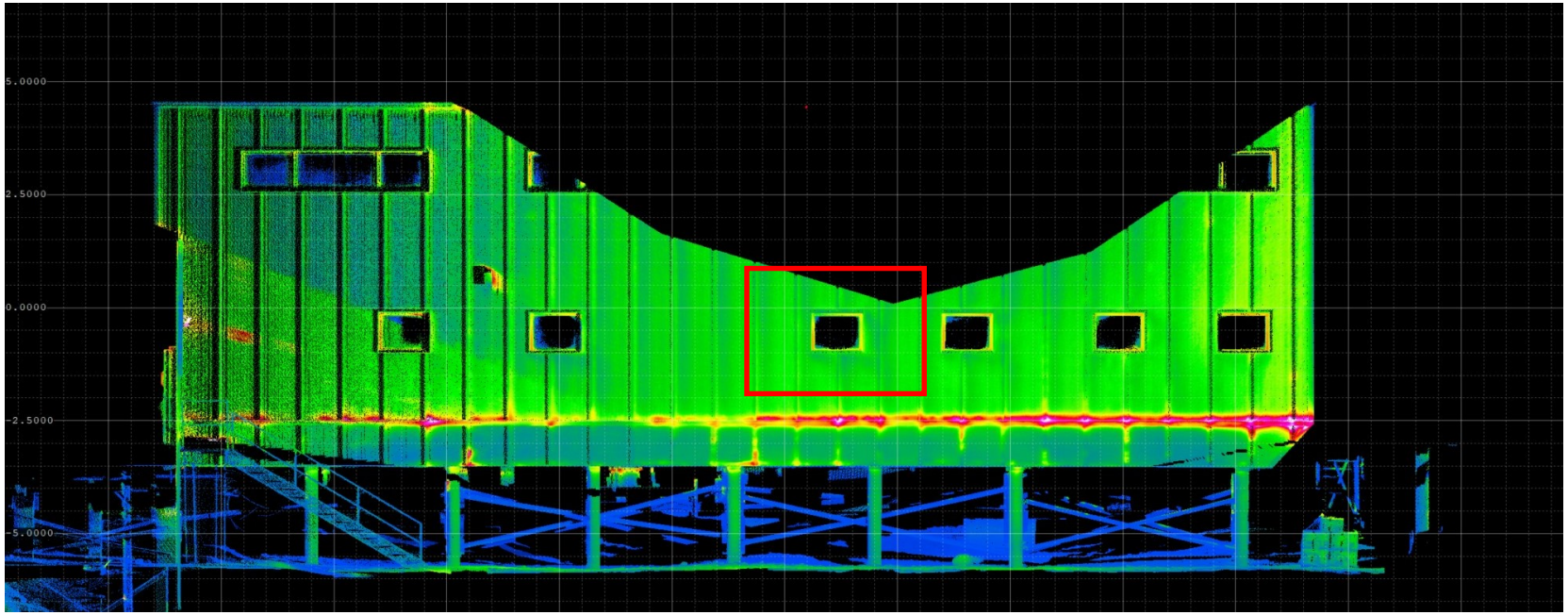




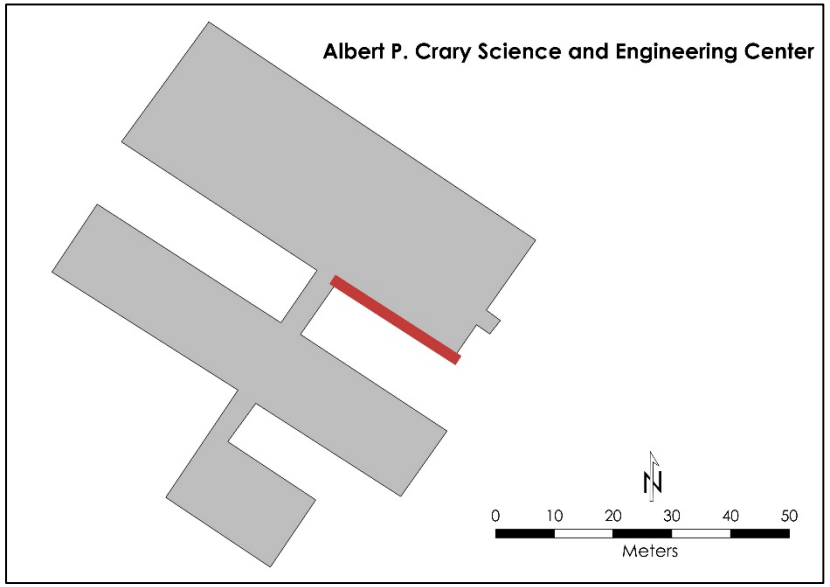
P1SE-W-04 -15◦C 5◦C

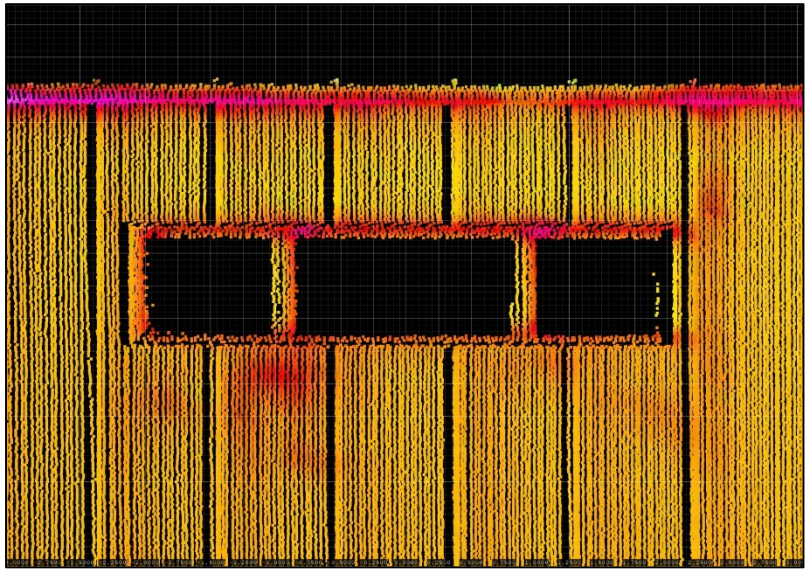


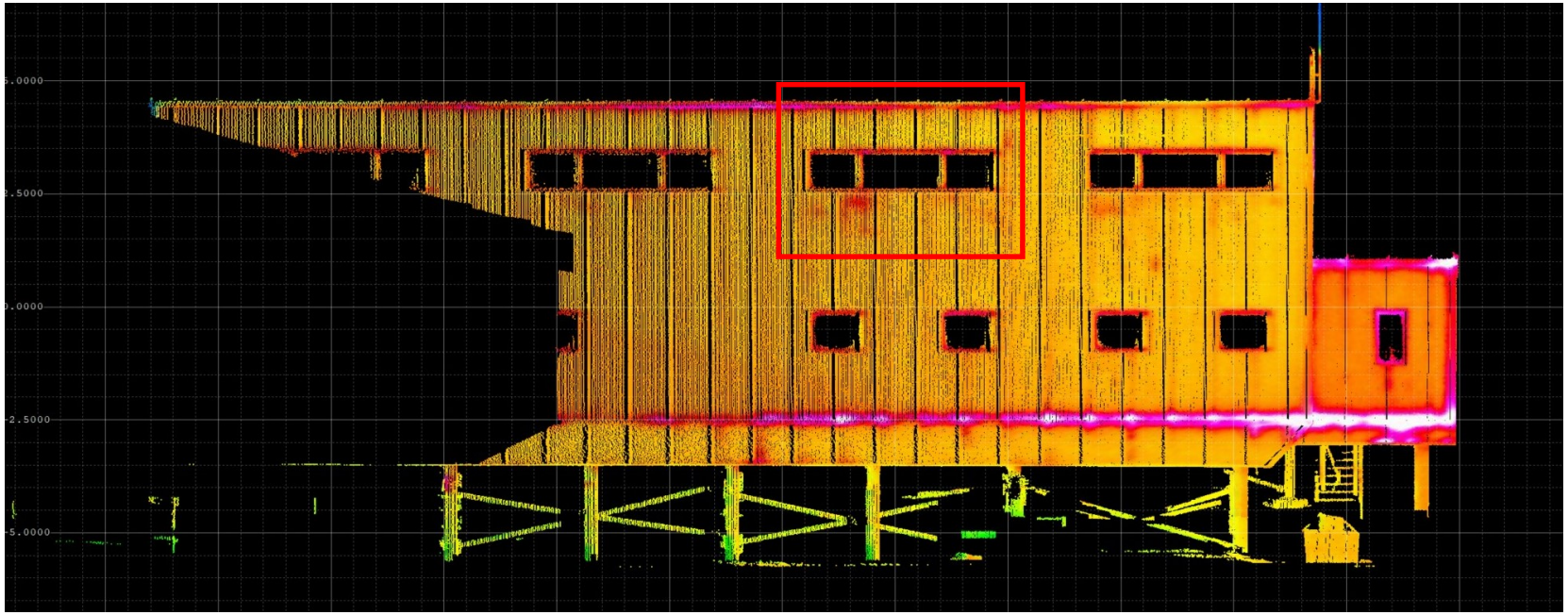




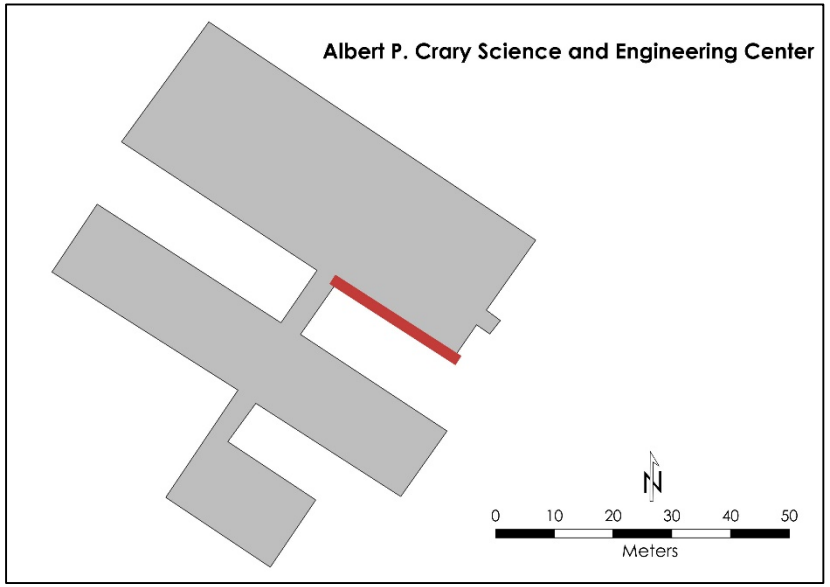
P1SE-W-05 -15◦C 5◦C

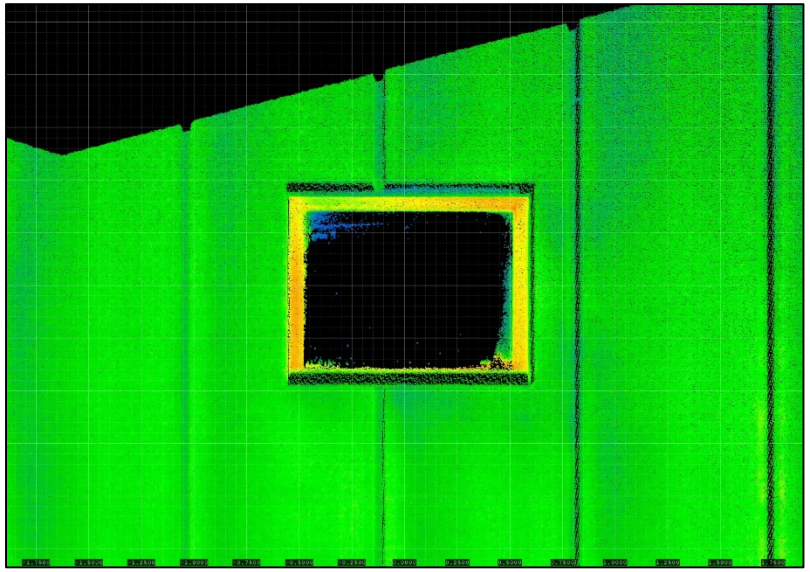


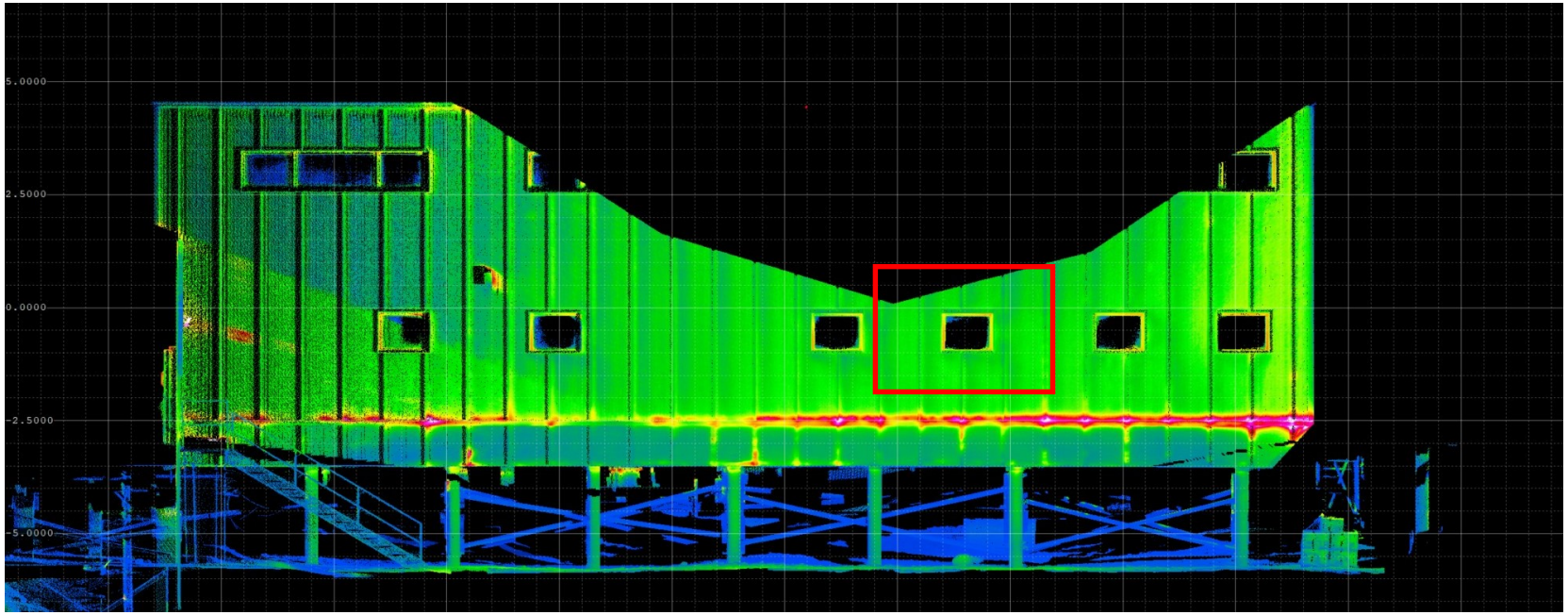




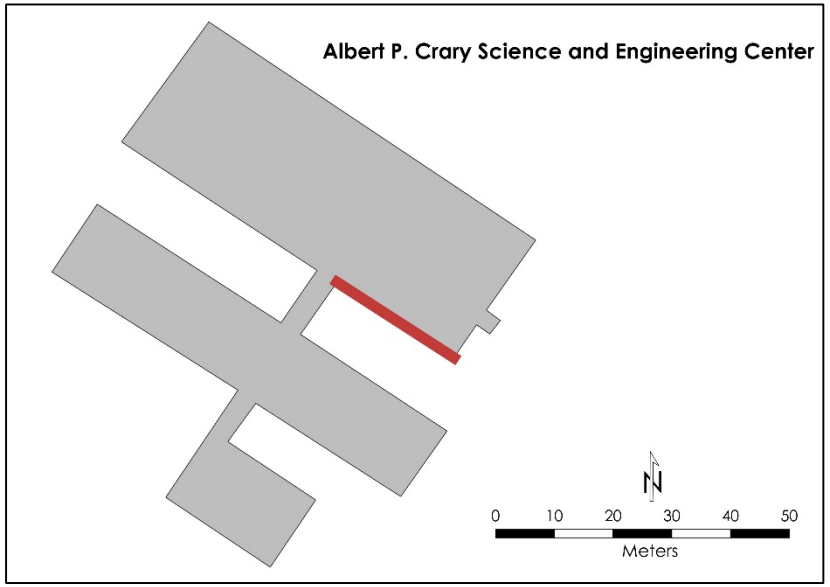
P1SE-W-06 -15◦C 5◦C

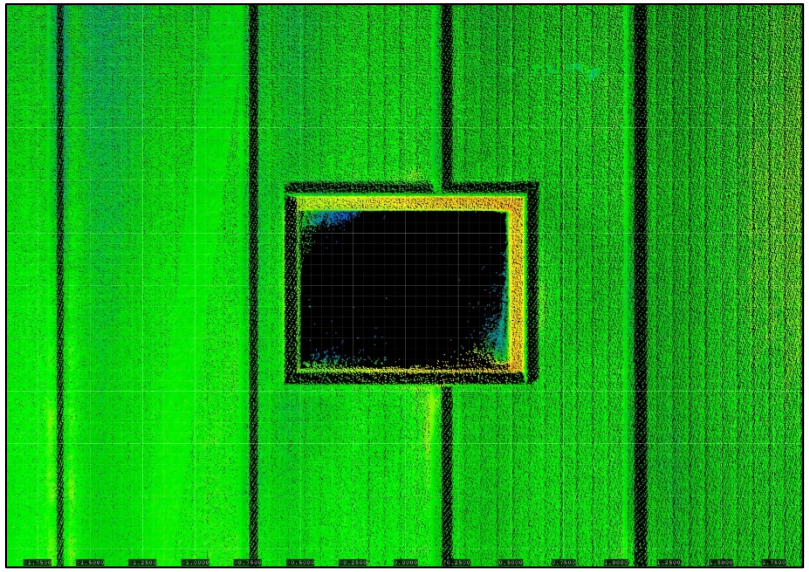


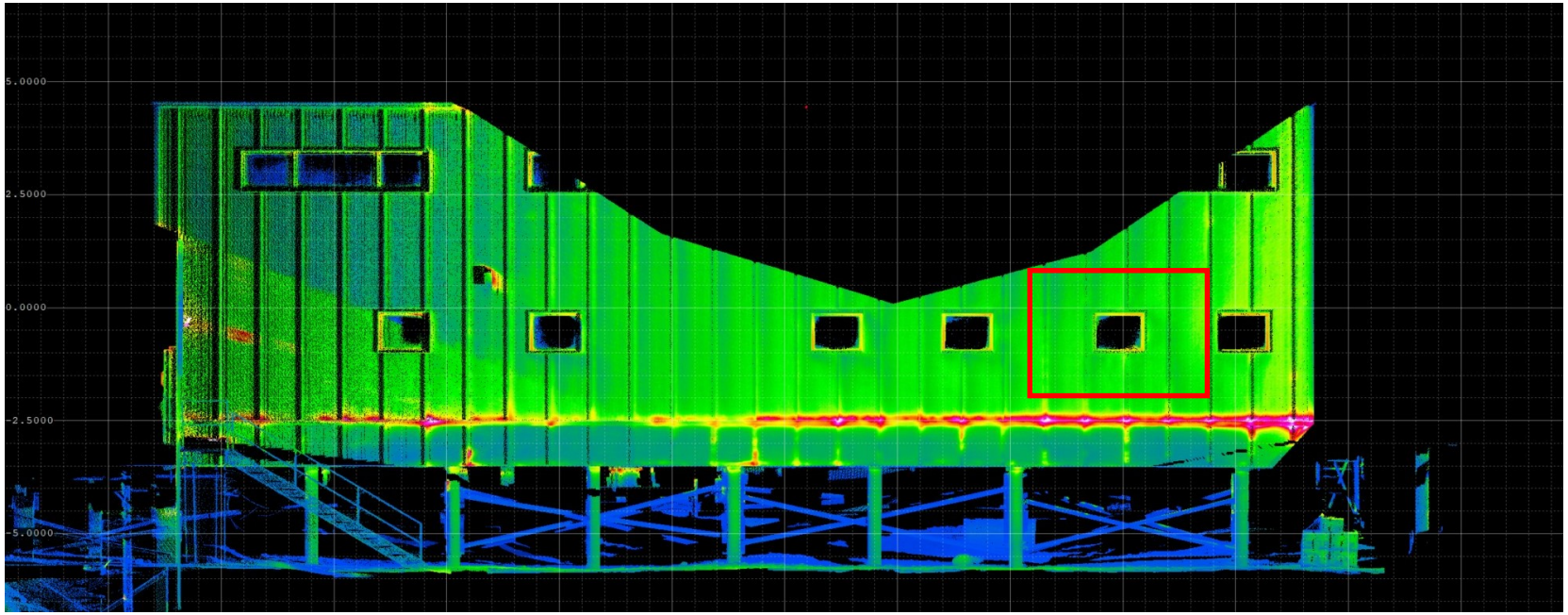




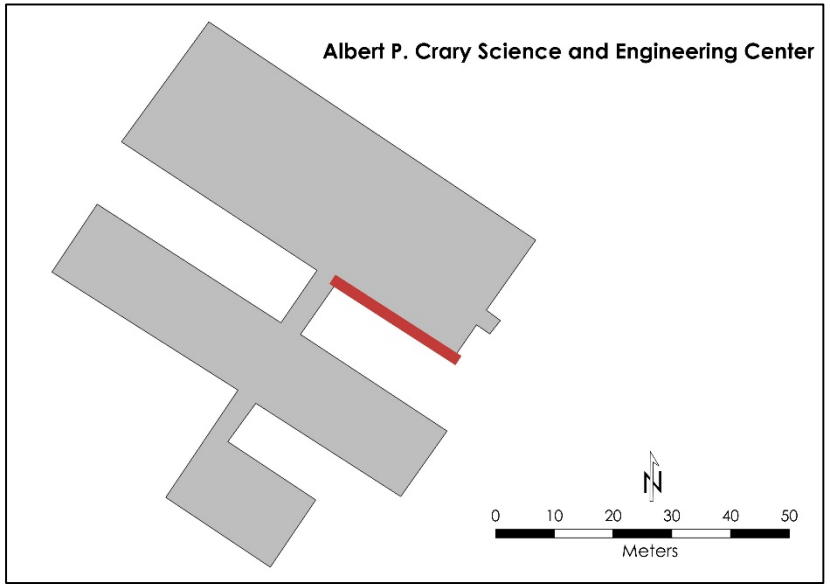
P1SE-W-07 -15◦C 5◦C

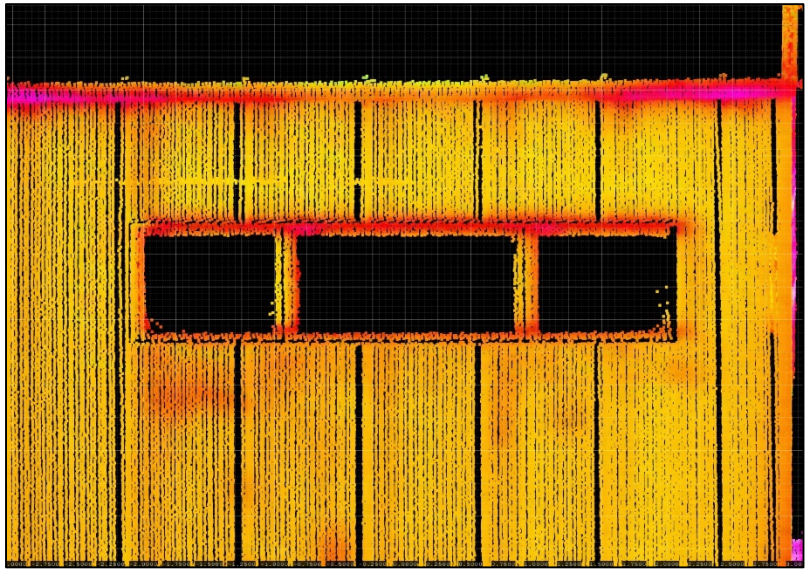


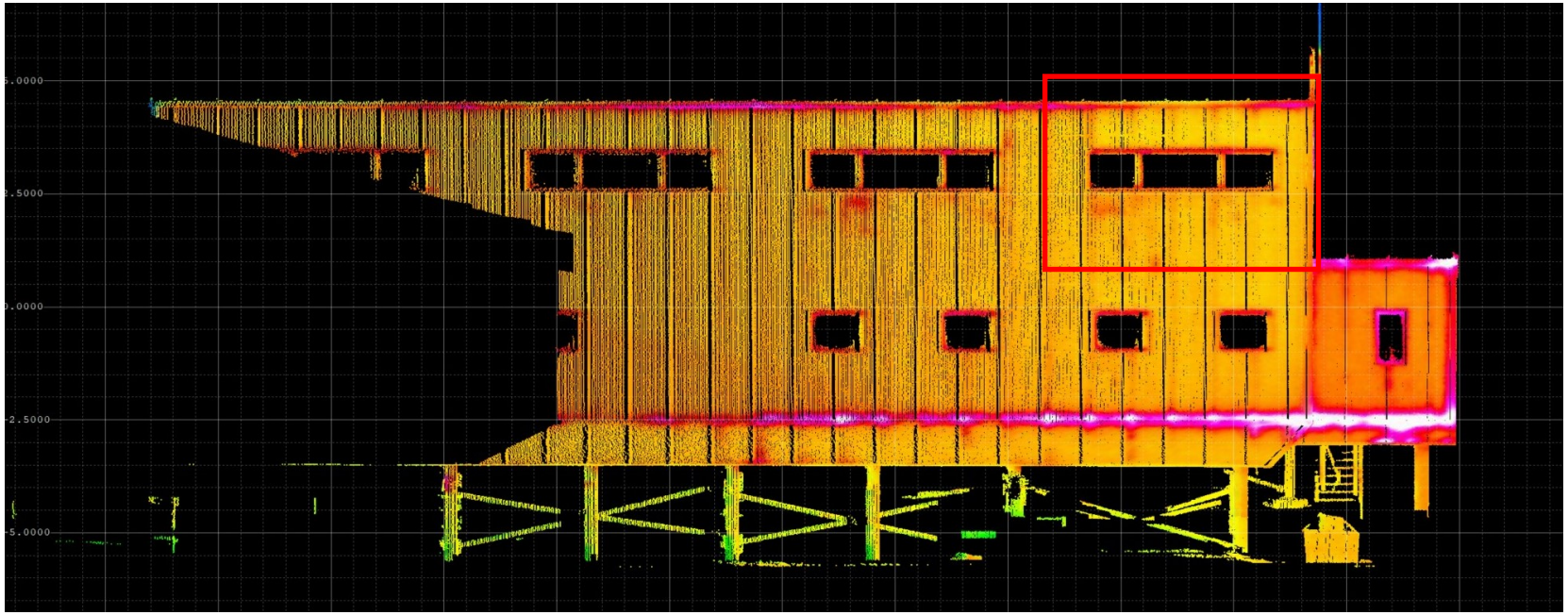




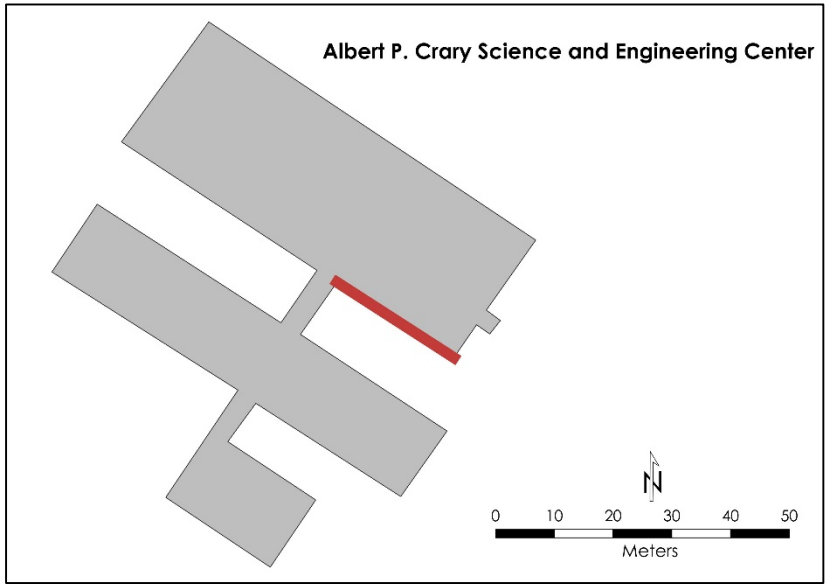
P1SE-W-08 -15◦C 5◦C

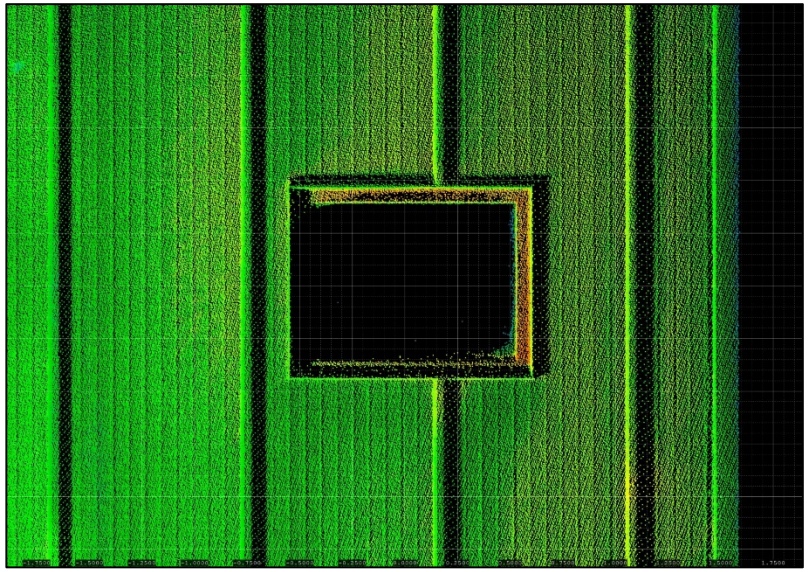


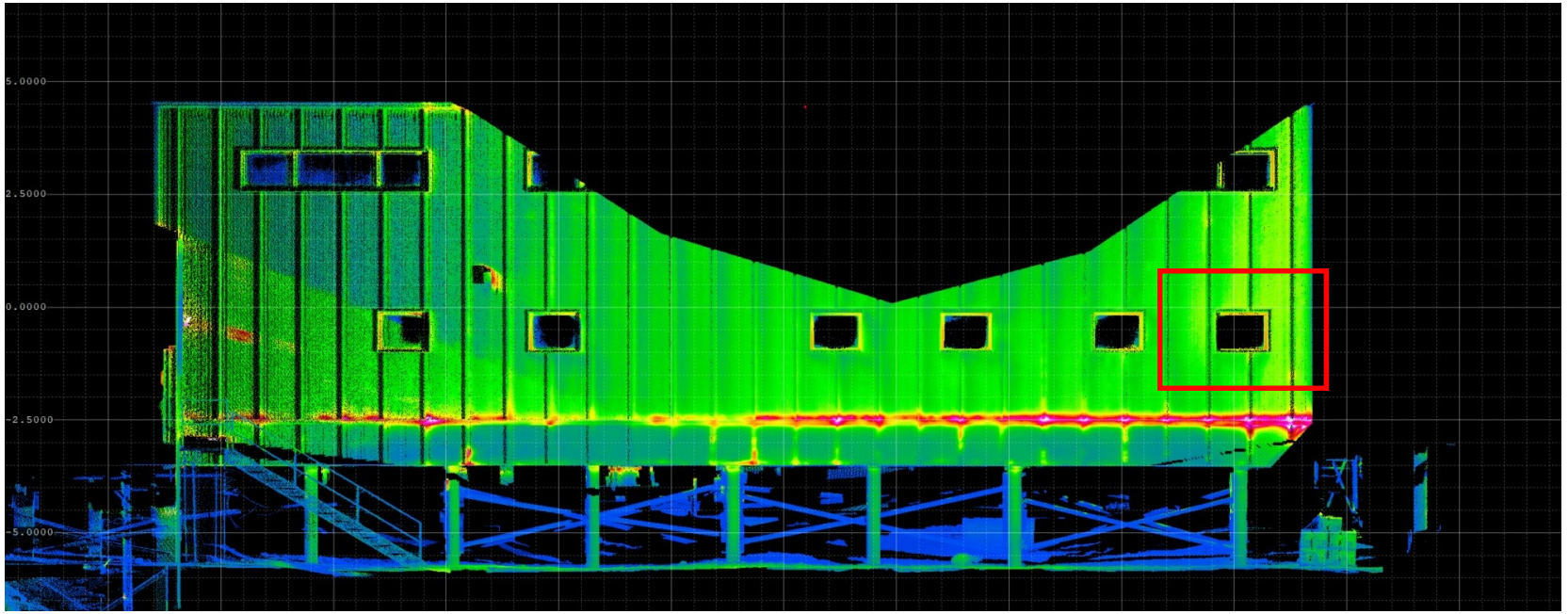




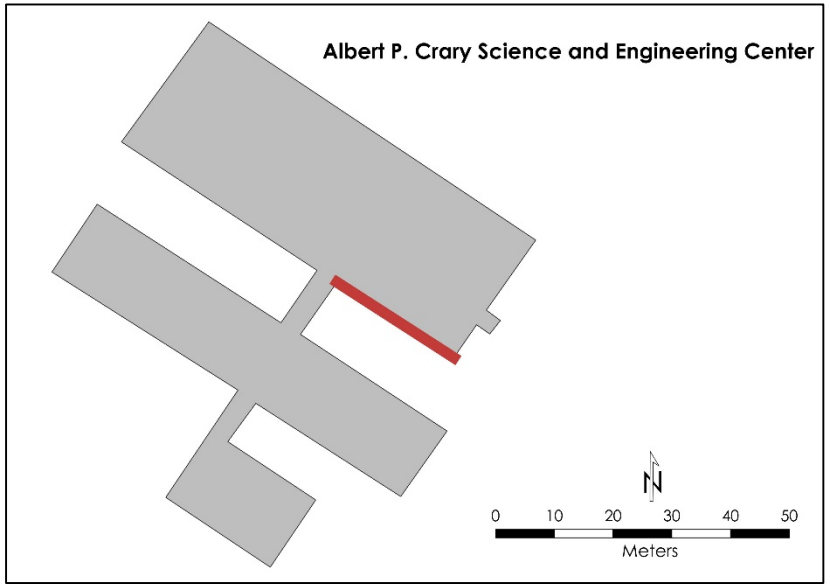
P1SE-W-09 -15◦C 5◦C

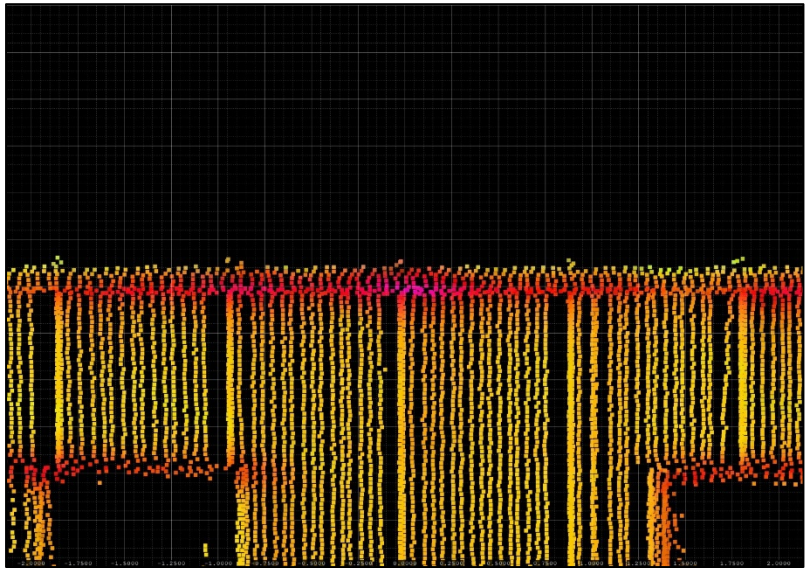


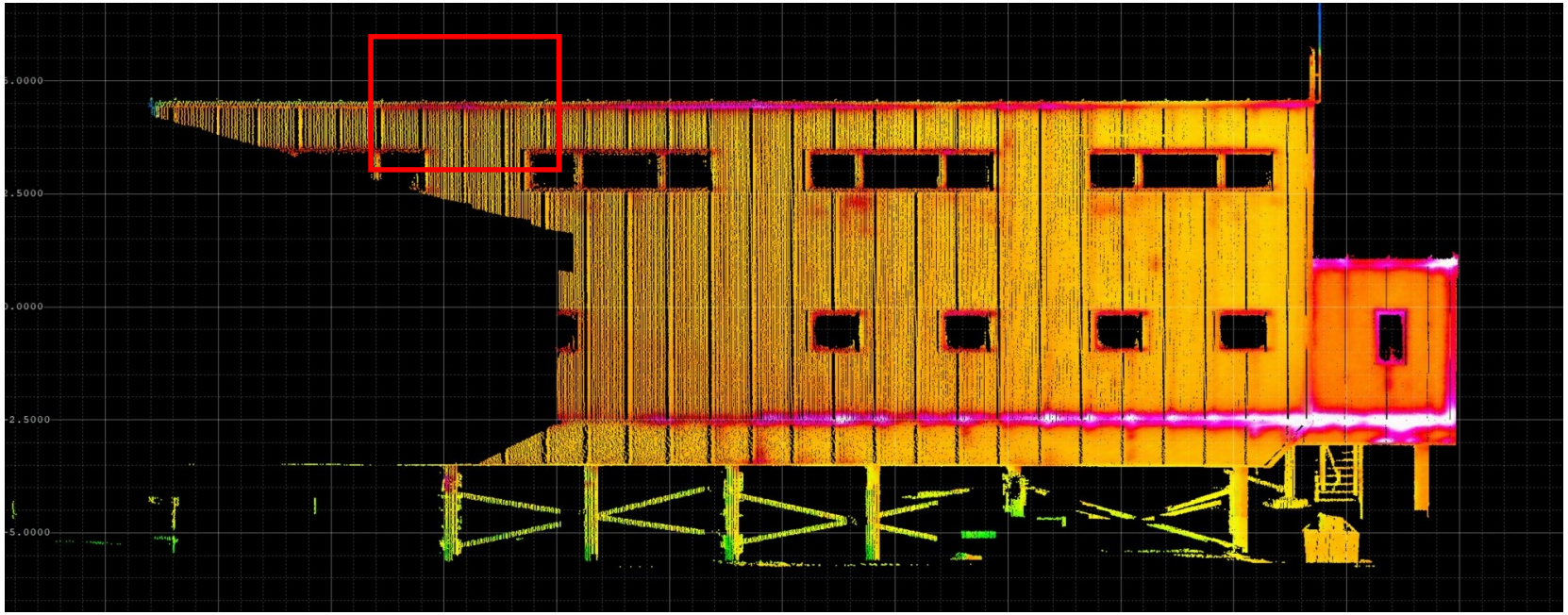




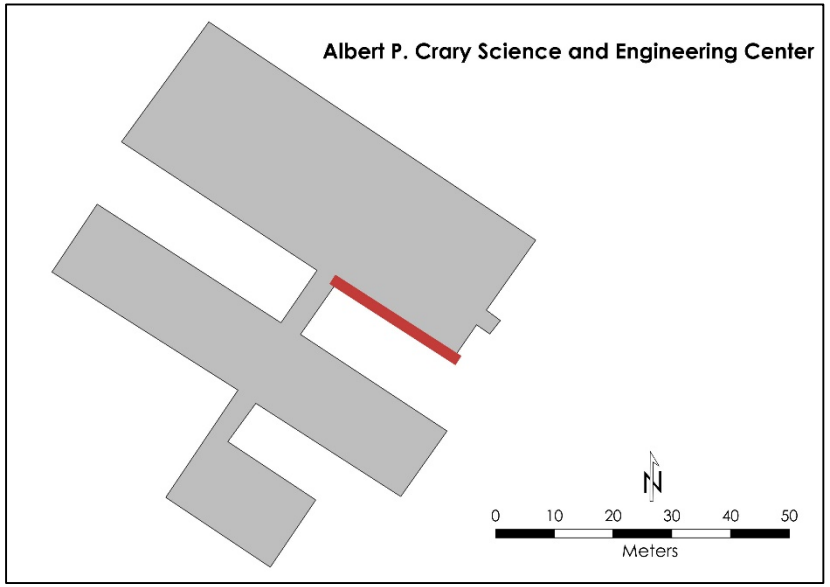
P1SE-W-10 -15◦C 5◦C

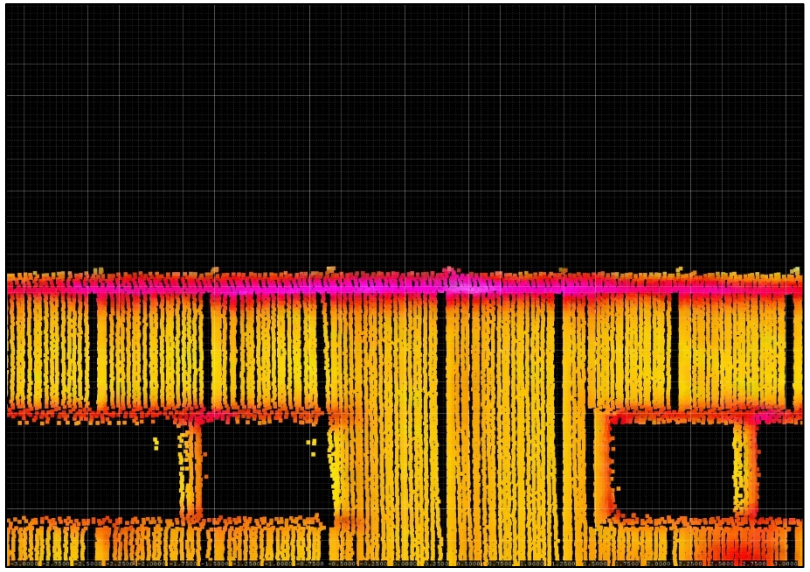


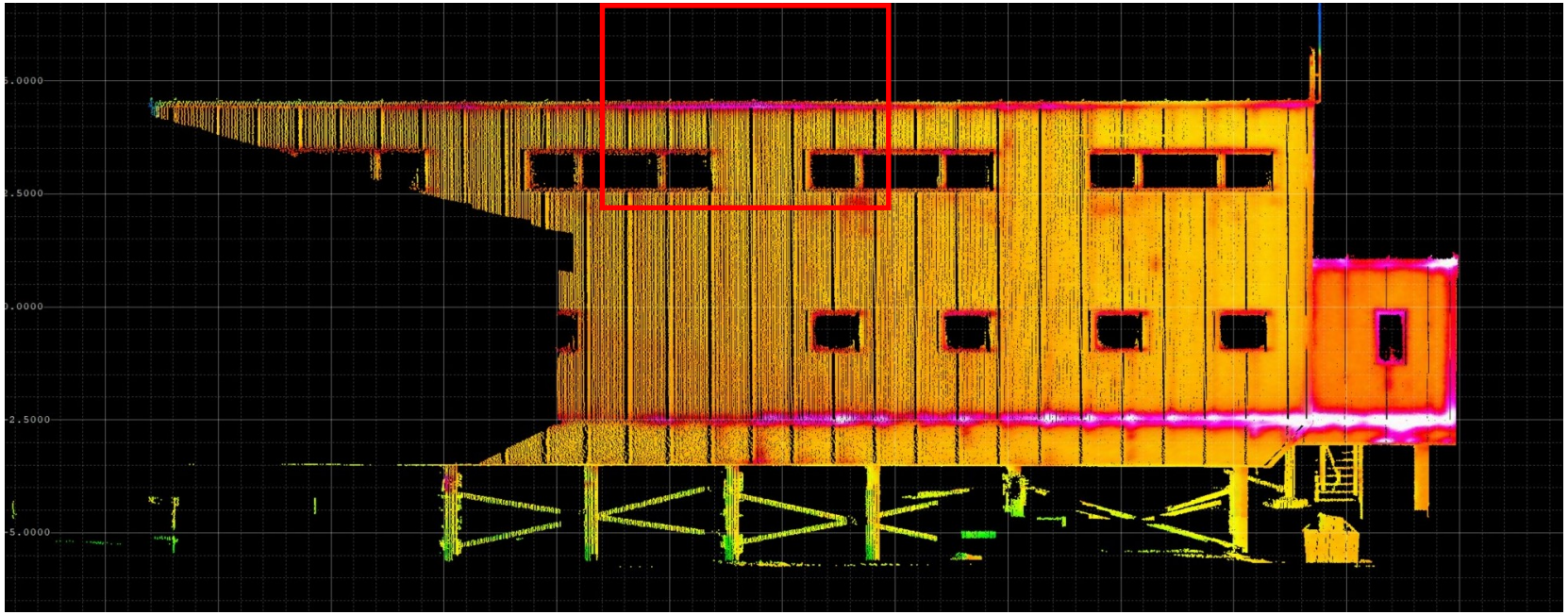




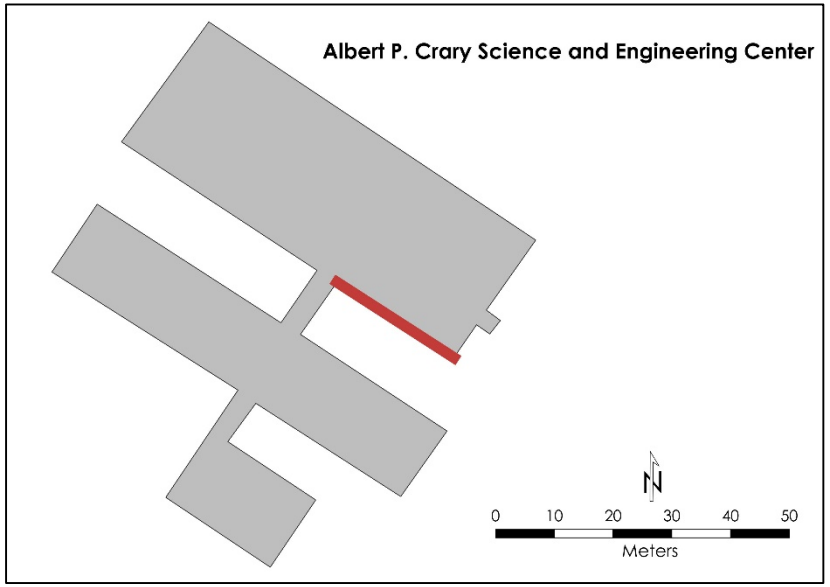
P1SE-TA-01 -15◦C 5◦C

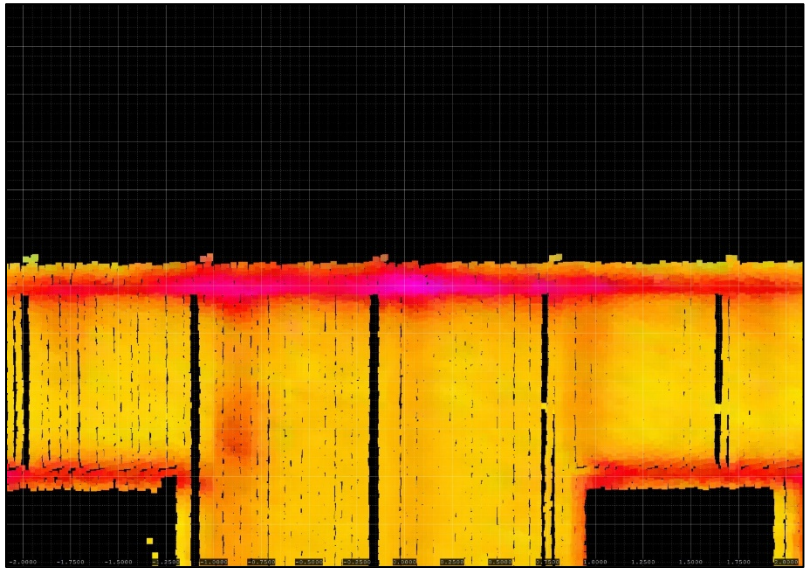


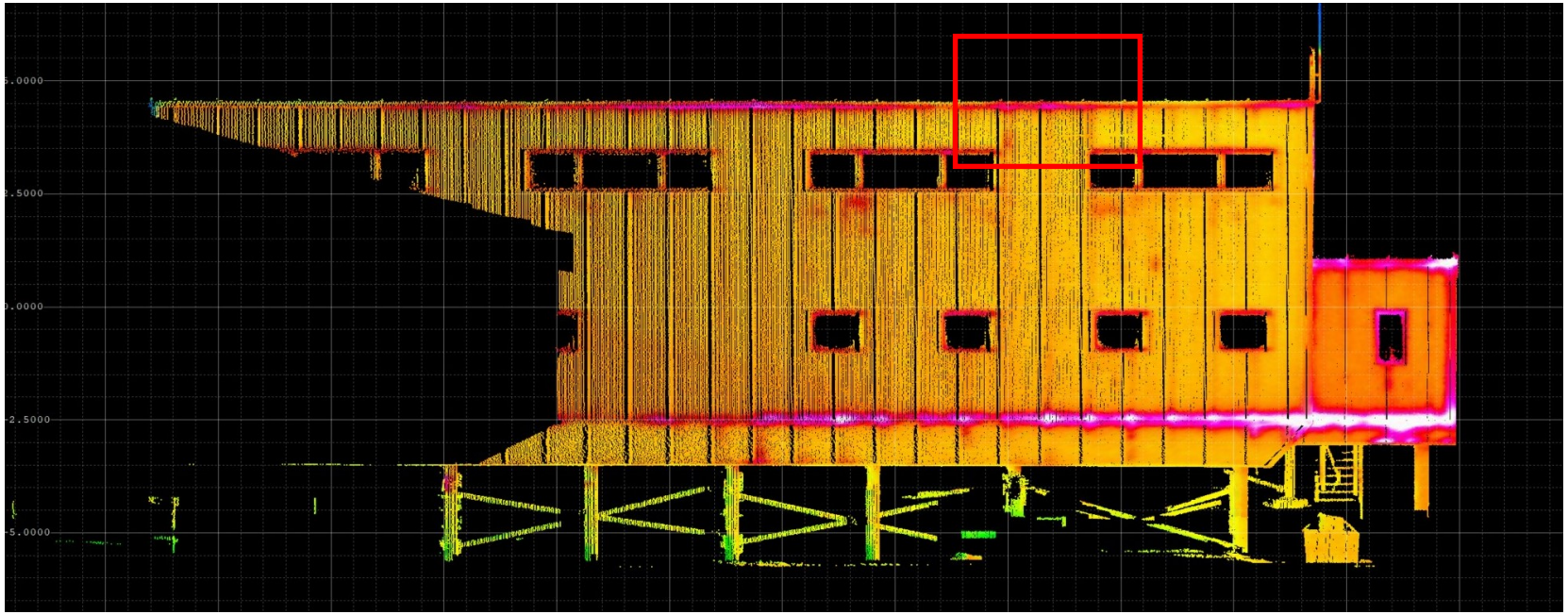




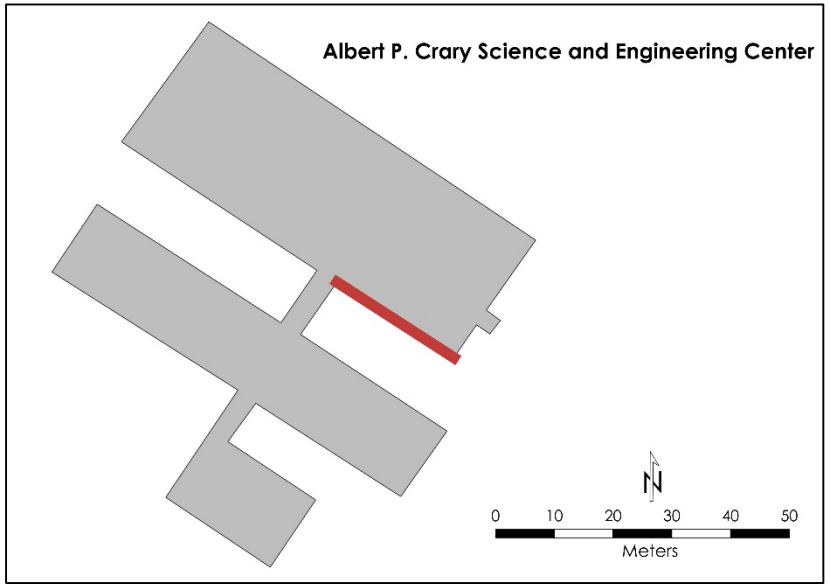
P1SE-TA-02 -15◦C 5◦C

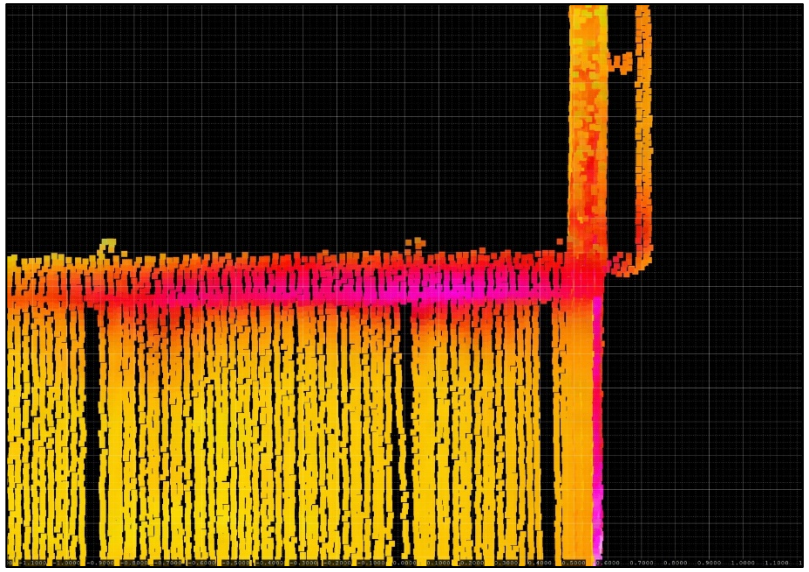


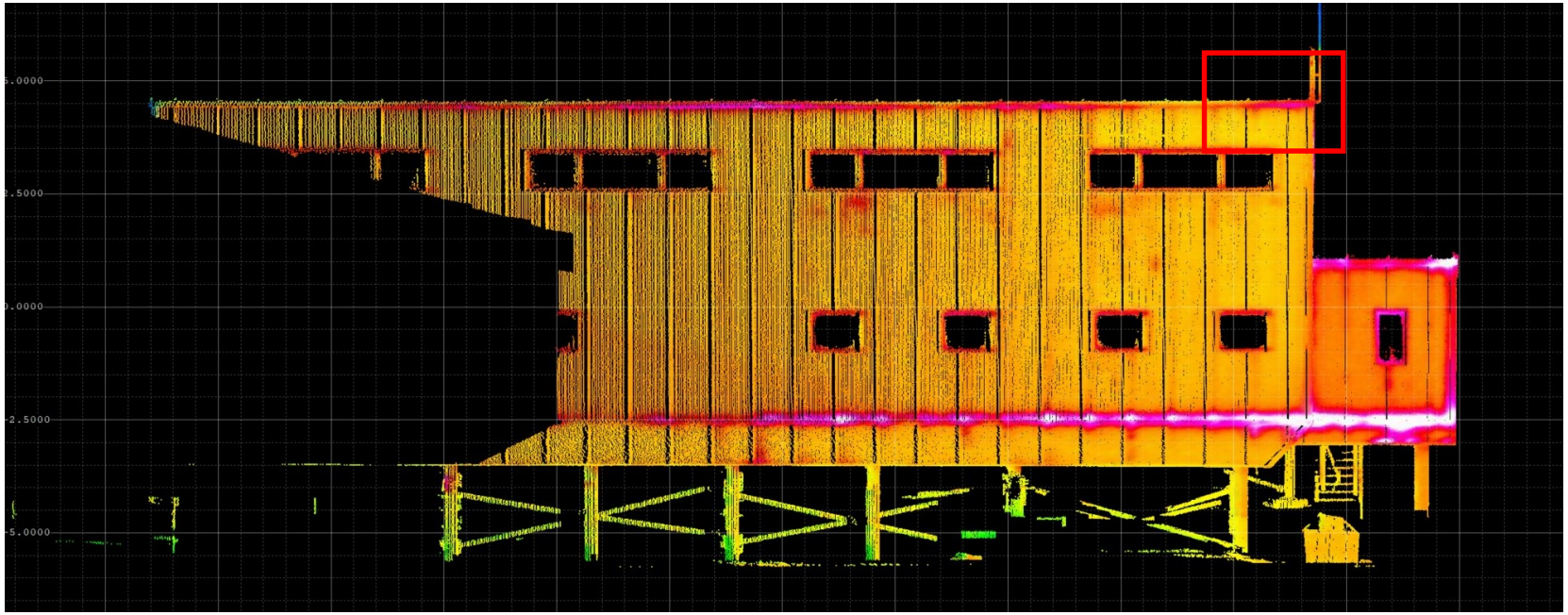




P1SE-TA-03 -15◦C 5◦C





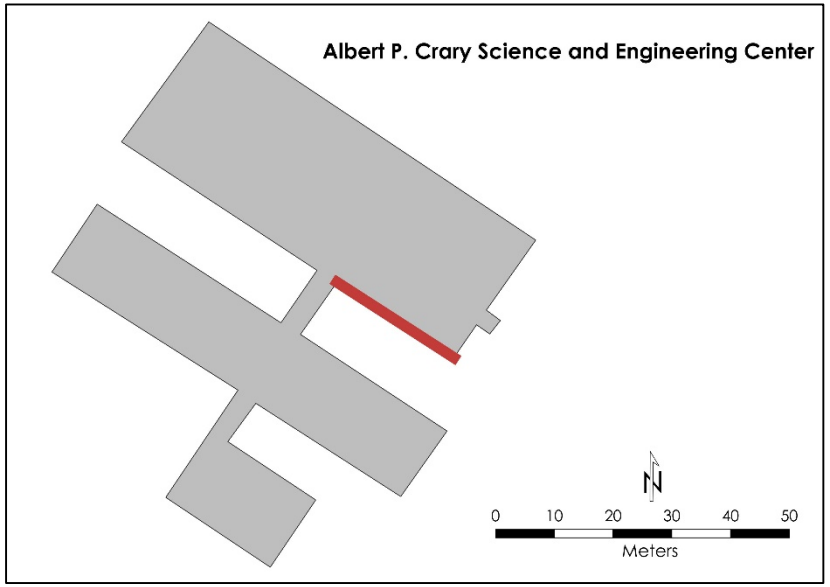


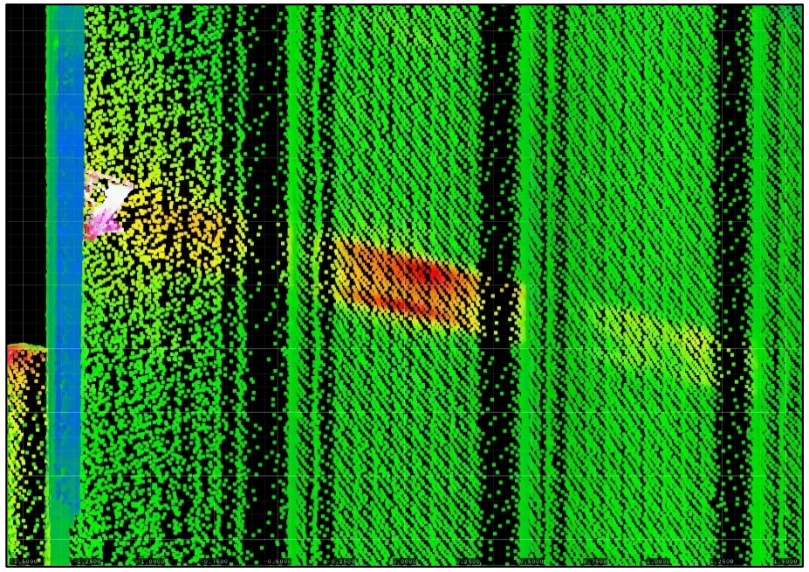
P1SE-TA-04

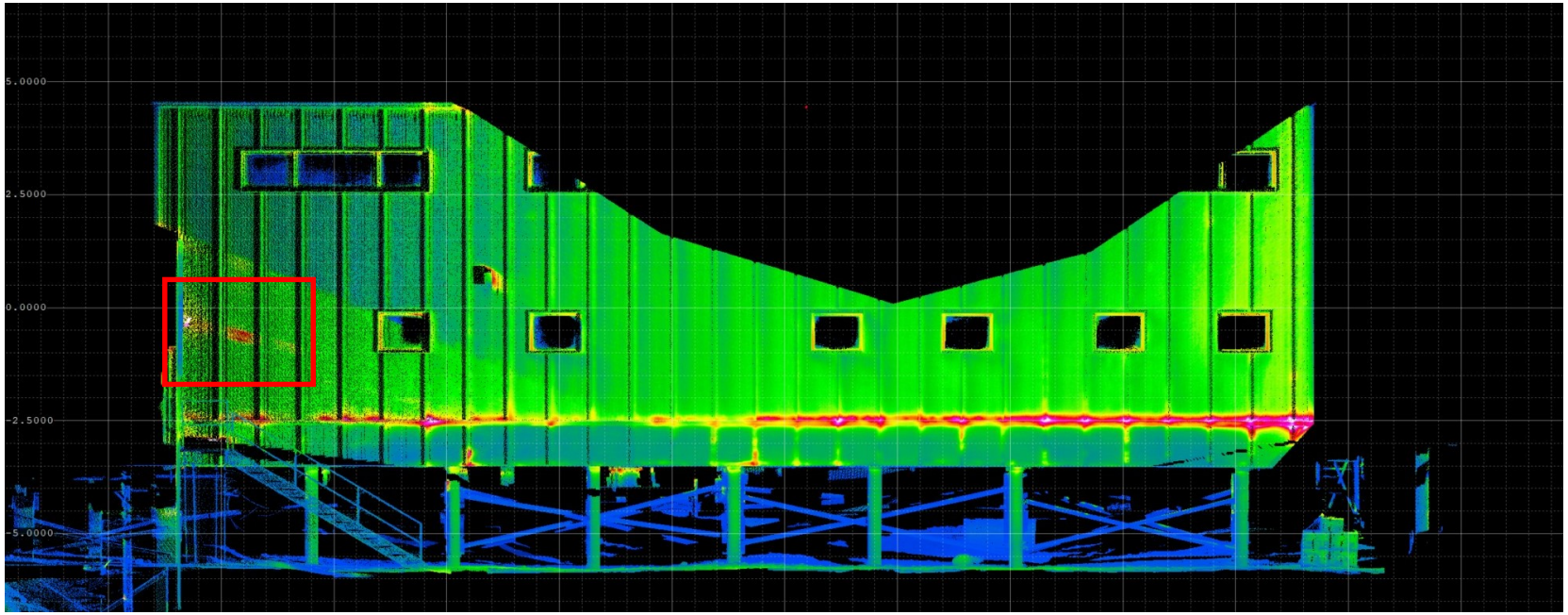
-15◦C



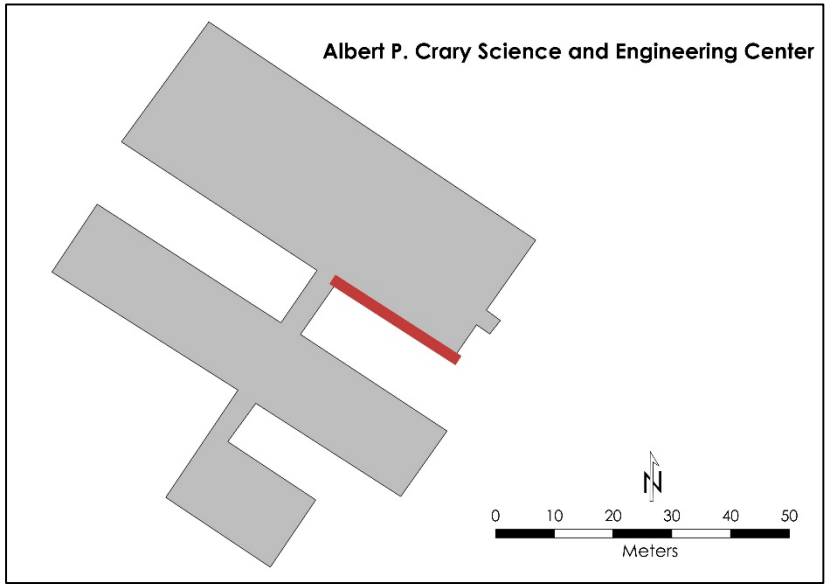
5◦C

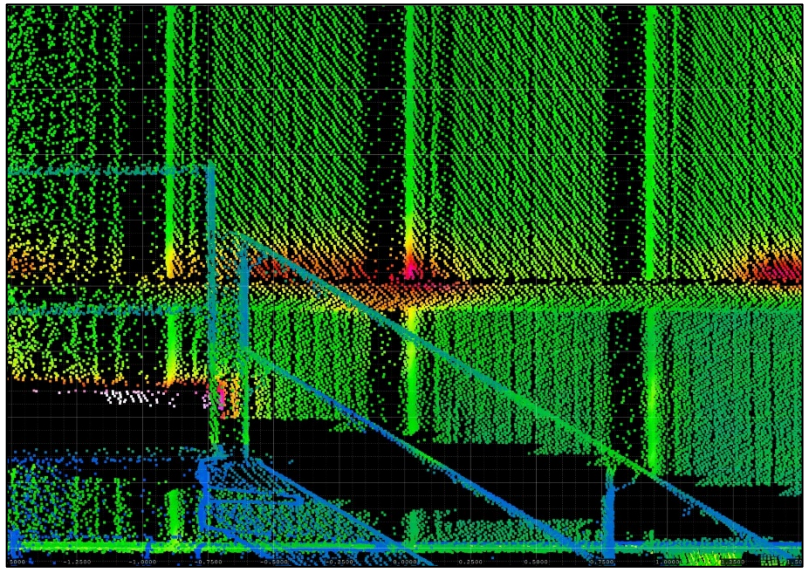


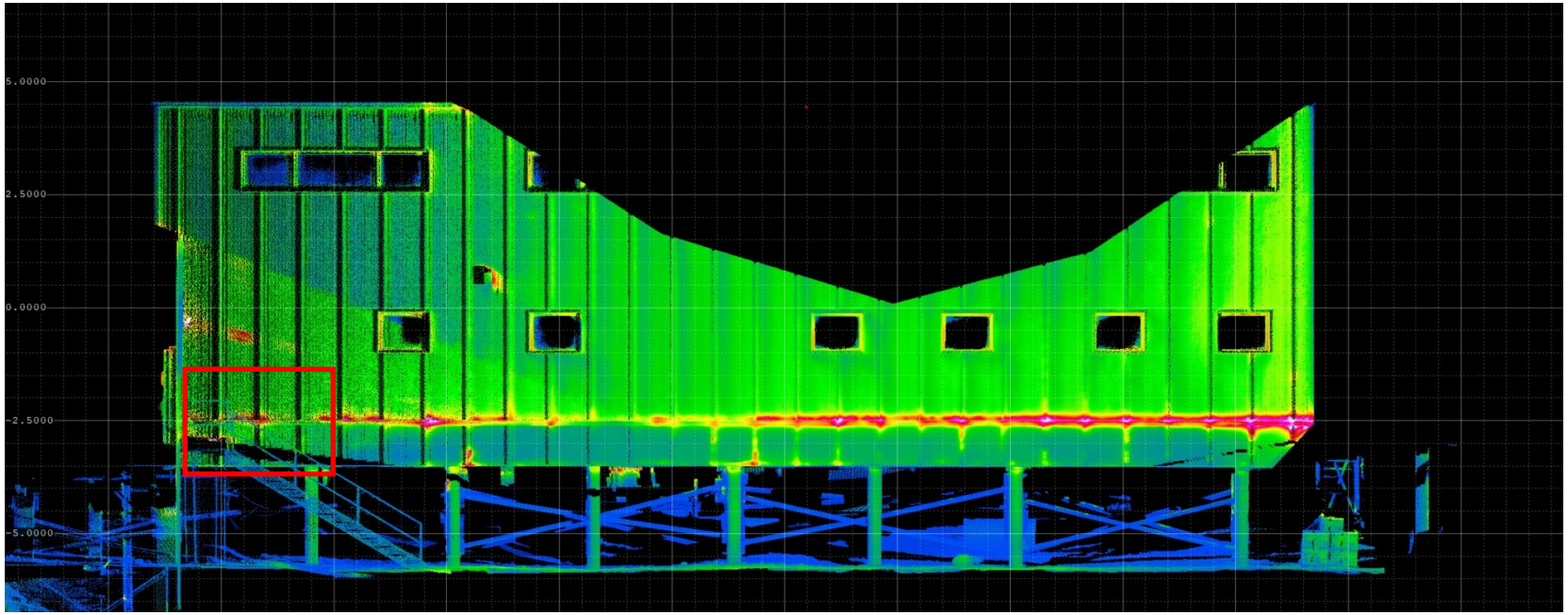




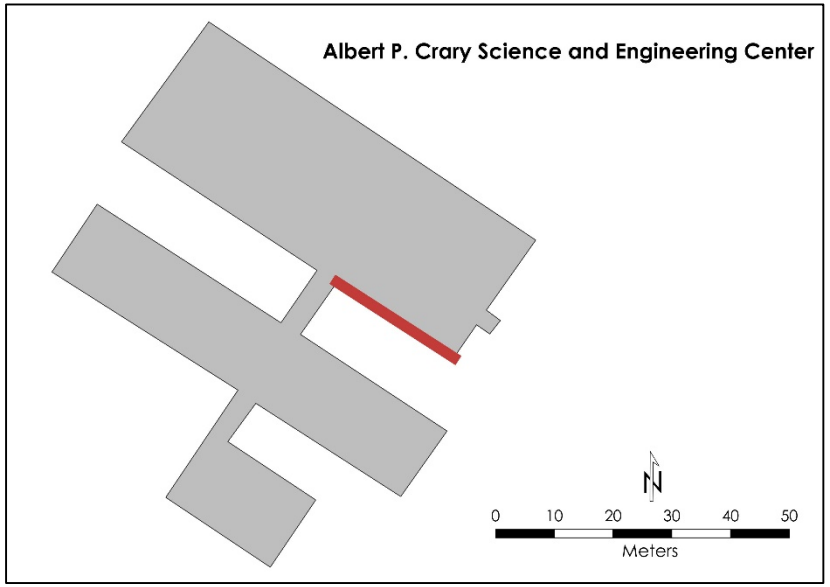
P1SE-TA-05 -15◦C 5◦C

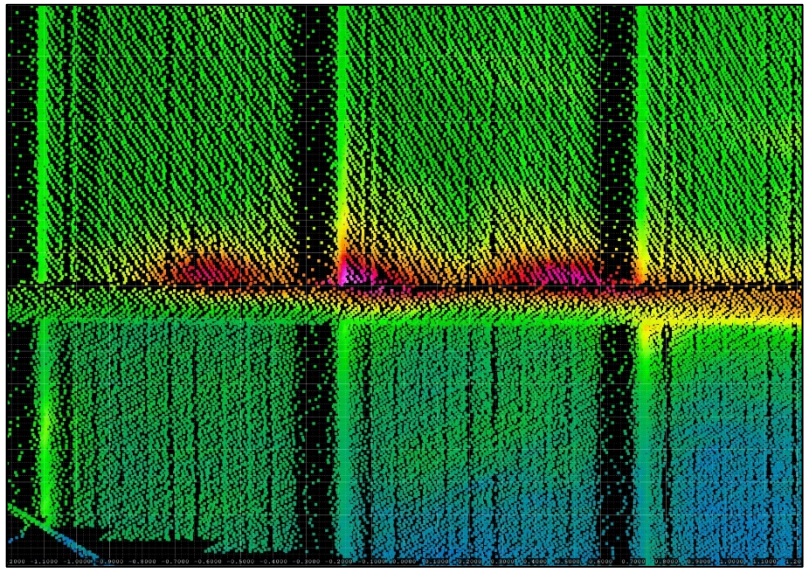


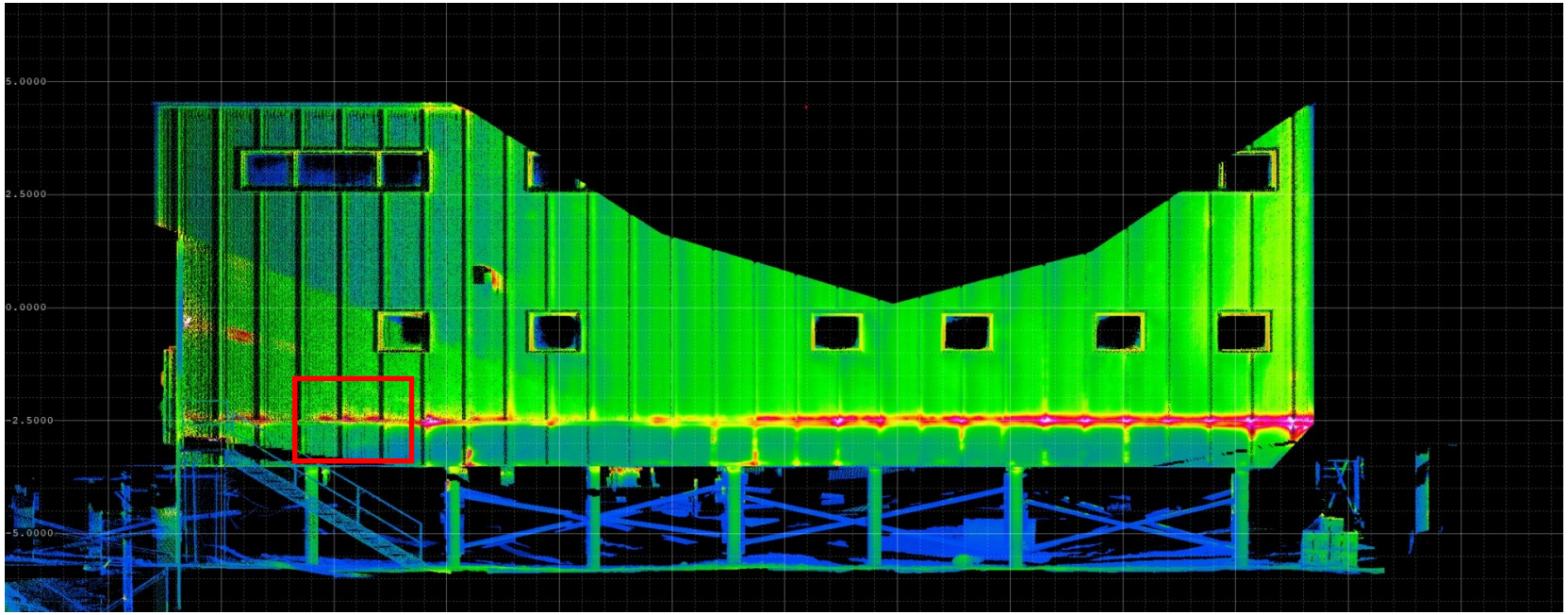




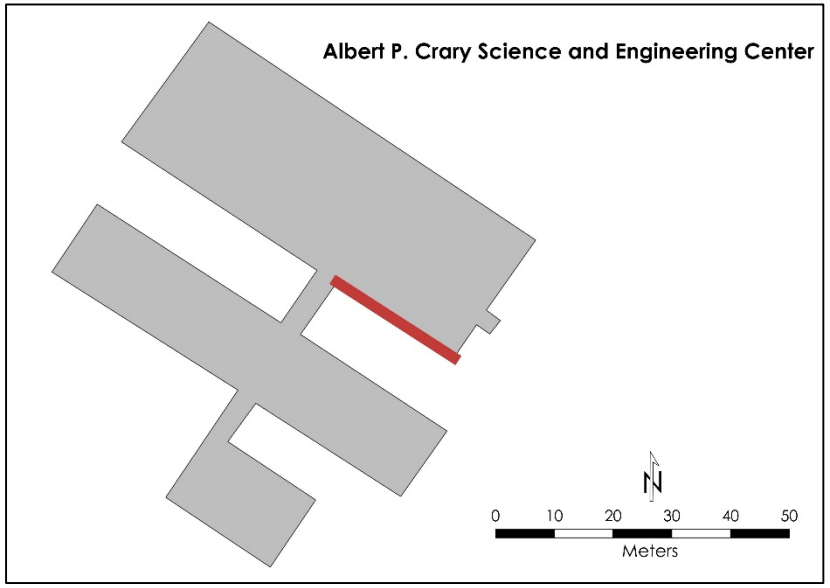
P1SE-TA-06 -15◦C 5◦C

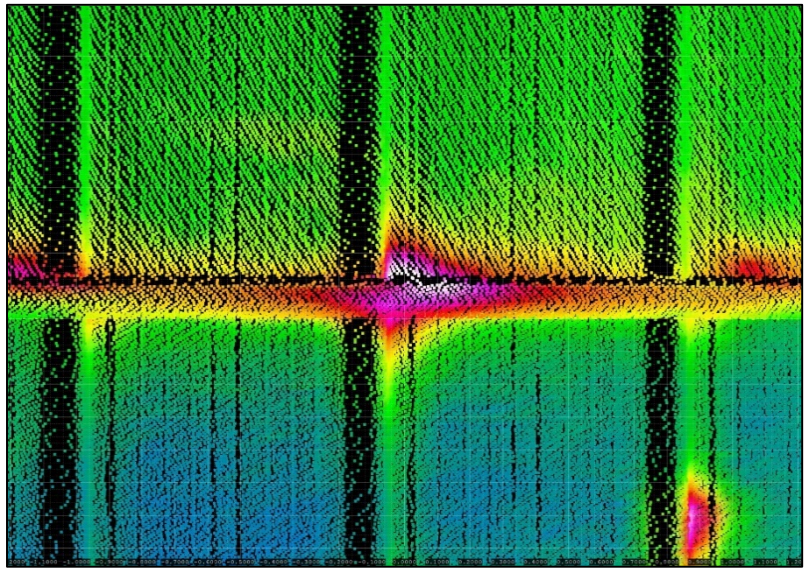


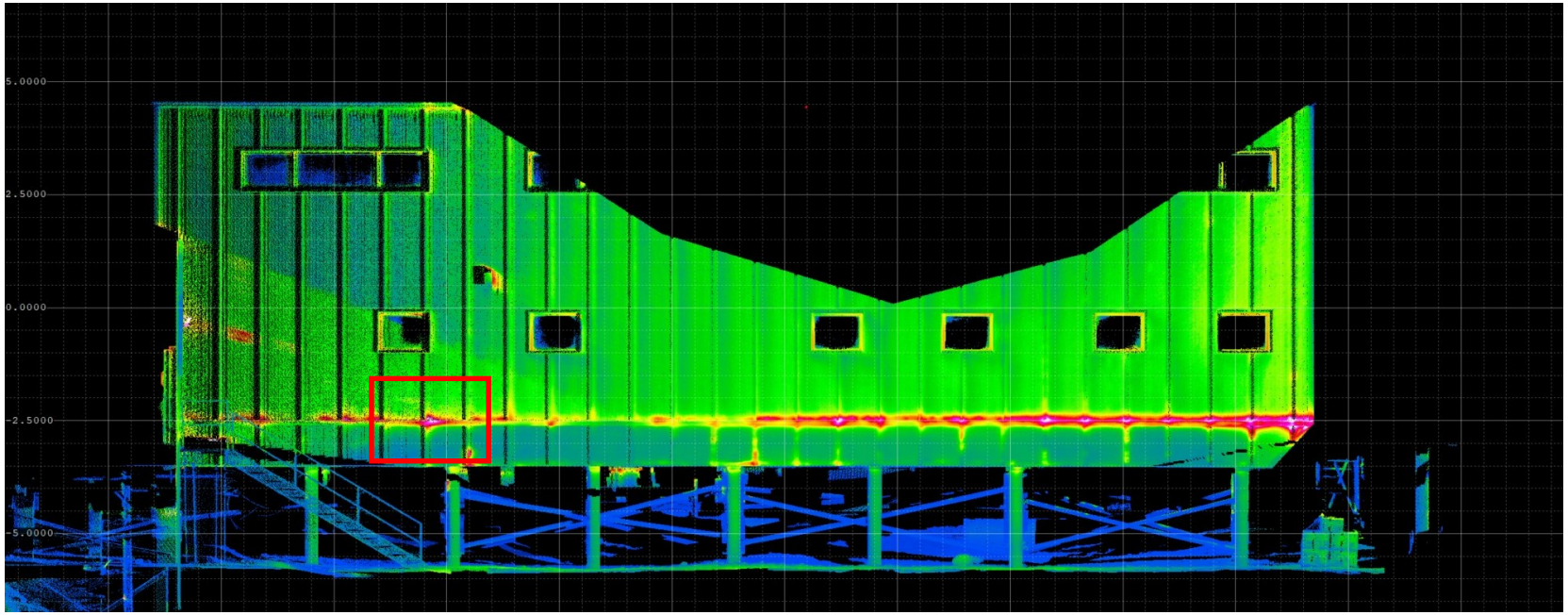




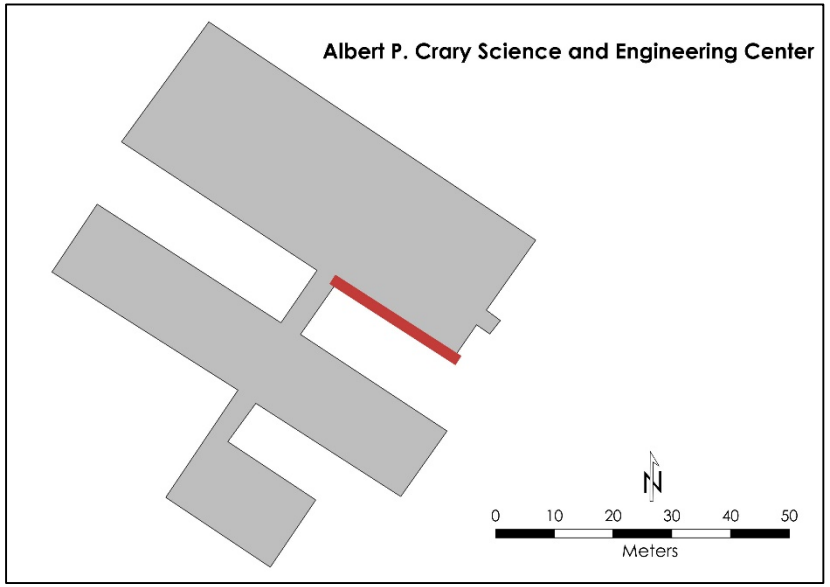
P1SE-TA-07 -15◦C 5◦C

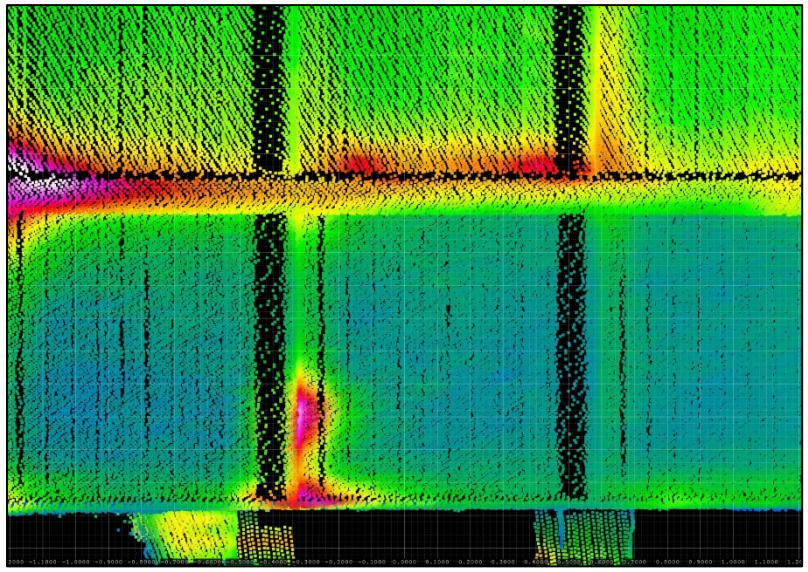


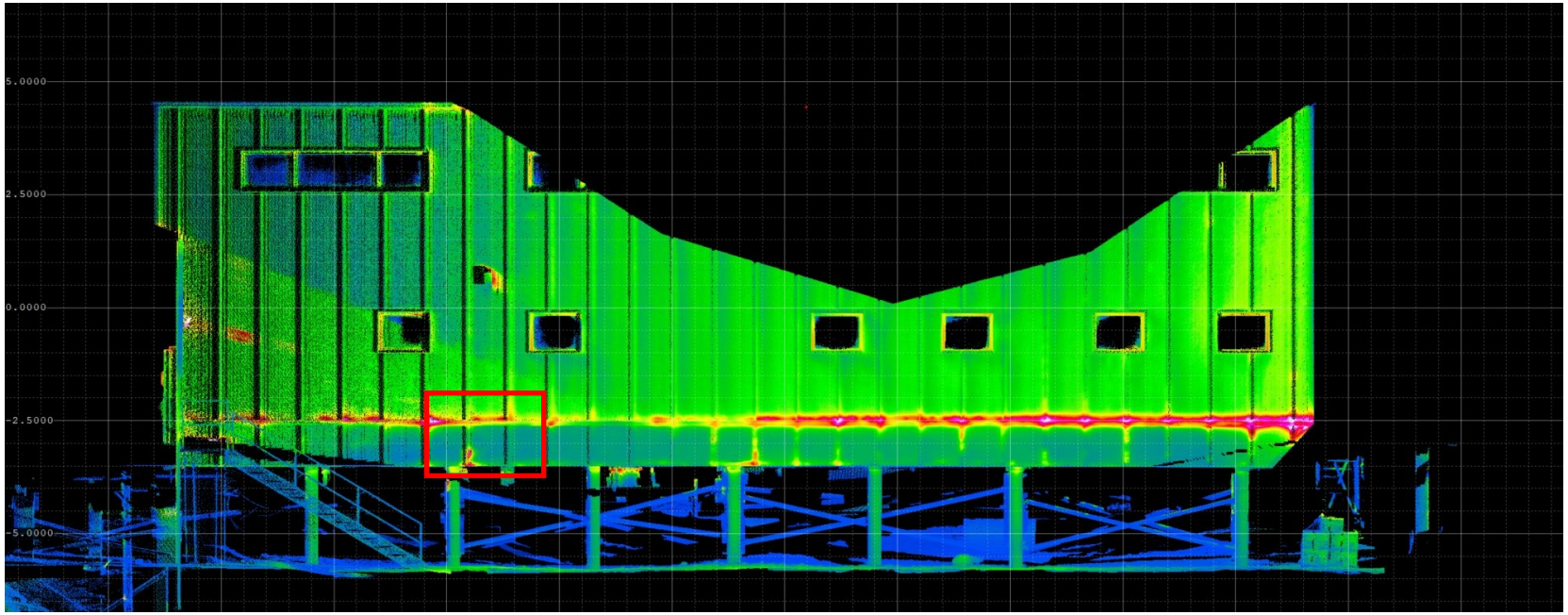




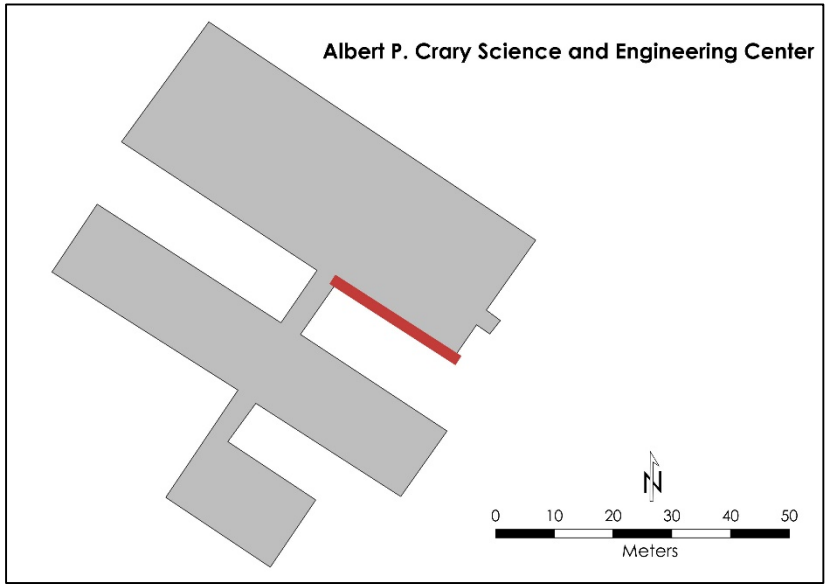
P1SE-TA-08 -15◦C 5◦C

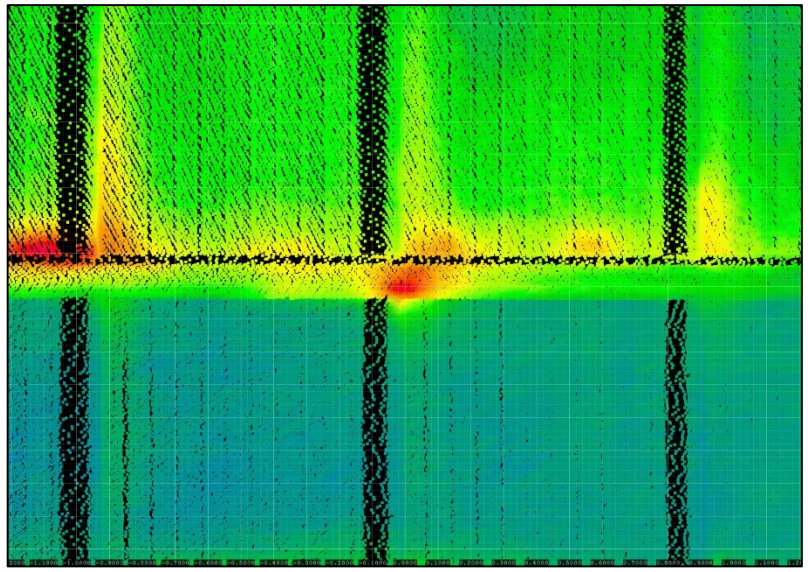


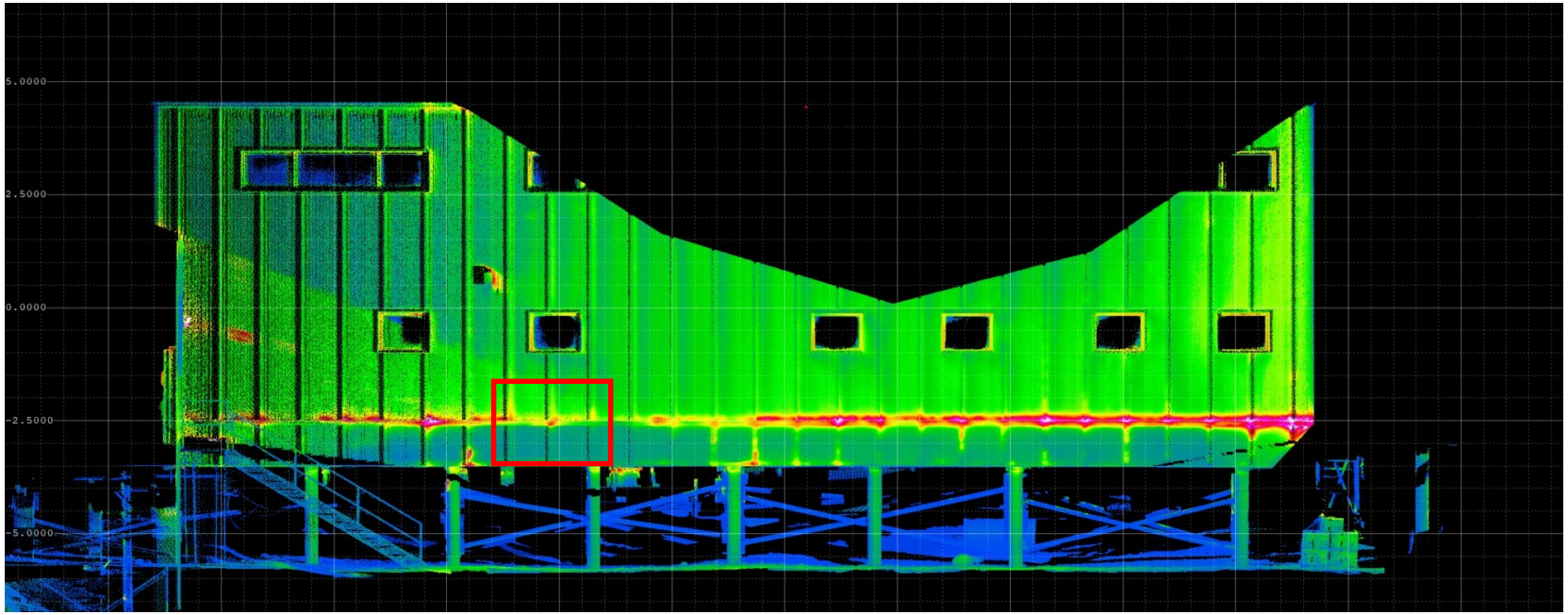




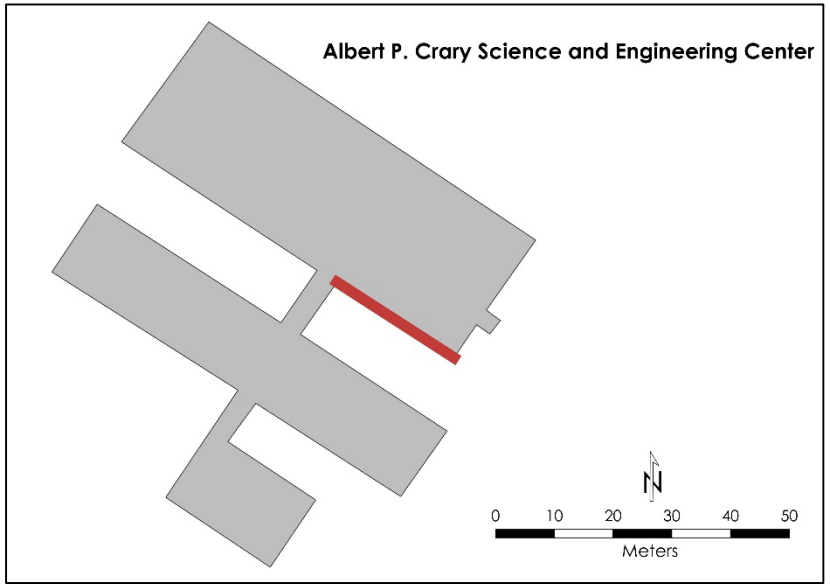
P1SE-TA-09 -15◦C 5◦C

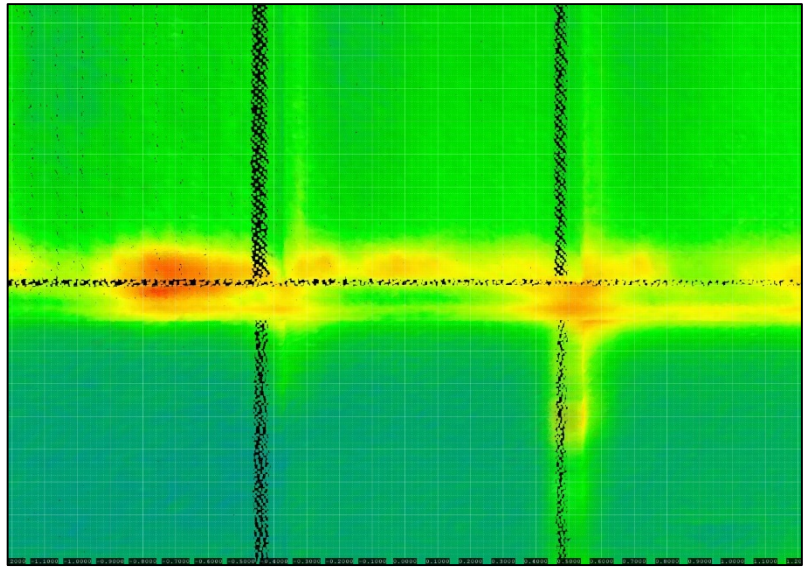


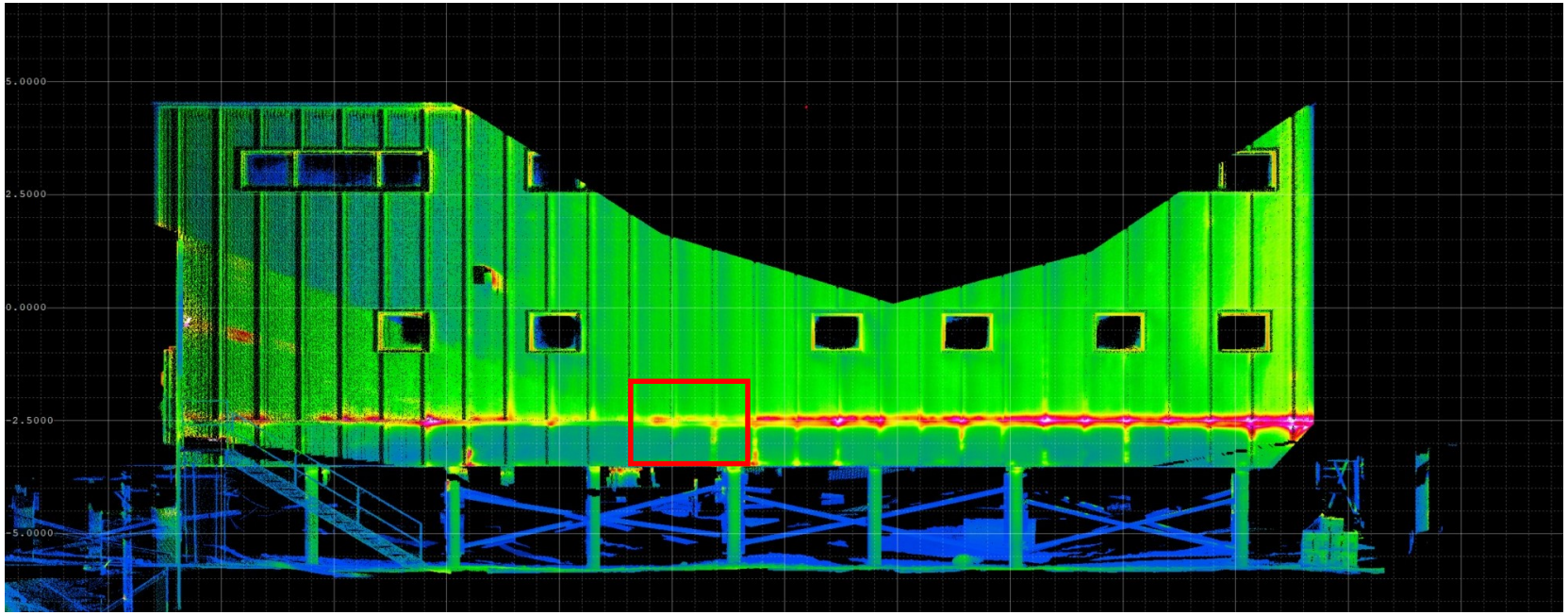




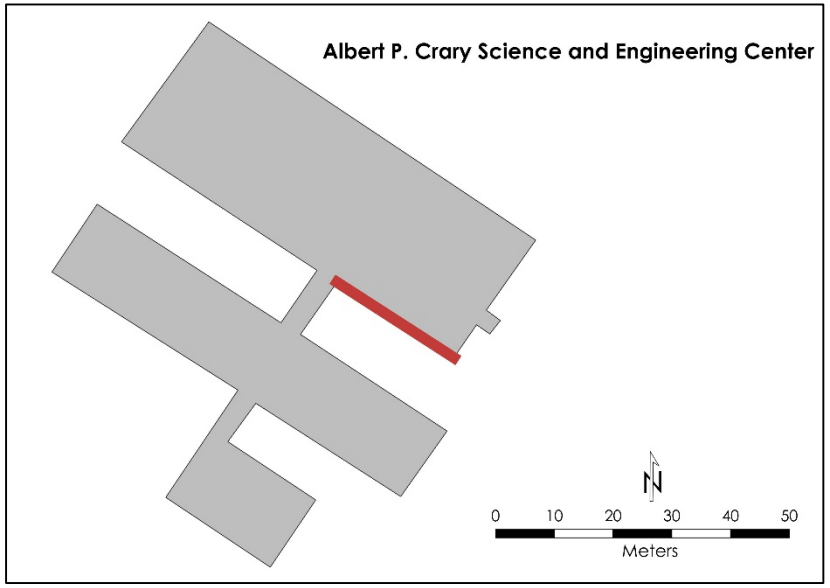
P1SE-TA-10 -15◦C 5◦C

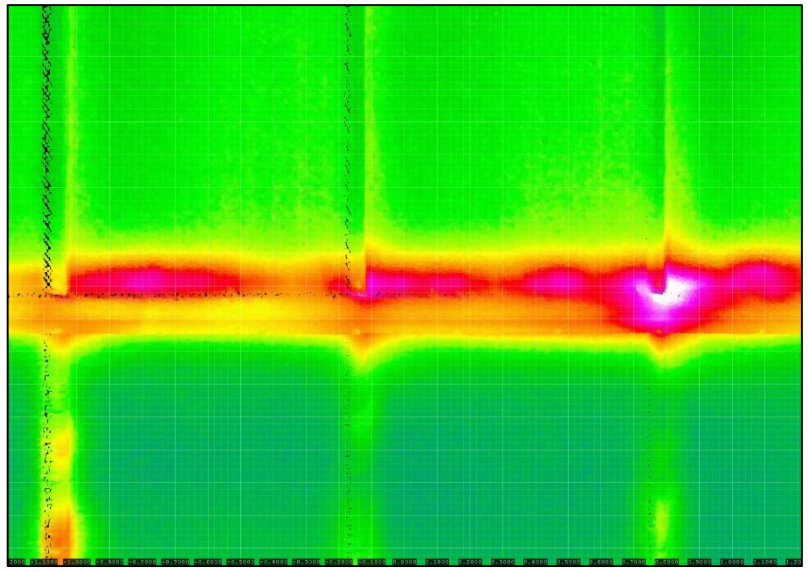


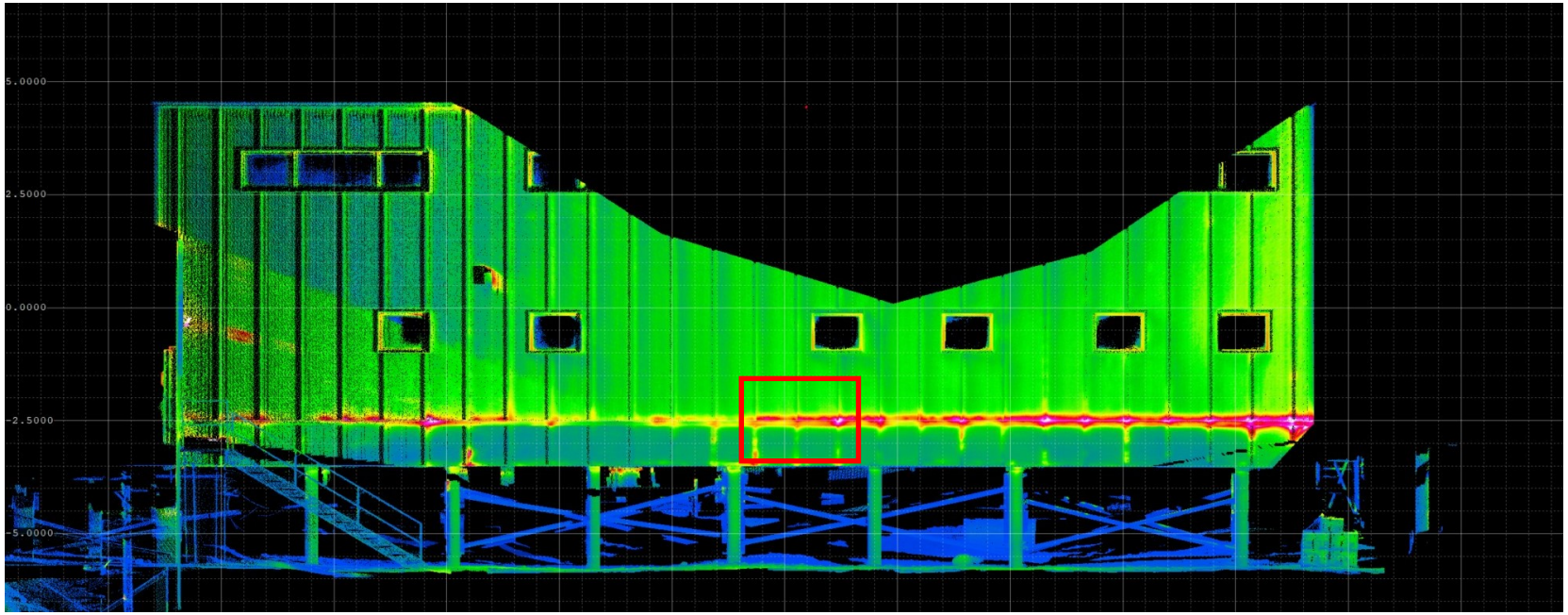




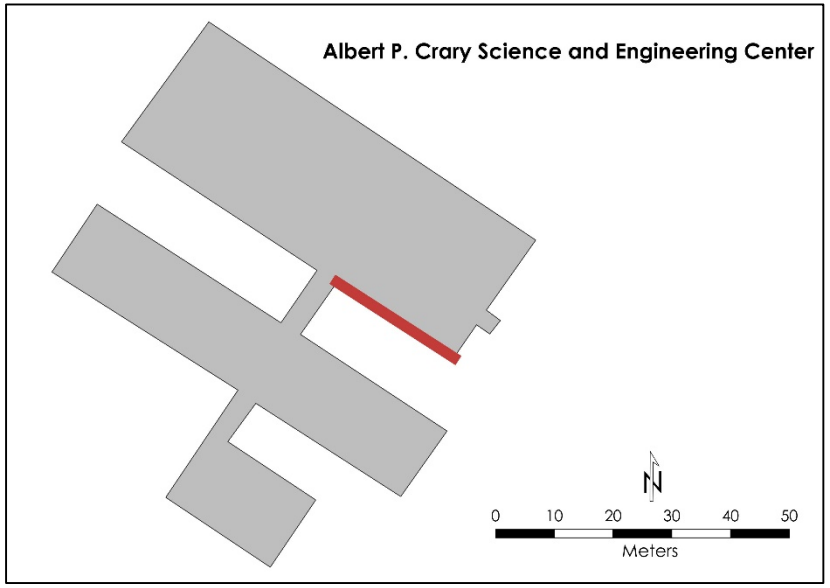
P1SE-TA-11 -15◦C 5◦C

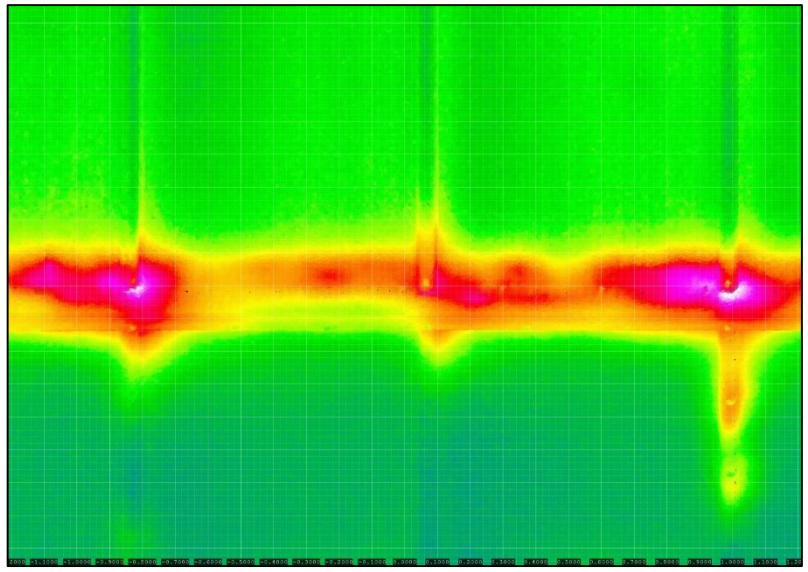


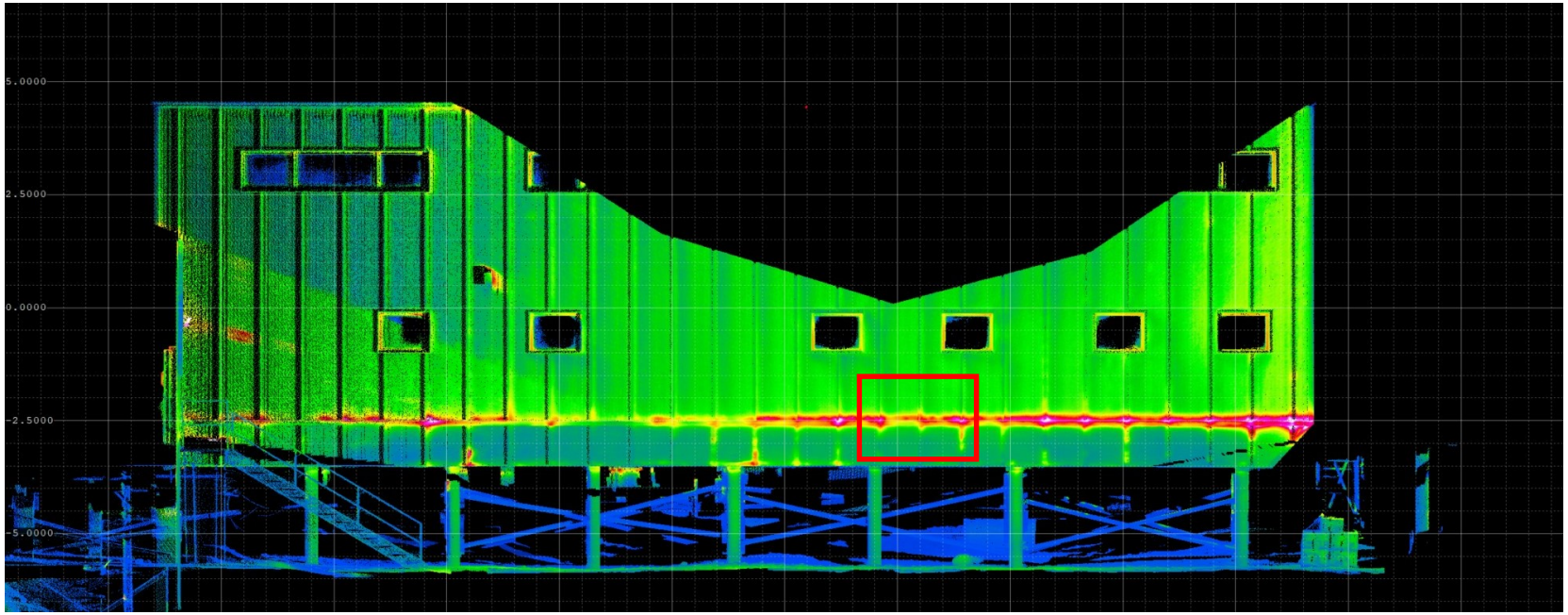




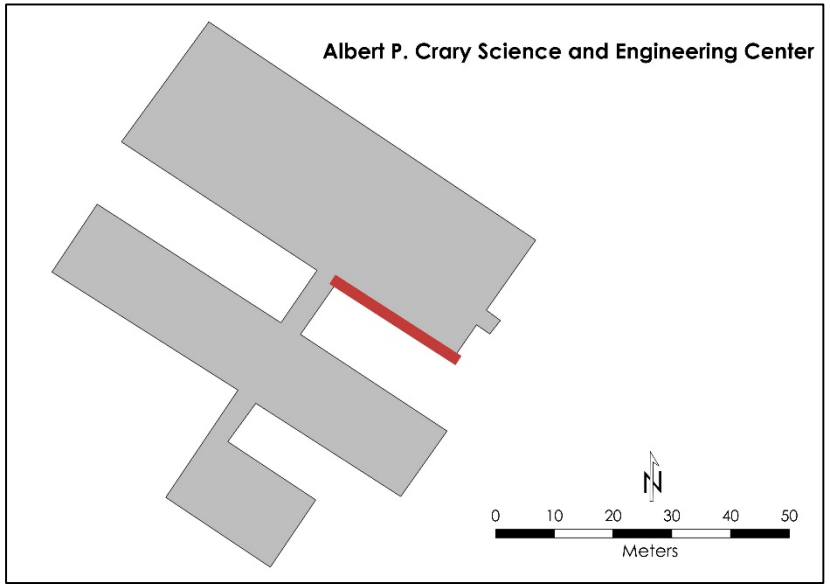
P1SE-TA-12 -15◦C 5◦C

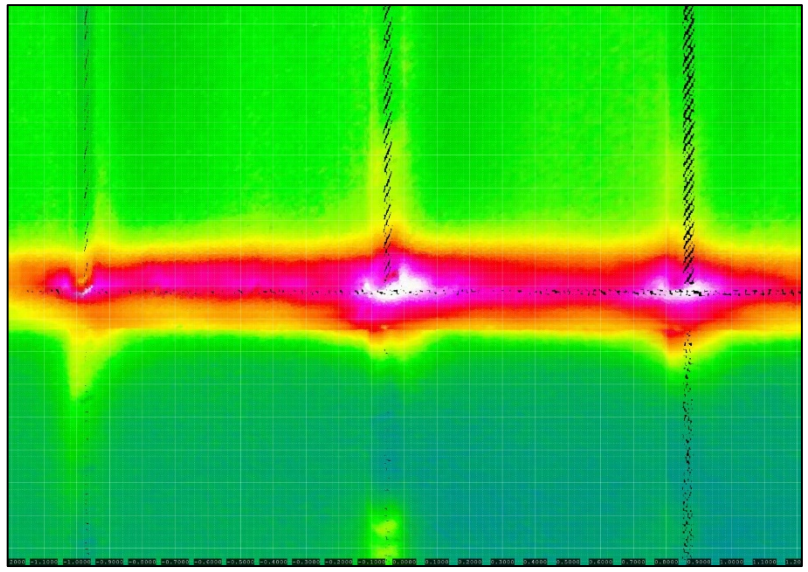


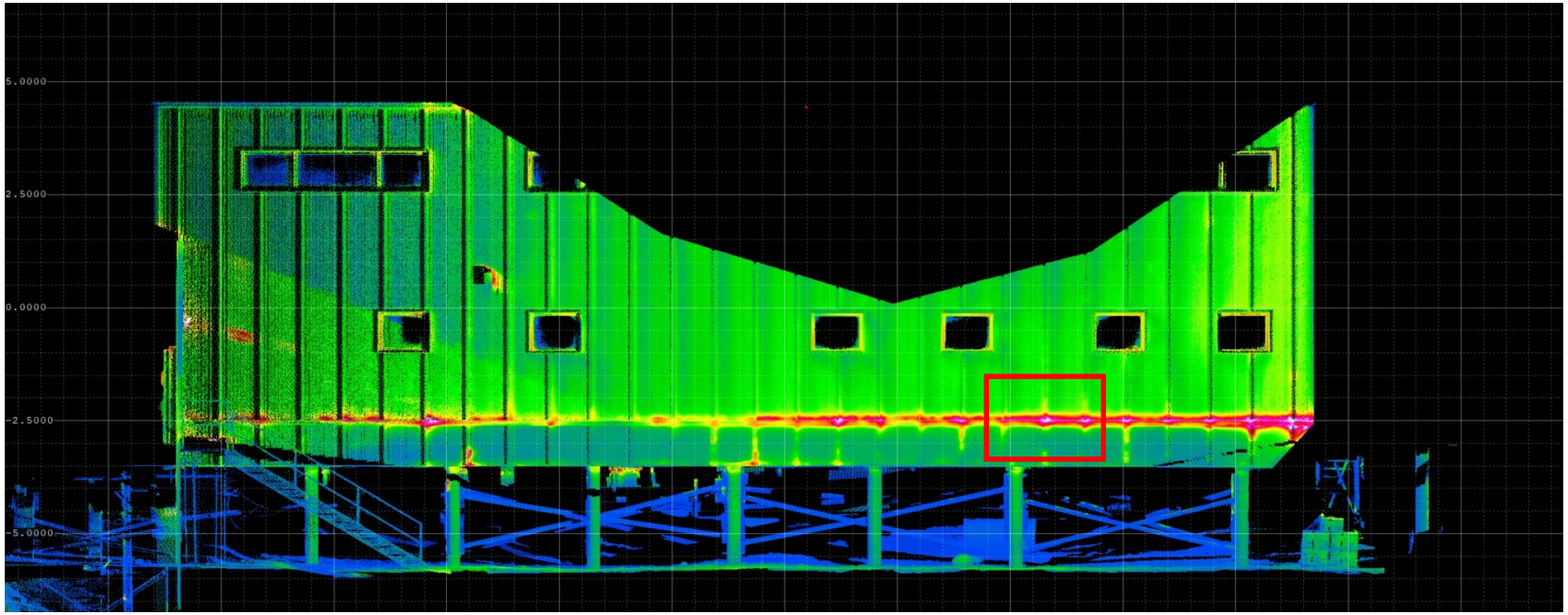




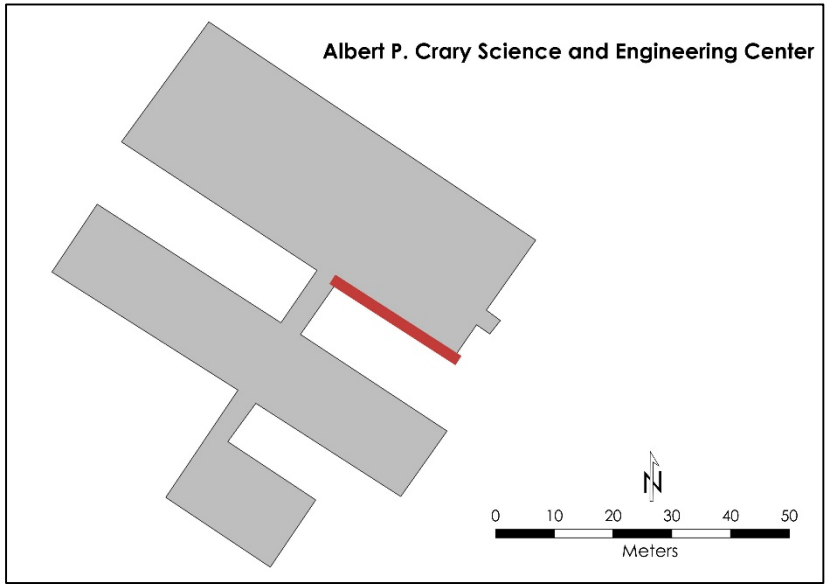
P1SE-TA-13 -15◦C 5◦C

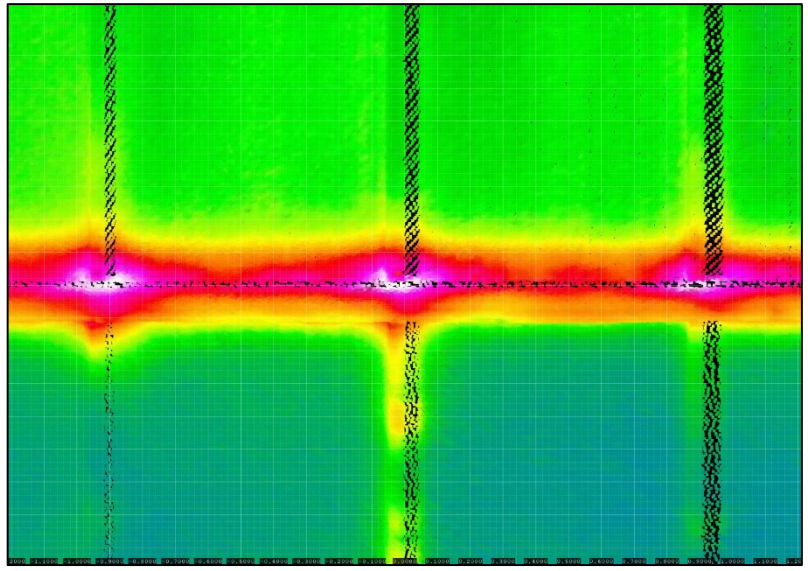


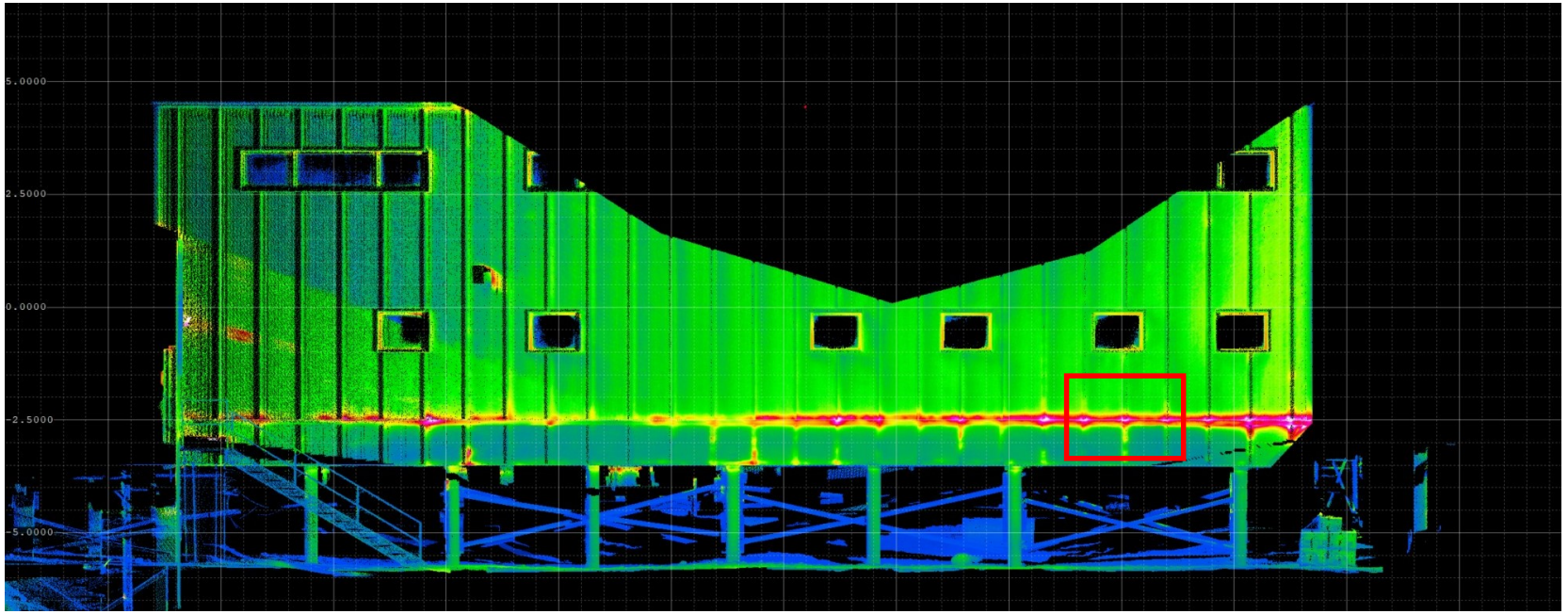




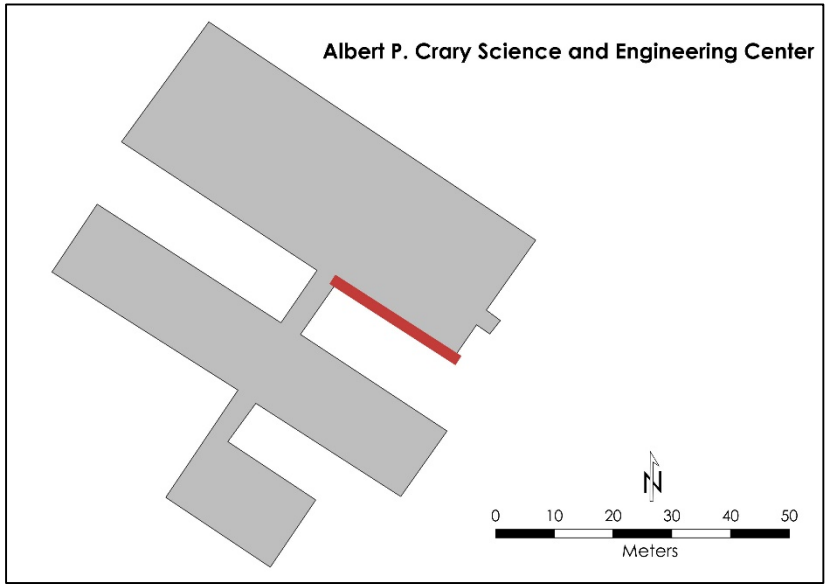
P1SE-TA-14 -15°C 5°C

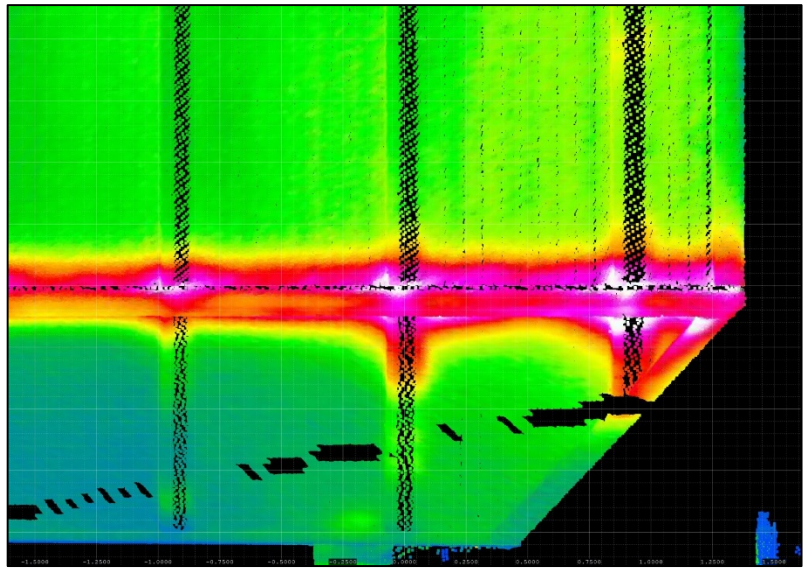


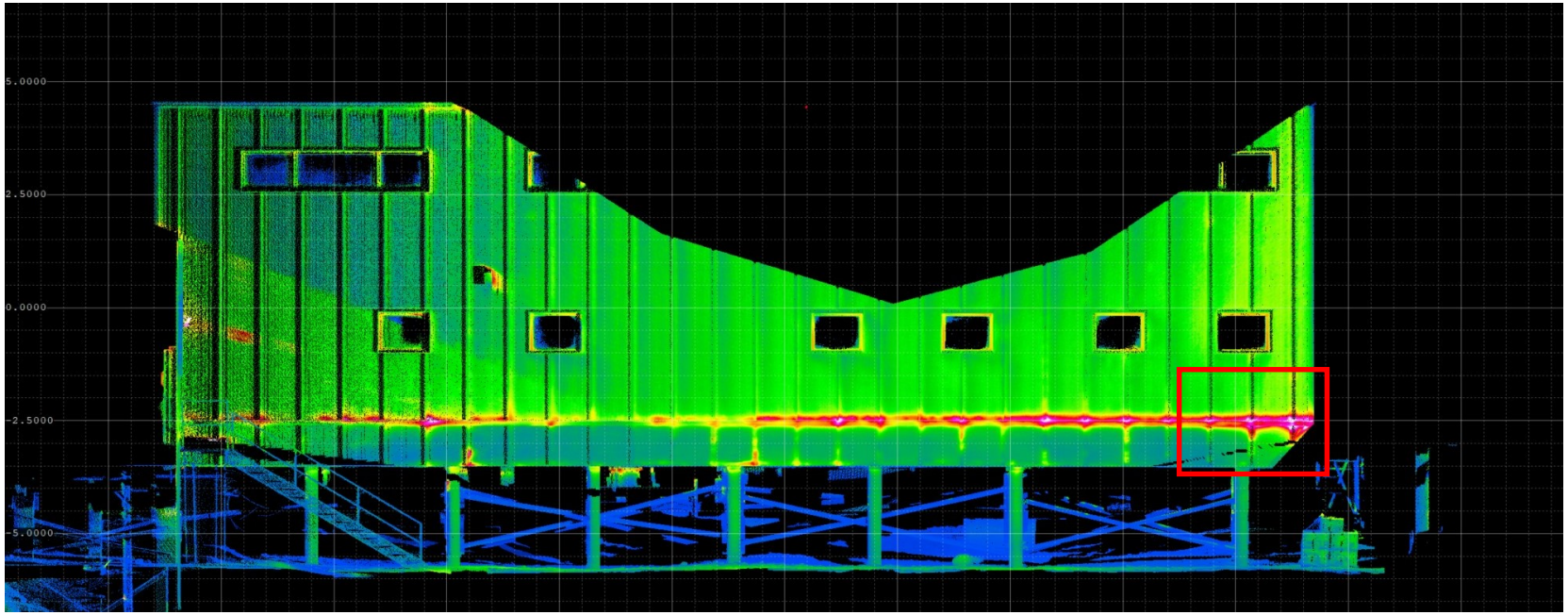




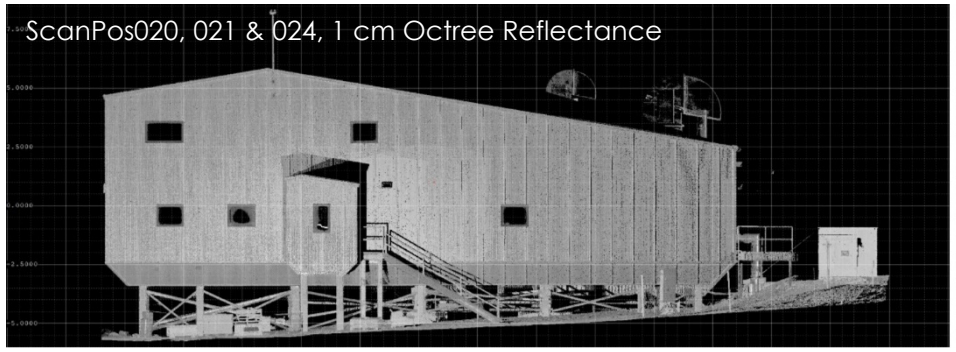
P1SE-TA-15 -15◦C 5◦C

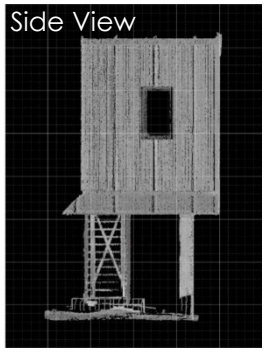


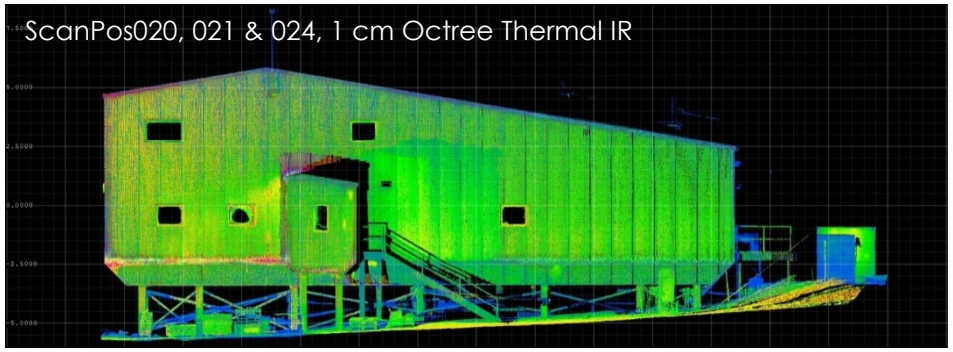


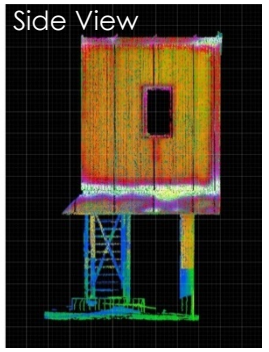


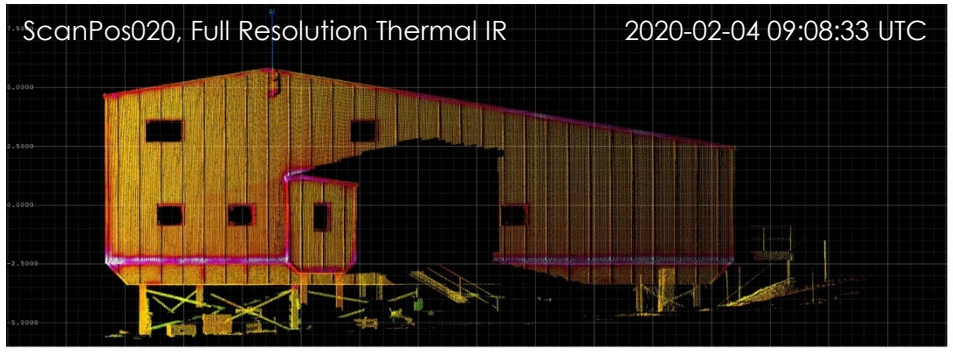
P1SE-TA-16 -15◦C 5◦C

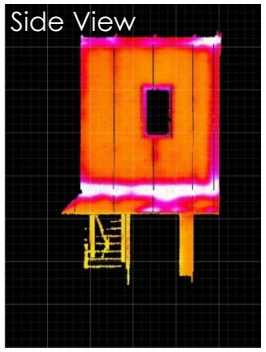


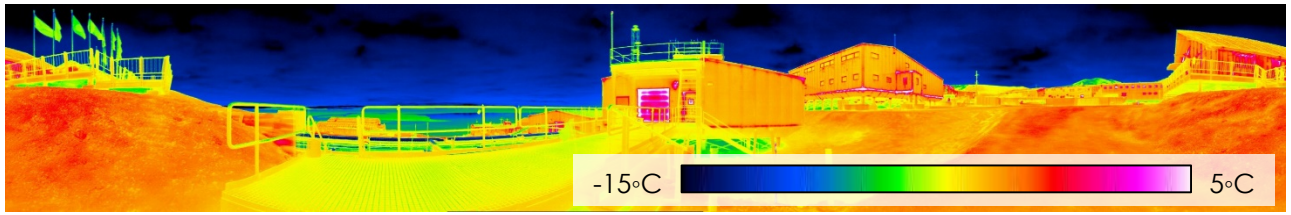




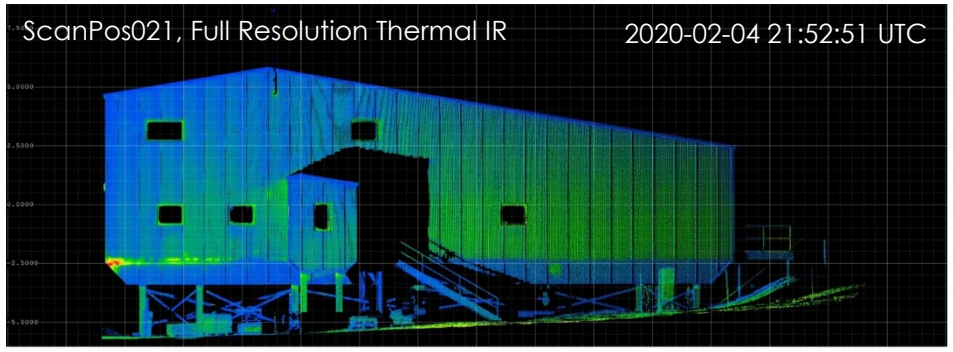


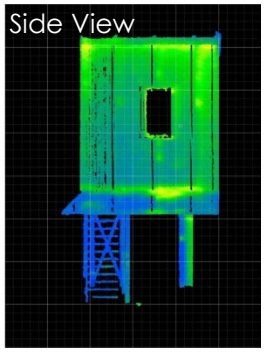


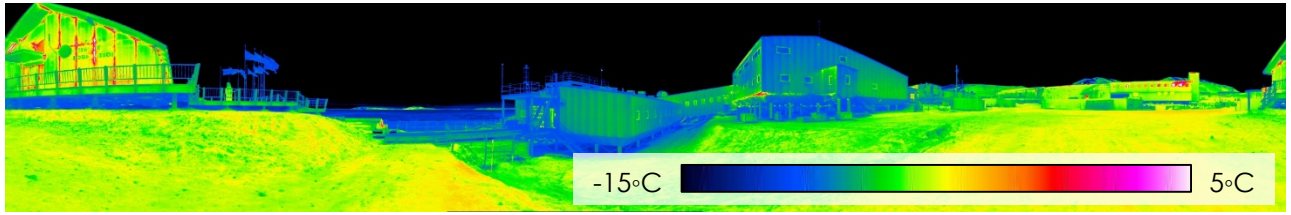




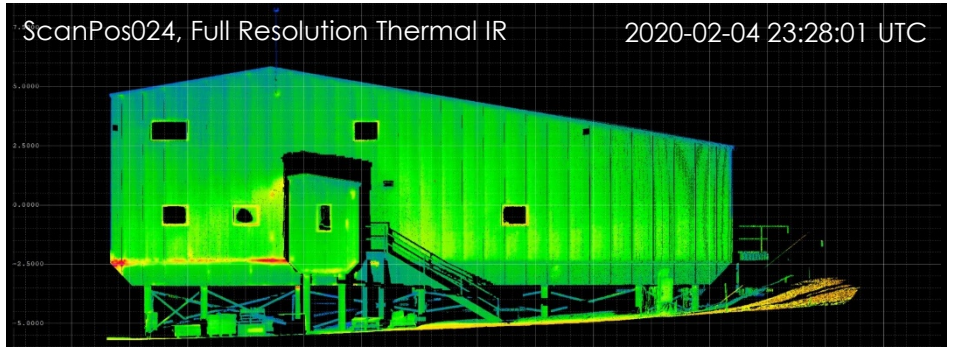
ScanPos020 – TIR Panorama

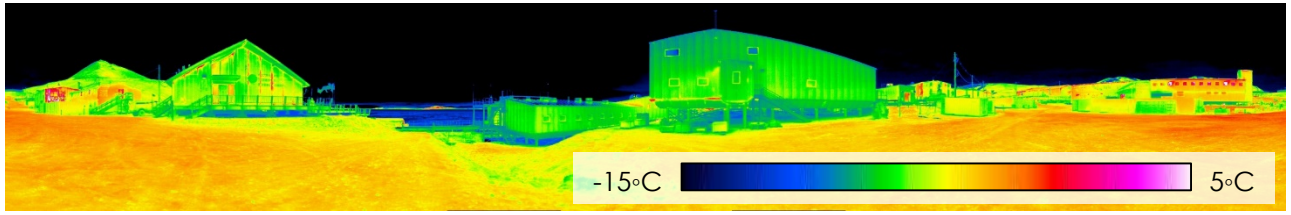




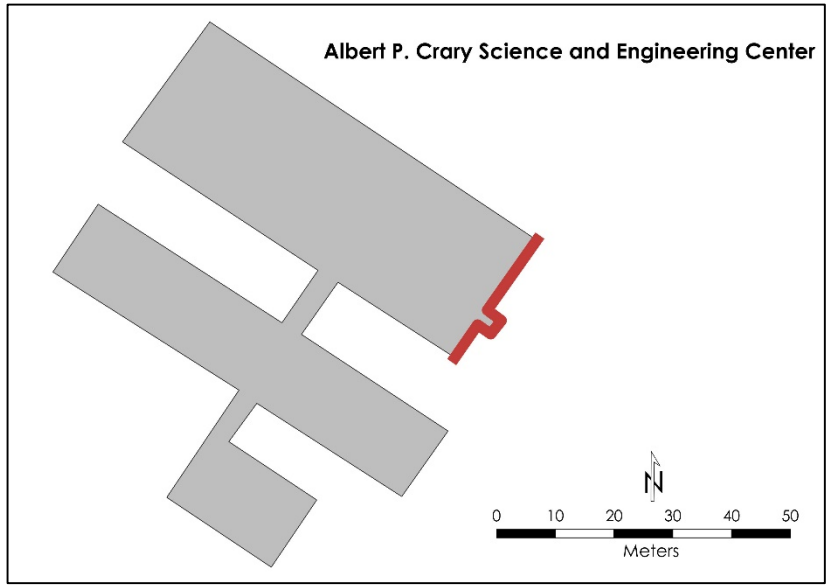


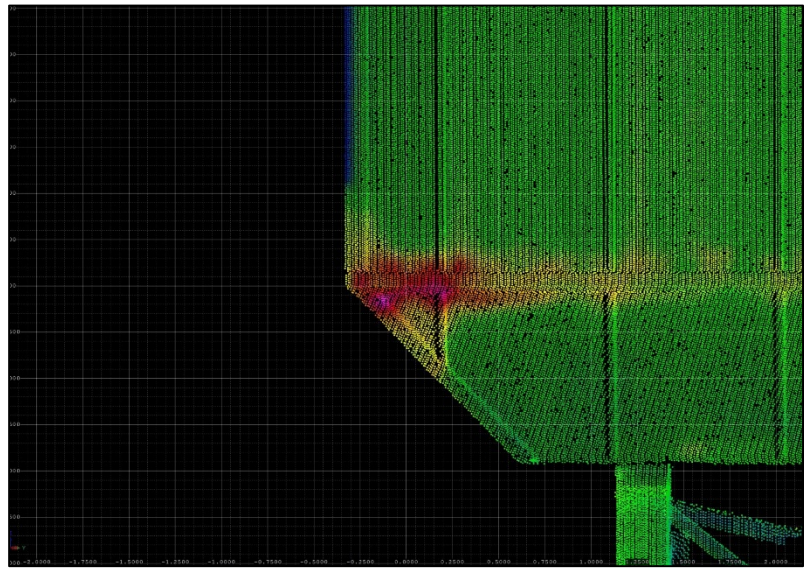
ScanPos021 – TIR Panorama

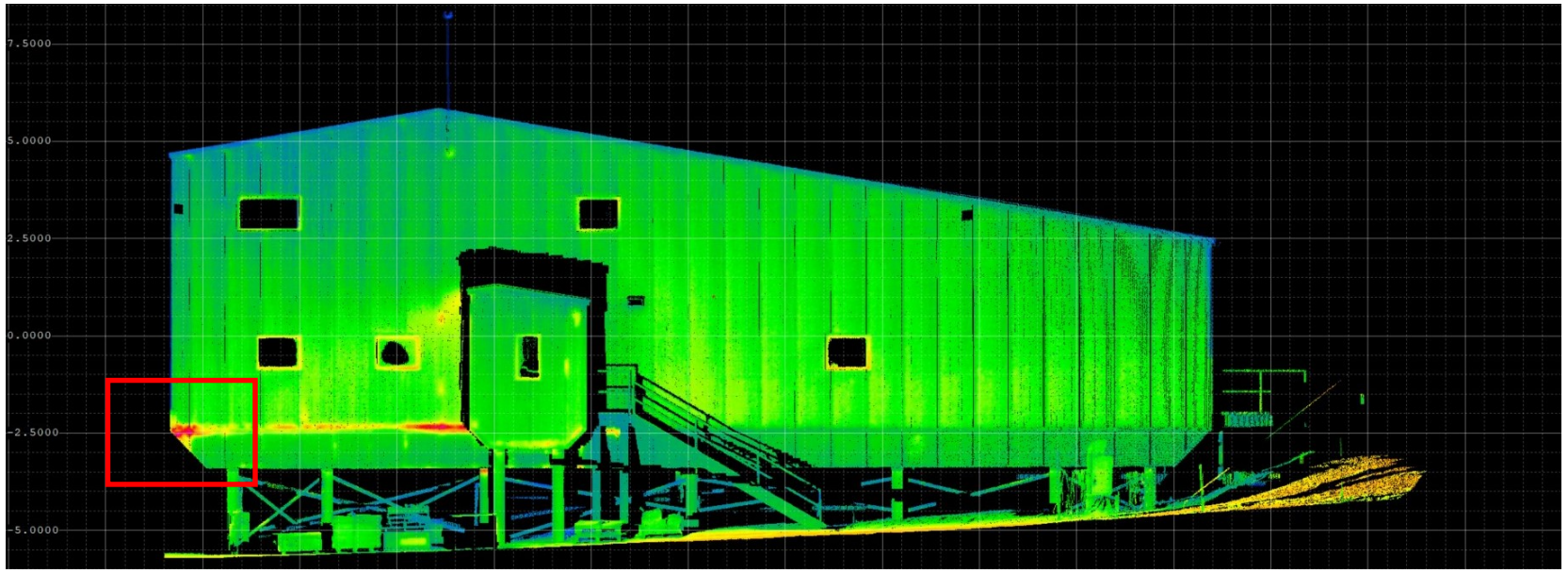




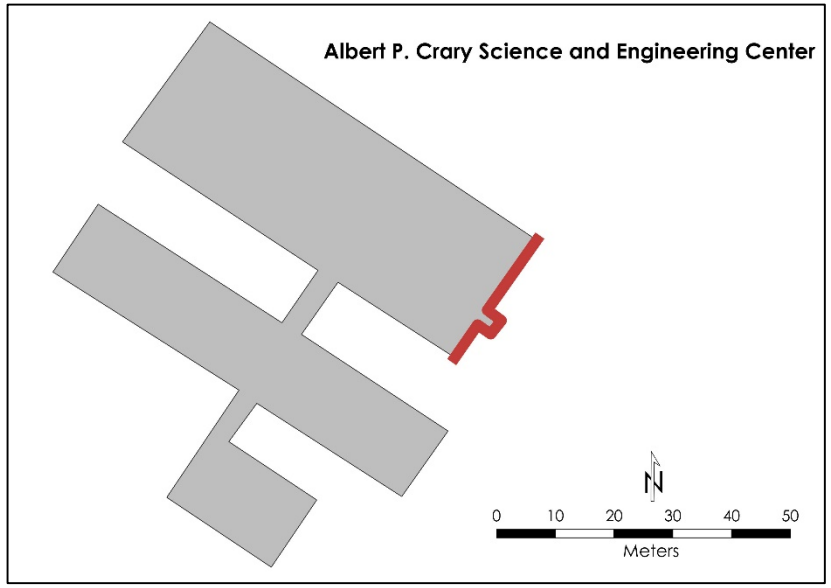
ScanPos024 – TIR Panorama

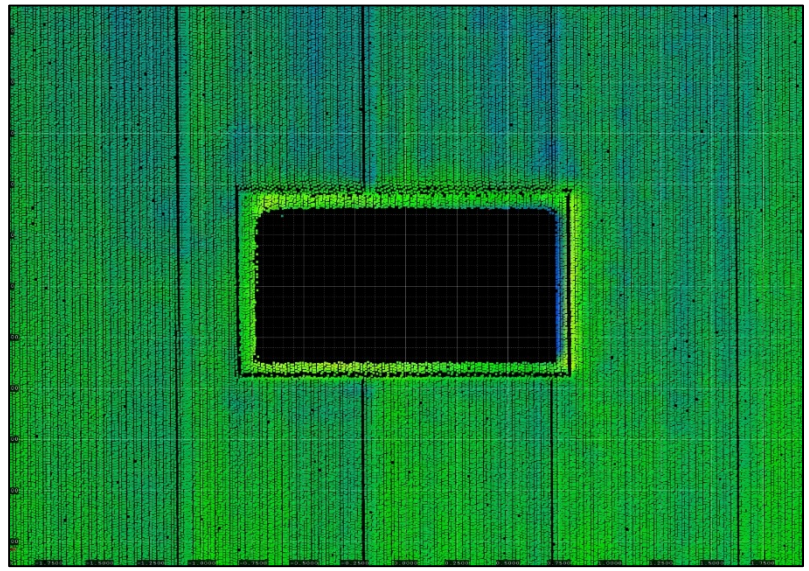


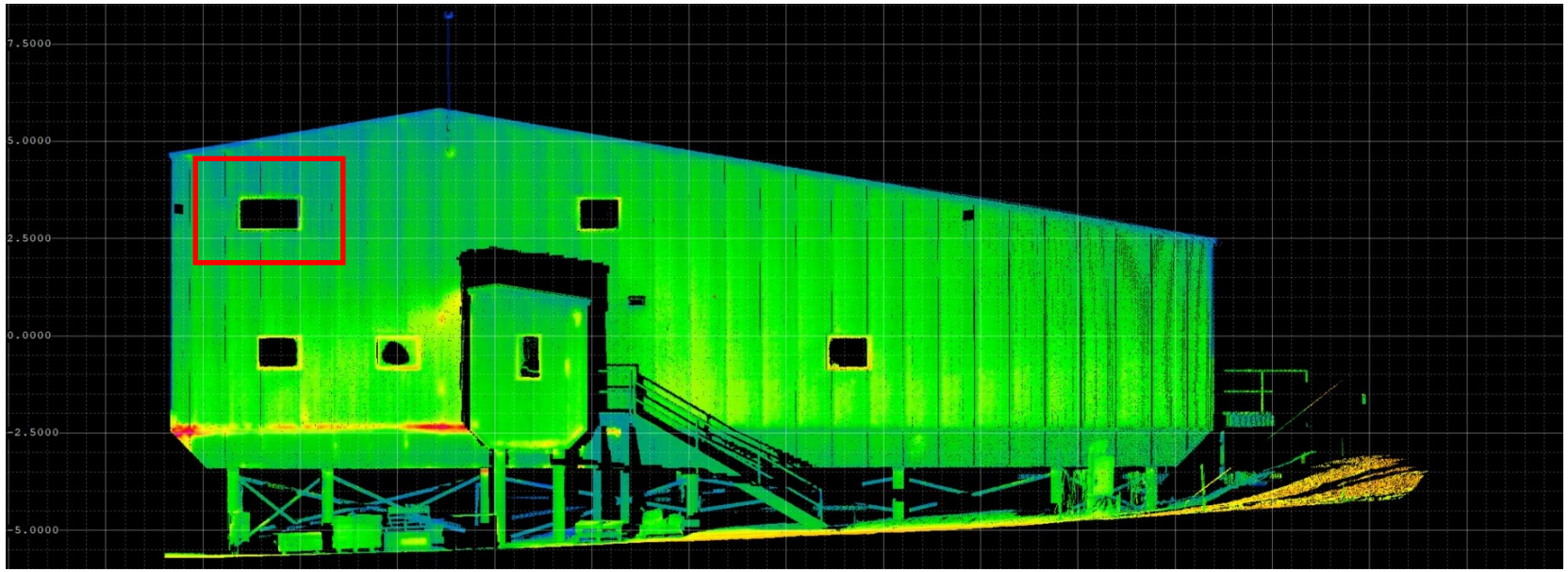




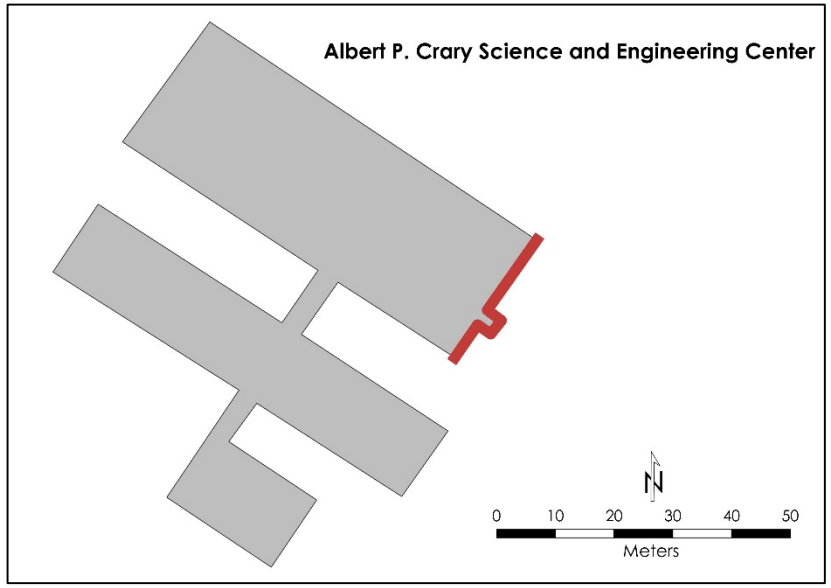
P1E-TA-01 -15◦C 5◦C

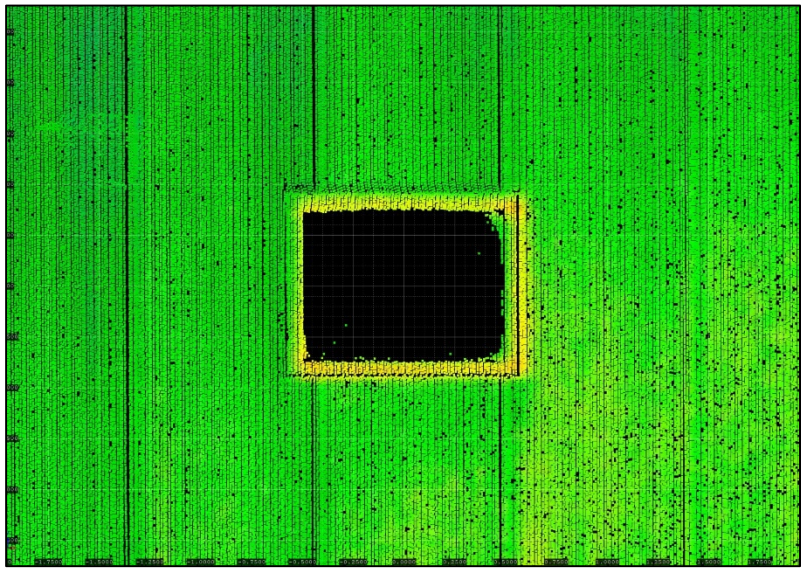


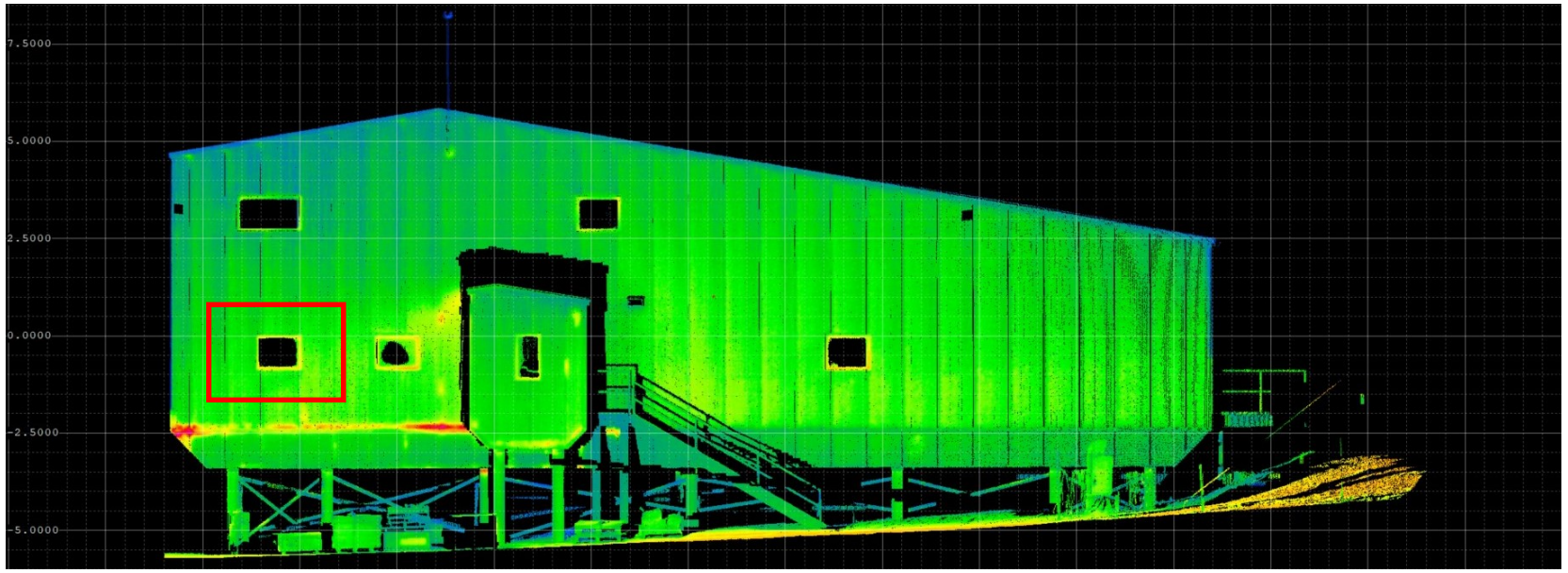




P1E-W-01 -15◦C 5◦C





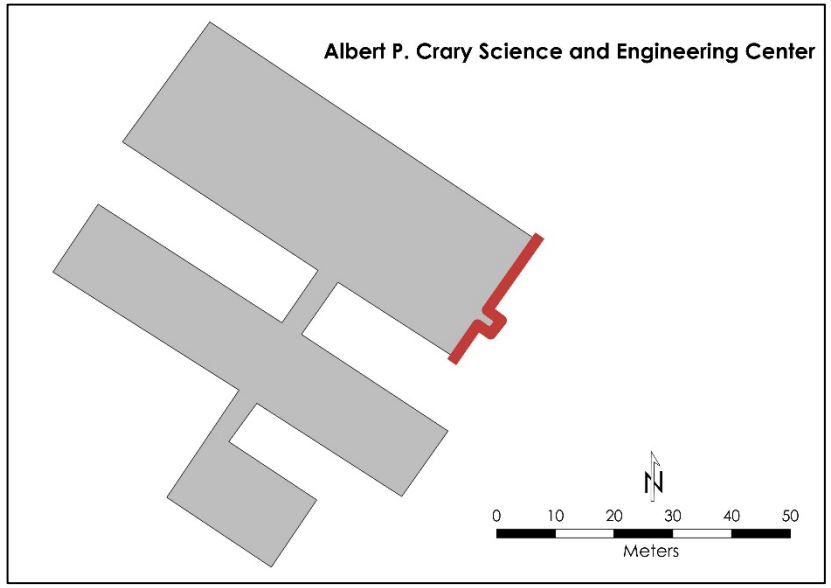


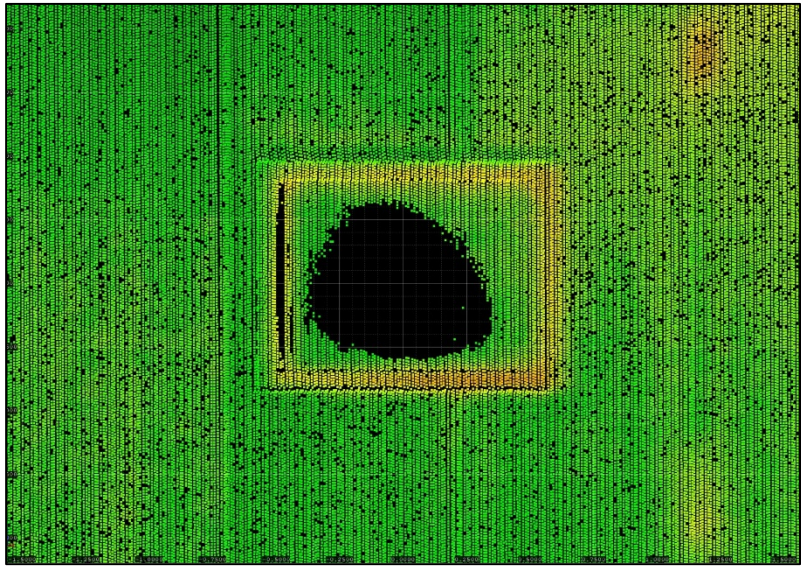
P1E-W-02

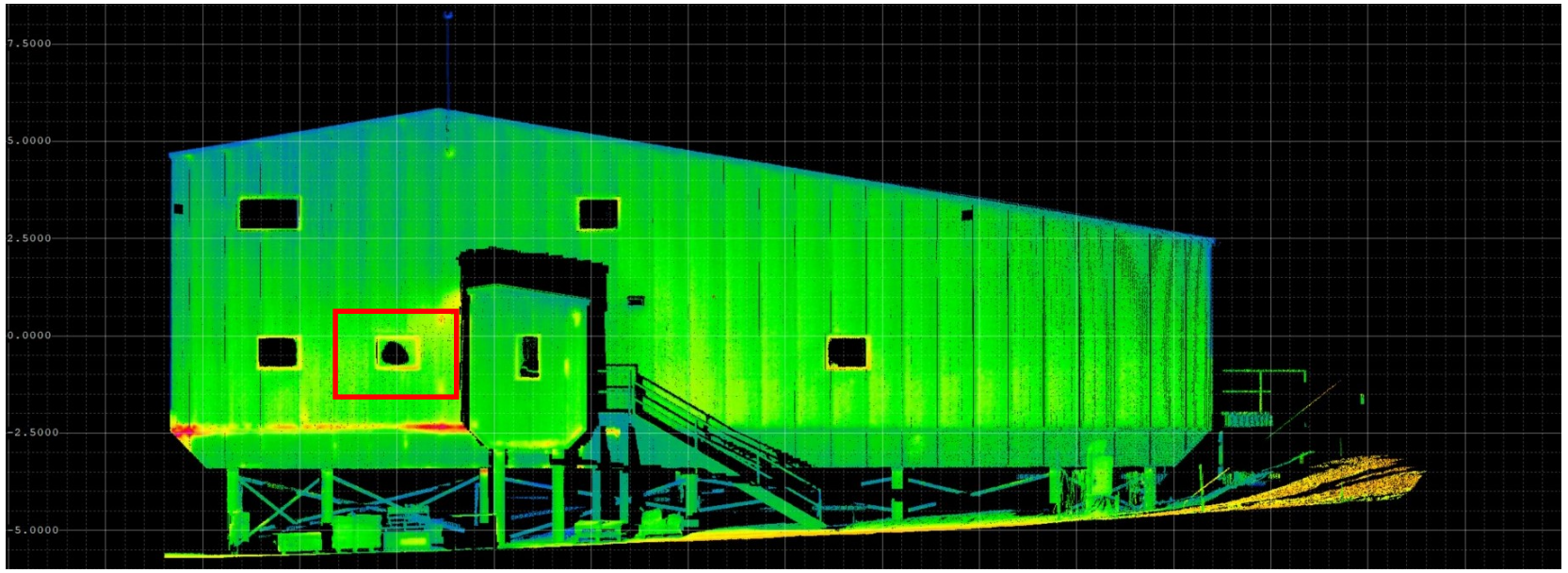
-15◦C



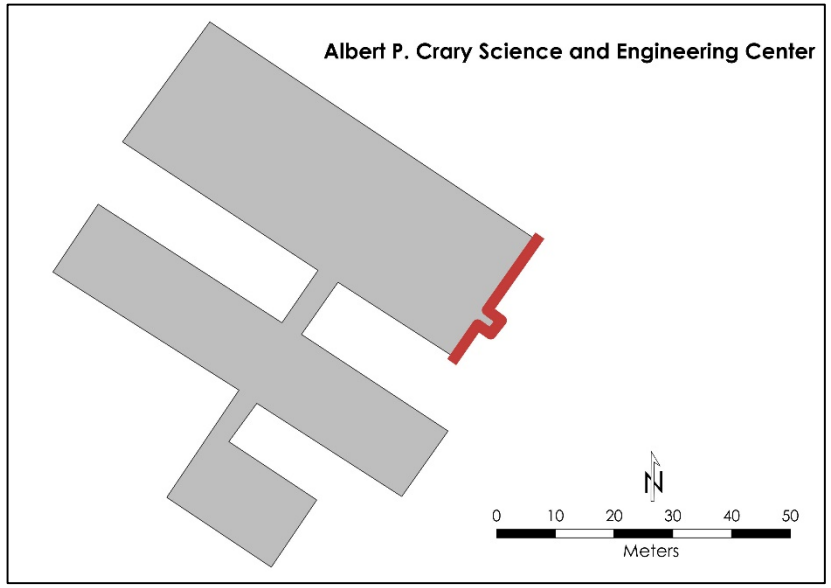
5◦C

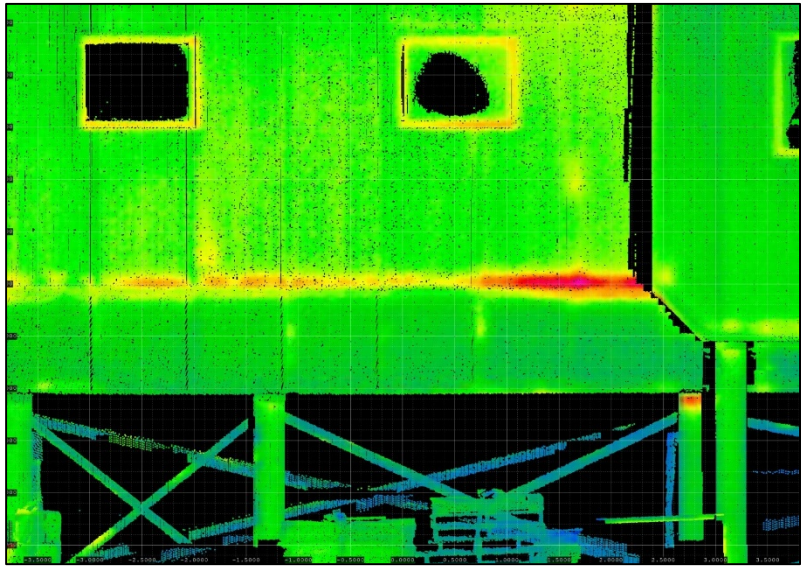


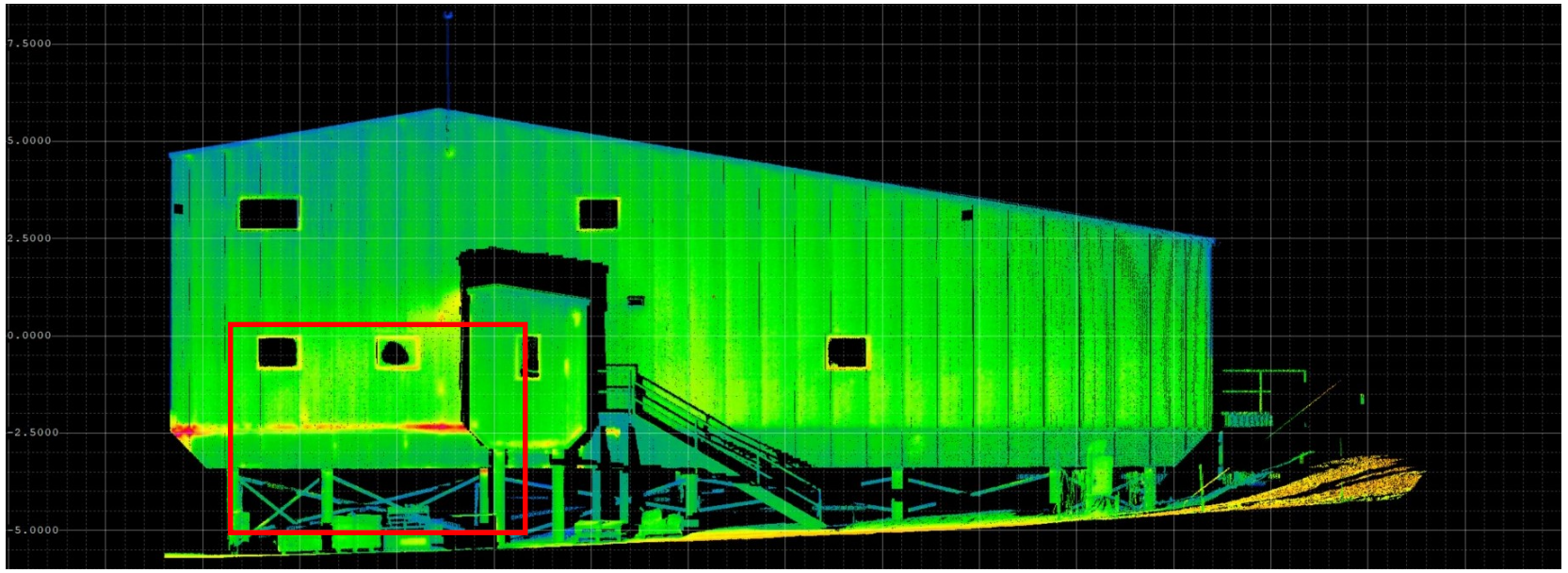




P1E-W-03 -15◦C 5◦C





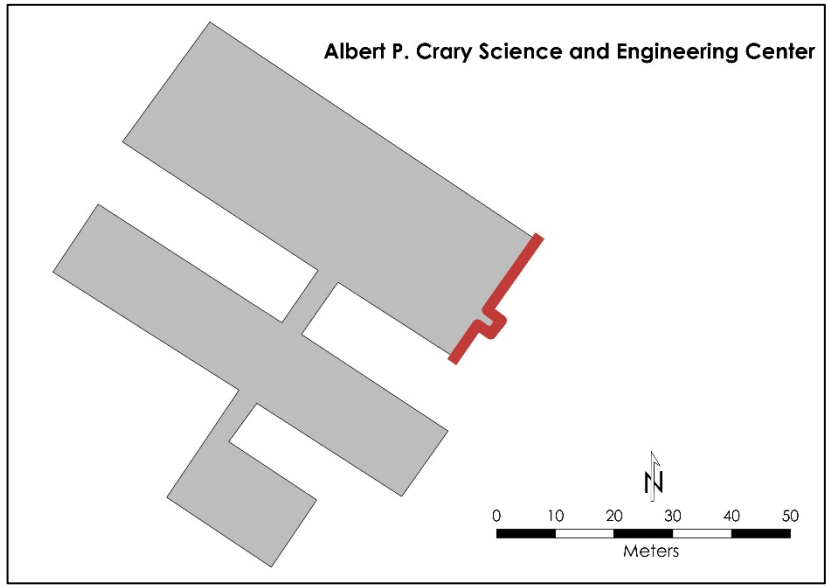


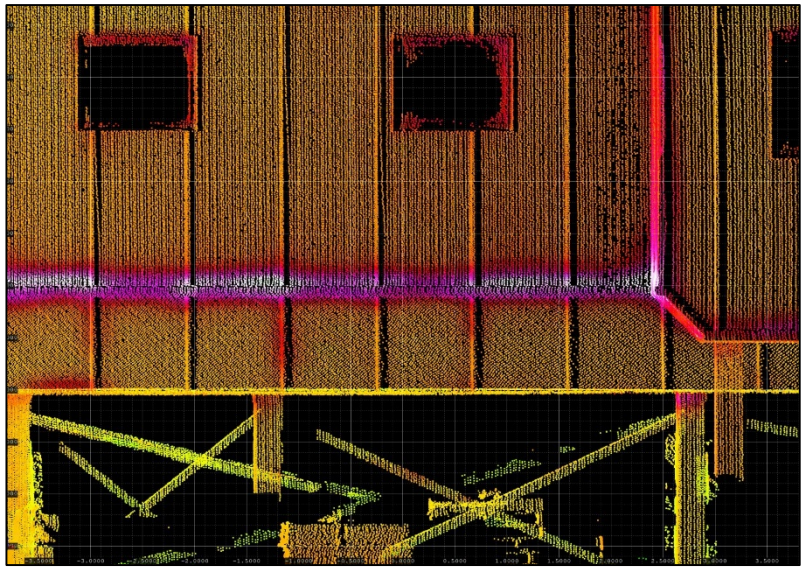
P1E-TA-02

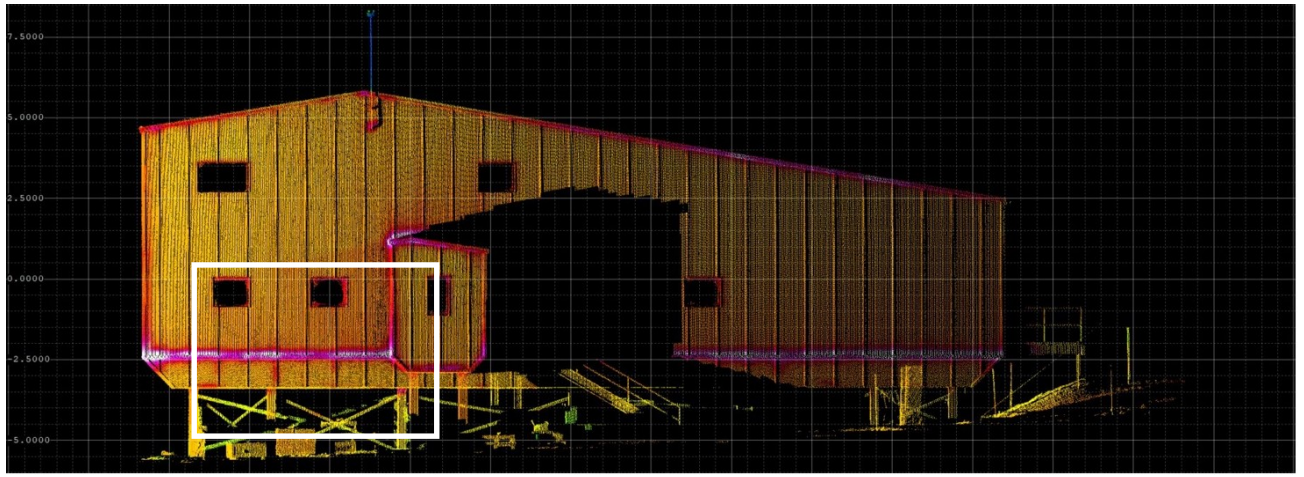
-15◦C

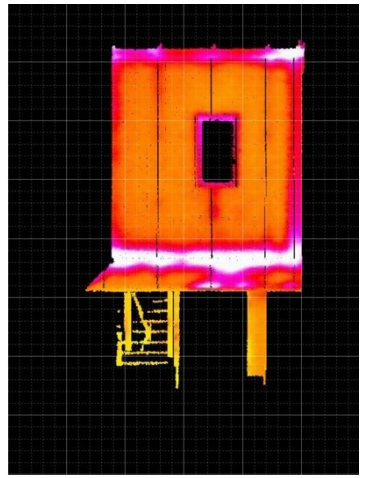


5◦C







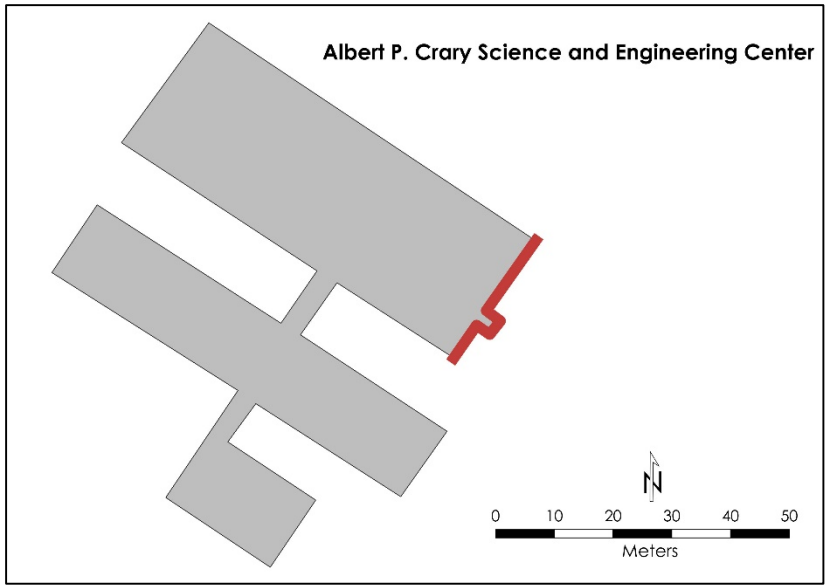


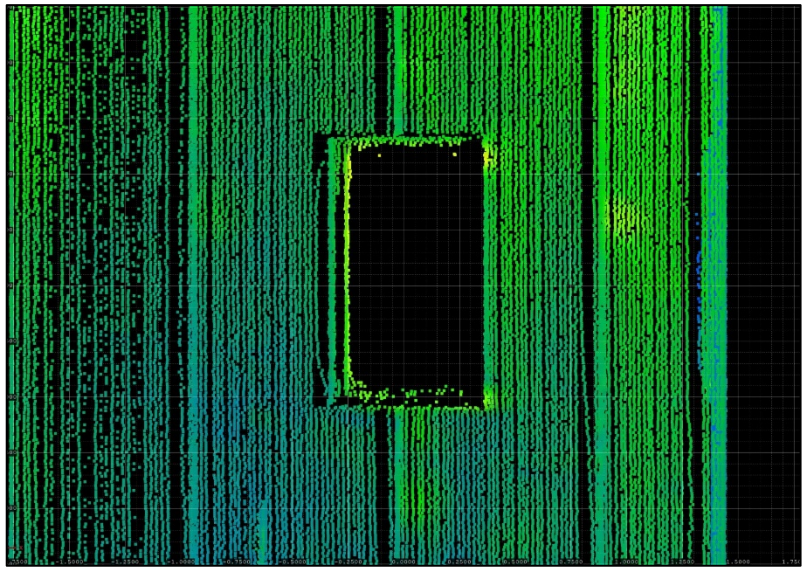
P1E-TA-02

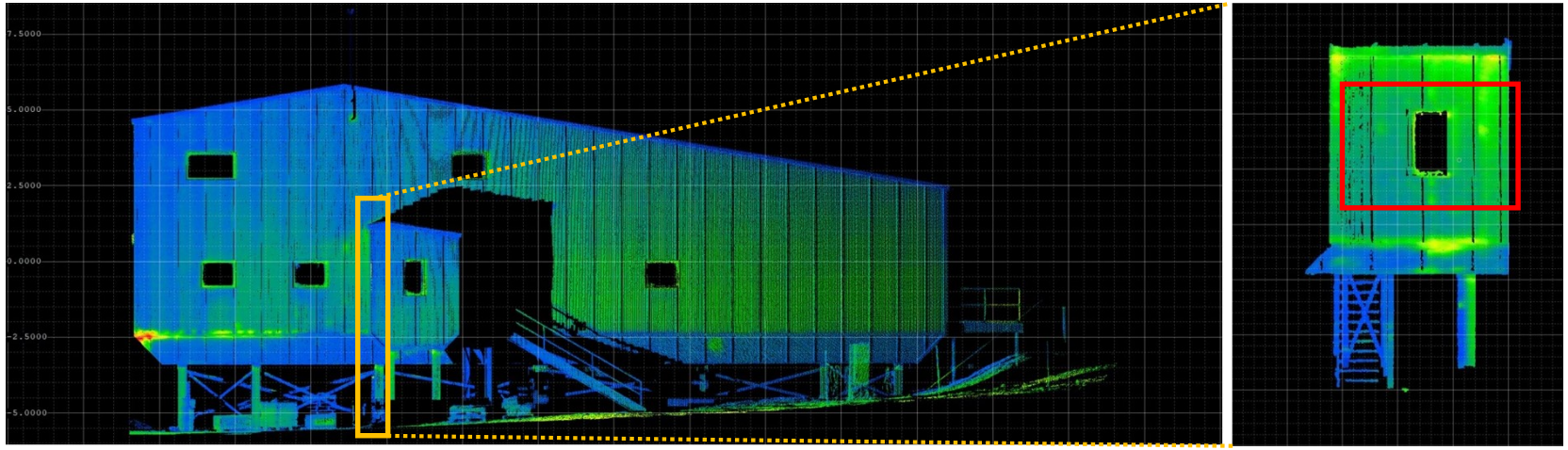
-15◦C



5◦C



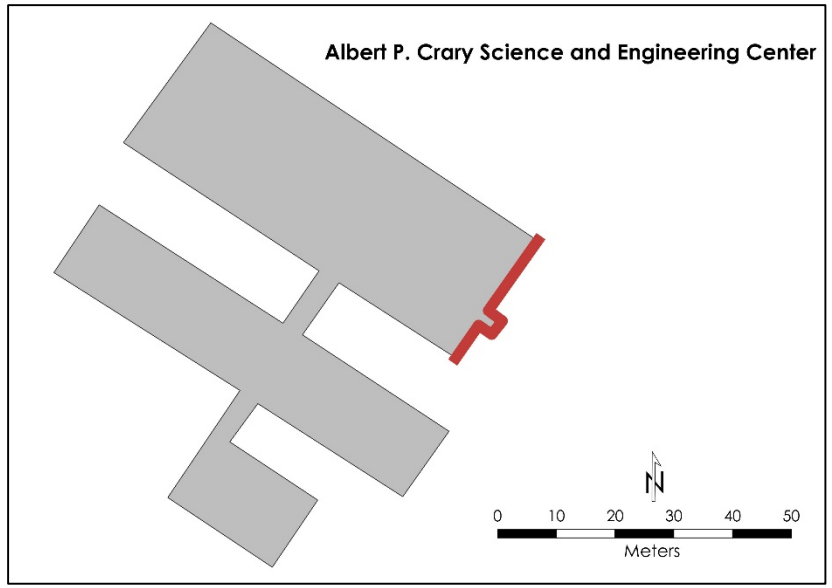


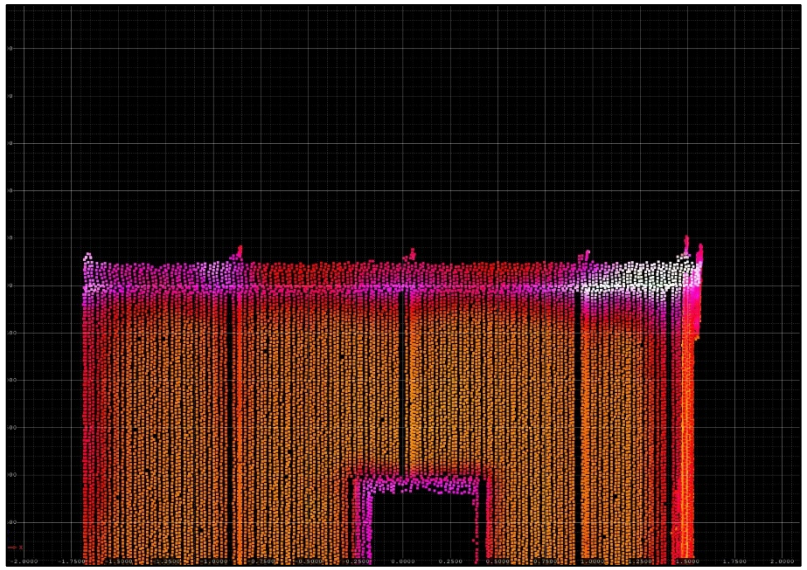


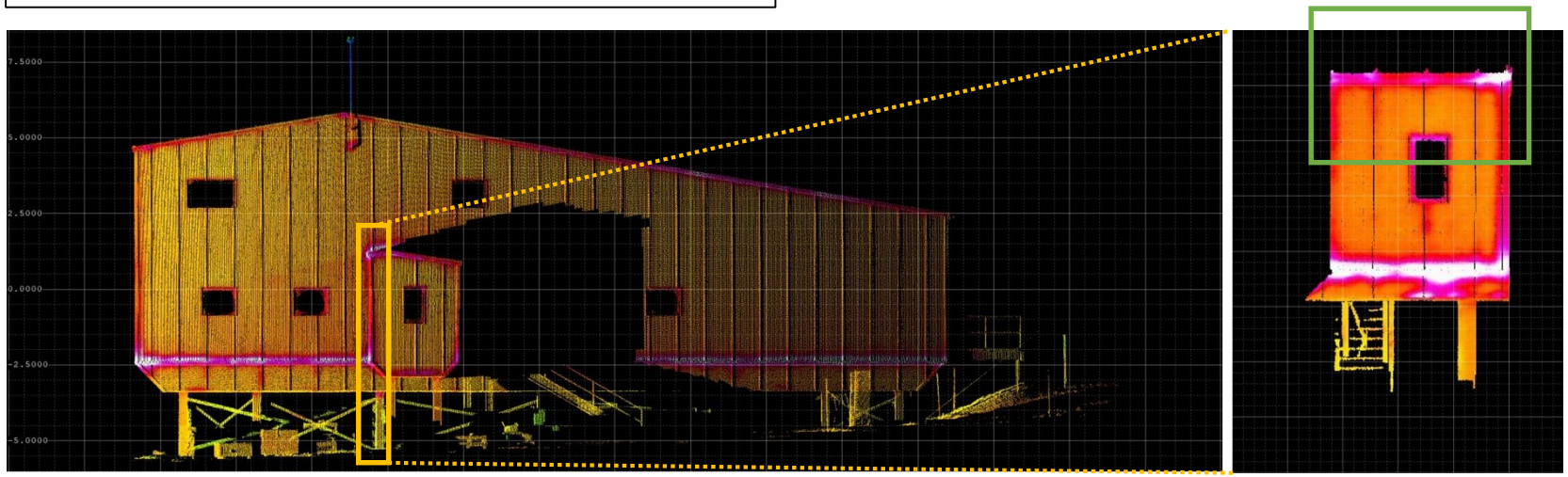
P1E-W-04

-15◦C

5◦C



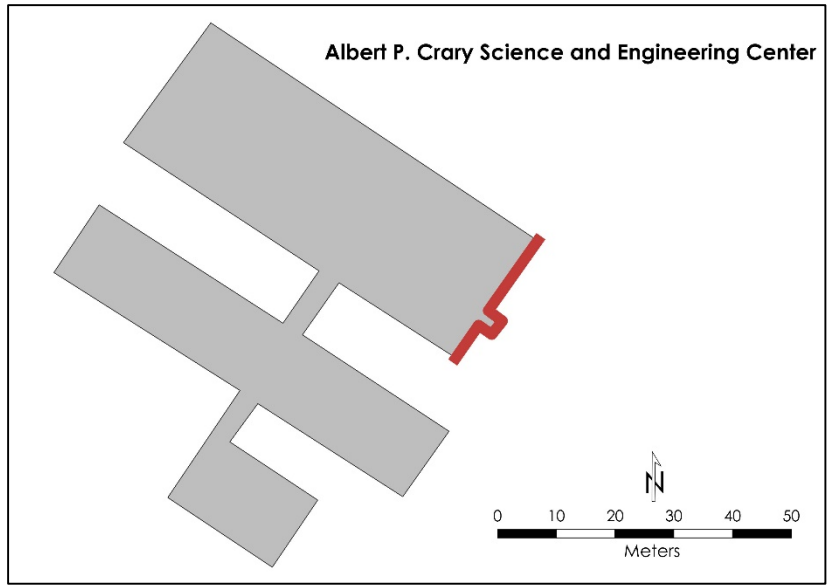


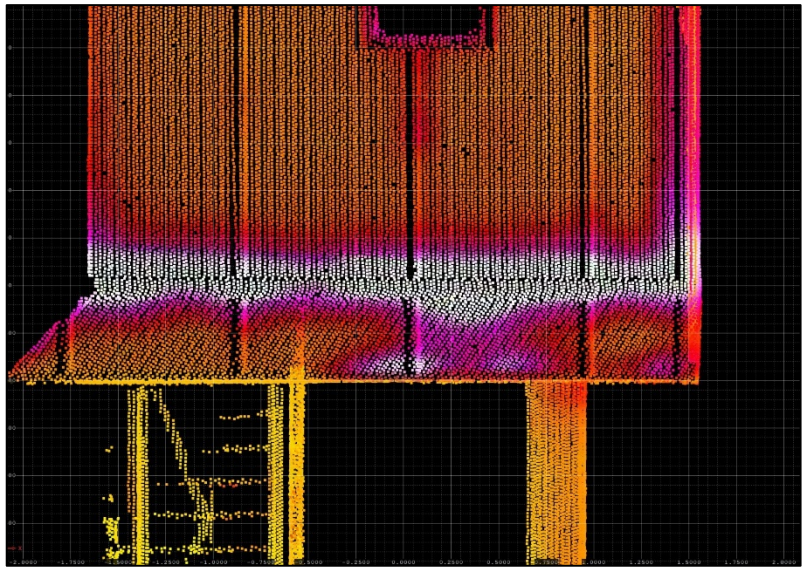


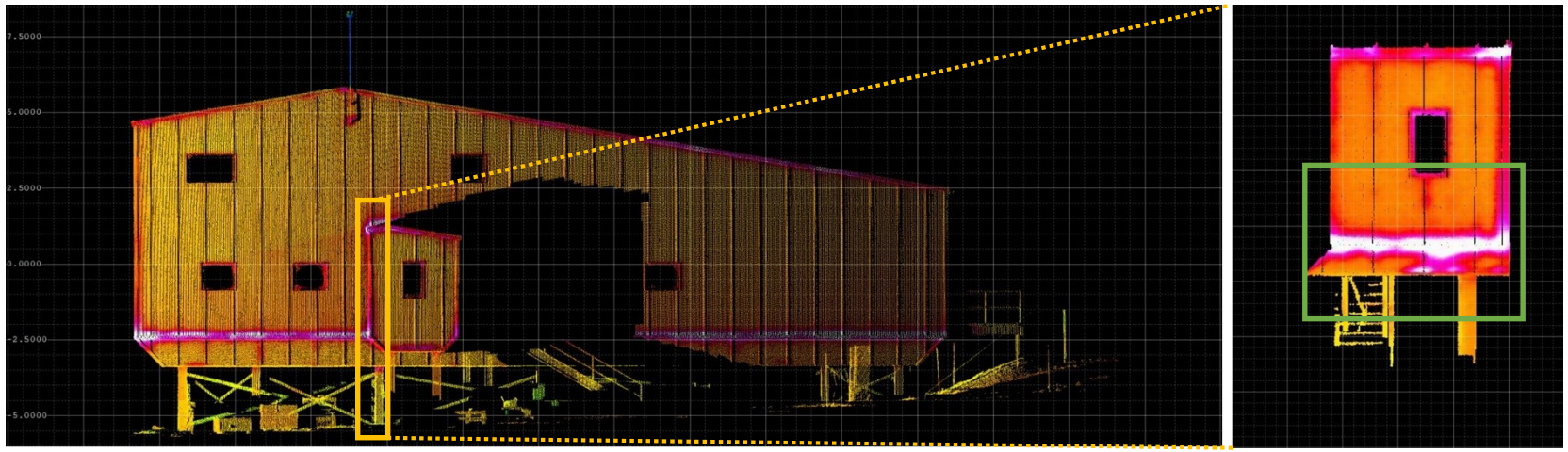
P1E-TA-03

-15◦C

5◦C



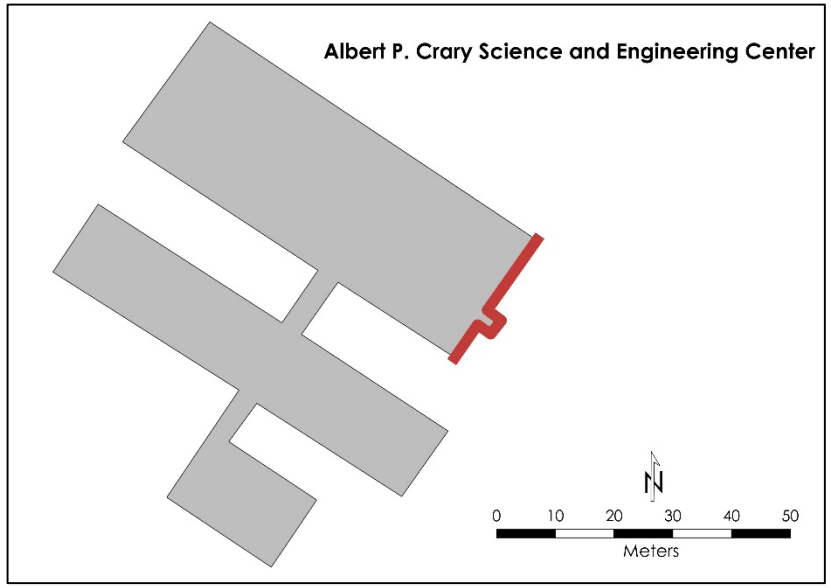


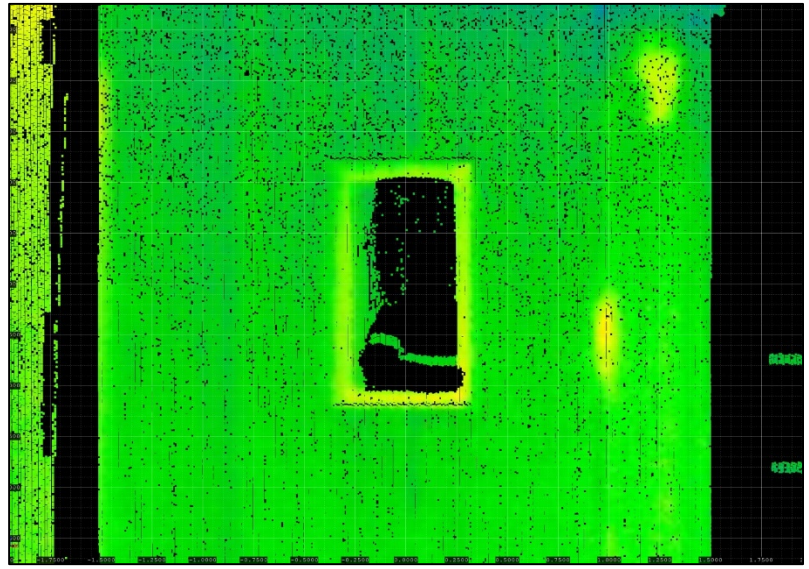


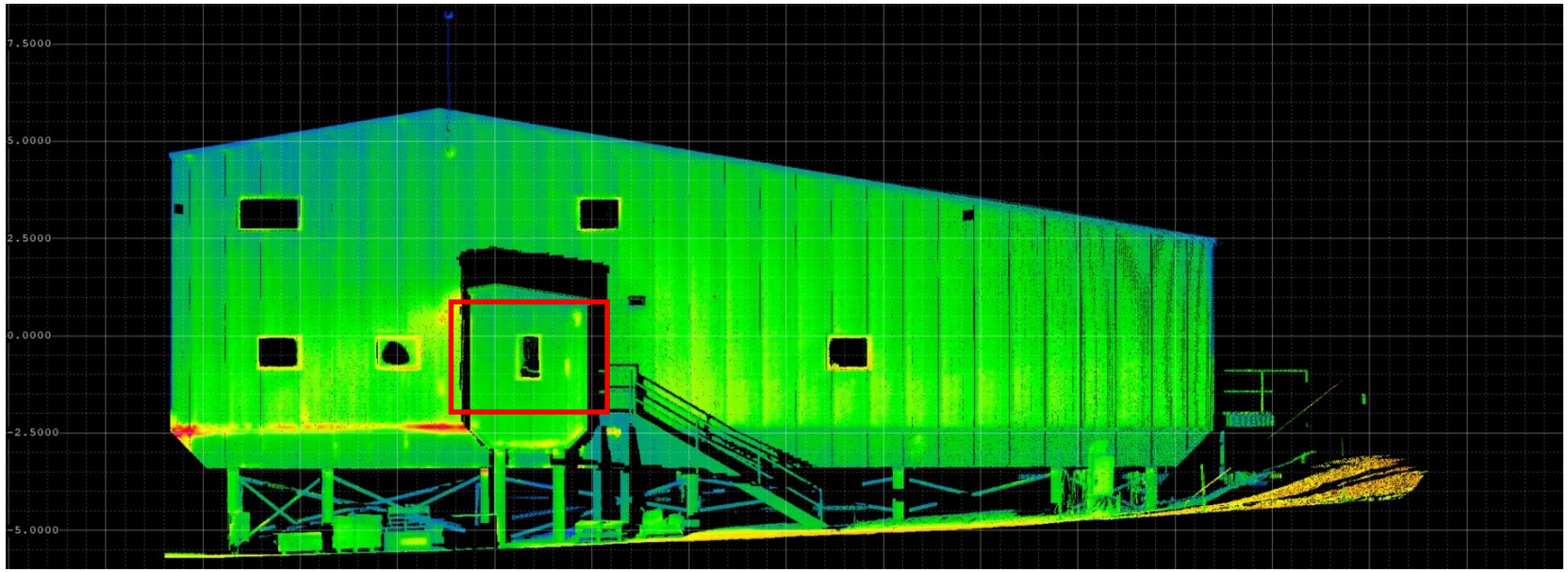
P1E-TA-04

-15◦C

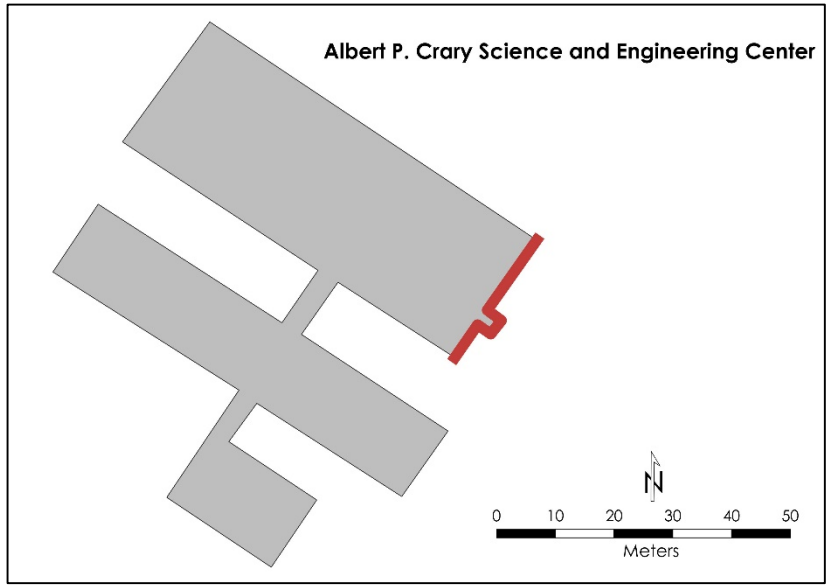
5◦C

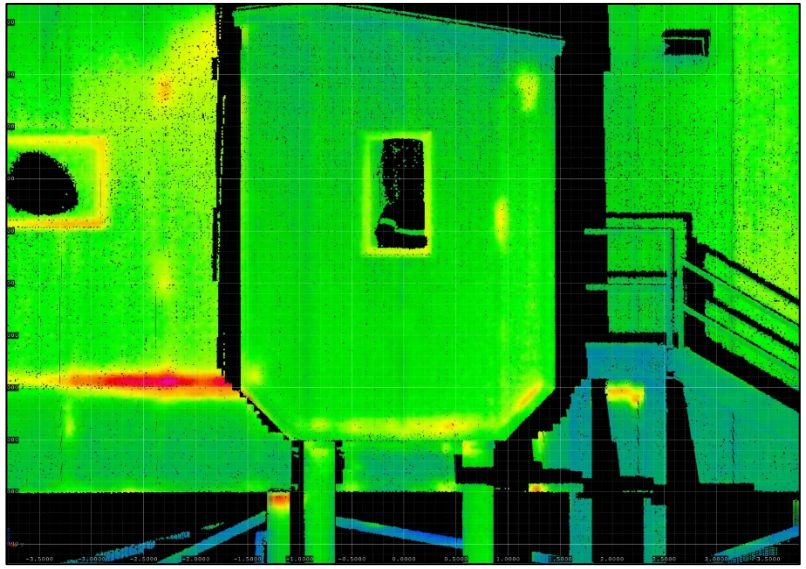


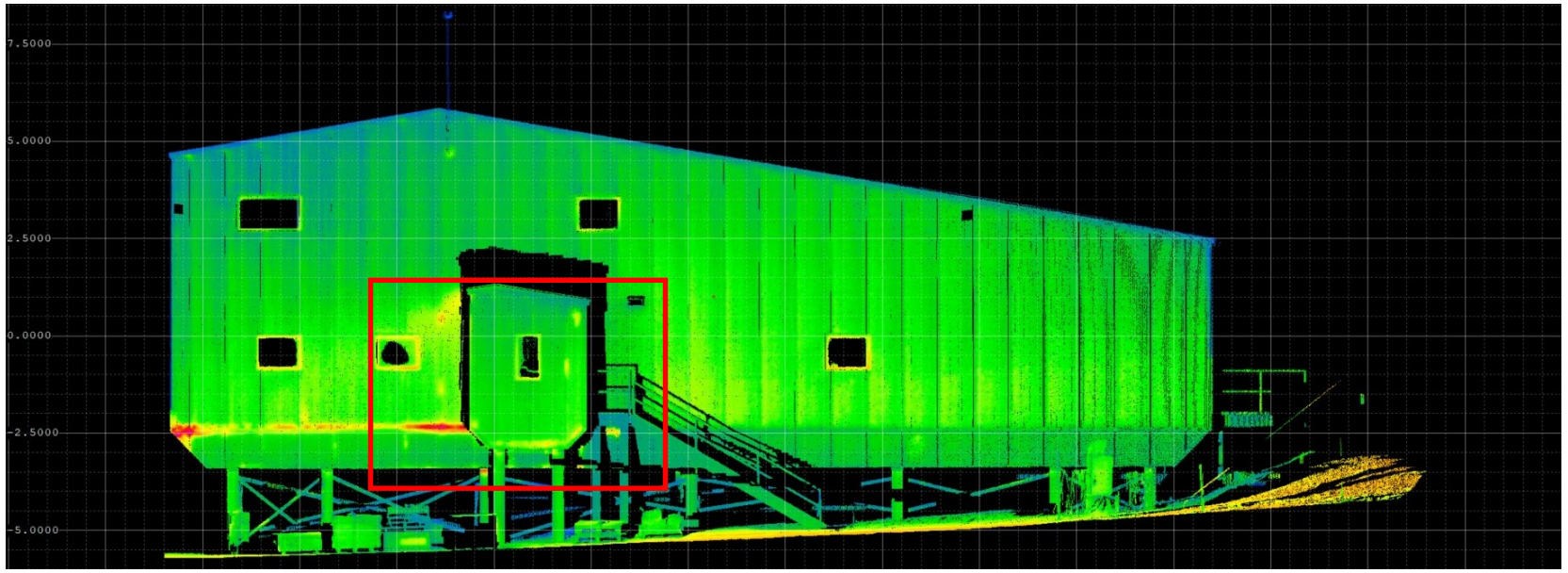




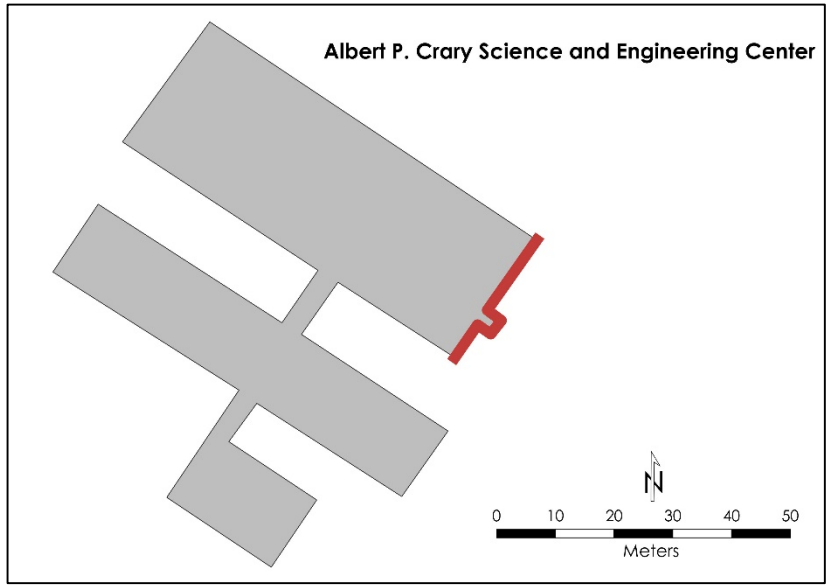
P1E-W-05 -15◦C 5◦C

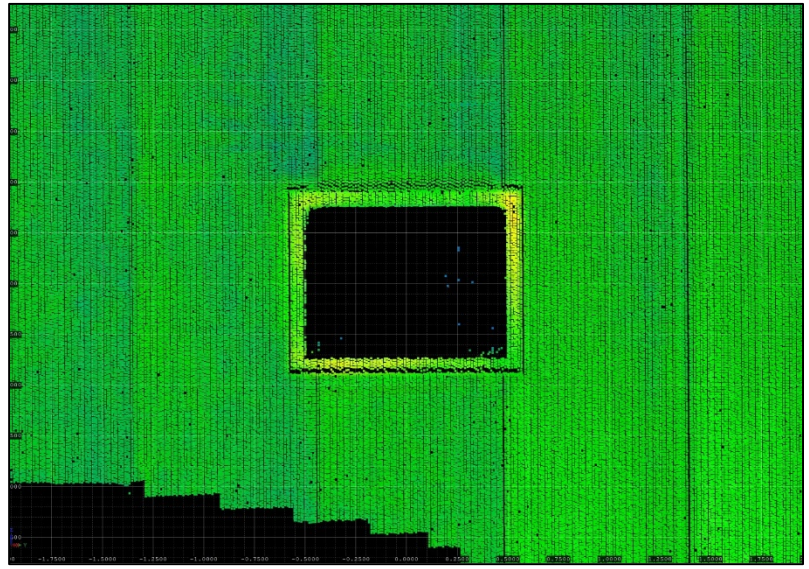


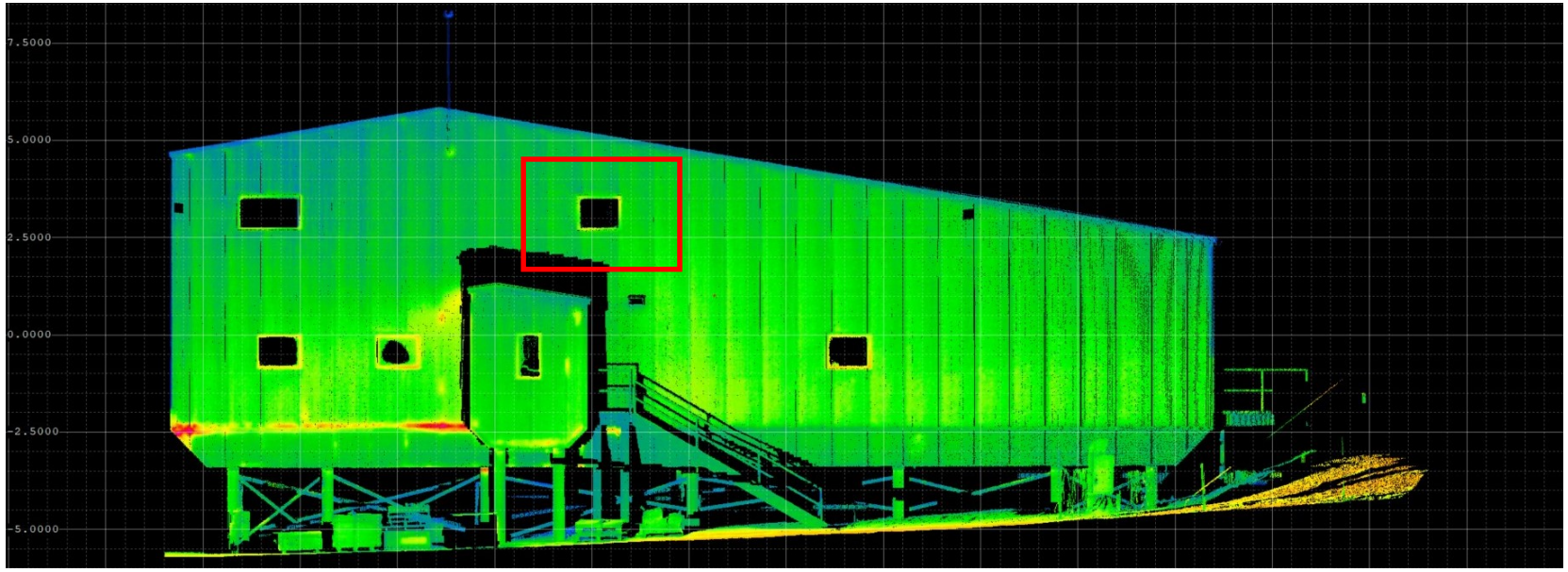




P1E-TA-05 -15◦C 5◦C





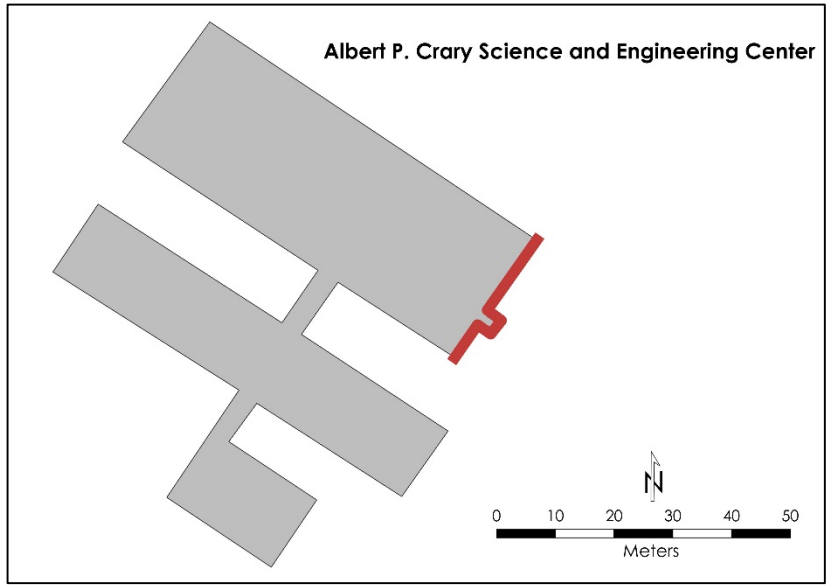


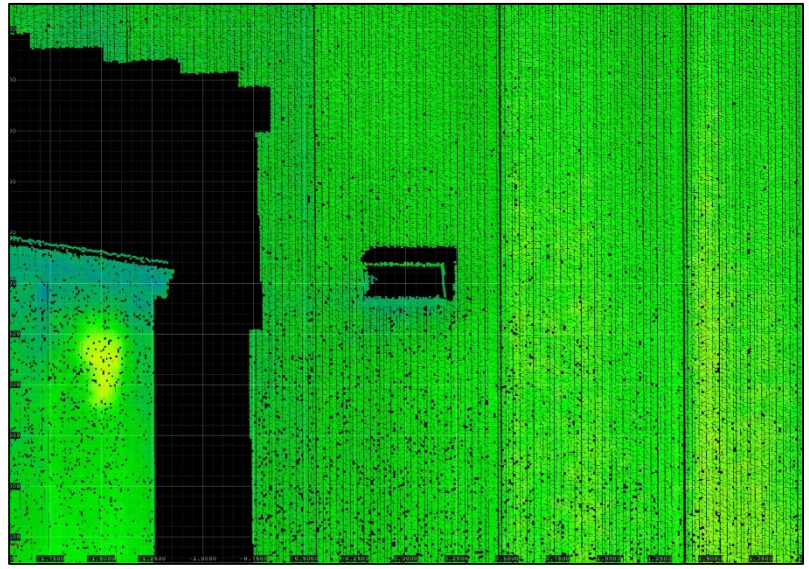
P1E-W-06

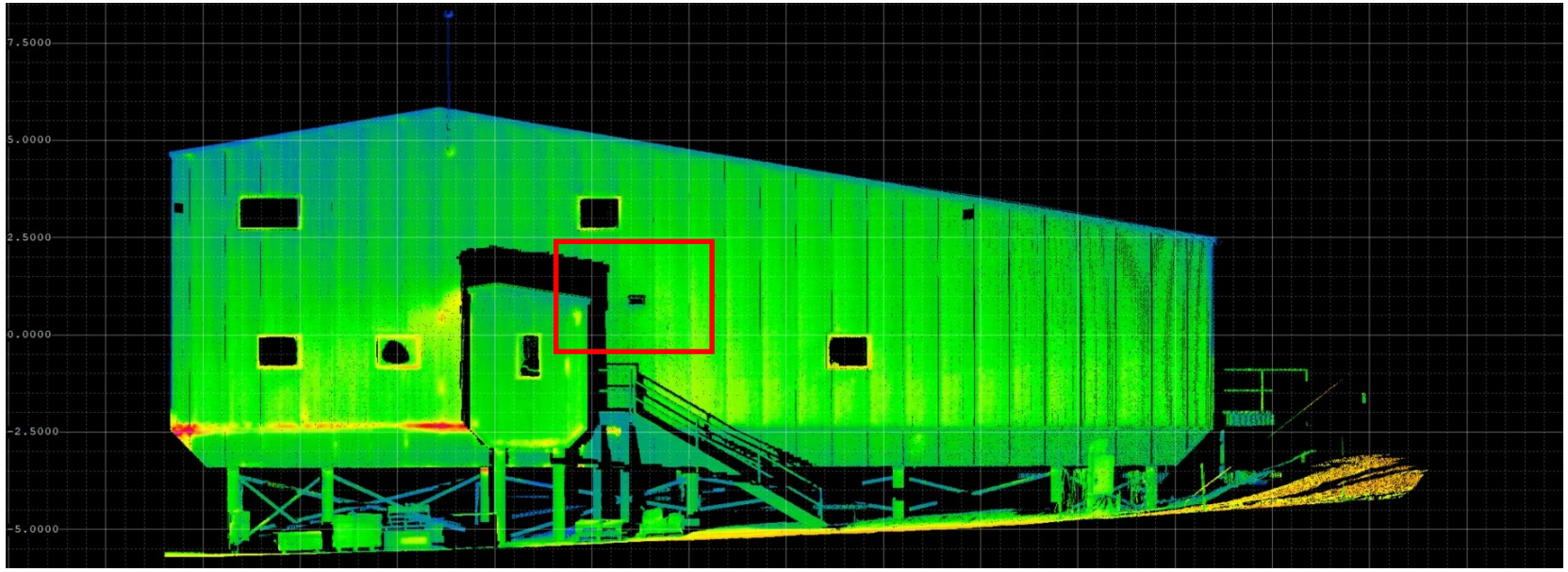
-15◦C



5◦C





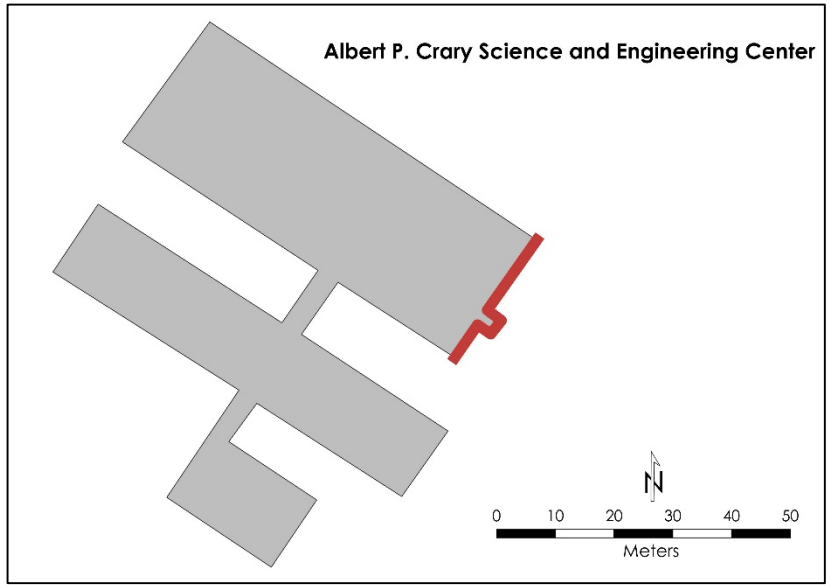


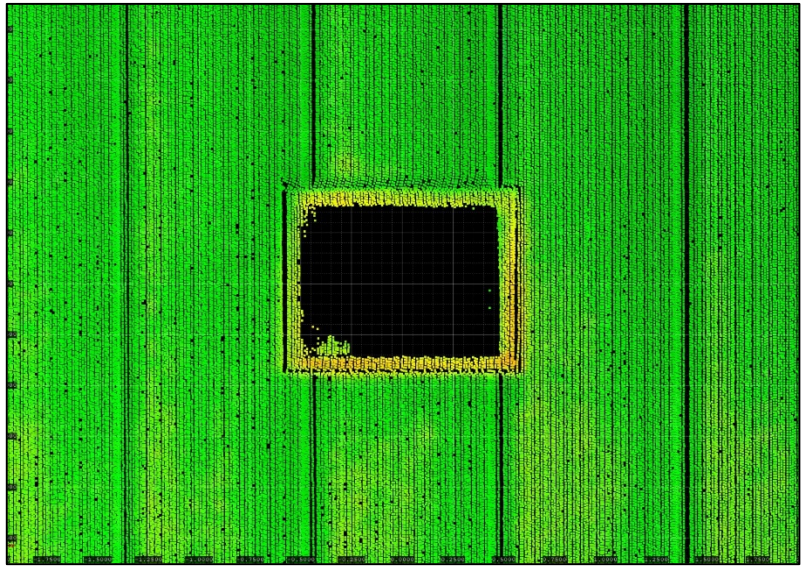
P1E-V-01

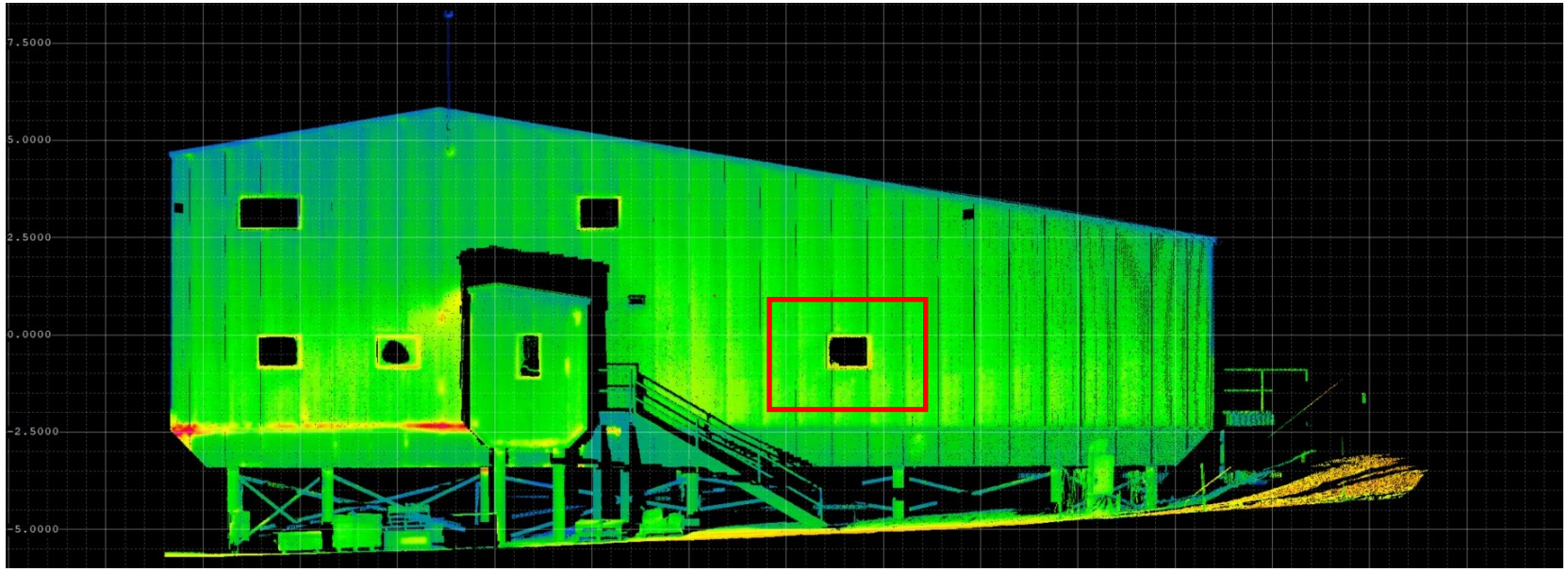
-15◦C



5◦C





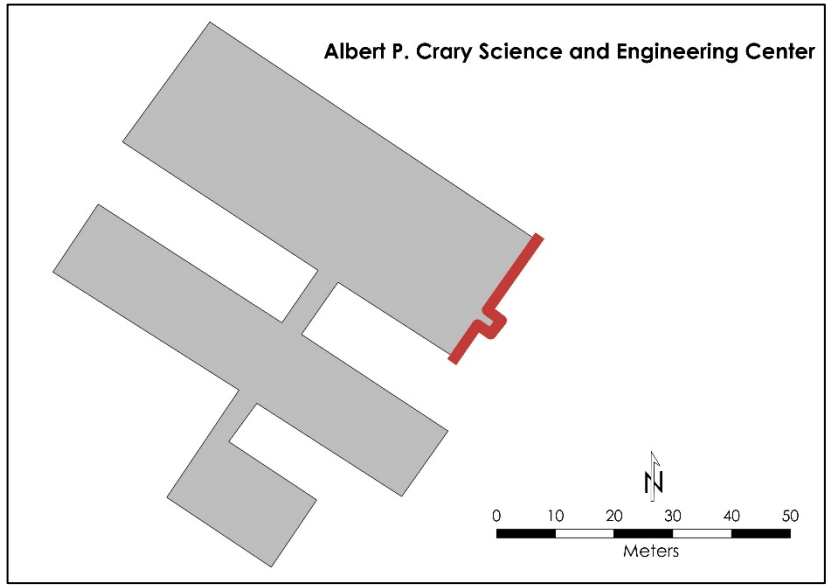


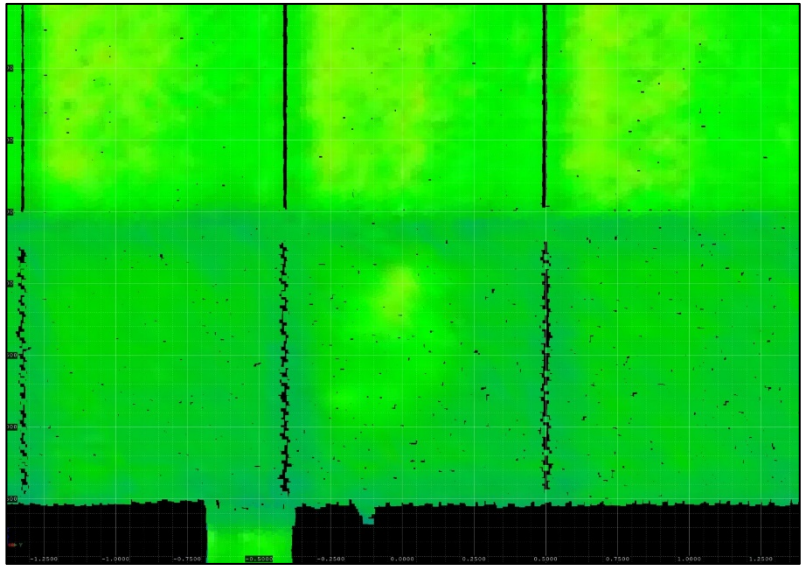
P1E-W-07

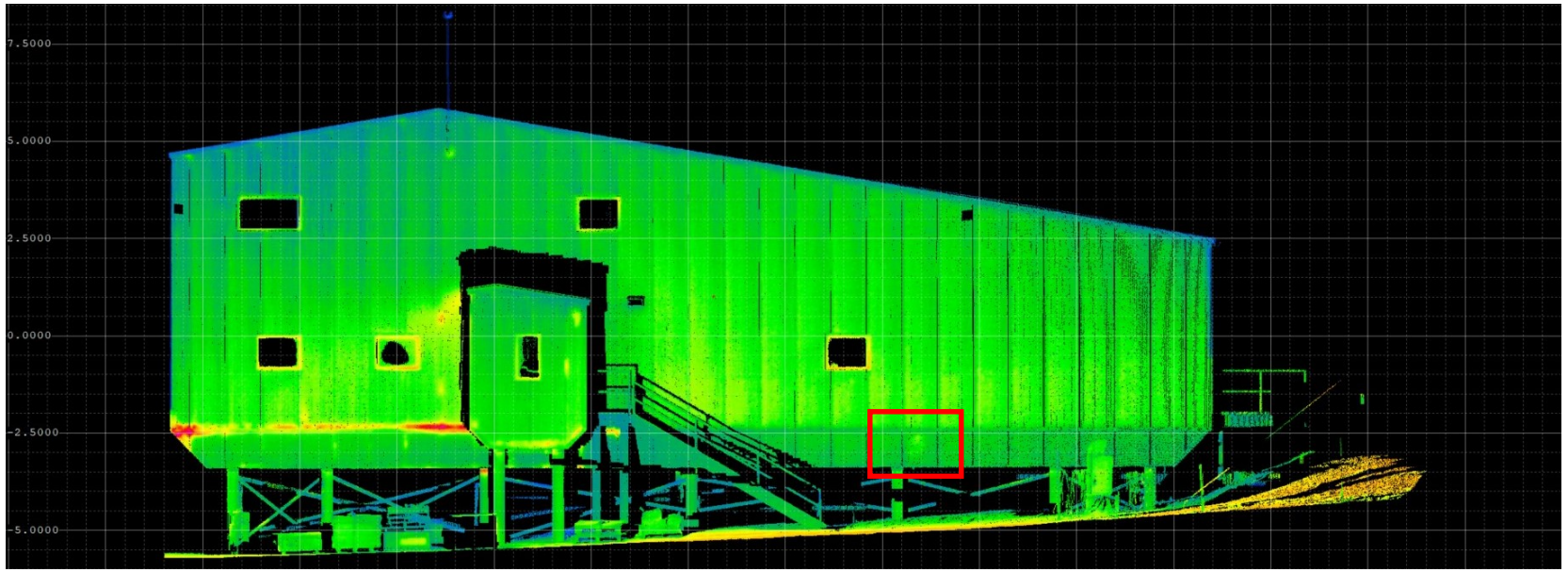
-15◦C



5◦C







P1E-TA-06 -15◦C 5◦C

REPORT DOCUMENTATION PAGE

Form Approved
OMB No. 0704-0188

Public reporting burden for this collection of information is estimated to average 1 hour per response, including the time for reviewing instructions, searching existing data sources, gathering and maintaining the data needed, and completing and reviewing this collection of information. Send comments regarding this burden estimate or any other aspect of this collection of information, including suggestions for reducing this burden to Department of Defense, Washington Headquarters Services, Directorate for Information Operations and Reports (0704-0188), 1215 Jefferson Davis Highway, Suite 1204, Arlington, VA 22202-4302. Respondents should be aware that notwithstanding any other provision of law, no person shall be subject to any penalty for failing to comply with a collection of information if it does not display a currently valid OMB control number. PLEASE DO NOT RETURN YOUR FORM TO THE ABOVE ADDRESS.

1. REPORT DATE (DD-MM-YYYY)	2. REPORT TYPE	3. DATES COVERED (From - To)
March 2022	Final Report	FY20–FY22

4. TITLE AND SUBTITLE
Continued Investigation of Thermal and Lidar Surveys of Building Infrastructure: Crary Lab and Wet Utility Corridor, McMurdo Station, Antarctica

5a. CONTRACT NUMBER

5b. GRANT NUMBER

5c. PROGRAM ELEMENT

6. AUTHOR(S)
Adam L. LeWinter, Elias J. Deeb, Dominic L. Filiano, and David C. Finnegan

5d. PROJECT NUMBER

5e. TASK NUMBER

5f. WORK UNIT NUMBER

7. PERFORMING ORGANIZATION NAME(S) AND ADDRESS(ES)
U.S. Army Engineer Research and Development Center (ERDC)
Cold Regions Research and Engineering Laboratory (CRREL)
72 Lyme Road
Hanover, NH 03755-1290

8. PERFORMING ORGANIZATION REPORT NUMBER
ERDC/CRREL TR-22-5

9. SPONSORING / MONITORING AGENCY NAME(S) AND ADDRESS(ES)
National Science Foundation, Office of Polar Programs
2415 Eisenhower Avenue
Alexandria, VA 22314

10. SPONSOR/MONITOR'S ACRONYM(S)
NSF

11. SPONSOR/MONITOR'S REPORT NUMBER(S)

12. DISTRIBUTION / AVAILABILITY STATEMENT
Approved for public release; distribution is unlimited.

13. SUPPLEMENTARY NOTES
Funded under Engineering for Polar Operations, Logistics, and Research (EPOLAR) Customer Order No. 1564557, ANT-19-11, "Continued Investigation of Thermal and Lidar Surveys of Building Infrastructure: Crary Lab and Wet Utility Corridor, McMurdo Station, Antarctica"

14. ABSTRACT

We conducted a combined lidar and thermal infrared survey from both ground-based and Unmanned Aerial System (UAS) platforms at McMurdo Station, Antarctica, in February 2020 to assess the building thermal envelope and infrastructure of the Crary Lab and the wet utility corridor (utilidor). These high-accuracy, coregistered data produced a 3-D model with assigned temperature values for measured surfaces, useful in identifying thermal anomalies and areas for potential improvements and for assessing building and utilidor infrastructure by locating and quantifying areas settlement and structural anomalies.

The ground-based survey of the Crary Lab was similar to previous work performed by the team at both Palmer (2015) and South Pole (2017) Stations. The UAS platform focused on approximately 10,500 linear-feet of utilidor throughout McMurdo Station. The datasets of the two survey areas overlapped, allowing us to combine them into a single, georeferenced 3-D model of McMurdo Station. Coincident exterior temperature and atmospheric measurements and Global Navigation Satellite System real-time kinematic surveys provided further insights.

Finally, we assessed the thermal envelope of the Crary Lab and the structural features of the utilidor. The resulting dataset is available for analysis and quantification.

15. SUBJECT TERMS
Building envelope, Buildings--Thermal properties--Testing, Digital elevation model, EPOLAR, Infrastructure, Lidar, Mapping, McMurdo Station (Antarctica), NSF, Optical radar, Point cloud, Thermal infrared, Unmanned aerial system

16. SECURITY CLASSIFICATION OF:			17. LIMITATION OF ABSTRACT	18. NUMBER OF PAGES	19a. NAME OF RESPONSIBLE PERSON
a. REPORT	b. ABSTRACT	c. THIS PAGE			19b. TELEPHONE NUMBER (include area code)
Unclassified	Unclassified	Unclassified	SAR	277	